INNOVATIVE TECHNOLOGIES FOR VERTICAL FARMING

EDITED BY: Jung Eek Son, Eiji Goto, Murat Kacira and Francesco Orsini

PUBLISHED IN: Frontiers in Plant Science

frontiers Research Topics

ISSN 1664-8714
ISBN 978-2-88976-388-7
DOI 10.3389/978-2-88976-388-7

About Frontiers

Frontiers is more than just an open-access publisher of scholarly articles: it is a pioneering approach to the world of academia, radically improving the way scholarly research is managed. The grand vision of Frontiers is a world where all people have an equal opportunity to seek, share and generate knowledge. Frontiers provides immediate and permanent online open access to all its publications, but this alone is not enough to realize our grand goals.

Frontiers Journal Series

The Frontiers Journal Series is a multi-tier and interdisciplinary set of open-access, online journals, promising a paradigm shift from the current review, selection and dissemination processes in academic publishing. All Frontiers journals are driven by researchers for researchers; therefore, they constitute a service to the scholarly community. At the same time, the Frontiers Journal Series operates on a revolutionary invention, the tiered publishing system, initially addressing specific communities of scholars, and gradually climbing up to broader public understanding, thus serving the interests of the lay society, too.

Dedication to Quality

Each Frontiers article is a landmark of the highest quality, thanks to genuinely collaborative interactions between authors and review editors, who include some of the world's best academicians. Research must be certified by peers before entering a stream of knowledge that may eventually reach the public - and shape society; therefore, Frontiers only applies the most rigorous and unbiased reviews.
Frontiers revolutionizes research publishing by freely delivering the most outstanding research, evaluated with no bias from both the academic and social point of view. By applying the most advanced information technologies, Frontiers is catapulting scholarly publishing into a new generation.

What are Frontiers Research Topics?

Frontiers Research Topics are very popular trademarks of the Frontiers Journals Series: they are collections of at least ten articles, all centered on a particular subject. With their unique mix of varied contributions from Original Research to Review Articles, Frontiers Research Topics unify the most influential researchers, the latest key findings and historical advances in a hot research area! Find out more on how to host your own Frontiers Research Topic or contribute to one as an author by contacting the Frontiers Editorial Office: frontiersin.org/about/contact

INNOVATIVE TECHNOLOGIES FOR VERTICAL FARMING

Topic Editors:
Jung Eek Son, Seoul National University, South Korea
Eiji Goto, Chiba University, Japan
Murat Kacira, University of Arizona, United States
Francesco Orsini, University of Bologna, Italy

Citation: Son, J. E., Goto, E., Kacira, M., Orsini, F., eds. (2022). Innovative Technologies for Vertical Farming. Lausanne: Frontiers Media SA.
doi: 10.3389/978-2-88976-388-7

Table of Contents

frontiers in Plant Science

ORIGINAL RESEARCH
published: 25 May 2021
doi: 10.3389/fpls.2021.649304

Improving the Fertigation of Soilless Urban Vertical Agriculture Through the Combination of Struvite and Rhizobia Inoculation in *Phaseolus vulgaris*

Verónica Arcas-Pilz[1], Felipe Parada[1], Gara Villalba[1,2], Martí Rufí-Salis[1,2], Antoni Rosell-Melé[3,4] and Xavier Gabarrell Durany[1,2]*

[1] Sostenipra Research Group (2017 SGR 1683), Institut de Ciència i Tecnologia Ambientals (CEX2019-000940-M), Universitat Autònoma de Barcelona, Barcelona, Spain, [2] Department of Chemical, Biological and Environmental Engineering, Universitat Autònoma de Barcelona, Barcelona, Spain, [3] Institut de Ciència i Tecnologia Ambientals, Universitat Autònoma de Barcelona, Barcelona, Spain, [4] Institució Catalana de Recerca i Estudis Avançats, Barcelona, Spain

OPEN ACCESS

Edited by:
Jung Eek Son, Seoul National University, South Korea

Reviewed by:
Pradeep Kumar, Central Arid Zone Research Institute (ICAR), India
Silvia Pampana, University of Pisa, Italy

***Correspondence:**
Gara Villalba
gara.villalba@uab.cat

Specialty section:
This article was submitted to Crop and Product Physiology, a section of the journal Frontiers in Plant Science

Received: *04 January 2021*
Accepted: *27 April 2021*
Published: *25 May 2021*

Citation:
Arcas-Pilz V, Parada F, Villalba G, Rufí-Salis M, Rosell-Melé A and Gabarrell Durany X (2021) Improving the Fertigation of Soilless Urban Vertical Agriculture Through the Combination of Struvite and Rhizobia Inoculation in Phaseolus vulgaris. Front. Plant Sci. 12:649304. doi: 10.3389/fpls.2021.649304

Soilless crop production is a viable way to promote vertical agriculture in urban areas, but it relies extensively on the use of mineral fertilizer. Thus, the benefits of fresher, local food and avoiding the transportation and packaging associated with food import could be counteracted by an increase in nutrient-rich wastewater, which could contribute to freshwater and marine eutrophication. The present study aimed to explore the use of mineral fertilizer substitutes in soilless agriculture. *Phaseolus vulgaris* (common bean) was fertilized with a combination of slow-releasing fertilizer struvite (a source of N, P, and Mg), which is a byproduct of wastewater treatment plants, and inoculation with Rhizobium (a N_2-fixing soil bacteria). The experiment included three bean-production lines: (A) 2 g/plant of struvite and rhizobial inoculation; (B) 5 g/plant of struvite and rhizobial inoculation, both irrigated with a Mg-, P-, and N-free nutrient solution; and (C) a control treatment that consisted of irrigation with a full nutrient solution and no inoculation. Plant growth, development, yields, and nutrient contents were determined at 35, 62, and 84 days after transplanting as well as biological N_2 fixation, which was determined using the ^{15}N natural abundance method. Treatments A and B resulted in lower total yields per plant than the control C treatment (e.g., 59.35 ± 26.4 g plant^{-1} for A, 74.2 ± 23.0 g plant^{-1} for B, and 147.71 ± 45.3 g plant^{-1} for C). For A and B, the nodulation and N_2 fixation capacities appeared to increase with the amount of initially available struvite, but, over time, deficient levels of Mg were reached as well as nearly deficient levels of P, which could explain the lower yields. Nevertheless, we conclude that the combination of struvite and N_2-fixing bacteria covered the N needs of plants throughout the growth cycle. However, further studies are needed to determine the optimal struvite quantities for vertical agriculture systems that can meet the P and Mg requirements throughout the lifetime of the plants.

Keywords: fertigation control, struvite, rhizobium, plant physiology, nutrient uptake, soilless agricultural system

INTRODUCTION

From 1950 to 2018, the population living in urban areas grew more than fourfold to an estimated 4.2 billion people. This unprecedented population increase has greatly increased global food demand, which has exerted great pressure on natural resources (United Nations, 2019). In response, new ways to efficiently produce vegetables while minimizing land use are being explored (Sanyé-Mengual et al., 2015, 2018). One of these initiatives is vertical farming with the use of soilless production systems with growing media or substrates (Sonneveld and Voogt, 2009), which would reduce the transportation and packaging of foodstuffs to cities (Sanyé et al., 2012). However, vertical agriculture relies extensively on the use of mineral fertilizer, which results in nitrates and phosphate being discharged into wastewater, which can contribute to freshwater and marine eutrophication (Anton et al., 2005; Gopalakrishnan et al., 2015; Sanjuan-Delmás et al., 2018).

This extensive use of mineral fertilizers affects not only the environment but can also be related to a high cost of production and extraction, as is the case for nitrogen fertilizers due to the Haber-Bosch process (Cherkasov et al., 2015) and for phosphorous due to phosphate rock extraction (Cordell and White, 2013). The widespread use of these nutrients has caused vertical farming to rely entirely on them, which thus makes this agricultural practice unsustainable in the long run. The high energy cost of synthetic nitrogen production and the ever-depleting sources of phosphate rock, when added to the environmental cost of their disposal and emissions to water and air (Rufí-Salís et al., 2020a,b), necessitates the search for alternatives to further implement these technologies in a sustainable way.

Many strategies have been described in recent years for the implementation of organic fertilization in vertical farming, which embraces a circular economy framework to reduce new resource inputs into cities. Some examples include fertilization that is based on gray water and urine (Ikeda and Tan, 1998; Karak and Bhattacharyya, 2011) and the use of biofertilizers such as Rhizobium for the cultivation of legumes (Kontopoulou et al., 2015; Savvas et al., 2018) for the plant nitrogen supply. Other methods describe the use of sewage sludge (Frossard et al., 1996), sewage sludge ash (Nanzer et al., 2014), and struvite (Rech et al., 2018) as alternative P sources. While these strategies may reduce the direct inputs of specific inorganic fertilizers, their use often results in lower crop yields and, in some cases, require more infrastructure for irrigation systems. These studies tend to focus on one particular nutrient alternative and do not consider the combination of alternative methodologies. Therefore, innovation to provide a solution for multiple mineral fertilizers while avoiding the addition of infrastructure as well as further environmental burdens due to local nutrient sourcing has not been widely studied.

Struvite ($MgNH_4PO_4.6H_2O$), which is a crystalline byproduct of wastewater treatment plants that formes by spontaneous or induced precipitation, usually contains high N and P concentrations (Rahman et al., 2014) and is regarded as a viable slow-releasing fertilizer due to its high P, Mg, and N contents, which average 12.5%, 9.9%, and 5.7%, respectively (Ahmed et al., 2018) and are suitable for plant growth (Degryse et al., 2017; Ahmed et al., 2018). Due to struvite's high nutrient concentrations, there are many ongoing efforts to optimize induced precipitation to make wastewater a valuable resource for providing a P alternative to the use of the depleting phosphate rock (Massey et al., 2007; Cordell et al., 2009; Talboys et al., 2016; Degryse et al., 2017).

A further positive aspect of struvite as an agricultural fertilizer substitute is its slow solubility in granular form (Talboys et al., 2016) under alkaline and neutral pH soil conditions (Bhuiyan et al., 2007). Thus, the risks of nutrient leaching and water eutrophication are rather small under these conditions when struvite is compared to common readily soluble fertilizers (Ahmed et al., 2018). Furthermore, the removal of approximately 30–40% of N and P from wastewater to produce this substance can prevent eutrophication in urban water cycles (González Ponce et al., 2009; Antonini et al., 2012). The granular form of struvite also causes it to be easily manageable and could be applied in larger-scale productions by mixing it with soil or applying it to the substrates in hydroponic production systems. The use of struvite has already been tested in agriculture as a substitute for phosphate from other sources and has shown promising results with low or even no yield losses reported (González Ponce et al., 2009; Cabeza et al., 2011; Liu et al., 2011; Ackerman et al., 2013; Degryse et al., 2017; Ahmed et al., 2018).

Although struvite already contains N that is available to plants, legumes have high N demands (McKey, 1994). Therefore, the average N contents in struvite would not be sufficient for soilless crops to achieve commercial yields and would require a second source of N to do so. This N could be obtained from Rhizobium, which is capable of forming an endosymbiotic interaction with leguminous plants by entering root cells and forming nodules. These nodules enable atmospheric N_2 fixation and ammonia (NH_3) formation. Plants benefit from the bacteria that generate these compounds, while the bacteria can profit from photosynthesis-derived compounds (Long, 1989). This symbiosis, on the other hand, may entail a major requirement of nutrients from the plant, such as phosphorous, to satisfy the needs of the bacteria and successful nodulation (Olivera et al., 2004). Possible N_2 fixation depends on successful rhizobial root colonization, which is influenced by diverse factors, such as phosphorous fertilization, salinity, drought, and initial N availability (Araújo et al., 2007; Ntatsi et al., 2018; Savvas et al., 2018).

Rhizobium as a second source of N was chosen due to the lower inputs needed to achieve nitrogen intake by plants (Gopalakrishnan et al., 2015). When using the N_2-fixing bacterium, Rhizobium, in hydroponic cultivation, Kontopoulou et al. (2017) described the need to apply initial N fertilization until nodulation in the root medium occurs, to further encourage nodulation and therefore N fixation, plant growth, and production. Even though previous studies have reported lower production capacities for N_2-fixing plants than for common beans with N fertilization (Olivera et al., 2004; Kontopoulou et al., 2017), a combination of the two N sources (e.g., struvite and N_2-fixing bacteria) was used to determine the

possibility of overcoming such lower yields (Pampana et al., 2017; Savvas et al., 2018).

To determine how effective the two alternative fertilizers are in providing N to plants, the ^{15}N natural abundance method was employed to determine the source of N throughout the experiment (Shearer and Kohl, 1989). While plants with N that is acquired from symbiotic atmospheric N_2 fixation show the lower richness of the ^{15}N isotope, which corresponds to the atmospheric abundance (0.3663%), plant tissues that are subjected to other N sources can exhibit greater amounts of the ^{15}N isotope, which depend on the N fertilizer applied (Robinson, 2001).

The present study aimed to add to this growing pool of knowledge on vertical urban agriculture by exploring the use of mineral fertilizer substitutes struvite and rhizobium combined in an effort to reduce emissions of simultaneously N and P to the environment in urban vertical agriculture. This combination also aims to optimize crop yields while avoiding the installation of additional infrastructure. In this study, we analyzed the growth, development, and production of the common bean (*Phaseolus vulgaris*), which was fertilized with a combination of the slow-releasing fertilizer, struvite, and the soil bacteria, Rhizobium. A combination of these alternative fertilizers can be implemented easily in terms of cost and space and promotes nutrient recycling within cities.

MATERIALS AND METHODS

Experimental Site, Materials, and Growth Conditions

This experiment was conducted in the Rooftop Greenhouse Laboratory (RTG-Lab) of the Environmental Science and Technology Building (ICTA-UAB), which is located in the Universitat Autònoma de Barcelona Campus (42°29′24″ E, 45°94′36″ N) (Sanjuan-Delmás et al., 2018). The bean variety used in this experiment was *Phaseolus v. Pongo*, which had previously been germinated in a commercial greenhouse 10 days before transplanting in the RTG-Lab. The production system was soilless with a perlite substrate in 40 L bags and the use of fertigation through a 2 L/h drip irrigation system.

Bean seeds were treated with a commercial product (e.g., Nadicom GmbH©) which contained a mixture of *Rhizobium phaseoli* and *Rhizobium giardinii* strains for inoculation before planting. The inoculation procedure was an exposure of the plant seeds with the liquid commercial product before planting. A total of 5 days after the seedling was transplanted into the perlite substrate, 5 ml liquid commercial mix was added to each plant, therefore ensuring the presence of the bacteria in the substrate. Once the plants were inoculated, they were irrigated with an Mg-, P-, and N-free solution (**Supplementary Table 1b**), and application of K_2SO_4 was increased to adjust for the K requirements. The control plants, on the other hand, were irrigated with a full nutrient solution. These nutrient concentrations were maintained throughout the entire experiment. The crops were irrigated four times a day for 3 min, which provided a total amount of 400 ml per day per plant.

The inoculated plants were treated with two different struvite amounts placed inside the perlite bag around the root area and surface, varying the concentration of P and N available to the plant from struvite: (A) 2 g (1.02 mmol of P and 0.46 mmol of N) of granulated struvite per plant and (B) 5 g (2.57 mmol of P and 1.15 mmol of N) of granulated struvite per plant. The amount of struvite that was best for growth was determined in a previous experiment conducted in the same i-RTG in which 2.57 mmol P was deemed sufficient for common bean fertilization to reach an equivalent level of commercial production as that of mineral-fertilized beans. To ensure no struvite loss due to runoff, each plant was planted inside an additional 1 L bag containing perlite and the corresponding amount of struvite, with small holes to allow water drainage.

Each treatment was arranged randomly in four rows with 16 plants each (four perlite bags with 4 plants per bag were planted in a frame with an area of 0.125 m^2), which resulted in a total of 64 plants per treatment (e.g., A, B, and Control), with 192 plants in total (**Supplementary Figure 1b**). Due to the irrigation and leachate recovery systems, randomization could only be achieved for entire lines of four bags.

The plants were germinated and transplanted in duplicate and were thinned to one plant at 21 days after transplanting (DAT).

Greenhouse conditions were monitored during the entire experiment with T107 sensing devices (Campbell Scientific) that were placed along the cropping area to measure temperature, relative humidity, and radiation (see **Supplementary Table 2b**). To ensure proper plant irrigation drainage volumes, the pH and electrical conductivity levels of the leachate were recorded every day for each irrigation line.

The phenological stages of the bean plants were determined each week. This information was assessed to identify plant growth, development, and productivity over time and provided a clear view of the plant cycle, growth, and production peaks that enabled accurate comparisons of plant development between treatments and the control. This was performed by counting leaves, flower buttons, and open flowers. The number of ripened bean pods was also counted and weighed for each harvest. These measurements were performed for each of the eight plants that were in the two middle bags of each row (see **Supplementary Figure 1b**) and started 14 DAT. To ensure uniform counting, leaves under 5 cm length were not considered, and only fully formed flower buttons with white coloration and fully open flowers were counted. For the bean pods, a minimum length of 11 cm was used for harvesting, while bean pods shorter than this were retained for the next harvest. The average numbers and bean pod weights per treatment were then calculated for each week. At the same time and on a weekly basis, chlorophyll content measurements were performed (with a SPAD CCM-200 plus; Opti-Sciences, Inc.) on the same eight plants in the center of each row.

Description of Plant Sampling Methods

To determine the changes in plant development as well as nutritional states and ^{15}N concentrations, samples were taken during the three different crop stages. The first sampling took place 35 DAT, immediately before bean pod production started;

the second sampling took place 62 DAT, during the productive phase of the plants; and the last sampling took place 84 DAT, at the end of the productive stage, which marked the last day of the experiment.

The samples consisted of eight randomly chosen plants per treatment (excluding the eight central plants of each row that were kept for phenological analysis). Each plant was washed with deionized water, excess water was dried off and each plant was separated into the four main organs: leaves, shoots, roots, and nodules. These were then weighed separately to determine their fresh weights (FW). All organs were placed separately in envelopes and left to dry in an oven at 65°C until stabilized dry weights (DW) were obtained, which occurred after approximately 7–8 days. The means of the obtained values were calculated for each treatment, each organ, and time. The numbers of nodules were counted prior to drying to determine the mean nodulation of each plant. In addition, fruit samples from each treatment were taken at three different times (49, 62, and 77 DAT), which closely matched the three plant harvests.

Moreover, 25% of the total sampled leaves for each plant were separated to determine their areas before the drying process. To do so, these fresh leaves were scanned with a reference pixel to obtain leaf areas using ImageJ software (Rueden et al., 2017). These leaf areas were further extrapolated to 100% of the leaf biomass of the plant. The leaf area index (LAI) was then calculated by dividing the total leaf area by the area of the planting frame of our crop ($0.125 m^2$).

Nitrogen Isotopic ($\delta^{15}N$) Analysis

The goal of inoculating treatments A and B with Rhizobium was for the plants to indirectly fix N_2 from the air and meet their N needs in this way. To determine how much of the N assimilated by the plants came from the atmosphere, we used the natural abundance method (Shearer and Kohl, 1989) to identify the origin of the N that was obtained by the plants, which in our case, should be either struvite or atmospheric N. While treatments A and B were actively inoculated with Rhizobium strains and fertilized with struvite containing N, the control treatment was fertilized through standard N fertilization that was administered through irrigation. Additional nitrogen sources were not considered due to the laboratory conditions and production of inert perlite.

Analysis was performed with an elemental analyzer isotopic ratio mass spectrometer (EA-IRMS; Thermo Fisher Scientific). The devices used were a Flash EA 1112 analyzer and Delta V Advantage spectrometer that was coupled with a Conflo III interface. The plant and struvite samples were weighed in tin capsules and were introduced into the EA-IRMS system to obtain the $\delta^{15}N$ values, as calculated with the following equation (Eq. 1) (Robinson, 2001):

$$\delta^{15}N = \frac{Sample\ atom\ \%^{15}N - 0.3663}{0.3663} \times 1000$$

Equation 1: $\delta^{15}N$ is the natural tracer for our N sources, the sample atom %15N is the previously obtained value of our plant sample, and the value 0.3663 is a standard value that represents the percentage of ^{15}N in the atmosphere.

$\delta^{15}N$ values provide an indication of the N sources in plant tissues. Values close to 0 indicate that the plant N sources are mainly due to atmospheric N_2 fixation, while higher values can be interpreted as indicating mixed sources or those dominated by the N obtained from struvite. The $\delta^{15}N$ value obtained for the struvite used in the experiment was 7.1‰. To determine the relative contributions from the two sources considered, we used Eq. 2, which yields an estimate of the percentage of N that was derived from N_2- fixation (%Ndfa) (Shearer and Kohl, 1993; Unkovich et al., 2002; Arndt et al., 2004)

$$\%Ndfa = \frac{\delta^{15}N\ Source\ 2 - \delta^{15}N\ Sink}{\delta^{15}N\ Source\ 2 -'\ B' value} \times 100$$

Equation 2: %Ndfa (nitrogen derived from N_2 fixation from the atmosphere), δ15N Source 2 (‰) corresponds to the δ15N value of struvite, δ15N Sink (‰) corresponds to the δ15N value from the sample, and the "B" value corresponds to the δ15N of N_2 fixation taking into account possible fractionation.

The "B" value is the isotopic fractionation observed in N_2-fixing *P. vulgaris* was set to –1.16‰, which corresponded to the lowest $\delta^{15}N$ value obtained (Shearer and Kohl, 1989; Peoples et al., 2002; Kermah et al., 2018) and was similar to the values determined by Kontopoulou et al. (2017) in common bean that was fertilized without N and inoculated with Rhizobium.

The biologically fixed nitrogen (BNF) levels were further calculated with the obtained %Ndfa values as well as the obtained values for the nitrogen contents in the plants. To extrapolate to kg/ha, a theoretical plant density of eight plants/m^2 was used.

Finally, the nitrogen use efficiency (NUE) for all treatments was estimated. The methodology that was followed to perform these calculations was given by Weih (2014), who provided a tool to successfully calculate the NUE. To accomplish this, the information provided was as follows:

- N content at the initial stage of the plant in g/m^2 (previous to the main production stage at 35 DAT),
- N content at the main productive stage in g/m^2 (chosen at 84 DAT),
- N content in the harvested yield in g/m^2,
- Biomass yield g/m^2,
- Added N to the soil in g/m^2 (in this case, perlite).

Plant Nutritional Analysis

Dried and ground plant organs were weighed (up to 0.25 g) and digested using a single reaction chamber microwave (Milestone Ultrawave) with concentrated HNO_3. The digested samples were then diluted with 1% HNO_3 (v/v) and were analyzed by optical spectrometry (ICP-OES) (Perkin-Elmer, Optima 4300DV). All samples were weighed, digested, and analyzed in duplicate.

Statistical Analysis

All statistical analyses in this experiment were performed with R studio software. Data normality in our values was tested with Shapiro-Wilk test $p > 0.05$, and to ensure homogeneity of variance the Levene test was performed $p > 0.05$. When both criteria were validated Duncan's multiple range test was

used to assess the statistical significance of treatments. The Kruskal-Wallis test was used for no parametric data. The significance between the treatments was tested for each harvest time separately.

RESULTS

Phenology, Biomass, and Yield

Weekly recordings of the phenological growth of the bean plants exhibited differences among all treatments (**Figure 1**). In this figure, we can see the evolution throughout the crop development of biomass production as well as flower production and finally bean pod production. The control plants (Treatment C) showed greater biomass growth and faster development in their transitions from flower buttons to open flowers and bean pod production. Although the treatment performances were similar in the earlier growth stages, once the production stage started, greater differences were observed.

At 40 DAT and 50 DAT, treatments A and B began to perform worse for leaf production as well as for the formation and opening of flower buttons than the control plants (C). Between 60 DAT and 70 DAT, a second production peak can be seen for the control treatment as well as rapid generation of flower buttons, while treatments A and B showed a declining pattern for bean pod production.

Table 1 shows the changes in the plant measurement results that were conducted on the sampled plants at three different developmental stages. While the first period of plant sampling, 35 DAT, showed very few significant differences among the treatments (only in the case of dry weight), the later samplings at 62 and 84 DAT showed greater differences between treatments. At this point, the leaf and shoot dry weights were greater for the control treatment, as was the measured leaf area index. The only parameter without significant differences among treatments throughout the entire experiment was the root dry weight at 62 DAT. The dry weights of the nodules exhibited persistent, significant differences for the three samplings among treatments A and B and control treatment C and reached maximum values of 0.16 g, 0.12 g, and 0.05 g for treatments A, B, and C, respectively. On the other hand, treatment B (with higher struvite quantities) also exhibited significantly greater numbers of nodules as well as higher weights than the other two treatments during the third sample period.

When examining the SPAD measurements (**Supplementary Figure 2b**), some differences in chlorophyll content were observed throughout the experiment. Initially, we can see a significant difference between the A and B treatments and the control marking a greater chlorophyll content in the latter that is sustained until 35 DAT. From 42 DAT to 63 DAT, the chlorophyll content in treatments A and B increases while treatment C remains stable. While differences toward the end of the experiment remain small, we can appreciate a greater chlorophyll content in the struvite fertilized treatments.

The final production amounts that were obtained for all three treatments were 1899.2 g, 2375.6 g, and 4726.7 g of green bean pods for treatments A, B, and C, respectively. Although the plants treated with struvite and rhizobium produced approximately half the yield of the mineral-fertilized plants, it is important to note that they were healthy throughout the experiment. The average yields provided per plant were $59.35 \pm 26.4\ g^{a}\ plant^{-1}$ for A, $74.24 \pm 23.0\ g^{a}\ plant^{-1}$ for B, and $147.71 \pm 45.3\ g^{b}\ plant^{-1}$ for the control treatment C. These production differences can also be seen in **Figure 1** where the obtained yields are shown as a function of time and show greater production peaks and a more rapid ability to develop flower buttons and open flowers after each harvest.

$\delta^{15}N$, %Ndfa and Biologically Fixed N

The results obtained for the $\delta^{15}N$ values of plant tissues and bean pods as seen in **Figure 2** (and **Supplementary Figure 3b**) show great variability in the enrichment of all organs except for the nodules. While treatment C showed clear enrichment over time, the pattern for treatments A and B was the opposite. For the nodules, all three treatments exhibited clear enrichment over time. Treatment B exhibited intermediate $\delta^{15}N$ values that were between those of A and C, with decreasing $\delta^{15}N$ values that were not as abrupt when compared to the tissues that were exposed to treatment A. It was also interesting to observe that the major decrease in $\delta^{15}N$ values for treatment A occurred between days 35 and 62 after transplanting and remained rather constant at 84 DAT. For the plants in treatment B, the value at 62 DAT did not fall as drastically and experienced a more significant change at 84 DAT.

When calculating the percentage of fixed atmospheric N during our three sampling periods, we obtained the values shown in **Figure 3**. This figure shows the approximate percentages of N that were derived from atmospheric fixation relative to the total N obtained by the plants.

As shown in the figure, the percentages of fixed N_2 in all three tissues were higher for the plants in treatment A, with values of 65-80% at 35 DAT, which reached 90% by the end of the experiment (84 DAT). On the other hand, treatment B exhibited lower values throughout the experiment, with initial values close to 50% to 60% (35 DAT), which reached final values of 80% at 84 DAT.

While the plants with less struvite in the root medium (treatment A) increased their percentages of fixed N_2 more rapidly (from 70% (35 DAT) to 90% (62 DAT) in the leaves), the plants in treatment B took longer to reach this value (from 60% (35 DAT) to 71% (62 DAT) in leaves). This corresponds to the results for the $\delta^{15}N$ values shown in **Figure 2**.

Table 2 shows the results of the estimations of biological fixed nitrogen (BNF) contents expressed in kg/ha. These results show the extrapolations of total N found in the plants for each treatment to kg/ha values. The N percentages that were of atmospheric origin (obtained previously) were further used to attain the kg/ha of biologically fixed nitrogen for each treatment as well as the N from struvite that was used by the plants.

Here, we can see that as the percentages of atmospheric-derived N and total N that were found in the plants increased, as well as the kg/ha values of biologically fixed N. While the plants in

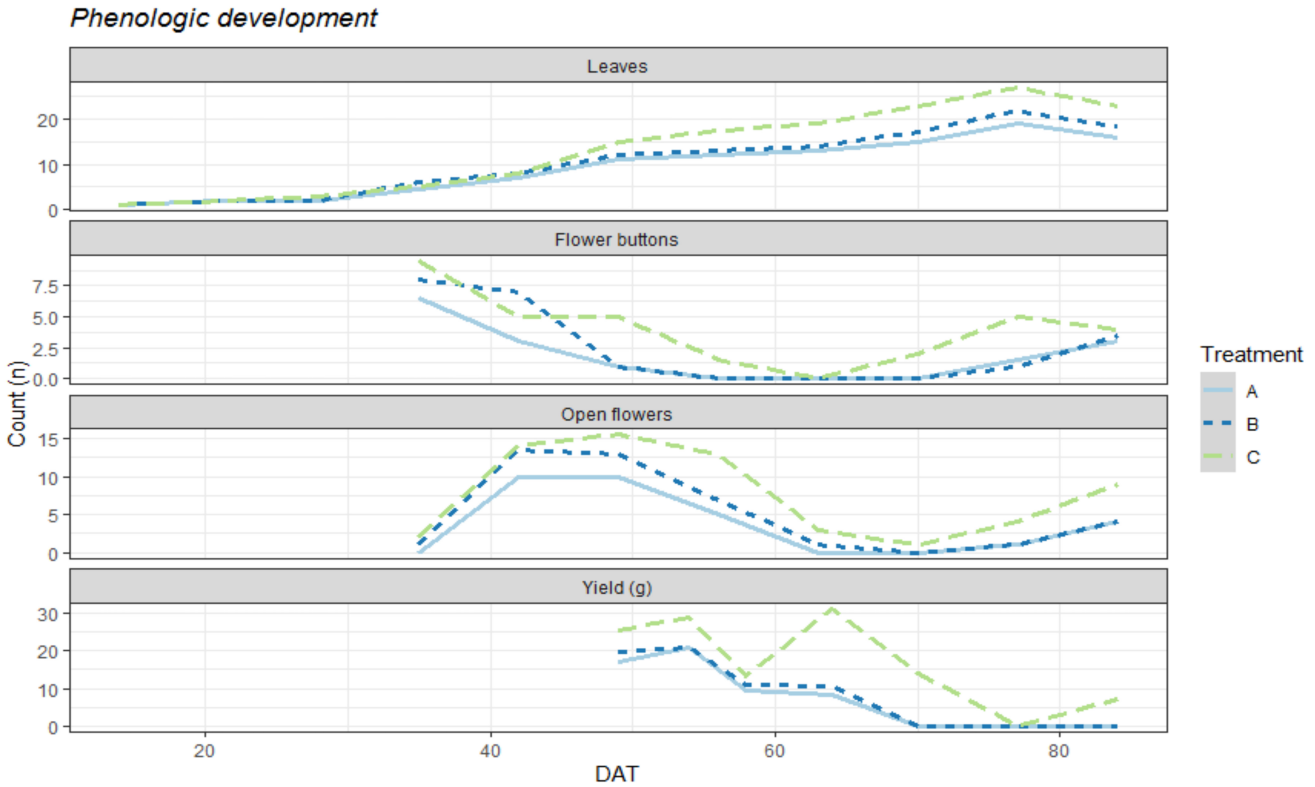

FIGURE 1 | Graphic representation of the mean numerical count per plant for each organ (Leaves, flower buttons, open flowers) and yield in g/plant on a weekly basis, DAT representing the days after transplanting inside the iRTG. The colors represent the three treatments: A = N.free solution with Rhizobium inoculation and 2g of struvite per plant. B = N.free solution with Rhizobium inoculation and 5g of struvite per plant. C = Complete nutrient solution without struvite and no inoculation treatment.

TABLE 1 | Results for the mean values (n = 8) per plant of fresh weight (FW) and dry weight (DW) of the different organs as well as the Leaf Area Index (LAI) m^2 $plant^{-1}$ of the three treatments (A = 2g Struvite + Rhizobium; B = 5g Struvite + Rhizobium; C = Control) in three different time periods: 35 DAT (1), 62 DAT (2), and 84 DAT (3).

	Leaf DW (g) per plant	Shoot DW (g) per plant	Roots DW (g) per plant	Nodules n per plant	Nodules DW per plant (g)	LAI
(1)						
A	$1.12^{a} \pm 0.22$	$0.46^{a} \pm 0.08$	$0.44^{a} \pm 0.10$	$132.50^{a} \pm 80.35$	$0.16^{b} \pm 0.07$	$0.57^{a} \pm 0.12$
B	$1.31^{a} \pm 0.46$	$0.56^{a} \pm 0.19$	$0.51^{a} \pm 0.15$	$156.75^{a} \pm 60.82$	$0.12^{b} \pm 0.06$	$0.62^{a} \pm 0.23$
C	$1.33^{a} \pm 0.57$	$0.58^{a} \pm 0.18$	$0.53^{a} \pm 0.14$	$148.75^{a} \pm 48.23$	$0.05^{a} \pm 0.02$	$0.65^{a} \pm 0.27$
(2)						
A	$3.97^{a} \pm 1.25$	$2.02^{a} \pm 0.72$	$0.80^{a} \pm 0.28$	$127.88^{a} \pm 63.85$	$0.14^{b} \pm 0.09$	$1.28^{a} \pm 0.51$
B	$3.69^{a} \pm 1.53$	$2.24^{a} \pm 1.01$	$0.87^{a} \pm 0.34$	$172.25^{a} \pm 132.66$	$0.15^{b} \pm 0.14$	$1.29^{a} \pm 0.64$
C	$6.44^{b} \pm 3.09$	$3.85^{b} \pm 1.95$	$0.95^{a} \pm 0.44$	$82.25^{a} \pm 62.47$	$0.01^{a} \pm 0.01$	$2.64^{b} \pm 1.33$
(3)						
A	$5.86^{a} \pm 2.96$	$3.09^{a} \pm 1.45$	$1.77^{a} \pm 0.79$	$136.88^{b} \pm 106.31$	$0.15^{b} \pm 0.13$	$1.74^{a} \pm 0.92$
B	$7.40^{a} \pm 2.17$	$4.53^{a} \pm 1.48$	$2.49^{a} \pm 0.57$	$186.25^{c} \pm 48.79$	$0.24^{b} \pm 0.11$	$1.80^{a} \pm 0.67$
C	$11.11^{b} \pm 1.51$	$6.91^{b} \pm 1.42$	$3.35^{b} \pm 0.88$	$39.13^{a} \pm 24.76$	$0.02^{a} \pm 0.02$	$3.72^{b} \pm 0.87$

Significant differences ($p < 0.05$) between treatments marked with different letter (a,b,c).

treatment A had higher values of biologically fixed N during the first two sampling periods at 84 DAT, the increase in the fixation percentage and total N in the plants in treatment B increased their amounts of biologically fixed N. On the other hand, the use of N from struvite increased only for treatment B and remained constant for treatment A.

Nutrient Content

The nutrient contents in the aboveground plant organs are presented in **Figure 4** (**Supplementary Figure 5b** for differences between harvests). The observed concentrations of nutrients in leaves for the three treatments were at sufficient levels except for the less than optimal Mg^{2+} concentrations at 62 DAT for

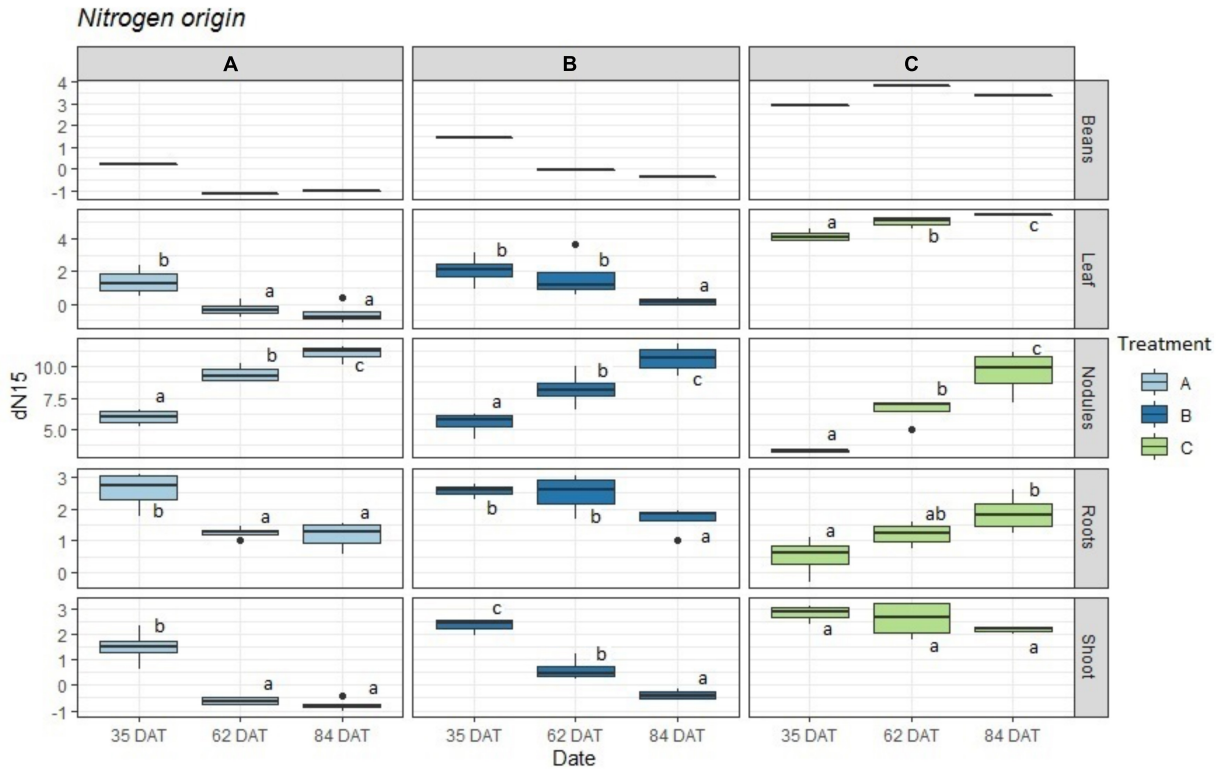

FIGURE 2 | Boxplot representing the obtained $\delta^{15}N$ values ($n = 4$) for treatments: A = 2g of struvite + Rhizobium inoculation + P, Mg, N-free nutrient solution, B = 5g of struvite + Rhizobium inoculation + P, Mg, N-free nutrient solution and C = standard nutrient solution - Rhizobium inoculation. These observed values are given by plant organs in three different time periods: 35 days after transplanting, 62 days after transplanting, and 84 days after transplanting. Significant differences ($p < 0.05$) between dates marked with different letter (a,b,c).

treatments A and at 84 DAT for treatments A and B and were close to deficient levels P in both treatments A and B at 62 and 84 DAT according to Hochmuth et al. (2018). In the case of N, in both leaf and shoot tissues, no deficient levels were found for any of the treatments, and no significant differences were found among treatments. On the other hand, a clear decline in P and Mg^{2+} over time can be seen for treatments A and B in the leaves as well as for P in the shoots. The control treatment (C), on the other hand, remained stable.

Supplementary Figure 4b also indicates the total nutrient contents that are bound to the total biomass of the sampled plants. Here, it is apparent that treatment B, with more struvite, provided results that were between those of the other treatments. In the case of Mg at 35 DAT in leaves, treatment B showed levels as high as those for the control treatment, but while the latter remained constant over time, both A and B decreased. The same trend can be seen for P in both leaves and shoots. In the case of N, we can see an increase for all treatments that was faster for control C, while A and B increased in a similar fashion.

Finally, the NUEs obtained for all three treatments were 1.32 g/g, 0.55 g/g, and 0.29 g/g for A, B, and C, respectively. The calculation methodology considered that N was in the soil, while the fixed nitrogen was not considered; therefore, the use efficiency can be very different for all three treatments.

DISCUSSION

Plant Growth and Development

The results indicate that once the first production peak was reached, the control plants were more capable of continuing to produce flower buttons, while the inoculated and struvite-fertilized plants took longer. The relationship between their development and the amount of struvite given to the plants seems to be directly correlated. Generally, the biomass and bean pod production was higher in the control plants, while treatment B had a greater amount of struvite (5 g). Treatment A, with the lowest amount of struvite (2 g), was determined to be the treatment with the lowest growth and production rates. These findings agree with those presented in previous literature (Nanjareddy et al., 2014), for which lower KNO_3 availability was directly linked to a reduction in leaf and flower formation. This reduction also seemed to be related to the P and Mg availability over time due to struvite depletion, considering that the initial performance was similar in all three treatments.

By observing the SPAD measurements, the chlorophyll contents in all three treatments indicated that the N contents in the leaves were not strongly affected by the treatments but rather the LAI. Lower P availability resulted in a reduction in LAI as well as in overall plant growth, which was observed in

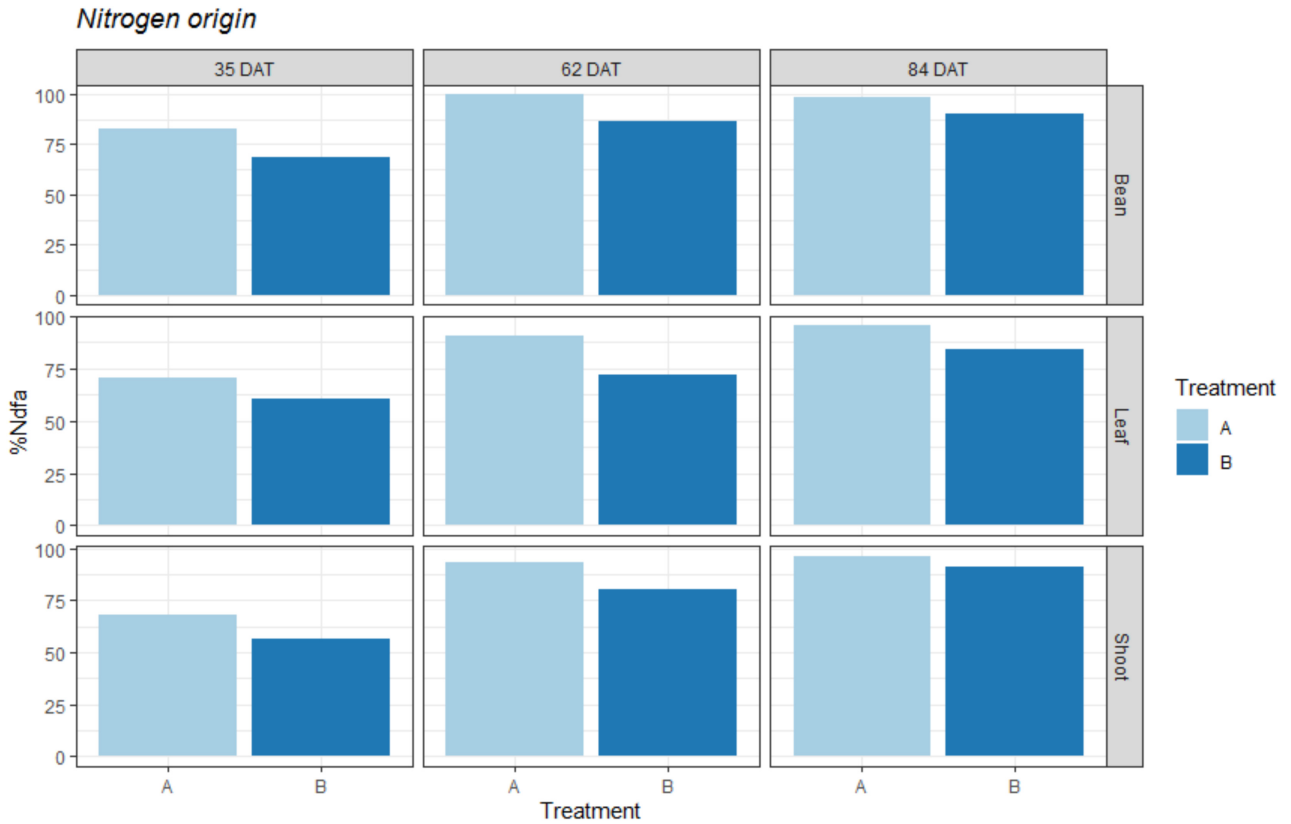

FIGURE 3 | Percentage of Nitrogen derived from atmospheric N2 fixation (%Ndfa) represented for treatments: A = 2g of struvite + Rhizobium inoculation + P, Mg, N-free nutrient solution, and B = 5g of struvite + Rhizobium inoculation + P, Mg, N-free nutrient solution. These observed values are given for two plant organs (leaf; shoot) as well as the bean pods in three different time periods: 35 days after transplanting, 62 days after transplanting, and 84 days after transplanting.

treatments A and B. These differences were not as great as those for root weights (compared to the other plant organs), which have been reported in the previous literature to be less affected by P reductions (Chaudhary and Fujita, 1998; Rao et al., 2008).

The lower nodule dry weights in the control treatment, compared to treatments A and B, have previously been reported in other studies, in which the nodule fresh and dry weights were found to be considerably reduced when inorganic NO_3^- fertilization was not restricted (Nanjareddy et al., 2014; Kontopoulou et al., 2017). On the other hand, other authors report that the nodule number was not affected when exposing the crop to mineral and organic N sources but rather affected in size and weight (Pampana et al., 2017).

The increasing nodule numbers and weights throughout the experiment for the B treatment (with greater struvite), when compared to treatment A, confirm Kontopoulou et al. (2017). findings that low initial N fertilization can restrict successful colonization. These differences, however, could also be due to the lower P amounts in treatment A compared to treatment B since P is a limiting factor for successful nodulation (Olivera et al., 2004).

The lower bean productivities were similar to those in the study reported by Olivera et al. (2004), where bean production with lower P fertilization and Rhizobia inoculation turned out to be insufficient to reach production levels as high as those of conventionally fertilized beans. However, struvite fertilization seemed to increase the production of inoculated plants by up to 25% when treatments with 2 g and 5 g per plant were compared

TABLE 2 | Results for percentage of Nitrogen derived from atmospheric N_2 fixation (%Ndfa) in plant, Total amount of N in plant expressed in kg/ha (Leaves+Shoot+Root+Beans) and Biologically fixed N expressed in kg/ha.

Date	Treatment	% Ndfa plant^{-1}	Total N in plant kg/ha	Kg/ha biologically fixed N	Kg/ha N from struvite
35 DAT	*A*	68%	7.5 ± 1.0^a	5.4 ± 1.0^a	2.2
	B	60%	8.6 ± 2.2^a	5.3 ± 1.4^a	3.3
62 DAT	*A*	89%	24.7 ± 5.0^a	22.9 ± 4.0^b	1.8
	B	73%	24.6 ± 6.2^a	18.7 ± 5.1^a	5.9
84 DAT	*A*	90%	27.3 ± 12.8^a	25.4 ± 13.0^a	1.9
	B	82%	35.0 ± 9.2^a	29.2 ± 7.8^a	5.8

Results given for three treatments (n = 8 each) (A) 2g of struvite + Rhizobium inoculation + P, Mg, N-free nutrient solution (B) 5g of struvite + Rhizobium inoculation + P, Mg, N-free nutrient solution at three different time periods. 35 days after transplanting, 62 days after transplanting and 84 days after transplanting. Significant differences ($p < 0.05$) between treatments marked with different letter (a,b,c).

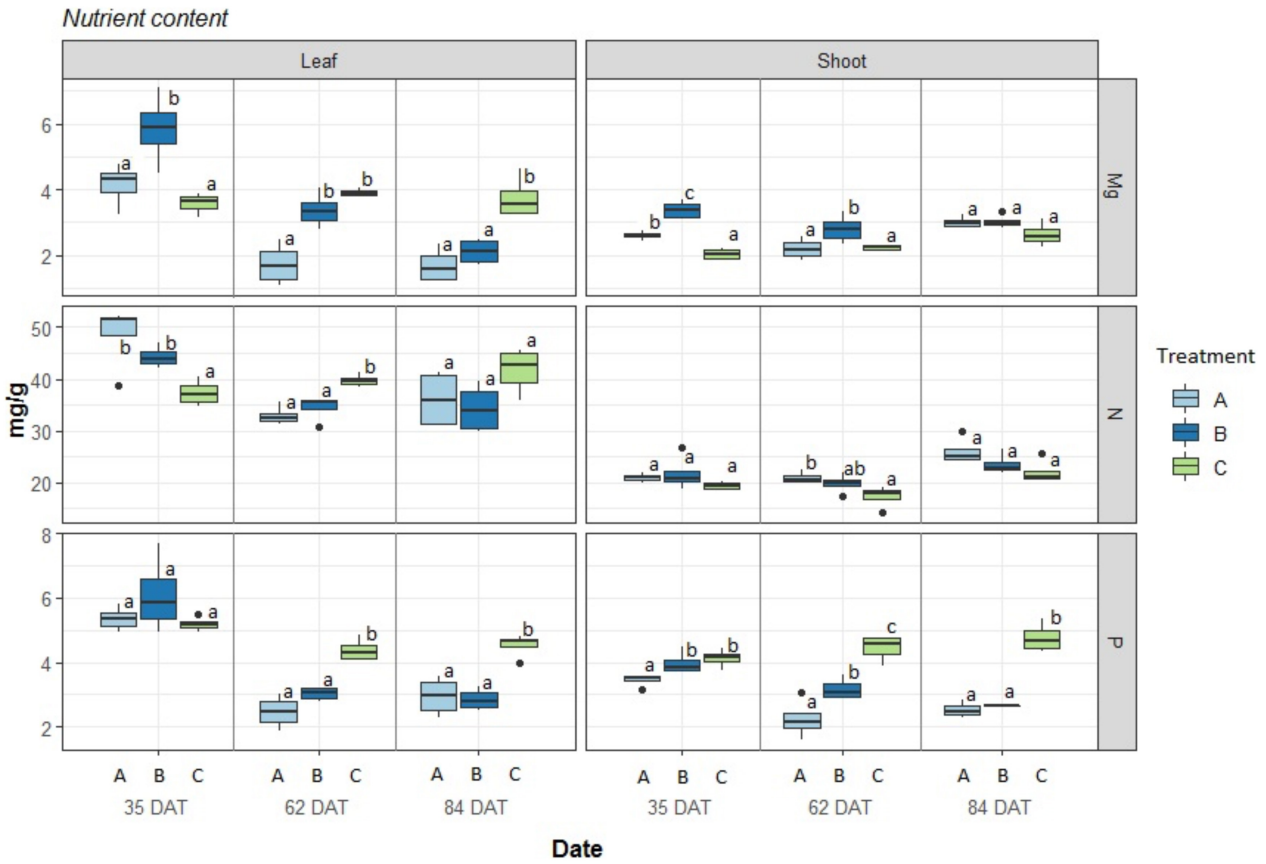

FIGURE 4 | Nutrient concentration in Phaseolus vulgaris leaves and shoots, expressed in mg/g. Boxplot (n = 4) results given for three treatments: A = 2g of struvite + Rhizobium inoculation + P, Mg, N-free nutrient solution, B = 5g of struvite + Rhizobium inoculation + P, Mg, N-free nutrient solution and, C = standard nutrient solution - Rhizobium inoculation at three different time periods: 35 days after transplanting, 62 days after transplanting, and 84 days after transplanting. Significant differences ($p < 0.05$) between treatments marked with different letter (a,b,c).

(59.35 ± 26.4 g plant^{-1} in treatment A and 74.23 ± 23.0 g plant^{-1} in treatment B).

The effect of the struvite treatment on the increasing nodule number and dry weight indicates successful nodulation and a greater fixation capacity with the given N. The slow release of N has presented itself as sufficient to increase the nodulation capacity as well as production capacity, without inhibiting N^2 fixation by the bacteria.

The Effect on Atmospheric N Fixation Capacity

The aboveground organs showed a clear pattern throughout the three measurements in terms of N assimilation. ^{15}N enrichment levels in the A and B treatments were lower than that in the C treatment, which means that treatments A and B obtained most of their N from the atmosphere. This difference became even greater as time progressed and reflected a greater dependence on N_2 fixation in the A and B treatments. The differences between these two treatments (A and B) themselves can be due to the greater availability of struvite in the root medium and therefore a greater availability of initial N and P for treatment B than for treatment A (Olivera et al., 2004; Kontopoulou et al., 2017).

The $\delta^{15}N$ reductions in treatments A and B over time corresponded to the availability of N provided by the struvite, assuming that it decreased over time. These reductions can be seen when the NO_3^- concentrations in the drained water were examined (see **Supplementary Table 3b**). While initially greater amounts of N were detected in the leached water, by the end of the experiment, very low concentrations were seen. Therefore, while the $\delta^{15}N$ values for the control treatment C remained constant over time (except in the nodules), the $\delta^{15}N$ values for treatments A and B decreased progressively over time, which corresponded to the available N that was provided by struvite in the root medium.

This information indicates that a change in the source of N for the plants took place during the time span of 35 to 62 DAT. We can therefore assume that the availability of struvite and therefore N in the root medium was depleted mainly during that time, which forced the plants to rely on atmospheric N_2 fixation. The results obtained for %Ndfa also confirm that the levels of N_2 fixation increased over time in both treatments.

The indicated timespan of 35 to 63 DAT corresponds to the initial pod production of the plant, maximizing its nutritional needs. Therefore, an N and P source capable to uphold these needs during this stage must be contemplated. As seen in **Supplementary Table 3b** a major reduction of NO_3^- in the leachate water is found between day 35 and 49 for treatments A and B, indicating that the administered struvite was insufficient to further support a greater production.

The nodules appeared to be highly enriched with ^{15}N during all three harvests, especially for treatments A and B. These results agree with previous literature that attributes this enrichment to the export of ^{15}N-depleted ureides and import of ^{15}N-enriched amino acids. Nevertheless, these values do not have a great effect on the total plant enrichment if the nodule biomass is considered (Shearer and Kohl, 1986; Unkovich, 2013; Craine et al., 2015).

The quantity of fixed nitrogen did not reach 40-50 kg/ha, which corresponds to low ranges, as reported in previous research (Farid and Navabi, 2015). While treatment A, with less struvite, had higher BNF values at the first two sampling times, treatment B's BNF value had increased by the end of the experiment. These findings are in agreement with those mentioned in the literature, where BNF was found to be restricted in the presence of plant-available NO_3^-, and the BNF values increased during the mature stages of the plant with sufficient NO_3^- fertilization during early plant growth (Müller et al., 1993; Hungria et al., 2006; Kontopoulou et al., 2017).

Plant Health and Nitrogen Assimilation

We conclude that all treatments had sufficient N since there were minimal differences in N concentrations in the shoots and leaves during plant growth and at the end of the experiment, as was also found by Kontopoulou et al. (2015). We consider that the lower yields were caused by the reduced uptake of K^+ and Mg^{2+} cations, which was cased by the electrochemical imbalance generated by the reduced presence of NO_3^- in the root medium. This idea is reinforced by the results shown in **Supplementary Figure 4b**, where N gradually increased in all three treatments throughout the experiment, which indicated that fixation was taking place for treatments A and B. The values increased from less than 0.1 g N at 35 DAT up to 0.2 g at 84 DAT for both the A and B treatments.

The slight increase in K by the end of the experiment in the plants with less struvite (treatment A) was most likely due to the lower availability of the Mg^{2+} cation, which facilitated cation uptake (Marschner, 2002).

The declining N concentrations in the leachates led us to believe that the decreases in P and Mg concentrations in the aboveground organs could also be related to the depletion of struvite in the medium. This depletion occurred faster in treatment A than in treatment B, which was related to the initial amounts of struvite provided in each treatment (2 g and 5 g, respectively). It was seen that for the inoculated plants, greater amounts of P were needed to support symbiosis and nodulation, as has also been observed by other researchers (Olivera et al., 2004; Ntatsi et al., 2018; Savvas et al., 2018). Whether the additional required P can be assimilated by adding more struvite to the substrate is worth pursuing in future studies.

These findings lead to the concept that a lack of N is not the limiting factor that is entirely responsible for the lower yields of the A and B treatments, but the limiting factor is instead the progressive loss of P and Mg in the root medium as well as the reduced cation uptake. When examining the NUEs that were obtained for all treatments, it is evident that plants with lower N inputs have greater use efficiency. This difference is very clear in treatment A with a three-times higher efficiency compared to treatment B. These differences can also be influenced by atmospheric N fixation, which was not provided as "Soil" N in the calculation tool (Weih, 2014). A higher fixation capacity can therefore generate a higher NUE, which corresponds to our BNF results.

For production on larger-scale vertical farms, fertilization with struvite and Rhizobium seems possible, especially with greater struvite quantities, as in treatment B, which shows great compatibility with soil bacteria and produces larger yields than those crops fertilized with only 2 g of struvite. The initial fixation capacity of the control treatment and appearance of nodules during the first sampling stage indicate that nodulation could occur even with naturally occurring Rhizobium, which could simplify the fertilization process in soil-based agriculture. A limitation for larger-scale production could be providing precise applications of struvite in the root areas. As seen in this study, there were large production differences between the applications of 2 g and 5 g of struvite, and large-scale production in a vertical farm would mean precise weighting of the struvite amounts per plant and direct applications to each rhizosphere of each plant. As stated by Degryse et al. (2017), the location of this slow-releasing fertilizer can have a great impact on successful nutrient delivery to plants. These could thus be highly time- and resource-consuming applications.

CONCLUSION

This work aimed to study the feasibility of using struvite and inoculation with Rhizobium bacteria as alternative Mg, N, and P fertilization methods for vertical agriculture systems. For this purpose, we quantified the nitrogen sources, production, and evolution of the phenological stages of *Phaseolus vulgaris* with Rhizobium inoculation and different quantities of struvite and compared the results to a control treatment. Three main conclusions can be drawn from this study.

First, both alternative fertilizer treatments supplied the necessary nutrients to fulfill the plant cycle in soilless growing media. The lower yields compared to the control suggest the necessity for evaluating higher struvite quantities to fulfill plant requirements to achieve higher yields. Since previous experiments conducted with struvite suggested successful performance with 5 g/plant, its combination with the soil bacteria, Rhizobium, causes this quantity to be insufficient due to the additional nutritional requirements of the bacteria. This can be seen by the great reduction in yields of treatments A and B in comparison to the control.

Second, while nodulation seemed to not be hindered by nitrogen input through struvite in the root medium, it did not

significantly improve it either, although BNF appeared to increase in the later stages for plants grown under the treatment with a greater initial quantity of struvite.

Third, the limiting factor for struvite-fertilized and rhizobia-inoculated treatments did not seem to be nitrogen, which was maintained at sufficient concentrations in the plants throughout the experiment, but rather was potassium, due to the lower uptake capacity that was caused by an electrochemical imbalance that was generated by the reduced presence of NO_3^- in the root medium as well as by magnesium and phosphorus, given that struvite depletion was reflected by the reduced plant nutrient concentrations over time.

An increase in the amount of applied struvite might be a solution for a more sustained phosphorus and magnesium supply for vertical agriculture but could also interfere with the nodulation capacity of the plants. Furthermore, we encourage the addition of nutrients in the form of anions to ensure the electrochemical balance in the root area in case NO_3^- is removed. In this sense, further studies should aim to determine the optimal struvite quantities for hydroponic bean production in combination with Rhizobium inoculation.

DATA AVAILABILITY STATEMENT

The raw data supporting the conclusions of this article will be made available by the authors, without undue reservation.

AUTHOR CONTRIBUTIONS

VA-P contributed to the conceptualization, performed the methodology, carried out the formal analysis and data curation, and wrote the original draft. FP performed the methodology, carried out the data curation, and wrote, reviewed, and edited the manuscript. MR-S performed the methodology, wrote, reviewed, and edited the manuscript. GV contributed to the conceptualization, performed the methodology, wrote, reviewed, and edited the manuscript, supervised the data, and carried out the funding acquisition. AR-M performed the methodology and reviewed and edited the manuscript. XG contributed to the conceptualization, performed the methodology, wrote, reviewed, and edited the manuscript, supervised the data, and carried out the funding acquisition. All authors contributed to the article and approved the submitted version.

FUNDING

The authors are grateful to the Spanish Ministry of Economy, Industry, and Competitiveness (Spain) for the grant that was awarded to VA-P (FPI-MINECO 2018), the National Commission for Scientific and Technological Research (Chile) for the grant that was awarded to FP (PFCHA-CONICYT 2018 – Folio 72180248), and Universitat Autònoma de Barcelona for awarding a research scholarship to MR-S (PIF-UAB 2017). This work was supported by the Spanish Ministry of Economy, Industry, and Competitiveness (AEU/FEDER)-[CTM2016-75772-C3-1-R] and the "María de Maeztu" program for Units of Excellence in R&D [MDM-2015-0552] [CEX2019-000940-M]. This research received funding from the European Union's Horizon 2020 research and innovation program under grant agreement No 862663 (FoodE) and ERC grant agreement n° 818002 URBAG, which was awarded to GV. The publication reflects the authors' views. The Research Executive Agency (REA) is not liable for any use that may be made of the information contained therein.

SUPPLEMENTARY MATERIAL

The Supplementary Material for this article can be found online at: https://www.frontiersin.org/articles/10.3389/fpls.2021.649304/full#supplementary-material

REFERENCES

Ackerman, J. N., Zvomuya, F., Cicek, N., and Flaten, D. (2013). Evaluation of manure-derived struvite as a phosphorus source for canola. *Can. J. Plant Sci.* 93, 419–424. doi: 10.4141/cjps2012-207

Ahmed, N., Shim, S., Won, S., and Ra, C. (2018). Struvite recovered from various types of wastewaters: characteristics, soil leaching behaviour, and plant growth. *Land Degrad. Dev.* 29, 2864–2879. doi: 10.1002/ldr.3010

Anton, A., Montero, J. I., Muñoz, P., and Castells, F. (2005). LCA and tomato production in Mediterranean greenhouses. *Int. J. Agric. Resour. Gov. Ecol.* 4, 102–112. doi: 10.1504/IJARGE.2005.007192

Antonini, S., Arias, M. A., Eichert, T., and Clemens, J. (2012). Greenhouse evaluation and environmental impact assessment of different urine-derived struvite fertilizers as phosphorus sources for plants. *Chemosphere* 89, 1202–1210. doi: 10.1016/j.chemosphere.2012.07.026

Araújo, A. S. F., Monteiro, R. T. R., and Carvalho, E. M. S. (2007). Effect of composted textile sludge on growth, nodulation and nitrogen fixation of soybean and cowpea. *Bioresour. Technol.* 98, 1028–1032. doi: 10.1016/j.biortech.2006.04.028

Arndt, S. K., Kahmen, A., Arampatsis, C., Popp, M., and Adams, M. (2004). Nitrogen fixation and metabolism by groundwater-dependent perennial plants in a hyperarid desert. *Oecologia* 141, 385–394. doi: 10.1007/s00442-004-1655-7

Bhuiyan, M. I. H., Mavinic, D. S., and Beckie, R. D. (2007). A solubility and thermodynamic study of struvite. *Environ. Technol.* 28, 1015–1026. doi: 10.1080/09593332808618857

Cabeza, R., Steingrobe, B., Römer, W., and Claassen, N. (2011). Effectiveness of recycled P products as P fertilizers, as evaluated in pot experiments. *Nutr. Cycl. Agroecosyst.* 91:173. doi: 10.1007/s10705-011-9454-0

Chaudhary, M. I., and Fujita, K. (1998). Comparison of phosphorus deficiency effects on the growth parameters of mashbean, mungbean, and soybean. *Soil Sci. Plant Nutr.* 44, 19–30. doi: 10.1080/00380768.1998.10414423

Cherkasov, N., Ibhadon, A. O., and Fitzpatrick, P. (2015). A review of the existing and alternative methods for greener nitrogen fixation. *Chem. Eng. Process.* 90, 24–33. doi: 10.1016/j.cep.2015.02.004

Cordell, D., and White, S. (2013). Sustainable phosphorus measures: strategies and technologies for achieving phosphorus security. *Agronomy* 3, 86–116. doi: 10.3390/agronomy3010086

Cordell, D., Drangert, J. O., and White, S. (2009). The story of phosphorus: global food security and food for thought. *Glob. Environ. Change* 19, 292–305. doi: 10.1016/j.gloenvcha.2008.10.009

Craine, J. M., Brookshire, E. N. J., Cramer, M. D., Hasselquist, N. J., Koba, K., Marin-Spiotta, E., et al. (2015). Ecological interpretations of nitrogen isotope ratios of terrestrial plants and soils. *Plant Soil* 396, 1–26. doi: 10.1007/s11104-015-2542-1

Degryse, F., Baird, R., da Silva, R. C., and McLaughlin, M. J. (2017). Dissolution rate and agronomic effectiveness of struvite fertilizers – effect of soil pH, granulation and base excess. *Plant Soil* 410, 139–152. doi: 10.1007/s11104-016-2990-2

Farid, M., and Navabi, A. (2015). N 2 fixation ability of different dry bean genotypes. *Can. J. Plant Sci.* 95, 1243–1257. doi: 10.4141/CJPS-2015-084

Frossard, E., Sinaj, S., and Dufour, P. (1996). Phosphorus in urban sewage sludges as assessed by isotopic exchange. *Soil Sci. Soc. Am. J.* 60, 179–182. doi: 10.2136/sssaj1996.03615995006000010029x

González Ponce, R., López-de-Sá, E. G., and Plaza, C. (2009). Lettuce response to phosphorus fertilization with struvite recovered from municipal wastewater. *HortScience* 44, 426–430.

Gopalakrishnan, S., Sathya, A., Vijayabharathi, R., Varshney, R. K., Gowda, C. L., and Krishnamurthy, L. (2015). Plant growth promoting rhizobia: challenges and opportunities. *3 Biotech* 5, 355–377. doi: 10.1007/s13205-014-0241-x

Hochmuth, G., Maynard, D., Vavrina, C., Hanlon, E., and Simonne, E. (2018). Plant tissue analysis and interpretation for vegetable crops in Florida. *Hortic. Sci. Dep.* 2012:55.

Hungria, M., Franchini, J. C., Campo, R. J., Crispino, C. C., Moraes, J. Z., Sibaldelli, R. N. R., et al. (2006). Nitrogen nutrition of soybean in Brazil: contributions of biological N 2 fixation and N fertilizer to grain yield. *Can. J. Plant Sci.* 86, 927–939. doi: 10.4141/p05-098

Ikeda, H., and Tan, X. (1998). Urea as an organic nitrogen source for hydroponically grown tomatoes in comparison with inorganic nitrogen sources. *Soil Sci. Plant Nutr.* 44, 609–615. doi: 10.1080/00380768.1998.10414484

Karak, T., and Bhattacharyya, P. (2011). Human urine as a source of alternative natural fertilizer in agriculture: a flight of fancy or an achievable reality. *Resour. Conserv. Recycl.* 55, 400–408. doi: 10.1016/j.resconrec.2010.12.008

Kermah, M., Franke, A. C., djei-Nsiah, S. A., Ahiabor, B. D. K., Abaidoo, R. C., and Giller, K. E. (2018). N2-fixation and N contribution by grain legumes under different soil fertility status and cropping systems in the Guinea savanna of northern Ghana. *Agric. Ecosyst. Environ.* 261, 201–210. doi: 10.1016/j.agee.2017.08.028

Kontopoulou, C. K., Giagkou, S., Stathi, E., Savvas, D., and Iannetta, P. P. M. (2015). Responses of hydroponically grown common bean fed with nitrogen-free nutrient solution to root inoculation with N2-fixing bacteria. *HortScience* 50, 597–602. doi: 10.21273/HORTSCI.50.4.597

Kontopoulou, C. K., Liasis, E., Iannetta, P. P. M., Tampakaki, A., and Savvas, D. (2017). Impact of rhizobial inoculation and reduced N supply on biomass production and biological N2 fixation in common bean grown hydroponically. *J. Sci. Food Agric.* 97, 4353–4361. doi: 10.1002/jsfa.8202

Liu, Y. H., Rahman, M., Kwag, J. H., Kim, J. H., and Ra, C. S. (2011). Eco-friendly production of maize using struvite recovered from swine wastewater as a sustainable fertilizer source. *Asian-Australas. J. Anim. Sci.* 24, 1699–1705. doi: 10.5713/ajas.2011.11107

Long, S. R. (1989). Rhizobium-legume nodulation: life together in the underground. *Cell* 56, 203–214. doi: 10.1016/0092-8674(89)90893-3

Marschner, H. (2002). "Ion uptake mechanisms of individual cells and roots: short-distance transport," in *Marschner's Mineral Nutrition of Higher Plants*, (Cambridge, MA: Academic Press), 6–78. doi: 10.1016/b978-0-08-057187-4.50008-4

Massey, M. S., Davis, J. G., Sheffield, R. E., and Ippolito, J. A. (2007). "Struvite production from dairy wastewater and its potential as a fertilizer for organic production in calcareous soils," in *Proceedings of the International Symposium on Air Quality and Waste Management for Agliculture, 16-19 September 2007*, (Broomfield, CO).

McKey, D. (1994). Legumes and nitrogen: the evolutionary ecology of a nitrogen-demanding lifestyle. *Adv. Legume Syst.* 5, 211–228. doi: 10.1007/s13398-014-0173-7.2

Müller, S., Pereira, P. A. A., and Martin, P. (1993). Effect of different levels of mineral nitrogen on nodulation and N2 fixation of two cultivars of common bean (*Phaseolus vulgaris* L.). *Plant Soil* 152, 139–143. doi: 10.1007/BF00016343

Nanjareddy, K., Blanco, L., Arthikala, M. K., Affantrange, X. A., Sánchez, F., and Lara, M. (2014). Nitrate regulates rhizobial and mycorrhizal symbiosis in common bean (*Phaseolus vulgaris* L.). *J. Integr. Plant Biol.* 56, 281–298. doi: 10.1111/jipb.12156

Nanzer, S., Oberson, A., Berger, L., Berset, E., Hermann, L., and Frossard, E. (2014). The plant availability of phosphorus from thermo-chemically treated sewage sludge ashes as studied by 33P labeling techniques. *Plant Soil* 377, 439–456. doi: 10.1007/s11104-013-1968-6

Ntatsi, G., Karkanis, A., Yfantopoulos, D., Olle, M., Travlos, I., Thanopoulos, R., et al. (2018). Impact of variety and farming practices on growth, yield, weed flora and symbiotic nitrogen fixation in faba bean cultivated for fresh seed production. *Acta Agric. Scand. B* 68, 619–630. doi: 10.1080/09064710.2018.1452286

Olivera, M., Tejera, N., Iribarne, C., Ocaña, A., and Lluch, C. (2004). Growth, nitrogen fixation and ammonium assimilation in common bean (*Phaseolus vulgaris*): effect of phosphorus. *Physiol. Plant.* 121, 498–505. doi: 10.1111/j.0031-9317.2004.00355.x

Pampana, S., Scartazza, A., Cardelli, R., Saviozzi, A., Guglielminetti, L., Vannacci, G., et al. (2017). Biosolids differently affect seed yield, nodule growth, nodule-specific activity, and symbiotic nitrogen fixation of field bean. *Crop Pasture Sci.* 68, 735–745. doi: 10.1071/CP17166

Peoples, M. B., Boddey, R. M., and Herridge, D. F. (2002). "Quantification of nitrogen fixation," in *Nitrogen Fixation at the Millennium*, ed. G. Jeffery Leigh (Amsterdam: Elsevier B.V.), 357–389. doi: 10.1016/b978-044450965-9/50013-6

Rahman, M. M., Salleh, M. A. M., Rashid, U., Ahsan, A., Hossain, M. M., and Ra, C. S. (2014). Production of slow release crystal fertilizer from wastewaters through struvite crystallization – a review. *Arab. J. Chem.* 7, 139–155. doi: 10.1016/j.arabjc.2013.10.007

Rao, I. M., Fredeen, A. L., and Terry, N. (2008). Leaf phosphate status, photosynthesis, and carbon partitioning in sugar beet: III. Diurnal changes in carbon partitioning and carbon export. *Plant Physiol.* 92, 29–36. doi: 10.1104/pp.92.1.29

Rech, I., Withers, R., Jones, D. L., and Pavinato, P. (2018). Solubility, diffusion and crop uptake of phosphorus in three different struvites. *Sustainability* 11:134. doi: 10.3390/su11010134

Robinson, D. (2001). δ15N as an integrator of the nitrogen cycle. *Trends Ecol. Evol.* 16, 153–162.

Rueden, C. T., Schindelin, J., Hiner, M. C., DeZonia, B. E., Walter, A. E., Arena, E. T., et al. (2017). ImageJ2: imageJ for the next generation of scientific image data. *BMC Bioinformatics* 18:529. doi: 10.1186/s12859-017-1934-z

Rufí-Salís, M., Parada, F., Arcas-Pilz, V., Petit-Boix, A., Villalba, G., and Gabarrell, X. (2020a). Closed-loop crop cascade to optimize nutrient flows and grow low-impact vegetables in cities. *Front. Plant Sci.* 11:596550. doi: 10.3389/fpls.2020.596550

Rufí-Salís, M., Petit-Boix, A., Villalba, G., Sanjuan-Delmás, D., Parada, F., Ercilla-Montserrat, M., et al. (2020b). Recirculating water and nutrients in urban agriculture: an opportunity towards environmental sustainability and water use efficiency? *J. Clean. Prod.* 261:121213. doi: 10.1016/j.jclepro.2020.121213

Sanjuan-Delmás, D., Llorach-Massana, P., Nadal, A., Ercilla-Montserrat, M., Muñoz, P., Montero, J. I., et al. (2018). Environmental assessment of an integrated rooftop greenhouse for food production in cities. *J. Clean. Prod.* 177, 326–337. doi: 10.1016/j.jclepro.2017.12.147

Sanyé, E., Oliver-Solà, J., Gasol, C. M., Farreny, R., Rieradevall, J., and Gabarrell, X. (2012). Life cycle assessment of energy flow and packaging use in food purchasing. *J. Clean. Prod.* 25, 51–59. doi: 10.1016/j.jclepro.2011.11.067

Sanyé-Mengual, E., Martinez-Blanco, J., Finkbeiner, M., Cerdà, M., Camargo, M., Ometto, A. R., et al. (2018). Urban horticulture in retail parks: environmental assessment of the potential implementation of rooftop greenhouses in European and South American cities. *J. Clean. Prod.* 172, 3081–3091. doi: 10.1016/J.JCLEPRO.2017.11.103

Sanyé-Mengual, E., Oliver-Solà, J., Montero, J. I., and Rieradevall, J. (2015). An environmental and economic life cycle assessment of rooftop greenhouse (RTG) implementation in Barcelona, Spain. Assessing new forms of urban agriculture from the greenhouse structure to the final product level. *Int. J. Life Cycle Assess.* 20, 350–366. doi: 10.1007/s11367-014-0836-9

Savvas, D., Ntatsi, G., Vlachou, M., Vrontani, C., Rizopoulou, E., Fotiadis, C., et al. (2018). Impact of different rhizobial strains and reduced nitrogen supply on growth, yield and nutrient uptake in cowpea grown hydroponically. *Acta Hortic.* 1227, 417–424. doi: 10.17660/ActaHortic.2018.1227.52

Shearer, G., and Kohl, D. H. (1986). N_2-fixation in field settings: estimations based on natural ^{15}N abundance. *Aust. J. Plant Physiol.* 13, 699–756. doi: 10.1016/0003-2697(92)90302-N

Shearer, G., and Kohl, D. H. (1989). "Natural 15N abundance as a method of estimating the contribution of biologically fixed nitrogen to N2-fixing

systems: potential for non-legumes," in *Proceedings of the Fourth International Symposium on 'Nitrogen Fixation with Non-Legumes', Rio de Janeiro, 23-28 August 1987*, eds F. A. Skinner, R. M. Boddey, and I. Fendrik (Dordrecht: Springer Netherlands), 289–299. doi: 10.1007/978-94-009-0889-5_33

Shearer, G., and Kohl, D. H. (1993). "Natural abundance of 15N: fractional contribution of two sources to a common sink and use of isotope discrimination," in *Nitrogen Isotope Techniques*, eds R. Knowles and T. H. Blackburn (Cambridge, CA: Academic Press), 89–125. doi: 10.1016/B978-0-08-092407-6.50009-2

Sonneveld, C., and Voogt, W. (2009). *Plant Nutrition of Greenhouse Crops*. Dordrecht: Springer Netherlands. doi: 10.1017/CBO9781107415324.004

Talboys, P. J., Heppell, J., Roose, T., Healey, J. R., Jones, D. L., and Withers, P. J. (2016). Struvite: a slow-release fertiliser for sustainable phosphorus management? *Plant Soil* 401, 109–123. doi: 10.1007/s11104-015-2747-3

United Nations (2019). World urbanization prospects the 2018 revision. *Demogr. Res.* 12, 197–236. doi: 10.4054/demres.2005.12.9

Unkovich, M. J. (2013). Isotope discrimination provides new insight into biological nitrogen fixatio. *New Phytol.* 198, 643–646.

Unkovich, M. J., Pate, J. S., Lefroy, E. C., and Arthur, D. J. (2002). Nitrogen isotope fractionation in the fodder tree tagasaste (*Chamaecytisus proliferus*) and assessment of N2 fixation inputs in deep sandy soils of Western Australia. *Funct. Plant Biol.* 27, 921–929. doi: 10.1071/pp99201

Weih, M. (2014). A calculation tool for analyzing nitrogen use efficiency in annual and perennial crops. *Agronomy* 4, 470–477. doi: 10.3390/agronomy4040470

Conflict of Interest: The authors declare that the research was conducted in the absence of any commercial or financial relationships that could be construed as a potential conflict of interest.

frontiers in Plant Science

ORIGINAL RESEARCH
published: 15 June 2021
doi: 10.3389/fpls.2021.675810

Effects of Artificially Reproduced Fluctuations in Sunlight Spectral Distribution on the Net Photosynthetic Rate of Cucumber Leaves

Ryo Matsuda, Hiroki Ito and Kazuhiro Fujiwara*

Department of Biological and Environmental Engineering, Graduate School of Agricultural and Life Sciences, The University of Tokyo, Tokyo, Japan

The effects of photosynthetic photon flux density (PPFD) fluctuations in sunlight have already been investigated; however, the spectral photon flux density distribution (SPD) has hardly been considered. Here, sunlight SPD fluctuations recorded for 200 min in October in Tokyo, Japan were artificially reproduced using an LED-artificial sunlight source system. The net photosynthetic rate (P_n) of cucumber leaves under reproduced sunlight was measured and compared with the P_n estimated from a steady-state PPFD–P_n curve for the same leaves. The measured and estimated P_n agreed except when the PPFD was low, where the measured P_n was lower than the estimated P_n. The ratio of measured P_n to estimated P_n was 0.94–0.95 for PPFD ranges of 300–700 μmol m^{-2} s^{-1}, while the value was 0.98–0.99 for 900–1,300 μmol m^{-2} s^{-1}, and the overall ratio was 0.97. This 3% reduction in the measured P_n compared with the P_n estimated from a steady-state PPFD–P_n curve was significantly smaller than the approximately 20–30% reduction reported in previous experimental and simulation studies. This result suggests that the loss of integral net photosynthetic gain under fluctuating sunlight can vary among days with different fluctuation patterns or may be non-significant when fluctuations in both PPFD and relative SPD of sunlight are taken into consideration.

Keywords: fluctuating light, light-emitting diode, light quality, LED artificial sunlight source system, photosynthetic photon flux density, spectral photon flux density distribution

OPEN ACCESS

Edited by:
Jung Eek Son,
Seoul National University,
South Korea

Reviewed by:
Theoharis Ouzounis,
Fluence Bioengineering, Inc.,
United States
Jeremy Harbinson,
Wageningen University and Research,
Netherlands

****Correspondence:***
Ryo Matsuda
amatsuda@mail.ecc.u-tokyo.ac.jp

Specialty section:
This article was submitted to Crop and Product Physiology, a section of the journal Frontiers in Plant Science

Received: *03 March 2021*
Accepted: *20 May 2021*
Published: *15 June 2021*

Citation:
Matsuda R, Ito H and Fujiwara K (2021) Effects of Artificially Reproduced Fluctuations in Sunlight Spectral Distribution on the Net Photosynthetic Rate of Cucumber Leaves. Front. Plant Sci. 12:675810. doi: 10.3389/fpls.2021.675810

INTRODUCTION

The spectral photon-flux-density distribution (SPD) is a distribution of photon flux density (PFD) per unit wavelength within a defined wavelength range. The SPD can be characterized by two aspects: the integral of spectral PFD and the relative SPD. As an index of the former factor, the photosynthetic PFD (PPFD), with an amount of PFD between 400 and 700 nm, is often used. The latter factor is the "shape" of the SPD curve and may sometimes be called light quality. As elements

Abbreviations: DC, direct current; g_s, stomatal conductance; LASS system, LED-artificial sunlight source system; LED, light-emitting diode; PFD, photon flux density; PPFD, photosynthetic PFD; SPD, spectral photon-flux-density distribution; P_n, net photosynthetic rate.

of the light environment, both PPFD (Boardman, 1977; Björkman, 1981) and relative SPD (McCree, 1972; Inada, 1976) significantly affect the net photosynthetic rate (P_n) of leaves.

The SPD of sunlight in open fields and greenhouses fluctuates during the daytime at various time scales, from seconds to hours, because of a change in solar altitude, clouds covering the sun, leaf movement due to wind, and so on. Recently, the effects of PPFD fluctuations on instantaneous leaf photosynthesis have been intensively studied (for reviews, see Kaiser et al., 2015, 2018; Yamori, 2016; Vialet-Chabrand et al., 2017a; Murchie et al., 2018; Slattery et al., 2018; Tanaka et al., 2019). Reportedly, photosynthetic performance under fluctuating PPFD conditions is different from that under constant PPFD conditions. Most previous studies employed simple periodic fluctuations in PPFD in which PPFD alternated between two PPFD levels (Leakey et al., 2002; Kono et al., 2014, 2017, 2020; Sejima et al., 2014; Kono and Terashima, 2016; Yamori et al., 2016; Yang et al., 2019; Bhuiyan and van Iersel, 2021) or a single event involving an increase or decrease in PPFD (Kaiser et al., 2016; Qu et al., 2016; Soleh et al., 2017; Zhang et al., 2019). Although these studies demonstrated the significance of physiological responses to fluctuating light, the PPFD fluctuation patterns differ from complex fluctuation patterns observed in open fields and greenhouses under sunlight.

Vialet-Chabrand et al. (2017b) reproduced a sunlight PPFD fluctuation measured on a relatively clear day using a light-emitting diode (LED) light source. The researchers measured a diurnal change in leaf P_n in *Arabidopsis thaliana* under the conditions where PPFD fluctuated below 1,500 μmol m^{-2} s^{-1} and compared it with the P_n predicted from the separately determined PPFD-response curve of steady-state P_n. They reported that the measured P_n tended to be lower than the predicted P_n and that the difference between the measured and predicted P_n integrated over the diurnal period was 19–30%. Similarly, model simulation studies reported that the daily integral net photosynthetic gain under sunlight where PPFD fluctuated was calculated as 21% lower than that estimated by assuming that steady-state photosynthesis was attained at any moment (Taylor and Long, 2017; Tanaka et al., 2019). The reduction in P_n by PPFD fluctuations was thought to be mainly attributed to the delayed response of photosynthesis to an increase in PPFD, i.e., photosynthetic induction. Photosynthetic induction comprises three processes: (i) the induction of photosynthetic electron transport reactions in the thylakoid membrane, (ii) the activities of Calvin cycle enzymes including ribulose-1,5-bisphosphate carboxylase/oxygenase (Rubisco), and (iii) gas diffusion conductance including stomatal opening, each has a different time to respond of approximately 1–2 min, 5–10 min, and 10–30 min, respectively (Pearcy, 1990; Tanaka et al., 2019; Kimura et al., 2020; Yamori et al., 2020). It has been considered increasingly important to understand the nature of photosynthesis under sunlight with fluctuating PPFD and its underlying physiological mechanisms for genetic improvements of related traits (e.g., Adachi et al., 2019; Kimura et al., 2020; Yamori et al., 2020). In addition, fluctuations in environmental factors other than PPFD (e.g., CO_2 concentration, air temperature, relative humidity) have also been discussed (Kaiser et al., 2015; Yamori, 2016). On the other hand, most of the current greenhouse crop growth models (e.g., TOMSIM, Heuvelink, 1995, 1999) calculate leaf P_n in changing environments using parameters obtained with the assumption of steady-state conditions. However, such models simulate crop growth reasonably well under a wide range of growth conditions (e.g., Heuvelink, 1999; Heuvelink and Dorais, 2005; Heuvelink et al., 2008), indirectly suggesting that steady-state photosynthetic parameters are not too inappropriate to simulate leaf P_n of greenhouse crops under sunlight. Furthermore, a recent simulation study stated that the daily integral net photosynthetic gain calculated considering the delayed response of photosynthesis to an increased PPFD under various patterns of diurnal sunlight PPFD fluctuation was, on average, only 3–6% lower than P_n calculated assuming a steady-state (Murakami and Jishi, 2021). Thus, further verification is needed as to whether the approximately 20–30% reduction in P_n is a typical value under various fluctuating light conditions.

In contrast to PPFD reproduction, relative SPD or "light quality," the other important aspect of sunlight SPD, has hardly been considered. For example, the light sources used in previous studies to artificially reproduce sunlight PPFD fluctuations were a commercial LED light source (Vialet-Chabrand et al., 2017b) and an LED light source attached to a commercial portable photosynthesis system (Adachi et al., 2019; Kimura et al., 2020; Yamori et al., 2020), of which the relative SPDs were completely different from those of sunlight. It is known that factors characterizing relative SPD, such as the proportions of blue, red, and far-red light and/or their ratios, are known to significantly influence instantaneous photosynthesis (e.g., Hogewoning et al., 2010; Murakami et al., 2016). Furthermore, Kono et al. (2017, 2020) clarified the importance of far-red light in the photosynthetic response to fluctuating PPFD; periodic PPFD fluctuations without far-red light caused photoinhibition of photosystem II, while it was suppressed when far-red light was added. Thus, it is strongly desired that not only PPFD but also the relative SPD of sunlight be reproduced when we evaluate the effects of sunlight fluctuation on photosynthesis and intend to extrapolate the results to open field or greenhouse crop production. On the other hand, investigating photosynthesis under sunlight in an actual open field or a greenhouse may be another option to elucidate the responses of photosynthesis to fluctuating light. However, such field experiments do not allow us to confirm the reproducibility of the results obtained. To ensure reproducibility, laboratory experiments under a controlled environment must be useful.

Fujiwara and Sawada (2006); Fujiwara et al. (2007), and Fujiwara and Yano (2011) have been developing an LED-artificial sunlight source (LASS) system. A second-generation LASS system (Fujiwara et al., 2013) can produce SPDs at the same level as full irradiation of ground-level sunlight, within a range of 380–940 nm, with a high approximation accuracy at the light outlet of 7.1 cm^2 (30 mmϕ). Moreover, it also has a time-varying (dynamic) light production program and can change the SPD at the light outlet to an arbitrarily modified SPD at an arbitrarily set time interval of more than 2 s. To our knowledge, this system is the most appropriate for elucidating the effects of sunlight SPD fluctuations, taking both PPFD and relative SPD

into consideration, as well as ensuring a high reproducibility of sunlight SPD fluctuations.

In this study, we measured sunlight SPD fluctuations and artificially reproduced them using the LASS system. Characteristics of the measured sunlight SPD fluctuations and reproducibility of PPFD and relative SPD with the LASS system were evaluated. Then, the P_n of cucumber leaves under reproduced sunlight was compared with the P_n estimated from a steady-state PPFD–P_n curve of the same leaves.

MATERIALS AND METHODS

Measurement of Fluctuations in Sunlight SPD

Fluctuations in sunlight SPD were measured at the top of a seven-storied building located in Bunkyo, Tokyo, Japan (35°43′N) with a spectroradiometer (MS-720, EKO Instruments Co., Ltd., Tokyo, Japan). The SPDs between 350 and 1,050 nm were measured and recorded once every 15 s. To protect the spectroradiometer from sudden strong wind and rain, it was placed in a box (450 mm × 450 mm × 300 mm) covered with a fluoropolymer film (F-CLEAN Clear, AGC Green-Tech Co., Ltd., Tokyo, Japan) with an almost constant spectral transmittance (>90%) within the wavelength range measured. Measurements were repeated several times from April to October 2017. Data collected from 11:10 to 14:30 on October 12, 2017, in which relatively large amplitudes and frequent fluctuations in PPFD were observed, were selected for reproduction. The measurement periods of 200 min (3 h and 20 min) corresponded to the maximum number of storable data (800) of the spectroradiometer.

Reproduction of Fluctuations in Sunlight SPD With an LED-Artificial Sunlight Source System

Hardware and software system configurations of the second-generation LASS system were described in detail in Fujiwara et al. (2013). The hardware system comprises a light source unit, an LED temperature control system, and an SPD control system (**Figure 1A**). The light source unit comprises an LED module containing 625 LEDs with 32 different peak wavelengths (385–910 nm) (**Figure 1B**) and a hollow conical reflection condenser that condenses and mixes light from the LEDs to the light outlet of 7.1 cm^2. The SPD control system comprises 32 direct current (DC) power supplies, a DC power supply controller, controller expansion units, and a laptop computer used to send voltage value signals to the DC power supply controller. The software installed in the computer enables production of the desired SPD at the light outlet by transmitting a set of appropriate, previously determined voltage signals to the DC power supply controller, which is then applied to each type of LED in the light source unit. According to the original procedure (Fujiwara et al., 2013), four-step procedures are taken to determine the set of appropriate voltages: (i) preparation of a voltage–spectral irradiance database; (ii) calculation of the set of appropriate voltages; (iii) re-approximation using feedback control; and (iv) light production. In this study, we did not use the re-approximation function. This function can minimize the difference in spectral distributions between the reproduced light and target light using feedback control with a spectroradiometer (Fujiwara et al., 2013). However, roughly 10 min was needed as one routine operation for each of the SPDs that we wanted to reproduce. In this study, we had 800 SPD data points to reproduce, and too much time was needed to finish the procedure; thus, we had to omit the third step for the use of the re-approximation function.

Plant Materials and Growth Conditions

Cucumber (*Cucumis sativus* L. 'Hokushin', Takii & Co., Ltd., Kyoto, Japan) seeds were sown into moistened rockwool cubes (AO36/40, ROCKWOOL B.V., Roermond, the Netherlands) in a plug tray. Then, the tray was placed in a temperature-controlled growth chamber (MIR-554-PJ, PHC Holdings Corp., Tokyo, Japan) equipped with an LED panel [HMW120DC6 (1N-40Y), Kyoritsu Densho Co., Ltd., Osaka, Japan] composed of phosphor-converted white LEDs (GSPW1651NSE-40Y-TR, Stanley Electric Co., Ltd., Tokyo, Japan) (**Figure 2**). The seedlings were grown at a PPFD of 300 μmol m^{-2} s^{-1} at the tops of plants for 16 h d^{-1} and air temperatures of 25/20°C (day/night). The growth chamber was ventilated with external air using an air pump with the number of air exchanges of 1.0 h^{-1}. At 7 days post-seeding, seedlings were transplanted onto rockwool cubes (Delta 6.5G, ROCKWOOL B.V.) and grown for another week under the same environmental conditions. The rockwool cubes were subirrigated once per day or every 2 days with a nutrient solution (prescription A, OAT Agrio Co., Ltd., Tokyo, Japan) at an electrical conductivity of 0.13 S m^{-1}.

Measurement of Leaf Gas Exchange Rates

The gas exchange rates of the first true leaves of the 13- to 15-day-old cucumber seedlings (**Figure 1C**) were measured using a portable photosynthesis system (LI-6400XT, LI-COR, Inc., Lincoln, United Kingdom). A leaf chamber of the portable photosynthesis system was not equipped with any light source provided by the manufacturer. The light outlet of the hollow conical reflection condenser of the LASS system was placed in contact with a surface of 2 × 3-cm transparent polypropylene film covering the leaf chamber (**Figure 1D**). Environmental conditions of the leaf chamber, other than PPFD, were set as follows: CO_2 concentration of incoming air was 420 μmol mol^{-1}, air temperature was 25°C, and relative humidity was 70%. The airflow rate to the leaf chamber was 500 μmol s^{-1}. Measurements consisted of (1) changes in gas exchange rates under the reproduced sunlight and (2) steady-state P_n in response to PPFD. For (1), leaves were first kept at a constant PPFD of 500 μmol m^{-2} s^{-1} with a reference sunlight spectrum, which is defined by IEC 60904-3:2019 (International Electrotechnical Commission, 2019), for 20 min. The reference sunlight spectrum is defined for the global (direct and diffuse) solar radiation and at an air mass of 1.5. Leaves were then irradiated with light with an SPD at the beginning (0 min) of the reproduced sunlight (PPFD

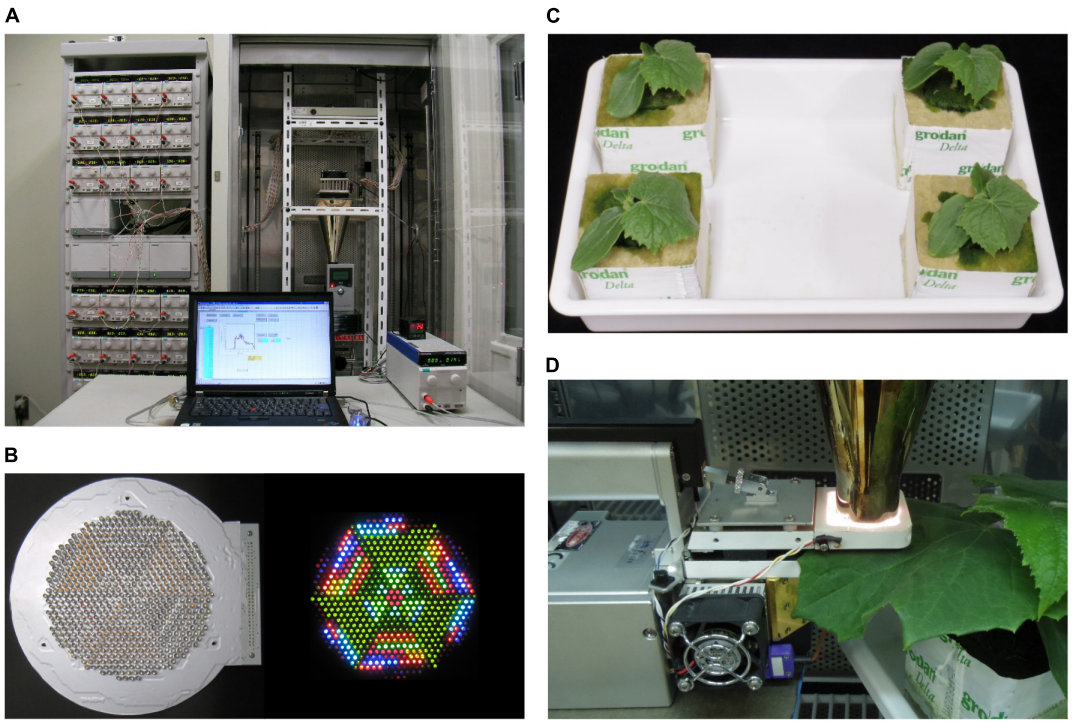

FIGURE 1 | (A) The LED-artificial sunlight source (LASS) system. Left: 32 DC power supplies, a DC power supply controller, and three controller expansion units in a rack; right: the light source unit comprising an LED module, a cooling unit of the LED temperature control system, and a hollow conical reflection condenser, and a spectroradiometer in a temperature-controlled chamber; bottom: a DC power supply and a PID controller of the LED temperature control system and a laptop computer. **(B)** Bottom views of the LED module when all LEDs are off (left) and on (right). **(C)** 13-day-old cucumber seedlings grown under phosphor-converted white LED light. **(D)** During the measurement of net photosynthetic rate (P_n), a part of a cucumber leaf was sandwiched in a leaf chamber of the portable photosynthesis system, and the surface of transparent film covering the top of the leaf chamber was placed in contact with the light outlet of the hollow conical reflection condenser of the LASS system.

ca. 1,200 μmol m^{-2} s^{-1}) for 20 min. Subsequently, leaves were irradiated with the reproduced sunlight for 200 min. The SPD was changed every 15 s. P_n and stomatal conductance (g_s) were recorded every 3 s, and five gas exchange measurement data (3, 6, 9, 12, and 15 s) were recorded for each SPD of light. The means of the gas exchange parameters collected at 12 and 15 s were regarded as corresponding to the SPD of light to minimize the effects of the transient responses of the LASS system and the portable photosynthesis system. The readings of the reference and sample infrared gas analyzers (IRGAs) were matched after the sample gas was temporarily passed through the reference IRGA once every 20 min. For (2), leaves were first kept at a constant PPFD of 400 μmol m^{-2} s^{-1} with a relative SPD of the reference sunlight for 20 min. Then, leaves were irradiated with light with a relative SPD of the reference sunlight at different PPFD levels in the following order: 1,200, 1,000, 800, 600, 400, 200, and 0 μmol m^{-2} s^{-1}. Each PPFD level was maintained for 20 min, and the mean P_n and g_s values for the last 5 min (15–20 min) were regarded as the steady-state values. Matching of the reference and sample IRGAs was carried out at 14–15 min after each PPFD level was attained.

We used 12 plants for measurements. Six plants were first subjected to measurement (1) followed by measurement (2), while the other six were subjected to measurements in the opposite order. Because no significant differences were found in the results between the two irradiation patterns, data for 12 plants were averaged irrespective of the irradiation pattern order.

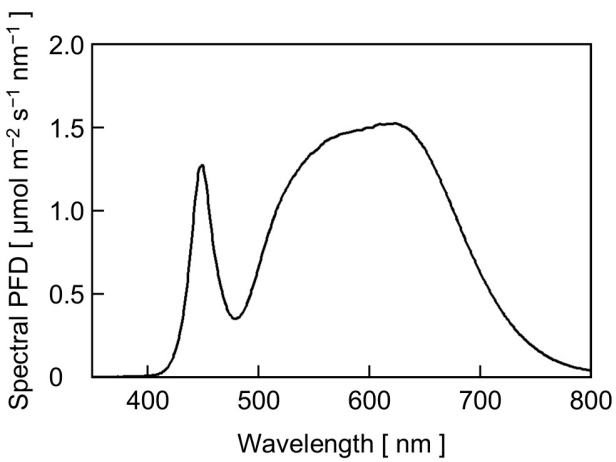

FIGURE 2 | The SPD of phosphor-converted white LED light for cucumber seedling growth at a PPFD of 300 μmol m^{-2} s^{-1}.

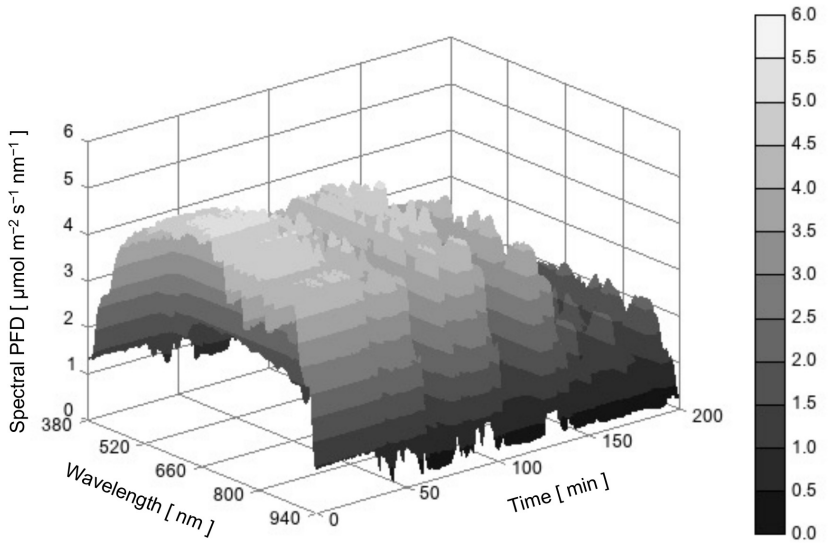

FIGURE 3 | Time course of sunlight SPD between 380 and 940 nm measured in Bunkyo, Tokyo, Japan (35°43'N) from 11:10 to 14:30 on October 12, 2017.

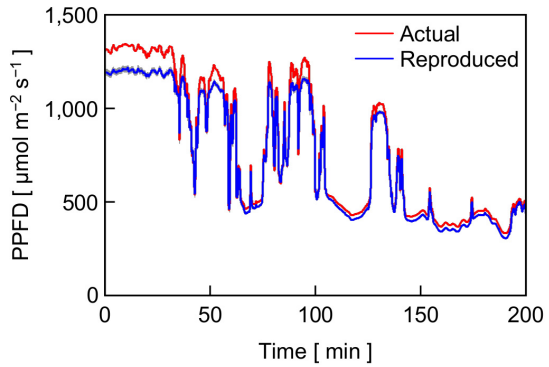

FIGURE 4 | Time course of PPFD of actual sunlight measured in Bunkyo, Tokyo, Japan (35°43'N) from 11:10 to 14:30 on October 12, 2017 and that of sunlight reproduced with the LASS system. The height of gray area at a given time represents the standard deviation of the PPFD of the reproduced sunlight (n = 12).

The steady-state P_n averaged for 12 plants in response to PPFD was fitted with the following nonrectangular hyperbolic function (Johnson and Thornley, 1984) using the least-squares method: $P_n = \{\phi I + P_{max} - [(\phi I + P_{max}) - 4\theta\phi I P_{max}]^{0.5}\} / 2\theta - R_d$, where I is PPFD, mol m^{-2} s^{-1}; ϕ is the initial slope, mol mol^{-1}; P_{max} is the maximum rate of gross photosynthetic rate, mol m^{-2} s^{-1}; θ is the convexity of the curve, dimensionless; and R_d is the dark respiratory rate, mol m^{-2} s^{-1}.

RESULTS AND DISCUSSION

Time Course of Sunlight SPD

Figure 3 is a three-dimensional surface plot showing the time course of SPD of actual sunlight between 380 and 940 nm. When focusing on PPFD (red line in **Figure 4**), the value was approximately 1,300 μmol m^{-2} s^{-1} at the beginning of measurement and then fluctuated in the range between 1,300 and 400 μmol m^{-2} s^{-1} because clouds sometimes covered the sun and direct solar radiation was largely attenuated. The relative SPD, or the shape of the SPD, may not be apparently different among times (**Figure 3**). However, sunlight with a lower PPFD tended to contain a relatively large number of photons below 600 nm and that with a higher PPFD tended to contain a relatively large number of photons above 700 nm (data not shown). Most likely, occasional reductions in PPFD by clouds that covered the sun enhanced the fraction of diffuse solar radiation from the sky in global solar radiation and the diffuse radiation was rich in light with a shorter waveband compared with direct radiation (Kume et al., 2018). Thus, both the PPFD and relative SPD of sunlight changed dynamically.

Reproduction of the Time Course of Sunlight SPD With the LED-Artificial Sunlight Source System

Figure 4 also shows the time course of the PPFD of reproduced sunlight with the LASS system averaged over 12 replications (a blue line). The PPFD of reproduced sunlight agreed with that of actual sunlight except that it was lower than that of actual sunlight when the actual sunlight PPFD was greater than 1,200 μmol m^{-2} s^{-1} (**Figure 4**). Overall, the difference in PPFD between actual and reproduced sunlight at a given time was minor and considered to be acceptable.

The relatively lower reproducibility of artificial sunlight PPFD in the high PPFD range was primarily due to the limited maximum output capacity of the LASS system, although it was reported that the LASS system could reproduce full irradiation of ground-level sunlight (Fujiwara et al., 2013). Specifically, there were two main reasons for the limitation generated in

this experiment. One reason was that we did not use the re-approximation function in this study (see section "Materials and Methods"). **Figure 5** shows the reference sunlight spectra with PPFDs of 1,600, 1,300, and 1,000 μmol m^{-2} s^{-1}, as well as those of reproduced sunlight without the re-approximation function. The extent of approximation of the reproduced sunlight to the reference sunlight spectrum declined as the target PPFD increased: the coefficients of variation calculated at every 1 nm between 380 and 940 nm were 13.6, 15.0, and 18.4% for 1,000, 1,300, and 1,600 μmol m^{-2} s^{-1}, respectively. The other reason was that the transparent polypropylene film (Propafilm C) covering the leaf chamber of the portable photosynthesis system significantly reduced the PPFD on the leaf surface. The spectral transmissivity of the film was approximately 85–90% between 380 and 940 nm and hardly dependent on wavelength (Meiwafosis Co., Ltd., personal communication), indicating that the film reduced SPDs within this range to a similar extent. However, the extent of sunlight SPD reproduction here must be the highest among those employed in previous experiments investigating the effects of fluctuating light on photosynthesis.

Time Course of Leaf Gas Exchange Rates Under Reproduced Sunlight

Figure 6A shows the time course of P_n in cucumber leaves measured under reproduced sunlight and P_n estimated from a PPFD-response curve of steady-state P_n in leaves of the same plants (**Figure 6C**). The measured and estimated P_n agreed well except when the PPFD was 500 μmol m^{-2} s^{-1} or lower (see **Figure 3**), where the measured P_n was lower than the estimated P_n. The time course of measured g_s (**Figure 6B**) resembled that of measured P_n, while the response of g_s to changes in PPFD appeared to be delayed relative to that of P_n. A slow response of g_s to a change in PPFD has been frequently reported (e.g., Lawson et al., 2012; Slattery et al., 2018). As a result, the amplitude of fluctuation appeared smaller in g_s than in P_n.

We grew cucumber seedlings under phosphor-converted white LEDs, of which relative SPD (**Figure 2**) was quite different from that of the reproduced sunlight (**Figure 5**). One notable difference was the spectral PFD of far-red light: the white LED light contained a less proportion of far-red light than the reproduced sunlight. In leaves grown under light containing less far-red light, light is preferentially absorbed by photosystem II (PSII) compared with photosystem I (PSI) ("PSII-light"), and the ratio of the amount of PSII to that of PSI (PSII/PSI ratio) decreases to counteract the imbalance excitation (Chow et al., 1990a,b; Melis, 1991; Walters and Horton, 1994, 1995; Wagner et al., 2008; Hogewoning et al., 2012). One might suggest that the shift of the growth light of "PSII-light" to the P_n measurement light of "PSI-light" affected the response of P_n to the sunlight SPD fluctuations. However, Murakami et al. (2016) showed that cucumber leaves grown under phosphor-converted white LED light supplemented with and without far-red LED light did not show a significant difference in steady-state P_n measured under reproduced sunlight. This suggests that the effect of the shift from "PSII-light" during growth to "PSI-light" for P_n measurement in this study was also not significant.

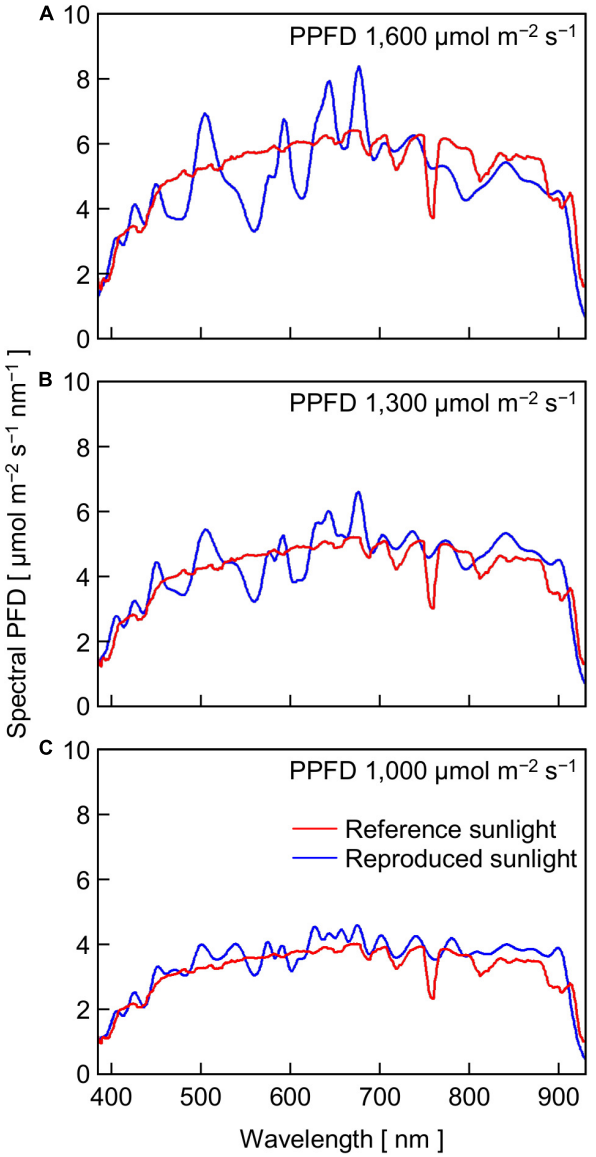

FIGURE 5 | The SPDs of reference sunlight at PPFDs of 1,600 **(A)**, 1,300 **(B)**, and 1,000 **(C)** μmol m^{-2} s^{-1} and reproduced sunlight of which SPDs were approximated to those of the reference sunlight with the LASS system.

Relationship Between the Ratio of Measured P_n to Estimated P_n and PPFD or the Change in PPFD

To further analyze the effect of reproduced sunlight PPFD on the difference between measured and estimated P_n, the ratio of measured P_n to estimated P_n was plotted against PPFD (**Figure 7A**). Overall, a large part of the ratio was distributed below 1, indicating that the measured P_n was generally lower than the estimated P_n. The ratio appeared to vary in an intermediate PPFD range of 400–700 μmol m^{-2} s^{-1} compared with lower and higher PPFD ranges. The linear regression was not statistically significant (r^2 = 0.195). We summarized these data by averaging

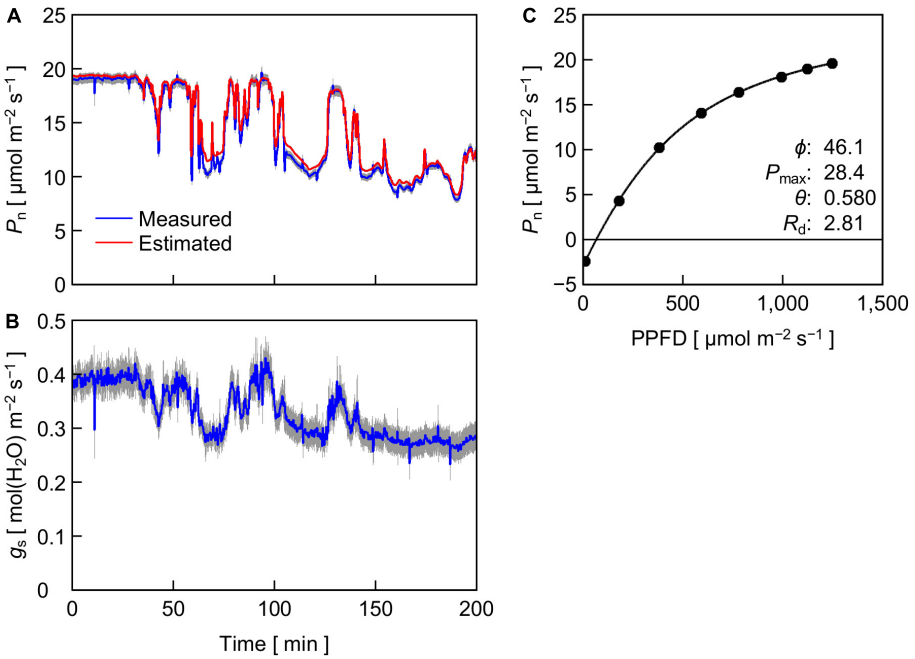

FIGURE 6 | (A,B) Time course of P_n **(A)** and stomatal conductance g_s **(B)** in cucumber leaves measured under reproduced sunlight. For P_n, values estimated from the steady-state PPFD-response curve of P_n **(C)** are also shown. The height of gray area at a given time represents the standard errors of the means for the measured values (n = 12). **(C)** Steady-state P_n in cucumber leaves in response to PPFD. Solid circles are the means of measured values (n = 12), and the line is a fitting curve with a nonrectangular hyperbolic function, of which parameter values are shown within the panel. Standard errors of the means are smaller than the diameter of the circles and are invisible.

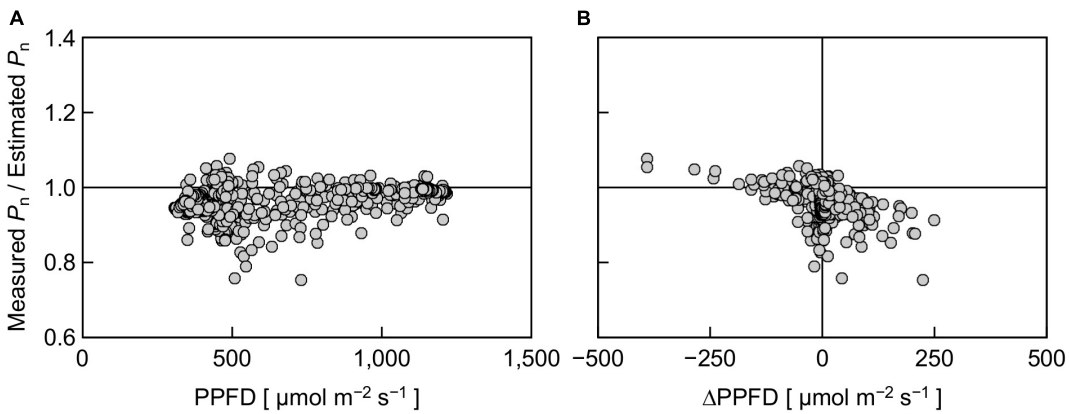

FIGURE 7 | The ratio of measured P_n to estimated P_n in response to PPFD at a given moment **(A)** and the ratio in response to a change in PPFD for 15 s (ΔPPFD) **(B)**. Positive and negative ΔPPFD values represent increases and decreases in PPFD, respectively.

the measured and estimated P_n, respectively, within every 200 μmol m^{-2} s^{-1} PPFD range between 300 and 1,300 μmol m^{-2} s^{-1} and computed the ratio (**Table 1**). The ratio was relatively low at low PPFDs; 0.95 and 0.94 for PPFD ranges of 300–500 and 500–700 μmol m^{-2} s^{-1}, respectively. On the other hand, this value was slightly higher at high PPFDs; 0.98 and 0.99 for 900–1,100 and 1,100–1,300 μmol m^{-2} s^{-1}, respectively. The overall ratio of measured P_n to estimated P_n between 300 and 1,300 μmol m^{-2} s^{-1} was 0.97, indicating that the reduction in P_n measured under reproduced sunlight compared with P_n estimated from the steady-state PPFD–P_n curve throughout the measurement was 3%.

This 3% reduction was significantly smaller than the 20–30% reduction reported in previous experimental (Vialet-Chabrand et al., 2017b) and simulation (Taylor and Long, 2017; Tanaka et al., 2019) studies but close to the 3–6% reduction on average reported by a more recent study employing comprehensive simulation over a wide range of diurnal PPFD fluctuations (Murakami and Jishi, 2021). There are several possible reasons for the difference between the values of calculated reduction. The first

TABLE 1 | The ratio of mean measured P_n to mean estimated P_n calculated in different PPFD ranges.

PPFD range (μmol m^{-2} s^{-1})	Measured P_n (μmol m^{-2} s^{-1})	Estimated P_n (μmol m^{-2} s^{-1})	Measured P_n/ estimated P_n
300–500	10.4	10.8	0.95
500–700	12.9	13.8	0.94
700–900	15.9	16.5	0.96
900–1,100	18.0	18.3	0.98
1,100–1,300	19.0	19.2	0.99
All (300–1,300)	14.3	14.7	0.97

reason is the relative SPD. Reproducing both the PPFD and the relative SPD of sunlight could reduce the difference between the measured and estimated P_n, compared with reproducing PPFD only. The second reason is the pattern of PPFD change. The difference between the measured and estimated P_n can depend on the pattern of PPFD change (Naumburg and Ellsworth, 2002). Murakami and Jishi (2021) also performed a simulation of diurnal courses of P_n under various PPFD fluctuation patterns of sunlight using a steady-state photosynthesis model and a dynamic photosynthesis model incorporating the response delay of P_n to an increase in PPFD. They showed that the difference in P_n calculated with the two models was largely dependent on the PPFD fluctuation pattern. The amplitudes of PPFD fluctuations in previous studies were ca. 100–2,000 μmol m^{-2} s^{-1} (Taylor and Long, 2017), 100–1,500 μmol m^{-2} s^{-1} (Vialet-Chabrand et al., 2017b), and 200–2,200 μmol m^{-2} s^{-1} (Tanaka et al., 2019), which are greater than those in the present study (400–1,300 μmol m^{-2} s^{-1}). According to our data, the difference between the measured and estimated P_n tended to be high under low PPFD conditions (**Figure 7A** and **Table 1**). The levels and duration of low PPFDs in the PPFD fluctuating pattern, in relation to the shape of the PPFD-response curve of P_n in leaves considered, may be important to account for the difference between the measured and estimated P_n. The third reason is the P_n measurement duration under fluctuating light. Vialet-Chabrand et al. (2017b) reported that when the overall PPFD level was high (mean: 460 μmol m^{-2} s^{-1}), the extent of measured P_n reduction compared with the estimated P_n became greater, especially after 4–6 h after the measurement started. However, when the mean PPFD was low (230 μmol m^{-2} s^{-1}), the reduction was apparent at the beginning of the measurement (Vialet-Chabrand et al., 2017b). The interactive effects of the fluctuating PPFD pattern and the timing at which the measured and estimated P_n started to significantly differ should be examined in detail in future work.

Finally, we evaluated the effect of PPFD change (ΔPPFD) on the ratio of measured P_n to estimated P_n (**Figure 7B**). There was a negative trend between the ratio and ΔPPFD; a large increase and decrease in PPFD tended to decrease and increase the ratio, respectively, although the linear regression was not statistically significant ($r^2 = 0.166$). This trend may partly reflect the response delay of the portable photosynthesis system. In particular, the overvalued P_n when ΔPPFD was negative was likely due to the response delay, as the response of P_n to a decrease in PPFD was reportedly faster than that to an increase in PPFD (Bhuiyan and van Iersel, 2021). On the other hand, this trend suggests that P_n estimated using the steady-state PPFD-response curve (**Figure 6C**) tended to be particularly undervalued under the fluctuating SPD condition when the rate of PPFD increase was high. A similar result was reported by Bhuiyan and van Iersel (2021) that it took a longer time until P_n reached a steady state when the extent of PPFD increase was high.

CONCLUSION

In this study, we reproduced a time course of sunlight SPD (both PPFD and relative SPD) using the LASS system. The P_n of cucumber leaves measured under the reproduced sunlight and that estimated from the steady-state PPFD–P_n curve of the same leaves were compared. The measured P_n tended to be lower than the estimated P_n under low PPFD conditions. The extent of measured P_n reduction compared with the estimated P_n averaged over all PPFD levels was 3%, which was smaller than the values of approximately 20–30% reported by previous studies (Taylor and Long, 2017; Vialet-Chabrand et al., 2017b; Tanaka et al., 2019). This finding suggests that the loss of integral net photosynthetic gain under fluctuating sunlight can vary among days with different fluctuation patterns or may be nonsignificant when fluctuations in both PPFD and relative SPD of sunlight are reproduced. More experimental observations of P_n under various patterns of reproduced fluctuating sunlight must be acquired and analyzed to discuss the quantitative importance of considering sunlight SPD fluctuations in leaf instantaneous photosynthesis.

DATA AVAILABILITY STATEMENT

The original contributions presented in the study are included in the article, further inquiries can be directed to the corresponding author.

AUTHOR CONTRIBUTIONS

RM conceived and designed the study and drafted the manuscript. HI acquired the data. HI and KF critically revised the manuscript. All authors analyzed the data and approved the final version.

FUNDING

This work was financially supported in part by JSPS KAKENHI (Grant No. 18H03966).

ACKNOWLEDGMENTS

We would like to thank Yasuomi Ibaraki, Akira Yano, and Shunsuke Kubo for helpful discussion and AGC Green-Tech Co., Ltd. for kindly providing the F-CLEAN Clear film.

REFERENCES

Adachi, S., Tanaka, Y., Miyagi, A., Kashima, M., Tezuka, A., Toya, Y., et al. (2019). High-yielding rice Takanari has superior photosynthetic response to a commercial rice Koshihikari under fluctuating light. *J. Exp. Bot.* 70, 5287–5297. doi: 10.1093/jxb/erz304

Bhuiyan, R., and van Iersel, M. (2021). Only extreme fluctuations in light levels reduce lettuce growth under sole source lighting. *Front. Plant Sci.* 12:619973. doi: 10.3389/fpls.2021.619973

Björkman, O. (1981). "Responses to different quantum flux densities," in *Physiological Plant Ecology I. Responses to the Physical Environment*, eds O. L. Lange, P. S. Nobel, C. B. Osmond, and H. Ziegler (Berlin: Springer-Verlag), 57–107.

Boardman, N. K. (1977). Comparative photosynthesis of sun and shade plants. *Annu. Rev. Plant Physiol.* 28, 355–377. doi: 10.1146/annurev.pp.28.060177.002035

Chow, W. S., Goodchild, D. J., Miller, C., and Anderson, J. M. (1990a). The influence of high levels of brief or prolonged supplementary far-red illumination during growth on the photosynthetic characteristics, composition and morphology of *Pisum sativum* chloroplasts. *Plant Cell Environ.* 13, 135–145. doi: 10.1111/j.1365-3040.1990.tb01285.x

Chow, W. S., Melis, A., and Anderson, J. M. (1990b). Adjustments of photosystem stoichiometry in chloroplasts improve the quantum efficiency of photosynthesis. *Proc. Natl. Acad. Sci. U.S.A.* 87, 7502–7506. doi: 10.1073/pnas.87.19.7502

Fujiwara, K., Eijima, K., and Yano, A. (2013). "Second-generation LED-artificial sunlight source system available for light effects research in biological and agricultural sciences," in *Proceedings of the 7th Lux Pacifica*, Bangkok, 140–145.

Fujiwara, K., and Sawada, T. (2006). Design and development of an LED-artificial sunlight source system prototype capable of controlling relative spectral power distribution. *J. Light Vis. Environ.* 30, 170–176. doi: 10.2150/jlve.30.170

Fujiwara, K., Sawada, T., Goda, S., Ando, Y., and Yano, A. (2007). An LED-artificial sunlight source system available for light effects research in flower science. *Acta Hortic.* 755, 373–380. doi: 10.17660/ActaHortic.2007.755.49

Fujiwara, K., and Yano, A. (2011). Controllable spectrum artificial sunlight source system using LEDs with 32 different peak wavelengths of 385–910 nm. *Bioelectromagnetics* 32, 243–252. doi: 10.1002/bem.20637

Heuvelink, E. (1995). Dry matter production in a tomato crop: measurements and simulation. *Ann. Bot.* 75, 369–379. doi: 10.1006/anbo.1995.1035

Heuvelink, E. (1999). Evaluation of a dynamic simulation model for tomato crop growth and development. *Ann. Bot.* 83, 413–422. doi: 10.1006/anbo.1998.0832

Heuvelink, E., Bakker, M., Marcelis, L. F. M., and Raaphorst, M. (2008). Climate and yield in a closed greenhouse. *Acta Hortic.* 801, 1083–1092. doi: 10.17660/ActaHortic.2008.801.130

Heuvelink, E., and Dorais, M. (2005). "Crop growth and yield," in *Tomatoes*, ed. E. Heuvelink (Wallingford: CABI Publishing), 81–144.

Hogewoning, S., Trouwborst, G., Maljaars, H., Poorter, H., van Ieperen, W., and Harbinson, J. (2010). Blue light dose–responses of leaf photosynthesis, morphology, and chemical composition of Cucumis sativus grown under different combinations of red and blue light. *J. Exp. Bot.* 61, 3017–3117. doi: 10.1093/jxb/erq132

Hogewoning, S. W., Wientjes, E., Douwstra, P., Trouwborst, G., van Ieperen, W., Croce, R., et al. (2012). Photosynthetic quantum yield dynamics: from photosystems to leaves. *Plant Cell* 24, 1921–1935. doi: 10.1105/tpc.112.097972

Inada, K. (1976). Action spectra for photosynthesis in higher plants. *Plant Cell Physiol.* 17, 355–365. doi: 10.1093/oxfordjournals.pcp.a075288

International Electrotechnical Commission (2019). *IEC 60904-3:2019, Photovoltaic Devices – Part 3: Measurement Principles for Terrestrial Photovoltaic (PV) Solar Devices with Reference Spectral Irradiance Data*. Available online at: https://webstore.iec.ch/publication/61084 (accessed March 2, 2021).

Johnson, I. R., and Thornley, J. H. M. (1984). A model of instantaneous and daily canopy photosynthesis. *J. Theor. Biol.* 107, 531–545. doi: 10.1016/S0022-5193(84)80131-9

Kaiser, E., Morales, A., and Harbinson, J. (2018). Fluctuating light takes crop photosynthesis on a rollercoaster ride. *Plant Physiol.* 176, 977–989. doi: 10.1104/pp.17.01250

Kaiser, E., Morales, A., Harbinson, J., Heuvelink, E., Prinzenberg, A. E., and Marcelis, L. F. M. (2016). Metabolic and diffusional limitations of photosynthesis in fluctuating irradiance in *Arabidopsis thaliana*. *Sci. Rep.* 6:31252. doi: 10.1038/srep31252

Kaiser, E., Morales, A., Harbinson, J., Kromdijk, J., Heuvelink, E., and Marcelis, L. F. M. (2015). Dynamic photosynthesis in different environmental conditions. *J. Exp. Bot.* 66, 2415–2426. doi: 10.1093/jxb/eru406

Kimura, H., Hashimoto-Sugimoto, M., Iba, K., Terashima, I., and Yamori, W. (2020). Improved stomatal opening enhances photosynthetic rate and biomass production in fluctuating light. *J. Exp. Bot.* 71, 2339–2350. doi: 10.1093/jxb/eraa090

Kono, M., Kawaguchi, H., Mizusawa, N., Yamori, W., Suzuki, Y., and Terashima, I. (2020). Far-red light accelerates photosynthesis in the low-light phases of fluctuating light. *Plant Cell Physiol.* 61, 192–202. doi: 10.1093/pcp/pcz191

Kono, M., Noguchi, K., and Terashima, I. (2014). Roles of the cyclic electron flow around PSI (CEF-PSI) and O2-dependent alternative pathways in regulation of the photosynthetic electron flow in short-term fluctuating light in Arabidopsis thaliana. *Plant Cell Physiol.* 55, 990–1004. doi: 10.1093/pcp/pcu033

Kono, M., and Terashima, I. (2016). Elucidation of photoprotective mechanisms of PSI against fluctuating light photoinhibition. *Plant Cell Physiol.* 57, 1405–1414. doi: 10.1093/pcp/pcw103

Kono, M., Yamori, W., Suzuki, Y., and Terashima, I. (2017). Photoprotection of PSI by far-red light against the fluctuating light-induced photoinhibition in *Arabidopsis thaliana* and field-grown plants. *Plant Cell Physiol.* 58, 35–45. doi: 10.1093/pcp/pcw215

Kume, A., Akitsu, T., and Nasahara, K. N. (2018). Why is chlorophyll b only used in light-harvesting systems? *J. Plant Res.* 131, 961–972. doi: 10.1007/s10265-018-1052-7

Lawson, T., Kramer, D. M., and Raines, C. A. (2012). Improving yield by exploiting mechanisms underlying natural variation of photosynthesis. *Curr. Opin. Biotechnol.* 23, 215–220. doi: 10.1016/j.copbio.2011.12.012

Leakey, A. D. B., Press, M. C., Scholes, J. D., and Watling, J. R. (2002). Relative enhancement of photosynthesis and growth at elevated CO2 is greater under sunflecks than uniform irradiance in a tropical rain forest tree seedling. *Plant Cell Environ.* 25, 1701–1714. doi: 10.1046/j.1365-3040.2002.00944.x

McCree, K. J. (1972). The action spectrum, absorptance and quantum yield of photosynthesis in crop plants. *Agric. Meteorol.* 9, 191–216. doi: 10.1016/0002-1571(71)90022-7

Melis, A. (1991). Dynamics of photosynthetic membrane composition and function. *Biochim. Biophys. Acta* 1058, 87–106. doi: 10.1016/S0005-2728(05)80225-7

Murakami, K., and Jishi, T. (2021). Appropriate time interval of PPFD measurement to estimate daily photosynthetic gain. *Funct. Plant Biol.* doi: 10.1071/FP20323 [Epub ahead of print],

Murakami, K., Matsuda, R., and Fujiwara, K. (2016). Interaction between the spectral photon flux density distributions of light during growth and for measurements in net photosynthetic rates of cucumber leaves. *Physiol. Plant.* 158, 213–224. doi: 10.1111/ppl.12421

Murchie, E. H., Kefauver, S., Araus, J. L., Muller, O., Rascher, U., Flood, P. J., et al. (2018). Measuring the dynamic photosynthome. *Ann. Bot.* 122, 207–220. doi: 10.1093/aob/mcy087

Naumburg, E., and Ellsworth, D. S. (2002). Short-term light and leaf photosynthetic dynamics affect estimates of daily understory photosynthesis in four tree species. *Tree Physiol.* 22, 393–401. doi: 10.1093/treephys/22.6.393

Pearcy, R. W. (1990). Sunflecks and photosynthesis in plant canopies. *Annu. Rev. Plant Physiol. Plant Mol. Biol.* 41, 421–453. doi: 10.1146/annurev.pp.41.060190.002225

Qu, M., Hamdani, S., Li, W., Wang, S., Tang, J., Chen, Z., et al. (2016). Rapid stomatal response to fluctuating light: an under-explored mechanism to improve drought tolerance in rice. *Funct. Plant Biol.* 43, 727–738. doi: 10.1071/FP15348

Sejima, T., Takagi, D., Fukuyama, H., Makino, A., and Miyake, C. (2014). Repetitive short-pulse light mainly inactivates photosystem I in sunflower leaves. *Plant Cell Physiol.* 55, 1184–1193. doi: 10.1093/pcp/pcu061

Slattery, R. A., Walker, B. J., Weber, A. P. M., and Ort, D. R. (2018). The impacts of fluctuating light on crop performance. *Plant Physiol.* 176, 990–1003. doi: 10.1104/pp.17.01234

Soleh, M. A., Tanaka, Y., Kim, S. Y., Huber, S. C., Sakoda, K., and Shiraiwa, T. (2017). Identification of large variation in the photosynthetic induction response among 37 soybean [*Glycine max* (L.) Merr.] genotypes that is not correlated with steady-state photosynthetic capacity. *Photosynth. Res.* 131, 305–315. doi: 10.1007/s11120-016-0323-1

Tanaka, Y., Adachi, S., and Yamori, W. (2019). Natural genetic variation of the photosynthetic induction response to fluctuating light environment. *Curr. Opin. Plant Biol.* 49, 52–59. doi: 10.1016/j.pbi.2019.04.010

Taylor, S. H., and Long, S. P. (2017). Slow induction of photosynthesis on shade to sun transitions in wheat may cost at least 21% of productivity. *Philos. Trans. R. Soc. B* 372:20160543. doi: 10.1098/rstb.2016.0543

Vialet-Chabrand, S., Matthews, J. S. A., McAusland, L., Blatt, M. R., Griffiths, H., and Lawson, T. (2017a). Temporal dynamics of stomatal behavior: modeling and implications for photosynthesis and water use. *Plant Physiol.* 174, 603–613. doi: 10.1104/pp.17.00125

Vialet-Chabrand, S., Matthews, J. S. A., Simkin, A. J., Raines, C. A., and Lawson, T. (2017b). Importance of fluctuations in light on plant photosynthetic acclimation. *Plant Physiol.* 173, 2163–2179. doi: 10.1104/pp.16.01767

Wagner, R., Dietzel, L., Bräutigam, K., Fischer, W., and Pfannschmidt, T. (2008). The long-term response to fluctuating light quality is an important and distinct light acclimation mechanism that supports survival of Arabidopsis thaliana under low light conditions. *Planta* 228, 573–587. doi: 10.1007/s00425-008-0760-y

Walters, R. G., and Horton, P. (1994). Acclimation of *Arabidopsis thaliana* to the light environment: changes in composition of the photosynthetic apparatus. *Planta* 195, 248–256. doi: 10.1007/BF00199685

Walters, R. G., and Horton, P. (1995). Acclimation of Arabidopsis thaliana to the light environment: regulation of chloroplast composition. *Planta* 197, 475–481. doi: 10.1007/BF00196669

Yamori, W. (2016). Photosynthetic response to fluctuating environments and photoprotective strategies under abiotic stress. *J. Plant Res.* 129, 379–395. doi: 10.1007/s10265-016-0816-1

Yamori, W., Kusumi, K., Iba, K., and Terashima, I. (2020). Increased stomatal conductance induces rapid changes to photosynthetic rate in response to naturally fluctuating light conditions in rice. *Plant Cell Environ.* 43, 1230–1240. doi: 10.1111/pce.13725

Yamori, W., Makino, A., and Shikanai, T. (2016). A physiological role of cyclic electron transport around photosystem I in sustaining photosynthesis under fluctuating light in rice. *Sci. Rep.* 6:20147. doi: 10.1038/srep20147

Yang, Y. J., Zhang, S. B., Wang, J. H., and Huang, W. (2019). Photosynthetic regulation under fluctuating light in field-grown Cerasus cerasoides: a comparison of young and mature leaves. *Biochim. Biophys. Acta Bioenerg.* 1860:148073. doi: 10.1016/j.bbabio.2019.148073

Zhang, Y., Kaiser, E., Zhang, Y., Yang, Q., and Li, T. (2019). Red/blue light ratio strongly affects steady-state photosynthesis, but hardly affects photosynthetic induction in tomato (*Solanum lycopersicum*). *Physiol. Plant.* 167, 144–158. doi: 10.1111/ppl.12876

Conflict of Interest: The authors declare that the research was conducted in the absence of any commercial or financial relationships that could be construed as a potential conflict of interest.

frontiers in Plant Science

ORIGINAL RESEARCH
published: 08 July 2021
doi: 10.3389/fpls.2021.667407

Blue and Far-Red Light Affect Area and Number of Individual Leaves to Influence Vegetative Growth and Pigment Synthesis in Lettuce

*Yuyao Kong and Krishna Nemali**

Department of Horticulture and Landscape Architecture, Purdue University, West Lafayette, IN, United States

Published work indicates that high percentage of blue light can enhance pigment levels but decreases growth, while addition of far-red light to growth light can increase quantum efficiency and photosynthesis in leafy greens. Combining high-energy blue light with low-energy far-red light may increase both vegetative growth and pigment levels. However, the effect of high-energy blue and low-energy far-red light on the vegetative growth and pigments synthesis is unclear. This information can be potentially useful for enhancing the levels of pigments with nutritional value (e.g., beta-carotene and anthocyanins) in the produce grown in vertical farms. We grew romaine lettuce (cv. Amadeus) under similar light intensity (approximately 130 $\mu mol \cdot m^{-2} \cdot s^{-1}$) but different proportions of red: blue: far-red including 90:10: 0 ("High-R"), 50: 50: 0 ("High-B"), and 42: 42: 16 ("High-B+FR") for 31 days. Results indicated that canopy area and leaf photosynthetic rate of lettuce plants was reduced in the High-B, thereby reducing plant growth. We did not observe photosynthesis enhancement in the High-B+FR. Instead, plants clearly showed photomorphogenic effects. The phytochrome photostationary state (PSS) decreased with far-red addition, resulting in reduced leaf number per plant. This was likely to shift the allocation of resources toward elongation growth for shade avoidance. Further, we observed an increase in the area of individual leaves, canopy area, and shoot dry weight in the High-B+FR. However, these appear to be an indirect consequence of decreased leaf number per plant. Our results also indicate that changes in expansion growth at individual leaf scale largely regulated pigment concentration in plants. As individual leaf area became smaller (e.g., High-B) or larger (e.g., High-B+FR), the levels of pigments including chlorophylls and beta-carotene increased or decreased, respectively. Area of individual leaves also positively influenced canopy area (and likely light interception) and shoots dry weight (or vegetative growth). Our study provides additional insights into the effects of high-energy blue and low-energy far-red light on individual leaf number and leaf growth, which appear to control plant growth and pigment levels in lettuce.

Keywords: controlled environment agriculture, photoinhibition, phytochrome photostationary state, light interception, proximity response

OPEN ACCESS

Edited by:
Jung Eek Son,
Seoul National University,
South Korea

Reviewed by:
Gaozhong Shen,
Pennsylvania State University (PSU),
United States
Julian C. Verdonk,
Wageningen University and Research,
Netherlands

***Correspondence:**
Krishna Nemali
knemali@purdue.edu

Specialty section:
This article was submitted to Crop and Product Physiology, a section of the journal Frontiers in Plant Science

Received: *13 February 2021*
Accepted: *14 June 2021*
Published: *08 July 2021*

Citation:
Kong Y and Nemali K (2021) Blue and Far-Red Light Affect Area and Number of Individual Leaves to Influence Vegetative Growth and Pigment Synthesis in Lettuce. Front. Plant Sci. 12:667407. doi: 10.3389/fpls.2021.667407

INTRODUCTION

Vertical farming involves growing food crops at multiple vertically stacked levels in controlled environments to maximize productivity per unit area (Despommier, 2010). The concept of vertical farming was mainly developed to produce food in urban areas where available space can be limited for growing crops. Vertical farming can aid in increasing the supply of fresh food, which is needed in many urban areas (Avgoustaki and Xydis, 2020). Because of its importance to food production, the industry is growing rapidly in the United States, with an estimated market value of $3 billion by 2024 (Qiu et al., 2020). At present, leafy greens such as lettuce are the major crops grown in vertical farms (Frazier, 2017). With developments in science and technology, the range of species, including vegetables, medicinal plants, and ornamentals, that can be grown in vertical farms is expected to increase in the future.

Plant pigments such as beta-carotene (precursor of vitamin A biosynthesis) and anthocyanins (aid in reducing inflammation and blood pressure, Karlsen et al., 2007; Jennings et al., 2012) have beneficial effects on human health. Nutrients consumed through plant-based foods are regarded as more efficacious than those consumed through supplements (Martin and Li, 2017). However, the levels of nutrients beneficial to human health are generally low in plants (Lako et al., 2007; Thoma et al., 2020). For example, a salad bowl of lettuce (approximately 60 g) can provide only a third of recommended daily allowance of vitamin A (Institute of Medicine US Panel on Micronutrients, 2001; USDA, 2019). Breeding efforts to improve the levels of nutrients in leafy greens is at its infancy. The current research focus in the area of vertical farming is on increasing crop productivity and optimizing resource-use during production. Relatively less effort is being made to explore the potential of vertical farms to supply nutrient-dense foods to urban population. Given this, environmental manipulation appears to be the only viable option for enhancing the level of healthy nutrients in leafy greens.

Light emitting diode (LED) lights with a wide range of customized light spectra are used to grow plants in vertical farms (Kong et al., 2019). Spectral composition of light can significantly affect pigment levels in plants (Amoozgar et al., 2017; Naznin et al., 2019; Camejo et al., 2020). Addition of high-energy blue light is usually associated with increased accumulation of pigments such as carotenoids and anthocyanins (Li and Kubota, 2009; Johkan et al., 2010; Ouzounis et al., 2015; Amoozgar et al., 2017), and chlorophylls (Cope et al., 2013; Fan et al., 2013; Zhen and Bugbee, 2020). However, blue light is less efficient at driving photosynthesis than red light (McCree, 1972). Plants exposed to excess blue light show decreased leaf expansion (Hernandez and Kubota, 2016; Craver et al., 2020; Kusuma et al., 2020), stem elongation, and growth (Ohashi-Kaneko et al., 2007; Fan et al., 2013; Kang et al., 2016; Craver et al., 2020). Blue light is also involved, *via* cryptochrome receptors, in de-etiolation of hypocotyls and photoperiodic responses related to flowering (Yu et al., 2010), and phototropism (Ahmad et al., 1998) in plants. Far-red light addition enhanced quantum efficiency (or efficiency with which absorbed light is used in photosynthesis) when supplemented with light containing shorter wavelengths of photosynthetically active radiation (Zhen and van Iersel, 2017). It was reported that the absorbed far-red photons (700–750 nm) were equally efficient for photosynthesis when combined with photosynthetically active radiation (400–700 nm; Zhen and Bugbee, 2020). Increases in leaf area and canopy light interception (Park and Runkle, 2017; Kang et al., 2019; Zhen and Bugbee, 2020) were reported with far-red addition. However, far-red addition resulted in a decrease in the levels of carotenoids and anthocyanins (Li and Kubota, 2009; Stutte and Edney, 2009), and chlorophylls (Meng and Runkle, 2019; Zhen and Bugbee, 2020).

Moreover, far-red light has been associated with photomorphogenic effects associated with shade avoidance (e.g., stem elongation) in plants (Ballaré et al., 1990; Gommers et al., 2012; Yang and Li, 2017). A small increase in the proportion of far-red light in the environment can elicit "proximity" shade responses in plants, prior to actual canopy shading by neighbors (Martinez-Garcia et al., 2014). Based on the published research (Lorrain et al., 2008; Martinez-Garcia et al., 2014; Yang and Li, 2017), shade stimulus is perceived by phytochrome (P) receptor. The receptor exists in two photo-convertible forms i.e., red light absorbing P_r (inactive) and far-red light absorbing P_{fr} (active) form. The P_r form converts to P_{fr} upon absorption of red light and the P_{fr} form reverts to P_r form after absorbing far-red light or in the dark. Among the important light signaling components, phytochrome interacting factors (PIFs) play an important role in shade avoidance response. The activation of PIFs is necessary for eliciting shade avoidance responses such as elongation. A lower proportion of P_{fr} form in plants results in activation of PIFs and subsequent gene expression required for shade avoidance responses. This happens when relatively more P_{fr} converts to P_r form, i.e., when plants are exposed to far-red light.

Addition of low-energy far-red light to growth spectrum containing relatively high proportion of high-energy blue light may increase photosynthesis, crop growth rate, and pigment concentration in the produce grown in vertical farms. However, addition of far-red light may elicit photomorphogenic responses including elongation and may have little direct impact on photosynthesis in the long-term. Shade-avoidance responses due to far-red exposure may lower levels of pigments in the cells, as additional resources are needed for the elongation growth. Further, elongation growth may decrease plant quality. The interactive effects of high-energy blue light and low-energy far-red light on vegetative growth and pigment levels in plants is unclear. This information is important to exploit the benefits of blue and far-red spectrum in vertical farming. The objectives of the study were to quantify the effects of blue and combination of blue and far-red spectrum on vegetative growth and pigment concentration and to understand how light composition affects the interplay between vegetative growth and pigment synthesis in lettuce plants.

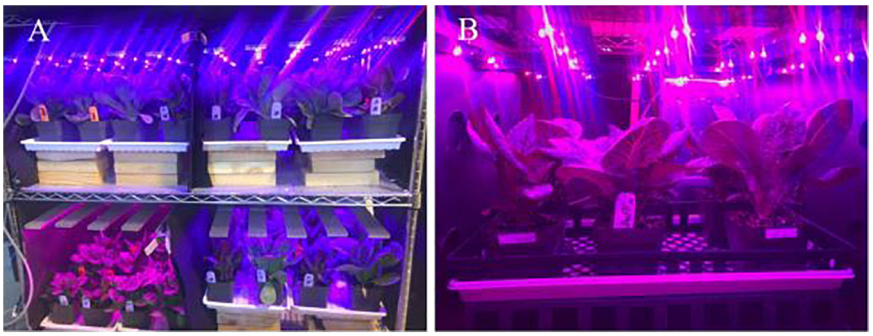

FIGURE 1 | (A) Experimental setup used in the study showing different experimental units. **(B)** A closeup picture of one experimental unit.

TABLE 1 | Total light intensity (400–750 nm), phytochrome photostationary state (PSS), and spectral composition of light in different treatments.

Treatment	Intensity	PSS	Spectral composition		
			Blue	Red	Far-red
	($\mu mol \cdot m^{-2} \cdot s^{-1}$)			(%)	
High-R	128.9 (1.67) a	0.90 (0.0008) a	8.3 (0.39) c	91.7 (0.39) a	0 (0.00) b
High-B	132.2 (1.44) a	0.86 (0.0008) b	47.2 (0.24) a	52.8 (0.24) b	0 (0.00) b
High-B+FR	138.1 (1.52) a	0.78 (0.0008) c	41.6 (0.20) b	41.5 (0.28) c	16.9 (0.12) a

Percentages of photons associated with broadband blue (400–500 nm), red (600–699 nm), and far-red (700–750 nm) light are shown. Values represent least square means and standard errors (±) (in parenthesis).

MATERIALS AND METHODS

Plant Production, Growing System, and Environmental Conditions

Romaine lettuce (*Lactuca sativa* cv. Amadeus) was grown from seed purchased from Paramount Seeds Company (Stuart, FL, United States). The selected variety has green foliage (i.e., contain low level of anthocyanins) and low crop yield (Miller et al., 2020), making it suitable for studying treatment effects on pigment levels and vegetative growth. Seeds were germinated in plug flats (72-cell; 3.5 cm × 3.5 cm × 5.9 cm, 30.2 mL per cell, Landmark Plastic, Akron, OH, United States) filled with a soilless substrate (80% peat, 15% perlite, and 5% vermiculite, BM-2, Berger, Saint Modeste, QC, Canada). The plug flats were placed under mist for 7 days to ensure uniform germination. Light treatments started immediately after germination (see section "Treatments"). After 10 days, seedlings in each light group were transplanted into square pots (10.6 cm × 10.6 cm × 8.4 cm, 943 mL, Kord Products Ltd., Brampton, ON, Canada) filled with the same soilless substrate used in the germination trays and arranged in a predetermined experimental design (see section "Experimental Design and Statistical Analyses"). Plants were harvested after 31 days from transplanting.

The vertical growing system was custom-built using chrome-wire shelves (1.22 m × 0.61 m × 1.37 m, H-6948, Uline, Pleasant Prairie, WI, United States) and LED fixtures. Each shelf had two levels spaced 0.6 m apart. Each level was further divided into two grow spaces (0.61 m × 0.61 m, of 0.37 m^2) and each grow space housed plants in pots (**Figure 1**). Customized LED fixtures (0.6 m × 0.6 m, Applied Electronic Materials, Fort Wayne, IN, United States) with different spectral composition were fastened to the chrome-wire shelves in each grow space. The light fixtures had separate circuits for blue (450 ± 18 nm), red (660 ± 19 nm), and far-red (730 ± 30 nm) LEDs (Oslon SSL, Osram, Munich, Germany). Each light fixture comprised of five individual bars (60 cm long), each containing six LEDs of a given wavelength. The LEDs were spaced 10 cm apart in the circuit and emitted light at 120° angle from the source. The intensities of red, blue, and far-red wavebands emitted from each fixture were adjusted using a controller (Time-Keeper MAX, Touch-Plate Light Controls, Fort Wayne, IN, United States). The LED fixtures were hung 0.5 m above the pots in each grow space.

Plants were grown using sole-source lighting from the LED fixtures. As the vertical growing system was located in a greenhouse, it was covered with two layers of black cloth (WeedBlock, Jobes Co., Waco, TX, United States) that allowed air movement but blocked sunlight to ensure a sole-source LED lighting environment for plants. Average day/night air temperature, daily light integral, photoperiod, and relative humidity during the study were 21.7 ± 1.43/19.5 ± 0.81°C, 11.4 ± 0.17 $mol \cdot m^{-2} \cdot d^{-1}$, 24 h, and 62 ± 12.5%, respectively. Overhead irrigation with a fertilizer solution was provided as needed during the production to avoid any drought stress. Plants were fertigated with a water-soluble fertilizer containing 20N-4.4P-16.6K (20-10-20, Peters Professional, Summerville, SC, United States) at an electrical conductivity (EC) level of 1.7 ± 0.04 $dS \cdot m^{-1}$ and pH of 5.8 ± 0.04.

Treatments

Plants were grown under three light treatments with different spectral composition and similar light intensity (**Figure 2** and **Table 1**). Light treatments comprised of different percentages red: blue: far-red light in the total light including 90: 10: 0 ("High-R"), 50: 50: 0 ("High-B"), and 42: 42: 16 ("High-B+FR"). Black plastic sheets (0.61 m × 0.4 m, HomeDepot, Atlanta, GA, United States) were used to separate the grow spaces in each shelf and contain the dispersed light within each treatment. The total light intensity (400–750 nm) ranged between 129 and 138 $\mu mol \cdot m^{-2} \cdot s^{-1}$ in different treatments (**Table 1**).

Measurements

Air temperature (°C) was measured in each experimental unit (see section "Experimental Design and Data Analyses") using thermistors (ST-110, Apogee Instruments, Logan, UT, United States) connected to a data logger (CR1000, Campbell Sci. Logan, UT, United States). Total incident light intensity (I_{tot}, $\mu mol \cdot m^{-2} \cdot s^{-1}$) and spectral composition were measured at plant height using a spectroradiometer (SS-110, Apogee Instruments, Logan, UT, United States) with a hemispherical field-of-view (180°). From spectroradiometer measurements, broadband intensities of blue, red, and far-red wavelengths (I, $\mu mol \cdot m^{-2} \cdot s^{-1}$) were calculated by adding intensities of individual wavelengths between 400–499 nm, 600–699 nm, and 700–750 nm, respectively. Percentage of blue, red, and far-red photons in the total light was calculated as $100 \times \frac{I}{I_{tot}}$.

The proportion of P_{fr} to total phytochrome in plants was calculated as phytochrome photostationary state (PSS) using spectral composition and intensity of light received by plants (Sager et al., 1988; Stutte, 2009):

$$PSS = \frac{\sum_{400}^{750} (N_\lambda \sigma_{r\lambda})}{\left(\sum_{400}^{750} N_\lambda \sigma_{r\lambda} + \sum_{400}^{750} N_\lambda \sigma_{fr\lambda}\right)}$$

Where N_λ is light intensity ($mol \cdot s^{-1} \cdot m^{-2}$) at each wavelength ($\lambda$). The σ_{r_λ} and σ_{fr_λ} are phytochrome photochemical cross-sections for red and far-red absorbing states ($m^2 \cdot mol^{-1}$) at each λ based on measurements made by Sager et al. (1988) on isolated phytochrome. The λ levels used in the calculation were 400, 425, 450, 475, 500, 600, 625, 660, 675, 700, 725, 730, and 750 nm. The N_λ was measured by a spectroradiometer (SS-110, Apogee Instruments, Logan, UT, United States).

Leaf photosynthetic rate (LPR, $\mu mol \cdot m^{-2} \cdot s^{-1}$) was measured as described by Long et al. (1996) on the youngest fully expanded leaf during the last week before harvest using an open gas exchange system with CO_2, humidity, temperature, and light control (LI-6400XT, Li-Cor Biosciences, Lincoln, NE, United States). A clear-top leaf chamber was used to measure leaf gas exchange rate in different light treatments. This allowed us to measure leaf gas exchange under similar spectral composition and intensity of light incident on the plants in a given treatment. A reference CO_2 concentration of 400 $\mu mol \cdot mol^{-1}$, RH of 60%, and air temperature of 25°C were maintained during the measurement inside the leaf chamber. Measurements were recorded when gas exchange reached steady state, which occurred between 2 and 3 min after enclosing the leaf inside the chamber.

A representative plant from the center of each experimental unit was used to measure canopy area (CA, $cm^2 \cdot plant^{-1}$), leaf area (LA, $m^2 \cdot plant^{-1}$), shoot fresh weight (SFW, $g \cdot plant^{-1}$), and shoot dry weight (SDW, $g \cdot plant^{-1}$) at harvest. CA was measured as described by Adhikari and Nemali (2020) on the 31st day of the study using an imaging system (TopView phenotyping system, Aris B.V. Eindhoven, Netherlands). The distance between the camera and top of the plant was maintained similar during measurements. The software of the image station automatically segmented plants from the background, measured plant pixel area, and converted plant pixel area to CA by multiplying with a magnification factor (100) specific to the imaging system. Number of leaves on each plant (L_N) was counted prior to harvest. Plants were harvested at the base of the shoot and SFW was measured. Leaves were separated from plants and LA was measured by running separated leaves through the rollers of a leaf area meter (LI-3100C,

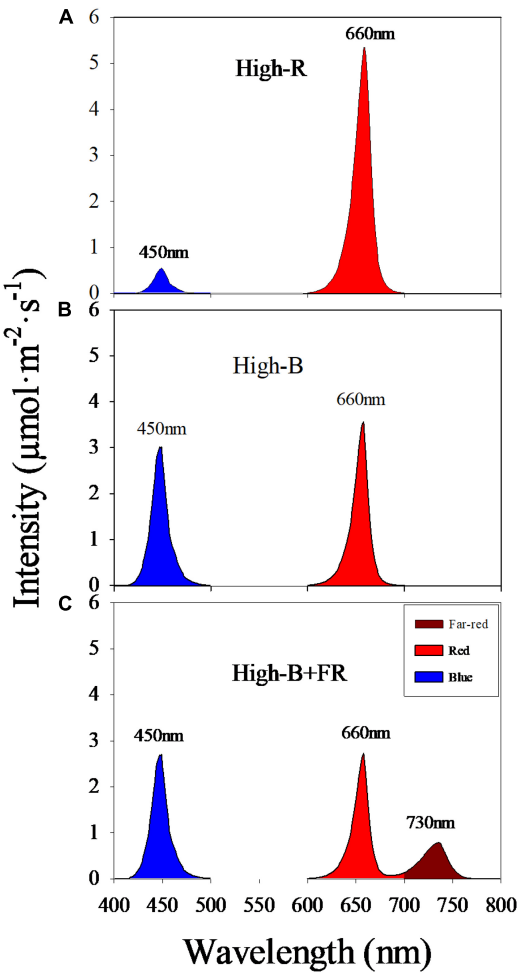

FIGURE 2 | Spectral composition in different light treatments: **(A)** red: blue: far-red = 90: 10: 0 ("High-R"), **(B)** red: blue: far-red = 50: 50: 0 ("High-B"), and **(C)** red: blue: far-red = 42: 42: 16 ("High-B+FR"). Peak wavelength numbers are shown for each broadband.

FIGURE 3 | Representative romaine lettuce plants from different light treatments. **(a)** High-R, **(b)** High-B, and **(c)** High-B+FR treatments. See **Table 1** for a description of treatments.

TABLE 2 | Effect of different light treatments (see **Table 1** for treatment description) on shoot fresh weight (SFW), shoot dry weight (SDW), leaf area (LA), canopy area (CA), leaf photosynthesis rate (LPR), leaf number (L_N), and average area of a single leaf (LA_s) in green romaine lettuce.

Measurement	Treatment		
	High-R	High-B	High-B+FR
SFW (g·plant^{-1})	151.7 (7.09) a	136.9 (7.09) b	138.2 (7.09) b
SDW (g·plant^{-1})	9.8 (0.52) a	8.1 (0.52) b	9.0 (0.52) a
LA (m^2·plant^{-1})	0.208 (0.0100) a	0.191 (0.0100) a	0.182 (0.0100) b
$\log_{10}$(CA)	1.96 (0.056) a	1.81 (0.056) b	1.94 (0.056) a
LPR (μmol·m^{-2}·s^{-1})	4.5 (0.25) a	3.6 (0.25) a[1]	3.5 (0.25) a[2]
L_N (plant^{-1})	19.7 (0.88) a	18.7 (0.88) a	11.3 (0.88) b
LA_s(m^2)	0.008 (0.0009) b	0.007 (0.0009) b	0.012 (0.0009) a

Least square means and standard errors (±) (in parenthesis) are shown. Least square means followed by different letters are statistically different at $P \leq 0.05$.
[1] $P_{\text{High-R vs High-B}} = 0.062$.
[2] $P_{\text{High-R vs High-B+FR}} = 0.052$.

Li-Cor Biosciences, Lincoln, NE, United States). Area of a single leaf (LA_s, m^2) was calculated as the ratio of total leaf area to leaf number. Separated leaves and remaining plant material were dried in a forced-air oven set to 70°C for 1 week to measure SDW.

Levels of chlorophylls (Chl), including chlorophyll-*a* (Chl_a) and chlorophyll-*b* (Chl_b), and beta-carotene (β-carotene) were measured as described by Nagata and Yamashita (1992). Plant samples collected from each experimental unit was used to analyze plant pigments at harvest stage. Two mature leaves from a plant were flash-frozen in liquid nitrogen and ground into fine power using a mortar and pestle. Approximately 0.2 g of the ground tissue was extracted with 1.8 ml acetone-hexene (2:3, v/v) solvent until the tissue turned white. Then the samples were centrifuged at 12,000 rpm for 3 min using a benchtop centrifuge (Sorvall Legend Micro 21 micro-centrifuge, Thermo Fisher Scientific, Waltham, MA, United States). The supernatant was then applied to a 1.4 ml quartz cuvette (Fisher Scientific, Waltham, MA, United States) to measure the absorption at 663, 645, 505, and 453 nm using a spectrophotometer (GENESYS 180 UV-Vis, Thermo Fisher Scientific, Waltham, MA, United States). The concentration of pigments was calculated on a fresh weight basis (mg·100 g^{-1}) as follows:

$$Chl_a = [0.999 \times A_{663}] - [0.0989 \times A_{645}]$$
$$Chl_b = [-0.328 \times A_{663}] + [1.77 \times A_{645}]$$
$$Chl = Chl_a + Chl_b$$
$$\beta\text{-carotene} = [0.216 \times A_{663}] - [1.22 \times A_{645}] - [0.304 \times A_{505}] + [0.452 \times A_{453}]$$

Anthocyanins were extracted from the same leaf samples used for Chl and β-carotene analyses. A total of 0.1 g of the ground tissue was extracted using 4 ml of pre-cooled (4°C) 1% HCL-methanol solution (v/v) in tubes covered with aluminum foil, and placed in a refrigerator (dark) maintained at 4°C for 20 min. The mixed solution in the tubes was shaken several times during extraction. Later it was centrifuged at 12,000 rpm for 3 min using a benchtop centrifuge (Sorvall Legend Micro 21 microcentrifuge). The supernatant was then applied to 1.5 ml cuvettes (Fisher Scientific, Waltham, MA, United States). Optical density (OD) were measured at 530 nm (OD_{530}) and 600 nm (OD_{600}) using the spectrophotometer (GENESYS 180 UV-Vis). The difference of OD between 530 and 600 nm was used to estimate a relative measure of anthocyanins concentration on a fresh weight basis (ΔOD·100 g^{-1}) as follows:

$$\text{Anthocyanins} = (OD_{530}\text{-}OD_{600})$$

Concentration of above pigments was also expressed on a leaf area basis (mg or ΔOD × m^{-2}) as follows:

$$\left[\text{Pigment}_{\text{area basis}}\right] = \frac{\left[\text{Pigment}_{\text{fresh weight basis}}\right]}{100} \times \frac{\text{FW}}{\text{LA}}$$

Experimental Design and Statistical Analyses

There were two experiments in the study. Both experiments were laid out using a randomized block design. Light treatments were randomly allotted in each replication. An experimental unit comprised of a set of three plants belonging to a light treatment, replicated three and four times in experiments 1 and 2, respectively. Photosynthesis measurements were made in experiment 1 while Anthocyanin and L_N were measured

TABLE 3 | Effect of different light treatments (see **Table 1** for treatment description) on the levels of anthocyanins, beta-carotene (β-carotene), chlorophylls (Chl) and ratio of chlorophyll-*a* to chlorophyll-*b* [$Chl_{(a/b)}$] in green romaine lettuce.

Measurement	Treatment					
	High-R	High-B	High-B+FR	High-R	High-B	High-B+FR
	Fresh weight basis (ΔOD or mg·100 g^{-1})			Leaf area basis (ΔOD or mg·m^{-2})		
Anthocyanins	0.012 (0.0037) a	0.013 (0.0037) a	0.009 (0.0037) a	0.069 (0.0181) a	0.072 (0.0181) a	0.051 (0.0181) a
β-carotene	5.98 (0.693) ab	6.99 (0.693) a	4.85 (0.693) b	46.1 (4.71) ab	50.7 (4.71) a	40.1 (4.71) b
Chl	63.6 (6.78) ab	70.7 (6.78) a	54.4 (6.78) b	453.1 (46.13) a	488.6 (46.13) a	406.8 (46.13) a[1]
$Chl_{(a/b)}$	2.44 (0.063) a	2.42 (0.063) a	2.26 (0.063) b	–	–	–

Data was expressed on both fresh weight and leaf area basis. Least square means and standard errors (±) (in parenthesis) are shown. Least square means followed by different letters are statistically different at $P \leq 0.05$.
[1] $P_{High-B\ vs\cdot High-B+FR} = 0.077$.

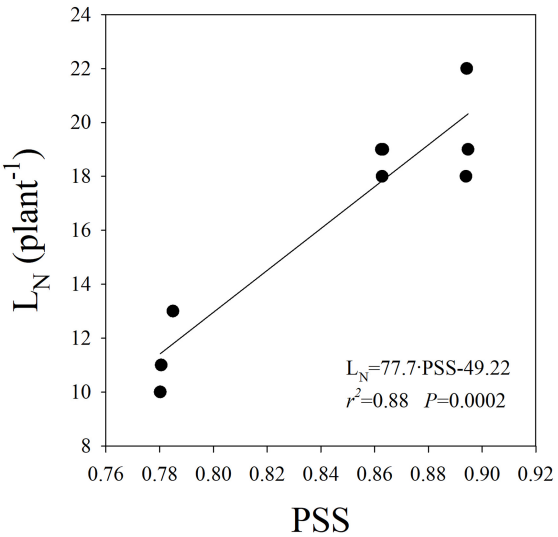

FIGURE 4 | Linear relationship between leaf number (L_N) and phytochrome photostationary state (PSS) in romaine lettuce. A linear regression was fitted to data from three light treatments and three replications per treatment.

in experiment 2. All the other measurements were made in both the experiments. Data were analyzed using a linear-mixed model (MIXED procedure) of statistical analysis software (SAS ver 9.4, Cary, NC, United States). Treatments were considered as fixed effects while both replications and experiments were considered as random effects in the model. Least-square means were separated using Tukey's honestly significant difference (HSD) procedure. Relationship between any two variables was tested using both the linear and quadratic regression procedures of SAS. A pre-determined alpha value of 5% (P-value ≤ 0.05) was considered statistically significant for all analyses.

RESULTS AND DISCUSSION

Light Spectral Composition

Average instantaneous light intensity received by the plants was not statistically different and within 10 μmol·m^{-2}·s^{-1} among different light treatments (**Table 1**). However, spectral composition significantly varied among different light treatments (**Figure 2**). The actual percentages of red, blue, and far-red light were slightly different from the intended treatment values (**Table 1**). Further, small standard errors of least square means indicate that total light intensity and light composition were highly consistent among different replications belonging to a light treatment. The PSS values were significantly different among the three light treatments, with highest in High-R, followed by High-B, and lowest in the High-B+FR. This indicates that phytochrome equilibrium differed among treatments and suggests that the relative amount of P_{fr} to total phytochrome was likely highest in the High-R, followed by High-B, and lowest in the High-B+FR treatment.

Morphological, Growth, and Physiological Differences

Plants appeared visually different in the High-B and High-B+FR treatments compared to High-R treatment (**Figure 3**). Plants and individual leaves were generally smaller in the High-B treatment compared to High-R and High-B+FR treatments. These differences may indicate lower LPR and/or light interception in High-B treatment. In the High-B+FR treatment, plants had both elongated and expanded leaves. In addition, plants were pale with fewer leaves in the High-B+FR compared to the other treatments. The canopy was open with relatively less intra-canopy shading in the High-B+FR treatment. These phenotypic characteristics may indicate that plants in the High-B+FR exhibited shade avoidance responses.

Shoot fresh weight was significantly higher in the High-R than High-B and High-B+FR treatments (**Table 2**). There were no significant differences in SFW between High-B and High-B+FR treatments. The SFW of plants increased by 9.8 and 8.8%, respectively, in the High-R compared to High-B and High-B+FR. Whereas SDW of plants was significantly lower in the High-B treatment compared to the other treatments and not different between High-R and High-B+FR treatments. The increase in SDW of plants in the High-B+FR and High-R compared to High-B was 13% and 18%, respectively. A decrease in both

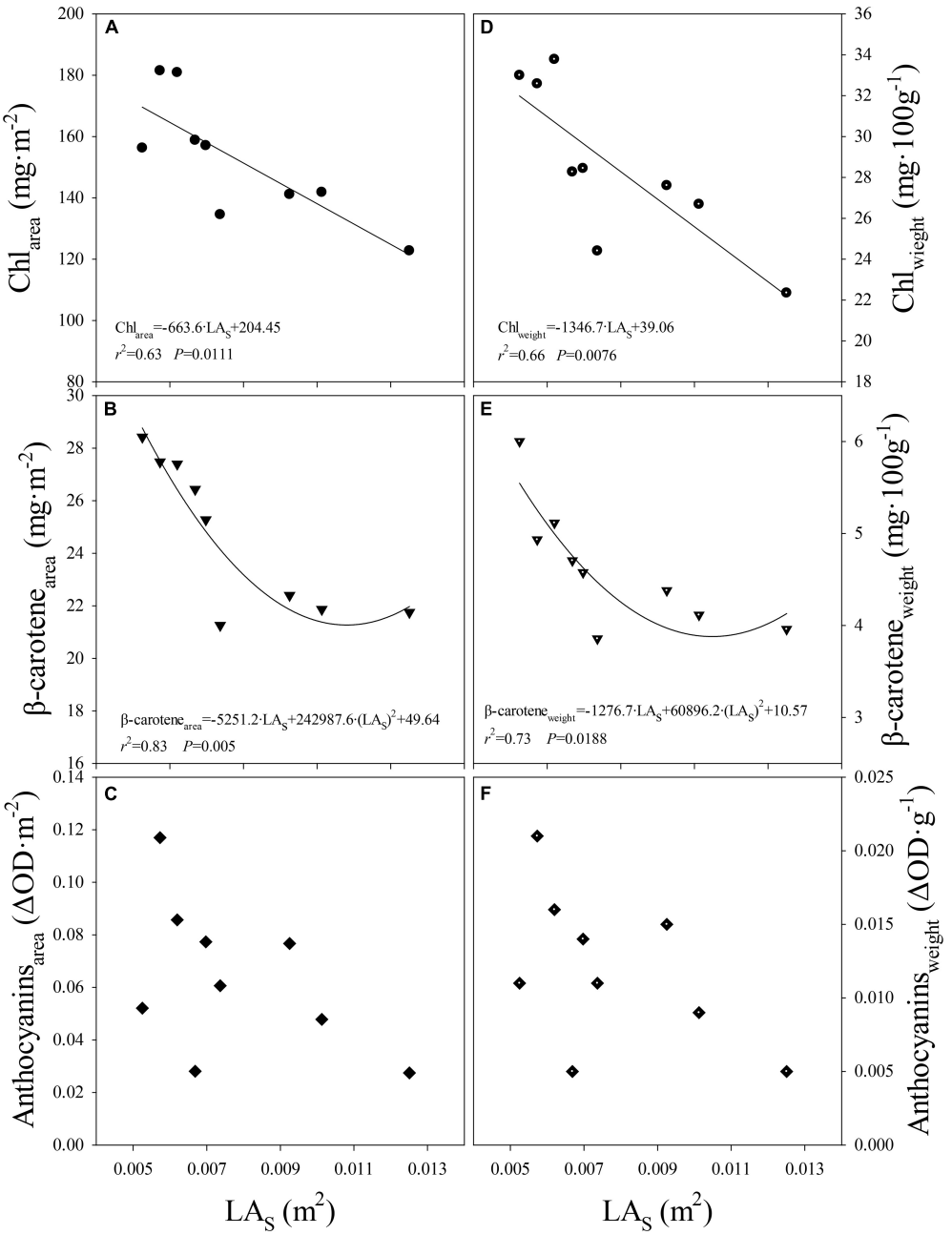

FIGURE 5 | Relationship between **(A)** level of chlorophylls per unit leaf area (Chl_{area}) and average area of a single leaf (LA_s), **(B)** level of beta-carotene per unit leaf area (β-$carotene_{area}$) and LA_s, **(C)** level of anthocyanins per unit leaf area ($Anthocyanins_{area}$) and LA_s, **(D)** levels of chlorophylls per unit fresh weight (Chl_{weight}) and LA_s, **(E)** level of beta-carotene per unit fresh weight (β-$carotene_{weight}$) and LA_s, **(F)** level of anthocyanins per unit fresh weight ($Anthocyanins_{weight}$) and LA_s in romaine lettuce. Data from three light treatments and three replications per treatment are shown. A linear regression was fitted to data in panels **(A,D)** and a quadratic regression was fitted to data in panels **(B,E)**.

SFW and SDW of plants in the High-B compared to High-R indicates slower growth rate in the High-B treatment. Further, the results indicate that reduced growth rate in High-B was reversed by the addition of far-red light. No differences in SFW but an increase in SDW in the High-B+FR than High-B suggest increased shoot water content in High-B than High-B+FR. Similarly, decrease in SFW in High-B+FR but no differences in SDW between High-B+FR and High-R suggest a decrease in shoot water content of plants in the High-B+FR compared to High-R.

Leaf area of plants was not different between the High-R and High-B and significantly lower in the High-B+FR treatment (**Table 2**). These results indicate a lack of association between LA and SDW. Although LPR was not statistically different among

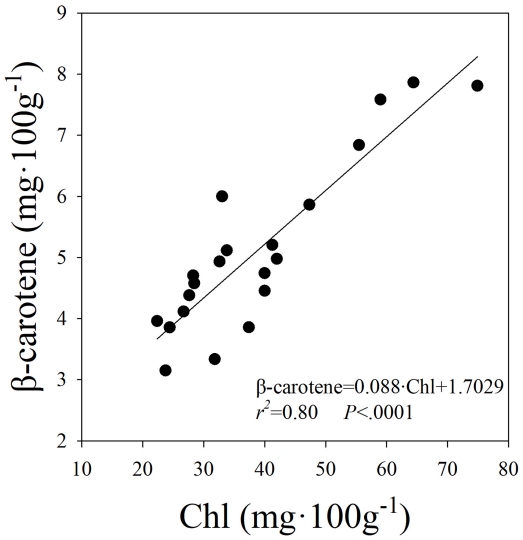

FIGURE 6 | Linear relationship between the levels of beta-carotene (β-carotene) and chlorophylls (Chl) in romaine lettuce. A linear regression was fitted to data from three treatments and all seven replications from two experiments.

treatments, it was numerically higher in the High-R compared to High-B (P = 0.062) and High-B+FR (P = 0.052) (**Table 2**). There were no statistical differences in LPR between High-B and High-B+FR treatments. Further, this indicates that the addition of far-red light to high percentage of blue light did not "enhance" LPR of lettuce in the long-term. In addition, the results indicate that LPR is highly sensitive to high-energy blue light as lower LPR was observed in both treatments with high percentage of blue light (i.e., High-B and High-B+FR). However, CA responses were similar to those observed for SDW. Log transformed CA was not significantly different between the High-R and High-B+FR treatments but significantly lower in the High-B treatment, similar to that of SDW. A lower CA in the High-B treatment may suggest that plants intercepted less incident light and an increase in CA in the High-B+FR compared to High-B indicate that plants intercepted more incident light.

Vegetative growth is related to both light interception by the canopy and light use in photosynthesis (He et al., 2019; Liao et al., 2019). Because LA, CA, and LPR were highest, maximum vegetative growth was observed in the High-R treatment (**Table 2**). Other studies also reported that high percentage of red light can efficiently drive photosynthesis, promote leaf expansion, stem elongation, and dry mass gain in plants (Gómez and Izzo, 2018; Kusuma et al., 2020). Shoot growth was lowest in the High-B treatment likely due to significant decrease in CA and numerical decrease in LPR, compared to the High-R treatment. The CA measurement in our study is proportional to the non-shaded leaf area. In other studies, CA was related to light interception (Zhen and Bugbee, 2020) and biomass production (Zhu et al., 2010; Jones et al., 2015) in plants. Thus, lower CA likely contributed in part to decreased growth in the High-B than High-R. Blue light was found to be photosynthetically less efficient than red light (McCree, 1972; Cope et al., 2013; Kusuma et al., 2020). Therefore, lower LPR also likely contributed to decreased growth in the High-B than High-R. Although LPR decreased in High-B+FR, an increase in CA was observed in this treatment suggesting increased light interception (**Table 2**). The absorbed far-red photons (700–750 nm) can be equally efficient for photosynthesis when combined with photosynthetically active radiation (400–700 nm) (Zhen and Bugbee, 2020). Collectively these can explain increased dry weight in the High-B+FR compared to High-B.

The percentage of blue light in the High-B (47.2%) was much higher than the recommended level of 10–15% of total light (Hoenecke et al., 1992; Son and Oh, 2013; Ouzounis et al., 2014; Runkle, 2016). High-energy blue light was reported to increase oxidative stress (Ohnishi et al., 2005), resulting in damage to photosynthetic machinery. Anthocyanins are synthesized in the cytosol (Tanaka et al., 2008), absorb blue and green wave bands (Pietrini and Massaeei, 1998; Kusuma et al., 2020), and

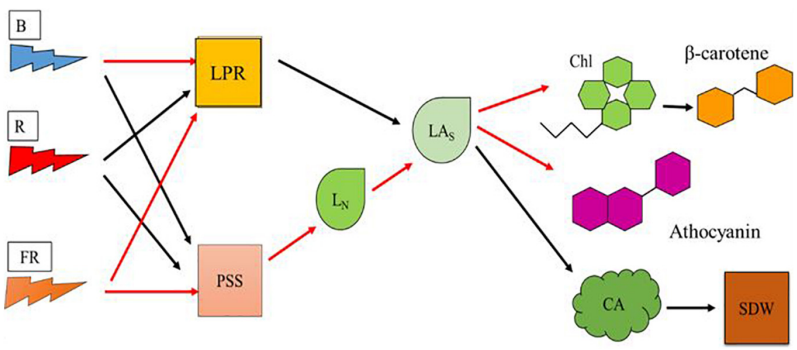

FIGURE 7 | A model showing the effects of blue, red, and far-red radiation on physiological responses at cellular and leaf scales that affect vegetative growth and pigment synthesis in romaine lettuce. Model parameters include blue light (B), red light (R), far-red light (FR), leaf photosynthesis rate (LPR), phytochrome photostationary state (PSS), average leaf number per plant (L_N), average area of individual leaf (LA_s), chlorophylls level (Chl), beta-carotene level (β-carotene), anthocyanins level, canopy area (CA), and shoot dry weight (SDW). Black and red arrows indicate positive and negative relationships, respectively, between two parameters.

screen photosynthetic machinery from damage due to high-energy radiation (Close and Beadle, 2003; Hughes et al., 2012). Anthocyanins function by attenuating the light that reaches chloroplasts (Gould et al., 1995; Mendez et al., 1999; Smillie and Hetherington, 1999; Close, 2001; Zhang et al., 2010). We observed no differences in anthocyanins between High-B and High-R and decrease between High-R and High-B+FR. It is possible that the decreases in LPR in High-B and High-B+FR treatments are likely due to a large fraction of photosynthetically less efficient blue radiation (McCree, 1972) in these treatments. Enhancement in LPR was reported with the addition of far-red light to broadband white light due to simultaneous activation of both photosystem II and I reaction centers (Zhen and van Iersel, 2017). There were no differences in LPR between High-B+FR and High-B, indicating no enhancement of photosynthesis due to addition of far-red light to high-energy blue radiation in our study. Chl_a, an integral component of the reaction center of photosystem (Horton et al., 2002; Fromme et al., 2006), was significantly lower [based on $Chl_{(a/b)}$ ratio, **Table 3**] in the High-B+FR than High-B. In addition, β-carotene levels were significantly lower in in the High-B+FR than High-B (**Table 3**). β-carotene is mostly present in the reaction center of photosystem (Härtel and Grimm, 1998; Ruiz-Sola and Rodríguez-Concepción, 2012) and aid in absorbing light in the range of 450–570 nm where Chl absorption declines (Ruiz-Sola and Rodríguez-Concepción, 2012). Collectively, these may have partly contributed to lack of photosynthesis enhancement in the High-B+FR treatment.

Leaf Number and Individual Leaf Area

A significant reduction in L_N was observed in the High-B+FR compared to High-B and High-R treatments (**Table 2**). The result indicates a decrease in leaf primordia in plants with the addition of far-red light. There was a linear and positive relationship between L_N and PSS (**Figure 4**), indicating that L_N increased with increasing P_{fr} to total phytochrome in plants. As P_{fr} increases with increasing red light incident on plants, the results indicate that high proportion of red light increases L_N. Previously, decrease in L_N due to far-red addition in lettuce was reported (Meng and Runkle, 2019). There was no association between LA or CA and L_N (data not shown), indicating leaf development happened independent of leaf primordia number or initiation in plants. The linear and positive relationship between L_N and PSS (**Figure 4**) indicates that lower L_N in the High-B+FR is likely associated with lower phytochrome equilibrium or increased proportion of P_r to total phytochrome in the High-B+FR treatment due to increased far-red light. Plants use increased proportion of far-red light in the environment as an indicator of proximity of neighbors and respond by exhibiting suit of traits (e.g., elongation) that reduce future canopy shading (Ballaré et al., 1990; Gommers et al., 2012; Yang and Li, 2017). The "proximity response" can happen even due to a slight decrease in red to far-red ratio and does not require a reduction in the intensity of total or red light (Martinez-Garcia et al., 2014). Increased proportion of far-red light (which lowers PSS value) resulted in reduced leaf primordia (Carabelli et al., 2007; Yang and Li, 2017) and increased elongation growth (Lorrain et al., 2008; Martinez-Garcia et al., 2014; Yang and Li, 2017). Thus, reduced L_N in the High-B+FR is most likely due to increased proportion of far-red light in this treatment.

A significantly higher LA_s was observed in the High-B+FR compared to High-R and High-B treatments (**Table 2**). This means, leaf lamina of individual leaves expanded more in the High-B+FR treatment compared to other treatments. The plants in the High-B+FR likely exhibited proximity responses but were not "truly" exposed to shade during growth. Due to decreased L_N and reduced leaf layers (**Figure 3**), there likely was little intra-canopy shading and increased light interception in the High-B+FR. As plants did not experience shade or low light intensity after initiating shade responses, products of photosynthesis were available continuously to a small number of leaves, thereby resulting in expansion growth of individual leaves. This is the likely reason for increased LA_s in the High-B+FR than High-B. The LPR was not different between High-B and High-B+FR, but products of photosynthesis were distributed to relatively more number of leaves in the High-B, resulting in smaller LA_s. Thus, the increased CA or LA_s in the High-B+FR than High-B is likely a consequence of reduced L_N and continued photosynthesis, albeit at a lower rate. Meng and Runkle (2019) and Zhen and Bugbee (2020) indicated that increased vegetative growth with far-red addition was related to increased canopy photon capture. Our results agree with the above two studies. In addition, our results point to the additional fact that increased SDW from increased CA in the High-B+FR is an indirect consequence of a negative effect of far-red light on L_N in lettuce.

Plant Pigments

On a fresh weight basis, the levels of β-carotene and Chl were highest in the High-B, intermediate in the High-R, and lowest in the High-B+FR treatment (**Table 3**). Anthocyanins levels were not statistically different but trended similar to other pigments. The levels of β-carotene and Chl in the High-B was higher by 31 and 23%, respectively, than High-B+FR treatment. Pigment differences expressed on a leaf area basis were generally similar to those expressed on fresh weight basis. The level of β-carotene was highest in the High-B, intermediate in the High-R, and lowest in the High-B+FR (**Table 3**). The levels of anthocyanins and Chl were not statistically different when expressed on a leaf area basis. The levels trended lower in High B+FR. These results indicate that high percentage of blue light can increase pigments levels in romaine lettuce. Pigments were consistently lower in the High-B+FR than High-B in spite of exposure to relatively high percentage of blue light (42%) in the High-B+FR treatment. This indicates that far-red light has more influence on plant responses than blue light in the High-B+FR treatment. The $Chl_{(a/b)}$ ratio was significantly lower in the High-B+FR compared to other treatments, while no differences were observed between the High-R and High-B treatments (**Table 3**). This suggests that lower level of Chl in the High-B+FR treatment is likely due to relatively larger decrease in the concentration of Chl_a than Chl_b.

When data from all light treatments were pooled, negative linear and quadratic relationships were observed between the level of Chl or β-carotene expressed on leaf area or fresh weight basis and LA_s, respectively (**Figures 5A,B,D,E**). Although

the response was not significant, similar trend was observed between anthocyanins levels per unit leaf area or fresh weight and LA_s (**Figures 5C,F**). This indicates that, regardless of light composition, pigment levels per unit leaf area decreased as LA_s increased. Further, this indicates that the differences in pigment levels can be explained mostly by changes in the LA_s. In other words, levels of pigments were regulated likely at the individual leaf scale. As LA_s became smaller (e.g., High-B treatment), the pigment levels increased and as the LA_s became larger (e.g., High-B+FR treatment), a decrease in pigment levels was observed. This is likely because resources for leaf expansion and pigment synthesis share a common source, i.e., glucose from photosynthesis. For example, precursors of anthocyanin (e.g., malonyl CoA; Tanaka et al., 2008), and Chl, and β-carotene (e.g., pyruvate and glyceraldehyde 3-phosphate; Meier et al., 2011; Ruiz-Sola and Rodríguez-Concepción, 2012) are formed in glycolysis that uses glucose from photosynthesis as the substrate (Horton et al., 2002). However, more work is needed to further understand the involved biochemical mechanisms.

A linear and positive relationship was observed between the level of Chl and β-carotene expressed on fresh weight basis (**Figure 6**). These results suggest that the increase in the level of Chl was associated with an increase in the level of β-carotene in plants. Both Chl and β-carotene synthesis were shown to be upregulated by blue light (Fu et al., 2012; Tuan et al., 2017) and dependence of β-carotene synthesis on biosynthesis of Chl was previously reported (Bohne and Linden, 2002; Fu et al., 2012). Further, coordinated transcription of phytoene synthase and many isoprenoid biosynthesis genes was shown to be critical for regulating biosynthesis of carotenoids and Chl (Meier et al., 2011) and involvement of a STAY-GREEN protein for regulation of lycopene and β-carotene biosynthesis during ripening processes was reported in tomato (Luo et al., 2013). The linear relationship between β-carotene and Chl in our study suggests that the proportionate change in both pigments was not different among the light treatments in our study. Similar to our results, Härtel and Grimm (1998) indicated that β-carotene to Chl ratio remained mostly unchanged in tobacco under low and high light environments. These results indicate that factors that increase Chl (e.g., tissue nitrogen concentration) can likely increase β-carotene levels in leaves.

CONCLUSION

Our objectives were to understand the effects of high-energy blue and low-energy far-red on vegetative growth and pigment synthesis in plants. In our study, effects of light composition on vegetative growth and pigment synthesis appear to be mediated by L_N and LA_s (**Figure 7**). Romaine lettuce plants provided with high proportion of blue light showed decreased growth and increased levels of Chl and β-carotene. Plants provided with high proportion of blue radiation showed decreased LPR, likely due to lower photosynthetic efficiency of blue light. Addition of far-red light to high proportion of blue light resulted in relatively more photomorphogenic effects on plants. We observed morphological changes including lower L_N and increase in the LA_s in plants exposed to far-red light. Addition of low-energy far-red light to high-energy blue light did not enhance LPR. When L_N increases without a change in LPR as in the High-B compared with High-B+FR, the products of photosynthesis are distributed to larger number of leaves thereby resulting in smaller LA_s. Whereas when L_N decreases without change in LPR as in High-B+FR compared to High-B, the products of photosynthesis will be allocated to a fewer number of leaves thereby resulting in larger LA_s. The High-R treatment showed positive effects on both LPR and L_N, resulting in LA_s intermediate to that of the High-B and High-B+FR treatments. Larger LA_s in the High-B+FR likely resulted in larger CA (and likely increased light interception) and SDW. Whereas, intermediate LA_s coupled with increased LPR in High-R, likely resulted in increased SDW. In contrast, smaller LA_s and decreased LPR likely resulted in smaller CA and SDW in the High-B. Pigment levels increased with decreasing LA_s and decreased with increasing LA_s. Because of this, the levels of Chl and β-carotene (and anthocyanins likely) were highest in the High-B, followed by the High-R, and lowest in the High-B+FR treatment. The results from this study indicate that high-energy blue and low-energy far-red light affect the number and expansion of individual leaves differently, thereby influencing both vegetative growth and pigment synthesis in lettuce. We hope that the information generated in this study can aid in increasing our understanding of plant responses to high-energy blue and low-energy far-red radiation and optimizing lighting environment in vertical farms.

DATA AVAILABILITY STATEMENT

The raw data supporting the conclusions of this article will be made available by the authors, without undue reservation.

AUTHOR CONTRIBUTIONS

YK performed the experimental design, experimentation, data collection, data analyses, and manuscript preparation. KN contributed to project leadership, funding, experimental design, data analyses, and manuscript preparation. Both authors contributed to the article and approved the submitted version.

REFERENCES

Adhikari, R., and Nemali, K. (2020). A novel method for estimating nitrogen stress in plants using smartphones. *Horticulturae* 6:74. doi: 10.3390/horticulturae6040074

Ahmad, M., Jarillo, J. A., Smirnova, O., and Cashmore, A. R. (1998). Cryptochrome blue-light photoreceptors of *Arabidopsis* implicated in phototropism. *Nature* 392, 720–723. doi: 10.1038/33701

Amoozgar, A., Mohammadi, A., and Sabzalian, M. R. (2017). Impact of light-emitting diode irradiation on photosynthesis, phytochemical composition and

mineral element content of lettuce cv. *Grizzly*. *Photosynthetica* 55, 85–95. doi: 10.1007/s11099-016-0216-8

Avgoustaki, D. D., and Xydis, G. (2020). Indoor vertical farming in the urban nexus context: business growth and resource savings. *Sustainability* 12:1965. doi: 10.3390/su12051965

Ballaré, C. L., Scopel, A. L., and Sánchez, R. A. (1990). Far-red radiation reflected from adjacent leaves: an early signal of competition in plant canopies. *Science* 247, 329–332. doi: 10.1126/science.247.4940.329

Bohne, F., and Linden, H. (2002). Regulation of carotenoid biosynthesis genes in response to light in *Chlamydomonas reinhardtii*. *Biochim. Biophys. Acta (BBA) Gene Struct. Expression* 1579, 26–34. doi: 10.1016/S0167-4781(02)00500-6

Camejo, D., Frutos, A., Mestre, T., Piñero, M. D. C., Rivero, R. M., and Martínez, V. (2020). Artificial light impacts the physical and nutritional quality of lettuce plants. *Hort Envi Biotech.* 61, 69–82. doi: 10.1007/s13580-019-00191-z

Carabelli, M., Possenti, M., Sessa, G., Ciolfi, A., Sassi, M., Morelli, G., et al. (2007). Canopy shade causes a rapid and transient arrest in leaf development through auxin-induced cytokinin oxidase activity. *Genes Dev.* 21, 1863–1868. doi: 10.1101/gad.432607

Close, D. C. (2001). *Cold-Induced Photoinhibition, Pigment Chemistry, Growth and Nutrition of EUCALYPTUSNITENS and E. Globulus Seedlings During Establishment*. Ph.D. Thesis. Hobart AUS: University of Tasmania.

Close, D. C., and Beadle, C. L. (2003). The ecophysiology of foliar anthocyanin. *Bot. Rev.* 69, 149–161. doi: 10.1663/0006-8101(2003)069[0149:teofa]2.0.co;2

Cope, K. R., Snowden, M. C., and Bugbee, B. (2013). Photobiological interaction of blue light and photosynthetic photon flux: effects of monochromatic and broad-spectrum light sources. *Photochem. Photobiol.* 90, 574–584. doi: 10.1111/php.12233

Craver, J. K., Nemali, K., and Lopez, R. G. (2020). Acclimation of growth and photosynthesis in petunia seedlings exposed to high-intensity blue radiation. *J. Amer. Soc. Hort. Sci.* 145, 152–161. doi: 10.21273/JASHS04799-19

Despommier, D. (2010). *The Vertical Farm: Feeding the World in the 21st Century*. New York, NY: Thomas Dunne Books.

Fan, X., Zang, J., Xu, Z., Guo, S., Jiao, X., Liu, X., et al. (2013). Effects of different light quality on growth, chlorophyll concentration and chlorophyll biosynthesis precursors of non-heading Chinese cabbage (*Brassica campestris* L.). *Acta Physiol. Plant* 35, 2721–2726. doi: 10.1007/s11738-013-1304-z

Frazier, I. (2017). The Vertical Farm." The New Yorker, 9 January. Available online at: https://www.newyorker.com/magazine/2017/01/09/the-vertical-farm (accessed December 2, 2020).

Fromme, P., Yu, H. Q., DeRuyter, Y. S., Jolley, C., Chauhan, D. K., Melkozernov, A., et al. (2006). Structure of photosystems I and II. *C.R. Chimie.* 9, 188–200. doi: 10.1016/j.crci.2005.06.039

Fu, W., Guðmundsson, Ó, Paglia, G., Herjólfsson, G., Andrésson, ÓS., Palsson, B. Ø, et al. (2012). Enhancement of carotenoid biosynthesis in the green microalga *Dunaliella salina* with light-emitting diodes and adaptive laboratory evolution. *Appl. Microbiol. Biotechnol.* 97, 2395–2403. doi: 10.1007/s00253-012-4502-5

Gómez, C., and Izzo, L. G. (2018). Increasing efficiency of crop production with LEDs. *AIMS Agric. Food* 3, 135–153. doi: 10.3934/agrfood.2018.2.135

Gommers, C. M. M., Visser, E. J. W., Onge, K. R. S., Voesenek, L. A. C. J., and Pierik, R. (2012). Shade tolerance: when growing tall is not an option. *Trends in Plant Science.* 18, 1360–1385. doi: 10.1016/j.tplants.2012.09.008

Gould, K., Kuhn, D., Lee, D., and Oberbauer, S. (1995). Why leaves are sometimes red. *Nature.* 378, 241–242. doi: 10.1038/378241b0

Härtel, H., and Grimm, B. (1998). Consequences of chlorophyll deficiency for leaf carotenoid composition in tobacco synthesizing glutamate 1-semialdehyde aminotransferase antisense RNA: dependency on developmental age and growth light. *J. Exp. Bot.* 49, 535–546. doi: 10.1093/jxb/49.320.535

He, J., Qin, L., and Chow, W. S. (2019). Impacts of LED spectral quality on leafy vegetables: productivity closely linked to photosynthetic performance or associated with leaf traits? *Int. J. Agric. Biol. Eng.* 12, 16–25. doi: 10.25165/j.ijabe.20191206.5178

Hernandez, R., and Kubota, C. (2016). Physiological responses of cucumber seedlings under different blue and red photon flux ratios using LEDs. *Environ. Exp. Bot.* 121, 66–74. doi: 10.1016/j.envexpbot.2015.04.001

Hoenecke, M. E., Bula, R. J., and Tibbitts, T. W. (1992). Importance of 'Blue' photon levels for lettuce seedlings grown under red-light-emitting diodes. *HortScience* 27, 427–430. doi: 10.21273/HORTSCI.27.5.427

Horton, P., O'Dea, M. A., Davison, P., Lee, P. J., Walters, R. G., Wentworth, M., et al. (2002). "Dynamic behavior of the light harvesting antenna of photosystem II," in *Proceedings of the 12th International Congress on Photosynthesis*, (Brisbane).

Hughes, N. M., Burkey, K. O., Cavender-Bares, J., and Smith, W. K. (2012). Xanthophyll cycle pigment and antioxidant profiles of winter-red (anthocyanic) and winter-green (acyanic) angiosperm evergreen species. *J. Exp. Bot.* 63, 1895–1905. doi: 10.1093/jxb/err362

Institute of Medicine US Panel on Micronutrients (2001). *Dietary Reference Intakes for Vitamin A, Vitamin K, Arsenic, Boron, Chromium, Copper, Iodine, Iron, Manganese, Molybdenum, Nickel, Silicon, Vanadium, and Zinc. Washington (DC): National Academies Press (US). 4. Vitamin A*. Washington DC: National Academies Press.

Jennings, A., Welch, A. A., Fairweather-Tait, S. J., Kay, C., Minihane, A.-M., Chowienczyk, P., et al. (2012). Higher anthocyanin intake is associated with lower arterial stiffness and central blood pressure in women. *Am. J. Clin. Nutr.* 96, 781–788. doi: 10.3945/ajcn.112.042036

Johkan, M., Shoji, K., Goto, F., Hashida, S., and Yoshihara, T. (2010). Blue light-emitting diode light irradiation of seedlings improves seedling quality and growth after transplanting in red leaf lettuce. *HortScience* 45, 1809–1814. doi: 10.21273/HORTSCI.45.12.1809

Jones, M. B., Finnan, J., and Hodkinson, T. (2015). Morphological and physiological traits for higher biomass production in perennial rhizomatous grasses grown on marginal land. *GCB Bioenergy* 7, 375–385. doi: 10.1111/gcbb.12203

Kang, W. H., Kim, J. W., and Son, J. E. (2019). Growth and photomorphogenesis of cucumber plants under artificial solar and high pressure sodium lamp with additional far-red light. *Protect. Horticul. Plant Factory* 28, 86–93. doi: 10.12791/KSBEC.2019.28.1.86

Kang, W. H., Park, J. S., Park, K. S., and Son, J. E. (2016). Leaf photosynthetic rate, growth, and morphology of lettuce under different fractions of red, blue, and green light from light-emitting diodes (LEDs). *Hort. Environ. Biotech.* 57, 573–579. doi: 10.1007/s13580-016-0093-x

Karlsen, A., Retterstøl, L., Laake, P., Paur, I., Kjølsrud-Bøhn, S., Sandvik, L., et al. (2007). Anthocyanins inhibit nuclear factor- κ B activation in monocytes and reduce plasma concentrations of pro-inflammatory mediators in healthy adults. *J. Nutr.* 137, 1951–1954. doi: 10.1093/jn/137.8.1951

Kong, Y., Nemali, A., Mitchell, C., and Nemali, K. (2019). Spectral quality of light can affect energy consumption and energy-use efficiency of electrical lighting in indoor lettuce farming. *HortScience* 54, 865–872. doi: 10.21273/HORTSCI13834-18

Kusuma, P., Pattison, P. M., and Bugbee, B. (2020). From physics to fixtures to food: current and potential LED efficacy. *Horticul. Res.* 7:56. doi: 10.1038/s41438-020-0283-7

Lako, J., Trenerry, V. C., Wahlqvist, M., Wattanapenpaiboon, N., Sotheeswaran, S., and Premier, R. (2007). Phytochemical flavonols, carotenoids and the antioxidant properties of a wide selection of Fijian fruit, vegetables and other readily available foods. *Food Chem.* 101, 1727–1741. doi: 10.1016/j.foodchem.2006.01.031

Li, Q., and Kubota, C. (2009). Effects of supplemental light quality on growth and phytochemicals of baby leaf lettuce. *Environ. Exp. Bot.* 67, 59–64. doi: 10.1016/j.envexpbot.2009.06.011

Liao, Z., Scheepens, J. F., Li, W., Wang, R., and Zheng, Y. (2019). Biomass reallocation and increased plasticity might contribute to successful invasion of *Chromolaena odorata*. *Flora* 256, 79–84. doi: 10.1016/j.flora.2019.05.004

Long, S. P., Farage, P. K., and Garcia, R. L. (1996). Measurement of leaf and canopy photosynthetic CO2 exchange in the field. *J. Exp. Bot.* 47, 1629–1642. doi: 10.1093/jxb/47.11.1629

Lorrain, S., Allen, T., Duek, P. D., Whitelam, G. C., and Fankhauser, C. (2008). Phytochrome-mediated inhibition of shade avoidance involves degradation of growth-promoting bHLH transcription factors. *Plant J.* 53, 312–323. doi: 10.1111/j.1365-313X.2007.03341.x

Luo, Z., Zhang, J., Li, J., Yang, C., Wang, T., Ouyang, B., et al. (2013). A STAY-GREEN protein SlSGR1 regulates lycopene and β-carotene accumulation by interacting directly with SlPSY1 during ripening processes in tomato. *New Phytol.* 198, 442–452. doi: 10.1111/nph.12175

Martin, C., and Li, J. (2017). Medicine is not health care, food is health care: plant metabolic engineering, diet and human health. *New Phytol.* 216, 699–719. doi: 10.1111/nph.14730

Martinez-Garcia, J. F., Gallemi, M., Molina-Contreras, M. J., Llorente, B., Bevilaqua, M. R. R., and Quail, P. H. (2014). The shade avoidance syndrome in *Arabidopsis*: the antagonistic role of phytochrome A and B differentiates vegetation proximity and canopy shade. *PLoS One* 9:e109275. doi: 10.1371/journal.pone.0109275

McCree, K. J. (1972). The action spectrum, absorptance and quantum yield of photosynthesis in crop plants. *Agric. Meteorol.* 9, 191–216. doi: 10.1016/0002-1571(71)90022-7

Meier, S., Tzfadia, O., Vallabhaneni, R., Gehring, C., and Wurtzel, E. T. (2011). A transcriptional analysis of carotenoid, chlorophyll and plastidial isoprenoid biosynthesis genes during development and osmotic stress responses in *Arabidopsis* thaliana. *BMC Syst. Biol.* 5:77. doi: 10.1186/1752-0509-5-77

Mendez, M., Jones, D. G., and Manetas, Y. (1999). Enhanced UV-B radiation under field conditions increases anthocyanin and reduces the risk of photoinhibition but does not affect growth in the carnivorous plant *Pinguicula vulgaris*. *New Phytol.* 144, 275–282. doi: 10.1046/j.1469-8137.1999.00511.x

Meng, Q., and Runkle, E. S. (2019). Far-red radiation interacts with relative and absolute blue and red photon flux densities to regulate growth, morphology, and pigmentation of lettuce and basil seedlings. *Sci. Horticul.* 255, 269–280. doi: 10.1016/j.scienta.2019.05.030

Miller, A., Langenhoven, P., and Nemali, K. (2020). *Performance of Lettuce Varieties in Greenhouse Hydroponic Production*. Available online at: https://www.extension.purdue.edu/extmedia/HO/HO-310-W.pdf (accessed October 18, 2020).

Nagata, M., and Yamashita, I. (1992). Simple method for simultaneous determination of chlorophyll and carotenoids in tomato fruit. *Nippon Shokuhin Kogyo Gakkaishi* 39, 925–928. doi: 10.3136/nskkk1962.39.925

Naznin, M. T., Lefsrud, M., Gravel, V., and Azad, M. O. K. (2019). Blue light added with red LEDs enhance growth characteristics, pigments content, and antioxidant capacity in lettuce, spinach, kale, basil, and sweet pepper in a controlled environment. *Plants* 8:93. doi: 10.3390/plants8040093

Ohashi-Kaneko, K., Takase, M., Kon, N., Fujiwara, K., and Kurata, K. (2007). Effect of light quality on growth and vegetable quality in leaf lettuce, spinach and komatsuna. *Environ. Conreol. Biol.* 45, 189–198. doi: 10.2525/ecb.45.189

Ohnishi, N., Allakhverdiev, S. I., Takahashi, S., Higashi, S., Watanabe, M., Nishiyam, Y., et al. (2005). Two-step mechanism of photodamage to photosystem II: step 1 occurs at the oxygen-evolving complex and step 2 occurs at the photochemical reaction center. *Biochemistry* 44, 8494–8499. doi: 10.1021/bi047518q

Ouzounis, T., Frette, X., Rosenqvist, E., and Ottosen, C.-O. (2014). Spectral effects of supplementary lighting on the secondary metabolites in roses, chrysanthemums, and campanulas. *J. Plant Physiol.* 171, 1491–1499. doi: 10.1016/j.jplph.2014.06.012

Ouzounis, T., Razi Parjikolaei, B., Fretté, X., Rosenqvist, E., and Ottosen, C.-O. (2015). Predawn and high intensity application of supplemental blue light decreases the quantum yield of PSII and enhances the amount of phenolic acids, flavonoids, and pigments in *Lactuca sativa*. *Front. Plant Sci.* 6:19. doi: 10.3389/fpls.2015.00019

Park, Y., and Runkle, E. S. (2017). Far-red radiation promotes growth of seedlings by increasing leaf expansion and whole-plant net assimilation. *Environ. Exp. Bot.* 136, 41–49. doi: 10.1016/j.envexpbot.2016.12.013

Pietrini, F., and Massaeei, A. (1998). Leaf anthocyanin content changes in *Zea mays* L. grown at low temperature: significance for the relationship between quantum yield of PSII and the apparent quantum yield of CO2 assimilation. *Photosyn. Res.* 58, 213–219. doi: 10.1023/A:1006152610137

Qiu, J., Bayabil, H. K., and Li, Y. (2020). *Indoor Vertical Farming Systems for Food Security and Resource Sustainability. IFAS Extension*. Gainesville FL: University of Florida, doi: 10.32473/edis-fr429-2020

Ruiz-Sola, M. Á, and Rodríguez-Concepción, M. (2012). carotenoid biosynthesis in *Arabidopsis*: a colorful pathway. *Arabidopsis Book* 10:e0158. doi: 10.1199/tab.0158

Runkle, E. S. (2016). *Red Light and Plant Growth.* Michigan State University Extension Floriculture Team. Available online at: http://flor.hrt.msu.edu/assets/Uploads/Redlight3.pdf (accessed December 7, 2020).

Sager, J. C., Smith, W. O., Edwards, J. L., and Cyr, K. L. (1988). Photosynthetic efficiency and phytochrome photoequilibria determination using spectral data. *Trans. ASAE* 31, 1882–1889. doi: 10.13031/2013.30952

Smillie, R. M., and Hetherington, S. E. (1999). Photoabatement by anthocyanin shields photosynthetic systems from light stress. *Photosynthetica* 36, 451–463. doi: 10.1023/A:1007084321859

Son, K.-H., and Oh, M.-M. (2013). Leaf shape, growth, and antioxidant phenolic compounds of two lettuce cultivars grown under various combination of blue and red Light-emitting Diodes. *HortScience* 48, 988–995. doi: 10.21273/HORTSCI.48.8.988

Stutte, G. W. (2009). Light-emitting diodes for manipulating the phytochrome apparatus. *HortScience* 44, 231–234. doi: 10.21273/HORTSCI.44.2.231

Stutte, G. W., and Edney, S. (2009). Photoregulation of bioprotectant content of rend leaf lettuce with light-emitting diodes. *HortScience* 44, 79–82. doi: 10.21273/HORTSCI.44.1.79

Tanaka, Y., Sasaki, N., and Ohmiya, A. (2008). Biosynthesis of plant pigments: anthocyanins, betalains and carotenoids. *Plant J.* 54, 733–749. doi: 10.1111/j.1365-313X.2008.03447.x

Thoma, F., Somborn-Schulz, A., Schlehuber, D., Keuter, V., and Deerberg, G. (2020). Effects of light on secondary metabolites in selected leafy greens: a review. *Front. Plant Sci.* 11:497. doi: 10.3389/fpls.2020.00497

Tuan, P. A., Park, C. H., Park, W. T., Kim, Y. B., Kim, Y. J., Chung, S. O., et al. (2017). Expression level of carotenoid biosynthetic genes and carotenoid production in the callus of scutellaria baicalensis exposed to white, blue, and red light-emitting diodes. *Appl. Biol. Chem.* 60, 591–596. doi: 10.1007/s13765-017-0314-8

USDA (2019). Available online at: https://fdc.nal.usda.gov/fdc-app.html#/food-details/169247/nutrients (accessed December 23, 2020).

Yang, C., and Li, L. (2017). Hormonal regulation in shade avoidance. *Front. Plant Sci.* 8:1527. doi: 10.3389/fpls.2017.01527

Yu, X., Liu, H., Klejnot, K., and Lin, C. (2010). The cryptochrome blue light receptors. *Arabidopsis Book*. 8:e0135. doi: 10.1199/tab.0135

Zhang, K., Yu, H., Shi, K., Zhou, Y., Yu, J., and Xia, X. (2010). Photoprotective roles of anthocyanins in *Begonia semperflorens*. *Plant Sci.* 179, 202–208. doi: 10.1016/j.plantsci.2010.05.006

Zhen, S., and Bugbee, B. (2020). Substituting far-red for traditionally defined photosynthetic photons results in equal canopy quantum yield for CO2 fixation and increased photon capture during long-term studies: implications for re-defining PAR. *Front. Plant Sci.* 11:581156. doi: 10.3389/fpls.2020.581156

Zhen, S., and van Iersel, M. W. (2017). Far-red light is needed for efficient photochemistry and photosynthesis. *J. Plant Physiol.* 209, 115–122. doi: 10.1016/j.jplph.2016.12.004

Zhu, X., Long, S., and Ort, D. R. (2010). Improving photosynthetic efficiency for greater yield. *Ann. Rev. Plant Biol.* 61, 235–261. doi: 10.1146/annurev-arplant-042809-112206

Conflict of Interest: The authors declare that the research was conducted in the absence of any commercial or financial relationships that could be construed as a potential conflict of interest.

frontiers in Plant Science

ORIGINAL RESEARCH
published: 08 July 2021
doi: 10.3389/fpls.2021.667456

Quantitative Analysis of UV-B Radiation Interception and Bioactive Compound Contents in Kale by Leaf Position According to Growth Progress

Hyo In Yoon[1†], Hyun Young Kim[1†], Jaewoo Kim[1] and Jung Eek Son[1,2]*

[1]Department of Agriculture, Forestry and Bioresources (Horticultural Science and Biotechnology), Seoul National University, Seoul, South Korea, [2]Research Institute of Agriculture and Life Sciences, Seoul National University, Seoul, South Korea

UV-B (280–315 nm) radiation has been used as an effective tool to improve bioactive compound contents in controlled environments, such as plant factories. However, plant structure changes with growth progress induce different positional distributions of UV-B radiation interception, which cause difficulty in accurately evaluating the effects of UV-B on biosynthesis of bioactive compounds. The objective of this study was to quantitatively analyze the positional distributions of UV-B radiation interception and bioactive compound contents of kales (*Brassica oleracea* L. var. *acephala*) with growth progress and their relationships. Short-term moderate UV-B levels did not affect the plant growth and photosynthetic parameters. Spatial UV-B radiation interception was analyzed quantitatively by using 3D-scanned plant models and ray-tracing simulations. As growth progressed, the differences in absorbed UV-B energy between leaf positions were more pronounced. The concentrations of total phenolic compound (TPC) and total flavonoid compound (TFC) were higher with more cumulative absorbed UV-B energy. The cumulative UV energy yields for TFC were highest for the upper leaves of the older plants, while those for TPC were highest in the middle leaves of the younger plants. Despite the same UV-B levels, the UV-B radiation interception and UV-B susceptibility in the plants varied with leaf position and growth stage, which induced the different biosynthesis of TFC and TPC. This attempt to quantify the relationship between UV-B radiation interception and bioactive compound contents will contribute to the estimation and production of bioactive compounds in plant factories.

Keywords: flavonoids, phenolic content, plant structure, three-dimensional analysis, ultraviolet yield, vertical farm

OPEN ACCESS

Edited by:
Brian Farneti,
Fondazione Edmund Mach, Italy

Reviewed by:
Houcheng Liu,
South China Agricultural University, China
Lars Olof Björn,
Lund University, Sweden

***Correspondence:**
Jung Eek Son
sjeenv@snu.ac.kr

†These authors have contributed equally to this work and share first authorship

Specialty section:
This article was submitted to Crop and Product Physiology, a section of the Frontiers in Plant Science

Received: *13 February 2021*
Accepted: *07 June 2021*
Published: *08 July 2021*

Citation:
Yoon HI, Kim HY, Kim J and Son JE (2021) Quantitative Analysis of UV-B Radiation Interception and Bioactive Compound Contents in Kale by Leaf Position According to Growth Progress. Front. Plant Sci. 12:667456. doi: 10.3389/fpls.2021.667456

INTRODUCTION

Brassica vegetable crops are known to have beneficial effects on human health (Heimler et al., 2007; Podsędek, 2007; Francisco et al., 2017). Among them, kale (*Brassica oleracea* L. var. *acephala*), which is a rich source of health-promoting phytochemicals, such as polyphenols and carotenoids (Olsen et al., 2009; Walsh et al., 2015), has been widely cultivated and consumed for several centuries (Šamec et al., 2019). Recently, to improve individual phytochemicals, the

nutritional contents and profiles of *Brassica* vegetables have been studied (Krumbein et al., 2010; Ishida et al., 2014). As strategies for optimizing and balancing these profiles, manipulation of environmental factors has been attempted (Oh et al., 2009; Davies and Espley, 2013). Variations in the amounts and patterns of compounds have been attributed to abiotic stress factors, including temperature, drought, salinity, and ultraviolet (UV) radiation (Ramakrishna and Ravishankar, 2011; Linić et al., 2019; Podda et al., 2019; Toscano et al., 2019). In particular, UV-B (280–315 nm) has a great impact on plant defense mechanisms and is used as an effective tool to increase bioactive compound contents over short-term periods in various crops (Czégény et al., 2016; Escobar-Bravo et al., 2017; Yavaş et al., 2020).

Many previous studies have focused on the effects of UV-B energy (dosage) levels on bioactive compounds in many crops for application in controlled environments, such as plant factories (Martínez-lüscher et al., 2013; Hectors et al., 2014; Zhao et al., 2020). UV-B levels have been determined from the energy emitted by UV-B light sources (Bian et al., 2014; Acharya et al., 2016). However, plant responses to UV-B are driven not by the energy released but by the energy absorbed by leaves (Meyer et al., 2009), which changes with leaf position (Morales et al., 2011). UV-B exposure on upper leaves was more advantageous for absorbing light, but lower leaves had no choice but to receive the transmitted light in the plant canopy (Filella and Peñuelas, 1999). In *Arabidopsis*, the light capture efficiency of simulated leaves with spiral phyllotaxis increased with leaf order (Strauss et al., 2020). Therefore, the accumulation pattern of UV-B absorbing compounds should be considered with respect to leaf position (Grammatikopoulos et al., 1999; Liakoura et al., 2003).

In most previous studies, accumulation of bioactive compounds according to leaf position has been interpreted as an influence of UV-B susceptibility that is related to leaf age (Behn et al., 2011; Majer and Hideg, 2012; Holub et al., 2019). Considering the three-dimensional (3D) plant structure, bioactive compounds at each leaf were determined with UV-B radiation interception as well as with leaf age in kale (Yoon et al., 2021). As plant growth progresses, changes in lighting distance (Kim et al., 2020b) or planting density (Portes and Melo, 2014; Xue et al., 2015) can affect the spatial distribution of light interception for whole plants, which is directly related to plant growth and biomass production. Accumulation of bioactive compounds is regulated by the overall developmental stages of whole plants as well as by the specific developmental state of each leaf (Lois, 1994). In particular, under UV-B exposure, secondary metabolites are affected by plant developmental ages in pak choi (Heinze et al., 2018). Therefore, plant growth progress may cause large variations in absorbed UV-B based on leaf position as well as the UV sensitivity due to leaf age. Their influences on metabolite accumulation cannot be distinguished without quantification of the absorbed UV-B energy distribution.

Recently, the light distribution for a whole plant was quantitatively analyzed using 3D plant models and ray-tracing simulation analysis (Kim et al., 2020a,b). However, spatial analysis of light distribution has not been applied to UV-B radiation. These methods allow interpretations of absorbed UV-B distributions based on plant structure. This study hypothesized that, for individual plants, light interception depends on leaf position as well as growth stage, which will affect UV-B-induced biosynthesis of bioactive compounds. The objective of this study was to quantitatively analyze the positional distributions of UV-B radiation interception and bioactive compound contents of kales with growth progress and their relationships using 3D analysis.

MATERIALS AND METHODS

Plant Materials and Growth Conditions

Kale seeds (*B. oleracea* L. var. *acephala*, "Manchoo collard," Asia Seed Company, Seoul, South Korea) were sown and germinated on sponge cubes by hydroponic methods under fluorescent lamps at a photosynthetic photon flux density of 150 μmol m^{-2} s^{-1}. After the first leaf appeared, the seedlings were supplied with a nutrient solution for *Brassica* modified from a previous study (Choi et al., 2005): N 137.8, P 30.9, K 140.9, Ca 104.6, Mg 54.8, Fe 2.76, Cu 0.02, Zn 0.05, Mn 0.68, B 0.50, and Mo 0.01 mg l^{-1}, at an electrical conductivity (EC) of 0.6 dS m^{-1}. At 4 weeks after germination, seedlings were transplanted into plant factory modules with a deep flow technique system, and each module was 150 H × 80 W × 50 L (cm) in size. The modules were maintained at 24°C/20°C light/dark temperatures, 70% relative humidity, and 500 μmol mol^{-1} CO_2 concentration. The transplanted plants were irradiated with light-emitting diodes (LEDs) at 200 μmol m^{-2} s^{-1} over a waveband of 400–700 nm for a 16 h light period and were supplied with 1.2 dS m^{-1} EC nutrient solution. The spectrum of the LED for growth was measured using a spectroradiometer (Blue-Wave spectrometer, StellarNet Inc., Tampa, FL, United States) in the range of 380–900 nm (**Figure 1A**). Three plants per treatment were harvested at 14 days after transplanting (DAT), and two plants per treatment were harvested at 28 DAT.

Growth Characteristics

Fresh leaf weights were determined at harvest with three replicates per treatment, and dry leaf weights were measured after drying in an oven for 120 or 168 h for the 14 DAT and 28 DAT plants, respectively. After photographing all leaves, total plant leaf areas were calculated with the image analysis software ImageJ (National Institutes of Health, Bethesda, MD, United States). Leaf positions (upper, middle, and lower leaves) were determined in the order from youngest to oldest, and consisted of 3, 2, and 2 leaves at 14 DAT and 3–4, 3, and 3 leaves at 28 DAT, respectively.

UV-B Treatment

All plants were irradiated with supplemental UV-B LEDs (Ericson Company Ltd., Bucheon, South Korea) with 1.2 W m^{-2}

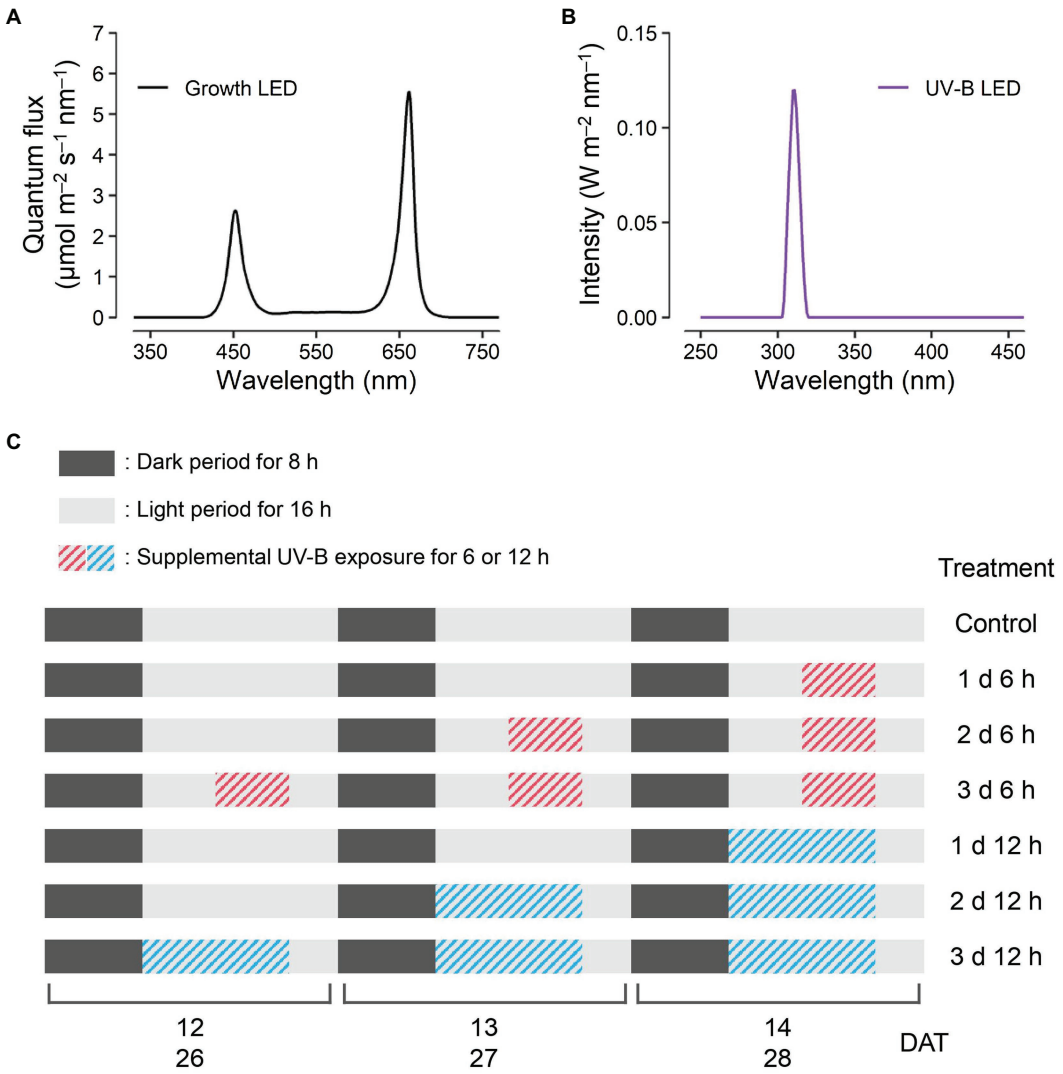

FIGURE 1 | Experimental design. Light spectra of the red, blue, and white light-emitting diodes (LEDs) for plant growth **(A)** at 200 μmol m^{-2} s^{-1} over a waveband of 400–700 nm and UV-B LED **(B)** of 1.2 W m^{-2} at a spectrum peak of 310 nm. The schedules of UV-B treatments **(C)** consisting of supplemental UV-B exposures of 6 and 12 h per day for 1, 2, and 3 days before harvest were the same for both harvest dates at 14 and 28 days after transplanting (DATs).

at a spectrum peak approximately 310 nm. The irradiance and spectrum of UV-B LEDs were measured by a UV sensor (MU-200, Apogee Instruments Inc., Logan, UT, United States) and the spectroradiometer in the range of 250–400 nm (**Figure 1B**). UV-B exposure periods were 6 and 12 h per day for 1, 2, and 3 days before harvest, which resulted in a total of six treatments (e.g., 1 d 6 h, 1 d 12 h, 2 d 6 h, 2 d 12 h, 3 d 6 h, and 3 d 12 h), and the experimental setup is shown in **Figure 1C**. The cumulative UV-B doses of six treatments were 21.6, 43.2, 43.2, 86.4, 64.8, and 129.6 kJ m^{-2} for 3 days, respectively, which are equivalent to biologically effective UV-B radiation ($UV\text{-}B_{BE}$) doses of 2.1, 4.2, 4.2, 8.4, 6.3, and 12.6 kJ m^{-2} for 3 days, respectively. $UV\text{-}B_{BE}$ was calculated using a plant action spectrum in the UV range (Flint and Caldwell, 2003). After UV-B exposure, all plants had a recovery time of 4 h per day. At the end of 14 and 28 DAT, the plants from all treatments were harvested simultaneously.

Chlorophyll Fluorescence

Chlorophyll fluorescence was measured for 30 min dark-adapted leaves using a chlorophyll fluorescence meter (Handy PEA fluorometer, Hansatech, Kings Lynn, United Kingdom) according to a previous study (Rapacz, 2007). At 14 and 28 DATs, all measurements were performed after the recovery time with three replicates per treatment and leaf position. Measurements were performed using a saturating pulse of 1,500 μmol m^{-2} s^{-1} for 1 s to determine the minimal fluorescence (F_0) and maximal fluorescence (F_m) values. The maximal photochemical efficiency of photosystem II (F_v/F_m) was calculated as $(F_m - F_0)/F_m$.

Bioactive Compounds and Antioxidant Capacity

Total Phenolics

Total phenolic compounds (TPCs) were measured by the Folin-Ciocalteu colorimetric method (Ainsworth and Gillespie, 2007). Powdered samples (50 mg) were mixed with 1 ml of 80% methanol, incubated for 48 h in the dark at room temperature and centrifuged at 1.1×10^4 *g* for 10 min. Supernatants of samples (50 µl) were collected in 2 ml microtubes and were then mixed with 750 µl of 10% Folin-Ciocalteu solution and 135 µl of distilled water using a vortexer. After mixing, 600 µl of 700 mm Na_2CO_3 was added, and the samples were then incubated for 2 h at room temperature. Sample absorbances were read at 765 nm using a spectrophotometer (PhotoLab 6100 VIS, Weilheim, Germany). The standard unit for TPC was expressed as milligrams of gallic acid equivalent per gram of dry weight (mg GAE g^{-1} DW).

Total Flavonoids

Total flavonoid compound (TFC) amounts were measured by an aluminum chloride colorimetric method (Dewanto et al., 2002; Lee et al., 2012). Powdered samples (50 mg) were mixed with 1 ml of 80% methanol, incubated for 24 h in the dark at 4°C, and centrifuged at 1.1×10^4 *g* for 10 min. The supernatants (50 µl) of the samples were collected in 2 ml microtubes, and 135 µl of distilled water and 45 µl of 5% $NaNO_2$ were added. Ninety microliters of 10% $AlCl_3$ and 300 µl of 1 M NaOH were added after 5 and 6 min, respectively, and 165 µl of distilled water was then added. After incubating for 30 min, sample absorbances were then read at 510 nm using a spectrophotometer, and the standard unit for TFC was expressed as milligrams of catechin acid equivalent per gram of dry weight (mg CE g^{-1} DW).

Antioxidant Capacity

Total antioxidant capacity was measured using the 2, 2-diphenyl-1-picrylhydrazyl (DPPH) assay method (Brand-Williams et al., 1995; Andarwulan et al., 2010). A DPPH solution was prepared with 500 ml of 80% methanol and 12 mg of DPPH. Powdered samples (50 mg) were mixed with 1 ml of 80% methanol, incubated for 48 h in the dark at room temperature and centrifuged at 1.1×10^4 *g* for 10 min. Supernatants (50 µl) were then collected in 2 ml microtubes, and 1.95 ml of DPPH solution was added. After incubating for 30 min, the sample absorbances were then read at 517 nm by the spectrophotometer and used methanol as the blank. Antioxidant activity was expressed as radical scavenging activity (RSA), which was calculated using the following equation:

$$RSA\left(\%\right) = \left(A_{control\,517nm} - A_{sample\,517nm}\right) / A_{control\,517nm} \times 100 \quad (1)$$

where the $A_{\text{control 517 nm}}$ and $A_{\text{sample 517 nm}}$ are the absorbances of the samples at 517 nm without and with leaf extracts, respectively.

Light Interception With 3D Plant Structure

Light interceptions of kale plants were analyzed using 3D-scanned plant models and ray-tracing simulation analysis method (Kim et al., 2020a,b; Yoon et al., 2021). The detailed procedure and condition from scan to simulation were described in **Supplementary Figure S1**.

Construction of 3D-Scanned Plant Models

The plants were scanned with a high-resolution portable 3D scanner (GO!SCAN50TM, CREAFORM, Lévis, Quebec, Canada). The scanner resolution was set at 2 mm. The scanned plants were randomly selected as one plant per treatment (Control, $UV_{6\ h}$ and $UV_{12\ h}$) before and after treatment, and a total of six scanned models were generated at each growth stage. The scanned data were exported to 3D mesh data with its scanning software (VXelement, CREAFORM). Holes and noise in the mesh data were fixed, and segmented mesh data were reconstructed to a surface model to perform ray-tracing simulations by reverse engineering software (Geomagic Design X, 3D Systems, Rock Hill, SC, United States).

Ray-Tracing Simulation

For the ray-tracing simulations, the transmittance and reflectance of each leaf position and module material were measured using the spectroradiometer with an integrating sphere (IC-2, StellarNet Inc.) in a range of 250–700 nm to determine optical properties for the plant models (**Supplementary Figure S1**). A virtual growth bed and LED bars were reconstructed using 3D computer-aided design software (Solidworks, Dassault Systèmes, Vélizy-Villacoublay, France) with the same size and layout as the actual growth environment. Twenty-four or twelve surface models of scanned plants were placed on the virtual growth bed equal to the actual planting density for each growth stages, 14 or 28 DAT, respectively. Ray-tracing simulations were performed by using a ray-tracing software (Optiworks, OTIS Inc., La Farlède, France). After setting up all leaf surface models as separate detectors, the simulation outputs were averaged according to leaf position and treatment. All simulation results are presented as the average light interceptions in the photosynthetically active radiation (PAR) range of 400–700 nm and the UV range of 250–400 nm.

Statistical Analysis

Comparison of mean value were performed with one-way or two-way ANOVA and Tukey's HSD test to assess the effects of treatments or leaf positions with R software (R 1.2.5, R Foundation, Vienna, Austria). The UV energy yields for TPC and TFC contents were considered as the increase rate based on cumulative absorbed UV energy, and the increase rates compared to the control were regressed into a nonlinear regression as follows:

$$Increase\ rate\ of\ TPC\ or\ TFC\left(\%\right) = a / \Delta UV + b \quad (2)$$

where a and b are the regression coefficients for the relationships between bioactive compounds and absorbed UV. ΔUV is the UV absorbed on leaves in each treatment. Linear and nonlinear regressions were conducted with Python (Python 3.6.7, Python Software Foundation, Wilmington, United States).

RESULTS

Plant Growth

The plant growth characteristics did not show any significant differences among the treatments at either growth stage during cultivation (**Figure 2**). In the $UV_{12\ h}$ treatments (e.g., 1 d 12 h, 2 d 12 h, and 3 d 12 h), fresh leaf weights and dry leaf weights slightly decreased with the UV-B exposure period at 28 DAT (**Figures 2C–F**), and leaf areas were 10–25% lower than those of the control (**Figures 2A,B**). F_v/F_m values at 14 and 28 DATs were 0.82–83 in all treatments and did not differ among treatments (data not shown). Therefore, UV-B levels did not affect the growth or photochemical efficiency in all treatments.

Vertical Distributions of PAR and UV Radiation Interception

Photosynthetically active radiation and UV radiation interceptions were simulated well with the 3D structure of the plants, i.e., leaf positions and leaf angles (**Figure 3**). Radiation interception levels increased with plant height and leaf position in the order of upper, middle, and lower leaves for both growth stages (**Figure 4**). Plants at 14 DAT had lower plant heights but the leaves at each position received higher light intensities compared to those at 28 DAT (**Figure 4A**). At 14 DAT, the absorbed UV levels of the upper leaves were 12.1 and 54.5% higher than those of the middle and lower leaves, respectively (**Figure 4B**). The differences in absorbed UV light between leaf positions were more pronounced at 28 DAT, for which the UV radiation interceptions of the upper leaves were 34.1 and 88.8% higher than those of the middle and lower leaves, respectively.

Bioactive Compounds and Antioxidant Capacity

TFC and TPC concentrations and antioxidant capacity (RSA) were higher with greater UV-B doses and higher leaf positions (**Figure 5**). Only on the upper leaves at 14 DAT were the TFC and TPC levels significantly higher than those at other positions (**Figures 5A,C,E**), while those at 28 DAT increased

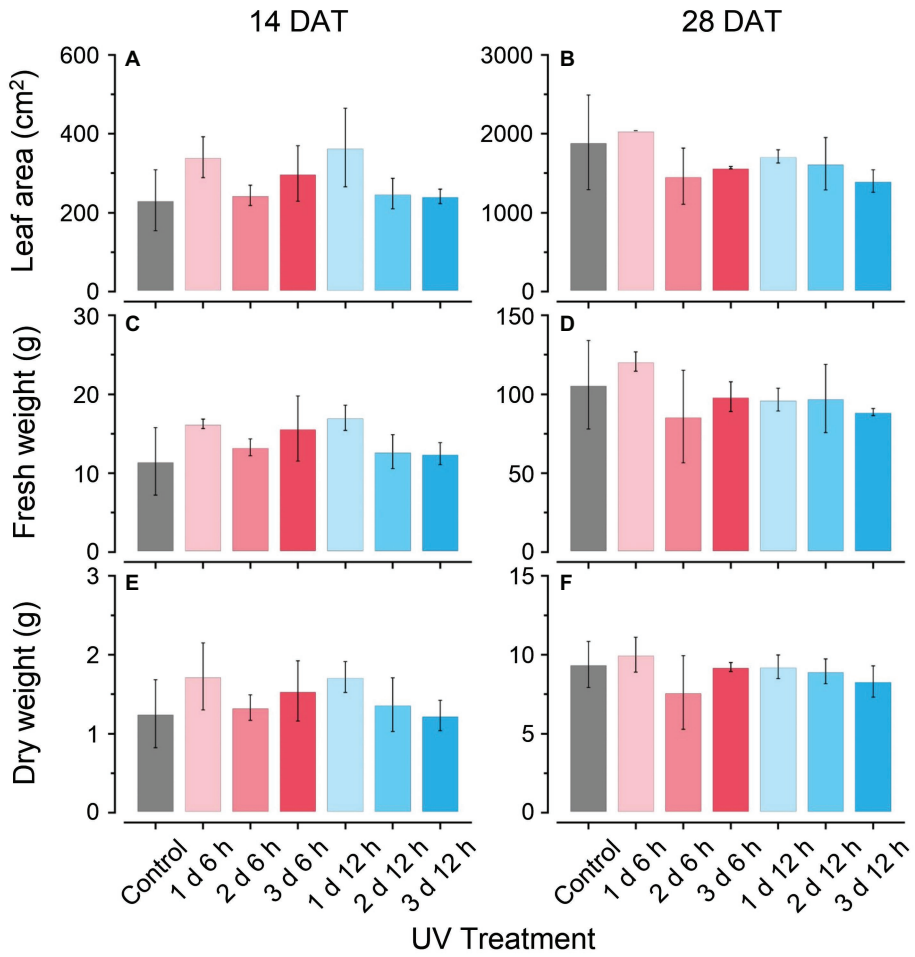

FIGURE 2 | Total leaf areas **(A,B)**; leaf fresh weights **(C,D)**; and dry weights **(E,F)** of kales grown under the control and UV-B treatments at 14 and 28 days after transplanting (DATs). Vertical vars indicate the standard deviation of mean. Refer to **Figure 1C** for the UV treatments.

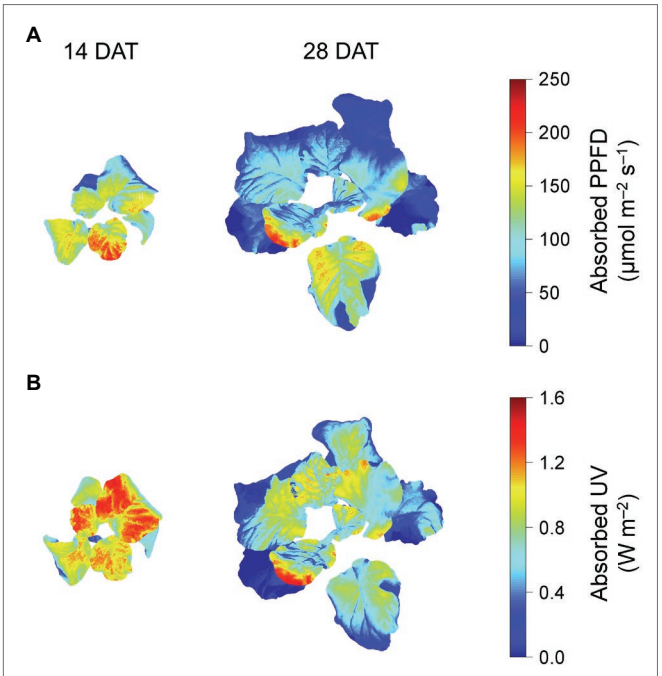

FIGURE 3 | Representative light interception distributions on 3D-scanned kale models at 14 and 28 days after transplanting (DATs). Each light interception represents the photosynthetic photon flux density (PPFD) absorbed at at 400–700 nm **(A)** and UV absorbed at 250–400 nm **(B)**.

significantly in the order of upper, middle, and lower leaves (**Figures 5B,D,F**). In all treatments at 14 DAT, the TFC and TPC levels in the upper leaves were 35.9–63.1% and 29.6–55.2% higher than those of the other leaves, respectively. At 28 DAT, those values in the upper leaves were 29.3–36.8% and 70.1–82.6% higher than those of the other leaves, respectively. Overall, the TFC, TPC, and RSA values for the 2 d 12 h and 3 d 12 h treatments were higher than those for the control at both growth stages.

Relationships Between UV Light Interception and Bioactive Compounds

Across all data, the TPC and TFC concentrations relative to the cumulative amounts of UV absorbed for 3 days showed linear relationships at each leaf position (**Figure 6**). The coefficients of determination (R^2) of the linear regressions are shown in **Table 1**. As growth progressed from 14 to 28 DATs, the gradients of TFC levels against absorbed UV increased slightly for the upper leaves (**Figures 6A,B**). In contrast, the gradients of TPC levels for the upper leaves decreased by 25% but only increased by 13.8% in the middle leaves at 28 DAT compared to those at 14 DAT.

Changes in TFC and TPC levels relative to cumulative absorbed UV amounts were regressed according to leaf positions and growth stages using rectangular hyperbolic equations (**Figure 7**; Eq. 2). The R^2 values of these nonlinear regressions are shown in **Table 1**. The patterns of increase rates, i.e., the cumulative UV energy yields, were dependent on the type of bioactive compound. UV yields for TFC were highest in the upper leaves at 28 DAT (**Figure 7B**), but those among leaf positions did not differ noticeably at 14 DAT (**Figure 7A**). On the other hand, UV yields for TPC were highest in the middle leaves at both growth stages and decreased for all leaf positions at 28 DAT compared to those at 14 DAT (**Figures 7C,D**).

DISCUSSION

Effect UV-B Radiation on Plant Growth

In most previous studies, growth inhibition in UV-B-acclimated plants was observed for numerous species (Hofmann et al., 2001; Jansen, 2002; Hectors et al., 2007). As growth progressed, all growth characteristics under UV-B exposure were slightly lower than those of the control (**Figure 2**). In addition, F_v/F_m values for all treatments remained at 0.82–83, which indicated normal growth conditions (Baker, 2008). In this study, the UV-B_{BE} doses were 2.1 or 4.2 kJ m^{-2} d^{-1} in $UV_{6\ h}$ and $UV_{12\ h}$ treatment, and the daily light integral in the PAR range was 11.5 mol m^{-2} d^{-1}. These unrealistic ratios of UV-B_{BE} and PAR for a day are far from those under sunlight (Bornman et al., 2019). The photon ratio of 1.3% between the UV-B (not UV-B_{BE}) and PAR also differed from sunlight, which is less than 0.2% (Robson et al., 2019). Despite of the higher UV-B/PAR ratio, the short-term UV-B duration was not sufficient to affect the growth and photosystem II activity. These results were consistent with the previous results, which did not have a negative effect on the growth of kale exposed to UV-B radiation for 2–3 days before harvest (Yoon et al., 2020, 2021).

UV-B Radiation Interception With Growth Progress

Several studies have determined the spatial distributions of light interception in plant canopies by use of a mathematical or functional structural plant model in soybean, maize, and tomato (Wells et al., 1993; Stewart et al., 2003; Sarlikioti et al., 2011). Similar to the previous results, UV radiation interception increased with leaf height and leaf position for both growth stages (**Figures 3, 4**). However, average light interception decreased with growth progress for all leaf positions (**Figure 4B**). In contrast, the previous reports for taller crops showed higher light interception than for shorter crops with growth progress (Xue et al., 2015; Cabrera-Bosquet et al., 2016). Unlike natural light, the narrow radiation ranges of artificial light sources, such as LEDs in controlled environments, affects the irradiation area depending on lighting distance and planting conditions. Calculation based on the scanned plant models, the distance of the upper, middle, and lower leaves from the light source was 29, 30, 33 cm at 14 DAT and 24, 27, 30 cm at 28 DAT, respectively (data not shown). In the center of an empty growth chambers, the light intensities of LED modules increased as the lighting distance increased from 15 to 45 cm (Hitz et al., 2019). Under the LED arranged vertically above lettuce plants, the total light interception also increased as the lighting distance

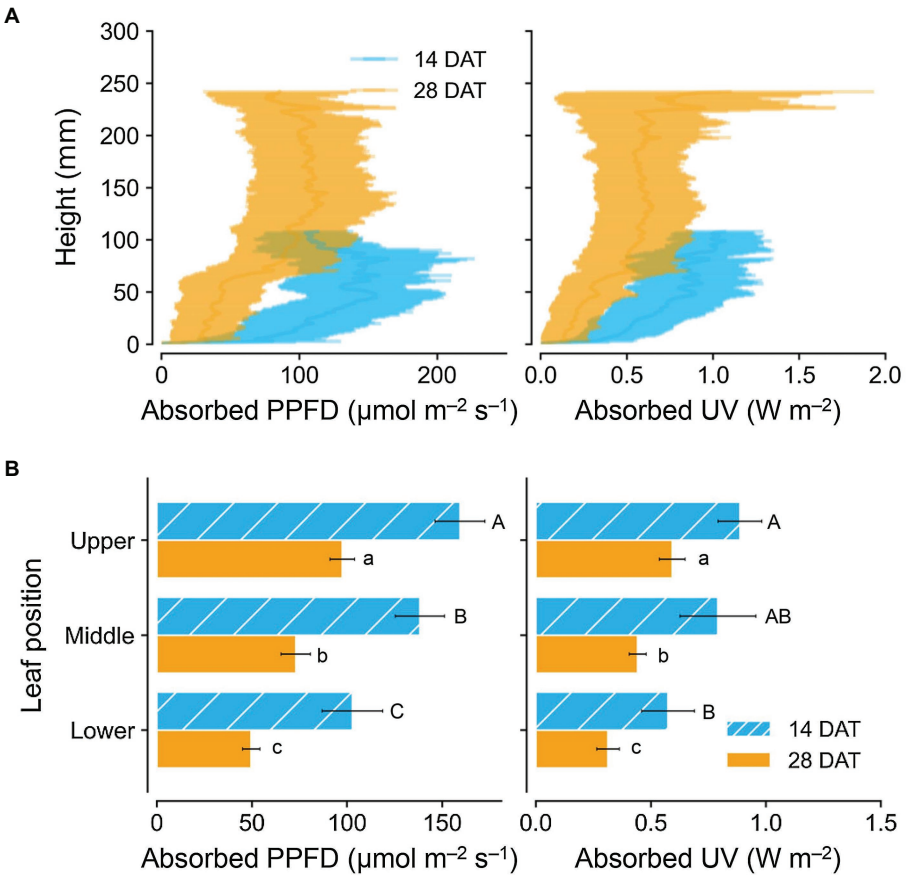

FIGURE 4 | Vertical distributions of light interception on kales according to plant heights **(A)** and leaf positions **(B)** at 14 and 28 days after transplanting (DATs). Each light interception represents the photosynthetic photon flux density (PPFD) absorbed at 400–700 nm and UV absorbed at 250–400 nm. Vertical vars indicate the standard error of mean (n = 2; average of 12 and 6 plant models for 14 and 28 DATs, respectively). Different letters represent significant differences between leaf position at $p < 0.05$ by two-way ANOVA and Tukey's HSD test.

increased from 20 to 35 cm (Kim et al., 2020b). Therefore, although the upper leaves at 28 DAT were irradiated closer to the UV LEDs compared to those at 14 DAT, the average light interception would have been relatively low due to less overlap of radiation. As growth progresses, higher leaf density, which called leaf area index, causes shading at the single or canopy level and reduces UV-B radiation interception along with the narrow radiation range of LEDs. In this study, planting densities used in the simulation and actual cultivation were 24 and 12 plants per one bed at 14 and 28 DAT, respectively, which correspond to 22.2 and 11.1 plants per m^2 (**Supplementary Figure S1**). Due to the growth progress, the leaf area indexes were 0.40 and 1.60 calculated as total leaf area per one bed area (m^2/m^2). Similarly, Kang et al. (2019) found in paprika that the estimated light interception rapidly decreased with a relative increase of surrounding plants. Due to the higher leaf area index, leaf angles in the middle leaves were twisted close to 90° or overlapped with each other and thus prevented irradiation. Similar to *Arabidopsis*, which has spiral phyllotaxis leaves at intervals of 137.5°, kale's overlapping leaves within individual plants affect light interception patterns (Strauss et al., 2020). Therefore, these results showed that the growth progression, along with self-shading or neighboring plants, alters the positional distributions of light interception under UV LEDs.

Phenolic Compound With UV-B Radiation Interception

UV-B has been used to irradiate various crops to enhance bioactive compound contents in controlled environments (Czégény et al., 2016; Yavaş et al., 2020). In this study, the longer daily time and duration of UV-B exposure, i.e., greater cumulative UV-B dose, induced higher TFC and TPC levels (**Figure 5**). Similarly, a UV-B dose-dependent response of biosynthesized secondary metabolites was found in St. John's wort and sweet basil with continuous or repeated UV-B exposure (Brechner et al., 2011; Mosadegh et al., 2018). However, the UV-dose dependence of TFC and TPC at 28 DAT appeared only in the upper leaves, which were exposed to higher UV-B intensities (**Figures 4, 5**). As growth progressed, similar to the vertical distribution of light interception, the differences in UV-B-induced TFC and TPC among leaf positions became highly distinct (**Figure 5**). This result suggested that the patterns

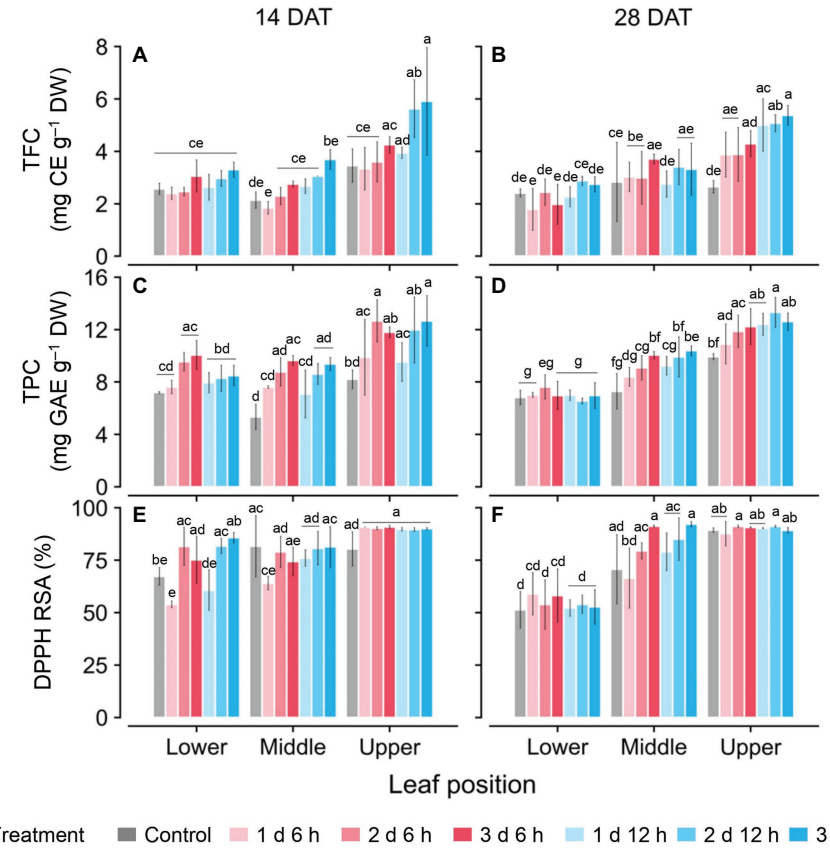

FIGURE 5 | Concentrations of total flavonoid compounds (TFC; **A,B**); total phenolic compounds (TPC; **C,D**); and antioxidant capacity represented as DPPH radical scavenging activities **(E,F)** of kales grown under control and UV-B treatments according to leaf positions at 14 and 28 days after transplanting (DATs). Vertical vars indicate the standard deviation of mean, $n = 3$. Different letters represent significant differences for each parameter at $p < 0.05$ by two-way ANOVA and Tukey's HSD test. Refer to **Figure 1C** for the UV-B treatments.

of bioactive compound accumulation were affected by UV radiation interception patterns according to plant structure. A previous study indicated that flavonol profiles were highly associated with characteristics that were related to canopy structure and light interception (Martínez-Lüscher et al., 2019). One of the main flavonoids, catechins, in an albino tea cultivar, significantly decreased with plant shading, which was associated with DNA methylation involved in the flavonoid biosynthesis pathway (Xu et al., 2020). In this study, RSA levels in the upper leaves were also highest for both growth stages (**Figures 5E,F**). Antioxidant capacity is an indicator that can indirectly show a plant's physiological ability of its leaves (Blum-Silva et al., 2015). Phenolic acids and flavonoids containing catechol structures have been highly correlated with their radical scavenging capacity (Ayaz et al., 2008; Zietz et al., 2010; Fiol et al., 2012).

UV-B Stress Susceptibility According to Leaf Developmental Age

Developmental age of leaves, as well as UV-B energy, determines antioxidant capacity and flavonoid accumulation, and thereby cause within-individual heterogeneity of UV-B response (Csepregi et al., 2017; Yoon et al., 2021). Heinze et al. (2018) reported that phenolic and hydroxycinnamic acids accumulated to higher levels in plants with mature leaves than in plants with younger leaves, which indicated that they can also be applied to mature and young leaves in individual plants. In addition, the growth progress caused large variations in leaf age within plants. In this study, TFC and TPC levels in lower (older) leaves at 28 DAT showed the lowest values among treatments (**Figures 5C,D**). RSA levels in lower leaves at 28 DAT were significantly lower than those at 14 DAT (**Figures 5E,F**). Even for the same position, the leaf ages of the lower leaves were at least 2 weeks at 14 DAT and were at least 4 weeks at 28 DAT. Similarly, younger leaves also exhibited higher antioxidant capacities than older leaves in grapevines (Majer and Hideg, 2012). The linear correlations between TPC and TFC levels and cumulative UV absorbed for 3 days were clearly distinguished by leaf position and age (**Figure 6**). The gradient of the regression line, i.e., the increase rate of TPC and TFC against UV energy, was interpreted as the age-dependent UV-B stress susceptibility (**Figure 7**). As growth progressed, the TFC increase rate in the upper leaves increased noticeably (**Figure 7B**).

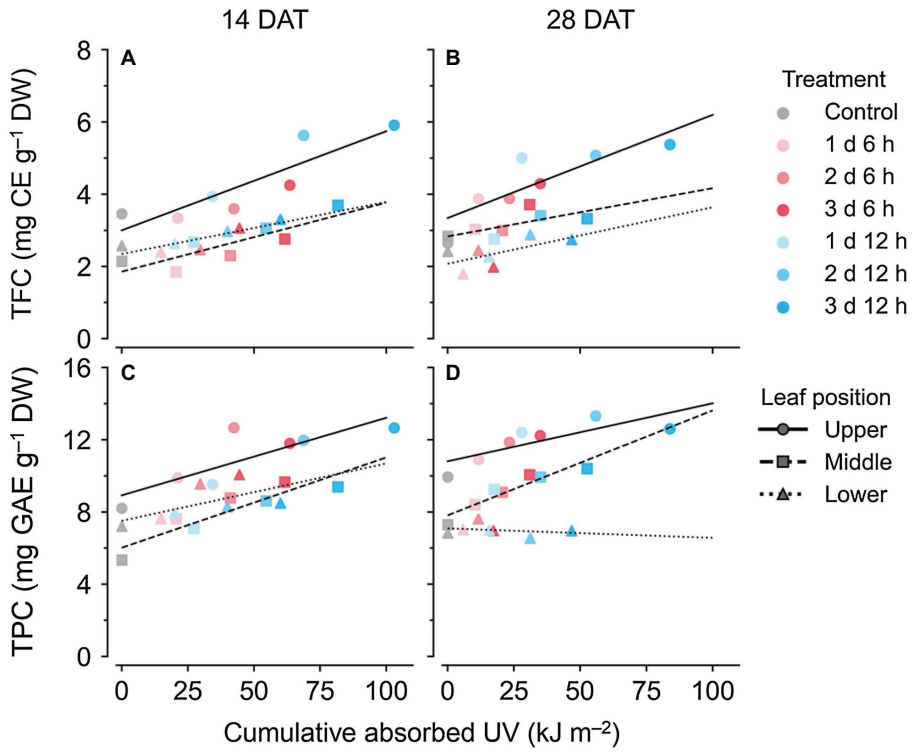

FIGURE 6 | Relationships between compound concentrations and cumulative absorbed UV for 3 days of kales grown under the control and UV-B treatments according to leaf position and growth stage; total flavonoid compounds (TFC; **A,B**) and total phenolic compounds (TPC; **C,D**) at 14 **(A,C)** and 28 **(B,D)** days after transplanting (DATs). The cumulative absorbed UV means the integration of UV irradiation absorbed by each leaf for 3 days. Refer to **Figure 1C** for the UV-B treatments and **Table 1** for R^2 of the linear regression.

TABLE 1 | Coefficients of determination (R^2) from linear regressions for bioactive compound contents and from nonlinear regressions for change rates with cumulative absorbed UV for 3 days according to leaf position and growth stage. Refer to Eq. 2 for the nonlinear regression equation.

Growth stage	Leaf position	Linear regression		Nonlinear regression	
		TFC[z]	TPC[y]	TFC	TPC
14 DAT[x]	Upper	0.79	0.70	0.64	0.59
	Middle	0.73	0.84	0.66	0.74
	Lower	0.73	0.39	0.71	0.37
28 DAT	Upper	0.73	0.64	0.59	0.84
	Middle	0.45	0.87	0.34	0.91
	Lower	0.41	0.07	0.61	0.11

[z]TFC, total flavonoid compounds; [y]TPC, total phenolic compounds; and [x]DAT, days after transplanting.

In other words, young leaves had the highest UV-B susceptibility for TFC, which was consistent with the previous findings of general stress susceptibility with leaf age (Sperdouli and Moustakas, 2014; Moustaka et al., 2015; Kanojia et al., 2020). As growth progressed, the TFC and TPC increase rates increased or decreased for all leaf positions, but the actual concentrations were similar between 14 and 28 DAT (**Figures 5, 7**). These results were caused by both higher UV-B light interceptions at 14 DAT and higher concentrations with growth progress in the control without UV-B exposure. This tendency is consistent with the results of a previous study, which showed the increases in TFC, TPC, and total glucosinolate contents in kale without UV-B exposure in plant factories (Yoon et al., 2019).

Potential of UV Energy Yield for Phenolic Profiles in 3D Plant Structure

In general, the radiation use efficiency is obtained as the slope of the regression line for biomass accumulated with PAR light intercepted by a plant (Chakwizira et al., 2014). Accordingly, the slope of the regression line of the accumulated TPC or TFC content with absorbed UV energy can be regarded as UV energy yield (**Figures 6, 7**). Canopy distributions of nitrogen (N) and phosphorus, whose levels remained constant or gradually decreased in aging leaves, were inferred to be related to UV energy yields for TFC and TPC (Coleman, 1986; Chakwizira et al., 2011). Radiation use efficiency was determined not only by canopy N distributions but also by leaf N allocations in the thylakoid light-harvesting proteins of *Brassica* crops (Fletcher et al., 2013; Liu et al., 2020). In this study, the cumulative UV energy yields for TFC or TPC accumulation were determined by plant ages as well as by leaf ages (**Figure 7**). Although the actual leaf ages of the upper leaves were the same at approximately 1–2 weeks from their appearance between 14 and 28 DATs, the TFC increase rate was markedly higher at 28 DAT (**Figures 7A,B**). In contrast, the UV-B increase rate for TPC was highest in the middle leaves (**Figures 7C,D**). The result

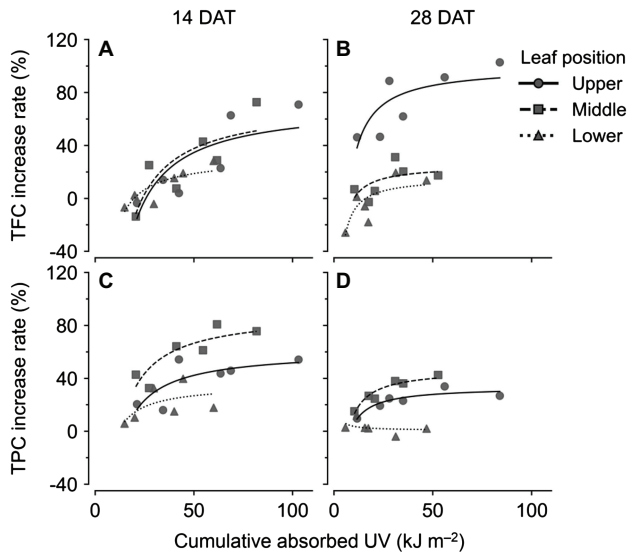

FIGURE 7 | Nonlinear regression for increase rates of compound concentrations compared to the control with cumulative absorbed UV for 3 days of kales according to leaf positions and growth stages; total flavonoid compounds (TFC; **A,B**) and total phenolic compounds (TPC; **C,D**) at 14 **(A,C)** and 28 **(B,D)** days after transplanting (DATs). The cumulative absorbed UV means the integration of UV irradiation absorbed by each leaf for 3 days. Refer to Eq. 2 for the nonlinear regression equation, and **Table 1** for R^2 of the nonlinear regression.

was consistent with a previous study, which showed that the TPC increase rate in the middle leaf was the highest because younger leaves had higher TPC even without UV-B exposure (Yoon et al., 2021). Similarly, UV-B-induced metabolite accumulations depended on chemical structure as well as chalcone synthase activity (Neugart et al., 2012; Ghasemzadeh et al., 2016). Despite the predominance of UV energy yield in the middle leaves at 28 DAT (**Figure 7D**), actual TPC concentrations were significantly higher in the upper leaves (**Figure 5D**). If the amount of UV radiation interception in the middle leaves was not intercepted by the upper leaves at 28 DAT, TPC concentrations in the middle leaves could be higher than those in the upper leaves. Therefore, the UV-B-induced bioactive compound contents in the plant structure can be estimated when the age-dependent cumulative UV energy yields and distributions of UV-B radiation interception are considered simultaneously.

Application to Bioactive Compound Production in Plant Factories

Several studies about modeling the light environment perceived by the plant organs using various techniques, such as 3D plant model and Monte Carlo ray-tracing, have been focused on light interception in the PAR range (Vos et al., 2010). Recently, Kim et al. (2020a) demonstrated the structural accuracy of 3D-scanned parametric model and their application for estimating photosynthetic rates as well as light interception of sweet pepper. Kim et al. (2020b) applied the same technique to lettuce canopy in plant factories with electrical lighting, which allowed the interpretation and evaluation of light use efficiency according to planting density and lighting condition. In the same way, our previous study applied the radiation interception analysis to the UV-B range and confirmed that the UV-B radiation interception of a whole plant determines intraindividual distribution of phenolic contents in kales along with leaf age (Yoon et al., 2021). In this study, we suggested the concept of UV energy yield for phenolic contents in short-term UV-B exposure and showed its applicability to other crops with self- or neighboring shading at various plant stages in controlled environments. In a further step, the UV-induced accumulation of bioactive compounds can be estimated for various plants and lighting condition, such as wavelengths, shape, arrangement, and distance. For example, the UV sensitivity of TPC was unexpectedly highest in the middle leaves at both growth stages (**Figure 7**). Considering the largest proportion of the middle leaves in plants, further studies are possible on the lateral UV-B irradiation method that focuses on the middle leaves.

From a commercial point of view, maximizing production efficiency against input costs is more important than the output itself. The annual production of TPC and TFC in plant factories could be estimated using the content per plant at various growth stages without neighboring shading, which could determine the optimal harvest time (Yoon et al., 2019). Chowdhury et al. (2021) reported that health-promoting components, specifically glucosinolates and anthocyanin, in kale grown in a plant factory can be estimated through spectral reflectance. Similar to these studies, the annual production of UV-B-induced bioactive compounds can be estimated through UV-B radiation interception analysis. Ultimately, the application of 3D plant model and radiation interception analysis will enable us to evaluate the UV illumination strategies to maximize production vs. UV energy or electrical input in commercially controlled environments.

CONCLUSION

The positional distributions of UV-B radiation interception and bioactive compound contents in kale leaves were quantitatively analyzed with 3D-scanned plant models and 3D light analysis. Concentrations of total flavonoid and phenolic compounds showed their highest values in the upper leaves for both growth stages. As growth progressed, variations in absorbed UV-B, as well as UV susceptibility, at each leaf position became evident. This study confirmed that biosynthesis of bioactive compounds in plant structures was determined by UV-B radiation interception and cumulative UV-B energy yield based on leaf position, leaf age, and plant growth stage. This attempt to quantitatively analyze the relationships between secondary metabolites and UV-B light interception can be applied to model bioactive compound production in plant factories.

DATA AVAILABILITY STATEMENT

The raw data supporting the conclusions of this article will be made available by the authors, without undue reservation.

AUTHOR CONTRIBUTIONS

HY, HK, and JS designed the research and prepared the manuscript. HY and HK performed the experiments. HY, HK, and JK analyzed the data. HY, JK, and JS revised and edited the manuscript. All authors contributed to the article and approved the submitted version.

FUNDING

This work was supported by the Korea Institute of Planning and Evaluation for Technology in Food, Agriculture, Forestry and Fisheries (IPET) through the Agriculture, Food and Rural Affairs Research Center Support Program funded by the Ministry of Agriculture, Food and Rural Affairs (MAFRA; 717001–07-1-HD240).

SUPPLEMENTARY MATERIAL

The Supplementary Material for this article can be found online at https://www.frontiersin.org/articles/10.3389/fpls.2021.667456/full#supplementary-material

REFERENCES

Acharya, J., Rechner, O., Neugart, S., Schreiner, M., and Poehling, H.-M. (2016). Effects of light-emitting diode treatments on *Brevicoryne brassicae* performance mediated by secondary metabolites in Brussels sprouts. *J. Plant Dis. Prot.* 123, 321–330. doi: 10.1007/s41348-016-0029-9

Ainsworth, E. A., and Gillespie, K. M. (2007). Estimation of total phenolic content and other oxidation substrates in plant tissues using Folin-Ciocalteu reagent. *Nat. Protoc.* 2, 875–877. doi: 10.1038/nprot.2007.102

Andarwulan, N., Batari, R., Sandrasari, D. A., Bolling, B., and Wijaya, H. (2010). Flavonoid content and antioxidant activity of vegetables from Indonesia. *Food Chem.* 121, 1231–1235. doi: 10.1016/j.foodchem.2010.01.033

Ayaz, F. A., Hayirlioglu-Ayaz, S., Alpay-Karaoglu, S., Grúz, J., Valentová, K., Ulrichová, J., et al. (2008). Phenolic acid contents of kale (*Brassica oleraceae* L. var. *acephala* DC.) extracts and their antioxidant and antibacterial activities. *Food Chem.* 107, 19–25. doi: 10.1016/j.foodchem.2007.07.003

Baker, N. R. (2008). Chlorophyll fluorescence: a probe of photosynthesis *in vivo*. *Annu. Rev. Plant Biol.* 59, 89–113. doi: 10.1146/annurev.arplant.59.032607.092759

Behn, H., Schurr, U., Ulbrich, A., and Noga, G. (2011). Development-dependent UV-B responses in red oak leaf lettuce (*Lactuca sativa* L.): Physiological mechanisms and significance for hardening. *Eur. J. Hortic. Sci.* 76, 33–40.

Bian, Z. H., Yang, C., and Ke, W. (2014). Effects of light quality on the accumulation of phytochemicals in vegetables produced in controlled environments: a review. *J. Sci. Food Agric.* 95, 869–877. doi: 10.1002/jsfa.6789

Blum-Silva, C. H., Chaves, V. C., Schenkel, E. P., Coelho, G. C., and Reginatto, F. H. (2015). The influence of leaf age on methylxanthines, total phenolic content, and free radical scavenging capacity of *Ilex paraguariensis* aqueous extracts. *Rev. Bras. Farmacogn.* 25, 1–6. doi: 10.1016/j.bjp.2015.01.002

Bornman, J. F., Barnes, P. W., Robson, T. M., Robinson, S. A., Jansen, M. A., Ballaré, C. L., et al. (2019). Linkages between stratospheric ozone, UV radiation and climate change and their implications for terrestrial ecosystems. *Photochem. Photobiol. Sci.* 18, 681–716. doi: 10.1039/C8PP90061B

Brand-Williams, W., Cuvelier, M. E., and Berset, C. (1995). Use of a free radical method to evaluate antioxidant activity. *LWT Food Sci. Technol.* 28, 25–30. doi: 10.1016/S0023-6438(95)80008-5

Brechner, M. L., Albright, L. D., and Weston, L. A. (2011). Effects of UV-B on secondary metabolites of St. John's wort (*Hypericum perforatum* L.) grown in controlled environments. *Photochem. Photobiol.* 87, 680–684. doi: 10.1111/j.1751-1097.2011.00904.x

Cabrera-Bosquet, L., Fournier, C., Brichet, N., Welcker, C., Suard, B., and Tardieu, F. (2016). High-throughput estimation of incident light, light interception and radiation-use efficiency of thousands of plants in a phenotyping platform. *New Phytol.* 212, 269–281. doi: 10.1111/nph.14027

Chakwizira, E., Brown, H. E., and De Ruiter, J. M. (2014). Radiation-use efficiency for forage kale crops grown under different nitrogen application rates. *Grass Forage Sci.* 70, 620–630. doi: 10.1111/gfs.12150

Chakwizira, E., Moot, D. J., Scott, W. R., Fletcher, A. L., and Maley, S. (2011). Leaf development, radiation interception and radiation-use efficiency of kale crops supplied with different rates of banded or broadcast phosphorus fertiliser. *Crop Pasture Sci.* 62, 840–847. doi: 10.1071/CP10359

Choi, K. Y., Seo, T. C., and Suh, H.-D. (2005). Development of nutrient solution for hydroponics of *Cruciferae* leaf vegetables based on nutrient-water absorption rate and the cation ratio. *Prot. Hortic. Plant Fact.* 14, 288–296.

Chowdhury, M., Ngo, V.-D., Islam, M. N., Ali, M., Islam, S., Rasool, K., et al. (2021). Estimation of glucosinolates and anthocyanins in kale leaves grown in a plant factory using spectral reflectance. *Horticulturae* 7:56. doi: 10.3390/horticulturae7030056

Coleman, J. S. (1986). Leaf development and leaf stress: increased susceptibility associated with sink-source transition. *Tree Physiol.* 2, 289–299. doi: 10.1093/treephys/2.1-2-3.289

Csepregi, K., Coffey, A., Cunningham, N., Prinsen, E., Hideg, É., and Jansen, M. A. K. (2017). Developmental age and UV-B exposure co-determine antioxidant capacity and flavonol accumulation in *Arabidopsis* leaves. *Environ. Exp. Bot.* 140, 19–25. doi: 10.1016/j.envexpbot.2017.05.009

Czégény, G., Mátai, A., and Hideg, É. (2016). UV-B effects on leaves-oxidative stress and acclimation in controlled environments. *Plant Sci.* 248, 57–63. doi: 10.1016/j.plantsci.2016.04.013

Davies, K., and Espley, R. (2013). Opportunities and challenges for metabolic engineering of secondary metabolite pathways for improved human health characters in fruit and vegetable crops. *New Zeal. J. Crop Hortic. Sci.* 41, 154–177. doi: 10.1080/01140671.2013.793730

Dewanto, V., Xianzhong, W., Adom, K. K., and Liu, R. H. (2002). Thermal processing enhances the nutritional value of tomatoes by increasing total antioxidant activity. *J. Agric. Food Chem.* 50, 3010–3014. doi: 10.1021/jf0115589

Escobar-Bravo, R., Klinkhamer, P. G. L., and Leiss, K. A. (2017). Interactive effects of UV-B light with abiotic factors on plant growth and chemistry, and their consequences for defense against arthropod herbivores. *Front. Plant Sci.* 8:278. doi: 10.3389/fpls.2017.00278

Filella, I., and Peñuelas, J. (1999). Altitudinal differences in UV absorbance, UV reflectance and related morphological traits of *Quercus ilex* and *Rhododendron ferrugineum* in the Mediterranean region. *Plant Ecol.* 145, 157–165. doi: 10.1023/A:1009826803540

Fiol, M., Adermann, S., Neugart, S., Rohn, S., Mügge, C., Schreiner, M., et al. (2012). Highly glycosylated and acylated flavonols isolated from kale (*Brassica oleracea* var. *sabellica*) - structure-antioxidant activity relationship. *Food Res. Int.* 47, 80–89. doi: 10.1016/j.foodres.2012.01.014

Fletcher, A. L., Johnstone, P. R., Chakwizira, E., and Brown, H. E. (2013). Radiation capture and radiation use efficiency in response to N supply for crop species with contrasting canopies. *F. Crop. Res.* 150, 126–134. doi: 10.1016/j.fcr.2013.06.014

Flint, S. D., and Caldwell, M. M. (2003). A biological spectral weighting function for ozone depletion research with higher plants. *Physiol. Plant.* 117, 137–144. doi: 10.1034/j.1399-3054.2003.1170117.x

Francisco, M., Tortosa, M., Martínez-Ballesta, M. D. C., Velasco, P., García-Viguera, C., and Moreno, D. A. (2017). Nutritional and phytochemical value of *Brassica* crops from the Agri-food perspective. *Ann. Appl. Biol.* 170, 273–285. doi: 10.1111/aab.12318

Ghasemzadeh, A., Ashkani, S., Baghdadi, A., Pazoki, A., Jaafar, H. Z. E., and Rahmat, A. (2016). Improvement in flavonoids and phenolic acids production and pharmaceutical quality of sweet basil (*Ocimum basilicum* L.) by ultraviolet-B irradiation. *Molecules* 21:1203. doi: 10.3390/molecules21091203

Grammatikopoulos, G., Petropoulou, Y., and Manetas, Y. (1999). Site-dependent differences in transmittance and UV-B-absorbing capacity of isolated leaf

epidermes and mesophyll in *Urginea maritima* (L.) Baker. *J. Exp. Bot.* 50, 517–521.

Hectors, K., Prinsen, E., De Coen, W., Jansen, M. A. K., and Guisez, Y. (2007). *Arabidopsis thaliana* plants acclimated to low dose rates of ultraviolet B radiation show specific changes in morphology and gene expression in the absence of stress symptoms. *New Phytol.* 175, 255–270. doi: 10.1111/j.1469-8137.2007.02092.x

Hectors, K., Van Oevelen, S., Geuns, J., Guisez, Y., Jansen, M. A. K., and Prinsen, E. (2014). Dynamic changes in plant secondary metabolites during UV acclimation in *Arabidopsis thaliana*. *Physiol. Plant.* 152, 219–230. doi: 10.1111/ppl.12168

Heimler, D., Isolani, L., Vignolini, P., Tombelli, S., and Romani, A. (2007). Polyphenol content and antioxidative activity in some species of freshly consumed salads. *J. Agric. Food Chem.* 55, 1724–1729. doi: 10.1021/jf0628983

Heinze, M., Hanschen, F. S., Wiesner-Reinhold, M., Baldermann, S., Gräfe, J., Schreiner, M., et al. (2018). Effects of developmental stages and reduced UVB and low UV conditions on plant secondary metabolite profiles in pak choi (*Brassica rapa* subsp. *chinensis*). *J. Agric. Food Chem.* 66, 1678–1692. doi: 10.1021/acs.jafc.7b03996

Hitz, T., Henkeb, M., Graeff-Hönningera, S., and Munza, S. (2019). Three-dimensional simulation of light spectrum and intensity within an LED growth chamber. *Comput. Electron. Agric.* 156, 540–548. doi: 10.1016/j.compag.2018.11.043

Hofmann, R. W., Campbell, B. D., Fountain, D. W., Jordan, B. R., Greer, D. H., Hunt, D. Y., et al. (2001). Multivariate analysis of intraspecific responses to UV-B radiation in white clover (*Trifolium repens* L.). *Plant Cell Environ.* 24, 917–927. doi: 10.1046/j.1365-3040.2001.00749.x

Holub, P., Nezval, J., Štroch, M., Špunda, V., Urban, O., Jansen, M. A. K., et al. (2019). Induction of phenolic compounds by UV and PAR is modulated by leaf ontogeny and barley genotype. *Plant Physiol. Biochem.* 134, 81–93. doi: 10.1016/j.plaphy.2018.08.012

Ishida, M., Hara, M., Fukino, N., Kakizaki, T., and Morimitsu, Y. (2014). Glucosinolate metabolism, functionality and breeding for the improvement of Brassicaceae vegetables. *Breed. Sci.* 64, 48–59. doi: 10.1270/jsbbs.64.48

Jansen, M. A. K. (2002). Ultraviolet-B radiation effects on plants: induction of morphogenic responses. *Physiol. Plant.* 116, 423–429. doi: 10.1034/j.1399-3054.2002.1160319.x

Kang, W. H., Hwang, I., Jung, D. H., Kim, D., Kim, J., Kim, J. H., et al. (2019). Time change in spatial distributions of light interception and photosynthetic rate of paprika estimated by ray-tracing simulation. *Prot. Hortic. Plant Fact.* 28, 279–285. doi: 10.12791/KSBEC.2019.28.4.279

Kanojia, A., Gupta, S., Benina, M., Fernie, A. R., Mueller-Roeber, B., Gechev, T., et al. (2020). Developmentally controlled changes during *Arabidopsis* leaf development indicate causes for loss of stress tolerance with age. *J. Exp. Bot.* 71, 6340–6354. doi: 10.1093/jxb/eraa347

Kim, D., Kang, W. H., Hwang, I., Kim, J., Kim, J. H., Park, K. S., et al. (2020a). Use of structurally-accurate 3D plant models for estimating light interception and photosynthesis of sweet pepper (*Capsicum annuum*) plants. *Comput. Electron. Agric.* 177:105689. doi: 10.1016/j.compag.2020.105689

Kim, J., Kang, W. H., and Son, J. E. (2020b). Interpretation and evaluation of electrical lighting in plant factories with ray-tracing simulation and 3D plant modeling. *Agronomy* 10:1545. doi: 10.3390/agronomy10101545

Krumbein, A., Schonhof, I., Smetanska, I., Scheuner, E. T., Rühlmann, J., and Schreiner, M. (2010). Improving levels of bioactive compounds in *Brassica* vegetables by crop management strategies. *Acta Hortic.* 856, 37–48. doi: 10.17660/ActaHortic.2010.856.4

Lee, M.-J., Lim, S., Kim, J., and Oh, M.-M. (2012). Heat shock treatments induce the accumulation of phytochemicals in kale sprouts. *J. Hortic. Sci. Technol.* 30, 509–518. doi: 10.7235/hort.2012.12094

Liakoura, V., Bornman, J. F., and Karabourniotis, G. (2003). The ability of abaxial and adaxial epidermis of sun and shade leaves to attenuate UV-A and UV-B radiation in relation to the UV absorbing capacity of the whole leaf methanolic extracts. *Physiol. Plant.* 117, 33–34. doi: 10.1034/j.1399-3054.2003.1170104.x

Linić, I., Šamec, D., Grúz, J., Vujčić Bok, V., Strnad, M., and Salopek-Sondi, B. (2019). Involvement of phenolic acids in short-term adaptation to salinity stress is species-specific among *Brassicaceae*. *Plan. Theory* 8:155. doi: 10.3390/plants8060155

Liu, T., Pan, Y., Lu, Z., Ren, T., and Lu, J. (2020). Canopy light and nitrogen distribution are closely related to nitrogen allocation within leaves in *Brassica napus* L. *F. Crop. Res.* 258:107958. doi: 10.1016/j.fcr.2020.107958

Lois, R. (1994). Accumulation of UV-absorbing flavonoids induced by UV-B radiation in *Arabidopsis thaliana* L. I. mechanisms of UV-resistance in *Arabidopsis thaliana* L. *Planta* 194, 498–503. doi: 10.1007/BF00714462

Majer, P., and Hideg, É. (2012). Developmental stage is an important factor that determines the antioxidant responses of young and old grapevine leaves under UV irradiation in a green-house. *Plant Physiol. Biochem.* 50, 15–23. doi: 10.1016/j.plaphy.2011.09.018

Martínez-Lüscher, J., Brillante, L., and Kurtural, S. K. (2019). Flavonol profile is a reliable indicator to assess canopy architecture and the exposure of red wine grapes to solar radiation. *Front. Plant Sci.* 10:10. doi: 10.3389/fpls.2019.00010

Martínez-lüscher, J., Morales, F., Delrot, S., Sánchez-díaz, M., and Gomés, E. (2013). Short- and long-term physiological responses of grapevine leaves to UV-B radiation. *Plant Sci.* 213, 114–122. doi: 10.1016/j.plantsci.2013.08.010

Meyer, S., Louis, J., Moise, N., Piolot, T., Baudin, X., and Cerovic, Z. G. (2009). Developmental changes in spatial distribution of in vivo fluorescence and epidermal UV absorbance over *Quercus petraea* leaves. *Ann. Bot.* 104, 621–633. doi: 10.1093/aob/mcp144

Morales, L. O., Tegelberg, R., Brosché, M., Lindfors, A., Siipola, S., and Aphalo, P. J. (2011). Temporal variation in epidermal flavonoids due to altered solar UV radiation is moderated by the leaf position in *Betula pendula*. *Physiol. Plant.* 143, 261–270. doi: 10.1111/j.1399-3054.2011.01511.x

Mosadegh, H., Trivellini, A., Ferrante, A., Lucchesini, M., Vernieri, P., and Mensuali, A. (2018). Applications of UV-B lighting to enhance phenolic accumulation of sweet basil. *Sci. Hortic.* 229, 107–116. doi: 10.1016/j.scienta.2017.10.043

Moustaka, J., Tanou, G., Adamakis, I. D., Eleftheriou, E. P., and Moustakas, M. (2015). Leaf age-dependent photoprotective and antioxidative response mechanisms to paraquat-induced oxidative stress in *Arabidopsis thaliana*. *Int. J. Mol. Sci.* 16, 13989–14006. doi: 10.3390/ijms160613989

Neugart, S., Zietz, M., Schreiner, M., Rohn, S., Kroh, L. W., and Krumbein, A. (2012). Structurally different flavonol glycosides and hydroxycinnamic acid derivatives respond differently to moderate UV-B radiation exposure. *Physiol. Plant.* 145, 582–593. doi: 10.1111/j.1399-3054.2012.01567.x

Oh, M. M., Trick, H. N., and Rajashekar, C. B. (2009). Secondary metabolism and antioxidants are involved in environmental adaptation and stress tolerance in lettuce. *J. Plant Physiol.* 166, 180–191. doi: 10.1016/j.jplph.2008.04.015

Olsen, H., Aaby, K., and Borge, G. I. A. (2009). Characterization and quantification of flavonoids and hydroxycinnamic acids in curly kale (*Brassica oleracea* L. *Convar. acephala* var. *sabellica*) by HPLC-DAD-ESI-MS^n. *J. Agric. Food Chem.* 57, 2816–2825. doi: 10.1021/jf803693t

Podda, A., Pollastri, S., Bartolini, P., Pisuttu, C., Pellegrini, E., Nali, C., et al. (2019). Drought stress modulates secondary metabolites in *Brassica oleracea* L. *convar. acephala* (DC) Alef, var. *sabellica* L. *J. Sci. Food Agric.* 99, 5533–5540. doi: 10.1002/jsfa.9816

Podsędek, A. (2007). Natural antioxidants and antioxidant capacity of *Brassica* vegetables: a review. *LWT Food Sci. Technol.* 40, 1–11. doi: 10.1016/j.lwt.2005.07.023

Portes, T. D. A., and Melo, H. C. D. (2014). Light interception, leaf area and biomass production as a function of the density of maize plants analyzed using mathematical models. *Acta Sci. Agron.* 2, 457–463. doi: 10.4025/actasciagron.v36i4.17892

Ramakrishna, A., and Ravishankar, G. A. (2011). Influence of abiotic stress signals on secondary metabolites in plants. *Plant Signal. Behav.* 6, 1720–1731. doi: 10.4161/psb.6.11.17613

Rapacz, M. (2007). Chlorophyll a fluorescence transient during freezing and recovery in winter wheat. *Photosynthetica* 45, 409–418. doi: 10.1007/s11099-007-0069-2

Robson, T. M., Aphalo, P. J., Banaś, A. K., Barnes, P. W., Brelsford, C. C., Jenkins, G. I., et al. (2019). A perspective on ecologically relevant plant-UV research and its practical application. *Photochem. Photobiol. Sci.* 18, 970–988. doi: 10.1039/C8PP00526E

Šamec, D., Urlić, B., and Salopek-Sondi, B. (2019). Kale (*Brassica oleracea* var. *acephala*) as a superfood: review of the scientific evidence behind the statement. *Crit. Rev. Food Sci. Nutr.* 59, 2411–2422. doi: 10.1080/10408398.2018.1454400

Sarlikioti, V., De Visser, P. H. B., and Marcelis, L. F. M. (2011). Exploring the spatial distribution of light interception and photosynthesis of canopies by means of a functional–structural plant model. *Ann. Bot.* 107, 875–883. doi: 10.1093/aob/mcr006

Sperdouli, I., and Moustakas, M. (2014). Leaf developmental stage modulates metabolite accumulation and photosynthesis contributing to acclimation of *Arabidopsis thaliana* to water deficit. *J. Plant Res.* 127, 481–489. doi: 10.1007/s10265-014-0635-1

Stewart, D. W., Costa, C., Dwyer, L. M., Smith, D. L., Hamilton, R. I., and Ma, B. L. (2003). Canopy structure, light interception, and photosynthesis in maize. *Agron. J.* 95, 1465–1474. doi: 10.2134/agronj2003.1465

Strauss, S., Lempe, J., Prusinkiewicz, P., Tsiantis, M., and Smith, R. S. (2020). Phyllotaxis: is the golden angle optimal for light capture? *New Phytol.* 225, 499–510. doi: 10.1111/nph.16040

Toscano, S., Trivellini, A., Cocetta, G., Bulgari, R., Francini, A., Romano, D., et al. (2019). Effect of preharvest abiotic stresses on the accumulation of bioactive compounds in horticultural produce. *Front. Plant Sci.* 10, 1–17. doi: 10.3389/fpls.2019.01212

Vos, J., Evers, J. B., Andrieu, B., Chelle, M., and De Visser, P. H. B. (2010). Functional–structural plant modelling: a new versatile tool in crop science. *J. Exp. Bot.* 61, 2101–2115. doi: 10.1093/jxb/erp345

Walsh, R. P., Bartlett, H., and Eperjesi, F. (2015). Variation in carotenoid content of kale and other vegetables: a review of pre- and post-harvest effects. *J. Agric. Food Chem.* 63, 9677–9682. doi: 10.1021/acs.jafc.5b03691

Wells, R., Burton, J. W., and Kilen, T. C. (1993). Soybean growth and light interception: response to differing leaf and stem morphology. *Crop Sci.* 33, 520–524. doi: 10.2135/cropsci1993.0011183X003300030020x

Xu, P., Su, H., Jin, R., Mao, Y., Xu, A., Cheng, H., et al. (2020). Shading effects on leaf color conversion and biosynthesis of the major secondary metabolites in the albino tea cultivar "Yujinxiang." *J. Agric. Food Chem.* 68, 2528–2538. doi: 10.1021/acs.jafc.9b08212

Xue, H., Han, Y., Li, Y., Wang, G., Feng, L., Fan, Z., et al. (2015). Spatial distribution of light interception by different plant population densities and its relationship with yield. *F. Crop. Res.* 184, 17–27. doi: 10.1016/j.fcr.2015.09.004

Yavaş, İ., Ünay, A., Ali, S., and Abbas, Z. (2020). UV-B radiations and secondary metabolites. *J. Agric. Sci. Technol.* 8, 147–157. doi: 10.24925/turjaf.v8i1.147-157.2878

Yoon, H. I., Kim, J. S., Kim, D., Kim, C. Y., and Son, J. E. (2019). Harvest strategies to maximize the annual production of bioactive compounds, glucosinolates, and total antioxidant activities of kale in plant factories. *Hortic. Environ. Biotechnol.* 60, 883–894. doi: 10.1007/s13580-019-00174-0

Yoon, H. I., Kim, H. Y., Kim, J., and Son, J. E. (2021). Quantitative analysis of UV-B radiation interception in 3D plant structures and intraindividual distribution of phenolic contents. *Int. J. Mol. Sci.* 22:2701. doi: 10.3390/ijms22052701

Yoon, H. I., Kim, D., and Son, J. E. (2020). Spatial and temporal bioactive compound contents and chlorophyll fluorescence of kale (*Brassica oleracea* L.) under UV-B exposure near harvest time in controlled environments. *Photochem. Photobiol.* 96, 845–852. doi: 10.1111/php.13237

Zhao, B., Wang, L., Pang, S., Jia, Z., Wang, L., Li, W., et al. (2020). UV-B promotes flavonoid synthesis in *Ginkgo biloba* leaves. *Ind. Crop. Prod.* 151:112483. doi: 10.1016/j.indcrop.2020.112483

Zietz, M., Weckmüller, A., Schmidt, S., Rohn, S., Schreiner, M., Krumbein, A., et al. (2010). Genotypic and climatic influence on the antioxidant activity of flavonoids in kale (*Brassica oleracea* var. *sabellica*). *J. Agric. Food Chem.* 58, 2123–2130. doi: 10.1021/jf9033909

Conflict of Interest: The authors declare that the research was conducted in the absence of any commercial or financial relationships that could be construed as a potential conflict of interest.

frontiers in Plant Science

REVIEW
published: 11 August 2021
doi: 10.3389/fpls.2021.691651

Response of Plant Rhizosphere Microenvironment to Water Management in Soil- and Substrate-Based Controlled Environment Agriculture (CEA) Systems: A Review

Bo Tan[1], Yihan Li[1], Tiegang Liu[1], Xiao Tan[1], Yuxin He[1], Xueji You[2,3], Kah Hon Leong[4], Chao Liu[1] and Longguo Li[1]**

[1] State Key Laboratory of Hydraulics and Mountain River Engineering, College of Water Resource and Hydropower, Sichuan University, Chengdu, China, [2] Department of Hydraulic Engineering, College of Civil Engineering, Tongji University, Shanghai, China, [3] Department of Civil, Architectural and Environmental Engineering, The University of Texas at Austin, Austin, TX, United States, [4] Department of Environmental Engineering, Faculty of Engineering and Green Technology, Universiti Tunku Abdul Rahman, Kampar, Malaysia

OPEN ACCESS

Edited by:
Francesco Orsini, University of Bologna, Italy

Reviewed by:
Giuseppe Carlo Modarelli, University of Naples Federico II, Italy
Daniel I. Leskovar, Texas A&M University, United States

***Correspondence:**
Chao Liu
liuchao@scu.edu.cn
Longguo Li
lilongguo@scu.edu.cn

Specialty section:
This article was submitted to Crop and Product Physiology, a section of the journal Frontiers in Plant Science

Received: *23 April 2021*
Accepted: *16 July 2021*
Published: *11 August 2021*

Citation:
Tan B, Li Y, Liu T, Tan X, He Y, You X, Leong KH, Liu C and Li L (2021) Response of Plant Rhizosphere Microenvironment to Water Management in Soil- and Substrate-Based Controlled Environment Agriculture (CEA) Systems: A Review. Front. Plant Sci. 12:691651. doi: 10.3389/fpls.2021.691651

As natural agroecology deteriorates, controlled environment agriculture (CEA) systems become the backup support for coping with future resource consumption and potential food crises. Compared with natural agroecology, most of the environmental parameters of the CEA system rely on manual management. Such a system is dependent and fragile and prone to degradation, which includes harmful bacteria proliferation and productivity decline. Proper water management is significant for constructing a stabilized rhizosphere microenvironment. It has been proved that water is an efficient tool for changing the availability of nutrients, plant physiological processes, and microbial communities within. However, for CEA issues, relevant research is lacking at present. The article reviews the interactive mechanism between water management and rhizosphere microenvironments from the perspectives of physicochemical properties, physiological processes, and microbiology in CEA systems. We presented a synthesis of relevant research on water–root–microbes interplay, which aimed to provide detailed references to the conceptualization, research, diagnosis, and troubleshooting for CEA systems, and attempted to give suggestions for the construction of a high-tech artificial agricultural ecology.

Keywords: controlled environment agriculture (CEA), water management, rhizosphere microenvironment, microbe, root exudates

INTRODUCTION

The rapid expansion of modern cities has brought unprecedented challenges to sustainable development. It has caused urban complex diseases, such as environmental pollution and resource shortages (Despommier, 2011; Xie et al., 2017). While agroecology is suffering tremendous damage, requirements for the quality of agricultural products are getting higher, thus creating

a contradictory situation within the current agroecological system (Orsini et al., 2013). In particular, with reference to European food safety policy, many countries and regions have stricter requirements for food safety and hygiene, labeling rules, regulations on plant health, control of pesticide residues, and food additives. Environmental issues bring people to contemplate the future of agriculture. As one of the solutions, high-tech agricultural technology is currently known as the manifestation of sustainable intensification (Pretty, 2018). It has taken the lead in large-scale development in developed regions, including the Americas and Europe. Through the construction of urban high-tech agricultural projects, one can solve the problems of climate change and urban food supply efficiently (Fatemeh et al., 2018; Fricano and Davis, 2019; Farhangi et al., 2020).

Controlled environment agriculture (CEA) is becoming a backup technology to cope with resource consumption and potential agricultural environmental deterioration in the future (Despommier, 2011). In CEA systems, the key parameters of production are artificially controlled. By controlling light, temperature, CO_2, and humidity, indoor environments can become feasible for the growth of plants inside built-up spaces (Fatemeh et al., 2018; Farhangi et al., 2020). Various environmentally controlled structures can be classified as CEA systems, including soil-based CEA systems (e.g., high tunnels, greenhouses, growth chambers, and warehouse farming) and soilless cultivation (e.g., hydroponics, aeroponics) (Niu and Masabni, 2018).

Through long-term development and practices, CEA represents highly dependent modern agricultural technology. If a CEA system has more controllable environmental factors, correspondingly, it has a higher degree of closure and system integrity (Shi et al., 2009; Despommier, 2011; Hong et al., 2014; Wang et al., 2017; Fatemeh et al., 2018; Singh H. et al., 2020). The practice has shown that, under precise artificial regulation, water consumption can be reduced by 90%, and the yield can reach 20 times than that of incumbent agricultural production practices (Barbosa et al., 2015; Fatemeh et al., 2018). However, high-energy consumption, poor nutrient condition stability, the potential proliferation of pathogenic bacteria, and degradation of system productivity, etc., could be the mixture of uncontrollable factors that hampers CEA development (Hosseinzadeh et al., 2017; Niu and Masabni, 2018; Salazar-Moreno et al., 2020).

The popularization of CEA requires great effort, especially from developing countries where the substrate-based low-to-medium-cost CEA systems have not yet formed an industrial scale. The main technical difficulty lies in the scarcity of implementation standards for planting substrate management. The rhizosphere is the most valuable constituent of a CEA system (Zhang et al., 2019), and water is responsible for substrate decomposition, mass balance, and energy conversion. It is also vital for the microbial community (Singh et al., 2011; Arikan and Pirlak, 2016). At this stage, we propose that the first step is to establish an understanding of the nature of the rhizosphere microenvironment based on water management.

As growing cycles of replanting can be very short (e.g., less than 4 weeks for some leafy greens) in CEA systems, replant disease and negative legacy effects during certain planting generations can be significant due to nutrient consumption, rhizosphere bacterial community reshaping, and unfavorable rhizodeposition (Yuan et al., 2018; Sun et al., 2019; Yao et al., 2020). There were clear legacy effects from moisture regimes prior to planting on soil, specifically in terms of physicochemical properties, plant growth and nutrition, and the formation of microbial responsiveness (Cavagnaro, 2016). Hence, while CEA systems satisfy plant growth, proper management of substrate water still needs to improve by increasing the input of endogenous organic matter, reducing the demand for exogenous mineral nutrients, and enhancing beneficial biological activity (Jain et al., 2020). Water management is, therefore, a challenge with significant influence on the availability and sustainability of the planting substrate (Qin et al., 2019) that plays a vital role in both eliminating negative legacy effects and maintaining the long-term health of the rhizosphere for the whole system. Hence, water management is of great importance for successive planting generations (de Zeeuw et al., 2011; Poncet et al., 2015; Napawan and Townsend, 2016). The aim of water management in CEA in this review is to (1) regulate the availability of nutrients in the rhizosphere microenvironment, (2) regulate the physiological processes of plants, and (3) construct the microbial community structure for system benign output.

In this review, first, we summarize the advances and distribution of practical CEA systems worldwide, emphasize the characteristics of rhizosphere microenvironments and the role of water management in CEA systems, and analyze the influences on the physicochemical properties of the substrate, including aeration, solute dissolution, nutrient availability, transformation, and consumption. Next, we consider the effect of water content variation on the biochemical processes of the rhizosphere, address the interaction of root exudation and rhizosphere moisture stabilization, and discuss the rhizosphere water stress tolerance under water-limited conditions. Afterward, we analyze the influence of water content variation on microbial community structure and discuss the influences on microbial population, nutrient type, metabolism, and proliferation. Accordingly, we then summarize relative practice cases, showing that establishing a reasonable and stable rhizosphere microbial community structure is beneficial to the benign output of the CEA system. Then, we address the model characterization for microbial traits for microenvironment interaction and discuss the interplay of the abovementioned regulatory phenomena. Finally, we conclude by discussing the limitations and technical challenges of the current research on CEA systems, proposing two issues on the possibility and potential for future science and technology to improve water management of CEA, and offering suggestions about the construction of high-tech artificial agricultural ecologies for the future. The literature retrieval report related to this review was attached to **Supplementary Material**.

While we attempted to synthesize the available literature by summarizing results into practicable management methods, we acknowledge that there are many factors that may further affect the microenvironment that we were not able to introduce in detail, including root exudation patterns and responses in mixed communities, relationships between plant signal and microbial response, molecular mechanisms of host plants against

pathogens, growth-promoting characteristics of endophytic bacteria and rhizobacteria, etc. (Ullah et al., 2019; de Vries et al., 2020; Williams and de Vries, 2020; Yadav et al., 2020).

Furthermore, our understanding of the response of rhizosphere microenvironments to artificial water management is hampered by the fact that there is only a very limited number of available studies on how water conditions in CEA relate to substrate physicochemical properties, root physiological processes, and rhizosphere microbiology; of those studies that do concern this topic, only a modest proportion focuses on controlled environments. In this review, we argue that an increased understanding of the complex feedback between water management and rhizosphere microenvironment evolution will pave the way for the conceptualization, construction, research, diagnosis, and troubleshooting of CEA systems.

CONCEPT AND CHARACTERISTICS OF CEA SYSTEMS

Understanding of the CEA System

Modern controlled environment agriculture has become an emerging form of land use in many developed regions (Sanye-Mengual et al., 2018), and the emergence is caused by the need to meet growing centralized demand for agricultural products and requirements for higher food security (Eigenbrod and Gruda, 2015). Advanced agriculture systems provide opportunities to improve food supply, the health of residents, the local economy, social integration, and environmental sustainability altogether (Orsini et al., 2013). An emerging CEA system has some notable characteristics: resource intensiveness, controllability, environmental fragility, high energy consumption, and high output.

Meanwhile, the CEA system usually has different manifestations. In vertical agriculture, plant growth substrates are strictly isolated and the system regulates nutrients to achieve clean, efficient, and high yield (Despommier, 2011; Fatemeh et al., 2018). In plastic greenhouse agriculture, the soil ecosystem is not completely isolated because the water, solutes, and microbes in the greenhouse soil still have interactions with the external environment, but the air composition is controlled, especially for some greenhouses with good airtightness (Shi et al., 2009; Hong et al., 2014; Wang et al., 2017; Singh H. et al., 2020). In closed hydroponic agriculture, plants are cultivated by using a mixture of nutrient salts and water instead of soil. The water is under treatment while circulation, therefore, the interaction between plant roots and the rhizosphere microenvironment is eliminated (Hosseinzadeh et al., 2017).

In a narrow sense, a CEA system is a set of agricultural planting facilities established in a specific enclosure. However, spatial isolation cannot accurately differentiate its intrinsic properties from traditional cultivation systems (Orsini et al., 2013). Therefore, a more specific definition could be, an industrialized agriculture system established in an independent space to maintain the continuous and stable regulation of plant growth factors through intensive management, thereby achieving optimal agricultural production and system sustainability (Eigenbrod and Gruda, 2015; Burchi et al., 2018).

Advances and Distribution of Emerging CEA Practices Worldwide

In the context of the global agricultural revolution, the CEA system construction is meant to be combined with actual local conditions and social needs, and the functions of the CEA system are improving to serve the local food production (Napawan and Townsend, 2016; Clucas et al., 2018; Amato-Lourenco et al., 2020; Zulfiqar et al., 2020). Decades ago, in Israel, precision agriculture in greenhouses was employed for biological control (Boari et al., 2008). This approach allowed the irrigation system to be more compatible with the integrated treatment of biological control. In recent years, there has been a growing number of innovative treatments, using irrigation systems, such as the application of biosurfactants (Singh R. et al., 2020), generation of nanobubbles (Xiao et al., 2020), air injections (D'Alessio et al., 2020), and so on. In the Netherlands (Hemming et al., 2020), artificial intelligence (AI) algorithms and sensor data were used to determine climate set points and crop management strategies in greenhouse operations. Based on this technology, a greenhouse that could control ventilation, irrigation, heat, light, and CO_2 was developed to maximize the net profit. As shown in **Figure 1**, at present, many representative emerging CEA systems in the world are mainly distributed in North America, Europe, the Middle East, etc., and their development orientation is toward integration into the urban context, aerospace engineering, and exploration into the integration of emerging AI and Internet of Things (IoT), and so on (Fatemeh et al., 2018; Lakhiar et al., 2018; Hemming et al., 2020; Halgamuge et al., 2021; Shuyu et al., 2021).

Significance and Characteristics of the Soil- and Substrate-Based CEA Systems

Studies have shown that the development of CEA is driven by policy and economic factors (Hunold et al., 2016; Ghosh et al., 2018). On a global scale, however, the emerging CEA systems are currently incompatible with major food supplies due to high land prices and pollution in cities (Eigenbrod and Gruda, 2015). The soil- and substrate-based CEA systems, as a transitional form of traditional agriculture to agriculture industrialization, are integral parts of the agricultural supply chain in many parts of the world and are of central importance to research, technological improvement, and acceptance by the global agricultural economy. At the current stage of global CEA development, energy ratio and economic benefits are key factors (Farhangi et al., 2020; Hemming et al., 2020; Ntinas et al., 2020), while solid substrates have the advantages of low energy consumption, relatively high stability, and nutrient accumulation, which will have long-term existence in CEA development (Sanye-Mengual et al., 2018). Hence, compared with other forms of cultivation methods (the roots are in direct contact with the solution and air and do not adhere to solids), such as hydroponics

Netherlands (Amsterdam): High-tech urban agriculture was established to make growing food vertically inside built-up spaces feasible.

Netherlands (Bleiswijk): Greenhouse was tested to maximize net profit by controlling environmental factors via artificial intelligence (AI) techniques.

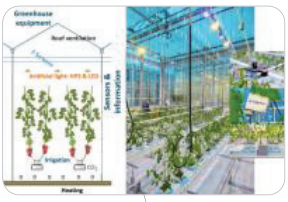

South Korea: Nutrient management was conducted for reducing the contaminant load on soil and groundwater from plastic greenhouse cultivation. This practice can serve as a baseline for the long-term monitoring of greenhouse nutrient loads.

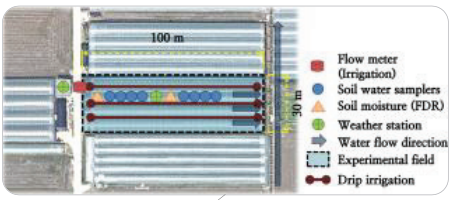

UK: Presented a glasshouse and growth chamber–based speed breeding approaches with supporting data from experimentation with several crops.

Germany: Study the optimization of LED lamp radiant energy control for plant management.

USA: Grew plants aeroponically without using pesticides that are sometimes necessary to control pathogens through using liquid biocontrol. Hence astronauts on the space shuttle would likely have to rely upon an on board aeroponics system to grow vegetables.

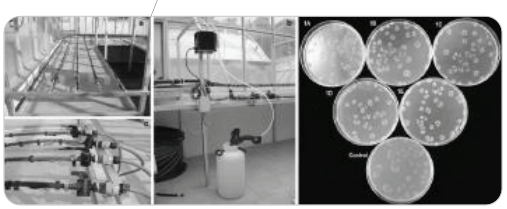

Israel: Biocontrol agents were used for plants and soil protection. The system could be used for soil release of biocontrol agents, to control all the bio-constraints constraints attacking or threatening the root system.

Turkey: High-tech greenhouses were employed for geothermal utilization. Based on a geothermal well at high temperatures and CO_2 application in a Venlotype greenhouse, high yields and a short payback period were achieved in terms of economic point of view.

FIGURE 1 | Exploration and application of controlled environment agriculture (CEA) systems worldwide. The figure compiled information based on the following references: Boari et al. (2008), Hong et al. (2014), Eigenbrod and Gruda (2015), Tuzel and Oztekin (2016), Ghosh et al. (2018), Lakhiar et al. (2018), Farhangi et al. (2020), Hemming et al. (2020).

and aeroponics, the use of solids as a growth substrate is still irreplaceable.

Considering the cost of the CEA system, managers always hope to improve its sustainability and expect to find more scientific approaches toward improving stability and resistance (Balafoutis et al., 2017; Al-Kodmany, 2018). A high-tunnel greenhouse is widely used in China (Shi et al., 2009). Research studies have shown that intensive production had a significant impact on soil and water quality. The rate and composition of fertilizers applied to vegetable plants were controlled for higher yield; meanwhile, it was equally important to protect the nutrient balance in rhizosphere soil and groundwater safety. In South Korea (Hong et al., 2014), the ecological safety of soil and groundwater was also closely considered during the implementation of plastic greenhouses. The substrate temperature is another factor that influences greenhouse cultivation. In Turkey, the CEA system (the main structure was a Venlo-type greenhouse, with 8 m width, 6 m gutter, and 7 m ridge

height) took advantage of its geothermal resource by using heat exchanger-based heating systems on geothermal wells (Tuzel and Oztekin, 2016). Such heating systems enabled the CEA to obtain high yields and short payback periods in terms of an economic point of view for long-season production.

However, current pilots are quite scattered worldwide, and no universal technical specifications and standards have been formed, resulting in slow promotion and weak reproducibility (Shamshiri et al., 2018). To address these problems, soil- and substrate-based cultivation is emphasized in the following sections of this review. Since we discussed the relationship between water and crop plants, many crops are relatively tall and with large biomasses (such as maize); traditional hydroponics and aeroponics have not yet been applied to many food crops. On the other hand, since the water is treated in the recycling process, hydroponics and aeroponics are generally not involved in the concept of the rhizosphere microenvironment. Therefore, the CEA system discussed in this study refers specifically to soil- or substrate-based cultivation. With these considerations, the CEA mainly refers to soil- and substrate-based systems unless otherwise specified in this study.

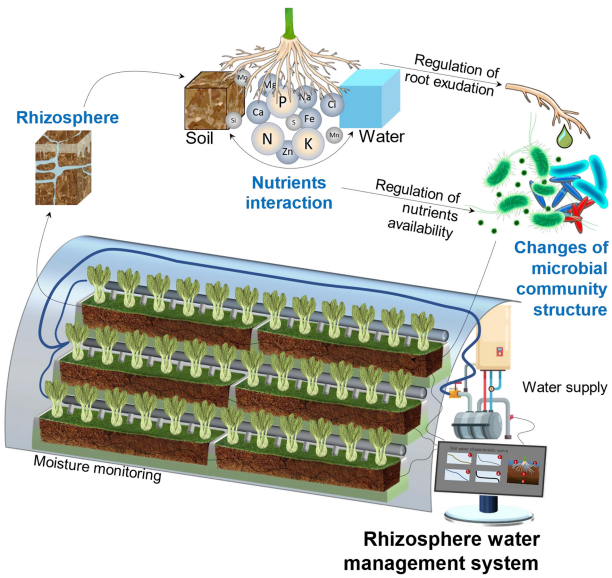

FIGURE 2 | Important influential units of a CEA system under rhizosphere water management (drawn by the authors).

The Issue of Water Management for the Growth Media in CEA Systems

Comparing with the emerging CEA systems, the underlying logic for the establishment of soil- and substrate-based CEA is sustainability and low-resource consumption, which require inheriting the traits of rhizosphere microenvironments from natural soil-plant interaction. Water management is a basic yet efficient method for building a stable rhizosphere microenvironment (Gao et al., 2019). In terms of cultivation, the difficulty of CEA development lies in the management of growth substrates, nutrition, and irrigation (Orsini et al., 2013; Hong et al., 2014). Water content variation also affects physical and chemical properties and root exudation and then drives microbes to change their resource utilization strategies under different nutrient conditions (Preece and Penuelas, 2016). As a result of these changes in rhizosphere microenvironments, microbial populations and community structures can be determined.

The practice has proven that growth media substrates can significantly change the water status of their rhizospheres as compared to soil (Banitalebi et al., 2019; Videgain-Marco et al., 2020). These materials include a wide range of organic- and mineral-based substrates (mineral wool, peat, coconut fiber, lignite, straw, composted bark and wood fiber, perlite, vermiculite, sandy soil, clayey soil, etc.) (Gajc-Wolska et al., 2008; Słowińska-Jurkiewicz and Jaroszuk-Sierocińska, 2011). The physical properties of these materials are varied, and such discrepancies give a great scope for using multiple components for combination. Wider ranges of properties, such as volumetric density (30–1,400 $kg{\cdot}m^{-3}$), porosity (45–99% vol), water-holding capacity (-10 cm H_2O, 15–85% vol), and air-holding capacity (–10-cm H_2O, 20–80% vol), can also be obtained to adapt to a particular planting pattern (Lazny et al., 2021).

Compared with natural agroecology, fragility is the major challenge for the sustainability of substrate-based CEA, which means that the system is less resistant to adversity, pests, diseases, and pathogenic bacteria (Niu and Masabni, 2018) and, thus, has to rely on precise and intensive management to maintain stability. As shown in **Figure 2**, the rhizosphere is the most important area of a CEA system. It refers to the small volume of soil or substrate that is directly influenced by root exudations and associated microbes (Pii et al., 2015; Ahmadi et al., 2017). Different from the microbial abundance in the natural ecological environment, which is dominated by a diversity of local plant species and stable microbiomes (Qin et al., 2019), a CEA system depends on planned artificial regulation, such as substrate selection, water management, crop rotation, soil heritage, and inoculation of symbiotic bacteria. A well-managed rhizosphere has a higher microbial abundance and provides good nutrient accessibility with higher turnover rates (Herman et al., 2006; Landi et al., 2006; Holz et al., 2018a).

Water management for growth media, which is one of the most basic projects for agriculture, is particularly important for CEA systems. Based on supporting plant growth, balancing the input of endogenous organic matter and demand for exogenous mineral nutrients is the key to the optimization of system stability and low-resource consumption (Qin et al., 2019). It is crucial to reduce the maintenance cost brought about by substrate renewal on one hand, but, more importantly, to serve a long-term, sustained, and high-yield artificial agriculture system by constructing a specific rhizosphere microenvironment (Philippot et al., 2013; Qin et al., 2019). Furthermore, proper water management should focus on the availability of nutrients related to microbiology, as it is crucial to fostering the presence of beneficial microbes and reducing the level of pathogenic microbes, thus achieving system sustainability and benign output (Fierer, 2017; Degrune et al., 2019).

EFFECT OF WATER MANAGEMENT ON THE AVAILABILITY OF THE CEA SUBSTRATE *VIA* AFFECTING ITS PHYSIOCHEMICAL PROPERTIES

Aeration and Solute Dissolution

In rhizosphere microenvironments, water content has a large influence on the physicochemical properties of the substrate. The overall resource utilization of the system is related to O_2 concentration (Chen et al., 2019b; Li Y. et al., 2020), solute transport and diffusion (Nobel and Cui, 1992; Carminati et al., 2009; Ahmadi et al., 2017), and substrate decomposition of microbes (Tang et al., 2016; Zhang et al., 2020). A deeper understanding of its operating mechanism is the prerequisite for proper management.

In saturated substrates, pores are filled with water and the nutrients are sufficiently dissolved and supplied to plants for uptake. However, stagnant water brings about anaerobic conditions. At this stage, organic matter, rhizosphere exudates, and other substances are used for anaerobic decomposition (Tang et al., 2016; Zhang et al., 2020). A longer anaerobic period may cause major changes to the structure of the substrate microenvironment system because the anaerobic conditions are conducive to the growth of anaerobic bacteria. Anaerobic experiments have observed an increase in the abundance of methane-producing archaea and a significant increase in methane emissions (Miller et al., 2001; Bao et al., 2014). Therefore, an increase in water content is conducive to improving the activity of anaerobes and the utilization of substrates (Tang et al., 2016), but, from another perspective, it exacerbates the net loss of organic carbon, which needs to be evaluated by system managers.

When water content drops to field water-holding capacity (50–80% of the saturated water content), aerobic conditions are initially formed. In this case, large pores are filled with air, which is conducive to the diffusion of O_2, and small pores are filled with water, which is conducive to the diffusion of soluble substrates. The soil or substrate emits a large amount of CO_2 through heterotrophic respiration. At this time, aerobic metabolic activity reaches its maximum, while the CO_2 flux is at the maximum (Zhou et al., 2014). In general, microbial activity at approximately moderate humidity (60% of water-filled pore space) is higher than activity at very wet or very dry conditions (Suseela et al., 2012).

As the substrate dries, the interconnection of pores promotes the formation of aerobic conditions. Meanwhile, roots shrink and partially detach from substrates, and air fills into the gaps between the roots and substrates. Consequently, the lower hydraulic conductivity induces the restriction of water and transport of nutrients to the roots and limits the activity of the rhizosphere microenvironment (Nobel and Cui, 1992; Carminati et al., 2009; Ahmadi et al., 2017). For substrates, solute transport and diffusion are reduced due to thinner water film and a more tortuous transfer path on a particle surface, thus limiting the rate of substrate diffusion to microbial cells (Stark and Firestone, 1995). Finally, concentrations of free ions in the residual solution increase, including calcium carbonate, sodium, potassium (K), phosphorus (P), and other redox-sensitive compounds (aluminum, iron, molybdenum, etc.) relevant to plants (Bouskill et al., 2016b).

Low water content causes a decrease in water potential in cells, thereby reducing hydration and activity in enzymes (Stark and Firestone, 1995), restricting the migration of enzymes for decomposers to decompose the substrate (Manzoni et al., 2012), thus inhibiting microbial activity. In general, a decrease in water content corresponds to a slowdown of biogeochemical processes in the rhizosphere microenvironment. Therefore, the rhizosphere microenvironment under water-saving measures undergoes resource redistribution, forcing microbes to change their way of resource utilization, such as carbon and nitrogen (N) utilization pathways (Schimel et al., 2007; Bachar et al., 2010).

Nutrient Availability

Variation in water content is one of the greatest impacts on the rhizosphere microenvironment (Fierer, 2017); as a result, nutrient availability is determined. Considering the nutritional requirements of the CEA system, it is necessary for managers to focus on the nutrient content of the substrates. It is an economic and environmentally friendly approach to maintaining a sustainable nutritional supply through water management.

Compared with the natural agricultural environment, nutrient availability in the CEA system is more sensitive to water changes (Niu and Masabni, 2018; Shamshiri et al., 2018). In natural systems, water affects the dynamics of nutrient availability by altering the balance between the death and growth of organisms; thus, the overall balance can be relatively stable in the long term (Blazewicz et al., 2014). However, the CEA system is not an ecosystem in any case; it largely relies on artificial control. For optimal nutrient conversion to production, it is important to coordinate fertilization with water management, because nutrients must be in an available form before roots can absorb them (Holland et al., 2018). The dry substrate has difficulty in providing available nutrients because the substrate has great matric potential for nutrients, which makes it impossible to uptake by the roots (Somma et al., 1998; Vetterlein and Jahn, 2004; Jin et al., 2015). This part of the nutrients is the nutrient pool of the substrate and is retained by 0.1–1.5 MPa of matric potential (an approximate wilting point). When water content increases, the potential decreases; thus, nutrients can be released for roots to absorb, including NH_4^+, NO_3^-, $H_2PO_4^{2-}$, HPO_4^{2-}, K^+, Ca^{2+}, Mg^{2+}, SO_4^{2-}, BO_3^{3-}, Cl^-, Cu^{2+}, Fe^{2+}, Fe^{3+}, Mn^{2+}, MoO_4^{2-}, Zn^{2+}, etc. (Kim et al., 2009). In addition to ion availability, organic matter in CEA systems is a key nutrient factor in sustainable operation. Water content affects respiration by changing the O_2 content, composition and activity of microbes, and utilization of substrates (Linn and Doran, 1984a; Williams, 2007; Zhou et al., 2014; Sierra et al., 2015), hence determining the decomposition of organic matter (Huang et al., 2016). The detailed transformation and consumption of macroelements, the complex interplay of microbial trophic type, substrate nutrition variation, and roots exudation in relation to water management are discussed in the following sections.

Macroelements Transformation and Consumption

A sustainable CEA system must have "living" substrates instead of inert substrates like rock wool or perlite; thus, the CEA system has strict requirements for nutrient use efficiency, which is a water–fertilizer coupling problem (Wang et al., 2018; Rasool et al., 2020). Within the limited rhizosphere, the transformation and consumption of macroelements are very sensitive to water content variation (Liu et al., 2015; Koch et al., 2020). Water management is even more important than fertilizer management in certain water-deficient conditions (Epie and Maral, 2018). N, P, and K are the most important macroelements, and their occurrences and transformations exhibit different characteristics in water content dynamics with the participation of microbes (Dhaliwal et al., 2019).

Nitrogen

Nitrogen exists in soil or substrate systems in many forms and changes (transforms) very easily from one formation to another (Cameron et al., 2013). The main forms of N include organic N, NH_4^+-N, and NO_3^--N. N is among the vital elements needed for plant growth. Since plants cannot use or take N directly from the air, uptake is through N forms that include ammonium and nitrate in substrates (Hachiya and Sakakibara, 2017). However, in the rhizosphere, their transformation process is related to nitrification and denitrification by microbes, while water is the key environmental factor to regulate this process and the transformation balance is closely related to rhizosphere water content variation (Chen et al., 2019b). The microbes involved are mainly ammonia-oxidizing archaea (AOA), ammonia-oxidizing bacteria (AOB), nitrite-oxidizing bacteria (NOB), etc. (Gleeson et al., 2010).

As for N transformation in the substrate, the importance of O_2 as a controlling factor in regulating the magnitude and pathway of N has been recognized (Wrage et al., 2001); however, O_2 concentrations are rarely measured in practice, and soil moisture content has generally been accepted as a measurable proxy for O_2 availability (Zhu et al., 2013). Water-filled pore space (WFPS) is a widely used moisture indicator, as it provides integrated information about water content, total porosity, and O_2 concentration of a soil or substrate system (Zhu et al., 2013; Qin et al., 2020). As shown in **Figure 3**, quick detection could be done by evaluating the N status based on WFPS and moisture content empirically or experimentally, because a gradual increase of the WFPS reflects the conversion of nitrification to denitrification. When the WFPS is 35–60%, O_2 diffusion is favorable, the metabolic activity of aerobic microbes is at its most vigorous, and nitrification is dominant. Among them, net N_2O emission is the lowest at approximately 40% WFPS (He et al., 2019), and more favorable conditions for nitrification is at 60% WFPS (Linn and Doran, 1984b; Skopp et al., 1990; Parton et al., 1996). When the WFPS is at 70–75%, O_2 dissolution and diffusion rates decrease significantly, and it is impossible to provide O_2 to aerobic microbes in time, which promotes denitrification and keeps the N_2O emission rate at a high level (Orwin et al., 2010). Among them, 70–75% WFPS is a favorable condition for N_2O emission. Denitrification consumes a large amount of NO_3^- and allows N_2O emission to reach its peak (Novosad and Kay, 2007; Qin et al., 2020). With increasing WFPS, O_2 diffusion into the soil becomes restricted and the proportion of soil volume, which is anaerobic, increases. Due to the high mobility of NO_3^-, it may quickly diffuse into a substrate compartment with low O_2 content, thereby providing substrate for biological denitrification. In addition, the massive production of NO_3^- also promotes the volatilization of NH_3. When WFPS is at 75–95%, the nitrification rate decreases significantly, and when WFPS is at approximately 80%, the denitrification effect could be at its utmost (Kool et al., 2011). When a substrate is nearly saturated (WFPS 90%), a large amount of NO_3^- is lost and the production of N_2O is mainly determined by NO_3^- denitrification. When WFPS is at 100–125%, it becomes extremely anaerobic (Qin et al., 2020). Complete denitrification may occur, and NO_3^- becomes the main substance for denitrification. As a result, N_2O is completely converted to N_2 under such anaerobic conditions (Zhu et al., 2013). This is because the anaerobic environment hinders the emission of N_2O and promotes its further reduction to N_2 (Qin et al., 2020).

Phosphorus

Phosphorus exists in various statuses and differs in its behavior and fate in soils or substrates (Hansen et al., 2004). Under water content variation, P has transformations among solution P (Sol-P), labile P (L-P), and non-labile P (NL-P). Sol-P is completely accessible for plants, but the bulk of P is virtually inaccessible, which can be described as NL-P. This fraction accounts for more than 90% of total P and is present as an insoluble and fixed form, including primary phosphate minerals, humus P, insoluble phosphate of calcium, iron and aluminum, and P fixed by hydrous oxides and silicate minerals (DeLonge et al., 2013). L-P is presented in phosphate precipitations and is held on substrate surfaces. It is also in rapid equilibrium with Sol-P. Consumption of Sol-P disturbs the equilibrium between Sol-P concentration and the L-P pool at a solid phase, which leads to supplementation for Sol-P (Bünemann, 2015).

Phosphorus in soil or substrate is mostly immobile and unavailable to plants and is further restricted when water availability is limited (Somaweera et al., 2017). Thus, the water content can be important to determining the P bioavailability and net primary productivity in planting systems (DeLonge et al., 2013). In general, higher water content is beneficial for the release of L-P and the improvement of P bioavailability, while, in saturation, reduction *via* anaerobic conditions may contribute to Sol-P release and result in the highest Sol-P concentration at wet extremes (Cournane et al., 2010).

The change of L-P content also follows a similar rule as Sol-P. Takahashi et al. (2016) found that L-P increased steadily when the water content was higher than the standard level (1 kg/kg) in incubated growth substrate. Epie and Maral (2018) suggested that L-P is best for root development, tillering, and growth when the water content is more than 75% field capacity; however, P availability is greatly reduced when the water content is less than 30% of field capacity. At this point, the effect of fertilization

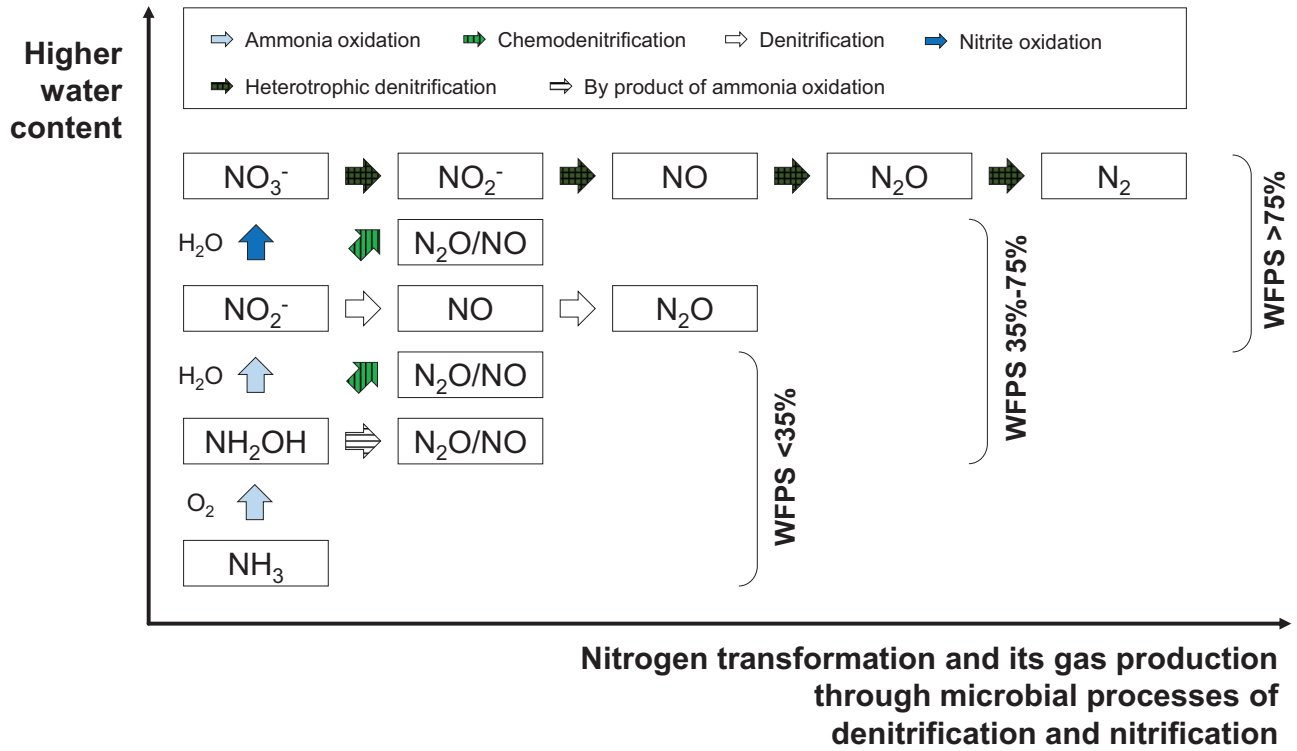

FIGURE 3 | A schematic diagram of the main pathways of nitrogen (N) transformation and its gas production vs. varied water content in substrate. The figure is remade by compilation of the following research: Bateman and Baggs (2005), Gleeson et al. (2010), Kool et al. (2011), Zhu et al. (2013).

is limited by water stress. Yang et al. (2009) indicated that an ideal L-P content was obtained at 50% of field capacity, as it was suitable for substrate phosphatase to enhance activity, and thus promoted the release of L-P from NL-P.

As irrigation after extreme drying, L-P content increased significantly; this phenomenon was found in Styles and Coxon (2006); DeLonge et al. (2013), and Sun et al. (2018). But it has to be noted that water content is positively related to L-P dissolution; meanwhile, it was regulated by microbial activities. Vandecar et al. (2011) found a delayed response of L-P release under high-water content (50–66%), while DeLonge et al. (2013) indicated that large pulses of water input may facilitate L-P release, but the process has an 8 days delay. Microbial activities play an important role in P mineralization and immobilization and consequently affect L-P supplementation and depletion. It is clear that wet-dry circulation affects L-P content *via* the alternation between community composition and acceleration of organic matter decomposition, thus enhancing P mineralization (Sun et al., 2018). Similar results demonstrated that microbial immobilization of P was stimulated initially; however, a time lag of up to 10 days was found due to subsequent mineralization (Campo et al., 1998).

Altogether, how does L-P release largely depend on antecedent and current substrate moisture conditions (Howard and Howard, 1993; Yuste et al., 2007). L-P can be increased in the short term by drying and rewetting, with its effect dependent on both the size and timing of water management (DeLonge et al., 2013).

Potassium

Potassium is another primary nutrient required by plants. K is found within plant cell solutions and is used for maintaining the turgor pressure of the cell (meaning it keeps the plant from wilting) (Abd El-Mageed et al., 2017; Abd El-Gayed and Bashandy, 2018). In addition, K plays a role in the proper functioning of stomata (cells located at the bottom of leaves that open and close to allow water vapor and waste gases to escape) and acts as an enzyme activator (Xu et al., 2020). In a given substrate, total K is almost certain because it depends on the presence of K, which bears primary and secondary minerals, namely, fixed or mineral K (Ghiri and Abtahi, 2011; Škarpa and Hlušek, 2012). Hence, managers are more concerned about how water content variation affects the transformation between soluble K (Sol-K) and exchangeable K (Ex-K).

Exchangeable-K is the major bioavailable form of K in substrates. There is rapid equilibrium between Sol-K and Ex-K, which can be described by the Gapon equation (Beckett and Nafady, 1967). The consumption of Sol-K at a root-solid matrix interface causes a readjustment of Ex-K to satisfy the equilibrium equation as mentioned above, releasing more Ex-K into solution, thereby buffering Sol-K against consumption.

With regard to Sol-K, higher water content is conducive to K dissolution while also contributing to K dilution, depending on the substrate components that adsorb K. Research from Abd-Elrahman and Taha (2018) showed that humates and sulfates have the strongest ability to hold Sol-K because they prevent K^+

ions from leaching, owing to the influence of multiple functional groups including carboxyl, phenol, and hydroxyl that, in turn, contribute to K^+ binding (Wang and Huang, 2001). Marchuk and Marchuk (2018) demonstrated that a high level of Sol-K has deleterious effects on the structural stability of a growth matrix, while the fraction of clay minerals could decrease cation exchange capacity and increase a mineral fraction of K, resulting in K fixation as a non-exchangeable form. As Ex-K diffusion and Sol-K are consumed, an ever-widening zone of K consumption spreads out from the root surface, leading to the development of a rhizosphere several millimeters in radius (Kuchenbuch et al., 1986; Hamoud et al., 2019). Therefore, the amount of K is closely related to the cation exchange capacity of the substrate.

In practice, Abd-Elrahman and Taha (2018) showed that soils amended with either humate or sulfate under 50% of the irrigation requirement recorded the highest increases in the fraction of Ex-K; however, increasing the irrigation water level from 75 to 100% led to a significant reduction in the Ex-K fraction, suggesting that the increasing level of water irrigation seemed to be of no further significant effect on the Ex-K content. Higher water content does not increase Ex-K content, and this result also applies to longer-term effects, as consistent results were found in the study by Škarpa and Hlušek (2012). As with the importance of Sol-K and Ex-K, fixed or mineral K is the K source for sustained supply. Ghiri and Abtahi (2011) suggested K-bearing minerals could be considered as the K pool; meanwhile, intentionally, K fixation by wetting and drying treatment could also be a practical method for conservative planting.

EFFECT OF WATER MANAGEMENT ON ROOT PHYSIOLOGICAL PROCESSES IN CEA

Root Growth and Exudation

Root exudates are fluids emitted through roots. These substances influence the rhizosphere around roots to inhibit harmful microbes and promote plant growth (Williams and de Vries, 2020). Root exudates contain a wide variety of molecules that are released into soil (Bobille et al., 2019). They act as signaling messengers that allow for communication between microbes and roots (Calvo et al., 2017). In CEA systems, rhizosphere exudation has more significance because the rhizosphere is bounded; hence, roots, microbes, exudates, and all sensitive substances are squeezed into the limited volume of a substrate cube. Thus, the impact of water changes is higher than in the natural environment (de Vries et al., 2020).

Plants release a large part of their photosynthetic products into soil or substrate through rhizodeposition, including low-molecular-weight compounds such as polysaccharides, amino acids, and organic acids (Fischer et al., 2010), and high-molecular-weight compounds such as mucoid biopolymers (Ahmadi et al., 2017). Most of the low-molecular-weight rhizosphere exudates are released from the growing tips of roots (Jones et al., 2009; Pausch and Kuzyakov, 2011). Root elongation is sensitive to water content variation and has an important influence on rhizodeposition due to major modification of the length and velocity of the exuding root zone (Sharp et al., 2004). An increase in rhizosphere water content enhances diffusion of exudate and increases its microbial decomposition (Holz et al., 2018a), while the diffusion has a strong influence on exudate distribution and the root exudation rate (Jones et al., 2004). The release and the diffusion capacity of exudates directly affect carbon distribution in the rhizosphere. Meanwhile, decomposition of rhizosphere exudates, root hair biomass, and adsorption capacity of microbes also affect the rhizosphere carbon content (Kuzyakov et al., 2003; Jones et al., 2009; Holz et al., 2018b).

However, limited irrigation quantities, a common water management measure in CEA systems, may cause water stress and initially promote redistribution of recently assimilated carbon, transfer it to roots, and synthesize rhizosphere exudates, whereas they may lead to a decrease in exudation intensity and ultimately weaken rhizodeposition (Sharp et al., 2004). They may affect the rhizodeposition process and change solute composition in the growth substrate in the long term.

Rhizosphere Allelopathy

Rhizosphere exudates are also known as allelochemicals and can have beneficial (positive allelopathy) or detrimental (negative allelopathy) effects on rhizosphere microenvironments (Scavo et al., 2019). Maintaining the beneficial rhizosphere allelopathy and reducing the allelochemicals phytotoxicity is of central importance. The exudates of allelochemicals are responsible for the recruitment of beneficial microbes through the alteration of the rhizosphere microenvironment, thus mitigating unfavorable conditions (Li et al., 2014; Holz et al., 2018a; Naylor and Coleman-Derr, 2018).

Rhizosphere microbes are inseparable from plant rhizosphere allelopathy because the secreted allelochemicals are accepted as the energy source for microbes (Holz et al., 2018a); meanwhile, the allelochemicals play a role in communicating with rhizosphere microbes as signal compounds (Shah and Smith, 2020). Rhizosphere microbes give different kinds of feedback to plants under various nutritional conditions, while water is the key to regulating the process. Generally, the rhizosphere microenvironment tends to recruit microbes that can produce plant hormones when the substrate is enriched with minerals and nutrients under water sufficiency, which is known as the eutrophication state (Pascault et al., 2013; Hartmann et al., 2017). On the contrary, insufficient rhizosphere water leads to the formation of oligotrophic conditions. Taking rhizosphere allelopathy into account, one could ascertain that the significance of water management is the opportunity to take advantage of the recruitment effect and achieve proper mineralization, nutrient dissolution, and plant absorption (He and Dijkstra, 2014).

To improve water use efficiency in CEA systems, deficit irrigation is commonly employed. Declining water content causes changes to plant physiology and biochemistry. Significant impact lies in the change of substrate pH, root morphology, the total amount of carbon input, and the rhizosphere exudates (including

soluble sugar, organic acid, mucilage, enzymes, and exfoliated cells, etc.) (Grierson and Adams, 2000; Marschner et al., 2005).

As with the changes in solution concentration, water deficiency is, essentially, a kind of osmotic stress on plant physiology. On the other hand, the bulk of situations of water deficiency increases enzyme activity during plant growth periods; meanwhile, it increases the concentration of organic acids in root exudates, thereby contributing to drought tolerance. Under water stress, the rhizosphere microenvironment of corn (*Zea mays* L.) has increased protease, catalase, alkaline phosphatase, and invertase activities. Osmotic stress increases the concentration of malic acid, lactic acid, acetic acid, succinic acid, citric acid, and maleic acid in root exudates (Song et al., 2012). Water deficiency enriches the root exudates of barley (*Hordeum vulgare* L.) with more proline, K, and phytohormone, which play important roles in promoting root growth osmotic protection and stress signal transduction (Calvo et al., 2017). Studies also showed the dependence of the microbial communities on activities of protease, urease, and phosphatase; these changes in substances are results of the rhizosphere allelopathy regulated by water (Marschner et al., 2005).

Water-stressed rhizosphere allelopathy could be an opportunity for one to make good use of it. Rhizosphere N-fixing bacteria have a higher N-dissolving ability under water shortage conditions, which is an approach to enhance plant growth (Knoth et al., 2014). Meanwhile, one can change the process of plant carbon assimilation, distribution, and deposition in the rhizosphere (Holz et al., 2018a), as well as the regulation of N mineralization (Akter et al., 2018). Detailed practical cases of water management with regard to the microbiome and production are discussed in Section "Microbial Community."

Rhizosphere Physiological Adaptation

Plants can adapt to varied rhizosphere hydro-environments by nature (Ahmed et al., 2018) because the rhizosphere exudation is responsible for the adjustment of plants to substrate moisture, especially when the water content is undergoing wet-dry circulation (Carminati et al., 2010; Ahmed et al., 2016). The exudate, commonly found to be mucilage, plays an important role in substrate moisture regulation. The exudation intensity is largely affected by water content, while, in turn, exudates affect soil or substrate hydrophilicity, thereby changing the moisture status, which is a unique process in rhizosphere microenvironments (Palta and Gregory, 1997; Sanaullah et al., 2012). In CEA systems, mucilage is easily spread throughout the planting substrates because the substrate cubes are generally kept to a minimum size. Hence, the mucilage is more significant for wettability regulation and water retention in the limited volume of a substrate cube.

As shown in **Figure 4**, continuous mucilage exudation is a kind of self-compensation under water stress. The mucilage increases the local moisture content in the root direction and ultimately compensates for the negative impact of water deficiency. It is a strategy to maintain rapid diffusion of exudates and high microbial activity (Holz et al., 2018a). The influence of rhizosphere exudates on the rhizosphere microenvironment starts from the contact part between root sheath and substrate. The root sheath has several important functions for water and nutrient absorption, especially under water stress (Hsiao and Xu, 2000). This is because the root sheath keeps the root system in contact with the substrate during the drying process, thereby enhancing the hydraulic connection between the root system and the substrate and creating a rhizosphere microenvironment that is compatible with water (Drenovsky et al., 2004; Kuzyakov and Blagodatskaya, 2015). Under water-deficient conditions, roots secrete polysaccharide mucilage to preserve relatively more water, but the mucilage reduces the substrate hydrophilicity. This, in turn, reduces water flux in the rhizosphere, and thereby reduces water consumption by roots (Zarebanadkouki and Carminati, 2014). When the rhizosphere is subsequently wetted again, the water content will be lower than that of the blank substrate because of the previously reduced hydrophilicity. This mechanism ensures the relative stability of the rhizosphere microenvironment during alternation of wetting-drying (Read et al., 1999), which has also been proved experimentally.

The mucilage secretion strongly affects the biophysical properties of the rhizosphere, which determines the ability of roots to extract water and nutrients from its growing substrate. The rhizoligand is a mucilage analog (such as the commercial surfactant of AC 1820 acrylate copolymer) that is defined as an addictive substance that increases the wettability of the rhizosphere and links the mucilage network to main intimate contact with the root surface. Ahmadi et al. (2017) used the exogenous rhizoligand to demonstrate the influence of rhizosphere exudates on substrate hydrophilicity during the wetting-drying cycle. It was found that the rhizoligand improved hydrophilicity and enhanced the communication between the rhizosphere microenvironment and plants, thereby making the root sheath more developed. Meanwhile, the activities of chitinase, sulfatase, and β-glucosidase were 4, 7.9, and 1.5 times greater, respectively, and biomass was 1.2-fold that of water-irrigated plants. By adjusting hydrophilicity, this approach harnesses water availability without using conventional irrigation methods (Ahmed et al., 2016; Ahmadi et al., 2018).

In controlled environment agriculture systems, water deficiency or moderate drought may be an approach to enhance the mass and energy utilization efficiency of the system (Sposito, 2013; Ahmed et al., 2018). Owing to the small rhizosphere space and concentrated allelochemical substances as described above, self-stabilization of moisture in the microenvironment can be fully utilized to achieve better results than traditional irrigation. One can realize optimized economical resource input by fully exploiting the potential instead of simply satisfying the greatest physiological needs of plants (Qin et al., 2019), which could be an innovative concept for CEA management.

EFFECT OF WATER MANAGEMENT ON RHIZOSPHERE MICROBIOLOGY IN CEA

Microbial Physiology

System designers of controlled environment agriculture need to guide the rhizosphere microbiology to a beneficial and sustainable status (Colla et al., 2017). In terms of water

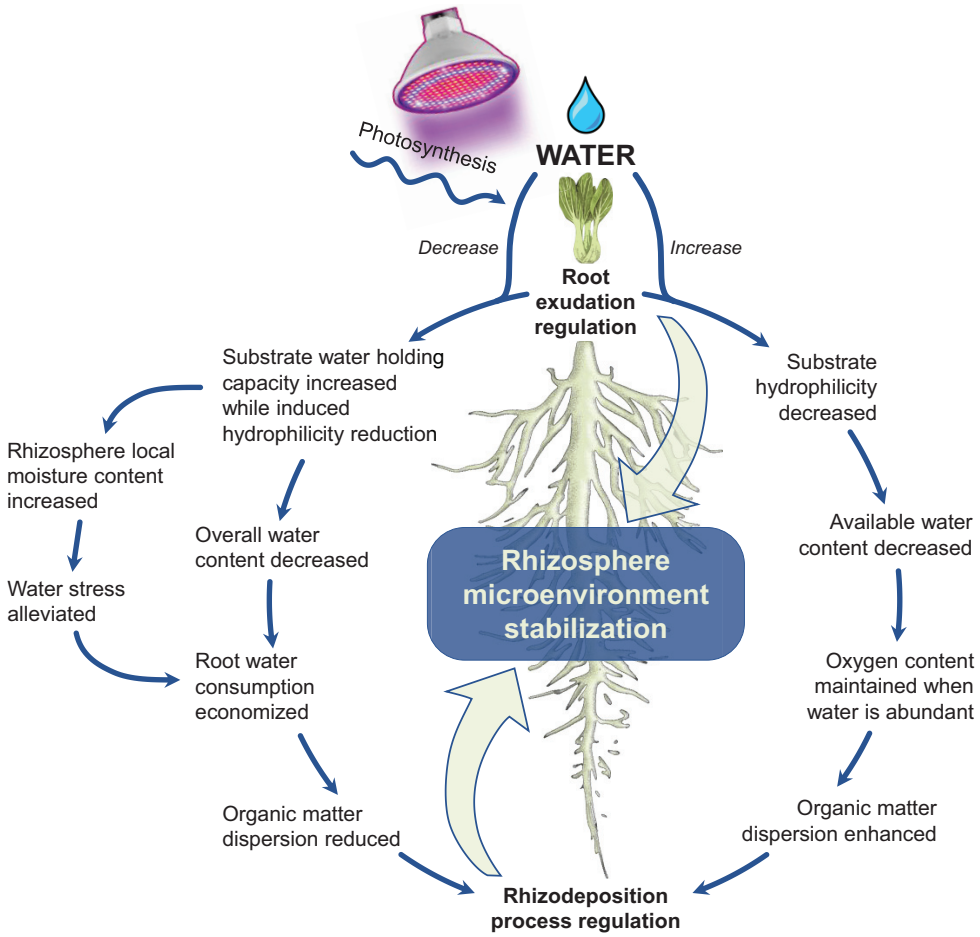

FIGURE 4 | A mechanism of rhizosphere microenvironment stabilization under water content variation (drawn by the authors).

management that acts upon rhizosphere microbial physiology, the main impact, in effect, is on carbon catabolism and cellular osmosis regulation (Vurukonda et al., 2016; Rajkumar et al., 2017). The regulatory significance lies in the regulation of hydrolytic enzymes and osmolytes production, which, in turn, influences the overall pattern of resource utilization (Blazewicz et al., 2014; Naseem et al., 2018; Sammauria et al., 2020).

Water saturation is favorable for facultative anaerobe to enhance substrate respiration and enzymatic degradation, which further increases the labile carbon fraction *via* carbon speciation. For instance, carbohydrates are particularly important in the carbon catabolism of a microbial community (Tate, 1979; Wilson et al., 2011; Fierer, 2017). It is clear that water saturation creates a nutrient-rich microenvironment and brings microbial proliferation; however, water deficiency can still stimulate the proliferation of oligotrophic bacteria in the dry rhizosphere (Naylor and Coleman-Derr, 2018); meanwhile, water use efficiency can be improved under relatively nutrient-poor conditions (Enebe and Babalola, 2018), despite the resource limitation for most microbes. On the other hand, as for the eutrophic microbes, water deficiency reduces microbial activity through dehydration and substrate limitation, and reduces the microbial metabolic process (Stark and Firestone, 1995); consequently, the formation of rhizosphere nutrients is determined.

As shown in **Figure 5**, microbes under varied nutritional conditions release extracellular enzymes that can regulate depolymerization and decomposition (Bouskill et al., 2016b; Igalavithana et al., 2017), thereby mediating the overall circulation rate of a nutritional substance (mainly carbon and N) in the rhizosphere (Frossard et al., 2000; Schimel and Bennett, 2004). For example, when the rhizosphere undergoes water deficiency, changes occur in the functional potential of microbial communities that are concomitant with an increase in hydrolase activity (Alster et al., 2013). As is exhibited from the data on functional gene regulation, the genes-encoding extracellular enzymes that degrade chitin, cellulose, lignin, pectin, and enzymes involved in hemicellulose (xylose) catabolism were of higher relative abundance in water deficiency; meanwhile, the specific activities of the corresponding classes of enzymes were also higher (Bouskill et al., 2016b).

Osmotic stress is the driving factor in the physiological processes depicted above. Specifically, as substrate dries and water potential drops, cells must accumulate solutes to reduce

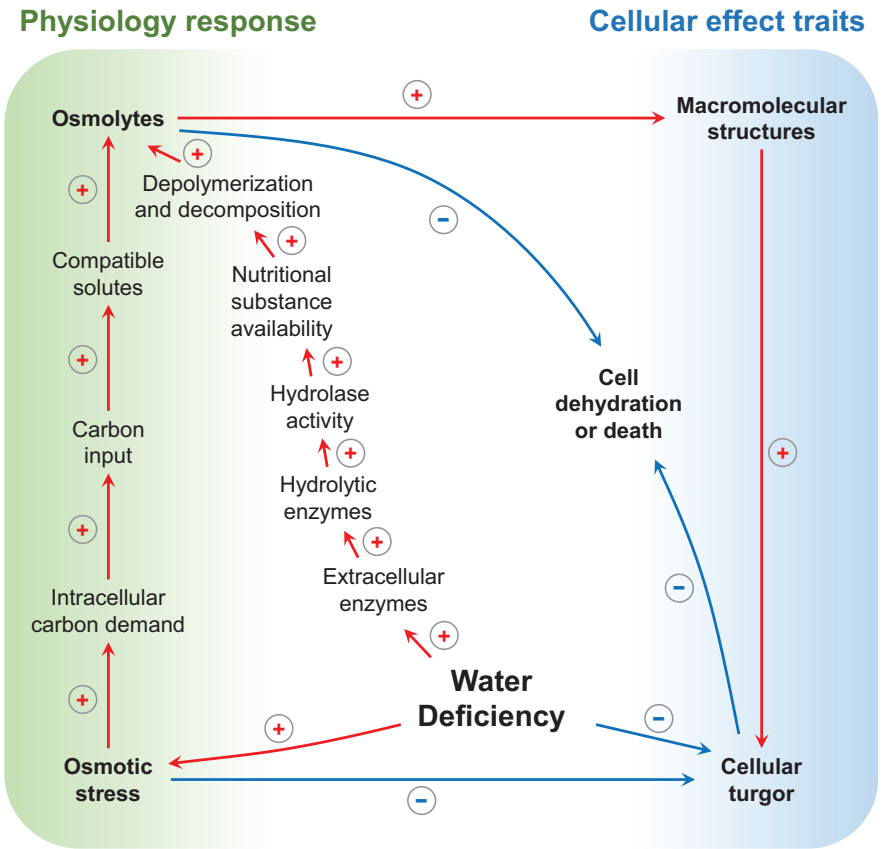

FIGURE 5 | Microbial physiology response and cellular effect traits under water deficiency. Arrows indicate influence processes, positive red signs represent increase or enhancement, and negative blue signs represent reduction (drawn by the authors).

their internal water potential to avoid dehydration or death (Schimel et al., 2007). Hence, the synthesis of osmolytes is necessary, and a large amount of carbon input is required. Under this circumstance, it was found that, as a response to osmotic stress, the intracellular carbon demand and production of compatible solutes increases (Bouskill et al., 2016b). For bacteria, amino compounds are typically used as osmolytes, such as proline, glutamine, and betaine (Csonka, 1989); while, for fungi, polyols, such as glycerol, erythritol, and mannitol, are used (Witteveen and Visser, 1995).

These physiological performances and adaptations are manifested in a dynamic process; microbes maintain cellular turgor and protect macromolecular structures by using osmolytes; meanwhile, these osmolytes regulate hydrolytic enzymes activity to acquire carbon for osmolytes synthesis and, ultimately, achieve the balance of carbon consumption and rhizodeposition (Welsh, 2000; Bouskill et al., 2016a; Vurukonda et al., 2016; Rajkumar et al., 2017; Naseem et al., 2018; Hartman and Tringe, 2019; Teijeiro et al., 2020).

Microbial Community

Different substrate configurations affect microbial traits, and a "living" substrate could retain stable and beneficial microbial communities. Fresh and easily degradable organic matter in the substrate stimulates microbial growth and serves as an energy source for microbes to synthesize extracellular enzymes that are capable of degrading recalcitrant organic matter, thus facilitating mineralization. This is based on the way microorganisms live in the substrate that was explained by the "co-metabolism" theory (Kuzyakov et al., 2000; Wang et al., 2015). Although we did not find a specific case study on a microbial community that was affected by varied substrates, there is emerging consensus on which variables are most likely to have marked effects on the microbial community.

An optimized ratio of substrate carbon/N for microbial mineralization is believed to be around 20, which is calculated by dividing the microbial carbon/N ratio (10) by the carbon assimilation yield of microbial biomass (0.5) (Recous et al., 1995; Manzoni et al., 2010). However, with the consumption of nutrients, the microbial community develops in different directions; not surprisingly, it generally does not lead to desired yield and sustainability if the dynamic of the microbial communities is underestimated. Fei et al. (2008) showed a notable increase in bacteria and actinomycetes and a significant decrease of fungi in surface soil-based greenhouses; that is, the ratio of bacteria to fungi increased. As the substrate was used for a long time, the microbial biomass showed a downward trend. In agronomic practices by Bonanomi et al. (2017),

soil with disinfestation treatments was used as the planting substrate for plastic tunnel farming systems. Mulching films were employed as a combination with microbial consortia, containing beneficial microbes (i.e., antagonistic fungi of the genus *Trichoderma*, mycorrhizal fungi of the genus *Glomus*, and the plant growth-promoting bacterium *Bacillus subtilis*). The application of beneficial microbes can indirectly increase water use efficiency by controlling soilborne pathogens and significantly increase root mycorrhizal colonization compared with untreated controls in all cropping cycles.

We hoped to understand the link between the microbial community and the substrate parameters. As shown in **Figure 6**, among multiple factors, in addition to pH, water content, quality and quantity of organic carbon, and the redox state are the most significant factors that have notable influences on the structure of microbial communities (Schimel et al., 2007; Lauber et al., 2009; Kuramae et al., 2011, 2012; Okegbe et al., 2014; Maestre et al., 2015; Prober et al., 2015; Fierer, 2017).

The driving factors that lead to the difference between CEA planting substrate and field soil could be varied. Due to the complexity of the natural soil system, measurements of bulk soil (ectorhizosphere) properties do not necessarily capture the microscale variations in soil properties that may drive spatial variation in soil microbial community composition (Fierer, 2017). A broad range of different microbial habitats coexists in field conditions; meanwhile, microbial communities and microbial taxa are preferentially associated with different surface vegetation. This is true for many mycorrhizal fungi, fungal plant pathogens, and some N-fixing bacteria (for example, *Rhizobium* spp.), which, typically, only associate with specific plant species. However, in CEA systems, the microbial community can be significantly regulated, which provides a basis for the application of growth-promoting bacteria (PGPB). A cluster of bacteria that colonize the root of the plant rhizosphere is termed the "PGPB" (Dhayalan and Sudalaimuthu, 2021). The role of PGPB in plant growth is of importance to water regulation because the PGPB could induce a plant to tolerate water deficit conditions *via* colonies in rhizospheres and endorhizospheres, and it could provide a wider range for water regulation in the system. Sandhya et al. (2010) proved that the plant biomass was enhanced through the inoculation of *Pseudomonas putida* under drought conditions. Armada et al. (2014) found that the concentration of proline in the *Lavandula* shoot was increased by inoculation of *Bacillus thuringiensis*, thereby promoting plant growth.

In controlled environment agriculture–planting substrates, moisture and aeration could be the most significant contributors to determining microbial composition. Water condition decides the O_2 content and nutrient availability (Drenovsky et al., 2004) and reshapes the community structure of eutrophicor oligotrophic microbes; as a result, the nutritional type of the microbes is determined (Hedenec et al., 2018). When water deficiency occurs, it is nutrient-poor but oxygen-rich in the substrate; thus, microbes die or enter dormancy and the overall activity tends to decrease. However, it sets up a stage for aerobic bacteria and/or oligotrophic bacteria (Blazewicz et al., 2014; Armstrong et al., 2016).

The different behaviors of Gram-positive bacteria and Gram-negative bacteria are a good example showing the community structural changes under water deficiency. Gram-positive bacteria are metabolically more "tenacious," as they can use recalcitrant compounds to produce extracellular enzymes (Treseder et al., 2011; Naylor and Coleman-Derr, 2018). *Actinomycetes*, the oligotrophic bacteria under the phylum Gram-positive bacteria, are metabolically versatile. They can degrade complex organic compounds, maintain high-carbon utilization efficiency, and form spores and filaments through cellular modification (osmotic protectants, dormancy) (Hartmann et al., 2017). These abilities ensure their survival and even dominance in the substrate with low-hydraulic connectivity and nutrient limitation (Wolf et al., 2013). Cell walls may render microbes more resistant to water potential decrease; for example, Gram-positive bacteria can survive in stress by producing strong, thick, and interlinked cell walls of peptidoglycan (Schimel et al., 2007). Another strategy for microbes to withstand stress is sporulation, which is considered a potential factor in observing the trend of abundance. Many genera in Gram-positive phyla are known as sporophytes, while the Gram-negative phyla have mostly lost the ability to sporulate during evolution (Tocheva et al., 2016).

Water content variation reshapes the microbial community structure significantly, while it has a minor effect on diversity (Bachar et al., 2010; Blazewicz et al., 2014). On the other hand, the different behaviors of bacteria and fungi under water deficiency merit attention, especially under long-term water stress. Bachar et al. (2010) showed that bacteria abundance had a decreasing trend with the degree of water deficiency; however, bacteria diversity had less relevance to water content. Acosta-Martinez et al. (2014) showed that 10 months of severe drought caused the fungal diversity index and OTUs to increase more than bacteria, and found that *Proteobacteria*, *Actinobacteria*, *Chloroflexi*, and *Nitrospirae* have higher abundance. While significant progress has been made in exploring the relationship between how water and nutrition shape microbial communities, the extent to which water affects rhizosphere plant-microbe interactions is still elusive. It remains to be seen which of the detected correlations will prove to be significant for microbial diversity and structural composition, and which will prove redundant (Aung et al., 2018; Qin et al., 2019; Jain et al., 2020).

As shown in **Table 1**, for the benign output of the system, there have been many attempts for different crops. To be sure, proper water management is conducive to the benign output of an agricultural system. There are constantly increasing practical experiences on this issue. The method of negative pressure irrigation is a water supply technology for water-saving and fertilizer utilization efficiency improvement, which emits water through a porous ceramic tube embedded in the rhizosphere. This method can consistently supply water, depending on the water consumption of the plants and soil tension (Long et al., 2018). Zhao et al. (2019) employed negative pressure irrigation to supply water in relation to soil matrix tension and water consumption during rapeseed (*Brassica chinensis* L.) planting. The rhizosphere water content was maintained within 9.7–11.7%, which was more stable than that of

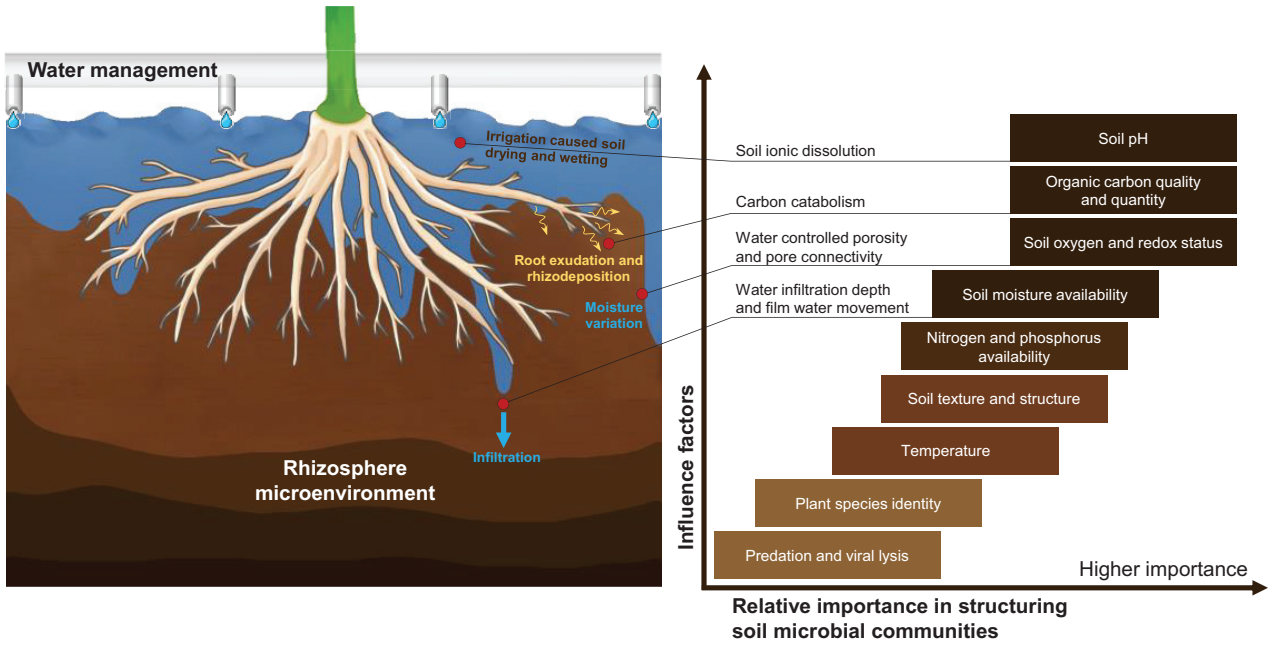

FIGURE 6 | The importance of water management in rhizosphere microenvironments and the factors that structure microbial communities. The box color qualitatively indicates the current understanding of the specific effects of certain factors on microbial communities; darker shades highlight reasonably well-understood factors. The figure is remade using the compilation of the following research studies: Schimel et al. (2007), Lauber et al. (2009), Kuramae et al. (2011, 2012), Okegbe et al. (2014), Maestre et al. (2015), Prober et al. (2015), Fierer (2017).

traditional water supply and drip irrigation. As a result, microbial diversity was increased, and the dominance of *Proteobacteria*, *Acidobacteria*, etc., was eliminated from the microenvironment. Other categories of bacteria flourished, including *Actinobacteria*, *Bacteroidetes*, *Verrucomicrobia*, *Firmicutes*, *Planctomycetes*. This method provided a stable microenvironment for improving the yield and quality of rapeseed, increased the N, P, and K content in plants, and contributed to improving water use efficiency.

Indeed, the water and the air in the microenvironment are linked. To explore the impact of aeration on the microbial community, Li Y. et al. (2020) conducted an artificial aeration experiment in the soil matrix and found that an aeration treatment increased the abundance of *Acidobacteria*, reduced the abundance of *Gammaproteobacteria*, and eliminated *Geobacteraceae* and *Halanaerobiaceae*. Studies have described that *Geobacteraceae* and *Halanaerobiaceae* are closely related to *Xanthomonas*, which is an important plant pathogen (Zhang et al., 2017; Li Y. et al., 2020). The aeration improved the connection of pores, which led to a decrease in solute transport capacity and nutrient availability. It must be noted that *Acidobacteria* is an oligotrophic bacteria, which is good at reproducing with low-carbon availability (Fierer et al., 2007). The *Acidobacteria* can participate in the biogeochemical cycle, exhibit metabolic activity, and finally dominate in number under such circumstances (Lee et al., 2008). Through artificial regulation, a better rhizosphere microenvironment is created, which increases ACE, Chao index, Shannon diversity index, root length, surface area, root tip, and activity.

However, it needs to be emphasized that proper water management is more than water saving. Li M. et al. (2020) compared two different irrigation methods, namely, subsurface drip irrigation and furrow irrigation, and found that, in the rhizosphere of drip irrigation, 28.3% of the tomato (*Solanum lycopersicum* L.) yield decreased. Water limitation induced a decrease in the potential activity of carbon cycle extracellular enzymes; meanwhile, an increase in the overall abundance of microbial functional genes was involved in the N cycle process. As a result, the carbon-to-N ratio was altered in the rhizosphere microenvironment. Furthermore, water stress increased the colonization of arbuscular mycorrhizal fungi, increasing root density. Finally, the biomass of tomato plants was allocated to a non-yielding part. Therefore, although water can be used to change the interaction between plants and microbes and root morphological traits, if there are mismatches in plant demand, resource availability, and microbial carbon-to-N ratios, the goal of sustainability for CEA will not be achieved.

Microbial Traits for Microenvironment Interaction

Currently, there is a lack of models that characterize the microbial traits in CEA systems. The relationships between the rhizosphere competitor, stress tolerator, and ruderal can be characterized by the C-S-R framework (Grime, 1977), and the C-S-R life history triangle is a good start in advancing trait-based microbial ecology; however, it does not map well on microbes (Malik et al., 2020). Global-scale research may shed light on this issue,

TABLE 1 | Cases of water management, using CEA systems or controlled agricultural techniques to explore the impact of the microbiome on yield.

Plant	Water management method	Effects on microbial communities in rhizosphere microenvironment	Application effect	References
Tomato (*Solanum lycopersicum* L.)	Irrigation combined with aeration.	The abundance of *Acidobacteria* increased and that of *Gammaproteobacteria* decreased in response to aeration treatments; conversely, *Geobacteraceae* and *Halanaerobiaceae* were eliminated.	The ACE, Chao index, Shannon diversity index, root length, surface area, tips, and activity all increased.	Li Y. et al. (2020)
Tomato (*Solanum lycopersicum* L.)	Subsurface drip irrigation combined with concentrated organic fertilizer application.	Higher mycorrhizal colonization rates, higher abundance of microbial N-cycling genes, and lower activities of carbon-degrading enzymes were found in the rhizosphere of surface drip irrigation plants compared to full irrigation.	Tomato plants produced shorter and finer root systems with higher densities of roots around the drip line, stems and leaves increased, however, marketable tomato yield decreased by 28.3%.	Li M. et al. (2020)
Maize (*Zea mays* L.)	Well-watered irrigation and water-stressed irrigation in field blocks.	Highly significant differences (approximately 2.6–3.9% of the variation in microbial community composition) were found due to water stress. Water stress-induced belowground bacterial and archaeal microbiomes dramatically change, which were relative abundance increase of *Actinobacteria* and *Saccharibacteria* in rhizosphere, and decrease of *Chloroflexi*, *Proteobacteria,* and *Cyanobacteria*.	Water-stressed irrigation significantly reduced maize growth and productivity, among which 28% reduction was found in grain yield as compared to well-water conditions.	Wang et al. (2020)
Rapeseed (*Brassica chinensis* L.)	Supplying water based on plant consumption by using negative pressure irrigation technique.	The dominance of *Proteobacteria* and *Acidobacteria* in the rhizosphere was eliminated, and other taxa thrive, including *Actinobacteria*, *Bacteroidetes*, *Verrucomicrobia*, *Firmicutes*, *Planctomycetes*, etc.	The yield and quality of rapeseed were improved, the content of nitrogen (N), phosphorus (P), and potassium (K) of the plant was increased, and the water consumption was reduced.	Zhao et al. (2019)
Bell pepper (*Capsicum annuum* cv. Revolution)	Drip irrigation (below ground surface) subjected to well-watered and deficit irrigation levels.	Extra moisture positively induced fungi abundance through improvement in plant aboveground performance. Microbial activity at the community level decreased with water content reduction. Bacteria were more sensitive to water input changes as compared to fungi.	Higher water input contributed to the increase of pepper yield but negatively affected substrate respiration. Deficit irrigation reduced yield by 12.0% compared to the well-watered treatment, while root responses also followed a similar pattern as fruit yield.	Qin et al. (2019)
Tomato (*Solanum lycopersicum* L.)	Surface drip irrigation combined with aeration.	Aeration slightly increased mean values of the abundance of bacteria, fungi, and actinomycetes, with average increases of 4.6, 5.5, and 3.4%, respectively, and the abundance increased as irrigation amount increased.	Total root length was significantly increased by 22.2% on average under aeration, meanwhile, total root surface area and volume under the aeration was 6.6% and 6.7% higher than that of the control, respectively. Dry biomass of tomato leaf, stem, fruit, and root increased as irrigation amount increased, and the effect was significant on leaf, fruit, and root.	Chen et al. (2019a)
Maize (*Zea mays* L.)	Two levels of water stress irrigation for pot experiment.	Soil pH was lower in the rhizosphere than bulk soil but was not affected by water deficiency.	Water stress significantly decreased the rhizosphere protease activity at elongation, tasseling and grain-filling stages, and reduced the rhizosphere alkaline phosphatase activity at tasseling and grain-filling stages.	Song et al. (2012)

such as earth system models (ESMs) (Wieder et al., 2013), but they exhibited high uncertainties because they omitted key biogeochemical mechanisms (Conant et al., 2011; Schmidt et al., 2011). Microbial traits mainly correlate with resource utilization with different strategies (Hall et al., 2018; Malik et al., 2020), and thereby influence the microenvironment. The MIcrobial-MIneral Carbon Stabilization (MIMICS) model incorporated copiotrophic and oligotrophic microbial functional groups and raised hypotheses involving the roles of substrate availability, community-level enzyme induction, and microbial physiological responses (Wieder et al., 2015). Several recent efforts have applied this framework to microbial systems, particularly in the context of anthropogenic-controlled environments (Ho et al., 2013; Krause et al., 2014; Fierer, 2017; Wood et al., 2018). Malik et al. (2020) reclassified multiple factors into three main microbial strategies, which were high yield (Y), resource acquisition (A), and stress tolerance (S), and conceptualized as the Y-A-S framework (**Figure 7**).

Since we have reviewed much of the impact of water content variation on the all-round characteristics of CEA in this study, it is more important to conceptualize trait-based microbial strategies so that system investment could

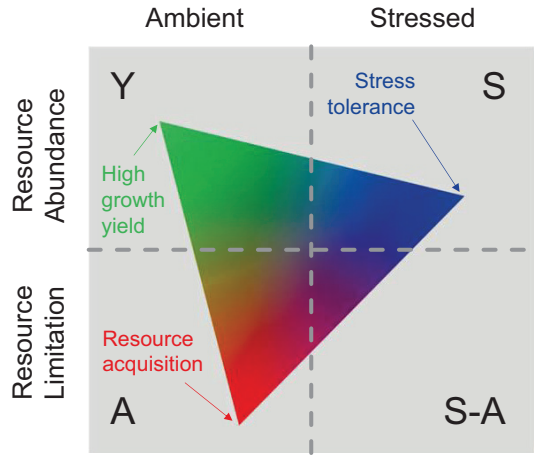

FIGURE 7 | A conceptual figure of the Y-A-S framework. The Y-A-S triangle was arrayed on the combinations and represented a hypothesized particular system. The meaning of the three strategies, including the high yield (Y: maximizes growth efficiency as a result of reduced investments in stress tolerance and resource acquisition), the resource acquisition (A: preferential investment for optimized resource acquisition), and stress tolerance (S: preferential investment in stress tolerance mechanisms) (Malik et al., 2020).

be estimated. For example, when we analyze the influence of water content variation on carbon cycling, we should consider the rhizosphere microenvironment traits as mentioned; these traits will interact with certain factors (root elongation, exudation, rhizodeposition, osmosis regulation, allelopathy, extracellular enzymes production, carbon decomposition, microbial community evolution, microbial residue chemistry, etc.) to determine long-term carbon storage in the substrate. If we evaluate this process under the Y-A-S framework (Malik et al., 2020), Y-strategists would contribute to rhizodeposition that can benefit substrate carbon accumulation. In contrast, A-strategies should contribute more to carbon decomposition through investment by enhancing microbial extracellular enzyme production (Schimel and Schaeffer, 2012; Kallenbach et al., 2016; Malik et al., 2019). On the other hand, S-strategists might depend on the type of stress compounds produced, such as osmolytes; meanwhile, it would contribute to root sheath elongation and microbial copiotrophic-oligotrophic functional alternation (Hsiao and Xu, 2000; Schimel et al., 2007; Bouskill et al., 2016b).

The same is true for other substance cycling/transformations in CEA systems, but the hindrance could be measuring and quantification (Malik et al., 2020). Current approaches have mostly focused on identifying taxonomic and functional responses to environmental changes. However, integration of these large datasets with process rate measurements remains a challenge, thereby making it difficult to link microbial composition and function with CEA systems (Krause et al., 2014; Rocca et al., 2015; Hall et al., 2018). Water variation could significantly affect rhizosphere respiration, microbial activity, and plant yield (Qin et al., 2019). Future frameworks could suggest the connection between water response and effect traits (de Vries et al., 2020).

CONCLUSION AND FUTURE PERSPECTIVES

Conclusion

In this review, we discussed the influence of water management on rhizosphere microenvironments in CEA systems, pointed out that water content variation affects the physicochemical properties of the rhizosphere substrate and changes the formation and availability of nutrients within it, thereby emphasizing the influences of macroelement transformation and consumption underwater content dynamics. Correspondently, the physiological processes in the rhizosphere are adaptively adjusted, which is achieved by the allelopathy of root exudates. In addition, from the perspective of microbiology, in rhizospheres, water content variation significantly affects microbial metabolism and proliferation, thereafter altering its nutrient type and community. The regulatory mechanism described above has important implications for CEA management. Water management can be used to seek advantages, avoid disadvantages, and establish a stable and replicable microbial microenvironment; furthermore, it could be one of the most important methodologies for benign output and sustainability for CEA systems.

Future Perspectives

While there are promising findings that have come out from extensive research and production practices conducted to date, the CEA system is still far from large-scale utilization. Concepts of dealing with the artificial agricultural environment and its systematization require innovation (Sigrimis et al., 2001). On global food issues, we are not yet ready to deal with major environmental changes (Alvarado et al., 2020). We hypothesize there are at least two key points worth considering for the theoretical development of CEA, namely, data integration and modeling. In this study, we presented a brief overview of the two issues and made suggestions for future research and the modern development of agriculture.

Improvement of Universally Applicable Water Management Reference for Various CEA Systems: Data Integration

For traditional agriculture in different parts of the world, water resources management has unique regional characteristics that are calculated based on local hydrology (Hisdal and Tallaksen, 2003). Although many studies have been carried out for different crops in different regions and under different conditions, it is often difficult to replicate the same planting environment in practice (Amitrano et al., 2019). For the future systemization and globalization of the CEA, the currently published pieces of the literature showed a lack of descriptive benchmarks and norms; as a result, one management method is difficult to replicate, which hinders relevant key issues from being comparatively studied in different regions (Casaregola et al., 2016; Ladau and Eloe-Fadrosh, 2019).

Therefore, a universally applicable water management reference is crucial. At this stage, researchers are advised to focus

on data acquisition for a series of key parameters, including water-related organic matter content, O_2 concentration, respiration, substrate utilization rate, microbial composition, and activity of the rhizosphere microenvironment (Linn and Doran, 1984a; Williams, 2007; Zhou et al., 2014; Sierra et al., 2015). It is necessary to track the evolution process of the microenvironment under different water management strategies and pay attention to the environmental context and the development stage of multiple specific systems. Furthermore, it would be very beneficial to establish a database of modern CEA systems and share monitoring data and reports, which will help to accelerate the research and development of high-tech artificial agricultural ecology.

Quantification of Relationships Between Plant Physiology and Biochemistry Underwater Management: Modeling

To date, there is little evidence of coupling between rhizosphere microenvironment variation and microbial functional traits that affect plant physiology underwater content variation (de Vries et al., 2020). On the other hand, due to microenvironment complexity and a lack of descriptions of benchmarks and norms, it is difficult to replicate a CEA system under different planting backgrounds and promote management methods with excellent performance.

Based on massive data acquired from water management references worldwide (Sigrimis et al., 2001), we need to further offer a platform to discover the relationship between plant physiology and biochemistry by addressing ecological questions on microbial community composition and rhizosphere biogeochemical functions (Wieder et al., 2015). By evaluating the regulatory effect of water control, it is necessary to group microbial diversity into simplified functional groups and demonstrate how community differences may have a significant influence on rhizosphere substance transport and transformation. This model is expected to parameterize and accurately simulate the rhizosphere biogeochemical function of the CEA, thus showing how functional traits interact with water content gradients and follow perturbations, including wettability of substrate, enzyme activity, and microbial community (Sardans and Penuelas, 2005; Moore et al., 2010).

AUTHOR CONTRIBUTIONS

BT and CL: conceptualization. BT and XT: resources. BT and YL: writing – original draft preparation. BT, YL, YH, XY, and KL: writing – review and editing. BT: visualization. TL, CL, and LL: supervision. CL and LL: project administration. CL and LL: funding acquisition. All authors contributed to the article and approved the submitted version.

FUNDING

This study was funded by the Key Research and Development Program of Sichuan Province (2019YFN0153), the Fundamental Research Funds for the Central Universities (2021SCU12037), the National Natural Science Foundation of China (51909175 and 42077175), the National Key R&D Program of China (2019YFE0114900), and Shanghai "Science and Technology Innovation Action Plan" Project (19230742400, 19ZR1459300, and 20dz1204502).

SUPPLEMENTARY MATERIAL

The Supplementary Material for this article can be found online at: https://www.frontiersin.org/articles/10.3389/fpls.2021.691651/full#supplementary-material

REFERENCES

Abd El-Gayed, S. S., and Bashandy, S. O. (2018). Effect of reduced irrigation and potassium fertilization on quantity and quality of Giza 95 cotton plants. *Egypt. J. Agron.* 40, 71–84.

Abd El-Mageed, T. A., El-Sherif, A. M. A., Ali, M. M., and Abd El-Wahed, M. H. (2017). Combined effect of deficit irrigation and potassium fertilizer on physiological response, plant water status and yield of soybean in calcareous soil. *Arch. Agron. Soil Sci.* 63, 827–840. doi: 10.1080/03650340.2016.1240363

Abd-Elrahman, S. H., and Taha, N. M. (2018). Comparison between organic and mineral sources of potassium and their effects on potassium fractions in clay soil and productivity of potato plants under water stress conditions. *Egypt. J. Soil Sci.* 58, 193–206. doi: 10.1007/bf01834812

Acosta-Martinez, V., Cotton, J., Gardner, T., Moore-Kucera, J., Zak, J., Wester, D., et al. (2014). Predominant bacterial and fungal assemblages in agricultural soils during a record drought/heat wave and linkages to enzyme activities of biogeochemical cycling. *Appl. Soil Ecol.* 84, 69–82. doi: 10.1016/j.apsoil.2014.06.005

Ahmadi, K., Razavi, B. S., Maharjan, M., Kuzyakov, Y., Kostka, S. J., Carminati, A., et al. (2018). Effects of rhizosphere wettability on microbial biomass, enzyme activities and localization. *Rhizosphere* 7, 35–42. doi: 10.1016/j.rhisph.2018.06.010

Ahmadi, K., Zarebanadkouki, M., Ahmed, M. A., Ferrarini, A., Kuzyakov, Y., Kostka, S. J., et al. (2017). Rhizosphere engineering: innovative improvement of root environment. *Rhizosphere* 3, 176–184. doi: 10.1016/j.rhisph.2017.04.015

Ahmed, M. A., Kroener, E., Benard, P., Zarebanadkouki, M., Kaestner, A., and Carminati, A. (2016). Drying of mucilage causes water repellency in the rhizosphere of maize: measurements and modelling. *Plant Soil* 407, 161–171. doi: 10.1007/s11104-015-2749-1

Ahmed, M. A., Zarebanadkouki, M., Ahmadi, K., Kroener, E., Kostka, S., Kaestner, A., et al. (2018). Engineering rhizosphere hydraulics: pathways to improve plant adaptation to drought. *Vadose Zone J.* 17, 1–12.

Akter, M., Deroo, H., Kamal, A. M., Kader, M. A., Verhoeven, E., Decock, C., et al. (2018). Impact of irrigation management on paddy soil N supply and depth distribution of abiotic drivers. *Agric. Ecosyst. Environ.* 261, 12–24. doi: 10.1016/j.agee.2018.03.015

Al-Kodmany, K. (2018). The vertical farm: a review of developments and implications for the vertical city. *Buildings* 8, 1–36.

Alster, C. J., German, D. P., Lu, Y., and Allison, S. D. (2013). Microbial enzymatic responses to drought and to nitrogen addition in a Southern California grassland. *Soil Biol. Biochem.* 64, 68–79. doi: 10.1016/j.soilbio.2013.03.034

Alvarado, K. A., Mill, A., Pearce, J. M., Vocaet, A., and Denkenberger, D. (2020). Scaling of greenhouse crop production in low sunlight scenarios. *Sci. Total Environ.* 707:136012. doi: 10.1016/j.scitotenv.2019.136012

Amato-Lourenco, L. F., Buralli, R. J., Ranieri, G. R., Hearn, A. H., Williams, C., and Mauad, T. (2020). Building knowledge in urban agriculture: the challenges of

local food production in Sao Paulo and Melbourne. *Environ. Dev. Sustain.* 23, 2785–2796. doi: 10.1007/s10668-020-00636-x

Amitrano, C., Arena, C., Rouphael, Y., De Pascale, S., and De Micco, V. (2019). Vapour pressure deficit: the hidden driver behind plant morphofunctional traits in controlled environments. *Ann. Appl. Biol.* 175, 313–325. doi: 10.1111/aab.12544

Arikan, S., and Pirlak, L. (2016). Effects of plant growth promoting rhizobacteria (PGPR) on growth, yield and fruit quality of sour cherry (*Prunus cerasus* L.). *Erwerbs Obstbau* 58, 221–226. doi: 10.1007/s10341-016-0278-6

Armada, E., Roldan, A., and Azcon, R. (2014). Differential activity of autochthonous bacteria in controlling drought stress in native *Lavandula* and *Salvia* plants species under drought conditions in natural arid soil. *Microb. Ecol.* 67, 410–420. doi: 10.1007/s00248-013-0326-9

Armstrong, A., Valverde, A., Ramond, J., Makhalanyane, T. P., Jansson, J. K., Hopkins, D. W., et al. (2016). Temporal dynamics of hot desert microbial communities reveal structural and functional responses to water input. *Sci. Rep.* 6:34434.

Aung, K., Jiang, Y., and He, S. Y. (2018). The role of water in plant-microbe interactions. *Plant J.* 93, 771–780.

Bachar, A., Al-Ashhab, A., Soares, M. I. M., Sklarz, M. Y., Angel, R., Ungar, E. D., et al. (2010). Soil microbial abundance and diversity along a low precipitation gradient. *Microb. Ecol.* 60, 453–461. doi: 10.1007/s00248-010-9727-1

Balafoutis, A., Beck, B., Fountas, S., Vangeyte, J., van der Wal, T., Soto, I., et al. (2017). Precision agriculture technologies positively contributing to GHG emissions mitigation, farm productivity and economics. *Sustainability* 9:1339. doi: 10.3390/su9081339

Banitalebi, G., Mosaddeghi, M. R., and Shariatmadari, H. (2019). Feasibility of agricultural residues and their biochars for plant growing media: physical and hydraulic properties. *Waste Manage.* 87, 577–589. doi: 10.1016/j.wasman.2019.02.034

Bao, Q., Xiao, K., Chen, Z., Yao, H., and Zhu, Y. (2014). Methane production and methanogenic archaeal communities in two types of paddy soil amended with different amounts of rice straw. *FEMS Microbiol. Ecol.* 88, 372–385. doi: 10.1111/1574-6941.12305

Barbosa, G. L., Gadelha, F. D. A., Kublik, N., Proctor, A., Reichelm, L., Weissinger, E., et al. (2015). Comparison of land, water, and energy requirements of lettuce grown using hydroponic vs. conventional agricultural methods. *Int. J. Environ. Res. Public Health* 12, 6879–6891. doi: 10.3390/ijerph120606879

Bateman, E. J., and Baggs, E. M. (2005). Contributions of nitrification and denitrification to N2O emissions from soils at different water-filled pore space. *Biol. Fertil. Soils* 41, 379–388. doi: 10.1007/s00374-005-0858-3

Beckett, P. H. T., and Nafady, M. H. M. (1967). Potassium-calcium exchange equilibria in soils – location of non-specific (Gapon) and specific exchange sites. *J. Soil Sci.* 18, 263–281. doi: 10.1111/j.1365-2389.1967.tb01505.x

Blazewicz, S. J., Schwartz, E., and Firestone, M. K. (2014). Growth and death of bacteria and fungi underlie rainfall-induced carbon dioxide pulses from seasonally dried soil. *Ecology* 95, 1162–1172. doi: 10.1890/13-1031.1

Boari, A., Zuccari, D., and Vurro, M. (2008). 'Microbigation': delivery of biological control agents through drip irrigation systems. *Irrig. Sci.* 26, 101–107. doi: 10.1007/s00271-007-0076-x

Bobille, H., Fustec, J., Robins, R. J., Cukier, C., and Limami, A. M. (2019). Effect of water availability on changes in root amino acids and associated rhizosphere on root exudation of amino acids in *Pisum sativum* L. *Phytochemistry* 161, 75–85. doi: 10.1016/j.phytochem.2019.01.015

Bonanomi, G., Chirico, G. B., Palladino, M., Gaglione, S. A., Crispo, D. G., Lazzaro, U., et al. (2017). Combined application of photo-selective mulching films and beneficial microbes affects crop yield and irrigation water productivity in intensive farming systems. *Agric. Water Manage.* 184, 104–113. doi: 10.1016/j.agwat.2017.01.011

Bouskill, N. J., Wood, T. E., Baran, R., Hao, Z., Ye, Z., Bowen, B. P., et al. (2016a). Belowground response to drought in a tropical forest soil. II. Change in microbial function impacts carbon composition. *Front. Microbiol.* 7:323. doi: 10.3389/fmicb.2016.00323

Bouskill, N. J., Wood, T. E., Baran, R., Ye, Z., Bowen, B. P., Lim, H. C., et al. (2016b). Belowground response to drought in a tropical forest soil. I. Changes in microbial functional potential and metabolism. *Front. Microbiol.* 7:525. doi: 10.3389/fmicb.2016.00525

Bünemann, E. K. (2015). Assessment of gross and net mineralization rates of soil organic phosphorus – a review. *Soil Biol. Biochem.* 89, 82–98. doi: 10.1016/j.soilbio.2015.06.026

Burchi, G., Chessa, S., Gambineri, F., Kocian, A., Massa, D., Milazzo, P., et al. (2018). "Information technology controlled greenhouse: a system architecture," in *Proceedings of the 2018 IoT Vertical and Topical Summit on Agriculture – Tuscany (IOT Tuscany)*, (Tuscany), 6.

Calvo, O. C., Franzaring, J., Schmid, I., Mueller, M., Brohon, N., and Fangmeier, A. (2017). Atmospheric CO_2 enrichment and drought stress modify root exudation of barley. *Global Change Biol.* 23, 1292–1304. doi: 10.1111/gcb.13503

Cameron, K. C., Di, H. J., and Moir, J. L. (2013). Nitrogen losses from the soil/plant system: a review. *Ann. Appl. Biol.* 162, 145–173. doi: 10.1111/aab.12014

Campo, J., Jaramillo, V. J., and Maass, J. M. (1998). Pulses of soil phosphorus availability in a Mexican tropical dry forest: effects of seasonality and level of wetting. *Oecologia* 115, 167–172. doi: 10.1007/s004420050504

Carminati, A., Moradi, A. B., Vetterlein, D., Vontobel, P., Lehmann, E., Weller, U., et al. (2010). Dynamics of soil water content in the rhizosphere. *Plant Soil* 332, 163–176.

Carminati, A., Vetterlein, D., Weller, U., Vogel, H., and Oswald, S. E. (2009). When roots lose contact. *Vadose Zone J.* 8, 805–809. doi: 10.2136/vzj2008.0147

Casaregola, S., Vasilenko, A., Romano, P., Robert, V., Ozerskaya, S., Kopf, A., et al. (2016). An information system for European culture collections: the way forward. *SpringerPlus* 5, 1–11. doi: 10.1080/0960085x.2021.1889346

Cavagnaro, T. R. (2016). Soil moisture legacy effects: impacts on soil nutrients, plants and mycorrhizal responsiveness. *Soil Biol. Biochem.* 95, 173–179. doi: 10.1016/j.soilbio.2015.12.016

Chen, H., Shang, Z., Cai, H., and Zhu, Y. (2019a). Irrigation combined with aeration promoted soil respiration through increasing soil microbes, enzymes, and crop growth in tomato fields. *Catalysts* 9:945. doi: 10.3390/catal9110945

Chen, H., Shang, Z., Cai, H., and Zhu, Y. (2019b). Response of soil N_2O emissions to soil microbe and enzyme activities with aeration at two irrigation levels in greenhouse tomato (*Lycopersicon esculentum Mill.*) fields. *Atmosphere* 10:72. doi: 10.3390/atmos10020072

Clucas, B., Parker, I. D., and Feldpausch-Parker, A. M. (2018). A systematic review of the relationship between urban agriculture and biodiversity. *Urban Ecosyst.* 21, 635–643. doi: 10.1007/s11252-018-0748-8

Colla, G., Hoagland, L., Ruzzi, M., Cardarelli, M., Bonini, P., Canaguier, R., et al. (2017). Biostimulant action of protein hydrolysates: unraveling their effects on plant physiology and microbiome. *Front. Plant Sci.* 8:2202. doi: 10.3389/fpls.2017.02202

Conant, R. T., Ryan, M. G., Agren, G. I., Birge, H. E., Davidson, E. A., Eliasson, P. E., et al. (2011). Temperature and soil organic matter decomposition rates - synthesis of current knowledge and a way forward. *Global Change Biol.* 17, 3392–3404. doi: 10.1111/j.1365-2486.2011.02496.x

Cournane, F. C., McDowell, R. W., and Condron, L. M. (2010). Effects of cattle treading and soil moisture on phosphorus and sediment losses in surface runoff from pasture. *N. Z. J. Agric. Res.* 53, 365–376. doi: 10.1080/00288233.2010.509903

Csonka, L. N. (1989). Physiological and genetic responses of bacteria to osmotic-stress. *Microbiol. Rev.* 53, 121–147. doi: 10.1128/mr.53.1.121-147.1989

D'Alessio, M., Durso, L. M., Williams, C., Olson, C. A., Ray, C., and Paparozzi, E. T. (2020). Applied injected air into subsurface drip irrigation: plant uptake of pharmaceuticals and soil microbial communities. *J. Environ. Eng.* 146:06019008. doi: 10.1061/(asce)ee.1943-7870.0001655

de Vries, F. T., Griffiths, R. I., Knight, C. G., Nicolitch, O., and Williams, A. (2020). Harnessing rhizosphere microbiomes for drought-resilient crop production. *Science* 368, 270–274. doi: 10.1126/science.aaz5192

de Zeeuw, H., van Veenhuizen, R., and Dubbeling, M. (2011). The role of urban agriculture in building resilient cities in developing countries. *J. Agric. Sci.* 1491, 153–163. doi: 10.1017/s0021859610001279

Degrune, F., Boeraeve, F., Dufrene, M., Cornelis, J., Frey, B., and Hartmann, M. (2019). The pedological context modulates the response of soil microbial communities to agroecological management. *Front. Ecol. Evol.* 7:261. doi: 10.3389/fevo.2019.00261

DeLonge, M., Vandecar, K. L., D'Odorico, P., and Lawrence, D. (2013). The impact of changing moisture conditions on short-term P availability in weathered soils. *Plant Soil* 365, 201–209. doi: 10.1007/s11104-012-1373-6

Despommier, D. (2011). The vertical farm: controlled environment agriculture carried out in tall buildings would create greater food safety and security for large urban populations. *J. Verbrauch. Lebensm.* 6, 233–236. doi: 10.1007/s00003-010-0654-3

Dhaliwal, S. S., Naresh, R. K., Mandal, A., Singh, R., and Dhaliwal, M. K. (2019). Dynamics and transformations of micronutrients in agricultural soils as influenced by organic matter build-up: a review. *Environ. Sustain. Indic.* 1-2:100007. doi: 10.1016/j.indic.2019.100007

Dhayalan, V., and Sudalaimuthu, K. (2021). Plant growth promoting rhizobacteria in promoting sustainable agriculture. *Glob. J. Environ. Sci. Manage.* 7, 1–18.

Drenovsky, R. E., Vo, D., Graham, K. J., and Scow, K. M. (2004). Soil water content and organic carbon availability are major determinants of soil microbial community composition. *Microb. Ecol.* 48, 424–430. doi: 10.1007/s00248-003-1063-2

Eigenbrod, C., and Gruda, N. (2015). Urban vegetable for food security in cities. A review. *Agron. Sustain. Dev.* 35, 483–498. doi: 10.1007/s13593-014-0273-y

Enebe, M. C., and Babalola, O. O. (2018). The influence of plant growth-promoting rhizobacteria in plant tolerance to abiotic stress: a survival strategy. *Appl. Microbiol. Biol.* 102, 7821–7835. doi: 10.1007/s00253-018-9214-z

Epie, K. E., and Maral, E. (2018). Shoot and root biomass, phosphorus and nitrogen uptake of spring wheat grown in low phosphorus and moisture content conditions in a pot experiment. *J. Plant Nutr.* 41, 2273–2280. doi: 10.1080/01904167.2018.1510000

Farhangi, M. H., Turvani, M. E., van der Valk, A., and Carsjens, G. J. (2020). High-tech urban agriculture in Amsterdam: an actor network analysis. *Sustainability* 12:3955. doi: 10.3390/su12103955

Fatemeh, K., Osman, M. T., Raheleh, A. J., and Ezaz, F. (2018). Opportunities and challenges in sustainability of vertical farming: a review. *J. Landsc. Ecol.* 11, 35–60. doi: 10.1515/jlecol-2017-0016

Fei, Y., Huang, Y., Yan, C., Chao, Y., and He, W. (2008). Influence of greenhouse cultivation on agricultural soil environment. *J. Agro Environ. Sci.* 27, 243–247.

Fierer, N. (2017). Embracing the unknown: disentangling the complexities of the soil microbiome. *Nat. Rev. Microbiol.* 15, 579–590. doi: 10.1038/nrmicro.2017.87

Fierer, N., Bradford, M. A., and Jackson, R. B. (2007). Toward an ecological classification of soil bacteria. *Ecology* 88, 1354–1364. doi: 10.1890/05-1839

Fischer, H., Eckhardt, K., Meyer, A., Neumann, G., Leinweber, P., Fischer, K., et al. (2010). Rhizodeposition of maize: short-term carbon budget and composition. *J. Plant Nutr. Soil Sci.* 173, 67–79. doi: 10.1002/jpln.200800293

Fricano, R., and Davis, C. (2019). How well is urban agriculture growing in the Southern United States? Trends and issues from the perspective of urban planners regulating urban agriculture. *J. Agric. Food Syst. Commun. Dev.* 9, 31–53.

Frossard, E., Condron, L. M., Oberson, A., Sinaj, S., and Fardeau, J. C. (2000). Processes governing phosphorus availability in temperate soils. *J. Environ. Qual.* 29, 15–23. doi: 10.2134/jeq2000.00472425002900010003x

Gajc-Wolska, J., Bujalski, D., and Chrzanowska, A. (2008). Effect of a substrate on yielding and quality of greenhouse cucumber fruits. *J. Elementol.* 13, 205–210.

Gao, X., Zhang, S., Zhao, X., and Long, H. (2019). Stable water and fertilizer supply by negative pressure irrigation improve tomato production and soil bacterial communities. *SN Appl. Sci.* 1:718.

Ghiri, M. N., and Abtahi, A. (2011). Potassium dynamics in calcareous vertisols of southern Iran. *Arid Land Res. Manag.* 25, 257–274. doi: 10.1080/15324982.2011.565857

Ghosh, S., Watson, A., Gonzalez-Navarro, O. E., Ramirez-Gonzalez, R. H., Yanes, L., Mendoza-Suarez, M., et al. (2018). Speed breeding in growth chambers and glasshouses for crop breeding and model plant research. *Nat. Protoc.* 13, 2944–2963. doi: 10.1038/s41596-018-0072-z

Gleeson, D. B., Mueller, C., Banerjee, S., Ma, W., Siciliano, S. D., and Murphy, D. V. (2010). Response of ammonia oxidizing archaea and bacteria to changing water filled pore space. *Soil Biol. Biochem.* 42, 1888–1891. doi: 10.1016/j.soilbio.2010.06.020

Grierson, P. F., and Adams, M. A. (2000). Plant species affect acid phosphatase, ergosterol and microbial P in a Jarrah (*Eucalyptus marginata* Donn ex Sm.) forest in south-western Australia. *Soil Biol. Biochem.* 32, 1817–1827. doi: 10.1016/s0038-0717(00)00155-3

Grime, J. P. (1977). Evidence for existence of three primary strategies in plants and its relevance to ecological and evolutionary theory. *Am. Nat.* 111, 1169–1194. doi: 10.1086/283244

Hachiya, T., and Sakakibara, H. (2017). Interactions between nitrate and ammonium in their uptake, allocation, assimilation, and signaling in plants. *J. Exp. Bot.* 68, 2501–2512.

Halgamuge, M. N., Bojovschi, A., Fisher, P. M. J., Le, T. C., Adeloju, S., and Murphy, S. (2021). Internet of things and autonomous control for vertical cultivation walls towards smart food growing: a review. *Urban For. Urban Gree.* 61:127094. doi: 10.1016/j.ufug.2021.127094

Hall, E. K., Bernhardt, E. S., Bier, R. L., Bradford, M. A., Boot, C. M., Cotner, J. B., et al. (2018). Understanding how microbiomes influence the systems they inhabit. *Nat. Microbiol.* 3, 977–982. doi: 10.1038/s41564-018-0201-z

Hamoud, Y. A., Wang, Z., Guo, X., Shaghaleh, H., Sheteiwy, M., Chen, S., et al. (2019). Effect of irrigation regimes and soil texture on the potassium utilization efficiency of rice. *Agronomy* 9:100. doi: 10.3390/agronomy9020100

Hansen, J. C., Cade-Menun, B. J., and Strawn, D. G. (2004). Phosphorus speciation in manure-amended alkaline soils. *J. Environ. Qual.* 33, 1521–1527. doi: 10.2134/jeq2004.1521

Hartman, K., and Tringe, S. G. (2019). Interactions between plants and soil shaping the root microbiome under abiotic stress. *Biochem. J.* 476, 2705–2724. doi: 10.1042/bcj20180615

Hartmann, M., Brunner, I., Hagedorn, F., Bardgett, R. D., Stierli, B., Herzog, C., et al. (2017). A decade of irrigation transforms the soil microbiome of a semi-arid pine forest. *Mol. Ecol.* 26, 1190–1206. doi: 10.1111/mec.13995

He, C., Manevski, K., Andersen, M. N., Hu, C., Dong, W., and Li, J. (2019). Abiotic mechanisms for biochar effects on soil N_2O emission. *Int. Agrophys.* 33, 537–546. doi: 10.31545/intagr/111605

He, M., and Dijkstra, F. A. (2014). Drought effect on plant nitrogen and phosphorus: a metaanalysis. *New Phytol.* 204, 924–931. doi: 10.1111/nph.12952

Hedenec, P., Rui, J., Lin, Q., Yao, M., Li, J., Li, H., et al. (2018). Functional and phylogenetic response of soil prokaryotic community under an artificial moisture gradient. *Appl. Soil Ecol.* 124, 372–378. doi: 10.1016/j.apsoil.2017.12.009

Hemming, S., de Zwart, F., Elings, A., Petropoulou, A., and Righini, I. (2020). Cherry tomato production in intelligent greenhouses-sensors and AI for control of climate, irrigation, crop yield, and quality. *Sensors* 20, 1–30.

Herman, D. J., Johnson, K. K., Jaeger, C. H. I., Schwartz, E., and Firestone, M. K. (2006). Root influence on nitrogen mineralization and nitrification in *Avena barbata* rhizosphere soil. *Soil Sci. Soc. Am. J.* 70, 1504–1511. doi: 10.2136/sssaj2005.0113

Hisdal, H., and Tallaksen, L. M. (2003). Estimation of regional meteorological and hydrological drought characteristics: a case study for Denmark. *J. Hydrol.* 281, 230–247. doi: 10.1016/s0022-1694(03)00233-6

Ho, A., Kerckhof, F., Luke, C., Reim, A., Krause, S., Boon, N., et al. (2013). Conceptualizing functional traits and ecological characteristics of methane-oxidizing bacteria as life strategies. *Environ. Microbiol. Rep.* 5, 335–345. doi: 10.1111/j.1758-2229.2012.00370.x

Holland, J. E., Bennett, A. E., Newton, A. C., White, P. J., McKenzie, B. M., George, T. S., et al. (2018). Liming impacts on soils, crops and biodiversity in the UK: a review. *Sci. Total Environ.* 610, 316–332. doi: 10.1016/j.scitotenv.2017.08.020

Holz, M., Zarebanadkouki, M., Kaestner, A., Kuzyakov, Y., and Carminati, A. (2018a). Rhizodeposition under drought is controlled by root growth rate and rhizosphere water content. *Plant Soil* 423, 429–442. doi: 10.1007/s11104-017-3522-4

Holz, M., Zarebanadkouki, M., Kuzyakov, Y., Pausch, J., and Carminati, A. (2018b). Root hairs increase rhizosphere extension and carbon input to soil. *Ann. Bot.* 121, 61–69. doi: 10.1093/aob/mcx127

Hong, E., Choi, J., Nam, W., Kang, M., and Jang, J. (2014). Monitoring nutrient accumulation and leaching in plastic greenhouse cultivation. *Agric. Water Manage.* 146, 11–23. doi: 10.1016/j.agwat.2014.07.016

Hosseinzadeh, S., Verheust, Y., Bonarrigo, G., and Van Hulle, S. (2017). Closed hydroponic systems: operational parameters, root exudates occurrence and related water treatment. *Rev. Environ. Sci. Biol.* 16, 59–79. doi: 10.1007/s11157-016-9418-6

Howard, D. M., and Howard, P. J. A. (1993). Relationships between CO_2 evolution, moisture-content and temperature for a range of soil types. *Soil Biol. Biochem.* 25, 1537–1546. doi: 10.1016/0038-0717(93)90008-y

Hsiao, T. C., and Xu, L. K. (2000). Sensitivity of growth of roots versus leaves to water stress: biophysical analysis and relation to water transport. *J. Exp. Bot.* 51, 1595–1616. doi: 10.1093/jexbot/51.350.1595

Huang, S., Sun, Y., Yu, X., and Zhang, W. (2016). Interactive effects of temperature and moisture on CO_2 and CH_4 production in a paddy soil under long-term different fertilization regimes. *Biol. Fertil. Soils* 52, 285–294. doi: 10.1007/s00374-015-1075-3

Hunold, C., Sorunmu, Y., Lindy, R., Spatari, S., and Gurian, P. L. (2016). Is urban agriculture financially sustainable? An exploratory study of small-scale market farming in Philadelphia, Pennsylvania. *J. Agric. Food Syst. Commun. Dev.* 7, 51–67.

Igalavithana, A. D., Lee, S. S., Niazi, N. K., Lee, Y., Kim, K. H., Park, J., et al. (2017). Assessment of soil health in urban agriculture: soil enzymes and microbial properties. *Sustainability* 9:310. doi: 10.3390/su9020310

Jain, A., Chakraborty, J., and Das, S. (2020). Underlying mechanism of plant-microbe crosstalk in shaping microbial ecology of the rhizosphere. *Acta Physiol. Plant.* 42:8.

Jin, K., Shen, J., Ashton, R. W., White, R. P., Dodd, I. C., Parry, M. A. J., et al. (2015). Wheat root growth responses to horizontal stratification of fertiliser in a water-limited environment. *Plant Soil* 386, 77–88. doi: 10.1007/s11104-014-2249-8

Jones, D. L., Hodge, A., and Kuzyakov, Y. (2004). Plant and mycorrhizal regulation of rhizodeposition. *New Phytol.* 163, 459–480. doi: 10.1111/j.1469-8137.2004.01130.x

Jones, D. L., Nguyen, C., and Finlay, R. D. (2009). Carbon flow in the rhizosphere: carbon trading at the soil-root interface. *Plant Soil* 321, 5–33. doi: 10.1007/s11104-009-9925-0

Kallenbach, C. M., Frey, S. D., and Grandy, A. S. (2016). Direct evidence for microbial-derived soil organic matter formation and its ecophysiological controls. *Nat. Commun.* 7:13630.

Kim, H., Sudduth, K. A., and Hummel, J. W. (2009). Soil macronutrient sensing for precision agriculture. *J. Environ. Monit.* 11, 1810–1824. doi: 10.1039/b906634a

Knoth, J. L., Kim, S., Ettl, G. J., and Doty, S. L. (2014). Biological nitrogen fixation and biomass accumulation within poplar clones as a result of inoculations with diazotrophic endophyte consortia. *New Phytol.* 201, 599–609. doi: 10.1111/nph.12536

Koch, M., Naumann, M., Pawelzik, E., Gransee, A., and Thiel, H. (2020). The importance of nutrient management for potato production part I: plant nutrition and yield. *Potato Res.* 63, 97–119. doi: 10.1007/s11540-019-09431-2

Kool, D. M., Dolfing, J., Wrage, N., and Van Groenigen, J. W. (2011). Nitrifier denitrification as a distinct and significant source of nitrous oxide from soil. *Soil Biol. Biochem.* 43, 174–178. doi: 10.1016/j.soilbio.2010.09.030

Krause, S., Le Roux, X., Niklaus, P. A., Van Bodegom, P. M., Lennon, J. T., Bertilsson, S., et al. (2014). Trait-based approaches for understanding microbial biodiversity and ecosystem functioning. *Front. Microbiol.* 5:251. doi: 10.3389/fmicb.2014.00251

Kuchenbuch, R., Claassen, N., and Jungk, A. (1986). Potassium availability in relation to soil-moisture. 2. Calculations by means of a mathematical simulation-model. *Plant Soil* 95, 233–243. doi: 10.1007/bf02375075

Kuramae, E. E., Yergeau, E., Wong, L. C., Pijl, A. S., van Veen, J. A., and Kowalchuk, G. A. (2012). Soil characteristics more strongly influence soil bacterial communities than land-use type. *FEMS Microbiol. Ecol.* 79, 12–24. doi: 10.1111/j.1574-6941.2011.01192.x

Kuramae, E., Gamper, H., van Veen, J., and Kowalchuk, G. (2011). Soil and plant factors driving the community of soil-borne microorganisms across chronosequences of secondary succession of chalk grasslands with a neutral pH. *FEMS Microbiol. Ecol.* 77, 285–294. doi: 10.1111/j.1574-6941.2011.01110.x

Kuzyakov, Y., and Blagodatskaya, E. (2015). Microbial hotspots and hot moments in soil: concept & review. *Soil Biol. Biochem.* 83, 184–199. doi: 10.1016/j.soilbio.2015.01.025

Kuzyakov, Y., Friedel, J. K., and Stahr, K. (2000). Review of mechanisms and quantification of priming effects. *Soil Biol. Biochem.* 32, 1485–1498. doi: 10.1016/s0038-0717(00)00084-5

Kuzyakov, Y., Raskatov, A., and Kaupenjohann, M. (2003). Turnover and distribution of root exudates of *Zea mays*. *Plant Soil* 254, 317–327.

Ladau, J., and Eloe-Fadrosh, E. A. (2019). Spatial, temporal, and phylogenetic scales of microbial ecology. *Trends Microbiol.* 27, 662–669. doi: 10.1016/j.tim.2019.03.003

Lakhiar, I. A., Gao, J., Syed, T. N., Chandio, F. A., Buttar, N. A., and Qureshi, W. A. (2018). Monitoring and control systems in agriculture using intelligent sensor techniques: a review of the aeroponic system. *J. Sensors* 2018:18.

Landi, L., Valori, F., Ascher, J., Renella, G., Falchini, L., and Nannipieri, P. (2006). Root exudate effects on the bacterial communities, CO_2 evolution, nitrogen transformations and ATP content of rhizosphere and bulk soils. *Soil Biol. Biochem.* 38, 509–516. doi: 10.1016/j.soilbio.2005.05.021

Lauber, C. L., Hamady, M., Knight, R., and Fierer, N. (2009). Pyrosequencing-based assessment of soil pH as a predictor of soil bacterial community structure at the continental scale. *Appl. Environ. Microbiol.* 75, 5111–5120. doi: 10.1128/aem.00335-09

Lazny, R., Mirgos, M., Przybyl, J. L., Nowak, J. S., Kunka, M., Gajc-Wolska, J., et al. (2021). Effect of re-used lignite and mineral wool growing mats on plant growth, yield and fruit quality of cucumber and physical parameters of substrates in hydroponic cultivation. *Agronomy* 11:998. doi: 10.3390/agronomy11050998

Lee, S., Ka, J., and Cho, J. (2008). Members of the phylum *Acidobacteria* are dominant and metabolically active in rhizosphere soil. *FEMS Microbiol. Lett.* 285, 263–269. doi: 10.1111/j.1574-6968.2008.01232.x

Li, M., Schmidt, J. E., LaHue, D. G., Lazicki, P., Kent, A., Machmuller, M. B., et al. (2020). Impact of irrigation strategies on tomato root distribution and rhizosphere processes in an organic system. *Front. Plant Sci.* 11:360. doi: 10.3389/fpls.2020.00360

Li, X., Rui, J., Xiong, J., Li, J., He, Z., Zhou, J., et al. (2014). Functional potential of soil microbial communities in the maize rhizosphere. *PLoS One* 9:e112609. doi: 10.1371/journal.pone.0112609

Li, Y., Niu, W., Zhang, M., Wang, J., and Zhang, Z. (2020). Artificial soil aeration increases soil bacterial diversity and tomato root performance under greenhouse conditions. *Land Degrad. Dev.* 31, 1443–1461. doi: 10.1002/ldr.3560

Linn, D. M., and Doran, J. W. (1984a). Aerobic and anaerobic microbial-populations in no-till and plowed soils. *Soil Sci. Soc. Am. J.* 48, 794–799. doi: 10.2136/sssaj1984.03615995004800040019x

Linn, D. M., and Doran, J. W. (1984b). Effect of water-filled pore-space on carbon-dioxide and nitrous-oxide production in tilled and nontilled soils. *Soil Sci. Soc. Am. J.* 48, 1267–1272. doi: 10.2136/sssaj1984.03615995004800060013x

Liu, C., Rubaek, G. H., Liu, F., and Andersen, M. N. (2015). Effect of partial root zone drying and deficit irrigation on nitrogen and phosphorus uptake in potato. *Agric. Water Manage.* 159, 66–76. doi: 10.1016/j.agwat.2015.05.021

Long, H., Zhang, H., Yue, X., and Zhang, R. (2018). Design and experiment of heavy liquid-type negative pressure valve used for negative pressure irrigation. *Trans. Chin. Soc. Agric. Eng.* 34, 85–92.

Maestre, F. T., Delgado-Baquerizo, M., Jeffries, T. C., Eldridge, D. J., Ochoa, V., Gozalo, B., et al. (2015). Increasing aridity reduces soil microbial diversity and abundance in global drylands. *Proc. Natl. Acad. Sci. U.S.A.* 112, 15684–15689. doi: 10.1073/pnas.1516684112

Malik, A. A., Martiny, J. B. H., Brodie, E. L., Martiny, A. C., Treseder, K. K., and Allison, S. D. (2020). Defining trait-based microbial strategies with consequences for soil carbon cycling under climate change. *ISME J.* 14, 1–9. doi: 10.1038/s41396-019-0510-0

Malik, A. A., Puissant, J., Goodall, T., Allison, S. D., and Griffiths, R. I. (2019). Soil microbial communities with greater investment in resource acquisition have lower growth yield. *Soil Biol. Biochem.* 132, 36–39. doi: 10.1016/j.soilbio.2019.01.025

Manzoni, S., Schimel, J. P., and Porporato, A. (2012). Responses of soil microbial communities to water stress: results from a meta-analysis. *Ecology* 93, 930–938. doi: 10.1890/11-0026.1

Manzoni, S., Trofymow, J. A., Jackson, R. B., and Porporato, A. (2010). Stoichiometric controls on carbon, nitrogen, and phosphorus dynamics in decomposing litter. *Ecol. Monogr.* 80, 89–106. doi: 10.1890/09-0179.1

Marchuk, S., and Marchuk, A. (2018). Effect of applied potassium concentration on clay dispersion, hydraulic conductivity, pore structure and mineralogy of two contrasting Australian soils. *Soil Till. Res.* 182, 35–44. doi: 10.1016/j.still.2018.04.016

Marschner, P., Grierson, P. F., and Rengel, Z. (2005). Microbial community composition and functioning in the rhizosphere of three Banksia species in native woodland in Western Australia. *Appl. Soil Ecol.* 28, 191–201. doi: 10.1016/j.apsoil.2004.09.001

Miller, W. D., Neubauer, S. C., and Anderson, I. C. (2001). Effects of sea level induced disturbances on high salt marsh metabolism. *Estuaries* 24, 357–367. doi: 10.2307/1353238

Moore, D., Kostka, S. J., Boerth, T. J., Franklin, M., Ritsema, C. J., Dekker, L. W., et al. (2010). The effect of soil surfactants on soil hydrological behavior, the plant growth environment, irrigation efficiency and water conservation. *J. Hydrol. Hydromech.* 58, 142–148. doi: 10.2478/v10098-010-0013-1

Napawan, N. C., and Townsend, S. A. (2016). The landscape of urban agriculture in California's capital. *Landsc. Res.* 41, 780–794. doi: 10.1080/01426397.2016.1151484

Naseem, H., Ahsan, M., Shahid, M. A., and Khan, N. (2018). Exopolysaccharides producing rhizobacteria and their role in plant growth and drought tolerance. *J. Basic Microbiol.* 58, 1009–1022. doi: 10.1002/jobm.201800309

Naylor, D., and Coleman-Derr, D. (2018). Drought stress and root-associated bacterial communities. *Front. Plant Sci.* 8:2223. doi: 10.3389/fpls.2017.02223

Niu, G., and Masabni, J. (2018). Plant production in controlled environments. *Horticulturae* 4, 1–4.

Nobel, P. S., and Cui, M. Y. (1992). Hydraulic conductances of the soil, the root soil air gap, and the root – changes for desert succulents in drying soil. *J. Exp. Bot.* 43, 319–326. doi: 10.1093/jxb/43.3.319

Novosad, N., and Kay, B. D. (2007). Water-filled microbially habitable pores: relation to denitrification. *Can. J. Soil Sci.* 87, 269–280. doi: 10.4141/s06-037

Ntinas, G. K., Dannehl, D., Schuch, I., Rocksch, T., and Schmidt, U. (2020). Sustainable greenhouse production with minimised carbon footprint by energy export. *Biosyst. Eng.* 189, 164–178. doi: 10.1016/j.biosystemseng.2019.11.012

Okegbe, C., Price-Whelan, A., and Dietrich, L. E. P. (2014). Redox-driven regulation of microbial community morphogenesis. *Curr. Opin. Microbiol.* 18, 39–45. doi: 10.1016/j.mib.2014.01.006

Orsini, F., Kahane, R., Nono-Womdim, R., and Gianquinto, G. (2013). Urban agriculture in the developing world: a review. *Agron. Sustain. Dev.* 33, 695–720.

Orwin, K. H., Bertram, J. E., Clough, T. J., Condron, L. M., Sherlock, R. R., O'Callaghan, M., et al. (2010). Impact of bovine urine deposition on soil microbial activity, biomass, and community structure. *Appl. Soil Ecol.* 44, 89–100. doi: 10.1016/j.apsoil.2009.10.004

Palta, J. A., and Gregory, P. J. (1997). Drought affects the fluxes of carbon to roots and soil in C-13 pulse-labelled plants of wheat. *Soil Biol. Biochem.* 29, 1395–1403. doi: 10.1016/s0038-0717(97)00050-3

Parton, W. J., Mosier, A. R., Ojima, D. S., Valentine, D. W., Schimel, D. S., Weier, K., et al. (1996). Generalized model for N_2 and N_2O production from nitrification and denitrification. *Global Biogeochem. Cycles* 10, 401–412.

Pascault, N., Ranjard, L., Kaisermann, A., Bachar, D., Christen, R., Terrat, S., et al. (2013). Stimulation of different functional groups of bacteria by various plant residues as a driver of soil priming effect. *Ecosystems* 16, 810–822. doi: 10.1007/s10021-013-9650-7

Pausch, J., and Kuzyakov, Y. (2011). Photoassimilate allocation and dynamics of hotspots in roots visualized by C-14 phosphor imaging. *J. Plant Nutr. Soil Sci.* 174, 12–19. doi: 10.1002/jpln.200900271

Philippot, L., Raaijmakers, J. M., Lemanceau, P., and van der Putten, W. H. (2013). Going back to the roots: the microbial ecology of the rhizosphere. *Nat. Rev. Microbiol.* 11, 789–799. doi: 10.1038/nrmicro3109

Pii, Y., Mimmo, T., Tomasi, N., Terzano, R., Cesco, S., and Crecchio, C. (2015). Microbial interactions in the rhizosphere: beneficial influences of plant growth-promoting rhizobacteria on nutrient acquisition process. A review. *Biol. Fertil. Soils* 51, 403–415. doi: 10.1007/s00374-015-0996-1

Poncet, C., Bresch, C., Fatnassi, H., Mailleret, L., Bout, A., Perez, G., et al. (2015). "Technological and ecological approaches to design and manage sustainable greenhouse production systems," in *Proceedings of the 29th International Horticultural Congress on Horticulture – Sustaining Lives, Livelihoods and Landscapes (IHC) / International Symposium on Innovation and New Technologies in Protected Cropping*, (Brisbane, QLD), 44–51.

Preece, C., and Penuelas, J. (2016). Rhizodeposition under drought and consequences for soil communities and ecosystem resilience. *Plant Soil* 409, 1–17. doi: 10.1007/s11104-016-3090-z

Pretty, J. (2018). Intensification for redesigned and sustainable agricultural systems. *Science* 362:908.

Prober, S. M., Leff, J. W., Bates, S. T., Borer, E. T., Firn, J., Harpole, W. S., et al. (2015). Plant diversity predicts beta but not alpha diversity of soil microbes across grasslands worldwide. *Ecol. Lett.* 18, 85–95. doi: 10.1111/ele.12381

Qin, H., Xing, X., Tang, Y., Zhu, B., Wei, X., Chen, X., et al. (2020). Soil moisture and activity of nitrite- and nitrous oxide-reducing microbes enhanced nitrous oxide emissions in fallow paddy soils. *Biol. Fertil. Soils* 56, 53–67. doi: 10.1007/s00374-019-01403-5

Qin, K., Dong, X., Jifon, J., and Leskovar, D. I. (2019). Rhizosphere microbial biomass is affected by soil type, organic and water inputs in a bell pepper system. *Appl. Soil Ecol.* 138, 80–87. doi: 10.1016/j.apsoil.2019.02.024

Rajkumar, M., Bruno, L. B., and Banu, J. R. (2017). Alleviation of environmental stress in plants: the role of beneficial *Pseudomonas* spp. *Crit. Rev. Environ. Sci. Technol.* 47, 372–407. doi: 10.1080/10643389.2017.1318619

Rasool, G., Guo, X., Wang, Z., Ali, M. U., Chen, S., Zhang, S., et al. (2020). Coupling fertigation and buried straw layer improves fertilizer use efficiency, fruit yield, and quality of greenhouse tomato. *Agric. Water Manage.* 239:106239. doi: 10.1016/j.agwat.2020.106239

Read, D. B., Gregory, P. J., and Bell, A. E. (1999). Physical properties of axenic maize root mucilage. *Plant Soil* 211, 87–91.

Recous, S., Robin, D., Darwis, D., and Mary, B. (1995). Soil inorganic N availability: effect on maize residue decomposition. *Soil Biol. Biochem.* 27, 1529–1538. doi: 10.1016/0038-0717(95)00096-w

Rocca, J. D., Hall, E. K., Lennon, J. T., Evans, S. E., Waldrop, M. P., Cotner, J. B., et al. (2015). Relationships between protein-encoding gene abundance and corresponding process are commonly assumed yet rarely observed. *ISME J.* 9, 1693–1699. doi: 10.1038/ismej.2014.252

Salazar-Moreno, R., Sánchez-Martínez, A. C., and López-Cruz, I. L. (2020). Indicators for assessing water, energy and labor use performance in a low-tech greenhouse. *Rev. Chapingo Ser. Hortic.* 26, 95–110. doi: 10.5154/r.rchsh.2019.09.018

Sammauria, R., Kumawat, S., Kumawat, P., Singh, J., and Jatwa, T. K. (2020). Microbial inoculants: potential tool for sustainability of agricultural production systems. *Arch. Microbiol.* 202, 677–693. doi: 10.1007/s00203-019-01795-w

Sanaullah, M., Chabbi, A., Rumpel, C., and Kuzyakov, Y. (2012). Carbon allocation in grassland communities under drought stress followed by C-14 pulse labeling. *Soil Biol. Biochem.* 55, 132–139. doi: 10.1016/j.soilbio.2012.06.004

Sandhya, V., Ali, S. Z., Grover, M., Reddy, G., and Venkateswarlu, B. (2010). Effect of plant growth promoting *Pseudomonas* spp. on compatible solutes, antioxidant status and plant growth of maize under drought stress. *Plant Growth Regul.* 62, 21–30. doi: 10.1007/s10725-010-9479-4

Sanye-Mengual, E., Specht, K., Krikser, T., Venni, C., Pennisi, G., Orsini, F., et al. (2018). Social acceptance and perceived ecosystem services of urban agriculture in Southern Europe: the case of Bologna, Italy. *PLoS One* 13:e0200993. doi: 10.1371/journal.pone.0200993

Sardans, J., and Penuelas, J. (2005). Drought decreases soil enzyme activity in a Mediterranean *Quercus ilex* L. forest. *Soil Biol. Biochem.* 37, 455–461. doi: 10.1016/j.soilbio.2004.08.004

Scavo, A., Abbate, C., and Mauromicale, G. (2019). Plant allelochemicals: agronomic, nutritional and ecological relevance in the soil system. *Plant Soil* 442, 23–48. doi: 10.1007/s11104-019-04190-y

Schimel, J. P., and Bennett, J. (2004). Nitrogen mineralization: challenges of a changing paradigm. *Ecology* 85, 591–602. doi: 10.1890/03-8002

Schimel, J. P., and Schaeffer, S. M. (2012). Microbial control over carbon cycling in soil. *Front. Microbiol.* 3:348. doi: 10.3389/fmicb.2012.00348

Schimel, J., Balser, T. C., and Wallenstein, M. (2007). Microbial stress-response physiology and its implications for ecosystem function. *Ecology* 88, 1386–1394. doi: 10.1890/06-0219

Schmidt, M. W. I., Torn, M. S., Abiven, S., Dittmar, T., Guggenberger, G., Janssens, I. A., et al. (2011). Persistence of soil organic matter as an ecosystem property. *Nature* 478, 49–56. doi: 10.1038/nature10386

Shah, A., and Smith, D. L. (2020). Flavonoids in agriculture: chemistry and roles in, biotic and abiotic stress responses, and microbial associations. *Agronomy* 10:1209. doi: 10.3390/agronomy10081209

Shamshiri, R. R., Kalantari, F., Ting, K. C., Thorp, K. R., Hameed, I. A., Weltzien, C., et al. (2018). Advances in greenhouse automation and controlled environment

agriculture: a transition to plant factories and urban agriculture. *Int. J. Agric. Biol. Eng.* 11, 1–22.

Sharp, R. E., Poroyko, V., Hejlek, L. G., Spollen, W. G., Springer, G. K., Bohnert, H. J., et al. (2004). Root growth maintenance during water deficits: physiology to functional genomics. *J. Exp. Bot.* 55, 2343–2351. doi: 10.1093/jxb/erh276

Shi, W., Yao, J., and Yan, F. (2009). Vegetable cultivation under greenhouse conditions leads to rapid accumulation of nutrients, acidification and salinity of soils and groundwater contamination in South-Eastern China. *Nutr. Cycl. Agroecosyst.* 83, 73–84. doi: 10.1007/s10705-008-9201-3

Shuyu, Y., Yirong, D., and Xiao, Z. (2021). Research and application of agricultural internet of things technology in intelligent agriculture. *J. Phys.* 1769:012020. doi: 10.1088/1742-6596/1769/1/012020

Sierra, C. A., Trumbore, S. E., Davidson, E. A., Vicca, S., and Janssens, I. (2015). Sensitivity of decomposition rates of soil organic matter with respect to simultaneous changes in temperature and moisture. *J. Adv. Model. Earth Syst.* 7, 335–356. doi: 10.1002/2014ms000358

Sigrimis, N., Antsaklis, P., and Groumpos, P. P. (2001). Advances in control of agriculture and the environment. *IEEE Control Syst. Mag.* 21, 8–12. doi: 10.1109/37.954516

Singh, H., Poudel, M. R., Dunn, B., Fontanier, C., and Kakani, G. (2020). Greenhouse carbon dioxide supplementation with irrigation and fertilization management of geranium and fountain grass. *Hortscience* 55, 1772–1780. doi: 10.21273/hortsci15327-20

Singh, J. S., Pandey, V. C., and Singh, D. P. (2011). Efficient soil microorganisms: a new dimension for sustainable agriculture and environmental development. *Agric. Ecosyst. Environ.* 140, 339–353. doi: 10.1016/j.agee.2011.01.017

Singh, R., Glick, B. R., and Rathore, D. (2020). Role of textile effluent fertilization with biosurfactant to sustain soil quality and nutrient availability. *J. Environ. Manage.* 268:110664. doi: 10.1016/j.jenvman.2020.110664

Škarpa, P., and Hlušek, J. (2012). Effect of years, fertilization and growing regions on the content and forms of potassium in soil. *J. Elementol.* 17, 305–315.

Skopp, J., Jawson, M. D., and Doran, J. W. (1990). Steady-state aerobic microbial activity as a function of soil-water content. *Soil Sci. Soc. Am. J.* 54, 1619–1625. doi: 10.2136/sssaj1990.03615995005400060018x

Słowińska-Jurkiewicz, A., and Jaroszuk-Sierocińska, M. (2011). "Horticulture substrates, structure and physical properties," in *Encyclopedia of Agrophysics*, eds J. Gliński, J. Horabik, and J. Lipiec (Dordrecht: Springer), 364–367. doi: 10.1007/978-90-481-3585-1_67

Somaweera, K. A. T. N., Suriyagoda, L. D. B., Sirisena, D. N., and De Costa, W. A. J. M. (2017). Growth, root adaptations, phosphorus and potassium nutrition of rice when grown under the co-limitations of phosphorus, potassium and moisture. *J. Plant Nutr.* 40, 795–812. doi: 10.1080/01904167.2016.1201497

Somma, F., Hopmans, J. W., and Clausnitzer, V. (1998). Transient three-dimensional modeling of soil water and solute transport with simultaneous root growth, root water and nutrient uptake. *Plant Soil* 202, 281–293.

Song, F., Han, X., Zhu, X., and Herbert, S. J. (2012). Response to water stress of soil enzymes and root exudates from drought and non-drought tolerant corn hybrids at different growth stages. *Can. J. Soil Sci.* 92, 501–507. doi: 10.4141/cjss2010-057

Sposito, G. (2013). Green water and global food security. *Vadose Zone J.* 12, 1–6. doi: 10.2136/vzj2013.02.0041

Stark, J. M., and Firestone, M. K. (1995). Mechanisms for soil moisture effects on activity of nitrifying bacteria. *Appl. Environ. Microbiol.* 61, 218–221. doi: 10.1128/aem.61.1.218-221.1995

Styles, D., and Coxon, C. (2006). Laboratory drying of organic-matter rich soils: phosphorus solubility effects, influence of soil characteristics, and consequences for environmental interpretation. *Geoderma* 136, 120–135. doi: 10.1016/j.geoderma.2006.03.017

Sun, D., Bi, Q., Li, K., Dai, P., Yu, Y., Zhou, W., et al. (2018). Significance of temperature and water availability for soil phosphorus transformation and microbial community composition as affected by fertilizer sources. *Biol. Fertil. Soils* 54, 229–241. doi: 10.1007/s00374-017-1252-7

Sun, D., Mullerova, V., Ardestani, M. M., and Frouz, J. (2019). Nitrogen fertilization and its legacy have inconsistent and often negative effect on plant growth in undeveloped post mining soils. *Soil Till. Res.* 195:104380. doi: 10.1016/j.still.2019.104380

Suseela, V., Conant, R. T., Wallenstein, M. D., and Dukes, J. S. (2012). Effects of soil moisture on the temperature sensitivity of heterotrophic respiration vary seasonally in an old-field climate change experiment. *Global Change Biol.* 18, 336–348. doi: 10.1111/j.1365-2486.2011.02516.x

Takahashi, S., Ihara, H., and Karasawa, T. (2016). Compost in pellet form and compost moisture content affect phosphorus fractions of soil and compost. *Soil Sci. Plant Nutr.* 62, 399–404. doi: 10.1080/00380768.2016.1198680

Tang, S., Cheng, W., Hu, R., Guigue, J., Kimani, S. M., Tawaraya, K., et al. (2016). Simulating the effects of soil temperature and moisture in the off-rice season on rice straw decomposition and subsequent CH4 production during the growth season in a paddy soil. *Biol. Fertil. Soils* 52, 739–748. doi: 10.1007/s00374-016-1114-8

Tate, R. L. (1979). Effect of flooding on microbial activities in organic soils - carbon metabolism. *Soil Sci.* 128, 267–273. doi: 10.1097/00010694-197911000-00002

Teijeiro, R. G., Belimov, A. A., and Dodd, I. C. (2020). Microbial inoculum development for ameliorating crop drought stress: a case study of *Variovorax paradoxus* 5C-2. *New Biotechnol.* 56, 103–113. doi: 10.1016/j.nbt.2019.12.006

Tocheva, E. I., Ortega, D. R., and Jensen, G. J. (2016). Sporulation, bacterial cell envelopes and the origin of life. *Nat. Rev. Microbiol.* 14, 535–542. doi: 10.1038/nrmicro.2016.85

Treseder, K. K., Kivlin, S. N., and Hawkes, C. V. (2011). Evolutionary trade-offs among decomposers determine responses to nitrogen enrichment. *Ecol. Lett.* 14, 933–938. doi: 10.1111/j.1461-0248.2011.01650.x

Tuzel, Y., and Oztekin, G. B. (2016). "Recent developments of vegetables protected cultivation in Turkey," in *Proceedings of the 6th Balkan Symposium on Vegetables and Potatoes*, (Zagreb), 435–441. doi: 10.17660/actahortic.2016.1142.66

Ullah, A., Nisar, M., Ali, H., Hazrat, A., Hayat, K., Keerio, A. A., et al. (2019). Drought tolerance improvement in plants: an endophytic bacterial approach. *Appl. Microbiol. Biol.* 103, 7385–7397. doi: 10.1007/s00253-019-10045-4

Vandecar, K. L., Lawrence, D., and Clark, D. (2011). Phosphorus sorption dynamics of anion exchange resin membranes in tropical rain forest soils. *Soil Sci. Soc. Am. J.* 75, 1520–1529. doi: 10.2136/sssaj2010.0390

Vetterlein, D., and Jahn, R. (2004). Gradients in soil solution composition between bulk soil and rhizosphere – in situ measurement with changing soil water content. *Plant Soil* 258, 307–317. doi: 10.1023/b:plso.0000016560.84772.d1

Videgain-Marco, M., Marco-Montori, P., Marti-Dalmau, C., Del Carmen Jaizme-Vega, M., Josep Manya-Cervello, J., and Javier Garcia-Ramos, F. (2020). Effects of biochar application in a sorghum crop under greenhouse conditions: growth parameters and physicochemical fertility. *Agronomy* 10:104. doi: 10.3390/agronomy10010104

Vurukonda, S. S. K. P., Vardharajula, S., Shrivastava, M., and SkZ, A. (2016). Enhancement of drought stress tolerance in crops by plant growth promoting rhizobacteria. *Microbiol. Res.* 184, 13–24. doi: 10.1016/j.micres.2015.12.003

Wang, F. L., and Huang, P. M. (2001). Effects of organic matter on the rate of potassium adsorption by soils. *Can. J. Soil Sci.* 81, 325–330. doi: 10.4141/s00-069

Wang, H., Boutton, T. W., Xu, W., Hu, G., Jiang, P., and Bai, E. (2015). Quality of fresh organic matter affects priming of soil organic matter and substrate utilization patterns of microbes. *Sci. Rep.* 5:10102.

Wang, H., Wu, L., Cheng, M., Fan, J., Zhang, F., Zou, Y., et al. (2018). Coupling effects of water and fertilizer on yield, water and fertilizer use efficiency of drip-fertigated cotton in northern Xinjiang, China. *Field Crop Res.* 219, 169–179. doi: 10.1016/j.fcr.2018.02.002

Wang, P., Marsh, E. L., Kruger, G., Lorenz, A., and Schachtman, D. P. (2020). Belowground microbial communities respond to water deficit and are shaped by decades of maize hybrid breeding. *Environ. Microbiol.* 22, 889–904. doi: 10.1111/1462-2920.14701

Wang, Q., Xu, J., Lin, H., Zou, P., and Jiang, L. (2017). Effect of rice planting on the nutrient accumulation and transfer in soils under plastic greenhouse vegetable-rice rotation system in southeast China. *J. Soil Sediment.* 17, 204–209. doi: 10.1007/s11368-016-1495-1

Welsh, D. T. (2000). Ecological significance of compatible solute accumulation by micro-organisms: from single cells to global climate. *FEMS Microbiol. Rev.* 24, 263–290. doi: 10.1111/j.1574-6976.2000.tb00542.x

Wieder, W. R., Bonan, G. B., and Allison, S. D. (2013). Global soil carbon projections are improved by modelling microbial processes. *Nat. Clim. Change* 3, 909–912. doi: 10.1038/nclimate1951

Wieder, W. R., Grandy, A. S., Kallenbach, C. M., Taylor, P. G., and Bonan, G. B. (2015). Representing life in the earth system with soil microbial functional traits in the MIMICS model. *Geosci. Model Dev.* 8, 1789–1808. doi: 10.5194/gmd-8-1789-2015

Williams, A., and de Vries, F. T. (2020). Plant root exudation under drought: implications for ecosystem functioning. *New Phytol.* 225, 1899–1905. doi: 10.1111/nph.16223

Williams, M. A. (2007). Response of microbial communities to water stress in irrigated and drought-prone tallgrass prairie soils. *Soil Biol. Biochem.* 39, 2750–2757. doi: 10.1016/j.soilbio.2007.05.025

Wilson, J. S., Baldwin, D. S., Rees, G. N., and Wilson, B. P. (2011). The effects of short-term inundation on carbon dynamics, microbial community structure and microbial activity in floodplain soil. *River Res. Appl.* 27, 213–225. doi: 10.1002/rra.1352

Witteveen, C. F. B., and Visser, J. (1995). Polyol pools in *Aspergillus-niger*. *FEMS Microbiol. Lett.* 134, 57–62. doi: 10.1111/j.1574-6968.1995.tb07914.x

Wolf, A. B., Vos, M., de Boer, W., and Kowalchuk, G. A. (2013). Impact of matric potential and pore size distribution on growth dynamics of filamentous and non-filamentous soil bacteria. *PLoS One* 8:e83661. doi: 10.1371/journal.pone.0083661

Wood, J. L., Tang, C., and Franks, A. E. (2018). Competitive traits are more important than stress-tolerance traits in a cadmium-contaminated rhizosphere: a role for trait theory in microbial ecology. *Front. Microbiol.* 9:121. doi: 10.3389/fmicb.2018.00121

Wrage, N., Velthof, G. L., van Beusichem, M. L., and Oenema, O. (2001). Role of nitrifier denitrification in the production of nitrous oxide. *Soil Biol. Biochem.* 33, 1723–1732. doi: 10.1016/s0038-0717(01)00096-7

Xiao, Y., Jiang, S. C., Wang, X., Muhammad, T., Song, P., Zhou, B., et al. (2020). Mitigation of biofouling in agricultural water distribution systems with nanobubbles. *Environ. Int.* 141:105787. doi: 10.1016/j.envint.2020.105787

Xie, H., Gao, M., Zhang, R., Xu, H., Wang, Y., and Deng, J. (2017). The subversive idea and its key technical prospect on underground ecological city and ecosystem. *Chin. J. Rock Mech. Eng.* 36, 1301–1313.

Xu, X., Du, X., Wang, F., Sha, J., Chen, Q., Tian, G., et al. (2020). Effects of potassium levels on plant growth, accumulation and distribution of carbon, and nitrate metabolism in apple dwarf rootstock seedlings. *Front. Plant Sci.* 11:904. doi: 10.3389/fpls.2020.00904

Yadav, V. K., Raghav, M., Sharma, S. K., and Bhagat, N. (2020). Rhizobacteriome: promising candidate for conferring drought tolerance in crops. *J. Pure Appl. Microbiol.* 14, 73–92. doi: 10.22207/jpam.14.1.10

Yang, J., Li, Z., Liang, Y., Zhang, L., and Li, W. (2009). Effects and their mechanisms of temperature and moisture on phosphorous transformation in black soil manured with different fertilizers. *Plant Nutr. Fertil. Sci.* 15, 1295–1302.

Yao, Y., Yao, X., An, L., Bai, Y., Xie, D., and Wu, K. (2020). Rhizosphere bacterial community response to continuous cropping of Tibetan barley. *Front. Microbiol.* 11:551444. doi: 10.3389/fmicb.2020.551444

Yuan, J., Zhao, J., Wen, T., Zhao, M., Li, R., Goossens, P., et al. (2018). Root exudates drive the soil-borne legacy of aboveground pathogen infection. *Microbiome* 6:156.

Yuste, J. C., Baldocchi, D. D., Gershenson, A., Goldstein, A., Misson, L., and Wong, S. (2007). Microbial soil respiration and its dependency on carbon inputs, soil temperature and moisture. *Global Change Biol.* 13, 2018–2035. doi: 10.1111/j.1365-2486.2007.01415.x

Zarebanadkouki, M., and Carminati, A. (2014). Reduced root water uptake after drying and rewetting. *J. Plant Nutr. Soil Sci.* 177, 227–236. doi: 10.1002/jpln.201300249

Zhang, R., Chen, L., Niu, Z., Song, S., and Zhao, Y. (2019). Water stress affects the frequency of Firmicutes, Clostridiales and Lysobacter in rhizosphere soils of greenhouse grape. *Agric. Water Manage.* 226:105776. doi: 10.1016/j.agwat.2019.105776

Zhang, X., Zhang, Q., Liang, B., and Li, J. (2017). Changes in the abundance and structure of bacterial communities in the greenhouse tomato cultivation system under long-term fertilization treatments. *Appl. Soil Ecol.* 121, 82–89. doi: 10.1016/j.apsoil.2017.08.016

Zhang, Y., Hou, W., Chi, M., Sun, Y., An, J., Yu, N., et al. (2020). Simulating the effects of soil temperature and soil moisture on CO_2 and CH_4 emissions in rice straw-enriched paddy soil. *Catena* 194:104677. doi: 10.1016/j.catena.2020.104677

Zhao, X., Gao, X., Zhang, S., and Long, H. (2019). Improving the growth of rapeseed (*Brassica chinensis* L.) and the composition of rhizosphere bacterial communities through negative pressure irrigation. *Water Air Soil Pollut.* 230:9.

Zhou, W., Hui, D., and Shen, W. (2014). Effects of soil moisture on the temperature sensitivity of soil heterotrophic respiration: a laboratory incubation study. *PLoS One* 9:e92531. doi: 10.1371/journal.pone.0092531

Zhu, X., Burger, M., Doane, T. A., and Horwath, W. R. (2013). Ammonia oxidation pathways and nitrifier denitrification are significant sources of N_2O and NO under low oxygen availability. *Proc. Natl. Acad. Sci. U.S.A.* 110, 6328–6333. doi: 10.1073/pnas.1219993110

Zulfiqar, F., Shang, J., Yasmeen, S., Wattoo, M. U., Nasrullah, M., and Alam, Q. (2020). Urban agriculture can transform the sustainable food security for urban dwellers in Pakistan. *GeoJournal* doi: 10.1007/s10708-020-10208-1

Conflict of Interest: The authors declare that the research was conducted in the absence of any commercial or financial relationships that could be construed as a potential conflict of interest.

Publisher's Note: All claims expressed in this article are solely those of the authors and do not necessarily represent those of their affiliated organizations, or those of the publisher, the editors and the reviewers. Any product that may be evaluated in this article, or claim that may be made by its manufacturer, is not guaranteed or endorsed by the publisher.

frontiers in Plant Science

REVIEW
published: 23 August 2021
doi: 10.3389/fpls.2021.668819

Vitamin B_{12} (Cobalamin) and Micronutrient Fortification in Food Crops Using Nanoparticle Technology

*Soojin Oh[1], Gareth Cave[2] and Chungui Lu[1]**

[1] School of Animal, Rural and Environmental Sciences, Nottingham Trent University, Nottingham, United Kingdom, [2] School of Science and Technology, Nottingham Trent University, Nottingham, United Kingdom

It is necessary to develop a resilient food supply that will withstand unexpected future shocks and deliver the required amounts of nutrients to consumers. By increasing the sustainability of food and agriculture, the food system will be able to handle challenges such as climate change, declining agricultural resources, growing population/urbanization, pandemics, and recessions/shortages. Micronutrient deficiency, otherwise called hidden hunger, is one of the major malnutrition consequences worldwide, particularly in middle- or low- income countries. Unlike essential mineral or nutrient compounds, micronutrients could be less of a priority due to their small levels of requirement. However, insufficient micronutrients caused critical adverse health symptoms and are excessively vital for young children's development. Therefore, there have been numerous attempts to enhance minerals and nutrients in food crops, including biofortification, food fortification, and supplementation. Based on several interventions involving micronutrients, modern technology, such as nanotechnology, can be applied to enhance sustainability and to reduce the food system's environmental impact. Previous studies have addressed various strategies or interventions to mitigate major micronutrient deficiency including iron, iodine, zinc, and vitamin A. Comparably small amounts of studies have addressed vitamin B_{12} deficiency and its fortification in food crops. Vitamin B_{12} deficiency causes serious adverse health effects, including in the nervous or blood systems, and occurs along with other micronutrient deficiencies, such as folate, iron, and zinc, worldwide, particularly in middle- and low-income countries. Mitigation for B_{12} deficiency has mainly focused on developing pharmacological and medical treatments such as vitamin B_{12} serum or supplements. Further studies are required to undertake a sustainable approach to fortify vitamin B_{12} in plant-based food sources for public health worldwide. This review paper highlights nanoparticle application as a promising technology for enhancing vitamin B_{12} without conventional genetic modification requirements. The nanoparticle can efficiently deliver the mineral/nutrient using coating techniques to targeted sites into the plant. This is mainly because nanoparticles have better solubility and permeability due to their nano size with high surface exposure. Vitamin B_{12}-coated nanoparticles would

OPEN ACCESS

Edited by:
Jung Eek Son,
Seoul National University,
South Korea

Reviewed by:
Dimitrios Savvas,
Agricultural University of Athens,
Greece
Hyo Gil Choi,
Kongju National University,
South Korea

***Correspondence:**
Chungui Lu
Chungui.Lu@ntu.ac.uk

Specialty section:
This article was submitted to Technical Advances in Plant Science, a section of the journal Frontiers in Plant Science

Received: *17 February 2021*
Accepted: *22 June 2021*
Published: *23 August 2021*

Citation:
Oh S, Cave G and Lu C (2021) Vitamin B_{12} (Cobalamin) and Micronutrient Fortification in Food Crops Using Nanoparticle Technology. Front. Plant Sci. 12:668819. doi: 10.3389/fpls.2021.668819

be absorbed, translocated, and accumulated by the plant and eventually enhance the bioavailability in food crops. Furthermore, by reducing adverse environmental effects, such as leaching issues that mainly occur with conventional fertilizer usage, it would be possible to develop more sustainable food fortification.

Keywords: biofortification, cobalamin (Cbl), food fortification, nanoparticle, vitamin B_{12}, vitamin B_{12} deficiency

INTRODUCTION

A healthy diet contains adequate amounts of macronutrients, including proteins, fats, and carbohydrates, and essential micronutrients, such as vitamins and minerals. However, the current global food system does not meet the universal requirement of adequate nutrition in food production, which directly influences human health. According to the Food and Agriculture Organization, over 690 million people worldwide are suffering hunger and nearly 750 million people have been exposed to food insecurity in 2019 (FAO et al., 2020). Globally, current food consumption shifts towards animal-based food and highly processed-products, while the consumption of fresh unprocessed-food products such as fruits and vegetables has increased inadequately (Bodirsky et al., 2020). The trends of food consumption have different patterns depending on socioeconomic status and geographical, cultural, and demographical traits. According to Agriculture and Rural Development in European Commission, the consumptions of high-value food, including meats and dairy products, has significantly increased in emerging economies like China. Meanwhile, the trends show a shift from red meat to plant-based food consumption including fruits and vegetables in developed economies countries such as Europe and North America (Agriculture and Rural Development, 2019). In middle- and high-income countries, plant-based diets (e.g., veganism or vegetarianism) have been rising along with increased concerns regarding climate change, environment issues, animal welfare, and health (Jones, 2020). According to Google Trends analysis, the interests regarding vegan/vegetarian diets have been simultaneously increasing worldwide, particularly in upper middle-income countries, along with the rising interest in veganism (19.54%) and vegetarianism (15.09%). The actual rates of plant-based diets has increased from 1.4 to 2% for vegan and 5% for vegetarian diets in the United States (Kamiński et al., 2020). These trends of plant-based diets also contribute to an incremental increase of plant-based sales in the U.S., up to 31.3% from 2017 to 2019 (Forgrieve, 2019). Thus, there are rising concerns regarding plant-based diets with low bioavailability of essential mineral/micronutrients such as iron, zinc, vitamin D, and fatty acids (Rizzo et al., 2016).

The nutrition transition shows a significant relation to malnutrition-related health effects (Bodirsky et al., 2020). Malnutrition is one of the major forms of food insecurity that refers to deficiencies and excesses or imbalances of nutrients or energy in human beings. Malnutrition symptoms include undernutrition, micronutrient deficiency, and obesity (WHO, 2020). Micronutrient deficiency is also known as hidden hunger due to the fact that its deficiency problem is generally asymptomatic but influences human health critically. In addition, micronutrient deficiency is highly related to food insecurity, which is a widespread issue in low-income and lower-middle-income countries such as Sub-Saharan Africa and South-Central and South-East Asia (Muthayya et al., 2013). The rationale underlying this is that these countries heavily rely on starchy staple foods such as cereals, tubers, and roots, and the overall availability of animal-based food is lower than that in high-income countries (FAO et al., 2020). The population groups at high risk for micronutrient deficiency include children under five and pregnant women, who have a considerable need for micronutrient supply for healthy development and growth. Child growth stunting is one of the major adverse symptoms due to malnutrition and it occurred in 21.3% or 144 million children in 2019 worldwide. Over 90% of stunted children lived in African or Asian countries accounting for 40–54% of all stunted children worldwide (FAO et al., 2020).

Among micronutrient deficiency, four major micronutrient deficiencies have been highlighted, namely iron, iodine, zinc, and vitamin A, which affect 2 billion people in the world (Ruel-Bergeron et al., 2015). Various strategies for these key micronutrient interventions have been developed and conducted worldwide through biofortification, food fortification, and supplementation (Khush et al., 2012). However, fortification of vitamin B_{12} has been less highlighted although its deficiency impacts on human health critically. Vitamin B_{12} deficiency is particularly common among vegetarians because animal-based food is the natural source for the B_{12}. It can cause neurological, hematological, and psychiatric symptoms and affect the formation of red blood cells and the normal functioning of the nervous system (Nakos, 2016). There has been extensive medicinal and pharmacological research

Abbreviations: AAS, atomic absorption spectrophotometer; Ado-Cbl, adenosyl cobalamin; BSA NPs, bovine serum albumin nanoparticles; Cbl, cobalamin; CN-Cbl, cyano cobalamin; DLS, dynamic light scattering; EDS, energy-dispersive X-ray spectrometry; ELS, electrophoretic light scattering; ENMs, engineered nanomaterials; FAO, Food and Agriculture Organisation; FE-SEM, Field Emission Scanning Electron Microscope; FTIR, Fourier transform infrared; H-Cbl, hydroxo cobalamin; HCl, hydrochloric acid; HCY, homocysteine pathway; His, histidine; HPLC-ICP-MS, high performance liquid chromatography – inductively coupled plasma mass spectrometry; ICP-OES, inductively coupled plasma optical emission spectroscopy; ICP-MS, inductively coupled plasma mass spectrometry; IF, intrinsic factor; LA-ICP-MS, laser ablation inductively coupled plasma mass spectroscopy; MALDI-MS, matrix-assisted laser desorption/ionization mass spectrometry; Me-Cbl, methyl cobalamin; NIH, National Institutes of Health; NPK, nitrogen–phosphorus–potassium; NTA, nanoparticle tracking analysis; NTDs, neural tube defections; RID, radioisotope dilution; RT-PCR, reverse transcription polymerase chain reaction; SAM, *S*-adenosylmethionine; SEM, scanning electron microscopy; SEM-EDX, scanning electron microscopy – energy dispersive X-ray analysis; SFY, stirred functional yogurt; TEM, transmission electron microscopy; TC, transcobalamin; UV-DRS, UV differential reflectance spectroscopy; WHO, World Health Organisation; XANES, X-ray absorption near edge structure; XRD, X-ray diffraction; XRF, X-ray fluorescence.

focusing on vitamin B_{12} supplementation. However, little is known about the specific uptake mechanism of vitamin B_{12} enrichment in living plants. Therefore, this review paper aims to review strategies for micronutrient fortification of food crops, particularly vitamin B_{12}, using nanotechnology. The objectives are to: (i) provide an overview of micronutrient interventions, (ii) determine a sustainable approach or technology for micronutrient fortification such as nanoparticle applications, and (iii) highlight the hydroponic system as a sustainable micronutrient fortification method for food crops.

CURRENT STRATEGIES OR INTERVENTIONS FOR MICRONUTRIENT DEFICIENCY

Biofortification for Micronutrient

Biofortification, as a complex process of developing new varieties of staple food crops, focuses on enhancing bioavailability of micronutrients through agronomic practices, breeding, or biotechnology techniques (Bouis and Saltzman, 2017; FAO, 2017). Biofortification includes three main approaches: agronomic practices, conventional breeding, and genetic modification technology (Thompson and Amoroso, 2010). In comparison to fertilizer development, biofortification can enhance up to the sufficient level of micronutrient/mineral in food crops without adverse environmental effects and it provides a cost-effective strategy for the long-term application with feasibility for underserved rural populations (Kaur et al., 2020). Biofortified crops have been widely adopted in low- and middle-income countries where staple crops, including cereals, tuberous roots, and legumes crops, are mainly consumed. For instance, vitamin A is fortified in various crops such as sweet potato, maize, cassava, banana, and plantain along with the enhancement of various agronomic traits including increased harvest yield and stress resistance. Iron has been fortified in legumes crops and pearl millet along with increased yield and disease resistance. In addition, zinc fortification has also been undertaken with wheat, rice, and maize (HarvestPlus and FAO, 2019).

Biofortification presents two main advantages: being cost-effective in the long-term and having the ability to spread to rural populations which are underserved (Bouis and Saltzman, 2017). Through various stages of biofortification, such as exploration development and delivery stages, the crop improvement activities are conducted considering applicability and cost-effectiveness worldwide, especially for low- and middle-income countries (Bouis and Saltzman, 2017; FAO, 2017). The main challenges for biofortification development consider three critical elements which are supply, policy, and demand. Agronomic traits should meet the micronutrient requirements and also biofortified crops should be supplied to both rural and urban consumers through supportive policies (Bouis and Saltzman, 2017). Supportive policy is necessary for further intervention program with sustainability. Consumer and growers' participation can also limit the biofortified food application which presents as an acceptance of biofortified crop produce. Also, conventional plant breeding or genetic engineering technology requires long-term development and adequate expenses. Utilizing the agronomic method has also highlighted the biofortification method which mainly focuses on fertilizers with micronutrients using nanotechnology. Davies (2018) stated that micronutrient-based nanoparticle application would be a great alternative for biofortification without further breeding or genetic variation by enhancing micronutrient content and crop quality. The study found that micronutrient contents including iron, zinc, and calcium are enhanced in potato, tomato, and chili pepper grown in hydroponic systems utilizing metal oxide nanoparticle which synthesized with amino acid, which enhances the stability of nanoparticle (Davies, 2018).

Food Fortification for Micronutrient

Food fortification refers to an approach to enhance essential micronutrient content by adding vitamins or minerals into food crops so that it contributes to fortifying the contents of nutrient/mineral and providing health benefits to the public (FAO, 2017). Food fortification technology positively regulates micronutrient deficiency and prevents malnutrition problems, especially in staple crops. Compared to supplementations, which generally require a large dose of micronutrients in the form of capsules, tablets, and syrups (Smith et al., 2006; Elemike et al., 2019), food fortification requires relatively small amounts of micronutrients. In comparison to supplementation which can easily cause overdoses (Elemike et al., 2019), food fortification provides adequate amounts of micronutrients to consumers from a mass scale to specific targeted scale (Smith et al., 2006). There are several opportunities and challenges in food fortification. First, fortified food would supply a better-quality diet within micronutrients which are necessary for women and children by reducing the requirements of supplementation. Second, fortified food for staple crops could contain micronutrients in a natural level. In addition, the application of fortified food could improve the nutritional status in a cost-effective way in a large population or targeted population worldwide.

Although food fortification has numerous impacts on the public diet, there are several challenges to be considered. First of all, although fortified food applies to the public or targeted group, a specific fortified food product might be consumed only by some part of the targeted group. It is required that adequate programs or advertisements regarding fortified food are given for the targeted group (Smith et al., 2006). Second, due to accessibility, there is a higher chance to access fortified food in urban areas compared to rural areas (Elemike et al., 2019). Therefore, research should focus not only on the fortification process but also on the distribution of fortified products. Third, fortified food generally targets young children and women due to their extra requirement of micronutrients. However, the amount of uptake of fortified food is relatively small in infants or young children. Therefore, they are less likely to consume recommended intakes compared to their requirement of micronutrients. In addition, further knowledge is required about the effect of interaction among nutrients when micronutrients are added. To achieve sustainable food fortification and its implementation, it is necessary to consider transdisciplinary aspects based on understanding the

effects of agriculture, environment, socioeconomic, and politics (Smith et al., 2006). Also, further supportive national scale involvement is vital for sustainable food fortification with increased bioavailability in the long term.

VITAMIN B_{12} (COBALAMIN)

Background

Physiochemical Traits of Vitamin B_{12} and Its Role in Human Health

Vitamin B_{12}, known as cobalamin (Cbl), is a water-soluble vitamin and it is synthesized by bacteria such as heterotrophic bacteria and most of the aerobic photosynthetic cyanobacteria (Tandon et al., 2017). Vitamin B_{12} mainly involves two enzymatic reactions, DNA synthesis and assimilation of inorganic carbon, which consequently influence on gene regulation, formation of blood cells, and metabolism of the nervous system (National Institute of Health, 2020). According to the National Institute of Health, the recommended daily amount of vitamin B_{12} is 0.4 mcg to 0.5–0.6 mcg for infants, 1.2–2.4 mcg for children to adolescence, and 2.4 mcg for adults (2.6 and 2.8 mcg for pregnancy and lactation respectively) (Pawlak et al., 2013; Nakos, 2016).

Vitamin B_{12} is originated by bacteria mainly found in the gastrointestinal tract of animals and it should be synthesized via the fermentation process of lactic acid (Jedut et al., 2021). There are two different vitamin B_{12}-biosynthetic routes for prokaryotes in nature based on their oxygen-dependency: aerobic and anaerobic pathways. For instance, *Paracoccus denitrificans* takes an aerobic (oxygen-dependent) pathway, whilst *Bacilus megaterium, P. shermanii,* and *Salmonella typhimurium* take anaerobic (oxygen-independent) pathways (Martens et al., 2002). Enteric bacteria, as the main source of vitamin B_{12}, is responsible for most vitamin B_{12} biosynthesis processes found in animals or humans. However, eukaryotes is merely linked to the metabolic process of vitamin B_{12} so that nematodes or animals acquire dietary vitamin B_{12} from vitamin B_{12}-producing bacteria (Lawrence et al., 2018). Vitamin B_{12} is a nutritional requirement for animals, whereas plants neither require nor synthesize it. Animals contain a vitamin B_{12}-dependent enzyme called methionine synthase (METH), such as methyl malonyl-CoA mutase or methionine synthase, whilst plants contain vitamin B_{12}-independent methionine synthase (METE) enzyme (Tandon et al., 2017). Only traceable amounts of vitamin B_{12} are found in plants due to a nitrogen-fixing actinobacteria, *Frankia anni,* which associates symbiotically with actinorhizal plants and contributes vitamin B_{12} (M. Nakos et al., 2017). Thus it is mainly found in animal-derived sources, including meat (e.g., ruminant or omnivorous animals), dairy, fish, and shellfish (Watanabe and Bito, 2018).

Vitamin B_{12} (Cobalamin) consists of central corrin rings containing four pyrrole rings around a central cobalt atom, a lower ligand (α-ligand) donated by 5,6-dimethylbenzimidazole (DMBI), and an upper ligand (β-ligand) synthesized from an adenosyl or methyl group (Nakos, 2016; Rizzo et al., 2016). Dependent on the different ligands on the upper surface of cobalt atoms, vitamin B_{12} is classified as four different chemical forms: (i) hydroxocobalamin(H-Cbl), (ii) Methylcobalamin (Me-Cbl), (iii) Cyanocobalamin (CN-Cbl), and (iv) adenosylcobalami (Ado-Cbl). As coenzymes in the cell, Me-Cbl and Ado-Cbl are the active forms of vitamin B_{12}. CN-Cbl and H-Cbl are provitamin forms requiring Me-Cbl or Ado-Cbl to be utilized by the cells (Rizzo et al., 2016). By participating in the metabolic homocysteine pathway (HCY), Me-Cbl acts a cofactor of methionine synthases. HCY pathway impacts on DNA synthesis and is involved in regenerating methyl donor *S*-adenosylmethionine (SAM). Methionine is required not only for SAM formation but also for metabolisms of DNA, RNA, proteins, and lipids (NIH, 2021). Ado-Cbl, as a cofactor of methylmalonyl-CoA mutase, is involved in metabolism of amino acid and fatty acid. Among the different chemical forms of vitamin B_{12}, cyanocobalamin (CN-Cbl), which is chemically manufactured, is the most stable form and is obtained by reacting natural cobalamin with cyanide. Therefore, CN-Cbl is the most widely used in food fortification, in nutrient formulas, and for pharmaceutical purposes (Nakos, 2016; Rizzo et al., 2016).

Vitamin B_{12} Absorption, Digestion, and Circulation in Humans

Vitamin B_{12} is predominately contained in animal-based food. Following food-cobalamin intake, vitamin B_{12} attaches to dietary animal protein produced from the salivary gland. In the stomach, dietary protein is released by the acidic environment of the stomach via proteolysis. Vitamin B_{12} binds to haptocorrin (R-protein) which is secreted by the salivary glands protecting vitamin B_{12} from acid degradation (Green et al., 2017). Pepsin and hydrochloric acid (HCl) are released from gastric secretion. In stomach, Intrinsic factor (IF) is also secreted, and it binds less strongly when gastric R-protein presents. In duodenum, hatocorrin degradation occurs and the pH is changed in favor of vitamin B_{12} binding to IF. Pancreatic enzymes degrade dietary vitamin B_{12} and haptocorrin complex to release free vitamin B_{12} and free vitamin B_{12} binds to IF and vitamin B_{12}-IF complex transport to ileum (Andrès et al., 2004). In the ileum, vitamin B_{12}-IF complex binds/enters to the cubam receptor which contains cubilin. Cubam receptor mediates endocytosis of vitamin B_{12}-IF complex (Stabler, 2013; Green et al., 2017; Surendran et al., 2018). After the IF and vitamin B_{12} are detached, vitamin B_{12} binds to transport proteins transcobalamin I, II, and III. Transcobalamin II (TCII) involves transportation of vitamin B_{12} to all cells in the human body. Vitamin B_{12} is consequently transported via the portal system. TCII-Cbl complex is absorbed by endocytosis and free vitamin B_{12} is enzymatically converted into its two coenzymatic forms: methyl-cobalamin (Me-Cbl) and adenosyl-cobalamin (Ado-Cbl). Most vitamin B_{12} is stored in the river and some vitamin B_{12} is secreted in bile which undergoes enterohepatic circulation (Andrès et al., 2004; Green, 2017; Green et al., 2017).

Previous studies pointed out several endogenous and exogenous factors that impact on the absorption of vitamin B_{12} in gastrointestinal metabolism and enterohepatic circulation (Andrès et al., 2004). Firstly, achlorhydria in stomach may be associated with cobalamin malabsorption, which is a lack of

hydrochloric acid in the gastric secretion in the stomach. Vitamin B_{12} malabsorption can be induced by insufficient IF along with chronic gastritis which may lead to megaloblastic anemia and neurological disorders (Andrès et al., 2004). Secondly, insufficient exocrine pancreatic can also influence vitamin B_{12} malabsorption owing to low pH in the small intestine and impaired degradation of haptocorrin due to pancreatic enzymes (Green et al., 2017). Thirdly, bacterial overgrowth, such as *Pseudomonas* spp. and *Klebsiella* spp., can influence vitamin B_{12} absorption in small intestine. Bacterial overgrowth may occur by gastrectomy, ileocolic intestinal resection, and secretion of impaired gastric acid (Andrès et al., 2004; Green et al., 2017). Lastly, genetic disorders associated with vitamin B_{12} deficiency is involved in plasma transportation and conversion to coenzyme forms (Andrès et al., 2004; **Figure 1**).

Vitamin B_{12} Deficiency

Vitamin B_{12} deficiency is characterized by low levels of circulating serum vitamin B_{12} and holo-transcobalamin (holoTC) along with elevated levels of total homocysteine in plasma and methylmalonic acid in serum or urine (Brito et al., 2018). Homocysteine, as an amino acid, is generated by the demethylation of methionine and is accumulated in blood when folate, vitamin B_{12}, and vitamin B_6 are insufficient (Tucker et al., 2004). Vitamin B_{12} deficiency is prevalent not only in lower-middle-income countries, but also in upper-middle-income countries. Geographically, the deficiency generally occurs in middle- or low-income countries due to the staple crop and plant-based diets and insufficient consumption of animal-based food (Titcomb and Tanumihardjo, 2019). Deficiency of vitamin B_{12}/iron causes pernicious anemia, mainly threatening pregnant women in South Asia and Sub-Sahara countries reaching 60 and 42% of children under five globally (Ritchie and Roser, 2017; **Figures 2**, **3**). Vitamin B_{12} deficiency is also prevalent in elderly, affecting up to 20% of people over 60 and approximately 6% of adults (younger than 60 years) in the United States and United Kingdom (NIH, 2021).

Populations at high risk for vitamin B_{12} deficiency include the elderly, children, pregnant women of reproductive age, patients (e.g., autoimmune diseases including pernicious anemia and atrophic gastritis), and those with malabsorption of food-cobalamin including those on strict vegetarian or vegan diets (Stabler, 2020). Within the elderly population, vitamin B_{12} malabsorption is mainly due to age-related gastric atrophy, which causes a reduction in acid and intrinsic factor (IF) (Rusher and Pawlak, 2013; **Figure 1**). Also, the populations with atrophic gastritis with low levels of stomach acid secretion generally have vitamin B_{12} malabsorption with certain gastric dysfunctions from food-bound vitamin B_{12} sources (Watanabe, 2007). Vitamin B_{12} deficiency is generally measured by serum methylmalonic acid (MMA) or the level of total plasma homocysteine which is normally lower than 200 or 250 pg/mL (NIH, 2021). Maternal vitamin B_{12} deficiency during the period and/or lactation increases the possibility of birth defects or growth retardation in infants (Brito et al., 2018). In addition, low levels of vitamin B_{12} in breastfeeding and insufficient maternal intake of animal-based food causes brain development defects and overall developmental regressions, particularly 4–6-month-old infants (Stabler, 2013).

Pathophysiology of vitamin B_{12} deficiency includes subclinical symptoms because vitamin B_{12} is stored at 1–5 mg in the human body which makes it difficult to diagnose deficiency (NIH, 2021). Vitamin B_{12} deficiency is often accompanied with other micronutrient deficiencies such as folate (as known as B_9), iron, zinc, and protein deficiencies (Stabler, 2020). In particular, various studies have highlighted the correlation between vitamin B_{12} and folate (Allen et al., 2010; Oakley and Tulchinsky, 2010). Folic acid fortification neither prevents nor treats vitamin B_{12} deficiency, but it also does not impact adversely on vitamin B_{12} deficiency (Oakley and Tulchinsky, 2010). Severe vitamin B_{12} deficiency induces megaloblastic anemia (abnormal nucleated red blood cells) and abnormal neurologic diseases (NIH, 2021). This deficiency also causes hematological and psychiatric adverse symptoms by affecting the formation of red blood cells and the normal functions of the nervous system (Nakos, 2016; Rizzo et al., 2016; Stabler, 2020). Previous research has highlighted several endogenous and exogenous effects on the absorption of vitamin B_{12}: (i) food-cobalamin malabsorption such as inadequate vitamin B_{12} levels due to inappropriate dietary intake or low bioavailability; (ii) malabsorption due to chronic disorder or autoimmune diseases including genetic disorders, pernicious anemia, atrophic gastric, malabsorption due to the overgrowth of *Helicobacter pylori,* or chronic alcoholism; and (iii) competition for vitamin B_{12} as a result of nitrous oxide exposure (Rusher and Pawlak, 2013; Stabler, 2013; Brito et al., 2018). Currently, patients suffering autoimmune diseases with vitamin B_{12} deficiency are recommended to be injected with 1000 μg of vitamin B_{12} several times weekly. Also, high-dose oral treatment is also recommended for patients providing effective treatments. Vitamin B_{12} replacement therapy via intramuscular administration was also conducted for treating vitamin B_{12} deficiency (Rusher and Pawlak, 2013; Stabler, 2013). However, it has been reported that deficiency symptoms are alleviated but not fully improved. Extensive medical and pharmacological research has focused on vitamin B_{12} supplementation. A more comprehensive study would be conducted on vitamin B_{12} enrichment in living plants.

Vitamin B_{12} Sources: Supplementations and Natural Food Sources

It is common to treat vitamin B_{12} deficiency with high-dose injection, oral treatments, and nasal gel spray with cyanocobalamin. Although the supplementations have a high level of vitamin B_{12} doses, it is generally believed to be safe since only limited amounts of vitamin B_{12} are stored in the human body (1.4–5.1 μg) (Doets et al., 2013; NIH, 2021). For instance, vitamin B_{12} is absorbed 50% from 1 μg oral dose and 20% from 5 μg dose and the absorption is decreased by saturation from vitamin B_{12}-IF complex in the ileum from 1 to 2% of an oral dose (Brito et al., 2018). Daily losses of vitamin B_{12} presents 3.8–20.7 μg in healthy populations (over 25 years old), which is 1.4–8.6 times higher than the required amount of vitamin B_{12} preventing deficiency (Doets et al., 2013).

Vitamin B_{12} is generally concentrated in animal-based sources such as meat, dairy products, eggs, fish, and shellfish (Bito et al.,

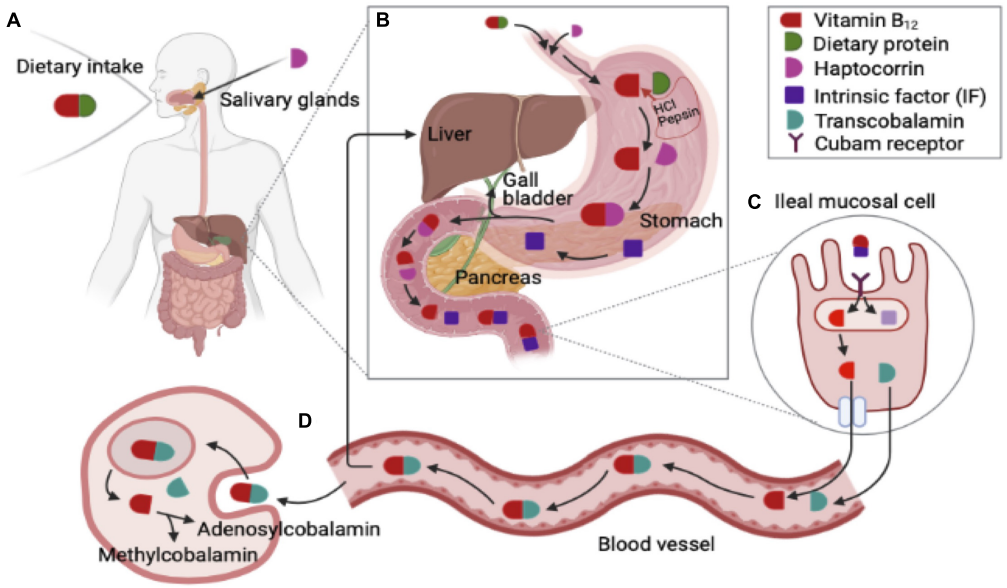

FIGURE 1 | Gastrointestinal metabolisms and enterohepatic circulation of vitamin B12 (Cobalamin) (Modified from Andrès et al., 2004; Stabler, 2013; Hunt et al., 2014; Green et al., 2017; Brito et al., 2018). **(A)** Dietary vitamin B_{12} attach to dietary animal protein produced from salivary gland. **(B)** Following food-cobalamin intake, dietary protein is released by acidic environment of the stomach via proteolysis, and vitamin B_{12} binds to haptocorrin (R-protein) which secreted by salivary glands protecting vitamin B_{12} from acid degradation. Pepsin and hydrochloric acid (HCl) from gastric secretion. In stomach, Intrinsic factor (IF) is also secreted, and it binds less strongly when gastric R-protein presents. In duodenum, hatocorrin degradation occurs and the pH is changed in favor of vitamin B_{12} binding to IF. Pancreatic enzymes degrade dietary vitamin B_{12} and haptocorrin complex to release free vitamin B_{12}. Then free vitamin B_{12} binds to IF and vitamin B_{12} -IF complex transport to ileum. **(C)** In ileum, IF-vitamin B_{12} complex binds/enters to the cubam receptor which consists of cubilin. Cubam receptor mediates endocytosis of IF-vitamin B_{12} complex. After the IF and vitamin B_{12} detaches, vitamin B_{12} binds to transport proteins transcobalamin I, II, and III. Transcobalamin II (TCII) involves transportation of B12 to all cells in the human body. Vitamin B_{12} is consequently transported via the portal system. **(D)** TCII- vitamin B_{12} complex is absorbed by endocytosis and free vitamin B_{12} is enzymatically converted into its two coenzymatic forms including methyl-cobalamin (Me-Cbl) and adenosyl-cobalamin (Ado-Cbl). Most of vitamin B_{12} stored in the river and some of vitamin B_{12} is secreted in bile, which undergoes enterohepatic circulation.

2013; Rizzo et al., 2016). According to Watanabe and Bito (2018), the meat and livers of ruminant animals contain higher amounts of vitamin B_{12} (cooked beef river contains 83 μg/100 g) than that found in omnivorous animals (Cooked chicken meat contains 0.4–0.6 μg/100 g). Traceable amounts of vitamin B_{12} are found in dairy products, such as milk (0.3–0.4 μg/100 g), egg (0.9–1.4 μg/100 g), shellfish (104 μg/100 g), and fish including salmon, trout, and tuna (3.0–8.9 μg/100 g) (Watanabe and Bito, 2018). Compared to animal-based food, plant-based food contains very low or negligible amounts of vitamin B_{12} (Nakos, 2016). For instance, only negligible amounts of vitamin B_{12} was found (<0.1 μg/100 g) in vegetables, including broccoli, asparagus, and mung bean sprouts (Watanabe and Bito, 2018).

Several studies have focused on plants, fungi, and algae with traceable amounts of vitamin B_{12} within these symbioses including edible mushrooms, edible algae, fermented soybeans (0.1–1.5 μg/100 g) and vegetables, and processed food such as cereal, bread, and beverages (Bito et al., 2016; Watanabe and Bito, 2018). The contents of vitamin B_{12} in edible plants is generally very low with different degrees of stability and bioavailability which contribute complex analysis of vitamin B_{12} (Nakos et al., 2017). Previous studies have emphasized that the biological activity of vitamin B_{12} is uncertain in most cases due to the limited availability of natural sources of vitamin B_{12} (Nakos et al., 2017). Therefore, further studies are required to focus on the fortification of vitamin B_{12} in food crops and evaluate their applicability in the dietary system.

Status of Vitamin B_{12} Supplementation/Fortification

Among micronutrient deficiencies, the amelioration of vitamin B_{12} deficiency is significantly less emphasized. Extensive research regarding vitamin B_{12} fortification has focused on supplementation for medical or pharmacological purposes. Supplements of vitamin B_{12} from multivitamin/minerals are generally 500–1,000 mcg of vitamin B_{12} with 2 and 1.3% of absorption respectively (NIH, 2021). Due to the IF-mediated gastrointestinal absorption and circulation system, vitamin B_{12} bioavailability decreased ranging from 1.5 to 2.0 μg per meal under physiologic conditions or food processing (Watanabe, 2007). In healthy populations, vitamin B_{12} bioavailability presents 42% from fish or meat (beef, lamb, and chicken), ranging from 56 to 89%, and although traceable amounts of vitamin B_{12} contents are found in the yolk, eggs have poor bioavailability compared to other vitamin B_{12}-contained food sources. Vitamin B_{12} bioavailability can be significantly degraded by dysfunctions such as atrophic gastritis with low levels of stomach acid secretion. According to Dietary Reference Intake, it is assumed that a healthy population with a normal

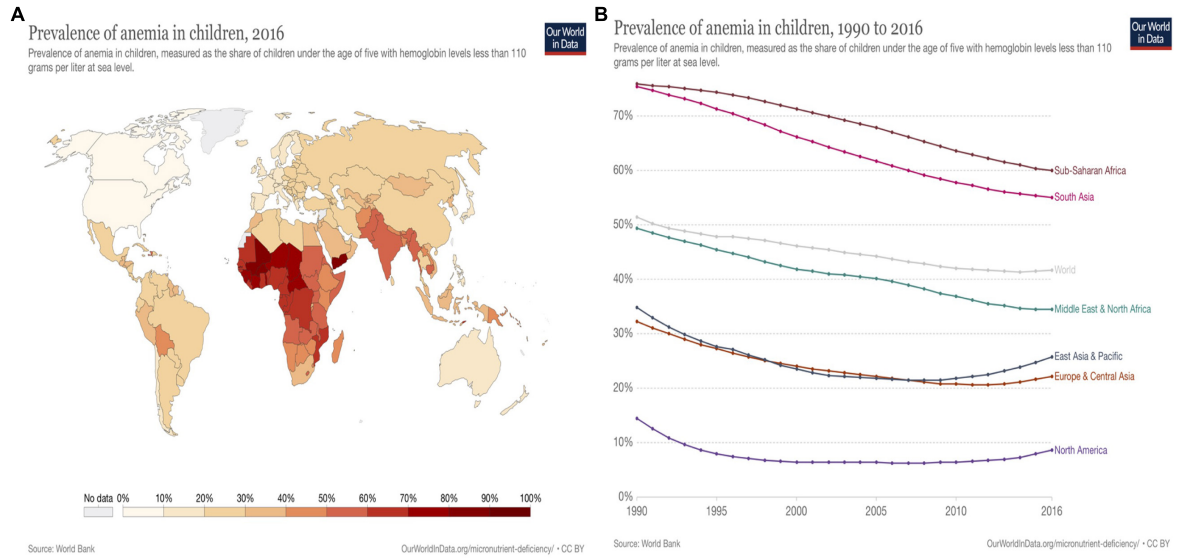

FIGURE 2 | Vitamin B_{12}/Iron deficiency: Anemia prevalence in children worldwide (Source: WorldBank; Ritchie and Roser, 2017). **(A)** Vitamin B_{12} /Iron deficiency: anemia prevalence in children worldwide, 2016| Anemia (B12/Fe deficiency) in children under five predominantly occurs in Sub-Saharan Africa regions with average 60% (28.8–86.2%) and Southern Asia 55% (16.9–83.5%) in 2016. The prevalence of anemia occurs less in North America (8.5–9.4%), Europe (12.1–27.1%), Central, East Asia (12.3–21.4%), and Oceania (13–48.4%). Prevalence of anemia relatively correlate to the values of gross domestic product (GDP). **(B)** Vitamin B_{12} /Iron deficiency: anemia prevalence in children worldwide, 1990 to 2016 | Prevalence of anemia (vitamin B_{12} /Fe deficiency) has been decreasing worldwide from 1990 to 2016 on average from 51 to 42%. However, it is still a significant issue in Sub-Saharan Africa and South Asia, who have approximately 60 and 55.1% respectively in 2016.

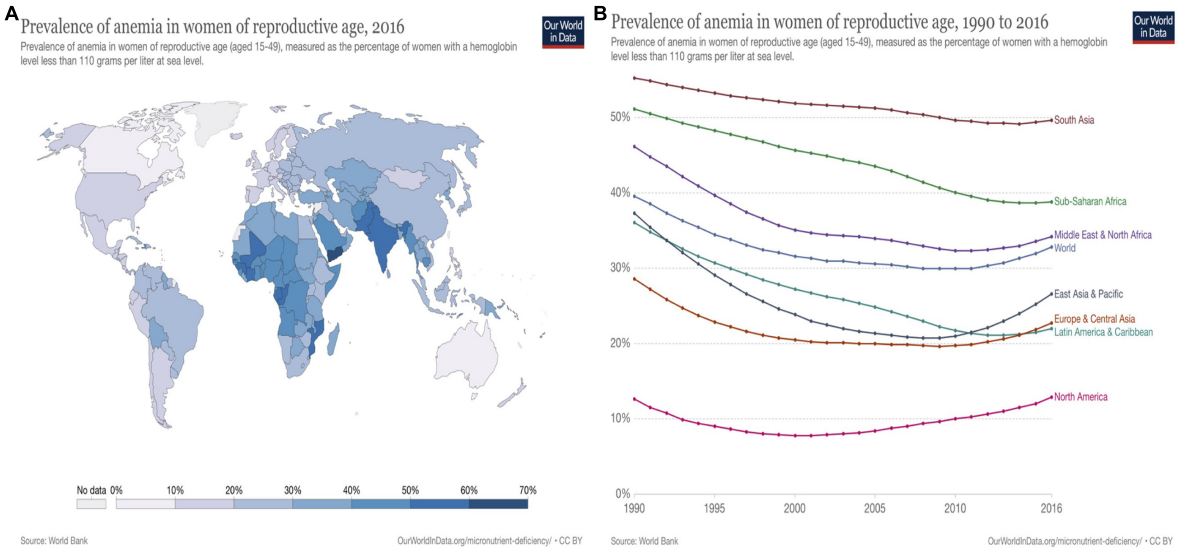

FIGURE 3 | Vitamin B12/Iron deficiency: Anemia prevalence in women of reproductive age worldwide (Source: WorldBank; Ritchie and Roser, 2017). **(A)** Vitamin B_{12}/Iron deficiency: anemia prevalence in women of reproductive age worldwide, 2016. Anemia (vitamin B_{12}/Fe deficiency) in women of reproductive age (aged between 15 and 49) mainly occurs in South Asia (24.2–69.6%) and Sub-Saharan Africa (23.2–59.1%), and Middle East and North Africa regions (23.4–49.5%). In particular, Yemen shows the highest rate with 69.6%. The prevalence of anemia in reproductive aged women occurs in comparatively low numbers in North America (9.5–14.6%), Latin America, the Caribbean (18.5–30.2%), Europe, and Eastern Asia (15.7–26.4%). **(B)** Vitamin B_{12} /Iron deficiency: anemia prevalence in women of reproductive age worldwide, 1990 to 2016. Prevalence of anemia (Vitamin B_{12}/Fe deficiency) has been decreased worldwide from 1990 to 2016 (39.60% to 34.23%). However, it slightly increased in several regions from 2013 to 2016 mainly in East and Central Asia, Pacific and Europe regions.

gastrointestinal function can absorb 40–50% of vitamin B_{12} from animal-based food sources (Watanabe, 2007). It is difficult to evaluate vitamin B_{12} bioavailability by quantifying active vitamin B_{12} or inactive corrinoids in certain foods, such as vitamin B_{12} fortified plant-based food. Therefore, for vitamin B_{12} fortification strategies, it is necessary to enhance the contents of vitamin B_{12}

in food sources along with the high bioavailability which is actual amounts of available uptake (Watanabe, 2007).

Little is known about vitamin B_{12} biofortification based on crops. However, a relatively limited number of studies have been conducted to investigate vitamin B_{12} fortification and understand their mechanisms of uptake/distribution in living plants. According to previous studies, several plants, fungi, and algae (e.g., Japanese radish sprouts, mushrooms, dry seaweed, and garden cress) absorb and translocate vitamin B_{12} if they are grown in nutrient-sufficient conditions with organic fertilizer or vitamin B_{12}-enriched growing media (Sato et al., 2004; Bito et al., 2013; Lawrence et al., 2018). One of the effective strategies to enhance the contents of vitamin B_{12} is flour fortification for a national scale with uniform dose. There are various processed food products that have been fortified with vitamin B_{12} such as cereal grain products (Tucker et al., 2004; Melo et al., 2020), dried soup powder, and powdered milk drink (Sanchez et al., 2013). Vitamin B_{12} can also be supplemented with fresh-cut fruits and vegetables for alleviating its deficiency in the population groups who are at high risk. A combination of vitamin B_{12} and chitosan is applied in fresh-cut salad mixes (melon, pineapple, and carrot) which are for 'ready-to-blend' beverages. According to Artés-Hernández et al. (2017), the study shows the fortified beverage contains up to 8.6 μg/1 kg of vitamin B_{12} along with an enhanced shelf-life.

Unlike widespread folate fortified wheat flour, there is inadequate case for vitamin B_{12} fortification with food crops in worldwide. Folic acid fortification has been successfully conducted, but it also increased the concerns about the possibility of neurological issues and deterioration of cognitive ability occurring with high folic acid supply and low level of vitamin B_{12} (Garrod et al., 2019). The study conducted by Garrod et al. (2019) aimed to quantify the bioavailability of fortified vitamin B_{12} in bread in five healthy elderly people aged over 60. The study shows that vitamin-B_{12}-fortified flour retains its bioavailability approximately 50% after the processes of fermentation and baking containing 2 μg/100 g. The study shows the healthy elderly can absorb sufficient vitamin B_{12} from the fortified bread addressing that the vitamin B_{12} fortified wheat (flour) can be a promising animal-based substitute with high-purity crystalline ^{14}C-vitamin B_{12} (Garrod et al., 2019). Further study would be required to investigate the absorption of fortified flour for different targeted subjects who have high risk of vitamin B_{12} deficiency such as children or pregnant women or larger populations of the elderly. According to Tucker et al. (2004), vitamin B complex fortified breakfast cereal contribute enhancement of their contents including vitamin B_6, B_9 (folate), and B_{12} (cobalamin). Fortified cereal significantly improves vitamin B_{12} concentrations and reduces the prevalence of high levels of plasma homocysteine from 13 to 3%. This study highlights that fortified cereal would be great vitamin B_{12} sources for general populations who frequently have poor vitamin status (Tucker et al., 2004). Tucker et al. (2004) pointed out that free vitamin B_{12}-fortified breakfast cereals presents better absorption compared to vitamin B_{12}-bound to proteins in food which may be due to the IF-mediated gastrointestinal metabolisms effects on vitamin B_{12} absorption. Vitamin B_{12} fortification is also targeted to adults aged over 50 years by using the microencapsulation approach (Melo et al., 2020). The study found that the application of the encapsulated vitamin B_{12} powder in yogurt (50 μg of vitamin B_{12} was added into 175 g of yogurt) successfully fortified vitamin B_{12}. The study compared Me-Cbl and CN-Cbl and the outcomes of the study show that CN-Cbl presents better stability throughout shelf-life. This study undertakes encapsulation technique for vitamin B_{12} fortification using spray-drying method to coat vitamin B_{12} with a maize starch-derived polymeric materials (Melo et al., 2020).

There are several in situ fortification methods for vitamin B_{12} in fermented plant-based food. In situ fortification with bacteria (*Propionibacterium freudenreichii* DSM 20271 and *Levilactobacillus brevis*) successfully enhances vitamin B_{12} contents in fermented cereal, pseudo-cereal (such as rice bran and buckwheat bran), and legume plants (Xie et al., 2021). Fermented legume materials contain 300–400 ng/g (dry weight) of vitamin B_{12} measured by ultra-high performance liquid chromatography and the results suggest that fermented crop materials can be a great potential alternative for plant-based food-cobalamin. This study also found that optimal pH condition for *P. freudenreichii* can increase the vitamin B_{12} contents in fermented grain materials. Further research would be needed to examine the contents of other micronutrients and minerals in the fermented crop materials using in situ fortification which is necessary to be considered for vitamin B_{12} amelioration along with other micronutrient deficiencies (Xie et al., 2021). Vitamin B_{12} also successfully fortified up to 0.97 μg/100 g in tempeh by *in situ* approach using *Propionibacterium freudenreichii* (Log 7 CFU/g) and *Rhizopus oryzae* spores (Log 4 CFU/g) (Wolkers – Rooijackers et al., 2018). This research determines the effect of in situ strategy on tempeh quality by analyzing the consumer acceptance traits including microbial composition, firmness, and volatile organic compounds to measure aroma quality. The result of the study shows that the fortification using both food-grade bacterium does not have any negative impact on the quality traits. However, it is also necessary for this study to analyze other micronutrient/mineral components that are highly related to vitamin B_{12} deficiency and fortification.

Vitamin B_{12} supplement programs and fortification strategies target reduction of vitamin B_{12} deficiency and further factors should be considered for successful vitamin B_{12} fortification: (i) actual concentration and bioavailability of vitamin B_{12} in fortified or supplemented sources; (ii) demographic, geographic, and socioeconomic traits of targeted groups, and (iii) effect of frequent- or over-dose of vitamin B_{12} (Carmel, 2008).

NANOPARTICLE TECHNOLOGY: A SUSTAINABLE APPROACH FOR MICRONUTRIENT/MINERAL ENHANCEMENT

Background on Nanoparticle Technology

Engineered nanomaterials (ENMs), called nanoparticles, feature at least one dimension ranging from 1 to 100 nm and consist of organic, inorganic, or hybrid materials (Shang et al., 2019).

Owing to their small particle size, nanoparticles have a large surface area and exhibit high solubility and mobility that is widely exploited for smart delivery for pharmaceutical, medical, and agricultural purposes (Shang et al., 2019). The size of ENMs corresponds to biological barriers such as a plant cell wall or membrane after root or foliar applications and to enable new smart delivery of nutrients or pesticides (Nair et al., 2010; Lowry et al., 2019). The characteristics of nanoparticles, such as structure or surface chemistry traits, should be selected properly for different functions or nanotechnological strategies (Lowry et al., 2019). Through interactions between nanoparticles and plants, including nutrient interactions, it is possible to enhance the nutritional quality of food crops by accumulating specific macro- and micronutrients.

The agronomical biofortification of food crops with micronutrients/minerals is a promising technique with a fast and easy way to mitigate inadequate essential nutrients/minerals in plants (Elemike et al., 2019). Nano-agrochemicals can be classified by their types or delivered nutrients, such as macronutrient and micronutrient fertilizers and macronutrient carriers (Singh Sekhon, 2014). Macronutrients, in particular NPK fertilizers, can be applied with nanoparticles in nanocapsule form, or particles can be coated with nutrients/minerals (such as in urea-coated zeolite chips) with slow release application to enhance the uptake and efficiency of fertilizer (Singh Sekhon, 2014). Nano-NPK fertilizer promotes crop harvest yield and growth quality, including the size or weight of edible vegetative parts and physiochemical compounds in several crops, such as wheat (Abdel-Aziz et al., 2016; Al-juthery and Al-Shami, 2019), potato (Rop et al., 2019), maize, kale, and capsicum crops (Rop et al., 2019). Among techniques involving nano-NPK fertilizers, such as the slow-release method or coating with nutrient ions, nano-NPK fertilizers shorten the life cycles of crops compared to conventional fertilizer application, which is highly relevant to increasing crop yield (Liu and Lal, 2015). Micronutrient-loaded nanoparticles may provide more favorable uptake or distribution of micronutrients in plants by providing slow release of the nutrient by plants or soils and reducing environmental pollution (e.g., leaching) or agroecology degradation (Elemike et al., 2019). Compared to conventional fertilizers, nanofertilizer can triple the nutrient effectiveness, reduce the requirement or usage of fertilizers applications, develop crops with stress resistance, and cause less adverse environmental impacts (e.g., leaching) (Elemike et al., 2019).

Micronutrient fertilizers are being developed with various micronutrient ions, such as Fe (Rameshraddy et al., 2017); Mn, Zn (Liu and Lal, 2015); and Cu (Trujillo-Reyes et al., 2014). Depending on the application method, nanoparticles synthesized with micronutrients differentially translocate and accumulate in leaves, shoots, and grains along with various effects on growth performance. For instance, hydroponic cultivation enables more efficient and effective root application of nanofertilizer (Jeyasubramanian et al., 2016). Nanofertilizers are also widely applied for foliar applications using spraying methods. Furthermore, nanofertilizer treatments can be conducted together, such as the combination of seed priming and foliar application of zinc oxide nanoparticles (ZnO NPs), which showed enhancement of seedling growth and increased biomass contents of chlorophyll and yield in rice (Rameshraddy et al., 2017).

Fortification Strategies of Vitamin B_{12} and Its Deficiency Relevant Micronutrient

Vitamin B_{12} Fortification Using Nanoparticle Technology

Vitamin B_{12} deficiency may be accompanied by high folate status presenting a negative association with adverse health consequences such as cognitive impairment and delaying nerve conductivity (Brito et al., 2018). According to Prueksaritanond et al. (2013), intramuscular inject of vitamin B_{12} along with the supplemented iron and folate significantly improve vitamin B_{12} deficiency. Thus, further strategies for vitamin B_{12} fortification should ameliorate folate, iron, and zinc deficiencies. Currently, nanocarriers have been applied for the pharmaceutical application of vitamin B_{12} for targeted smart delivery. Nanocarriers consist of organic/inorganic nanoparticles and are utilized for smart delivery as commonly used in the pharmaceutical industry. Nanoparticle applications offer innovative solutions to improve the sensitivity of measurement by enhancing the electromagnetic signal in metal nanoparticle due to their nanosize with surface plasmon resonance effect (Fidaleo et al., 2021). For vitamin B_{12} delivery, nanoparticles should be absorbed in the small intestinal tracts. There are several strategies for improving bioavailability using vitamin B_{12} nanocarriers with thiolate polyacrylic acid particles and nanoengineered polymeric capsules. However, there are increasing concerns regarding potential toxicity of nanoparticles. Further studies should address not only the mechanisms of uptake and transport and metabolisms *in vivo*, but also the safety applications dealing with the potential toxicity of nanoparticles.

Unlike for medical/pharmacological purposes, comparatively limited studies have been conducted for food/agriculture strategies. Seed priming techniques (Sato et al., 2004; Keshavarz and Moghadam, 2017) and a hydroponic system with vitamin B_{12}-enriched solution (Bito et al., 2013) have been utilized for vitamin B_{12} fortification in food crops (**Table 1**). Plants treated with high concentrations of vitamin B_{12} exhibit more favorable growth performance and an increased content of vitamin B_{12} in the crops (Keshavarz and Moghadam, 2017). The study found that vitamin B_{12} increases the resistance capacity against abiotic stress and reduces oxidative stress by providing an effective antioxidant and regulating osmotic balance. Common bean seeds soaked with 11 and 22 μm of vitamin B_{12} concentrations show enhanced chlorophyll contents, catalase, and peroxidase activity in the leaves in the condition of salt stress compared with control treatment. Also, the application of seed priming with 22 μm of vitamin B_{12} under saline conditions increase the level of proteins in the bean plants, whilst there was no effect of protein improvement under non-saline conditions. The outcome of this study highlights that the application of vitamin B_{12} enhances not only the salinity tolerance, but also effective photosynthetic biosynthesis by alleviating the adverse effect on photosynthesis pigments in salinity stress (Keshavarz and Moghadam, 2017).

Seed priming with vitamin B_{12}-enriched solution also increases the vitamin B_{12} contents in kaiware daikon sprout up to 1.5 μm/g in any concentration of vitamin B_{12} solutions ranging from 0 to 200 μg/ml (Sato et al., 2004). This study also addresses the possibility of reduction of vitamin B_{12} by cooking processes, such as boiling, and also highlights that prolonged boiling (3–10 min) will decrease the vitamin B_{12} contents in kaiware daikon. Based on this previous finding, further studies can be conducted to identify the effect of vitamin B_{12} enriched coated with micronutrient/mineral in food crops and how much vitamin B_{12} contents will be retained after cooking processes.

As demonstrated above, only a few previous studies focused on vitamin B_{12} fortification in food crops (Sato et al., 2004; Bito et al., 2013; Keshavarz and Moghadam, 2017; **Table 1**). Various studies only focused on the quantification and determination of vitamin B_{12} in food crops such as *Hippophae rhamnoides* berries (Nakos et al., 2017), edible algae (Kumudha, 2015), mushrooms (Watanabe et al., 2012, 2014; Bito et al., 2014, 2016), and fermented plant-based products (Watanabe et al., 2013). Titcomb and Tanumihardjo (2019) highlighted that high intake of vitamin B_{12} did not show adverse effects on human bodies. However, there are limitted studies on the effect of fortified vitamin B_{12} in the food crops and its specific health effects on human health. Further research would be required to identify sustainable fortification methods for vitamin B_{12} and its stability and effects on human health when it is digested or accumulated in the long term. Furthermore, it still remains challenging to quantify and determine exact vitamin B_{12} contents in food crops because vitamin B_{12} mainly exists as bound form in food crops with different degrees of stability (Nakos et al., 2017). Nakos et al. (2017) pointed out that immunoaffinity chromatography and HPLC analysis can provide quantitative chromatographic isolation of vitamin B_{12} in food crops. Further studies should distinguish between active or inactive analogs of vitamin B_{12} forms in food crops (Nakos et al., 2017).

Folate Fortification Using Nanoparticle Technology

In order to enhance the contents of vitamin B_{12} in food crops, the interrelated deficiencies should also be alleviated. Vitamin B_9, as known as folate, is involved in the synthetic mechanisms and methylations of nucleotides by intervening in cell multiplications and tissue growth. Vitamin B_{12} and folate presents an intimated connection via their cooperation in one-carbon metabolism and the hematological complications that are indistinguishable consequences/symptoms of deficiencies caused by either vitamin B_{12} or folate (Green, 2017). In vitamin B_{12} deficiency status, normal folate cycling disrupts the regeneration of methylenetetrahydrofolate, and it is required to sustain the synthesis of thymidine for replication of DNA. Since vitamin B_{12} is required for its conversion to tetrahydrofolate within the reaction of methionine synthase, folate becomes trapped as methyl-folate which ultimately causes functional folate deficiency (Green, 2017). Vitamin B_{12} deficiency decreases the activity of methionine synthase and subsequently reduces folate cycle intermediates, causing thymidine synthesis (Titcomb and Tanumihardjo, 2019).

TABLE 1 | Vitamin B_{12} fortification in food crop.

Plant	Method	Analysis tools	Media	Germ.	Seedling phenotype	Seedling growth	Yield	Nutrient	Toxicity	References
Cereal, pseudo-cereal and legume plants	In situ fortification with *Propionibacterium freudenreichii* and *Levilactobacillus brevis*	ICP-MS and Determination of pH, total titratable acids and contents of acids	Fermentation inoculation	N/A	N/A	N/A	N/A	↑	N/A	Xie et al., 2021
Common bean	Seed priming (0, 11, and 22 μM) and salinity stress application	Enzyme activity assay, chlorophyll and carotenoid assay, malondialdehyde assay and proline assay	In vitro	N/A	↑	↑	N/A	↑ (phenolic and protein)	N/A	Keshavarz and Moghadam, 2017
Kaiware daikon (Japanese radish sprout)	Soaking vitamin B_{12} solutions (0–200 μg/ml) and Heat treatment	Chemiluminescence assay method, supernatant fluid assay (E. coli 215 and L. *delbrueckii lactis* ATCC 7839)	In vitro	N/A	N/A	N/A	N/A	↑	N/A	Sato et al., 2004
Lettuce	CN-Cbl-loaded solution	Spectrophotometer, HPLC, Bioautography, Immunoaffinity column, LC/ESI-MS/MS	Hydroponic	N/A	N/A	N/A	N/A	↑(CN-Cbl)	N/A	Bito et al., 2013

Folate deficiency is prevalent worldwide and over 1.6 billion people are struggling with these deficiencies. Folate deficiency occurs along with iron deficiency and induces megaloblastic anemia in severe deficiency status due to reduced oxygen-carrying capacity (Titcomb and Tanumihardjo, 2019). However, fortification of folic acid, as a synthetic form of folate, has successfully mitigated folate deficiency. Unlike limited bioavailability of vitamin B_{12}, folic acid has over 85% bioavailability and folic acid has approximately 70% higher bioavailability than food folate (Dary, 2008). There are various folate fortified cereals and grains products aiming to reduce the incidence of neural tube defections (NTDs) (Crider et al., 2011). NTDs, as birth defects, occur when the neural tube is exposed to underlying neural tissue owing to the failure of closure during the early embryonic development. Mandatory folic acid fortification programs have been carried our in 53 countries and wheat flour is most widely fortified with folate (Crider et al., 2011). Food fortification with folic acid provides sufficient amounts of folic acid to meet individual and global requirements. However, fortified cereal grain products do not adequately reach all women of reproductive age. Furthermore, there are emerging concerns about the excessive intake of folic acid from the fortified food adversary impacts on pernicious anemia, known as vitamin B_{12} deficiency (Crider et al., 2011). For instance, vitamin B_{12} deficient people have a higher possibility of developing neurologic disorders from increased folic acid intake (Carmel, 2011).

A recent study conducted by Darwish et al. (2021) shows that folic acid and iron can be fortified via bovine serum albumin-nanoparticles in stirred functional yogurt (SFY) (BSA-NPs). BSA-NPs are coated with amino acids (lysine) allowing the positive/negative charge of molecules to absorb electro-statistically without any other compounds' intervention. BSA-NPs show stable applications and BSA-NPs loaded with folic acid/iron restore most of the monitored plasma iron parameters in SFY products. This fortified SFY retained iron and protein without adverse effects or architectural changes in the liver or kidney. Furthermore, it contributes to enhancing water-holding capacity, microstructure, and overall acceptability of sensors (Darwish et al., 2021). This study successfully introduces the nano-encapsulation technique for enhancing iron and folic acid addressing their physiochemical interaction between dairy food products.

Iron Fortification Using Nanoparticle Technology

As a co-factor in photosynthetic, iron is an essential nutrient for photosynthetic organisms involving various metabolic mechanisms such as electron transport chain (Davies, 2018). Iron deficiency is concomitant with vitamin B_{12} deficiency masking the macrocytosis, typically seen in vitamin B_{12} deficiency. Due to vitamin B_{12}/folate deficiencies, ineffective formation of the red cell is a block in iron utilization, causing increased serum iron levels. If the hemolytic anemia condition persisted, iron may be depleted and eventually cause iron deficiency anemia (Green, 2017). Iron and iron oxide nanoparticle (Fe- and Fe_2O_3 NPs) application has been widely conducted because Fe/Fe_2O_3 NPs enhance the development of shoots/roots, plant growth, and yields in potato, tomato plant (Shankramma et al., 2016), chili pepper (Davies, 2018), and bean seedlings (Duran et al., 2018; see **Table 2**). Iron bioavailability depends on the ferrous sulfate standards indicating high bioavailability in highly water-soluble compounds (Clarke, 1995).

Davies (2018) highlights that the application of nanoparticles with innovative synthesis methods successfully fortify iron, zinc, and calcium in potato, tomato, and chili pepper without requiring conventional breeding. Potato tubers were propagated with iron/iron oxide nanoparticle (FeNP/Fe_3O_4) coated with histidine (His) with an average of 4.732 nm (n^{-20}). FeNP + His solution was applied via the foliar application and hydroponic nutrient solution with 8, 12, and 16 mg/L concentration. The application of FeNP+His 16mg/L significantly increased the Fe contents in both potato skin and tuber owing to the nano size of the Fe+His penetrating and accumulating in the tuber. FeNP+His is also treated in tomato and chili pepper with different concentrations. All concentrations (6, 12, and 24mg/L) of FeNP+His significantly increased Fe contents in tomato with the greatest increase obtained by 6 mg/L. Furthermore, tomato treated with FeNP+His (particularly with 12 mg/L dose) showed increased weight in the ripened fruits and produced 146.38% more than control. FeNP + His with 6 mg/L contributes significantly to increasing the fresh weight of tomato from 287.21 501.08 g. Fe-fortified tomato displayed no phytotoxicity effects on excessive amounts of Fe treatment. In chili pepper trials, FeNP+His 6mg/L treatment increases plant height (70 nm) and fresh weight. Among various varieties of chili peppers, C. Chinese varieties gained a significant increase in Fe content with 6mg/L treatment. This study highlights that the hydroponic propagation contributes to fortifying micronutrient levels with advantageous conditions by providing adequate soil and compost substrates.

Zinc Fortification Using Nanoparticle Technology

Over 20% of the worldwide population could have risks of zinc deficiency based on the zinc intake and bioavailability estimations from food balance data obtained by the FAO (Smith et al., 2006). Zinc deficiencies widely occur in different geographical regions including South Asia (particularly in India and Bangladesh), Africa, and the Western Pacific. Zinc deficiency occurs along with iron deficiency, which is inhibited by phytates presence (Smith et al., 2006). Zinc and zinc oxide have been fortified in various food crops such as maize (Itroutwar et al., 2020), potato (Davies, 2018), soybean (Hoe et al., 2018), rice (Rameshraddy et al., 2017; Kasivelu et al., 2020), and barely (Seaman, 2017; **Table 2**).

Several studies present successful ZnO fortification in food crops using nanopriming and root/foliar application enhancing germination, plant growth, and harvest yield. Zn nanoparticle application also enhances the contents of zinc in potato and rice. Davies (2018) addressed the level of zinc in potato enhanced by zinc nanoparticle coated with histidine (ZnNP + His). The application of ZnNP + His presents a positive effect of tuber fortification due to significantly increased amounts of ZnO in potato tubers with 8 mg/L concentration in both hydroponic propagation system and compost media. However, ZnO is rapidly aggregated in an aqueous nutrient solution in hydroponic systems. The aggregation of nanoparticles is one

TABLE 2 | Micronutrient fortification relevant to vitamin B_{12} deficiency in food crops using nanoparticles: Iron (Fe) and Zinc (Zn).

Plant	NPs	NPs mass/size	Analysis tools	Media	Germ.	Seedling phenotype	Root Vigor	Yield	Nutrient	Toxicity	References
Potato and tomato	Fe_3O_4 NPs	8–32 mg/L, 3.62–20.18 nm	NPs synthesis (coating), SDR (spinning disc reactor), TEM, SEM, FTIR, ICP-OES and XRD	Hydroponic	N/A	↑ (Tuber)	↑	↑ (Tuber)	↑ (Fe in skin and tuber)	X (in Tomato)	Davies, 2018
Bean	Fe_3O_4 NPs and Fe_3O_4 -PEG NPs	1–1000 mg/ 11 nm and 12 nm	EDXRF, XRD, XRF, TEM, DLS, XANES and SEM-EDX	Seed priming	—	↑ (1 to 100 mg/L)	↑	↑	↑ (Seed coat and radicle)	O (in high concentration)	Duran et al., 2018
Tomato	Magnetic Fe_2O3 NPs	50–800 mg/L	UV-vis spectrophotometer, TEM and XRD	Greenhouse and hydroponic	↑	↑ (50–200 mg/L)	↑	N/A	↑ (Root hair, root tip)	O (in high concentration)	Shankramma et al., 2016
Maize	ZnO	10–200 mg/L, ∼37 nm	TEM, HR-SEM, measurement of seed germination and seedling parameters	Seed priming, in vitro	↑	↑	↑	N/A	N/A	X	Itroutwar et al., 2020
Maize and Rice	γ-Fe_2O_3 and ZnO	100–2000 ppm	SEM, UV-DRS, XRD, FT-IR, germination and vigor analysis	*In vitro*	↑	↑	↑	↑	N/A	N/A	Kasivelu et al., 2020
Potato	Zn	13.18–13.73 nm	NPs synthesis (coating), SDR (spinning disc reactor), TEM, SEM, FTIR, ICP-OES and XRD	Hydroponic	N/A	↑ (Tuber)	↓ (No. tuber)	↑	↑ (Zn in tubers)	↑ chance (in hydroponic)	Davies, 2018
Rice	Zn, ZnO and $ZnSO_4$ NPs	500–1500 ppm, 30 nm	Seed priming (1000 ppm) and foliar application, ICP-OES and RT-PCR analysis	*In vitro* (drought stress)	↑ (Zn, ZnO seed priming)	↑ (ZnO seed priming), ↓ (In high ZnO, $ZnSO_4$)	↑ (Zn seed priming)	↑ (ZnO > Zn)	↑ (ZnO > $ZnSO_4$)	O (1500 ppm of ZnO and $ZnSO_4$)	Rameshraddy et al., 2017
Soybean	Fe, ZnO, Cu and Co	5–500 mg/L, 40–40 nm	Morphological and cytological analysis,	*In vitro*	↑	↑	↑	N/A	N/A	↑ % of Zn	Hoe et al., 2018
Barely fodder	Teprosyn Zn/P	0.5–3.6 ml	LA-ICP-MS, MALDI-MS, HPLC-ICP-MS	Seed priming, hydroponic	↑	↑	↓	N/A	↑	N/A	(Seaman, 2017)

of the major issues because the size of the aggregated particle become larger which consequently reduces bioavailability of the nanoparticle. Also, increased ZnNP + His application can also cause phototoxic effects on food crops such as severe stunted leaves. Therefore, it is necessary to avoid ZnO aggregation and excessive applications for food fortification (Davies, 2018). Rameshraddy et al. (2017) also presents that ZnO nanoparticle application improves plant physiological growth (e.g., growth, yield, and quality), and enhances drought stress tolerance along with the increased contents of ZnO in rice. The study also highlights that high concentration of ZnO and $ZnSO_4$ (at 1500 ppm in both) significantly reduce rice seedling vigor which might cause toxicity (Rameshraddy et al., 2017).

Micronutrient Fortification for Plants Grown in Hydroponic and Aeroponic System

Hydroponic and aeroponic systems support effective fortification of micronutrients with high productivity and efficiency by providing optimized year-round production (Rouphael and Kyriacou, 2018). Hydroponic cultivation refers to the growing method based on the recirculated inorganic/organic nutrient solution instead of soil cultivation. In hydroponic systems, the plant roots are immersed partially or completely in a nutrient solution. On the other hand, aeroponic system exposes the plant roots to aerosol droplets containing micro-/macro-nutrient (Eldridge et al., 2020). In aeroponic systems, droplet size is one of the major parameters for determining the absorption effectiveness directly influencing plant growth and it can be classified into spray (over 100 μm), fog (1–100 μm), and mist (1–35 μm) (Niam and Sucahyo, 2020). Both hydroponic and aeroponic cultivations provide favorable environments for plant growth. Nanoparticles can be applied into nutrient solutions for hydroponic cultivation. Better absorption and translocation of nanoparticles was observed in plants grown in hydroponic systems compared to soil cultivation due to more conductive aggregation and dissolution of nanoparticles in roots zone in hydroponic system (Kranjc and Drobne, 2019). Some minerals/micronutrients present low mobility or are even unavailable to plants in the soil depending on the physicochemical characteristics including pH, composition, and electrical conductivity (Freire et al., 2020). Therefore, hydroponic cultivation systems can be an efficient strategy for vitamin B_{12} fortification by applying vitamin B_{12}-enriched nutrient solution precisely with nanoparticles coating techniques.

Bito et al. (2013) shows that vitamin B_{12}-loaded nutrients significantly improve the level of vitamin B_{12} in lettuce grown in hydroponic systems. Hydroponic growing systems have better management of water and nutrient supply without pathogen or bacteria risks or leaching issues. This study dissolves CN-Cbl into hydroponic nutrient solution at 5 μmol/L for lettuce growing. The results indicated the majority of CN-Cbl accumulated in leaves (86%) which may be a promising source of free CN-Cbl in food crops. Approximately 164.6 μg/g fresh weight of lettuce would provide the recommended daily allowance for vitamin B_{12} (2.4 μg/g). This study addressed the expected costs for CN-Cbl-nutrition solution for lettuce fortification which was calculated to be approximately U.S $0.06. Therefore, compared to conventional supplementary programs, it would be a cost-effective fortification strategy with an excellent source of free CN-Cbl for the populations who have plant-based diets or the elderly (Bito et al., 2013). One of the main challenges was to maintain the stability of CN-Cbl in hydroponic nutrient solution for future application by controlling light conditions (Bito et al., 2013). Additionally, the different concentrations of vitamin B_{12} variously impact crop growth performance and rate of vitamin B_{12} accumulation, so it is critical to identify the optimal concentration of vitamin B_{12} solution for fortification of living plants. Further study is required to undertake the actual bioavailability of vitamin B_{12} in fortified food crops.

Previous studies present successful approaches for sustainable fortification on food crops grown in hydroponic systems by enhancing mineral/micronutrient and non-essential micronutrients such as folate, iodine, and selenium. Watanabe et al. (2017) present that the contents of folate significantly increased approximately 1.8-fold in spinach with the applications of folate and phenylalanine in hydroponic cultivation. As non-essential micronutrients, selenium and iodine have been notably investigated by several previous studies. Puccinelli et al. (2021) showed that iodine was fortified in both basils and lettuces grown in closed-loop hydroponic cultivation with 10 μM potassium iodide-loaded nutrient solution. The outcome of the study presents that the growth rate of lettuces in aeroponic systems is much higher than in the hydroponic system, due to higher levels of dissolved oxygen in the nutrient solution in aeroponic systems. Therefore, aeroponics can provide an efficient growing system for nutrient fortification in plants with greater oxygen availability in the root zone, enhancing water and nutrients use efficiency.

Ultrasonic atomization aeroponic, as a novel hybrid system, enables more precise and effective control by producing very fine micro-size droplets (1–5 μm) of nutrient solution generated by ultrasonic atomization disks (Niam and Sucahyo, 2020). Therefore, nanoparticles can be applied into nutrient solution within ultrasonic atomization disk, and it would be possible to increase targeted micronutrients in food crops due to their better solubility and permeability. Further study would be useful to investigate the optimal droplet size, flow rate, and nutrient solution conditions such as temperature and nanoparticle application in aeroponic systems (Niam and Sucahyo, 2020). It is required to identify optimal nanoparticle application to fortify micronutrients in closed soilless cultivation such as in hydroponic and aeroponic systems, especially in ultrasonic atomization aeroponics. Also, efforts should be made for identifying adequate growing systems for food crops based on understanding of their genotypes and physiological characteristics.

Mechanisms of Uptake and Translocation of Nanoparticles in Plants

Factors Impacting the Uptake and Translocation of Nanoparticles in Plants

It is necessary to understand how the plant absorbs, transports, and accumulates the nanoparticle in order to enhance nutrient/mineral contents in food crops in targeted locations (such as edible parts of the food crops). Nanoparticle application

enables the effective smart-delivery functions owing to their high solubility and mobility (Shang et al., 2019). Several studies have been conducted to investigate the mechanisms of uptake, transport, and accumulation of micronutrient/mineral nanoparticle in living plants by applying integrated analytic methods such as microscopy and mass spectrometry. However, due to the complexity and interaction between nanoparticles and plants, exact mechanisms should be investigated. Additionally, various factors significantly impact the absorption and uptake of nanoparticles in living plants. First, the size of nanoparticles is one of the main restrictions for penetration into cell wall pores in plants, which are 5–20 nm wide (Pérez-de-Luque, 2017). Second, the type and chemical composition of nanoparticles have a great influence on the absorption or uptake of nanoparticles (Rico et al., 2011; Pérez-de-Luque, 2017).

Coating materials for nanoparticles and the chemical composition of their surfaces can also alter their absorption or accumulation in living plants (Schwab et al., 2016; Pérez-de-Luque, 2017). Third, plant species impact the speed of absorption and distribution of nanoparticles due to different plant physiological traits, such as the thickness or architecture of the barriers, including the size of the cell wall pore, Casparian strip, and xylem thickness (Cifuentes et al., 2010). For instance, paramagnetic-coated nanoparticles were applied to four different crops, wheat, pea, sunflower, and tomato, with results indicating that the nanoparticles accumulate in different plant locations, such as vascular tissues or trichomes (Schwab et al., 2016). The effects of ENMS on plants can be highlighted as dependent on crop life stages, including (i) germination and early seedling growth, (ii) post-transplant and further growth of seedlings, and (iii) mature/harvest stages (Servin and White, 2016). Finally, the method of application plays an important role in nanoparticle pathways in plants. Nanoparticles in terrestrial plants generally accumulate and aggregate at the root zone, which is greatly influenced by microenvironmental conditions, including symbiosis with bacteria or fungi (Schwab et al., 2016). According to Schwab et al. (2016), the application of foliar ENMs in soil via roots is particularly challenging due to the interaction between microorganisms in soils and additional complex soil conditions. Delivering ENMs via foliar application or seed coating may improve the uptake or distribution of ENMs in living plants. Further study is required to investigate the optimum application method of ENMs based on understanding the transdisciplinary factors of growing plants.

Uptake and Translocation of Nanoparticles in Plants

There are two primary paths for the uptake, translocation, and accumulation of nanoparticles: foliar and root (**Figure 4**). In foliar application, the cuticle is the major obstacle preventing nanoparticles from entering plant tissues due to the water resistance from waxy components. Therefore, the major route for nutrient uptake is via cuticular pathways, including lipophilic pathways. The lipophilic pathway involves diffusion via cuticular wax layers, whilst the hydrophilic pathway occurs via polar aqueous pores located in the cuticle or stomata in leaves: the "stomatal pathway." Uptake via the hydrophilic pathway is influenced by stomatal openings, such as the morphological traits of stomatal apertures in various plant species. After the stomatal pathway, nanoparticles are transported via the vascular pathway, consisting of the xylem and phloem systems. The direction of flow in the xylem system is from root to shoot, whilst the flow direction in the phloem system is from shoot to root. Thus, in foliar applications, nanoparticles are translocated only via the phloem system from leaves to roots. Accordingly, previous studies have found that nanoparticles can be transported via xylem and phloem systems. However, the mechanisms of nanoparticle translocation in xylem and phloem still require further investigation (Lv et al., 2019). Due to the size of the cuticular pore, which is approximately 2 nm in diameter, the stomatal pathway is the most likely route for nanoparticle translocation. Therefore, from foliar spraying application, nanoparticles can be found in leaf stomata and deeper plant tissues, such as phloem, with translocation (Lv et al., 2019).

Compared to foliar application, many more studies have focused on root application. In root application, nanoparticles passively cross the permeable cuticle region and the pores of the cell wall. There are several factors that influence the uptake of nanoparticles in plants via root application, such as nanoparticle size, fictionalization of surface (e.g., positive and negative charge), morphological traits, conditions of exposure, plant species and growth stage, root integrity, and rhizospheric processes (Lv et al., 2019). When applied in the root zone, there are several barriers that nanoparticles cross, including physiological barriers (e.g., root hair) or environmental conditions of the root (e.g., bacteria and mycorrhizae), mucilage/exudates, and cuticle of the root periderm. During interactions with barriers, nanoparticles penetrate the cell membrane by fluid-phase endocytosis, passive diffusion, or mechanical piercing and then accumulate in the mucilage, cuticle, and cell wall. Afterward, microorganisms, through processes such as mucilage exudation or biomineralization, assist nanoparticles in transport (Schwab et al., 2016).

Once nanoparticles penetrate the plant cell membrane through the pores of the roots, they start to diffuse by two pathways: (i) the space between the cell wall and plasma membrane and (ii) the intercellular space without penetrating the cell membrane (shown in **Figure 4**). Via penetration of roots, nanoparticles traverse from the root surface cuticle to intercellular structures, such as the epidermis, cortex, endodermis, and Casparian strip, and eventually penetrate the shoot via xylem (Lv et al., 2019). When nanoparticles approach the root epidermis, two major pathways have been previously investigated, namely the apoplast and symplast, connecting cell wall and intercellular spaces, and protoplasmic connections through ion channels (Pérez-de-Luque, 2017). The apoplastic pathway plays an important role in radial movement within plant tissues, and it allows nanoparticles to translocate upwards to the aerial part. In addition, once nanoparticles enter the central cylinder, they can move towards the aerial part via the transpiration stream through the xylem.

When the nanoparticles translocate through the apoplastic pathway, they face a barrier reaching the xylem through the root, which is called the Casparian strip and is mainly required in the symplastic pathway. The Casparian strip is a belt of cell wall components sealed by lipophilic hydrocarbons

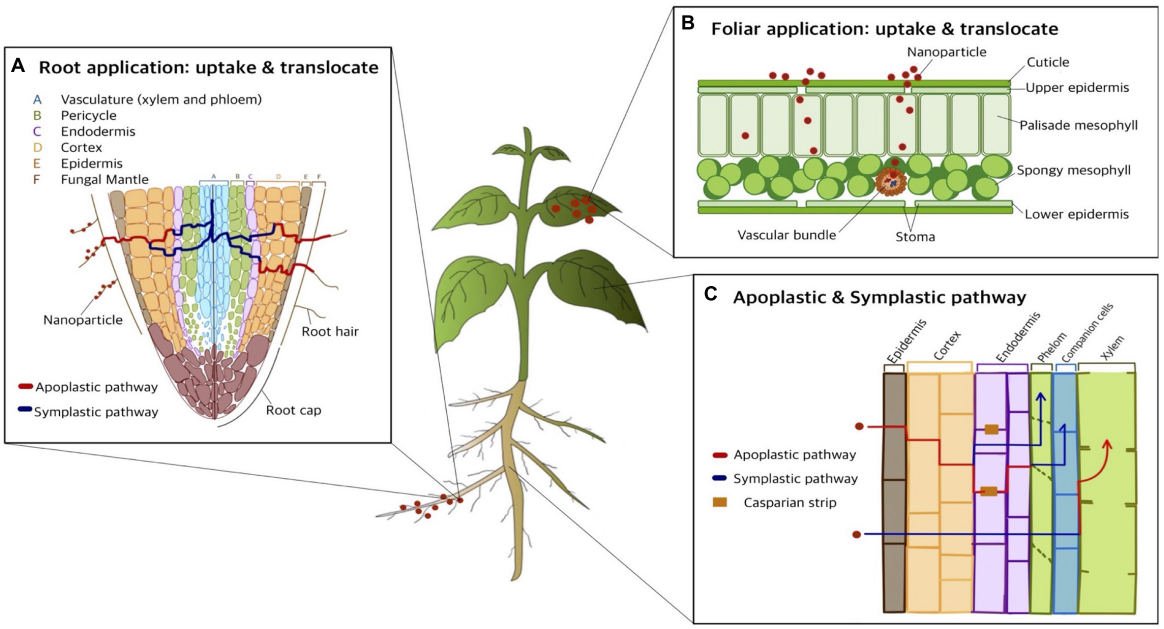

FIGURE 4 | Nanoparticle uptake and translocation in living plant: pathway of foliar spray and root application (modified from Pérez-de-Luque, 2017). **(A)** Root application: uptake and translocate. There are two pathways for uptake and transport of nanoparticles once the nanoparticles traverse the root hair: apoplastic pathway and symplastic pathway. **(B)** Foliar application: uptake and translocate. Nanoparticle can be applied via foliar spraying method allowing to uptake and accumulate the nanoparticle into leaves efficiently. **(C)** Apoplastic and symplastic pathway. When nanoparticles approach the root epidermis, two major pathways have been previously investigated: apoplast and symplast pathway. These allow the translocation of nanoparticles towards non-photosynthetic tissues and organs.

located adjacent to the vascular system. Casparian strips hamper nanoparticle translocation from roots to shoots if the particle size is too large (Cai et al., 2017; Lv et al., 2019). The symplastic pathway, which involves the movement of water and nutrients, utilizes the sieve tube elements in the phloem, allowing the translocation of nanoparticles towards non-photosynthetic tissues and organs. In the symplastic route, nanoparticles penetrate the cytoplasm or adjacent cells through plasmodesmata, which enables intercellular communication by linking the cytoplasm between adjacent cells. There are several hypotheses regarding symplastic pathways, involving aquaporins, ion channel interconnection, endocytosis, and breaking of membrane intubation. Endocytosis is the most feasible transmembrane pathway, including for nutrient uptake and microbial interactions (Lv et al., 2019). In root application, the nanoparticles are mainly translocated through the xylem but not the phloem and move from root to shoot and leaves (Pérez-de-Luque, 2017).

Nanoparticles are translocated and accumulate at different speeds and locations in plants based on their component materials (Pérez-de-Luque, 2017). Generally, nanoparticles accumulate in fruits, grains, flowers, or young leaves by traveling to the vascular system (Lu et al., 2008; Khot et al., 2012). Owing to advanced spectrometry or mass spectrometry techniques, it is possible to determine the overall uptake, translocation, and accumulation of nanoparticles in living plants. For instance, transmission electron microscopy (TEM), scanning electron microscopy (SEM), and X-ray spectroscopy analysis allow us to determine the sizes, shapes, and locations of nanoparticles in plant cells (Khot et al., 2012; Davies, 2018). Inductively coupled plasma optical emission spectroscopy (ICP-OES) and ICP-mass spectrometry (ICP-MS) precisely analyze nanoparticle compounds (Pérez-de-Luque, 2017). However, further studies should be conducted to identify the interaction between nanoparticles that are absorbed by plants and animals or humans that consume plants treated with nanoparticles (Pérez-de-Luque, 2017). Additionally, the uptake, distribution, and accumulation mechanisms vary and are greatly influenced by several components. Mozafar and Oertli (1992) found the uptake of vitamin B_{12} contents in soybean plants using the radioisotope dilution (RID) technique. By identifying vitamin B_{12} and vitamin B_{12}-binding sites, the study showed that vitamin B_{12} transport from vitamin B_{12}-enriched nutrient to soybean plants that was found in unifoliate, trifoliate leaves, and stems. Vitamin B_{12} transports rapidly from root to shoot and more vitamin B_{12} was accumulated in the leaves in the plants aerated with nitrogen.

Overall Opportunities and Challenges of Nanoparticle Applications for Food Crop

As a promising technology for sustainable agriculture, nanotechnology poses numerous opportunities. First, ENMs enhance the overall efficiency of water use and light and agrochemical use (Zhou et al., 2015). Increased water use efficiency is realized in nanofertilizer applications by increasing the retaining capacity, decreasing the loss amount, and

increasing the efficiency of utilization of water and nutrients (Giraldo et al., 2014). ENMs show the potential to increase light use efficiency in plants by augmenting chloroplast photosynthetic activities and enhancing chloroplast reactive oxygen species (ROS) (Giraldo et al., 2014). Agrochemical application shows significant enhancement of performance by decreasing adverse environmental effects, including leaching. Nanofertilizers constitute an alternative technique to the use of conventional fertilizers because they boost crop yield, quality, and tolerance to abiotic stress owing to their high efficiency (Kah et al., 2018). Compared to conventional fertilizer, nanofertilizer can increase crop production by approximately 20–30% and achieve similar levels of plant protection and nutrient enhancement with lower fertilizer usage (Kranjc and Drobne, 2019). Owing to their biochemical and physical characteristics, ENMs can be delivered precisely to the plant interior to enhance the uptake of nutrients and fertilizer (Lowry et al., 2019). Second, nanotechnology promotes soil sustainability by lowering additional fertilizer inputs via increased nutrient efficiency. Additionally, ENMs have the potential to increase fungi, which is beneficial for plant growth, or to encourage plant root vitality via nitrogen-fixing bacteria. Furthermore, nanotechnology enables the control of biotic stress such as pathogens or weed competitors and abiotic stress, including extreme temperature and water stress (Lowry et al., 2019).

There are several challenges for further deployment of nanotechnology in agri-food. One of the most significant challenges in nanotechnology is the potential risks and risk perceptions regarding nanoparticles (Lowry et al., 2019). Consumer perception and acceptance are negative towards ENMs in food crops. According to Giles et al. (2015), food product-integrated nanotechnology is less likely to be accepted by consumers than food packaging within nanotechnology. However, of most significant concern regarding ENM applications in agricultural food is that sectors have only focused on the input of nanoparticles as ingredients or additives to food products directly, whilst comparatively little concern has been aroused regarding nanoagrochemical applications, including nanofertilizers or nanopesticides. Furthermore, these observations indicate that the consumer accepts nanotechnology application in agricultural food production when perceived benefits outweigh the perceived risks. For the future application of nanotechnology in food crops, it is necessary to encourage marketing and commercialization for nanotechnology-processed food crops by increasing acceptance along with expert opinions regarding safety or acceptability (Giles et al., 2015). Further efforts should address and secure the availability of nano-agrochemicals within effective legislation and long-term risk assessment for the entire life cycle of nanoparticle application to food crops and further human/animal intake (Iqbal, 2019).

Additionally, although there have been several attempts, it is still necessary to investigate the interaction between ENMs and plants and to understand the mechanisms of uptake and translocation of nanoparticles in living plants (Nair et al., 2010; Pérez-de-Luque, 2017; Lowry et al., 2019). Precisely delivering ENMs remains a challenge considering precise target location, exact time of application, and appropriate dose of ENMs. Additionally, in nanoparticle applications, particle size plays an important role, influencing the translocation of nanoparticles in living plants. Nanoparticle size can be increased beyond the nano range and attain different shapes due to continuous aggregation which also may result in Ostwald ripening. Thus, synthesis process of nanoparticles should be developed to control nanosize and composition of nanoparticles, particularly when scaling up for commercial usages (Davies, 2018; Akbar et al., 2020). Davies (2018) presents a successful synthesis approach for producing stable sizes of nanoparticles ranging 3.62–20.18 nm for calcium oxide, 3–7.6 nm for iron oxide, and 7.03–15.41 nm for zinc oxide. The study exploited spinning disk reactor (SDR) to synthesize nanoparticles, which provided relatively rapid, efficient, and cost-effective synthesis process. SDR method allows the production of large amounts of nanoparticles with uniform size, and electrostatic coating method with histidine (amino acid) also enhances the mobility and solubility of metal oxide nanoparticle by enhancing retention capabilities and decreasing leaching issue (Davies, 2018). Further guidance documents and validated methods for nanoparticle size measurement should be established (Parisi et al., 2014).

CONCLUSION

Overall, this review paper suggests that nanoparticle technology would be a great sustainable strategy to mitigate vitamin B_{12} deficiency by providing efficient smart delivery of micronutrient/mineral to food crops. This review paper suggests several key findings:

(1) A sustainable vitamin B_{12} fortification approach should be balanced with other micronutrient/mineral deficiency focusing on not only increasing the contents but also the bioavailability of vitamin B_{12}.
(2) Nanoparticle technologies, such as seed priming and nanoparticle applications, can accelerate sustainable food fortification with better quality and yield by targeted macro- or micronutrient enhancement without further plant breeding or genetic technology.
(3) To develop food fortification along with nanoparticle applications, the participation of consumers and experts is significant. Further attempts should focus on enhancing the recognition of safety and applicability of nanotechnology for food crops along with investigations of the phytotoxicity and safety of nanoparticle application.
(4) Integration of hydroponic/aeroponic systems and nanoparticle applications is expected to be a promising technology for not only better productivity but also micronutrient fortification (e.g., vitamin B_{12}), which can be applied to vertical farming or indoor farming in future.

AUTHOR CONTRIBUTIONS

SO contributed to conception and review of the study, wrote first draft of the manuscript. SO, GC, and CL contributed to manuscript revision, read and approved the submitted version. All the authors contributed to the article and approved the submitted version.

REFERENCES

Abdel-Aziz, H., Hasaneen, M., and Omer, A. (2016). Nano chitosan-NPK fertilizer enhances the growth and productivity of wheat plants grown in sandy soil. *Span. J. Agric. Res.* 14:e0902. doi: 10.5424/sjar/2016141-8205

Agriculture and Rural Development (2019). *Global Food Supply and Demand, Consumer Trends, Trade Challenges. In EU Agricultural Markets Briefs*. Rome: FAO, 16.

Akbar, S., Tauseef, I., Subhan, F., Sultana, N., Khan, I., Ahmed, U., et al. (2020). An overview of the plant-mediated synthesis of zinc oxide nanoparticles and their antimicrobial potential. *Inorg. Nano Metal Chem.* 50, 257–271. doi: 10.1080/24701556.2019.1711121

Al-juthery, H., and Al-Shami, Q. (2019). The effect of fertigation with nano NPK fertilizers on some parameters of growth and yield of potato (*Solanum tuberosum* L.). *J. Agric. Sci.* 9, 225–232. doi: 10.33794/qjas.Vol9.Iss2.93

Allen, L. H., Rosenberg, I. H., Oakley, G. P., and Omenn, G. S. (2010). Considering the case for vitamin B12 fortification of flour. *Food Nutrit. Bull.* 31(1 Suppl.), 36–46. doi: 10.1177/15648265100311s104

Andrès, E., Loukili, N. H., Noel, E., Kaltenbach, G., Ben Abdelgheni, M., Perrin, A. E., et al. (2004). Vitamin B12 (cobalamin) deficiency in elderly patients. *CMAJ* 171, 251–259. doi: 10.1503/cmaj.1031155

Artés-Hernández, F., Formica-Oliveira, A. C., Artés, F., and Martínez-Hernández, G. B. (2017). Improved quality of a vitamin B12-fortified 'ready to blend' fresh-cut mix salad with chitosan. *Food Sci. Technol. Int.* 23, 513–528. doi: 10.1177/1082013217705036

Bito, T., Bito, M., Asai, Y., Takenaka, S., Yabuta, Y., Tago, K., et al. (2016). Characterization and quantitation of Vitamin B12 compounds in various *Chlorella* supplements. *J. Agric. Food Chem.* 64, 8516–8524. doi: 10.1021/acs.jafc.6b03550

Bito, T., Ohishi, N., Hatanaka, Y., Takenaka, S., Nishihara, E., Yabuta, Y., et al. (2013). Production and characterization of cyanocobalamin-enriched lettuce (*Lactuca sativa* L.) grown using hydroponics. *J. Agric. Food Chem.* 61, 3852–3858. doi: 10.1021/jf305033s

Bito, T., Teng, F., Ohishi, N., Takenaka, S., Miyamoto, E., Sakuno, E., et al. (2014). Characterization of vitamin B12 compounds in the fruiting bodies of shiitake mushroom (*Lentinula edodes*) and bed logs after fruiting of the mushroom. *Mycoscience* 55, 462–468. doi: 10.1016/j.myc.2014.01.008

Bodirsky, B. L., Dietrich, J. P., Martinelli, E., Stenstad, A., Pradhan, P., Gabrysch, S., et al. (2020). The ongoing nutrition transition thwarts long-term targets for food security, public health and environmental protection. *Scientific Reports* 10:19778. doi: 10.1038/s41598-020-75213-3

Bouis, H. E., and Saltzman, A. (2017). Improving nutrition through biofortification: a review of evidence from HarvestPlus, 2003 through 2016. *Glob. Food Sec.* 12, 49–58. doi: 10.1016/j.gfs.2017.01.009

Brito, A., Habeych, E., Silva-Zolezzi, I., Galaffu, N., and Allen, L. H. (2018). Methods to assess Vitamin B12 bioavailability and technologies to enhance its absorption. *Nutrit. Rev.* 76, 778–792. doi: 10.1093/nutrit/nuy026

Cai, F., Wu, X., Zhang, H., Shen, X., Zhang, M., Chen, W., et al. (2017). Impact of TiO2 nanoparticles on lead uptake and bioaccumulation in rice (*Oryza sativa* L.). *NanoImpact* 5, 101–108. doi: 10.1016/j.impact.2017.01.006

Carmel, R. (2008). Efficacy and safety of fortification and supplementation with vitamin B12: biochemical and physiological effects. *Food Nutrit. Bull.* 29, 177–187. doi: 10.1177/15648265080292S121

Carmel, R. (2011). Mandatory fortification of the food supply with cobalamin: an idea whose time has not yet come. *Bone* 23, 1–7. doi: 10.1007/s10545-010-9150-2.Mandatory

Cifuentes, Z., Custardoy, L., de la Fuente, J. M. D., Marquina, C., Ibarra, R., Rubiales, D., et al. (2010). Absorption and translocation to the aerial part of magnetic carbon-coated nanoparticles through the root of different crop plants. *J. Nanobiotechnol.* 8:26. doi: 10.1186/1477-3155-8-26

Clarke, R. (1995). *Annex 4–Micronutrient Fortification of Food: Technology and Quality Control. In Annex 4–Micronutrient Fortification of Food: Technology and Quality Control*. Rome: FAO.

Crider, K. S., Bailey, L. B., and Berry, R. J. (2011). Folic acid food fortification-its history, effect, concerns, and future directions. *Nutrients* 3, 370–384. doi: 10.3390/nu3030370

Darwish, A. M. G., Soliman, T. N., Elhendy, H. A., and El-Kholy, W. M. (2021). Nano-encapsulated iron and folic acid-fortified functional yogurt enhance anemia in albino rats. *Front. Nutrit.* 8:654624. doi: 10.3389/fnut.2021.654624

Dary, O. (2008). Establishing safe and potentially efficacious fortification contents for folic acid and vitamin B12. *Food Nutrit. Bull.* 29 2(Suppl.), 214–224. doi: 10.1177/15648265080292s126

Davies, K. (2018). *Biofortification of Potato (Solanum tuberosum) Using Metal Oxide Nanoparticles*. Available online at: http://irep.ntu.ac.uk/ (accessed November 20, 2020).

Doets, E. L., In't Veld, P. H., Szczecińska, A., Dhonukshe-Rutten, R. A. M., Cavelaars, A. E. J. M., Van 't Veer, P., et al. (2013). Systematic review on daily Vitamin B12 losses and bioavailability for deriving recommendations on Vitamin B12 intake with the factorial approach. *Ann. Nutr. Metab.* 62, 311–322. doi: 10.1159/000346968

Duran, N. M., Medina-Llamas, M., Cassanji, J. G. B., De Lima, R. G., De Almeida, E., Macedo, W. R., et al. (2018). Bean seedling growth enhancement using magnetite nanoparticles. *J. Agric. Food Chem.* 66, 5746–5755. doi: 10.1021/acs.jafc.8b00557

Eldridge, B. M., Manzoni, L. R., Graham, C. A., Rodgers, B., Farmer, J. R., and Dodd, A. N. (2020). Getting to the roots of aeroponic indoor farming. *New Phytol.* 228, 1183–1192. doi: 10.1111/nph.16780

Elemike, E. E., Uzoh, I. M., Onwudiwe, D. C., and Babalola, O. O. (2019). The role of nanotechnology in the fortification of plant nutrients and improvement of crop production. *Appl. Sci.* 9:499. doi: 10.3390/app9030499

FAO, IFAD, UNICEF, WFP and WHO (2020). *The State of Food Security and Nutrition in the World 2020. In The State of Food Security and Nutrition in the World 2020*. Rome: FAO, doi: 10.4060/ca9692en

FAO (2017). *Nutrition-Sensitive Agriculture and Food Systems in Practice. Options for Intervention. In Nutrition-Sensitive Agriculture and food Systems in practice. Options for Intervention*. Rome: FAO.

Fidaleo, M., Tacconi, S., Sbarigia, C., Passeri, D., Rossi, M., Tata, A. M., et al. (2021). Current nanocarrier strategies improve vitamin b12 pharmacokinetics, ameliorate patients' lives, and reduce costs. *Nanomaterials* 11:743. doi: 10.3390/nano11030743

Forgrieve, J. (2019). *Plant-Based Food Sales Continue To Grow By Double Digits, Fueled By Shift In Grocery Store Placement. Forbes*. 1–6. Available online at: https://www.forbes.com/sites/janetforgrieve/2019/07/16/plant-based-food-sales-pick-up-the-pace-as-product-placement-shifts/#119d3dd54f75 (accessed July 16, 2019)

Freire, M., Pereira, M., Lange, N., and Batista, L. (2020). "Biofortification of crop plants: a practical solution to tackle elemental deficiency," in *Sustainable Solutions for Elemental Deficiency and Excess in Crop Plants*, eds M. Freire, M. Pereira, N. Lange, and L. Batista (Singapore: Springer), 135–182. doi: 10.1007/978-981-15-8636-1_7

Garrod, M. G., Buchholz, B. A., Miller, J. W., Haack, K. W., Green, R., and Allen, L. H. (2019). Vitamin B12 added as a fortificant to flour retains high bioavailability when baked in bread. *Nucl. Instrum. Methods Phys. Res. B* 438, 136–140. doi: 10.1016/j.nimb.2018.05.042

Giles, E. L., Kuznesof, S., Clark, B., Hubbard, C., and Frewer, L. J. (2015). Consumer acceptance of and willingness to pay for food nanotechnology: a systematic review. *J. Nanopart. Res.* 17:464. doi: 10.1007/s11051-015-3270-4

Giraldo, J. P., Landry, M. P., Faltermeier, S. M., McNicholas, T. P., Iverson, N. M., Boghossian, A. A., et al. (2014). Plant nanobionics approach to augment photosynthesis and biochemical sensing. *Nat. Mater.* 13, 400–408. doi: 10.1038/nmat3890

Green, R. (2017). Vitamin B12 deficiency from the perspective of a practicing hematologist. *Blood* 129, 2603–2612. doi: 10.1182/blood-2016-10-569186.In

Green, R., Allen, L. H., Bjørke-Monsen, A. L., Brito, A., Guéant, J. L., Miller, J. W., et al. (2017). Vitamin B12 deficiency. *Nat. Rev. Dis. Prim.* 3:17040. doi: 10.1038/nrdp.2017.40

HarvestPlus and FAO (2019). *Biofortification: a Food-Systems Solution to Help End Hidden Hunger*. Rome: FAO.

Hoe, P. T., Mai, N. C., Lien, L. Q., Ban, N. K., Van Minh, C., Chau, N. H., et al. (2018). Germination responses of soybean seeds under Fe, ZnO, Cu and Co nanoparticle treatments. *Int. J. Agric. Biol.* 20, 1562–1568. doi: 10.17957/IJAB/15.0670

Hunt, A., Harrington, D., and Robinson, S. (2014). Vitamin B12 deficiency. *BMJ (Online)* 349, 1–7.

Iqbal, M. (2019). "Nano-fertilisers for sustainable crop production under changing climate_ A global perspective," in *Sustainable Crop Production*, Vol. 8, ed. M. Iqbal (London: InTechOpen), 1–13. doi: 10.5772/intechopen.89089

Itroutwar, P. D., Kasivelu, G., Raguraman, V., Malaichamy, K., and Sevathapandian, S. K. (2020). Effects of biogenic zinc oxide nanoparticles on seed germination and seedling vigor of maize (*Zea mays*). *Biocatal. Agric. Biotechnol.* 29:101778. doi: 10.1016/j.bcab.2020.101778

Jedut, P., Szwajgier, D., and Glibowski, P. (2021). Some plant food products present on the polish market are a source of Vitamin B12. *Appl. Sci.* 11:3601. doi: 10.3390/app11083601

Jeyasubramanian, K., Gopalakrishnan Thoppey, U. U., Hikku, G. S., Selvakumar, N., Subramania, A., and Krishnamoorthy, K. (2016). Enhancement in growth rate and productivity of spinach grown in hydroponics with iron oxide nanoparticles. *RSC Adv.* 6, 15451–15459. doi: 10.1039/c5ra23425e

Jones, L. (2020). *Veganism: Why are Vegan Diets on the Rise?–BBC News. In BBC News*. London: BBC News, 1–2.

Kah, M., Kookana, R. S., Gogos, A., and Bucheli, T. D. (2018). A critical evaluation of nanopesticides and nanofertilizers against their conventional analogues. *Nat. Nanotechnol.* 13, 677–684. doi: 10.1038/s41565-018-0131-1

Kamiński, M., Skonieczna-Żydecka, K., Nowak, J. K., and Stachowska, E. (2020). Global and local diet popularity rankings, their secular trends, and seasonal variation in Google Trends data. *Nutrition* 79-80:11075. doi: 10.1016/j.nut.2020.110759

Kasivelu, G., Selvaraj, T., Malaichamy, K., Kathickeyan, D., Shkolnik, D., and Chaturvedi, S. (2020). Nano-micronutrients [γ-Fe2O3(iron) and ZnO (zinc)]: green preparation, characterization, agro-morphological characteristics and crop productivity studies in two crops (rice and maize). *New J. Chem.* 44, 11373–11383. doi: 10.1039/d0nj02634d

Kaur, T., Rana, K. L., Kour, D., Sheikh, I., Yadav, N., Kumar, V., et al. (2020). "Microbe-mediated biofortification for micronutrients: present status and future challenges," in *New and Future Developments in Microbial Biotechnology and Bioengineering*, eds A. Rastegari, N. Yadav, and A. Yadav (Amsterdam: Elsevier Inc), 1–17. doi: 10.1016/b978-0-12-820528-0.00002-8

Keshavarz, H., and Moghadam, R. S. G. (2017). Seed priming with cobalamin (vitamin B12) provides significant protection against salinity stress in the common bean. *Rhizosphere* 3, 143–149. doi: 10.1016/j.rhisph.2017.04.010

Khot, L. R., Sankaran, S., Maja, J. M., Ehsani, R., and Schuster, E. W. (2012). Applications of nanomaterials in agricultural production and crop protection: a review. *Crop Prot.* 35, 64–70. doi: 10.1016/j.cropro.2012.01.007

Khush, G. S., Lee, S., Cho, J. ll, and Jeon, J. S. (2012). Biofortification of crops for reducing malnutrition. *Plant Biotechnol. Rep.* 6, 195–202. doi: 10.1007/s11816-012-0216-5

Kranjc, E., and Drobne, D. (2019). Nanomaterials in plants: a review of hazard and applications in the agri-food sector. *Nanomaterials* 9:1094. doi: 10.3390/nano9081094

Kumudha, A. (2015). Effect of different extraction methods on vitamin B12 from blue green algae, spirulina platensis. *Pharm. Anal. Acta* 6:337. doi: 10.4172/2153-2435.1000337

Lawrence, A. D., Nemoto-Smith, E., Deery, E., Baker, J. A., Schroeder, S., Brown, D. G., et al. (2018). Construction of fluorescent analogs to follow the uptake and distribution of cobalamin (Vitamin B 12) in bacteria, worms, and plants. *Cell Chem. Biol.* 25, 941.e–951.e. doi: 10.1016/j.chembiol.2018.04.012 941-951.e6,

Liu, R., and Lal, R. (2015). Potentials of engineered nanoparticles as fertilizers for increasing agronomic productions. *Sci. Total Environ.* 514, 131–139. doi: 10.1016/j.scitotenv.2015.01.104

Lowry, G., Avellan, A., and Gilbertson, L. (2019). Opportunities and challenges for nanotechnology in the agri-tech revolution. *Nat. Nanotechnol.* 14, 517–522. doi: 10.1038/s41565-019-0461-7

Lu, W., Dulal, S., Shuguang, W., Oleg, T., Anant Kumar, S., Hongtao, Y., et al. (2008). Effect of surface coating on the toxicity of silver nanomaterials on human skin keratinocytes. *Chem. Phys. Lett.* 23, 1–7. doi: 10.1038/jid.2014.371

Lv, J., Christie, P., and Zhang, S. (2019). Uptake, translocation, and transformation of metal-based nanoparticles in plants: recent advances and methodological challenges. *Environ. Sci. Nano* 6, 41–59. doi: 10.1039/C8EN00645H

Martens, J. H., Barg, H., Warren, M., and Jahn, D. (2002). Microbial production of vitamin B12. *Appl. Microbiol. Biotechnol.* 58, 275–285. doi: 10.1007/s00253-001-0902-7

Melo, L., Ng, C., Tsang, R., Singh, A. P., Kitts, D., and Lamers, Y. (2020). Development of novel Vitamin B12 fortified yogurts using isolated and microencapsulated Vitamin B12. *Proc. Nutr. Soc.* 79:2021. doi: 10.1017/s0029665120002128

Mozafar, A., and Oertli, J. J. (1992). Uptake of a microbially-produced vitamin (B12) by soybean roots. *Plant Soil* 139, 23–30. doi: 10.1007/BF00012838

Muthayya, S., Rah, J. H., Sugimoto, J. D., Roos, F. F., Kraemer, K., and Black, R. E. (2013). The global hidden hunger indices and maps: an advocacy tool for action. *PLoS One* 8:e67860. doi: 10.1371/journal.pone.0067860

Nair, R., Varghese, S. H., Nair, B. G., Maekawa, T., Yoshida, Y., and Kumar, D. S. (2010). Nanoparticulate material delivery to plants. *Plant Sci.* 179, 154–163. doi: 10.1016/j.plantsci.2010.04.012

Nakos, M., Pepelanova, I., Beutel, S., Krings, U., Berger, R. G., and Scheper, T. (2017). Isolation and analysis of vitamin B12 from plant samples. *Food Chem.* 216, 301–308. doi: 10.1016/j.foodchem.2016.08.037

Nakos, M. (2016). *Quantitative Determination of Vitamin B 12 in Plants [Gottfried Wilhelm Leibniz Universität Hannover]*. Available online at: https://www.repo.uni-hannover.de/bitstream/handle/123456789/8806/1024528006.pdf?sequence=1andisAllowed=y (accessed January 5, 2021).

National Institute of Health (2020). *Vitamin B12—Consumer*. Bethesda MD: National Institutes of Health.

Niam, A., and Sucahyo, L. (2020). Ultrasonic atomizer application for low cost aeroponic chambers (LCAC): A review. *IOP Conf. Ser. Earth Environ. Sci.* 542:012034. doi: 10.1088/1755-1315/542/1/012034

NIH (2021). *Vitamin B12_ Fact Sheet for Health professionals. Office of Dietary Supplements (ODS); National Institues of Health (NIH)*. Bethesda MD: National Institutes of Health, 1–13.

Oakley, G. P., and Tulchinsky, T. H. (2010). Folic acid and vitamin B12 fortification of flour: a global basic food security requirement. *Public Health Rev.* 32, 284–295. doi: 10.1007/BF03391603

Parisi, C., Vigani, M., and Rodriguez-Cerezo, E. (2014). *Proceedings of a Workshop on " Nanotechnology for the Agricultural sector?: From Research to the Field*. Brussels: European Union, 1–40. doi: 10.2791/80497

Pawlak, R., James, P. S., Raj, S., Cullum-Dugan, D., and Lucus, D. (2013). Understanding Vitamin B12. *Am. J. Lifestyle Med.* 7, 60–65. doi: 10.1177/1559827612450688

Pérez-de-Luque, A. (2017). Interaction of nanomaterials with plants: what do we need for real applications in agriculture? *Front. Environ. Sci.* 5:12. doi: 10.3389/fenvs.2017.00012

Prueksaritanond, S., Barbaryan, A., Mirrakhimov, A. E., Liana, P., Ali, A. M., and Gilman, A. D. (2013). A puzzle of hemolytic anemia, iron and vitamin B12 deficiencies in a 52-year-old male. *Case Rep. Hematol.* 2013:708489. doi: 10.1155/2013/708489

Puccinelli, M., Landi, M., Maggini, R., Pardossi, A., and Incrocci, L. (2021). Iodine biofortification of sweet basil and lettuce grown in two hydroponic systems. *Sci. Hortic.* 276:109783. doi: 10.1016/j.scienta.2020.109783

Rameshraddy, Pavithra, G. J., Rajashekar Reddy, B. H., Salimath, M., Geetha, K. N., and Shankar, A. G. (2017). Zinc oxide nano particles increases Zn uptake, translocation in rice with positive effect on growth, yield and moisture stress tolerance. *Indian J. Plant Physiol.* 22, 287–294. doi: 10.1007/s40502-017-0303-2

Rico, C. M., Majumdar, S., Duarte-Gardea, M., Peralta-Videa, J. R., and Gardea-Torresdey, J. L. (2011). Interaction of nanoparticles with edible plants and their possible implications in the food chain. *J. Agric. Food Chem.* 59, 3485–3498. doi: 10.1021/jf104517j

Ritchie, H., and Roser, M. (2017). *Micronutrient Deficiency. In Published online at OurWorldInData.org (Issue August 2017)*. 1. Available online at: https://ourworldindata.org/micronutrient-deficiency#citation (accessed December 18, 2020).

Rizzo, G., Laganà, A. S., Rapisarda, A. M. C., La Ferrera, G. M. G., Buscema, M., Rossetti, P., et al. (2016). Vitamin B12 among vegetarians: status, assessment and supplementation. *Nutrients* 8:767. doi: 10.3390/nu8120767

Rop, K., Karuku, G. N., Mbui, D., Njomo, N., and Michira, I. (2019). Evaluating the effects of formulated nano-NPK slow release fertilizer composite on the performance and yield of maize, kale and capsicum. *Ann. Agric. Sci.* 64, 9–19. doi: 10.1016/j.aoas.2019.05.010

Rouphael, Y., and Kyriacou, M. C. (2018). Enhancing quality of fresh vegetables through salinity eustress and biofortification applications facilitated

by soilless cultivation. *Front. Plant Sci.* 9:1254. doi: 10.3389/fpls.2018.01254

Ruel-Bergeron, J. C., Stevens, G. A., Sugimoto, J. D., Roos, F. F., Ezzati, M., Black, R. E., et al. (2015). Global update and trends of hidden hunger, 1995-2011: the hidden hunger Index. *PLoS One* 10:e0143497. doi: 10.1371/journal.pone.0143497

Rusher, D. R., and Pawlak, R. (2013). A review of 89 published case studies of vitamin B12 deficiency. *J. Hum. Nutr. Food Sci.* 1:1008.

Sanchez, H., Albala, C., Lera, L., Dangour, A. D., and Uauy, R. (2013). Effectiveness of the national program of complementary feeding for older adults in Chile on vitamin B12 status in older adults; secondary outcome analysis from the CENEX Study (ISRCTN48153354). *Nutr. J.* 12:124. doi: 10.1186/1475-2891-12-124

Sato, K., Kudo, Y., and Muramatsu, K. (2004). Incorporation of a high level of vitamin B12 into a vegetable, kaiware daikon (Japanese radish sprout), by the absorption from its seeds. *Biochim. Biophys. Acta Gen. Subj.* 1672, 135–137. doi: 10.1016/j.bbagen.2004.03.011

Schwab, F., Zhai, G., Kern, M., Turner, A., Schnoor, J. L., and Wiesner, M. R. (2016). Barriers, pathways and processes for uptake, translocation and accumulation of nanomaterials in plants–critical review. *Nanotoxicology* 10, 257–278. doi: 10.3109/17435390.2015.1048326

Seaman, C. (2017). *Investigation of Nutrient Solutions for the Hydroponic Growth of Plants Doctoral*. Sheffield: Sheffield Hallam University.

Servin, A. D., and White, J. C. (2016). Nanotechnology in agriculture: next steps for understanding engineered nanoparticle exposure and risk. *NanoImpact* 1, 9–12. doi: 10.1016/j.impact.2015.12.002

Shang, Y., Hasan, M. K., Ahammed, G. J., Li, M., Yin, H., and Zhou, J. (2019). Applications of nanotechnology in plant growth and crop protection: a review. *Molecules* 24:2558. doi: 10.3390/molecules24142558

Shankramma, K., Yallappa, S., Shivanna, M. B., and Manjanna, J. (2016). Fe2O3 magnetic nanoparticles to enhance S. lycopersicum (tomato) plant growth and their biomineralization. *Appl. Nanosci. (Switzerland)* 6, 983–990. doi: 10.1007/s13204-015-0510-y

Singh Sekhon, B. (2014). Nanotechnology in agri-food production: an overview. *Nanotechnol. Sci. Appl.* 7, 31–53. doi: 10.2147/NSA.S39406

Smith, M. E., Coffin, A. B., Miller, D. L., and Popper, A. N. (2006). Guidelines on food fortification with micronutrients. *J. Exp. Biol.* 209, 4193–4202. doi: 10.1242/jeb.02490

Stabler, S. (2020). "Present knowledge in nutrition," in *Present Knowledge in Nutrition*, 11th Edn, Vol. Volume 1, eds B. P. Marriott, D. F. Birt, V. A. Stallings, and A. A. Yates (Washington, DC: International Life Sciences Institute (ILSI)), 11. doi: 10.1016/c2018-0-02422-6

Stabler, S. P. (2013). Clinical practice. Vitamin B12 deficiency. *N. Engl. J. Med.* 368, 149–160. doi: 10.1056/NEJMcp1113996

Surendran, S., Adaikalakoteswari, A., Saravanan, P., Shatwaan, I. A., Lovegrove, J. A., and Vimaleswaran, K. S. (2018). An update on vitamin B12-related gene polymorphisms and B12 status. *Genes Nutr.* 13, 1–35. doi: 10.1186/s12263-018-0591-9

Tandon, P., Jin, Q., and Huang, L. (2017). A promising approach to enhance microalgae productivity by exogenous supply of vitamins. *Microb. Cell Factories* 16:219. doi: 10.1186/s12934-017-0834-2

Thompson, B., and Amoroso, L. (2010). "Combating micronutrient deficiencies: food-based approaches," in *Combating Micronutrient Deficiencies: Food-based Approaches*, eds B. Thompson and L. Amoroso (Rome: Food and Agriculture Organisation of the United Nations; CAB International), doi: 10.1079/9781845937140.0000

Titcomb, T. J., and Tanumihardjo, S. A. (2019). Global concerns with B vitamin statuses: biofortification, fortification, hidden hunger, interactions, and toxicity. *Compr. Rev. Food Sci. Food Safe.* 18, 1968–1984. doi: 10.1111/1541-4337.12491

Trujillo-Reyes, J., Majumdar, S., Botez, C. E., Peralta-Videa, J. R., and Gardea-Torresdey, J. L. (2014). Exposure studies of core-shell Fe/Fe3O4 and Cu/CuO NPs to lettuce (*Lactuca sativa*) plants: are they a potential physiological and nutritional hazard? *J. Hazard. Mater.* 267, 255–263. doi: 10.1016/j.jhazmat.2013.11.067

Tucker, K. L., Olson, B., Bakun, P., Dallal, G. E., Selhub, J., and Rosenberg, I. H. (2004). Breakfast cereal fortified with folic acid, vitamin B-6, and vitamin B-12 increases vitamin concentrations and reduces homocysteine concentrations: a randomized trial. *Am. J. Clin. Nutr.* 79, 805–811. doi: 10.1093/ajcn/79.5.805

Watanabe, F. (2007). Vitamin B12 sources and bioavailability. *Exp. Biol. Med.* 232, 1266–1274. doi: 10.3181/0703-MR-67

Watanabe, F., and Bito, T. (2018). Vitamin B12 sources and microbial interaction. *Exp. Biol. Med.* 243, 148–158. doi: 10.1177/1535370217746612

Watanabe, F., Schwarz, J., Takenaka, S., Miyamoto, E., Ohishi, N., Nelle, E., et al. (2012). Characterization of vitamin B12 compounds in the wild edible mushrooms black trumpet (*Craterellus cornucopioides*) and golden chanterelle (*Cantharellus cibarius*). *J. Nutr. Sci. Vitaminol.* 58, 438–441. doi: 10.3177/jnsv.58.438

Watanabe, F., Yabuta, Y., Bito, T., and Teng, F. (2014). Vitamin B12-containing plant food sources for vegetarians. *Nutrients* 6, 1861–1873. doi: 10.3390/nu6051861

Watanabe, F., Yabuta, Y., Tanioka, Y., and Bito, T. (2013). Biologically active vitamin B12 compounds in foods for preventing deficiency among vegetarians and elderly subjects. *J. Agric. Food Chem.* 61, 6769–6775. doi: 10.1021/jf401545z

Watanabe, S., Ohtani, Y., Tatsukami, Y., Aoki, W., Amemiya, T., Sukekiyo, Y., et al. (2017). Folate biofortification in hydroponically cultivated spinach by the addition of phenylalanine. *J. Agric. Food Chem.* 65, 4605–4610. doi: 10.1021/acs.jafc.7b01375

WHO (2020). *Fact Sheets: Malnutrition. Fact Sheets: Malnutrition*. Geneva: WHO.

Wolkers – Rooijackers, J. C. M., Endika, M. F., and Smid, E. J. (2018). Enhancing vitamin B12 in lupin tempeh by in situ fortification. *LWT* 96, 513–518. doi: 10.1016/j.lwt.2018.05.062

Xie, C., Coda, R., Chamlagain, B., Edelmann, M., Varmanen, P., Piironen, V., et al. (2021). Fermentation of cereal, pseudo-cereal and legume materials with *Propionibacterium freudenreichii* and *Levilactobacillus brevis* for vitamin B12 fortification. *LWT* 137:110431. doi: 10.1016/j.lwt.2020.110431

Zhou, L., Cai, D., He, L., Zhong, N., Yu, M., Zhang, X., et al. (2015). Fabrication of a high-performance fertilizer to control the loss of water and nutrient using micro/nano networks. *ACS Sustain. Chem. Eng.* 3, 645–653. doi: 10.1021/acssuschemeng.5b00072

Conflict of Interest: The authors declare that the research was conducted in the absence of any commercial or financial relationships that could be construed as a potential conflict of interest.

Publisher's Note: All claims expressed in this article are solely those of the authors and do not necessarily represent those of their affiliated organizations, or those of the publisher, the editors and the reviewers. Any product that may be evaluated in this article, or claim that may be made by its manufacturer, is not guaranteed or endorsed by the publisher.

frontiers in Plant Science

ORIGINAL RESEARCH
published: 21 October 2021
doi: 10.3389/fpls.2021.649283

A Transcriptome Analysis Revealing the New Insight of Green Light on Tomato Plant Growth and Drought Stress Tolerance

Zhonghua Bian[1,2], Yu Wang[2], Xiaoyan Zhang[3], Steven Grundy[2], Katherine Hardy[2], Qichang Yang[1] and Chungui Lu[2]**

[1] Photobiology Research Center, The Institute of Urban Agriculture, Chinese Academy of Agricultural Sciences, Chengdu, China, [2] School of Animal, Rural and Environment Sciences, Nottingham Trent University, Brackenhurst Campus, Nottingham, United Kingdom, [3] Institute of Industrial Crops, Jiangsu Academy of Agricultural Sciences, Nanjing, China

Light plays a pivotal role in plant growth, development, and stress responses. Green light has been reported to enhance plant drought tolerance via stomatal regulation. However, the mechanisms of green light-induced drought tolerance in plants remain elusive. To uncover those mechanisms, we investigated the molecular responses of tomato plants under monochromatic red, blue, and green light spectrum with drought and well-water conditions using a comparative transcriptomic approach. The results showed that compared with monochromatic red and blue light treated plants, green light alleviated the drought-induced inhibition of plant growth and photosynthetic capacity, and induced lower stomatal aperture and higher ABA accumulation in tomato leaves after 9 days of drought stress. A total of 3,850 differentially expressed genes (DEGs) was identified in tomato leaves through pairwise comparisons. Functional annotations revealed that those DEGs responses to green light under drought stress were enriched in plant hormone signal transduction, phototransduction, and calcium signaling pathway. The DEGs involved in ABA synthesis and ABA signal transduction both participated in the green light-induced drought tolerance of tomato plants. Compared with ABA signal transduction, more DEGs related to ABA synthesis were detected under different light spectral treatments. The bZIP transcription factor- HY5 was found to play a vital role in green light-induced drought responses. Furthermore, other transcription factors, including WRKY46 and WRKY81 might participate in the regulation of stomatal aperture and ABA accumulation under green light. Taken together, the results of this study might expand our understanding of green light-modulated tomato drought tolerance via regulating ABA accumulation and stomatal aperture.

Keywords: green light, stomatal aperture, ABA, drought stress, transcriptome, tomato

OPEN ACCESS

Edited by:
Eiji Goto,
Chiba University, Japan

Reviewed by:
Ki-Ho Son,
Gyeongsang National University, South Korea
Hideo Yoshida,
Chiba University, Japan

****Correspondence:***
Qichang Yang
yangqichang@caas.cn
Chungui Lu
chungui.lu@ntu.ac.uk

Specialty section:
This article was submitted to Crop and Product Physiology, a section of the journal Frontiers in Plant Science

Received: *04 January 2021*
Accepted: *23 September 2021*
Published: *21 October 2021*

Citation:
Bian Z, Wang Y, Zhang X, Grundy S, Hardy K, Yang Q and Lu C (2021) A Transcriptome Analysis Revealing the New Insight of Green Light on Tomato Plant Growth and Drought Stress Tolerance. Front. Plant Sci. 12:649283. doi: 10.3389/fpls.2021.649283

INTRODUCTION

In nature, plants often suffer from adverse environmental conditions, including drought, extreme temperature, heavy metal, and salinity stress. To survive under different stress conditions, plants must optimize their growth and development at the expense of yield loss. Drought is one of the most important prevalent abiotic

stresses that limits crop growth and productivity (Somerville, 2001; Lesk et al., 2016). With the global temperature increasing and worldwide population growth, the scarcity of water resources in agriculture will aggravate crop loss. The traditional producing staple foods could not meet the future food requirement due to the shortage of sufficiency irrigation water, and drought and/or unstable rainfall. Thus, new strategies for improving crop drought tolerance and water use efficiency are urgently needed for the next generation of agriculture (Chen et al., 2020).

Vertical Farming has been branded as the future of Food Production due to the environmental benefits and food security benefits (small geographical footprint, pesticide-free, water reuse, all year round growing) (Kalantari et al., 2020). However, there are still some issues that limit the wide commercialization of vertical farming, such as high energy cost, limited crop choice and lack of specialized crop varieties (Kozai and Niu, 2015). LEDs offer cheap, cool, controllable sources of light that can selectively and quantitatively provide different wavelengths that can activate discrete developmental pathways to change leaf area, thickness, stem length through photoreceptors include phytochrome and cryptochrome (Kozai and Niu, 2015). This provides us with a new opportunity to manipulate the quality and quantity of produce for markets and meet the demands of retailers. In order to understand the molecular mechanism leading to an increase in the resource use efficiency (light, water and nutrients). It is necessary to identify key genes (via transcriptomic analysis) which act as molecular markers and regulators for vertical framing (indoor farming) crop breeding.

It is reported that 70% of global freshwater is used for agriculture (Döll, 2009; FAO, 2012). Most of the water used in agriculture is lost to the atmosphere by evaporation and transpiration that is regulated by stomatal movement. Stomata are the important epidermal leaf pores in response to the water states of plants. It is evident that the early response of stomatal movement to drought stress can help plant survival sometimes through maintaining high relative water content (RWC) in leaves (Reddy et al., 2004). The plant hormone abscisic acid (ABA) is the key regulator of stomatal movement, which plays a pivotal role in plant's adaptive response to drought stress (Nakashima and Yamaguchi-Shinozaki, 2013). The ABA in plants is indirectly synthesized through the carotenoid pathway using β-carotene as a precursor (Schwartz and Zeevaart, 2010). The 9-cis-epoxycarotenoid dioxygenase (NCED) encoded by the homologous genes of *VIVIPAROUS14* (*VP14*), converses of 9′-cis-neoxanthin and 9′-cis-violaxanthin into xanthoxin in the plastid of plant cells. In the cytoplasm, the resulting xanthoxin will be further converted into two crucial enzymes: ABSCISIC ACID 2 (ABA2) and *Arabidopsis* aldehyde oxidase 3 (AAO3) (Chen et al., 2020). NCEDs are the rate-limiting enzymes of ABA synthesis. Overexpression of NCED related genes has been proved to enhance plant drought tolerance via increasing ABA levels to trigger stomatal closure and reduce transpiration (Wan et al., 2009; Lee and Luan, 2012). However, the decrease of stomatal aperture or stomatal closure caused by drought stress usually leads to a decrease in photosynthesis and finally results in a relatively low yield (Mafakheri et al., 2010). Thus, it is important to increase plant drought tolerance and concomitantly stabilize photosynthesis to minimize the drought-induced yield losses when carrying out stomatal regulation in crop production. Given the importance of endogenous ABA in regulating stomatal response to drought stress and the complexity of genetic engineering approaches used in enhancing plant drought stress tolerance, economic and innovative approaches are urgently needed for improving crop drought tolerance.

Light not only provides energy for driving photosynthesis but also works as a signal to regulate plant growth, development, and stress responses in a phytochrome-dependent manner (Wang et al., 2018). Light and ABA are integrated at the molecular level to regulate seed germination and seedling development. LONG HYPOCOTYL 5 (HY5, a bZIP transcription factor) plays an important role in integrating light signals with endogenous ABA pathways to help plants better adapt to environmental stresses (Chen et al., 2008; Xu et al., 2014). Recently, increasing numbers of studies demonstrate that endogenous ABA metabolism and/or ABA signaling pathway are subjected to the regulation of light spectra, including blue, red, and far-red light (Wang et al., 2018; Stawska and Oracz, 2019). In our previous studies, we found that green light enhanced tomato drought tolerance via altering stomatal aperture and ABA-dependent transcription factor-AREB1 (Bian et al., 2019). However, how green light induces ABA signals to regulate plant drought tolerance at the molecular level remains largely unclear.

Ribonucleic acid sequencing (RNA-seq) analysis based on next-generation sequencing is one of the main approaches of bioinformatics. RNA-seq is a good method for whole-transcriptome investigation (Cao et al., 2016). In this study, the molecular mechanism pathways and key genes of drought-treated tomato seedling response to green light were identified using RNA-seq analysis. Based on plant physiological responses and analyses of the Kyoto Encyclopedia of Genes and Genomes (KEGG) and Gene Ontology (GO) enrichment, a model of green light-enhanced tomato drought tolerance was proposed. Our present study could not only further facilitate our understanding of light spectra-regulated drought tolerance at the genome-wide level but also could identify key regulators and genes for improving stress tolerance of tomato grown under controlled environments.

MATERIALS AND METHODS

Plant Materials and Growth Conditions

Seeds of tomato (*Solanum Lycopersicum* L. cv. Ailsa Craig; wild type) were soaked in distilled water for 8 h and then grown in dark for 48 h. These germinated seeds were sown in rock wool cubes ($3 \times 3 \times 4$ cm^3) and grown under white LED light (Heliospectra RX30, Sweden) as our previous study (Bian et al., 2019) with photosynthetic photon flux density (PPFD) and photoperiod at 200 μmol $m^{-2}s^{-1}$ and 16 h, respectively, in an environmentally controlled growth chamber. The day/night temperature, air relative humidity, and CO_2 level were 25/20°C, 65%, and 400 μmol mol^{-1}, respectively. These seedlings were watered with half-strength Hoagland nutrition solution every other day.

Drought and Light Treatments

After around 28 days, similarly sized and healthy seedlings with five true leaves were transplanted into rock wool media (7.5 × 7.5 × 6.5 cm^3). The rock wool media were watered using half-strength Hoagland solution to reach their full water-holding capacity before these seedlings were transplanted. Throughout this whole experiment, these tomato seedlings were randomly grown under two watering regimes (well-watered and drought-stressed conditions) and concomitantly exposed to different light spectra. The two watering regimes: (1) well-watered, 90 ± 5% water-holding capacity of rock wools and (2) drought, stressed, non-watered until the plants showed severe drought stress symptoms–obvious turgor loss and wilting. The moisture of rock wools was monitored using every other day in proximity of the roots with a portable HH2 Moisture Meter connected to a WET sensor (Delta-T Device LTD, Cambridge, UK). The irrigation strategy was performed as the method described in the previous study (Wang et al., 2013; Bian et al., 2019). The light treatments included monochromatic red (peak at 660 nm), blue (peak at 450 nm) and green (peak at 530 nm) LED light (Heliospectra RX30, Sweden). The three different light treatments were combined with well-watered or drought conditions. In the first three treatments, plants were grown under well-watered conditions and exposed to monochromatic red light (RW), blue light (BW), or green light (GW) with PPFD at 200 μmol m^{-2} s^{-1}. In the other three were drought treatments. These drought-treated plants were irradiated with 200 μmol m^{-2} s^{-1} monochromatic red light (RD), blue light (BD), or green light (GD), respectively.

Plant Growth and Abscisic Acid Determination

After being treated for 9 days, the second fully expanded leaves from the top of plants were collected and immediately frozen in liquid nitrogen before being stored at −80°C. The extraction and determination of abscisic acid (ABA) were carried out as described by Balcke et al. (2012). Furthermore, another eight plants were randomly selected for the measurements of plant height, biomass, and leaf area measurements as the method of Bian et al. (2019). The leaf area was determined using a leaf area meter (LI-3000C, LI-COR, NE, USA).

Gas Exchange and Stomatal Aperture Determination

The second youngest and fully expanded leaves of plants under different treatments were used for gas exchange determination before (Day 0) and after treatment (Day 3, 6, and 9). The net photosynthesis (A_{net}) and chlorophyll fluorescent parameters were concomitantly measured using a portable photosynthesis system (LI-6800 F, LI-COR, Inc., Lincoln, NE). The light response curve of A_{net} was measured as the protocol of LI-6800F, and the light intensities were set as following: 0, 30, 50, 100, 200, 500, 800, and 1,200 μmol m^{-2} s^{-1}. The data obtained at the PPFD of 200 μmol $m^{-2}s^{-1}$ were used to analyze the photosynthetic performance of plants. During the gas exchange measurement, actinic light in the leaf chamber was provided by red and blue LED light sources (90% red, 10% blue), while the CO_2 level, air temperature, and airflow were set at 400 μmol mol^{-1}, 25°C, and 500 μmol s^{-1}, respectively. The light response curve fitting was carried out according to the methods of Thornley (1976). The responses of photosystem II (PSII) quantum efficiency (Φ_{PSII}) to the changes of PPFD were calculated as described by Baker (2008). The length and width of the stomata were determined using the method of Zeng et al. (2008). The stomatal aperture was calculated as the ratio of stomatal width to length.

Relative Water Content and Cell Membrane Stability

The method of Pan et al. (2012) was used to determine the relative water content (RWC) of plants treated with different light and water conditions. The cell membrane stability was expressed as the electrolyte leakage. The electrolyte leakage was determined as described by Jungklang et al. (2017). Briefly, five leaf discs punched from the second youngest and fully expanded leaves were put into a test tube with 20 ml of distal water and shaken every 5 min. After 30 min, the conductivity was measured using a conductivity meter. The total conductivity was measured after the test tubes were boiled for 15 min. The electrolyte leakage was calculated as the percentage of total conductivity.

RNA Extraction and Transcriptome Sequencing

After 9 days of treatments, the second fully expanded leaves from the top of randomly selected 12 plants (four plants per sample, three samples per treatment) were collected for RNA extraction. The total RNAs for transcriptome sequencing were extracted using an RNeasy Plant Mini RNA isolation kit (Qiagen, Hilden, Germany) according to the manufacturer's instructions. The quantity and purification of total RNAs were determined using a Nanodrop 2000C spectrophotometer (Thermo Scientific, USA) before and after the total RNAs were treated with 50 μl of RNase-free DNase I (Sigma-Aldrich, Poole, UK) at 37°C for 15 min. The integrity of total RNAs was rechecked using the Agilent Bioanalyzer 2100 system (Agilent Technologies, USA).

The total RNA extracted from each leaf sample was used for RNA-Seq library construction and sequencing by Biomics (Beijing) Biotech Co, Ltd. For the RNA sample preparations, 3 μg of RNA per sample was used as input material. The NEBNext® UltraTM RNA Library Prep Kit for Illumina® (NEB, USA) was used for generating sequencing as the manufacturer's instructions. Briefly, mRNA was purified from total RNA using poly-T oligo-attached magnetic beads. Fragmentation was carried out using divalent cations under elevated temperature in NEBNext First Strand Synthesis Reaction Buffer (5X). First-strand cDNA was synthesized using random hexamer primer and M-MuLV Reverse transcriptase (RNase H-), while the second strand cDNA was synthesized using DNA Polymerase I and RNase H. Remaining overhangs were converted into blunt ends via exonuclease/polymerase activities. The library fragments were purified with AMPure P system (Beckman Coulter, Beverly, USA) to select cDNA fragments of referentially 250∼300 bp in length. Then PCR was performed

TABLE 1 | The growth of tomato seedlings under different water and light spectral conditions (n = 6–8).

Treatments	Plant height (cm)	Leaf area (cm^2)	Dry weight (g)		
			Leaf	Stem	Leaf + stem
RW	27.23 ± 0.85 a	323.75 ± 18.07 a	0.53 ± 0.08 b	0.50 ± 0.05 a	1.03 ± 0.10 a
BW	24.74 ± 1.19 b	331.47 ± 39.76 ab	0.66 ± 0.03 a	0.48 ± 0.05 a	1.15 ± 0.08 a
GW	25.05 ± 1.02 b	272.44 ± 17.33 b	0.45 ± 0.09 b	0.32 ± 0.03 c	0.77 ± 0.12 b
RD	24.68 ± 1.39 b	221.36 ± 27.34 c	0.37 ± 0.06 b	0.33 ± 0.06 bc	0.70 ± 0.05 b
BD	21.84 ± 0.89 c	204.87 ± 16.48 c	0.43 ± 0.06 b	0.41 ± 0.03 b	0.84 ± 0.09 b
GD	24.81 ± 1.49 b	199.16 ± 29.01 c	0.37 ± 0.08 b	0.35 ± 0.03 bc	0.71 ± 0.12 b

The data are presented as Mean ± SEs. The different letters in each column indicate significant differences ($p < 0.05$) among treatments.

with Phusion High -Fidelity DNA polymerase, Universal PCR primers, and Index (X) Primer. Finally, the enriched cDNA libraries were assessed using the Agilent Bioanalyzer 2100 system before being sequenced on the HiSeq 6000 sequencing platform (Illumina, USA) to generate 125/150 bp paired-end reads.

Transcriptomic Analysis

The raw reads were cleaned by discarding the reads with adaptor contamination and low-quality reads (a quality score of $Q <$ 20). Clean reads from individual libraries of each group were mapped to the tomato reference genome Hisat2 v2.0.5 (Kim et al., 2015). The gene expression levels were estimated by the FPKM (fragments per kilobase of per millions of fragments mapped) of each gene calculated based on the length of the reads count mapped gene using RSEM (RNA-Seq by Expectation Maximization) module provided within the Trinity package (Trapnell et al., 2009). The DESeq2 R package (1.16.1) was used to carry out differential expression analysis of pairs of treatments (three biological replicates). The Benjamini and Hochberg's approach was used to adjust the resulting p-values for controlling the false discovery rate. Genes with an adjusted p-value < 0.05 and $|\log_2$ Fold Change$| < 1$ found by DESeq2 were assigned as differentially expressed between pairs of treatments. The analysis of the Gene Ontology (GO) and Kyoto Encyclopedia of Genes and Genomes (KEGG) pathways enrichment of differential expression genes (DEGs) were performed using the cluster Profiler R package was used to carry out (Tarazona et al., 2011). The GO and KEGG terms with corrected $p < 0.5$ were considered significantly enriched by DEGs between the two treatments.

Protein-protein Interaction Network and TF Regulatory Analysis

The PPI pairs of DEGs were extracted from STRING version 10.5 (Damian et al., 2017). Cytoscape version 3.8.0 was used to establish the PPI network of screened DEG (Shannon et al., 2003). The top five hub DEGs involved in the PPI network were identified from the network based on radiality by employing cytohubba (Chaudhary et al., 2019).

Validation of RNA-Seq Data by qRT-PCR Analysis

Ten DEGs were randomly selected for the validation of RNA-seq results by qRT-PCR. A total amount of 1 μg RNA, which was the same as that used for the RNA-seq sequence, was used for cDNA synthesis was performed through a RevertAid First Strand cDNA Synthesis Kit (Thermo Scientific, USA). The primers for these selected genes were designed by Primer Premier 6.0. Tomato Actin gene was employed as an internal reference gene (Li et al., 2016). The sequences of these primers are summarized in **Supplementary Table 1**. The qRT-PCR was performed on a CFX Connect™ Real-Time PCR Detection System (Bio-Rad, Hercules, CA, USA) with SsoFast™ EvaGreen® Supermix (Bio-Rad). The thermocycling conditions were set to 95°C for 30 s and 40 cycles of 95 C for 5 s, 56°C for 5 s, and 60°C for 5 s, followed by a melting curve (65–95°C). The qPCR was performed in triplicate, with three total RNA samples extracted from nine plants (three plants per sample). The relative gene expression levels of these selected genes were calculated using the $2^{-\Delta\Delta Ct}$ method (Shannon et al., 2003).

RESULTS

The Plant Growth of Tomato Exposed to Various Light Spectra Under Different Water Conditions

The growth of tomato seedlings was significantly affected by light spectra under both well-water and drought conditions (**Table 1**). Under the well-water condition, the plant height was highest under RW, followed by GW and then BW. The leaf area and plant dry weight of GW were lower than those under RW and BW. Except for the plant height and leaf dry weight, no significant differences were observed in those studied parameters between RW and BW. Drought led to significant decreases in plant height and dry weight of plants grown under red and blue light but showed slightly negative effects on those parameters of plants exposed to green light. Furthermore, the leaf area and dry weight of plants grown under RD, BD, and GD were comparable to each other. The leaf areas of RD, BD, and GD decreased by 31.61, 38.20, and 10.02%, while the total dry mass decreased by 32.03, 26.16, and 7.79% when compared with those parameters of RW, BW, and GW, respectively. These results indicate that green light

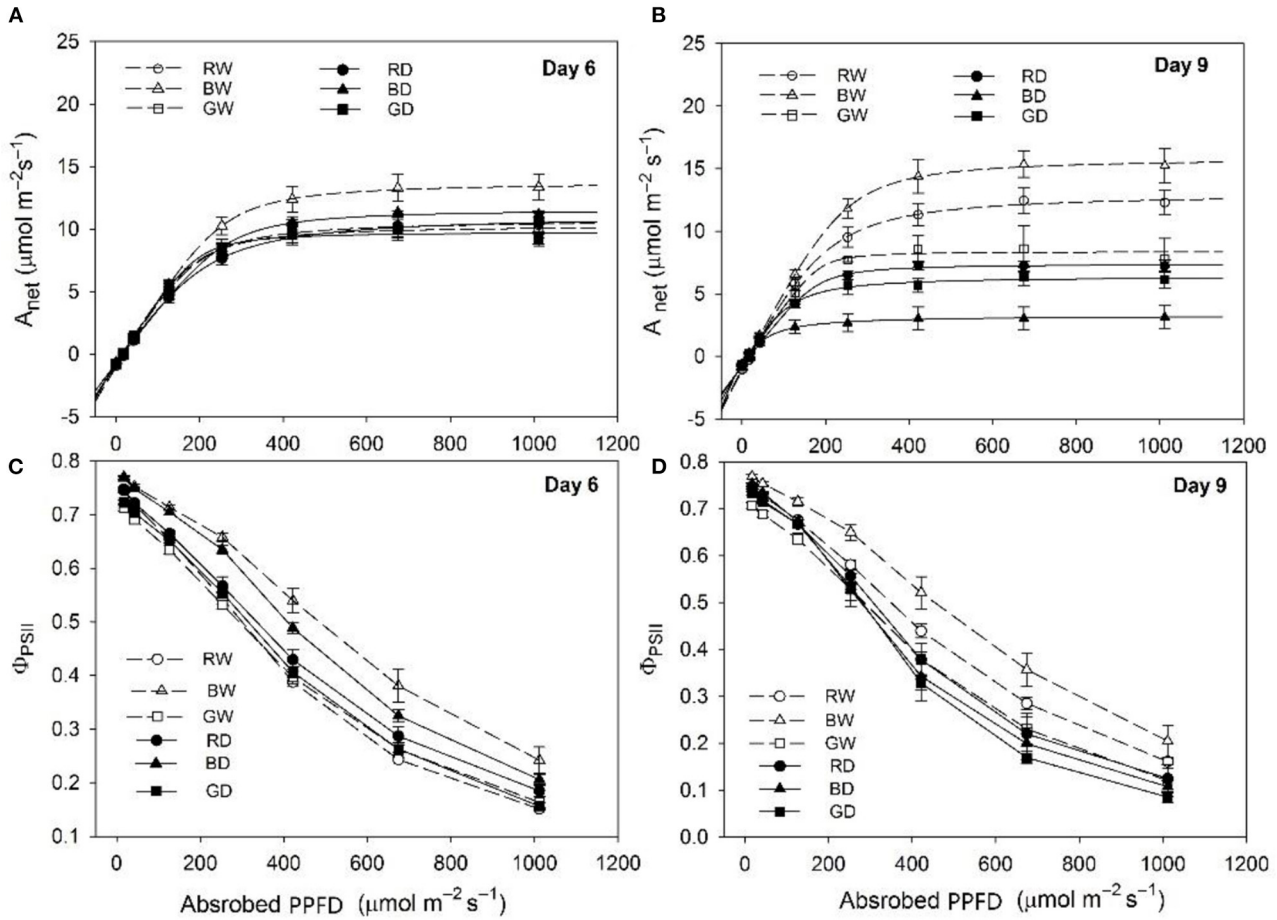

FIGURE 1 | The photosynthetic response of tomato seedlings under different water and spectral conditions. **(A,B)**, the changes of net photosynthetic rate (A_{net}) to increased light intensity; **(C,D)**, the changes of photosystem II (PSII) quantum efficiency (ϕ_{PSII}). RW, BW, and GW: well-water combined with red, blue, and green LED light, respectively; RD, BD, and GD: drought stress combined with red, blue, and green LED light, respectively. The photosynthetic photon flux density (PPFD) for all the treatments was 200 μmol m^{-2} s^{-1}.

counteracted the negative effects of drought stress on the tomato seedling growth.

The Photosynthetic Performance of Tomato Plants Exposed to Different Light Spectra

Drought stress led to marked decreases in max A_{net} and Φ_{PSII} of tomato plants under red and blue light. However, the levels of those parameters were comparable between GW and GD (**Figure 1**). Under well-watered conditions, the max A_{net} was highest under BW, flowed by RW and then GW throughout this study (**Figures 1A,B**). The changes of A_{net} with the increasing of light intensities (A-Q curve) were comparable among BD, RD, and GD at day 6 (**Figure 1A**), while the A-Q curve of plants under BD was markedly lower than those under RD and BD at day 9 (**Figure 1B**). Furthermore, Φ_{PSII} values of plants under different treatments decreased with the increase of light intensity. The values of Φ_{PSII} under BW and BD were higher than those under the other four treatments, while the Φ_{PSII} did not differ significantly among RW, GW, RD, and GW at day 6 (**Figure 1C**). The highest values of Φ_{PSII} were also observed under BW, followed by RW and GW, while values of this parameter under BD, RD, and GD were comparable to that under GW at day 9 (**Figure 1D**).

The Stomatal Responses and ABA Content of Tomato Plants Under Different Light Spectra

The g_s and Tr were markedly decreased between Day 6 and Day 9 (**Figures 2A,B**). The g_s showed a similar change tendency during the 9 days of treatments, but the g_s of plants under GD was lower than that under BD and RD (**Figure 2A**). Unlike g_s, Tr was significantly affected by light spectra. Under the well-watered condition, the Tr levels of plant leaves under GW were lower than those under RW and BW on day 6 and day 9. After 6 days of drought treatment, the Tr differed significantly

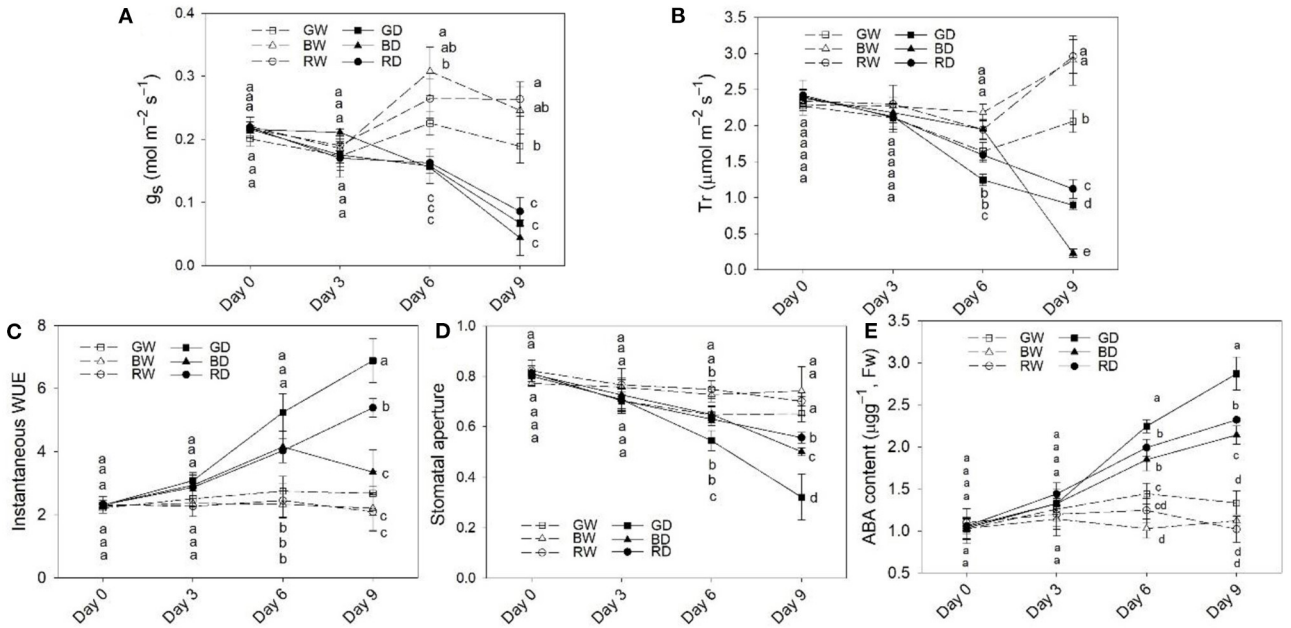

FIGURE 2 | The stomatal response, water use efficiency (WUE), and abscisic acid (ABA) content in leaves of plants under different water and light spectra condition. **(A,B)**, The responses of stomatal conductance (g_s) and transpiration rate (Tr) of plant leaves; **(C)**, The instantaneous WUE; **(D)**, stomatal aperture; **(E)**, ABA content in plant leaves after 9 days of treatment. RW, BW, and GW: well-water combined with red, blue, and green LED light, respectively; RD, BD, and GD: drought stress combined with red, blue, and green LED light, respectively. The PPFD for all the treatments was 200 μmol m^{-2} s^{-1}.

among drought treatments, with the highest values observed under BD, followed by RD, and then by GD, while Tr under BD was markedly lower than those under RD and GD on day 9 (**Figure 2B**). Drought stress led to increases in instantaneous WUE. The values of instantaneous WUE differed significantly among GD, BD, and RD with the highest value detected under GD, followed by RD and then BD (**Figure 2C**) at Day 9. Under the well-water condition, there were no marked differences in instantaneous WUE among different light spectra. Regardless of water conditions, the stomatal apertures of green light treated plants were lower than those under red and blue light between Day 6 and Day 9 (**Figure 2D**).

To verify the involvement of ABA in the response of plants to light spectra, the ABA content in tomato leaves of different treatments was determined. Under well-water conditions, the ABA content was comparable to each other, but the level of ABA under GW was slightly higher than that under BW and RW. However, under drought conditions, the ABA content was significantly affected by light spectra. The ABA content was highest under GD, followed by RD, while the lowest value was observed under BD from Day 6 to Day 9 (**Figure 2E**).

The Responses of Water Status and Plant Phenotype of Tomato Exposed Different Light Spectra

Drought for 9 days led to a marked increase in electrolyte leakage. The lowest electrolyte leakage was observed in green light treated plants under both well-watered and drought conditions. However, there was no significant difference in electrolyte leakage between red and blue light, as shown by the comparable values of this parameter between RW and BW, and between RD and DW (**Figure 3A**). When compared with the other four treatments, the RWC of BD and RD markedly decreased with the lowest value observed under BD. It is worth noting that no significant difference was observed in RWC between GW and GD (**Figure 3B**). These results indicate green light shows a positive function on enhancing the plant drought tolerance, as being further validated by the different wilting phenotypes of plants irradiated red, blue, green light under drought stress (**Figures 3C,D**).

Identification of DEGs of Tomato Seedlings Under Different Light Spectra by RNA-Seq

To further investigate key genes involved in the regulation of tomato seedling drought tolerance under different light spectra, we performed transcriptome analysis of plant leaves under red, blue, and green monochromatic light after 9 days of drought and well-watered treatment. A total of 3,850 DEGs was identified through pairwise comparisons. There were 601, 13, and 503 DEGs in the comparisons of GD vs. BD, GD vs. RD, and RD vs. BD, while 608, 505, and 1,616 DEGs were recorded when comparing GW vs. BW, GW vs. RW, and RW vs. BW (**Figure 4A**). Especially, 417, 8, and 307 DEGs were up-regulated, whereas 183, 5, and 196 DEGs were down-regulated in the comparison of GD vs. BD, GD vs. RD, and RD vs. BD, respectively. A total of 159, 6, and 51 DEGs were up-regulated

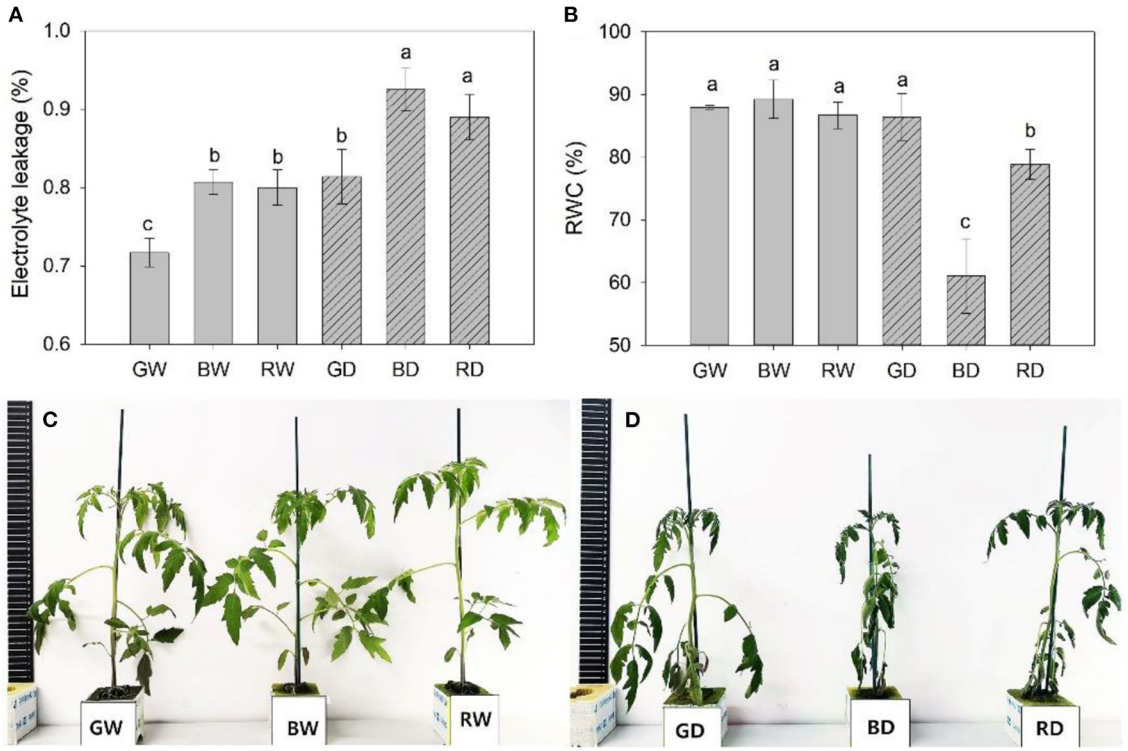

FIGURE 3 | The electrolyte leakage **(A)**, relative water content [RWC, **(B)**], and phenotype **(C,D)** of plants were treated with different water and light spectral condition for 9 days. RW, BW, and GW: well-water combined with red, blue, and green LED light, respectively; RD, BD, and GD: drought stress combined with red, blue, and green LED light, respectively. The PPFD for all the treatments was 200 μmol m^{-2} s^{-1}.

uniquely (**Figure 4B**), while the number of uniquely down-regulated DEGs were 98, 2, and 104 between GD and BD, GD and RD, and RD and BD, respectively (**Figure 4C**).

In addition, a hierarchical clustering analysis was performed to present a general overview of the expression pattern of DEGs (**Figure 4D**). Most of the genes with higher expression levels under drought stress displayed lower transcription levels under well-watered conditions and vice versa. Furthermore, the expression profile of most genes under blue light showed a great difference when compared with those of red and green light treated leaves, especially under drought stress. Notably, most DEGs presented different transcription profits between red and green light under well-watered conditions; whereas most identified genes showed a similar transcription pattern under drought stress (**Figure 4D**).

Functional Classification of DEGs Responses to Different Light Spectra Under Drought Stress

To reveal the function of green light-induced transcriptomes under drought stress, GO enrichment and KEGG pathway analysis were performed to categorize the DEGs. A total of 417, 10, and 386 DEG in the comparisons of GD vs. BD, GD vs. RD, and RD vs. BD were annotated into three major GO categories, respectively (**Supplementary Table 2**). In the comparison of GD vs. BD, the top 20 significantly enriched GO terms of DEGs were categorized into "biological process" and "cellular process" (**Figure 5A**). In the biological process category, the GO terms markedly enriched in the comparison of GD vs. BD included "oxidation-reduction process," "anthocyanin-containing compound metabolic process," and "maltose metabolic process," and "starch biosynthetic process." In the cellular process category, the significantly enriched GO terms were observed in "ammonium transmembrane transport," "oxidoreductase activity," and "1-deoxy-D-xylulose-5-phosphate" (**Figure 5A**). Compared with the other two comparisons, the enriched GO terms of the GD vs. RD comparison were not very complex. In the cellular component, "plasmodesma" was significantly enriched, while "sequence-specific DNA binding" and "DNA-binding transcription factors" were significantly enriched in the category of molecular function. Furthermore, the most significantly enriched GO terms of GD vs. RD comparison were identified in the processes of "defense response," "oxidation-reduction process," "protein phosphorylation," and "regulation of transcription" (**Figure 5B**). With respect to the comparison of RD vs. BD, the significant enriched GO terms in the biological process included "oxidation-reduction process," "anthocyanin-contained compounds," "thiamine biosynthetic process," and "flavonoid glucuronidation," while the top five most significantly enriched GO terms in the molecular function category was identified in the processes of "iron ion binding,"

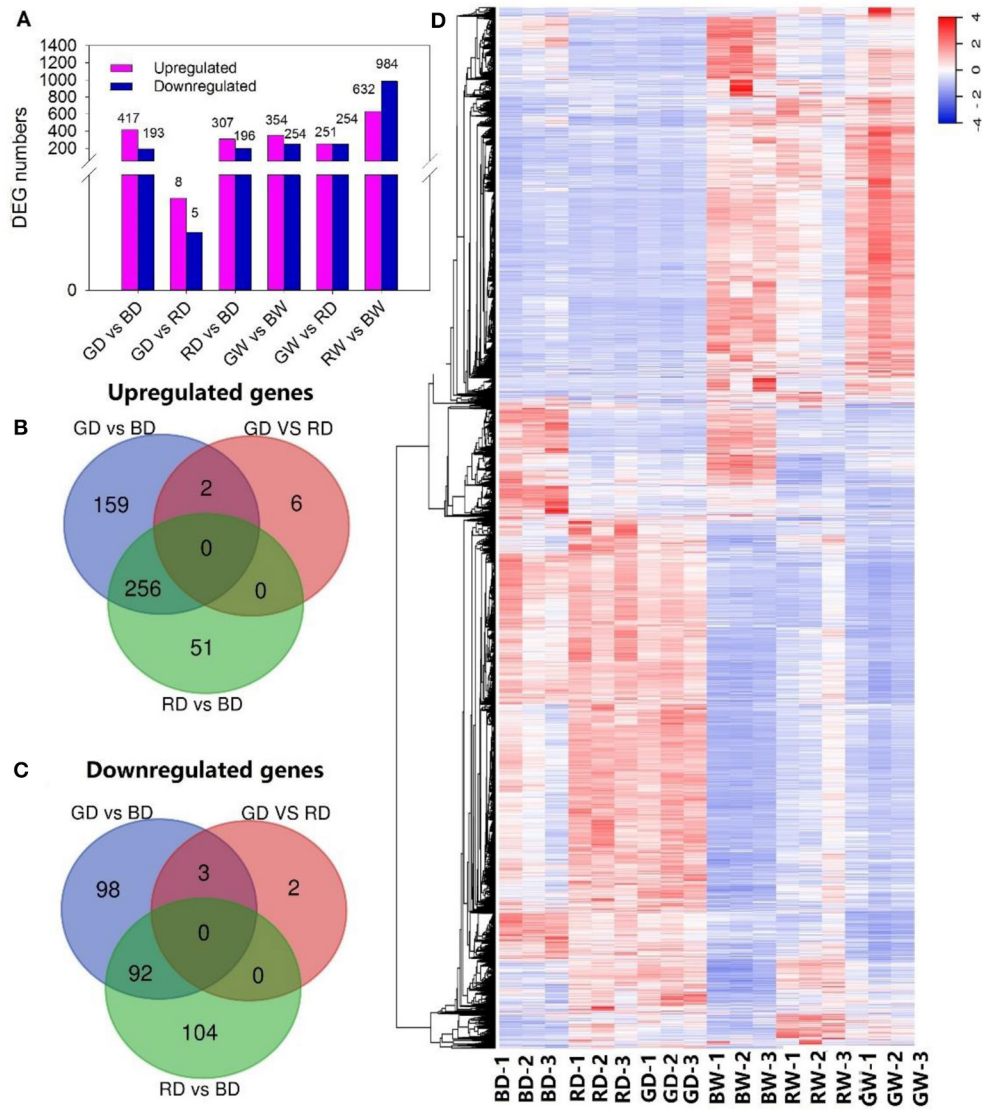

FIGURE 4 | The changes in gene expression profiles of tomato treated with different light spectra and water conditions. **(A)**, The number of DEGs between treatments; **(B,C)**, Venn diagram presenting up-regulated and down-regulated genes among plants exposed to different light spectra under drought conditions; **(D)**, Hierarchical clustering of DEGs, fragments per kilobase of transcript per million fragments mapped (FPKM), and relative expression of DEGs between different light and water treatments were calculated as $\log_2$ (FPKM) of differentially expressed genes, $\log_2$ (FPKM) of differentially expressed genes were calculated. A scale indicating the color assigned to $\log_2$ (FPKM) is shown to the right of the cluster.

"monooxygenase activity," "1-deoxy-D-xylulose-5-phosphate," "oxidoreductase activity," and "L-ascorbic acid-binding." In the category of the cellular compound, only "plastoglobule" was filtered into the top 20 significantly enriched GO terms in the RD vs. BD comparison (**Figure 5C**).

To further explore the biological functions of DEGs, the pathway enriched analysis based on the KEGG database was performed. When comparing each biological category, a higher number of DEGs were detected in the comparisons of GD vs. BD and RD vs. BD compared with GD vs. RD comparison, and the top 20 pathways in plants with the highest enrichment levels were listed in **Figure 6**. Among these KEGG pathways, DEGs in the comparison of GD vs. BD were mostly enriched in "phototransduction," "circadian entrainment," "calcium signaling pathway," "circadian rhythm-plant," and "plant hormone signal transduction" (**Figure 6A**). However, due to the less amount of DEGs detected in the comparison of GD vs. RD, the most significantly enriched pathway was detected in "arginine and proline metabolism" (**Figure 6B**). Furthermore, the top 5 pathways in enrichment degree were "phototransduction," "arginine and proline metabolism," "calcium signaling pathway," "circadian entrainment," and

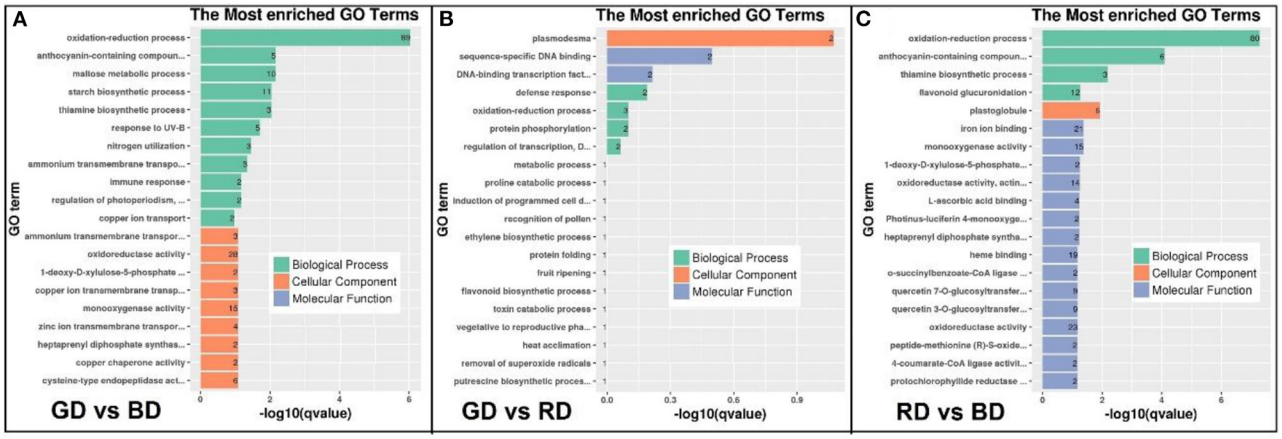

FIGURE 5 | The GO enrichment analysis of DEGs in the comparisons of GD vs. BD **(A)**, GD vs RD **(B)**, and RD vs. BD **(C)** in three main categories. BP, biological process; CC, cellular component; MF, molecular function.

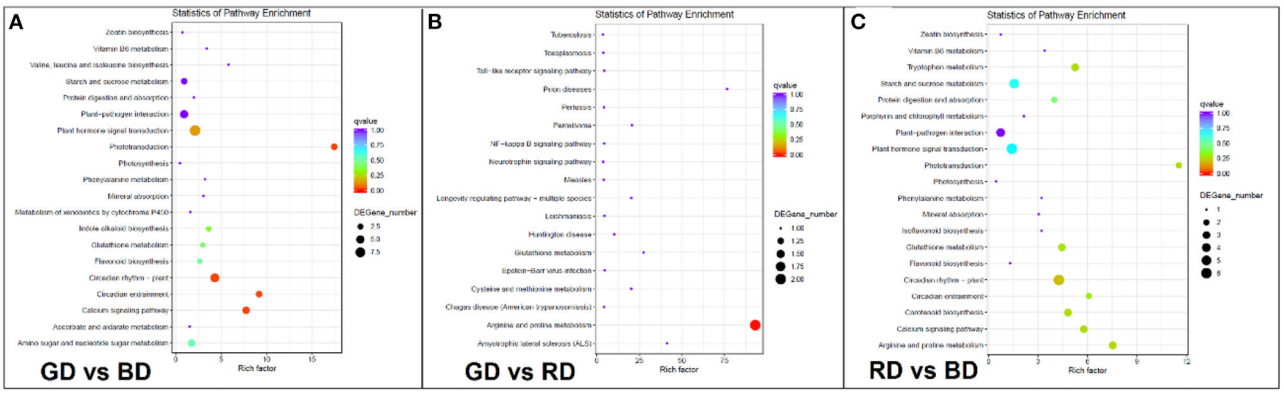

FIGURE 6 | KEGG pathway enrichment analysis of the annotated DEGs in the comparisons of GD vs BD **(A)**, GD vs. RD **(B)**, and RD vs. BD **(C)**. The Y-axis indicates the KEGG pathway, while the X-axis presents the enrichment factor, which is the ratio of DEGs enriched to specific KEGG pathways to DEGs enriched to all KEGG pathways. The dot size and the dot color indicate the number of DEGs of the pathway and q value, respectively.

"circadian rhythm-plant" under RD vs. BD comparison (**Figure 6C**).

Transcription Factors Identified by DEGs and PPI Network Analysis

The transcription factors among different comparisons were identified from DEGs and summarized in **Supplementary Table 3**. Among the DEGs of GD vs. BD comparison, 610 transcription factors were identified, including AP2/ERF (18), bHLH (16), bZIP (7), C2H2 (17), HSF (6), NAC (17), MYB/MYB-related (19), and WRKY (8). In the comparison of GD vs. RD, 13 transcription factor was identified, including AP2/ERF (1), C2H2 (1), WRKY (2), and SNF2 (1). Furthermore, there were 503 transcription factors detected in the comparison of RD vs. BD, including AP2/ERF (11), bHLH (15), bZIP (8), C2H2 (12), HSF (5), NAC (16), MYB/MYB-related (22), and WRKY (6).

To further investigate the hub genes involved in light spectral-induced drought tolerance, we first constructed the PPI network using screened DEG by Cytoscapeversion 3.8.0 (**Figure 7**). The top five hub proteins encoded by DEGs were further identified in the PPI network based on radiality analysis by employing cytohubba (**Supplementary Tables 4, 5**). In the comparison of GD vs. BD, two key hub proteins were identified in two sub-PPI networks. One of the key hub proteins-HY5 related gene (*Solyc08g061130.3*) was down-regulated, which directly acted with the other two hub protein: Solyc11g011980.3 (E3 ubiquitin-protein ligase COP1-like isoform X1) and Solyc02g070980.1 (chlorophyll a/b-binding protein Cab-1A). The other key hub gene-encoded protein was Solyc01g107730.3 (CycD3), which was directly affected by Solyc06g071830.2 (BTB/POZ and TAZ domain-containing protein 1) to participate in the regulation process of Solyc04g014470.3 (transcription factors, MYB20-like) (**Figure 7A**). In the comparison of RD vs. BD, Solyc08g061130.3 (transcription factors, HY5) was also identified

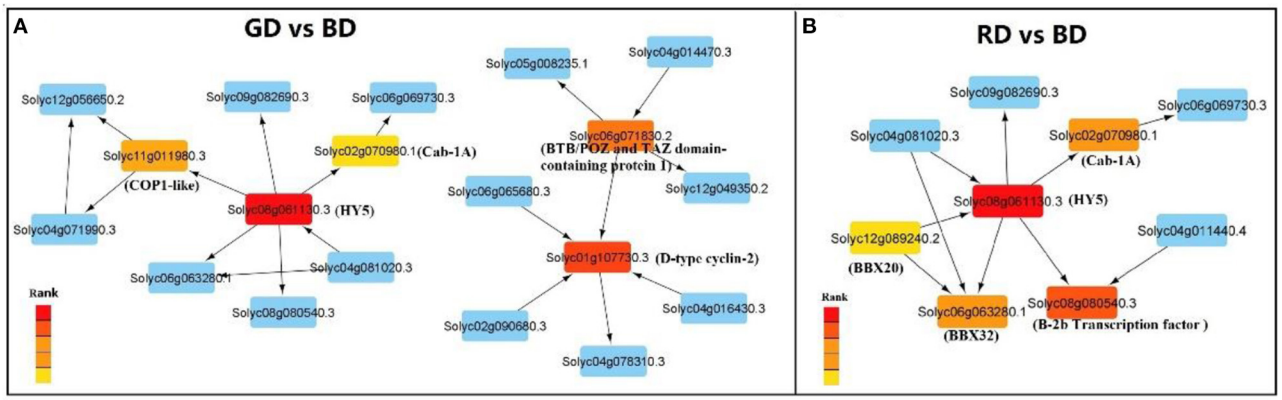

FIGURE 7 | Protein-protein interaction (PPI) network analysis based on the DEDs in the comparisons of "GD vs. BD" **(A)** and "RD vs. BD" **(B)**. Nodes depict proteins encoded by related genes and PPI are represented by edges in the network; the top five hub DEDs encoded proteins are represented by various colors (red: high rank; Yellow: low rank) in the PPI networks.

as the key hub protein, directly interacting with other four hub proteins: Solyc08g080540.3 (heat stress transcription factor, B-2b), Solyc02g070980.1 (chlorophyll a/b-binding protein Cab-1A), Solyc06g063280.1 (B-box zinc finger protein 32, BBX32), and Solyc12g089240.2 (B-box zinc finger protein 20, BBX20) (**Figure 7B**). Furthermore, no key hub proteins were identified by PPI analysis in GD vs. RD comparison due to the few DEGs detected in this comparison (**Supplementary Table 4**). These results indicate that HY5 might play role pivotal role in the light spectral-induced regulation of plant drought stress.

Differentially Expressed Genes Involved in ABA Metabolism and ABA Signal Transduction

Regardless of water conditions, the expression pattern of plant hormone metabolism and signaling pathway-related DEGs under green light was significant to those under red and blue light. More DEGs were involved in ABA metabolism, signaling, and responses (**Supplementary Figure 1**). To further investigate how ABA-related genes responded to different light spectra, the expression of ABA metabolism- and ABA signaling transduction-related genes were filtered from the DEGs and listed in **Figure 8**. Eight differentially expressed genes involved in ABA biosynthesis and one ABA signaling transduction-related gene were detected. Regardless of water conditions, the transcription level of the violaxanthin de-epoxidase related gene (*Solyc04g050930.3*, *VDE*) was highest under blue light, followed by green light and red light. The highest and lowest expression level of *NCED1* (*Solyc07g056570.1*) encoding 9-cis-epoxycarotenoid dioxygenase (NCED) was found under green light and red light, respectively (**Figures 8A,B**). Compared with blue light, *ABA2* (*Solyc12g056610.2*), encoding another important enzyme of ABA biosynthesis, was up-regulated under green light and red light. The cytochrome P450 monooxygenase (P450) encoded by *CYP707As*, plays an important role in the catabolism of ABA. Five *CYP707As* were identified under different light treatments. Regardless of water condition, three CYP707A related genes (*Solyc01g108210.3*, *Solyc04g080650.3*, and *Solyc08g005610.3*) were down-regulated under green light when compared with those under blue (**Figures 8A,B**). Under the well-water condition, the expression levels of *Solyc01g108210.3*, *Solyc04g071150*, *Solyc04g080650.3*, and *Solyc08g005610.3* under red light were lower than those under blue light (**Figure 8B**); however, only two identified *CYP707As* (*Solyc01g108210.3* and *Solyc04g071150*) were down-regulated under RD compared with those under BD. In addition, the PP2C related gene (*Solyc05g052520.3*) of plant leaves under green and red light was down-regulated compared with that of blue light treated plants (**Figures 8A,B**). These results suggest that the ABA biosynthesis, metabolism, and ABA signaling transduction are regulated by light spectra. Compared with red, green light not only enhances ABA biosynthesis and concomitantly reduces ABA degradation but is also involved in ABA signaling transduction in tomato plants, while green light is more efficient in promoting ABA biosynthesis in tomato seedlings.

Validation of Differently Expressed Genes by qPCR

The reliability of RNA-Seq data was verified by qRT-PCR using 10 randomly selected DEGs. The transcript profiles of these selected genes in the qRT-PCR analysis showed a similar pattern as being identified by the FPKM from RNA-seq under corresponding treatments (**Supplementary Figure 2**). These results confirm the reliability of RNA-Seq data.

DISCUSSION

Light is one of the most important environmental cues in the regulation of plant growth, development, and stress responses. A better understanding of the interaction between light and stress will provide useful information for helping both greenhouse and vertical farming production, with increasing crop production and concomitantly improving resource use efficiency. The present

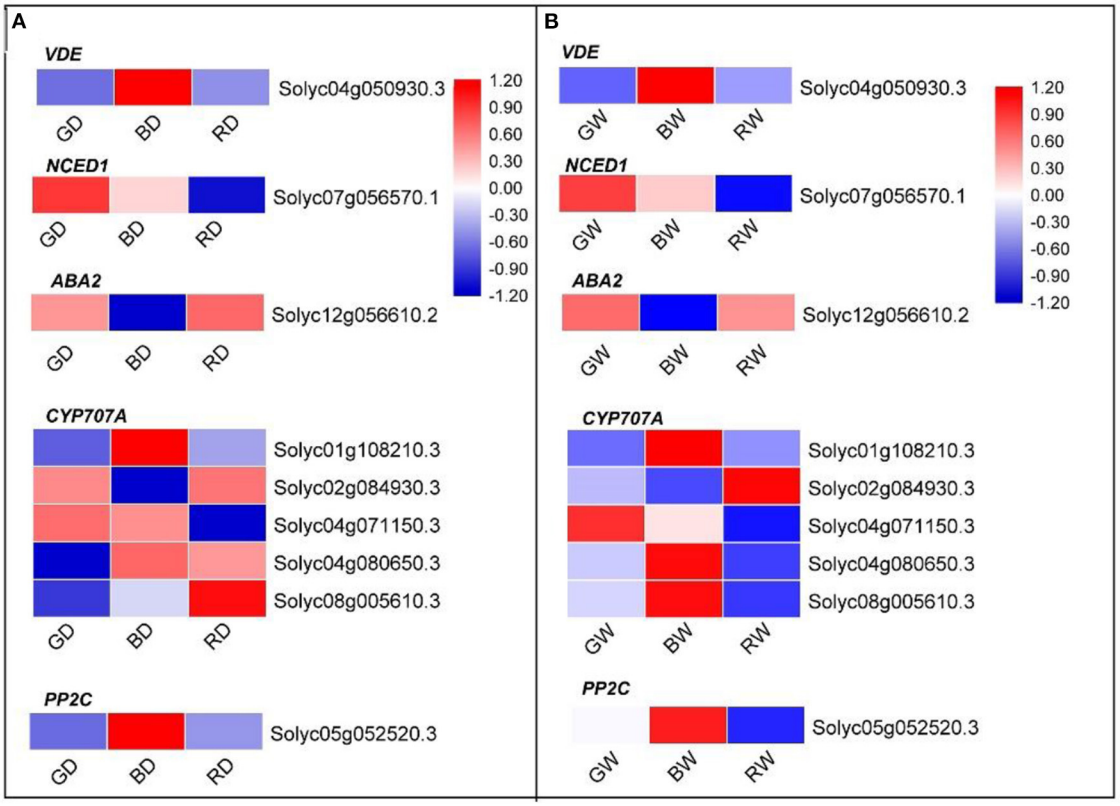

FIGURE 8 | The heatmap diagram of relative expression profiles of DEGs involved in ABA synthesis and ABA signaling transduction in response to red, blue, and green light under drought conditions **(A)** and well-water conditions **(B).** Gene expression is shown in a heatmap with color scale representing $\log_2$ (FPKM) (blue: low expression level; red: high expression level). A scale indicating the color assigned to $\log_2$ (FPKM) is shown to the right of the heatmap.

study aimed to explore the mechanism of green light on drought tolerance of tomato plants from a physiological and molecular perspective. For this purpose, this study investigated the effects of monochrome red, blue, and green light on photosynthetic performance, stomatal response, and endogenous ABA synthesis, and further characterize the differences in the transcriptome under drought stress.

In the present study, we found that compared with well-watered plants, the photosynthesis of red and blue light-treated plants was significantly decreased, while the photosynthetic capacity under green light showed a slight decline during 9 days of drought treatments (**Figure 1**). Together with comparable biomass of plants exposed to different light spectra under drought stress (**Table 1**) and the low electrolyte leakage under green light (**Figure 3A**), these results confirm the positive function of green light on alleviating drought stress-induced decreases in plant growth. This is consistent with our previous studies that green light showed positive effects on maintaining photosynthetic capacity and enhancing the stress tolerance of plants under continuous light and drought conditions (Bian et al., 2018, 2019).

Stomata are the gateway for CO_2 uptake and water loss from plant leaves by transpiration (Osakabe et al., 2014). Apart from being regulated by internal cues (e.g., phytohormones and Ca_2^+ signal), the stomatal aperture is controlled by external light spectra. In the present study, the g_s, Tr, and stomatal aperture of well-watered plants were lower under green light than those under red and blue light (**Figure 2**). These findings may lie in the fact that red and blue light facility stomata opening, while green light less efficient in promoting stomatal opening and strong green light suppressed the blue-light dependent stomatal opening (Frechilla et al., 2000; Shimazaki et al., 2007). However, the effect of light spectra on g_s was not in line with the changes of Tr and stomatal aperture under drought stress (**Figure 2**). In plants, transpiration is not only regulated by light-regulated stomatal aperture but also affected by other environmental factors, including soil and atmospheric moisture stresses (Durand et al., 2019). Furthermore, the g_s depends on the aperture, size, and density of stomata in plants (Monda et al., 2016). Thus, g_s of plants is not always correlated with Tr and stomatal aperture, especially under different abiotic stress conditions (Durand et al., 2019; Zhang et al., 2020).

Compared with RD and BD, the relatively higher instantaneous WUE and RWE and concomitantly lower electrolyte leakage and stomatal aperture under GD were further demonstrated our previous report that green light positively enhanced tomato plant drought stress tolerance via stomatal

regulation (Bian et al., 2019). As an important phytohormone, ABA plays a vital role in plant growth, development, and stress tolerance, such as stomatal regulation, cold, and drought tolerance (Chen et al., 2020). In this study, the relatively high ABA content in green light treated plants (**Figure 2E**) suggests that ABA may be involved in the green light-induced regulation of stomata and drought stress response. To reveal the underlying mechanism of green light in the regulation of drought tolerance, RNA-Seq analysis was employed to uncover the effects of light spectra on the global expression profiling of plants under drought stress. According to the basis of KEGG enrichment analysis, it was confirmed that "light transduction" and "plant hormone signal transduction" were involved in spectral regulation under drought stress (**Figure 6**). The related genes encoded the key enzymes of ABA synthesis, metabolism, and signaling were successfully filtered from the DEGs (**Figure 8**). Thompson et al. (2007) reported that overexpression of *LeNCED1* greatly reduced stomatal aperture through enhancing ABA synthesis in plant leaves. Furthermore, the ABA content can be mirrored by the expression of *ABA2*, another important gene in the ABA synthesis pathway (Tripathi et al., 2016). Therefore, regardless of water condition, the high ABA content and low stomatal aperture in green light-treated plants in the present study might be attributed to the up-regulated *NCED1* (*Solyc07g056570.1*) and *ABA2* (*Solyc12g056610.2*) compared with that under red and blue light, respectively (**Figure 8**).

The ABA content in plants depends on the balance between its biosynthesis and catabolism. Up-regulated *VDE* gene expression decreases ABA synthesis (Pastori et al., 2003). A cytochrome P450 monooxygenase (P450) encoded by *CYP707As* is a key enzyme in ABA catabolism (Kushiro et al., 2004). Our present study showed that *VDE* and most *CYP707As* identified from DEGs were up-regulated under blue, while most *CYP707As* under green light were down-regulated when compared with transcription levels under red and blue light under drought conditions (**Figure 8**). These results indicate that the relatively high ABA content under green light was attributed to green light-induced ABA synthesis and concomitantly a decrease of ABA catabolism.

ABA signal transduction plays a core role in ABA-dependent responses to abiotic stress. The signal transduction module of ABA is made up of three protein classes: Pyracbactin Resistance/Pyracbactin resistance-like/Regulatory Component of ABA Receptor (PYR/PYL/RCARs), Protein Phosphatase 2Cs (PP2Cs), and SNF1-related protein kinase 2s (SnRKs) (Danquah et al., 2014). PYR/PYL/RCARs are proved to be the ABA receptors, while PP2Cs and SnRKs act as the negative and positive regulators in ABA signaling, respectively (Park et al., 2009; Umezawa et al., 2010). The PP2C activity is inhibited by the PYR/PYL/RCAR-PP2C complex formation (Park et al., 2009; Santiago et al., 2009). The inhibition of PP2Cs activity allows SnRKs to actively target membrane proteins, ion channels, and transcription factors, and facilitate transcription of ABA-responsive genes, thereby regulating plant growth, development, and stress responses (Umezawa et al., 2010; Soon et al., 2012). Previous studies demonstrate that SnRK2.6 (open stomata, OST1) regulates fast ABA responses resulting in stomatal closure, which is inhibited by PP2Cs via dephosphorylation

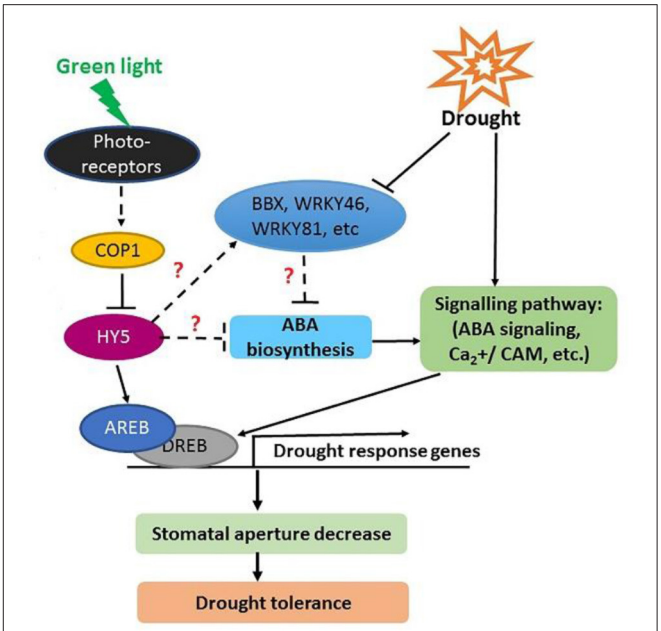

FIGURE 9 | A proposed model of green light enhances tomato drought tolerance.

of serine 175 (Umezawa et al., 2009; Vlad et al., 2009). In our present study, the significantly different transcription levels of one PP2C related gene (*Solyc05g052520.3*) under different light spectra suggest light spectra play important roles in ABA signal transduction. Together with the lower stomatal aperture (**Figure 2D**) and drought-induced damage under green light (**Figure 3**), the green-light induced drought tolerance in this present study may partly attribute to ABA signal transduction-induced the fast stomatal closure (**Figure 9**).

Transcription factors play pivotal roles in plant tolerance to various stresses through triggering or retarding downstream gene expression. Several stress-related transcription factors of bZIP, MYB/MYB-related, and WRKY were involved in the light spectral regulation under drought (**Supplementary Table 3**). According to the PPI network analysis, a bZIP family transcription factor, HY5, was identified as the hub gene in the regulation of light spectral on plant drought stress responses (**Figure 7**). In plants, HY5 integrates light signal and endogenous ABA to regulate plant development and stress tolerance (Xu et al., 2014). In addition, HY5 acts downstream of COP1 to suppresses ABA-regulated inhibition of seedling development (Yadukrishnan et al., 2020). Compared to blue light, green light led to down-regulation of HY5 related gene (**Supplementary Table 3**) but promoted ABA synthesis and signal transduction related gene expression (**Figure 8**), indicating that HY5 might act as a negative regulator in the green light-induced drought responses via modulating ABA synthesis and related signal transduction. To reveal this hypothesis, more detailed ongoing studies are still needed. Furthermore, WRKYs is another important transcription factor family and plays a

significant role in protecting plants against drought stress. Activated expression of *AtWRKY57* improves drought tolerance by elevation of ABA levels in *Arabidopsis* (Jiang et al., 2012). Jaffar et al. (2016) showed that overexpression of *CmWRKY10* in transgenic chrysanthemum plants improved tolerance to drought stress via up-regulating NCED related gene expression. Although no PPI network was constructed in the comparison of GD vs. RD because of few DEGs identified in this comparison, two important WRKY transcription factors, WRKY46 and WRKY81, were filtered and their related gene expressions were down-regulated by green light under drought conditions (**Supplementary Table 3**). Previous studies demonstrated that WRKY46 and WRKY81 were negative regulators for plant drought tolerance (Chen et al., 2017; Ahammed et al., 2020b), and their inhibition of drought tolerance is involved in the ABA-mediated pathway and the light-dependent stomatal opening in guard cells (Ding et al., 2014; Ahammed et al., 2020a). Compared with red light-treated plants, the down-regulated *WRKY46,* and *WRKY81* and relatively high ABA content with the up-regulated NCED related gene under green light suggest that *WRKY46* and *WRKY81* might indirectly be involved in the green light-induced drought tolerance via ABA-dependent pathway.

To date, the green light receptors have not been confirmed, but some studies indicate that green light might be involved in the regulation of plant growth and morphogenesis through the mediation of blue light receptors such as phototropin and cryptochrome (Bouly et al., 2007; Matthews et al., 2020). Based on the results of the present transcriptomic analysis and previous studies, a putative regulatory network of green-induced drought tolerance of tomato seedlings was proposed (**Figure 9**). Under green light radiation, the green light receptor perceives light signals and interacts with COP1, which directly regulates HY5. HY5 could interact with other transcription factors, like AREBs, DREBs, or WRKYs, to regulate the transcription of downstream genes involved in drought stress tolerance (He et al., 2018). Furthermore, green light promotes ABA accumulation via triggering the expression of ABA biosynthesis-related genes, such as *NCED*1 and *ABA2*, and meanwhile down-regulating the expression of ABA degradation-related gene-*CYP707A*. The resulting accumulated ABA induces signaling pathways, such as ABA signaling and Ca^{2+}/CaM, to enhance drought tolerance. Further studies at physiological and molecular levels should be conducted to provide more precise insight into the mechanisms of green light-induced drought tolerance. Successful identification of these key genes would give a great opportunity for breeding new varieties with high resources use efficiency or/and stress tolerance that are suitable to vertical farming.

CONCLUSION

The present study confirmed that green light has a positive function in alleviating the detrimental effects of drought stress on plant growth and photosynthetic capacity via stomatal aperture regulation. According to the analysis of the transcriptomic dataset, the identified those key genes encoding ABA synthesis and signaling revealed the involvement of the ABA-dependent pathway in green light-induced drought tolerance via stomatal regulation. The responses of transcription factors, including HY5, WRKY46, and WRKY81, to green light-induced drought responses, were also identified. The transcription data lay the groundwork for further revealing the mechanism of green light-induced stomatal movement and stress tolerance under drought conditions. However, further studies are needed to decipher the regulatory mechanisms of HY5, WRKY46, and WRKY81 in green light-induced drought tolerance. Furthermore, it is important to explore how genetic variation and phenotypic plasticity respond to abiotic stresses with allowing specific traits to be presented. We expect to be able to create an LED lighting system that can be programmed to generate an optimized wavelength recipe unique for each plant species.

DATA AVAILABILITY STATEMENT

The original contributions presented in the study are publicly available. This data can be found here: NCBI SRA database BioProject accession number PRJNA691997 (https://www.ncbi.nlm.nih.gov/bioproject/PRJNA691997).

AUTHOR CONTRIBUTIONS

ZB, CL, and QY conceived the original research plan and designed the experiment. ZB, YW, XZ, SG, and KH performed the experiments and analyzed the data. ZB and YW wrote the manuscript, while ZB and CL reviewed and edited the manuscript.

FUNDING

This research was financially funded by Institute of Urban Agriculture Internal Funding (S2021001), the Technology Innovation Program of the Chinese Academy of Agricultural Sciences (34-IUA-03), Nottingham Trent University Q&R Funding (01 ARE RA926), Science and the National Natural Science Foundation of China (No. 51708283), and the Natural Science Foundation of Jiangsu Province (No. BK20171011).

ACKNOWLEDGMENTS

We thank Beijing Biomics Biotech Co. Ltd. for the excellent technical help in bioinformatics analysis.

SUPPLEMENTARY MATERIAL

The Supplementary Material for this article can be found online at: https://www.frontiersin.org/articles/10.3389/fpls.2021.649283/full#supplementary-material

Supplementary Figure 1 | The Hierarchical clustering of plant hormone related DEGs of tomato treated with different light spectra and water conditions. Fragments per kilobase of transcript per million fragments mapped (FPKM), and relative expression of DEGs between different light and water treatments were calculated as log2 (FPKM) of differentially expressed genes, $\log_2$ (FPKM) of differentially expressed genes were calculated. A scale indicating the color assigned to $\log_2$ (FPKM) is shown to the right of the cluster.

Supplementary Figure 2 | The expression patterns of 10 randomly selected DEGs by RNA-Seq and qPCR. Gene expression is shown in a heatmap with color scale representing $\log_2$ (fold change) (blue: low expression level; red: high expression level). A scale indicating the color assigned to $\log_2$ (fold change) is shown to the right of the heatmaps.

Supplementary Table 1 | The details of the primers used for RNA-Seq data validation by qPCR.

Supplementary Table 2 | GO enrichment analysis.

Supplementary Table 3 | The transcription factor analysis of plants under drought stress by DEGs.

Supplementary Table 4 | Protein-protein interaction (PPI) network analysis based on the DEDs of the comparsion GD and BD.

Supplementary Table 5 | Protein-protein interaction (PPI) network analysis based on the DEDs of the comparsion RD and BD.

REFERENCES

Ahammed, G. J., Li, X., Mao, Q., Wan, H., Zhou, G., and Cheng, Y. (2020a). The SlWRKY81 transcription factor inhibits stomatal closure by attenuating nitric oxide accumulation in the guard cells of tomato under drought. *Physiol. Plant.* 172, 885–895. doi: 10.1111/ppl.13243

Ahammed, G. J., Li, X., Yang, Y., Liu, C., Zhou, G., Wan, H., et al. (2020b). Tomato WRKY81 acts as a negative regulator for drought tolerance by modulating guard cell H_2O_2-mediated stomatal closure. *Environ. Exp. Bot.* 171:103960. doi: 10.1016/j.envexpbot.2019.103960

Baker, N. R. (2008). Chlorophyll fluorescence: a probe of photosynthesis *in vivo*. *Annu. Rev. Plant Biol.* 59, 89–113. doi: 10.1146/annurev.arplant.59.032607.092759

Balcke, G. U., Handrick, V., Bergau, N., Fichtner, M., Henning, A., Stellmach, H., et al. (2012). An UPLC-MS/MS method for highly sensitive high-throughput analysis of phytohormones in plant tissues. *Plant Methods* 8:47. doi: 10.1186/1746-4811-8-47

Bian, Z. H., Yang, Q. C., Li, T., Cheng, R. F., Barnett, Y., and Lu, C. G. (2018). Study of the beneficial effects of green light on lettuce grown under short-term continuous red and blue light-emitting diodes. *Physiol. Plant.* 164, 226–240. doi: 10.1111/ppl.12713

Bian, Z. H., Zhang, X. Y., Wang, Y., and Lu, C. G. (2019). Improving drought tolerance by altering the photosynthetic rate and stomatal aperture via green light in tomato (*Solanum lycopersicum* L.) seedlings under drought conditions. *Environ. Exp. Bot.* 167:103844. doi: 10.1016/j.envexpbot.2019.103844

Bouly, J. P., Schleicher, E., Dionisio-Sese, M., Vandenbussche, F., Van Der Straeten, D., Bakrim, N., et al. (2007). Cryptochrome blue light photoreceptors are activated through interconversion of flavin redox states. *J. Biol. Chem.* 282, 9383–9391. doi: 10.1074/jbc.M609842200

Cao, X. N., Ma, F., Xu, T. T., Wang, J. J., Liu, S. C., Li, G. H., et al. (2016). Transcriptomic analysis reveals key early events of narciclasine signaling in Arabidopsis root apex. *Plant Cell Rep.* 35:2381–2401. doi: 10.1007/s00299-016-2042-7

Chaudhary, R., Balhara, M., Jangir, D. K., Dangi, M., Dangi, M., and Chhillar, A. K. (2019). In silico protein interaction network analysis of viru lence proteins associated with invasive aspergillosis for drug discovery. *Curr. Top Med. Chem.* 19, 146–155. doi: 10.2174/1568026619666181120150633

Chen, H., Zhang, J., Neff, M. M., Hong, S. W., Zhang, H., Deng, X. W., et al. (2008). Integration of light and abscisic acid signaling during seed germination and early seedling development. *PANS* 105, 4495–4500. doi: 10.1073/pnas.0710778105

Chen, J. N., Nolan, T. M., Ye, H. X., Zhang, M. C., Tong, H. N., Xin, P. Y., et al. (2017). Arabidopsis WRKY46, WRKY54, and WRKY70 transcription factors are involved in brassinosteroid-regulated plant growth and drought responses. *Plant Cell* 29, 1425–1439. doi: 10.1105/tpc.17.00364

Chen, K., Li, G. J., Bressan, R. A., Song, C. P., Zhu, J. K., and Zhao, Y. (2020). Abscisic acid dynamics, signaling, and functions in plants. *J. Integr. Plant Biol.* 62, 25–54. doi: 10.1111/jipb.12899

Damian, S., Morris, J. H., Helen, C., Michael, K., Stefan, W., Milan, S., et al. (2017). The STRING database in 2017: quality-controlled protein–protein association networks, made broadly accessible. *Nucleic Acids Res.* 45, 362–368. doi: 10.1093/nar/gkw937

Danquah, A., de Zelicourt, A., Colcombet, J., and Hirt, H. (2014). The role of ABA and MAPK signaling pathways in plant abiotic stress responses. *Biotechnol. Adv.* 32, 40–52. doi: 10.1016/j.biotechadv.2013.09.006

Ding, Z. J., Yan, J. Y., Xu, X. Y., Yu, D. Q., Li, G. X., Zhang, S. Q., et al. (2014). Transcription factor WRKY 46 regulates osmotic stress responses and stomatal movement independently in Arabidopsis. *Plant J.* 79, 13–27. doi: 10.1111/tpj.12538

Döll, P. (2009). Vulnerability to the impact of climate change on renewable groundwater resources: a global-scale assessment. *Environ. Res. Lett.* 4:035006. doi: 10.1088/1748-9326/4/3/035006

Durand, M., Brendel, O., Buré, C., and Le, T. D. (2019). Altered stomatal dynamics induced by changes in irradiance and vapour-pressure deficit under drought: impacts on the whole-plant transpiration efficiency of poplar genotypes. *New Phytol.* 222, 1789–1802. doi: 10.1111/nph.15710

FAO (2012). *Coping with Water Scarcity: An Action Framework for Agriculture and Food Security*. Rome: Food and Agriculture Organization of United States (FAO).

Frechilla, S., Talbott, L. D., Bogomolni, R. A., and Zeiger, E. (2000). Reversal of blue light-stimulated stomatal opening by green light. *Plant Cell Physiol.* 41, 171–176. doi: 10.1093/pcp/41.2.171

He, M., He, C. Q., and Ding, N. Z. (2018). Abiotic stresses: general defenses of land plants and chances for engineering multistress tolerance. *Front. Plant Sci.* 9:1771. doi: 10.3389/fpls.2018.01771

Jaffar, M. A., Song, A., Faheem, M., Chen, S., Jiang, J., Liu, C., et al. (2016). Involvement of CmWRKY10 in drought tolerance of chrysanthemum through the ABA-signaling pathway. *Int. J. Mol. Sci.* 17, 693. doi: 10.3390/ijms17050693

Jiang, Y., Liang, G., and Yu, D. (2012). Activated expression of WRKY57 confers drought tolerance in Arabidopsis. *Mol. Plant* 5, 1375–1388. doi: 10.1093/mp/sss080

Jungklang, J., Saengnil, K., and Uthaibutra, J. (2017). Effects of water-deficit stress and paclobutrazol on growth, relative water content, electrolyte leakage, proline content and some antioxidant changes in Curcuma alismatifolia Gagnep. cv. Chiang Mai Pink. *Saudi J. Biol. Sci.* 24, 1505–1512. doi: 10.1016/j.sjbs.2015.09.017

Kalantari, F., Nochiana, A., Darkhania, F., and Asif, N. (2020). The significance of vertical farming concept in ensuring food security for high-density urban areas. *J. Kejuruteraan* 32, 105–111. doi: 10.17576/jkukm-2020-32(1)-13

Kim, D., Langmead, B., and Salzberg, S. L. (2015). HISAT: a fast spliced aligner with low memory requirements. *Nat. Methods* 12, 357–360. doi: 10.1038/nmeth.3317

Kozai, M. T. T., and Niu, G. (2015). *Plant Factory: An Indoor Vertical Farming System for Efficient Quality Food Production*. Cambridge, MA: Academic Press.

Kushiro, T., Okamoto, M., Nakabayashi, K., Yamagishi, K., Kitamura, S., Asami, T., et al. (2004). The Arabidopsis cytochrome P450 CYP707A encodes ABA 8′-hydroxylases: key enzymes in ABA catabolism. *EMBO J.* 23, 1647–1656. doi: 10.1038/sj.emboj.7600121

Lee, S. C., and Luan, S. (2012). ABA signal transduction at the crossroad of biotic and abiotic stress responses. *Plant Cell Env.* 35, 53–60. doi: 10.1111/j.1365-3040.2011.02426.x

Lesk, C., Rowhani, P., and Ramankutty, N. (2016). Influence of extreme weather disasters on global crop production. *Nature* 529:84. doi: 10.1038/nature16467

Li, M. Q., Hasan, M. K., Li, C. X., Ahammed, G. J., Xia, X. J., Shi, K., et al. (2016). Melatonin mediates selenium-induced tolerance to cadmium stress in tomato plants. *J. Pineal Res.* 61, 291–302. doi: 10.1111/jpi.12346

Mafakheri, A., Siosemardeh, A., Bahramnejad, B., Struik, P., and Sohrabi, Y. (2010). Effect of drought stress on yield, proline and chlorophyll contents in three chickpea cultivars. *Aust. J. Crop Sci.* 4, 580. doi: 10.3316/informit.857341254680658

Matthews, J. S. A., Vialet-Chabrand, S., and Lawson, T. (2020). Role of blue and red light in stomatal dynamic behaviour. *J. Exp. Bot.* 71, 2253–2269. doi: 10.1093/jxb/erz563

Monda, K., Araki, H., Kuhara, S., Ishigaki, G., Akashi, R., Negi, J., et al. (2016). Enhanced stomatal conductance by a spontaneous Arabidopsis tetraploid, Me-0, results from increased stomatal size and greater stomatal aperture. *c*170 1435–1444. doi: 10.1104/pp.15.01450

Nakashima, K., and Yamaguchi-Shinozaki, K. (2013). ABA signaling in stress-response and seed development. *Plant Cell Rep.* 32,959–970. doi: 10.1007/s00299-013-1418-1

Osakabe, Y., Yamaguchi-Shinozaki, K., Shinozaki, K., and Tran, L. S. P. (2014). ABA control of plant macroelement membrane transport systems in response to water deficit and high salinity. *New Phytol.* 202, 35–44. doi: 10.1111/nph.12613

Pan, Y., Seymour, G. B., Lu, C., Hu, Z., Chen, X., and Chen, G. (2012). An ethylene response factor (ERF5) promoting adaptation to drought and salt tolerance in tomato. *Plant Cell Rep.* 31, 349–360. doi: 10.1007/s00299-011-1170-3

Park, S. Y., Fung, P., Nishimura, N., Jensen, D. R., Fujii, H., Zhao, Y., et al. (2009). Abscisic acid inhibits type 2C protein phosphatases via the PYR/PYL family of START proteins. *Science* 324,1068–1071. doi: 10.1126/science.1173041

Pastori, G. M., Kiddle, G., Antoniw, J., Bernard, S., Veljovic-Jovanovic, S., Verrier, P. J., et al. (2003). Leaf vitamin C contents modulate plant defense transcripts and regulate genes that control development through hormone signaling. *Plant Cell.* 15, 939–951. doi: 10.1105/tpc.010538

Reddy, A. R., Chaitanya, K. V., and Vivekanandan, M. (2004). Drought-induced responses of photosynthesis and antioxidant metabolism in higher plants. *J. Plant Physiol.* 161, 1189–1202. doi: 10.1016/j.jplph.2004.01.013

Santiago, J., Rodrigues, A., Saez, A., Rubio, S., Antoni, R., Dupeux, F., et al. (2009). Modulation of drought resistance by the abscisic acid receptor PYL5 through inhibition of clade A PP2Cs. *Plant J.* 60, 575–588. doi: 10.1111/j.1365-313X.2009.03981.x

Schwartz, S. H., and Zeevaart, J. A. (2010). "Abscisic acid biosynthesis and metabolism," in *Plant Hormones,* eds P. J. Davies (Dordrecht: Springer), 137–155. doi: 10.1007/978-1-4020-2686-7_7

Shannon, P., Markiel, A., Ozier, O., Baliga, N. S., Wang, J. T., Ramage, D., et al. (2003). Cytoscape: A Software Environment for Integrated Models of Biomolecular Interaction Networks. *London: Routledge*. doi: 10.1101/gr.1239303

Shimazaki, K. I., Doi, M., Assmann, S. M., and Kinoshita, T. (2007). Light regulation of stomatal movement. *Ann. Rev. Plant Biol.* 58, 219–247. doi: 10.1146/annurev.arplant.57.032905.105434

Somerville, C. (2001). Genetic engineering and water. *Science* 292:2217. doi: 10.1126/science.292.5525.2217

Soon, F. F., Ng, L. M., Zhou, X. E., West, G. M., Kovach, A., Tan, M. E., et al. (2012). Molecular mimicry regulates ABA signaling by SnRK2 kinases and PP2C phosphatases. *Science* 335, 85–88. doi: 10.1126/science.1215106

Stawska, M., and Oracz, K. (2019). phyB and HY5 are involved in the blue light-mediated alleviation of dormancy of arabidopsis seeds possibly via the modulation of expression of genes related to light, GA, and ABA. *Int. J. Mol. Sci.* 20:5882. doi: 10.3390/ijms20235882

Tarazona, S., García-Alcalde, F., Dopazo, J., Ferrer, A., and Conesa, A. (2011). Differential expression in RNA-seq: a matter of depth. *Genome Res.* 21, 2213–2223. doi: 10.1101/gr.124321.111

Thompson, A. J.,., Mulholland, B. J., Jackson, A. C., McKee, J. M., Hilton, H. W., et al. (2007). Regulation and manipulation of ABA biosynthesis in roots. *Plant Cell Environ.* 30, 67–78. doi: 10.1111/j.1365-3040.2006.01606.x

Thornley, J. H. (1976). *Mathematical Models in Plant Physiology*. London: Academic Press (Inc.) London, Ltd.

Trapnell, C., Pachter, L., and Salzberg, S. L. (2009). TopHat: discovering splice junctions with RNA-Seq. *Bioinformatics* 25, 1105–1111. doi: 10.1093/bioinformatics/btp120

Tripathi, P., Rabara, R. C., Reese, R. N., Miller, M. A., Rohila, J. S., Subramanian, S., et al. (2016). A toolbox of genes, proteins, metabolites and promoters for improving drought tolerance in soybean includes the metabolite coumestrol and stomatal development genes. *BMC Genomics* 17:102. doi: 10.1186/s12864-016-2420-0

Umezawa, T., Nakashima, K., Miyakawa, T., Kuromori, T., Tanokura, M., Shinozaki, K., et al. (2010). Molecular basis of the core regulatory network in ABA responses: sensing, signaling and transport. *Plant Cell Physiol.* 51, 1821–1839. doi: 10.1093/pcp/pcq156

Umezawa, T., Sugiyama, N., Mizoguchi, M., Hayashi, S., Myouga, F., Yamaguchi-Shinozaki, K., et al. (2009). Type 2C protein phosphatases directly regulate abscisic acid-activated protein kinases in Arabidopsis. *PNAS* 106, 17588–17593. doi: 10.1073/pnas.0907095106

Vlad, F., Rubio, S., Rodrigues, A., Sirichandra, C., Belin, C., Robert, N., et al. (2009). Protein phosphatases 2C regulate the activation of the Snf1-related kinase OST1 by abscisic acid in Arabidopsis. *Plant Cell* 21, 3170–3184. doi: 10.1105/tpc.109.069179

Wan, J., Griffiths, R., Ying, J., McCourt, P., and Huang, Y. (2009). Development of drought-tolerant canola (*Brassica napus* L.) through genetic modulation of ABA-mediated stomatal responses. *Crop Sci.* 49: 1539–1554. doi: 10.2135/cropsci2008.09.0568

Wang, F., Zhang, L., Chen, X., Wu, X., Xiang, X., Zhou, J., et al. (2018). SlHY5 integrates temperature, light and hormone signaling to balance plant growth and cold tolerance. *Plant Physiol.* 179, 749–760. doi: 10.1104/pp.18.01140

Wang, P., Sun, X., Li, C., Wei, Z., Liang, D., and Ma, F. W. (2013). Long-term exogenous application of melatonin delays drought-induced leaf senescence in apple. *J. Pineal Res.* 54, 292–302. doi: 10.1111/jpi.12017

Xu, D., Li, J., Gangappa, S. N., Hettiarachchi, C., Lin, F., Andersson, M. X., et al. (2014). Convergence of light and ABA signaling on the ABI5 promoter. *PLoS Genet.* 10:e1004197doi: 10.1371/journal.pgen.1004197

Yadukrishnan, P., Rahul, P. V., and Datta, S. (2020). HY5 suppresses, rather than promotes, abscisic acid-mediated inhibition of postgermination seedling development. *Plant Physiol.* 184:574. doi: 10.1104/pp.20.00783

Zeng, B., Wang, Q., and Tang, C. (2008). Anatomic analysis on heterosis in three transgenic bt pest-resistant hybrid cotton (*G. hirsutum* L.). *Acta Agronomica Sinica* 34, 496–505. doi: 10.3724/SP.J.1006.2008.00496

Zhang, X., Mei, X., Wang, Y., Huang, G., Feng, F., Liu, X., et al. (2020). Stomatal conductance bears no correlation with transpiration rate in wheat during their diurnal variation under high air humidity. *PeerJ* 8:e8927. doi: 10.7717/peerj.8927

Conflict of Interest: The authors declare that the research was conducted in the absence of any commercial or financial relationships that could be construed as a potential conflict of interest.

Publisher's Note: All claims expressed in this article are solely those of the authors and do not necessarily represent those of their affiliated organizations, or those of the publisher, the editors and the reviewers. Any product that may be evaluated in this article, or claim that may be made by its manufacturer, is not guaranteed or endorsed by the publisher.

frontiers in Plant Science

ORIGINAL RESEARCH
published: 11 November 2021
doi: 10.3389/fpls.2021.721512

Time-Series Growth Prediction Model Based on U-Net and Machine Learning in *Arabidopsis*

*Sungyul Chang[1], Unseok Lee[2], Min Jeong Hong[1], Yeong Deuk Jo[1] and Jin-Baek Kim[1]**

[1] Radiation Breeding Research Team, Advanced Radiation Technology Institute (ARTI), Korea Atomic Energy Research Institute (KAERI), Jeongeup-si, South Korea, [2] Smart Farm Research Center, Korea Institute of Science and Technology (KIST), Gangneung-si, South Korea

Yield prediction for crops is essential information for food security. A high-throughput phenotyping platform (HTPP) generates the data of the complete life cycle of a plant. However, the data are rarely used for yield prediction because of the lack of quality image analysis methods, yield data associated with HTPP, and the time-series analysis method for yield prediction. To overcome limitations, this study employed multiple deep learning (DL) networks to extract high-quality HTTP data, establish an association between HTTP data and the yield performance of crops, and select essential time intervals using machine learning (ML). The images of *Arabidopsis* were taken 12 times under environmentally controlled HTPP over 23 days after sowing (DAS). First, the features from images were extracted using DL network U-Net with SE-ResXt101 encoder and divided into early (15–21 DAS) and late (∼21–23 DAS) pre-flowering developmental stages using the physiological characteristics of the *Arabidopsis* plant. Second, the late pre-flowering stage at 23 DAS can be predicted using the ML algorithm XGBoost, based only on a portion of the early pre-flowering stage (17–21 DAS). This was confirmed using an additional biological experiment ($P < 0.01$). Finally, the projected area (PA) was estimated into fresh weight (FW), and the correlation coefficient between FW and predicted FW was calculated as 0.85. This was the first study that analyzed time-series data to predict the FW of related but different developmental stages and predict the PA. The results of this study were informative and enabled the understanding of the FW of *Arabidopsis* or yield of leafy plants and total biomass consumed in vertical farming. Moreover, this study highlighted the reduction of time-series data for examining interesting traits and future application of time-series analysis in various HTPPs.

Keywords: time series analysis, phenomics, high-throughput phenotyping (HTP), deep learning (DL), growth modeling, plant biomass, *Arabidopsis thaliana*

OPEN ACCESS

Edited by:
Francesco Orsini,
University of Bologna, Italy

Reviewed by:
Francesca Del Bonifro,
University of Bologna, Italy
Albino Maggio,
University of Naples Federico II, Italy

***Correspondence:**
Jin-Baek Kim
jbkim74@kaeri.re.kr

Specialty section:
This article was submitted to Technical Advances in Plant Science, a section of the journal Frontiers in Plant Science

Received: *07 June 2021*
Accepted: *08 October 2021*
Published: *11 November 2021*

Citation:
Chang S, Lee U, Hong MJ, Jo YD and Kim J-B (2021) Time-Series Growth Prediction Model Based on U-Net and Machine Learning in Arabidopsis. Front. Plant Sci. 12:721512. doi: 10.3389/fpls.2021.721512

INTRODUCTION

Food insecurity has threatened the survival of many people because of the desertification of arable land, global climate changes, population increase (Godfray et al., 2010), and spread of infectious disease worldwide (Laborde et al., 2020). To combat food insecurity, agricultural production approaches have not been revamped, wherein "digital agriculture" was proposed to overcome these challenges (Redmond Ramin et al., 2018b). Multiple studies examined this concept about agricultural production (Waltz, 2017). Regardless of the food production method

for growing field crops in indoor conditions, multiple challenges limit the implementation of this idea for the current agricultural production. The successful transformation requires digital plant phenotyping data and analysis tools (Granier and Vile, 2014). Determining plant performance in various situations requires various quantitative data to compare and make a decision (Großkinsky et al., 2015). Therefore, a description of the performance of a plant at a given time is important for the transformation of digital agriculture (Chawade et al., 2019).

Plant phenotype includes multiple aspects of plant science and its definitions vary in different plant science-related fields (Tardieu et al., 2017). Automated high-throughput phenotyping platform (HTPP) generates high-quality data (Lee et al., 2018) from multiple sensors (Fahlgren et al., 2015) and yields the complete life cycle of a plant (van Es et al., 2019). Moreover, rich phenotype data, based on time series generated from a single plant captured by HTPP, can provide insights into traits of interest. HTPP-generated data are used to investigate the salinity stress response in multiple rice cultivars and these data revealed that candidate genes can be resistant to salt-related stress (Al-Tamimi et al., 2016). However, many studies use only a small fraction of phenotype data for a fixed time point (Al-Tamimi et al., 2016; Chen et al., 2018) to associate phenotype data with interesting traits. This is primarily attributed to multiple plant scientists selecting measurement time that discriminates with notable traits in plant-related populations. Moreover, time-series analysis methods based on statistical models do not provide satisfying results (Boken, 2000). Recently, yield prediction for crop plants using machine learning (ML) algorithms from satellite or drone images provided high accuracies (Khaki et al., 2020). In these studies, the frequency of image acquisition is broad (days) and small changes over narrow (hours) time intervals are difficult to identify. Moreover, for determining phenotype changes over the plant life cycle, the examination of both narrow and broad time intervals is important (Tardieu et al., 2017). Novel time points with ML tools are essential because examining interesting traits from prior knowledge provides limited information on traits. The analysis and prediction of leaf area using time-series data at specific growth stages can establish prediction models for the growth pattern of a plant and essential time points. This study employed extreme gradient boost (XGBoost) for multiple time steps of forecast models. XGBoost, known as multiple additive regression trees, adds multiple decision trees to achieve the best outcome. XGBoost was used to analyze various classification and regression data not provided (Ji et al., 2019). It used multiple steps to make ensemble models for multiple time-step forecasts (Galicia et al., 2019). The additional benefits of using the ensemble models were the robustness and simplicity of modeling while forecasting (Dineva et al., 2020).

Machine learning-based analysis improved the extraction of projected area (PA) related to multiple agronomical traits. Many studies on the growth pattern of a plant are destructive, i.e., they harvest the plant to measure its weight. This method is labor-intensive, producing only a few time point measurements. HTPP gathers images related to plant weight in the PA with a high-frequency rate within a day. Moreover, the PA extracted from HTPP in this study showed a high correlation between images and biomass or photosynthetic capacity (Salas Fernandez et al., 2017). Similarly, multiple agricultural traits are directly or indirectly associated with PA (Yang et al., 2013; Araus and Cairns, 2014). Accurately extracting PA from the image of a plant is difficult because multiple size leaf areas are connected with thin branches in an overlapping manner (Lee et al., 2018). Previously, studies separated the plant area from background images, and the reported evaluation matrix shows that the accuracies of the segmentation of plants heavily depend on a specific dataset (Jiang and Li, 2020). ML algorithms, such as random forest (Lee et al., 2018), increase accuracy over conventional image regency approaches. Deep learning (DL) algorithms, such as U-Net, provide additional enhancement of semantic segmentation for biomedical (Ronneberger et al., 2015) and plant images (Chang et al., 2020). The U-Net architecture is composed of encoder and decoder architecture (**Figure 1E**). The first half of the architecture contained the encoder or backbone and extracts features from an image with multiple levels. The second half of the architecture, the decoder, uses features from the previous step. For separating object and background information, advanced encoders gather additional features from images and achieve higher accuracies (Hoeser and Kuenzer, 2020; Zhang et al., 2020). Hence, for segmenting, there is room for improvement because U-Net performs well in different soil conditions.

In this study, we examined the reduced time intervals for predicting PA and estimate FW at different growth stages. This study follows four steps. First, we applied the combination of DL for plant image semantic segmentation for better PA and features for plant shape. Second, ML-based prediction models used the extracted plant features to predict the PA at the early and late pre-flowering stages with biological replication. Third, we established a relationship between FW using PA in a pre-flowering stage. Finally, we compared the predicted FW with PAs from various training models and harvested FW at 23 days after sowing (DAS).

MATERIALS AND METHODS

Arabidopsis developmental stages were defined as growth stages with early vegetative stage, early pre-flowering, and late pre-flowering stages from the phenological development of a plant (Boyes et al., 2001). The images of plants were acquired at all growth stages. However, the early pre-flowering stage was used for the late pre-flowering stage growth pattern (**Figure 2A**). We repeated experiment II to validate the outcome of experiment I at 23 DAS. We estimated fresh weight (FW) from PA with harvested plants at the early pre-flowering stage and compared the predicted FW with training models and measured FW at 23 DAS.

Plant Materials and High-Throughput Phenotyping Setup

Arabidopsis thaliana was planted in the soil mixture and then moved to the HTPP with environmentally controlled conditions. The platform was programmed to obtain images with a 4K-RGB camera (Logitech, California, United States) every hour between 08:00 am and 7:00 pm during the photoperiod. A motorized

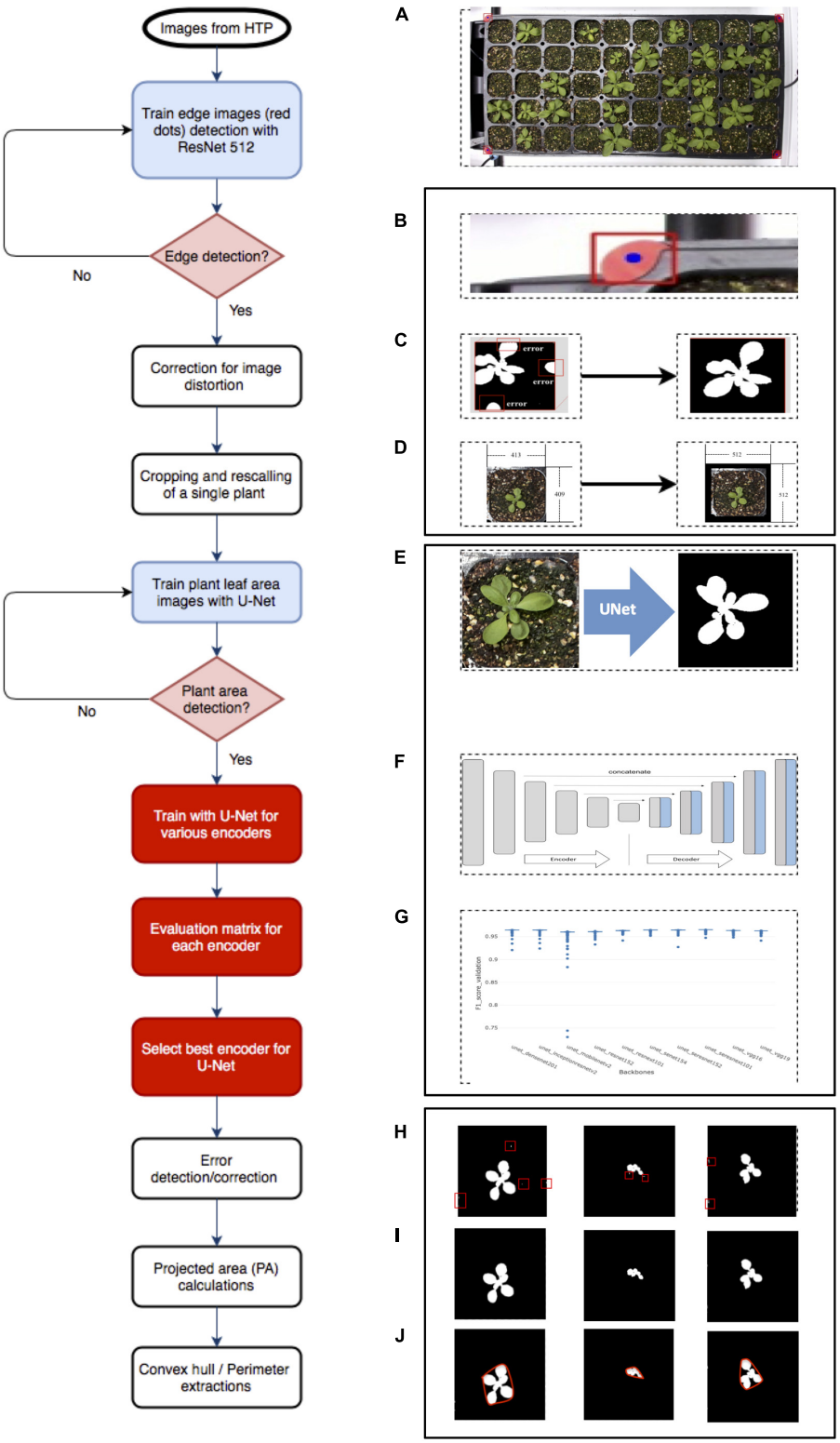

FIGURE 1 | Overview of *Arabidopsis* image analysis pipeline. There are three steps for image analysis. The first step is the preprocessing of raw images by **(A)** the acquisition of the raw image, **(B)** detecting reference point (red dot), **(C)** correcting images with the red dot, **(D)** cropping into single plant images, and rescaling. The second step is to train the **(E)** U-Net with various encoders and selecting encoders for the best result using the U-Net structure, **(F)** including encoder section, training network with various encoders, such as SE-RENext101, **(G)** comparing results from various encoders. The last step is the post-processing of images and exporting data using **(H)** error detection with a conditional random feature, **(I)** extract PA, and convex hull area, **(J)** perimeter.

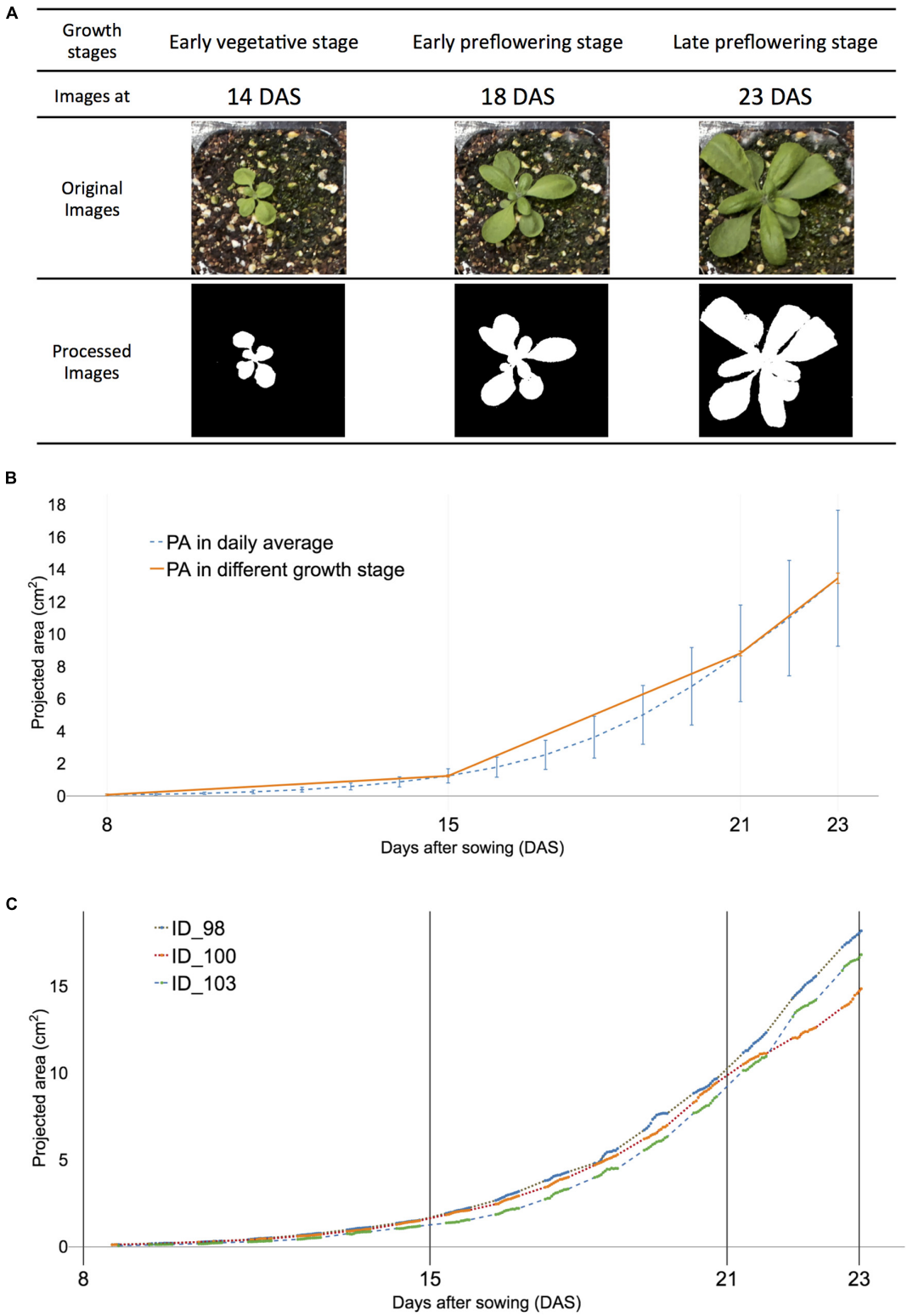

FIGURE 2 | Definition of early vegetative, early, and late pre-flowering stages were used in the study to visualize corresponding projected area (PA) of all and selected samples of *Arabidopsis*. **(A)** Visualized plant images at three growth stages: early vegetative [8–15 days after sowing (DAS)], early pre-flowering stage (15–21 DAS), and late pre-flowering stage (21–23 DAS). **(B)** The visualized growth pattern of all samples. Dashed blue lines indicate the average PA in each DAS. The orange solid line indicates PA at early vegetative, early, and late pre-flowering stages, respectively. **(C)** The visualized growth pattern of selected individual Arabidopsis samples of ID 98 (dot), ID 100 (dash with lines), and ID103 (dash). The actual measurement time point is displayed with solid lines in each sample.

irrigation dipper was connected to each tray and filled with water every 4 days over 4 weeks. Light-emitting diodes provided (Lumens, Seoul, South Korea) 16 h of lighting at 230 μmol/m^2/s. A more detailed description is available in the study by Chang et al. (2020).

Image Analysis Method and Evaluation of Semantic Segmentation

The image analysis pipeline was modified from the work of Chang et al. (2020) and comprised three parts. The first part was the pre-processing image step that detected edges of the tray (**Figure 1B**), corrected errors (**Figure 1C**), cropped, and saved individual plant images (**Figure 1D**). The second part was the segmentation process that tested U-Net (**Figure 1E**) with various encoders (**Figure 1F**) and selected a well-performed encoder (**Figure 1G**). The last part involved post-processing, which removed additional errors (**Figure 1H**) and extracted features from images (**Figures 1I,J**). This study tested multiple encoders using U-Net for more quality data from plant images.

Pre-processing of images was required for U-Net implementation. Firstly, we corrected image distortion of captured raw RGB tray images using four red markers in pre-processing; a tray image included 32- or 50-cell individual plants. Then, the corrected tray image was cropped for separating individual plants using the detected red marker coordinates (Chang et al., 2020 #74). The cropped images were properly scaled and padded for the U-net network size (512 × 512 dimensions). Secondly, the cropped, scaled, and padded RGB color image and mask image pairs were needed to train a semantic segmentation network; the mask image consisted of a black background and a white foreground (i.e., plant region). We selected an encoder such as Densenet, then performed training steps. Lastly, the cropped, scaled, and padded RGB color image inputs to the trained network, then only plant area was separated from backgrounds such as soil as an output (i.e., a mask image). Finally, the fully connected conditional random fields were applied to the segmented results for post-processing.

Cropped images were generated for image analysis, and 446 images were randomly selected to represent data for comparing different backbone approaches and source code available at Github (Yakubovskiy, 2019). Selected backbones are listed in **Supplementary Table 2**. To evaluate each backbone (encoder), data were randomly divided into two: 90 and 10% for training and data validation, respectively. Image augmentation such as flip, padding, blur, and sharpen using Python (Python software foundation, Beaverton, OR, United States) was performed to reinforce smaller training data (Buslaev et al., 2020). For each backbone, a total of 500 epochs of training was performed (Yakubovskiy, 2019). The trained model was evaluated using the validation dataset at the end of each epoch because an epoch has as many steps as training data.

Each model of the backbone was trained using binary dice and focal loss functions (Eqs 5, 7; we used beta value in Eq. 5). The dice and focal loss exhibited good performance for class imbalance problems (Milletari et al., 2016; Lin et al., 2017; Salehi et al., 2017; Zhu et al., 2019) [the class meant the foreground (plant part) and the background]. At the earlier stages of growth, the sizes of the plants were small. Therefore, the foreground class was much smaller, causing a class imbalance problem. To overcome this, we used a combination of loss functions during training.

The evaluation of the semantic segmentation used various methods such as the intersection-over-union (IoU) method (Yu et al., 2018). Eq. 1 shows that the IoU used calculates overlapped PA percentage using the intersection of the PA between the predicted (denoted by A) and ground-truth areas (denoted by B) over union PA between the predicted and ground-truth areas.

$$\text{IoU} = \frac{\text{Area}(A \cap B)}{\text{Area}(A \cup B)} \tag{1}$$

F1-scores were used for evaluating semantic segmentation in agriculture (Bargoti and Underwood, 2017) and can be calculated from Eqs 2–4. From the precision calculation, a true positive (TP) result indicated that the output correctly predicted the pixels in PA, while a false positive (FP) result indicated that the output falsely predicted the pixels in non-PA. A TP and a false negative (FN) result indicated that the output failed to predict pixels in PA. Various backbones with U-Net could correctly determine PA if the IoU score was >0.5. A higher number indicated a more accurate prediction from the model. To compare the results, IoU and F1 scores were measured and calculated average values were used.

$$\text{Precision (P)} = \frac{\text{TP}}{\text{TP} + \text{FP}} \tag{2}$$

$$\text{Recall (R)} = \frac{\text{TP}}{\text{TP} + \text{FN}} \tag{3}$$

$$F_\beta \text{ score} = \left(1 + \beta^2\right) \cdot \frac{\text{P} \cdot \text{R}}{(\beta^2 \cdot \text{P}) + \text{R}}, \beta = 1 \tag{4}$$

$$\text{Dice loss} = 1 - F_\beta \text{ score}, \beta = 1 \tag{5}$$

$$p_t = \begin{cases} p \text{ if } y = 1 \\ 1 - p \text{ otherwise} \end{cases} \tag{6}$$

$$\text{Focal loss}\left(p_t\right) = -\alpha_t \cdot (1-p_t)^\gamma \cdot \log\left(p_t\right), \alpha = 0.25, \gamma = 2 \tag{7}$$

$y \in \{\pm 1\}$ means ground-truth class and $p \in (0,1)$ is the estimated probability of the model for the class with label y = 1.

$$\text{Loss function} = \text{Dice loss} + \text{Focal loss} \tag{8}$$

Time-Series Data Definition and Projected Area Prediction Models Construction

This study measured a PA at the complete growth cycle of 232 plant samples. Experiments I and II measured 122 and 110 samples, respectively. The growth cycle range is 10–23 DAS with 165 time steps that include 12-time steps per day. The time data format was in a sequential order ranging from 1 to 165 because multiple time points were not present with the DAS format.

To express specific time points with DAS, the measured hours divided by 24 h were added after DAS. If images were taken 17 h at 23 DAS, the time point expressed as 23 DAS was (17/24 h). The training set was composed of a convex hull and compactness from extracted individual plant images.

Based on the phenological development of a plant, Boyes et al. (2001) defined *Arabidopsis* growth stages using the early vegetative stage, early and late pre-flowering stages with the Biologische Bundesanstalt, Bundessortenamt und CHemische Industrie (BBCH) scale. The growth stages of the early and late pre-flowering stages corresponded to 1.04 and 1.1 (**Figure 2A**) where the decimal point indicated the number of rosette leaves. The early vegetative stage was before 1.04. In our study, rosette leaves were manually counted for early and late flowering stages. The developmental stages and corresponding lengths of the early and late pre-flowering stages ranged from 15 to 21 and 21 to 24 DASs, respectively, and 60 to 140 and 141 to 165 time steps, respectively (**Table 1**), because inflorescence emerged at late 23 DAS in a partial plant population.

The early pre-flowering stage was then divided into six training data sets, in those with endpoints at 20 and 21 DAS, respectively. The first four training sets were based on the training window: 15, 16, 17, and 18 DAS, with corresponding time lengths of 80, 68, 56, and 44 time steps, respectively (**Table 1**). Each of the training sets contained an ID, date, day, month, and experiment number. **Figure 2C** (orange solid line at ID 100) shows the plot of the measurement of PA of plants in the controlled environment in the daylight period only.

The last two training sets (5 and 6) were based on the training windows starting with 16 and 17 DASs with the corresponding time steps of 55 and 43, respectively. A summary of the reference time points for each set is listed in **Table 1**, where the entire experiment was termed experiment I. To verify the repeatability, an additional entire experiment, which was termed experiment II, was repeated.

To examine the influence of various time lengths on the performance of the forecast model, a direct forecasting package called "forecastML" (Vienna, Austria) was utilized (Redell, 2020). The R forecast library required static (location) and non-static data (date and month). The period was set to 48 h. The overall scheme of the data structure is available (**Supplementary Figure 3A**). Individual model for each sample ID was constructed and evaluated as training 1 to 4 dataset (**Supplementary Figure 3B**) with multiple n-step ahead forecasting in training data hours, as shown in **Figure 3A**. The R code utilized in the analysis is available in the **Supplementary Material**. The mean absolute error (MAE) calculated the average errors using the sum of magnitude (absolute values) divided by the total samples (n), as shown in Eq. 9. The root means square error (RMSE) calculated average errors by identifying the total squared errors between the observed and the predicted values over n. The square root of mean squared errors was calculated using Eq. 10. The MAE and RMSE were the most used metrics for measuring the accuracy of time-series data (Cort and Kenji, 2005; Chai and Draxler, 2014).

$$\mathrm{MAE} = \frac{1}{\mathrm{n}}\sum_{j=1}^{\mathrm{n}} |\mathrm{y}_j - \hat{y}_j| \tag{9}$$

$$\mathrm{RMSE} = \sqrt{\frac{1}{\mathrm{n}}\sum_{j=1}^{\mathrm{n}} (\mathrm{y}_j - \hat{y}_j)^2} \tag{10}$$

For all training datasets, horizons for the combined forecasting at 1, 6, 12, 24, 36, 42, and 48 h were selected.

TABLE 1 | Summary of reference points of each dataset with two-time scales used in the study.

Training set	Reference timepoints			
	DAS with (Time steps)			
	Training period		Testing period	
	Start	End	Start	End
Training 1	15 (60)	21 (140)	21 (141)	23 (165)
Training 2	16 (72)	21 (140)	21 (141)	23 (165)
Training 3	17 (84)	21 (140)	21 (141)	23 (165)
Training 4	18 (96)	21 (140)	21 (141)	23 (165)
Training 5	16 (72)	20 (127)	20 (128)	23 (165)
Training 6	17 (84)	20 (127)	20 (128)	23 (165)

The time scale was recorded with the day format as days after sowing (DAS) with time steps. Moreover, the corresponding time steps are mention in the parenthesis next to the day format.

Trained Model Testing With Late Pre-flowering Stage Data

Individual PA forecasting models were constructed and tested for the late growth stage of the *Arabidopsis* plant. Four training models for various time intervals were then tested using testing sets ranging from 21 to 23 DAS (141–165 time steps), while two training models were tested with testing sets with a range of 20–23 DAS (133 to 165 time steps). **Table 1** lists the reference time points for each set.

Statistical Analysis

Statistical tests were performed using R (R Core Team, 2019). Three analyses were performed to verify that the forecast values from the ensemble model provided accurate output. The late growth time steps at 165 (23 DAS with 16 h) were selected for statistical analysis because inflorescence emerged at 23 DAS. First, an ANOVA test was used to determine if one or more datasets were different. The observed outputs were compared with the predicted values for six datasets. Non-significant datasets ($P < 0.01$) were selected and the homogeneity of variance for these sets was compared using Tukey's honestly significant difference at a family-wise confidence level of 95%. The correlations between observed and predicted values were tested using Spearman's rank coefficient (R).

Measurement and Estimated Fresh Weight

Previous studies indicated that strong relationships between FW and PA exist in *Arabidopsis* (Fahlgren et al., 2015).

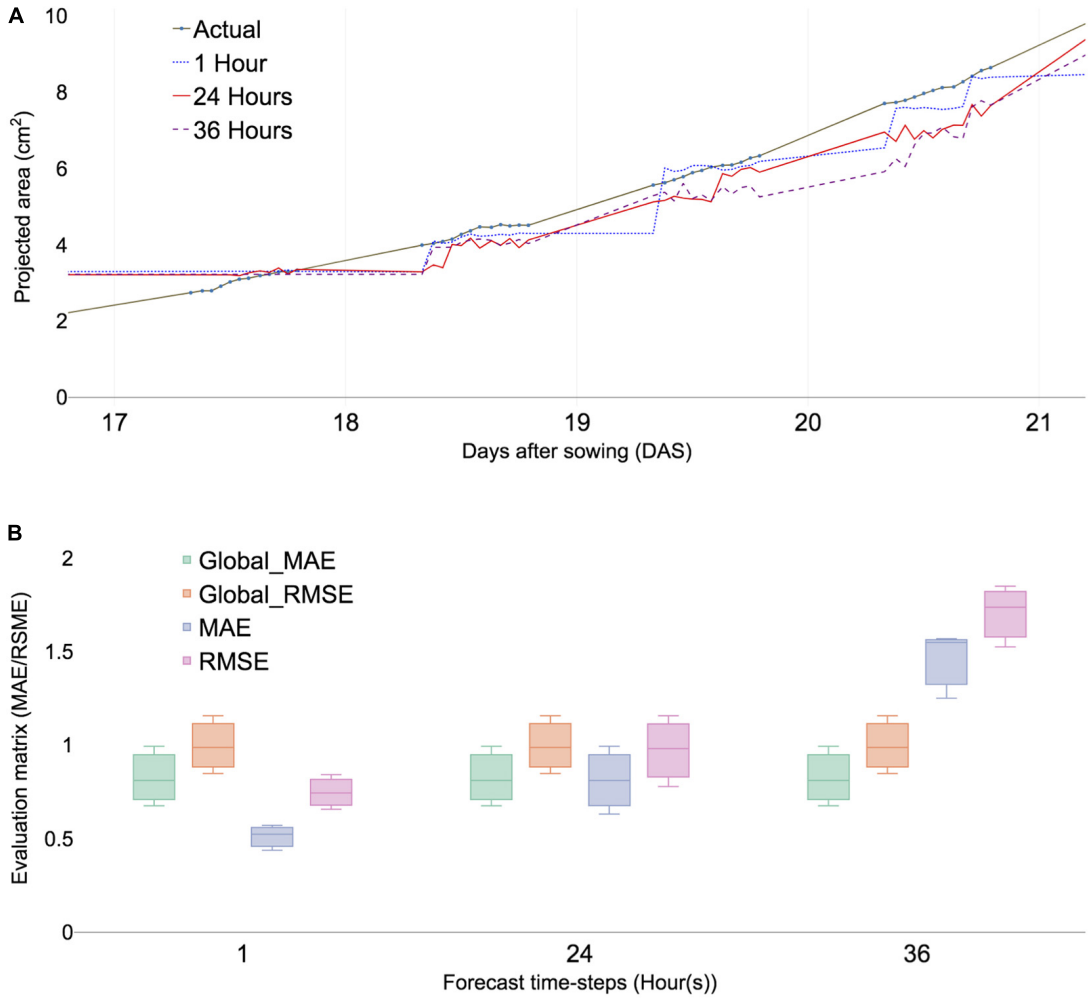

FIGURE 3 | Predicted PA and error calculation at 1-, 24-, and 36-h forecast window sing ML algorithms (XGBoost). **(A)** Comparing PA prediction with 17–21 DAS of ID 98. **(B)** Comparing evaluation matrices of mean absolute errors (MAE), root mean square error (RMSE) of three selected samples, namely, ID 98,100, and 103. Global MAE and RMSE are defined as average MAEs and RMSE of all forecast time steps.

Moreover, it was infeasible to harvest all representative plant images of 220,000 (165 time steps × 115 plants × 12 times per day). Therefore, plants were randomly selected and harvested among 112 plants from HTPP at 14, 17, and 20 DAS, respectively. Furthermore, 30 of 110 plants were randomly selected in experiment II at early 23 DAS because inflorescence emerged. Each plant was harvested and measured using the precision scientific balance (Ohaus, New Jersey, United States).

The following steps were required for establishing a relationship between FW and PA. First, a regression model was established to verify the relationship between FW and PA at the early pre-flowering stage using the data at 14, 17, and 20 DAS, respectively. Second, the regression model for the early pre-flowering stage was used to verify the predictability estimate of FW from PA in experiment II at 23 DAS. Third, FW was estimated from PA training models. Finally, the measured and predicted FW at 23 DAS were compared.

RESULTS

Evaluation of Semantic Segmentation

The image analysis pipeline "U-Net" used for DL algorithms yielded good results (Chang et al., 2020). However, minor errors were evident when the network distinguished moss from plant areas. Thus, this study incorporated a more flexible U-Net network with various backbones (encoders) from other published networks to improve the segmentation task (Jiang and Li, 2020). IoU scores predicted PA over true PA values and a score of 1 indicated a perfect match between the predicted and true values. F1 score calculated model accuracy by combining precision and recall output. Similarly, a score of 1 indicated the highest value for the evaluation. Results from the evaluation matrix showed a high association between the evaluation and validation data (**Table 2**), indicating that the up-to-date backbones such as the SE-ResNext101 exhibited a reduced error rate than VGG16. Furthermore, the residual module-based network such

TABLE 2 | Summary of an evaluation matrix for semantic segmentation of U-Net using various deep learning backbones (encoder).

Backbones	Model evaluation matrix		Validation matrix	
	IoU	F1-score	IoU	F1-score
VGG16	0.9384	0.9682	0.9272	0.9626
VGG19	0.9464	0.9724	0.9301	0.9637
SEResNet152	0.9665	0.9824	0.9323	0.9639
SEResNeXt101	0.9684	0.9839	0.9324	0.9648
SENet154	0.9697	0.9846	0.9314	0.9643
ResNet154	0.9565	0.9777	0.9259	0.9613
ResNeXt101	0.9623	0.9808	0.9281	0.9614
MoblieNetV2	0.9518	0.9749	0.9250	0.9608
InceptionResNetV2	0.9640	0.9817	0.9308	0.9637
DenseNet201	0.9609	0.9801	0.9310	0.9642

Two evaluation scores are shown in the table. Intersection-over-union (IoU) evaluation matrix and F1-score were calculated.

as ResNet154 provided a high-confidence F1-score of 0.9613. The distribution evaluation matrix was then visualized to determine whether the network architecture influenced that of the output. The results (**Supplementary Figure 1**) indicated that squeeze and excitation (SE) architecture provided the most accurate PA among all backbones. The total loss of each backbone showed the same result from the F1 score (**Supplementary Figure 1C**). These results indicated that U-Net with SE backbones could be used for segmentation in various crops.

Growth Pattern Analysis

The dynamic growth patterns were observed in *Arabidopsis* day and night (Wiese et al., 2007; van Es et al., 2019) and demonstrated that daylight growth was responsible for 70% of growth activities (Wiese et al., 2007). The overall growth pattern of the selected plant showed a somewhat linear trend for multiple growth stages (**Figure 2B**) and agreed well with previous studies on *Arabidopsis* (van Es et al., 2019). Three of 122 plant samples were selected and the dynamic growth pattern of the individual plants was compared (**Figure 2C**). Individual samples had distinct patterns from (orange solid line) one another and although the unmeasured night period varied, ID 98 had the fastest-growing rate ahead of ID100 and 102. However, its absolute growth rate (AGR) was the slowest at 20 DAS (**Supplementary Table 2**). Furthermore, the AGR of sample ID 100 grew fastest in selected samples of ID 98, 100, and 102; however, ID 102 was the fastest in afternoon time points. These results reveal that a dynamic growth habit can be observed within a 6-h time window. Consequently, the n-step forecast time was determined using multiples of 6 h and translated into 0.5 days because a 12-h-window was measured for a day.

Prediction of the Projected Area With Training Models

High-confidence data were obtained using the 165 time steps collected and an up-to-date DL network-based image analysis. The definition of Boyes et al. (2001) was adapted (**Figure 2A**) for defining the developmental stages of *Arabidopsis*. Results showed that the early vegetative stage had slight sample variations from the pre-flowering stage of the plant developmental phase (Boyes et al., 2001; **Figure 2B**). Thus, the period from the early pre-flowering stage was tested, and the prediction models were validated in the late pre-flowering stage. Time-series analysis required the predefined time steps for training and testing purposes. Algorithms only used information within the training window to build a model and predict future values in the pre-determined forecast window. Later, predicted values from the trained model were compared with measured PA with U-Net within testing data. Forecasting terminologies were used in the time series analysis because not all data have true values in future events such as weather forecasts. This study determined the training and testing windows for the plant developmental stages until flowering bud emerged at late 23 DAS. The forecasting window at 24 h indicated 2 days after 12 h defined 1 day in the dataset. Various forecasting windows were tested with baseline studies to compare predicted and true values at the end of the late pre-flowering stage.

Verifying the essential time for the prediction model, the total time data was divided into six training sets following the start and end dates of the training data. Training sets 1–4 and training sets 5 and 6 were selected based on the end date of 21 and 20 DAS, respectively. Similarly, they were selected from the start point from 15 to 18 and 16 to 17 DAS, respectively (**Table 1**).

The initial analysis was performed with time points ranging from 15 to 21 DAS. Forecasting multiple windows and combining models provided more reliable results; however, the selection of time steps depends on the dataset (Galicia et al., 2019). The errors of different combinations of time steps were calculated using multiple-error evaluation matrices. The forecast value showed a similar trend among the different forecast windows at 1, 6, 12, 24, 36, 42, and 48 h, respectively (**Supplementary Figure 2**), because growth variation was observed at least 6 h (**Supplementary Table 2**). PA prediction deviated with increased time intervals for forecast and forecasting window at 24 h provided an additional reliable prediction value than the 36 h window (**Figure 3A**). The result indicated that the optimal forecasting window ranged between 24 and 36 h (**Figure 3A**). The data structure of the study was performed for 12 h a day for measuring daylight growth, which corresponded to 36 h for 3 days. To summarize, forecast windows at 1, 6, 12, 24, 36, 42, and 48 h corresponded to 0.04, 0.5, 1, 2, 3, 3.5, and 4 days, respectively.

Time-series analysis used various result-testing tools such as MAE and RMSE. MAE is one of the most commonly used matrices for measuring the performance of forecast models. A smaller MAE indicated that the predicted values were closer to actual values (Tay and Cao, 2001). The effectiveness of time-series analysis with the ML model was checked using RMSE (Chen et al., 2006). Two absolute error evaluation matrices provided appropriate information because no negative values exist in the dataset. Selected subsamples from training models were compared with check time window selection and forecast evaluation within testing data. The MAE of each plant sample showed little differences in multiple forecast windows (**Figure 3B**) and the overall error rate called the global MAE was 0.25 (**Supplementary Figure 5A**). Moreover, the RMSE

of selected samples showed little differences (**Figure 3B**). All samples of MAEs were calculated using a forecasting window that ranged from 0.5 to 2 and a global MAE given as 0.7 (**Supplementary Figure 4B**). The result indicated that it served as a baseline MAE for other datasets.

A total of six training sets were generated from the endpoints of 20 and 21 DAS (**Table 1** and **Supplementary Figure 5F**). The training period of the training sets 5 and 6 started at 16 DAS (**Supplementary Figure 5F**). The MAE ranged from 0.5 to 1.7 with the mean of global MAE as 0.7 (**Supplementary Figure 4**). The prediction errors decreased slightly compared with the baseline training sets 1–4. Furthermore, the training sets 3 and 4 with training windows that started at 17 and 18 DAS, respectively, were compared to check their error rate decreased with a narrow time. The results from training sets 3 and 4 indicated a similar error rate with training sets 5 and 6 (**Supplementary Figures 5B–D**). The mean of MAE training sets 3 and 4 was 0.6 and 0.7, respectively (**Supplementary Figures 5C,D**), suggesting that limited intermediated time points for time-series analysis can be feasible for predicting late-stage growth patterns.

The endpoint of the training set 5 and 6 was shifted to the forecasting window at 20 DAS. Training set 5 started a time window at 16 DAS and the MAEs of 1, 6, 12, and 24 h n-step forecast showed similar ranges (0.5–1.5) compared with the training sets 1–4. In the same training set, MAE increase by >2 or more at 36 and 42 h of the forecast period. Finally, the training set 6 with a start date at 17 DAS exhibited increased MAEs over 3 at 36 and 42-h forecast.

Overall, MAEs were increased after 36 h (3 days) of forecasting windows among different training sets (**Figure 3B** and **Supplementary Figure 5F**). This result indicated that models would predict reliable PAs at the endpoint of late time point in the testing time steps (**Supplementary Table 3**).

Testing Trained Models With Late Pre-flowering Stage Data

This study forecasts the late pre-flowering stage using correlated features from the early pre-flowering. The growth forecast models for each training set (**Table 1**) were constructed and tested (**Supplementary Figure 6** and **Supplementary Table 3**). The test time included the late growth stage of the *Arabidopsis* plant, including 23 DAS at which the emergence of inflorescence occurs in certain plants. To forecast the target days at 23 DAS, the training sets 5 and 6 were forecasted 42 h or longer. The forecasting plot of training sets 5 and 6 demonstrated that prediction at least 42 h ahead of time was feasible (**Supplementary Figures 6E,F**). Sample ID 98 was selected and all the predicted values of the six training sets were compared to evaluate prediction efficiencies (**Figure 4A**). Training sets 1–4 showed a stable trend in the whole growth period but training sets 5 and 6 demonstrated decreased accuracies after the end of 22 DAS. The prediction of the training sets 1–4 demonstrated close to actual values in the late growth stage at 23 DAS at 5:00 pm (**Figure 4B**). Moreover, the global error rate showed a similar trend in training sets 1–4 but different in training sets 5 and 6 (**Figure 4C**), although the error rates were similar between sets 1–4 and training sets 5 and 6 before 36 h of forecast window (**Figure 4A**). The result indicated that training sets 1–4 forecast the growth pattern of the late pre-flowering stage at 23 DAS. The training set 3 that included only 5 days of data showed similar MAEs compared with the 7-day data in the training set 1. An essential time window of fewer than 5 days of data (17–21 DAS) was generated, which included the transitional window from early to late pre-flowering stages in *Arabidopsis*. The same time window was tested in the replication at experiment II.

In experiment II, the overall growth pattern was similar (**Figure 5A**) to experiment I (**Figure 2B**). HTTP stopped in the early hours of 23 DAS (23.37) because inflorescence was observed in the portion population ($n = 110$) and the 30 randomly selected plants for FW. Growth prediction models were constructed from 17 to 21 DAS (training set 3) and at 23 DAS, the t-test results of the observed and predicted values using the training dataset 3 were not different ($P > 0.01$). The Spearman's rank coefficient (R) of PA and the predicted PA of experiments I and II were calculated and compared. The coefficient (R) of experiment I was 0.868 (**Supplementary Figure 7A**) and that of experiment II was 0.872 (**Supplementary Figure 7B**). The coefficient of each experiment was similar ($P > 0.01$), thereby confirming the experimental reproducibility. Furthermore, an additional statistical test is provided in Section "Statistical Analysis of Validation Sets."

Statistical Analysis of Validation Sets

The low MAEs (**Supplementary Figure 5**) is a good indication of high accuracy-ML models and provide statistically inseparable results with limited time points. To confirm the effectiveness of limited time for forecasting late growth stages, certain statistical methods were tested. One time point was selected in the late growth stage for statistical analysis. The selected time point was 23 DAS at 17 h (23.71) because this time point corresponds to the flower bud formation. The ANOVA test indicated that at least one training set was significantly different ($P < 0.01$). T-test of the observed and predicted values using training sets 1–4 were not significantly different ($P > 0.01$), while training sets 5 and 6 were observed to be significantly different ($P < 0.01$). Tukey's honestly significant difference (HSD) test confirmed that all datasets of training sets 1–4 were not significantly different ($P > 0.01$) at 95% of family confidence level (**Supplementary Figure 8**). The result revealed that the time window ranges from 15 to 21 DAS were not different from the time-reduced windows from 17 to 21 DAS. In the experiment, I, the prediction of PA in the training 3 models was not significantly different from the actual PAs ($P > 0.01$) at 95% of family confidence level (**Figure 5B** and **Supplementary Figure 9**). Both experimental results confirm that 17–21 DASs was the essential time window for predicting at 23 DAS PAs. Furthermore, the selection of time intervals for HTPP was feasible because using a partial time interval was as effective as was using a whole interval in the early pre-flowering stage. This procedure might be applicable in detecting subtle differences in traits of interest where traits have expressed only a part of the life cycle of a plant. Moreover, focusing on a restricted time window of digital phenotyping data could alleviate the heavy burden of big-scale research projects because they require

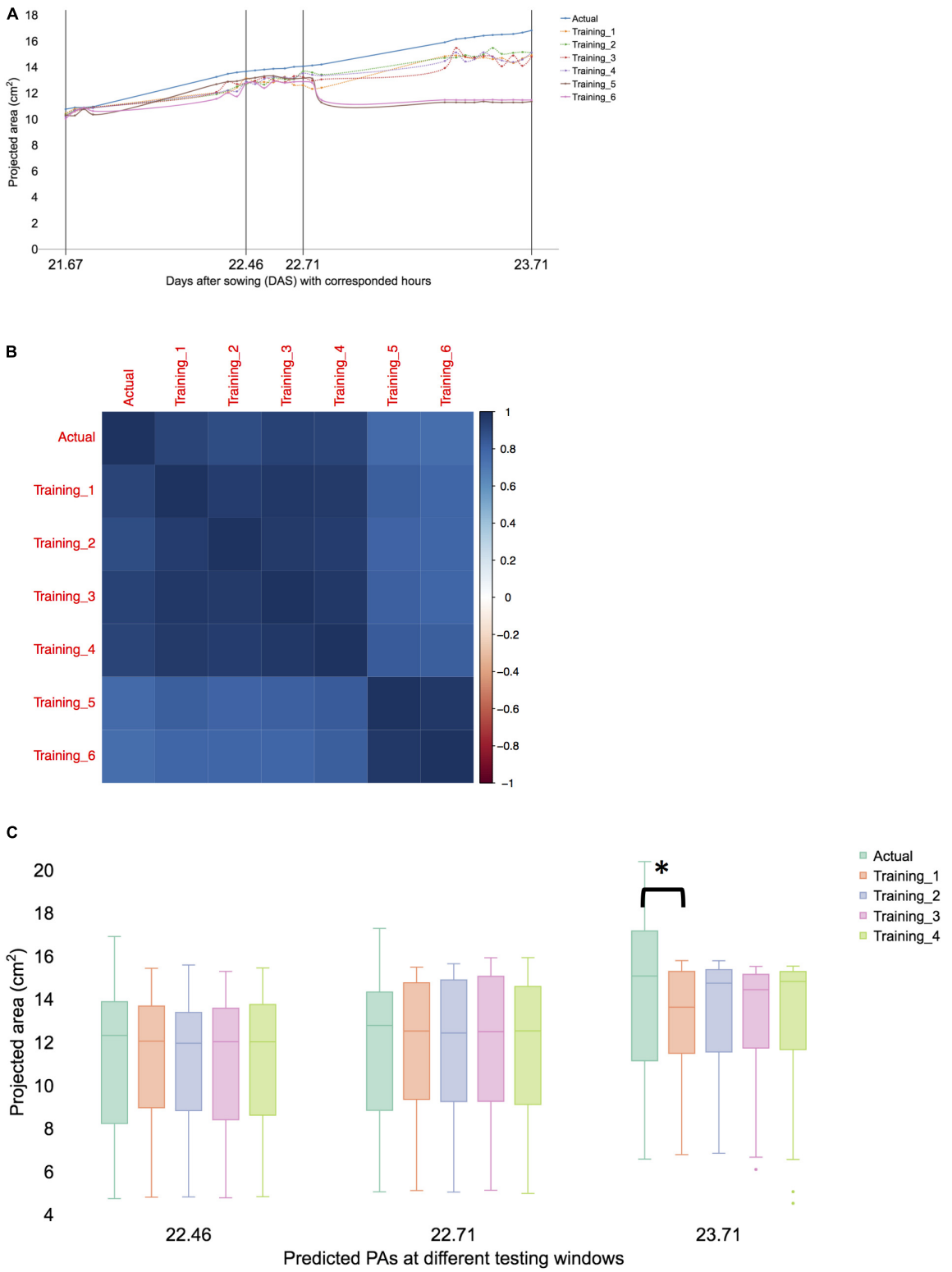

FIGURE 4 | Predicted total leaf area and error range from 21 to 23 DAS in selected and total samples. Time points format as format images were taken at DAS (DAS.hours). MAE was calculated using multiple time windows with various forecast time points. **(A)** Predicted values with multiple time windows of the dataset (**Figure 3**) at 21–23 DAS (validation time points) of sample ID 98. **(B)** Correlation plot of all samples at 23.71. Clustering and grouping with R library for arranged samples. **(C)** Predicted PAs with training sets 1–4 at the selected testing window are given as 22.26, 22.71, and 23.71. The result is shown in a boxplot of actual and predicted PAs from each testing model. We compared with *post hoc* statistical test (Tukey's HSD) and the significant result is showed with an asterisk.

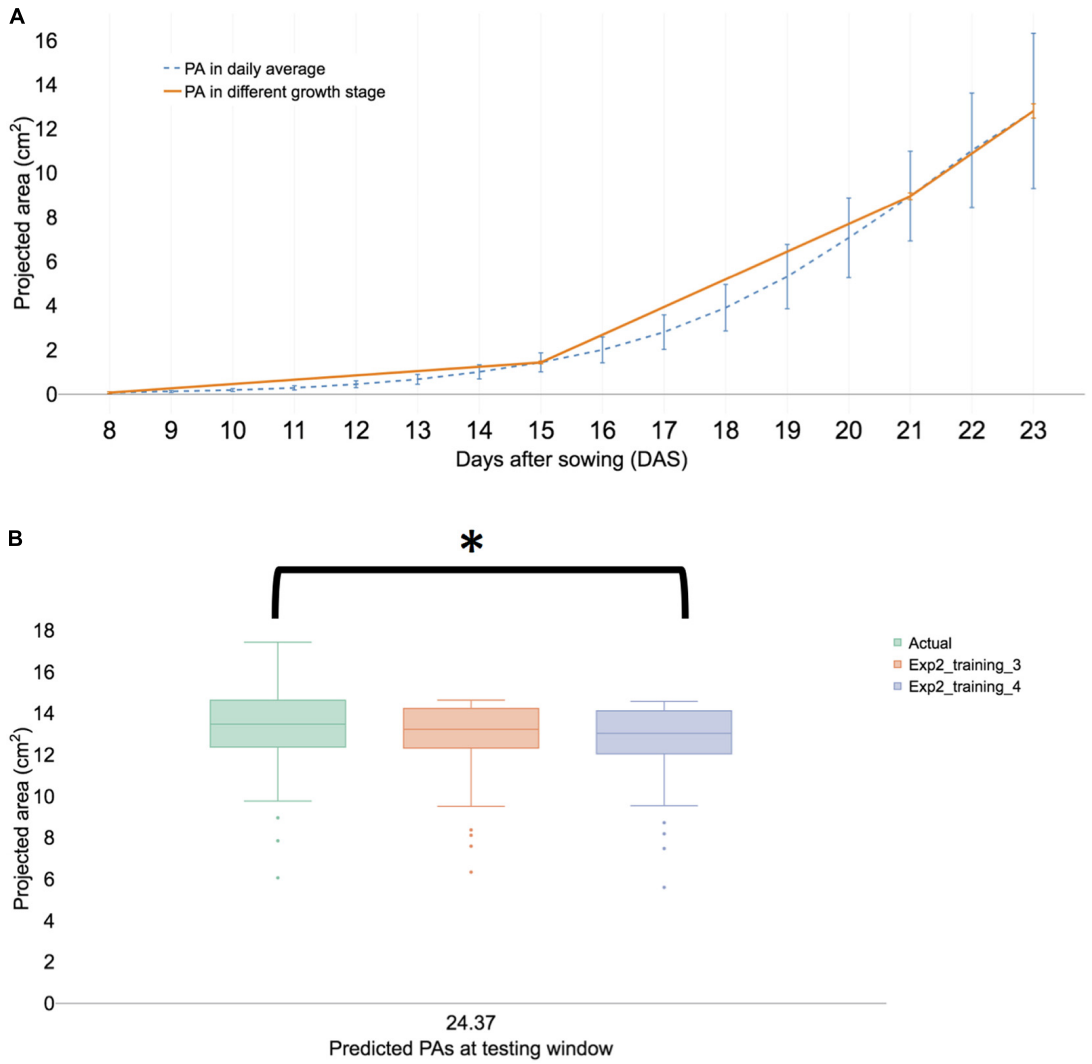

FIGURE 5 | Summary of a biological replication study at experiment II. **(A)** The visualized growth pattern of all samples of biological replication experiment including three growth stages. **(B)** Predicted PAs with training sets 3 and 4 with testing window at 23 DAS. The result is shown in a boxplot of actual and predicted PAs from each testing model. We then compared with *post hoc* statistical test (Tukey's HSD) and the significant result is shown with an asterisk.

considerable resources to obtain new information during the entire life cycle of a plant.

Estimated Fresh Weight Using the Projected Area

Fresh weight provided important information of interesting traits; however, the measuring data required the destruction of samples, and obtaining the corresponding time-series data was difficult.

Multiple steps were required to predict FW using PA. The initial step was to establish a relationship between FW and PA in a target plant species. First, time-series data required corresponded to FW at each time point, and the estimated FW was obtained from the regression model between FW and PA in *Arabidopsis*. Previously, studies demonstrated a highly correlated relationship between FW and PA (Walter et al., 2007; Faragó et al., 2018), and the results of our study suggest the same relationship between FW and PA in the range of 14–20 DAS (**Figure 6A**). Moreover, the correlation coefficient between FW and PA was 0.99 (**Figure 6A**). The next step was testing the established relationship in different growth stages. The regression model from the early pre-flowering stage for FW (R = 0.9683) was constructed and was used to estimate the FW of the late pre-flowering stage. Results indicated (**Supplementary Figure 10**) a high correlation coefficient value (R = 0.9382) compared with the measurement during harvest at 23 DAS. Moreover, the estimated FW from PA not only provided accurate values in the same growth stage but can also be applied to different growth stages. The last step was to compare with measured FW and predicted PA from the training models. PAs were predicted with the training model 3 (**Figure 5B**) and then FW was estimated using the regression from the previous step. Finally, the predicted FW was compared with the measurement

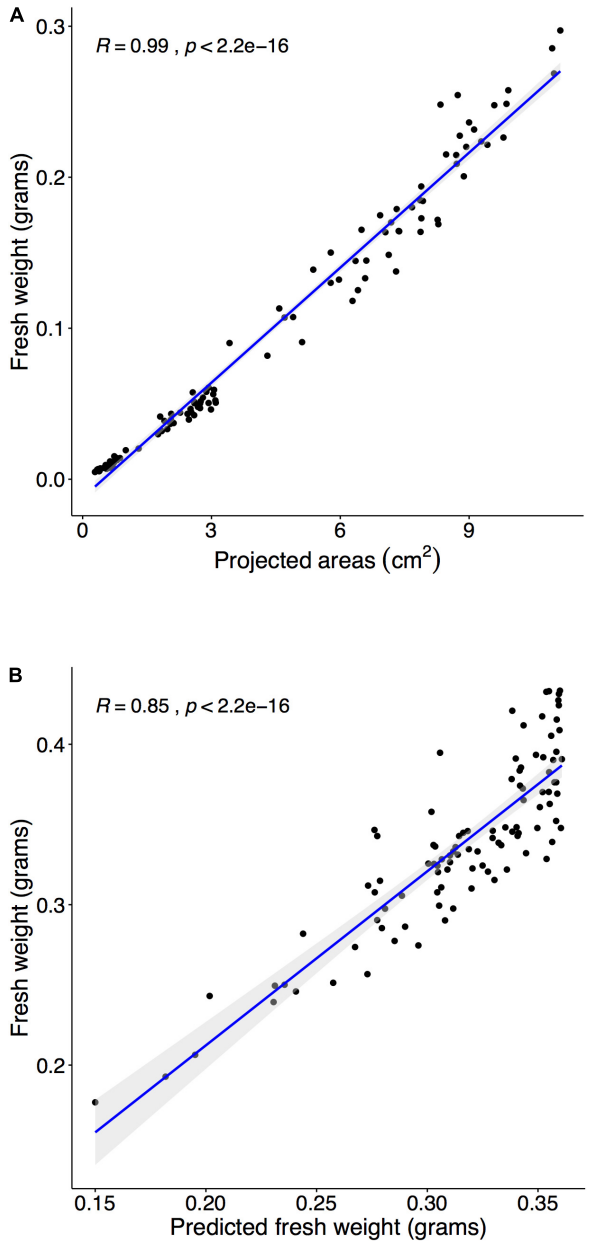

FIGURE 6 | Estimating fresh weight (FW) from the PA and predict FW with three training sets. Panel **(A):** Harvest and weight 110 plants within the pre-flowering stage (15, 18, and 20 DAS), and we compared measured FW and PA from the image analysis. The correlation between FW and PA was tested using Spearman's rank correlation coefficient (*R*). The coefficient's (*R*) confidence level at 95% was shaded in gray. **(A)** Comparison of PA and FW in the range of 14–21 DAS (*R* = 0.9904). **(B)** Randomly select 30 samples at experiment II and predicted PAs with training 3 model and then converted into estimated FW. Compared estimated FW and measured FW at 23 DAS (*R* = 0.9042).

during harvest at 23 DAS, and a high correlation coefficient (*R* = 0.8512) was observed (**Figure 6B**).

In summary, the new strategy showed that limited growth period ranges were required to predict the growth pattern of different developmental stages. The predicted PAs were confirmed in an independent study and the PAs were converted into highly accurate FW values.

DISCUSSION

Transforming into digital agriculture requires various digital (Redmond Ramin et al., 2018b; Weersink et al., 2018; Klerkx et al., 2019) and image data, which are essential data. The primary reason why digital agriculture is essential is to detect the health and performance of plants in real-time in various environments. RGB images provide quantitative data in plant breeding and production (Araus and Cairns, 2014). The early image analysis from the legacy method or early application of ML (Pan and He, 2008) yielded partial success and not many plant scientists benefited from the quantitative data from the extract from RGB images. Many studies of plant segmentation were published and the result was difficult since the environmental conditions (lights, view of camera, soil conditions) were not identical in each experiment (Jiang and Li, 2020). ML- and DL-based image pipeline showed superb qualities over outdated legacy methods. The image analysis pipeline from ML showed promising results in its application to semantic segmentation in the rosette plant species named *Youngia denticulata* (Lee et al., 2018). U-Net was applied to separate irradiated and wild-type *Arabidopsis* plants (Chang et al., 2020). Additionally, botanists showed interest to apply up-to-date DL in HTPP data analysis (Jiang and Li, 2020). The encoder and decoder portions of U-Net (**Figure 1E**) showed several performances in various environments (Zhang et al., 2020). The encoder provides valuable information on whether various encoders at U-Net yield different results for interesting traits (PA) in agriculture (Jiang and Li, 2020). We demonstrated a more flexible way of applying networks to images for plant phenotyping (**Figure 2**). The SE network architecture demonstrated the highest confidence level among various backbones (**Supplementary Figure 1**). VGG-16, a simple network, provides high accuracy for the IoU score at 0.94, indicating a 94% of the images were correctly predicted with the combination of simple networks. Thus, applying and using image processing with DL still held certain challenges because of the lack of significant computing resources such as graphical process units or tensor process units. In a limited resource-research scheme, it should be beneficial to apply a simple network and gradually move to more complex network schemes. Importantly, it would be interesting to examine a specific encoder that could provide superior performance to detect the organs of plants such as flowers or other targets for interesting traits.

Arabidopsis thaliana was selected because it is a model plant for scientists and is rich in several noteworthy information. Moreover, the growth pattern of the gene function (van Es et al., 2019) and stress responses (Dhondt et al., 2014) was analyzed using time series.

To incorporate time-series analysis in an *Arabidopsis* research, many challenges in extracting and analyzing data from OMICS, including phenomics data associated with developmental stages were experienced. Previously, studies suggested that the growth

pattern of long time steps provides valuable information on interesting traits (Dhondt et al., 2014); however, an additional investigation was not reported. Using complete time-series data is beneficial because dynamic growth habits were observed between 15 and 23 DAS (**Figure 2C**). Time-series data divided into developmental stages defined with the BBCH scale provided a more descriptive explanation (Boyes et al., 2001) and useful defined-data structure for analysis. To explain the end of the analysis, training and testing windows needed to be associated with developmental stages. Time-series analysis with XGBoost demonstrated better performance over other algorithms (Ji et al., 2019); however, this method was rarely used in biomass prediction or studying interesting traits. We applied multiple time steps with XGBoost and multiple correlated features to predict PA and the result was highly confident. A new analysis method that restricted time-series data within predefined developmental stages is helpful because relevant data on the relationship between or among different growth stages were accessible. Working with interesting traits with a full life cycle in a plant is time-consuming; therefore, it is possible to narrow down specific developmental stages using our method. Furthermore, our method can be used to reduce time intervals within the developmental stages. The method can be applied to predict traits of interest using HTPP data. Abiotic stress-related screening requires multiple resources because plants require testing over a long period. *Arabidopsis* plant showed stress effect after being exposed to the salt solution for 8 days (Geng et al., 2013). In the drought stress study, *Arabidopsis* demonstrated wilt symptoms after we stopped watering for 20 days. The total observation period of abiotic stress was ∼33 or 50% of the whole life cycle. A new method is beneficial to researchers who require to screen a larger number of samples using the HTTP because reduced time windows for a population provide extra time for screening another population.

The FW of a plant is an important selection criterion for bioenergy conversion using plants and other target materials. Since plant weight is obtained only after the growing plant is harvested or growth is completely stopped, understanding plant characteristics in a non-destructive method is a fundamentally essential research field in recent biology. Previous studies have demonstrated a positive correlation between FW and PA (Walter et al., 2007; Araus and Cairns, 2014; Faragó et al., 2018). Predicting FW from PA is plausible if there is a high correlation between two factors. A high correlation was found in our experiment and the estimated FW from PA using a different developmental stage was accurate (R = 0.93). The results indicated that the estimated FW in individual plants was possible from PA using time-series data and can be applied to predict FW or biomass in crops. FW of vegetable crops has essential information for the grower since FW of vegetables is a good indicator of yield at harvest. Vegetable crops are grown in vertical farming or controlled environment agriculture (CEA) and are important in food production and distribution, particularly during a virus outbreak where food movement is limited. Vertical farming produces more food in urban settings compared with field production (Benke and Tomkins, 2017). The estimation of FW using the visible spectrum is beneficial and should be incorporated into vertical farming. Though phenotype information, such as the leaf area index, has been used for plant status (Wang et al., 2017) in CEA, the estimated FW provides better plant status information and serves as a good yield indicator (Marondedze et al., 2018). In a plant factory setting, accurate yield prediction was performed with early time-series phenotyping data in lettuce (Nagano et al., 2019). We tested a model plant in the CEA for growth forecast with a limited time window and it yielded an accurate result (**Figure 6B**). A forecast of lettuce FW is possible but accurately predicting individual FW of lettuce is challenging because vertical farming production plants are tightly placed because the indoor farming space is limited (Redmond Ramin et al., 2018a). Advanced DL network using various encoders with U-Net provides more FW or PA-related features. Furthermore, more sophisticated DL for time-series analysis was promising in other fields, e.g., advanced DL-based network, long-short-time-memory (LSTM), or gate recurrent unit (GRU) outperformed the recurrent neural network (Khaki et al., 2020). A novel DL called temporal attention-based network (TCAN) can replace LSTM and GRU in certain tasks (Hoeser and Kuenzer, 2020; Jiang and Li, 2020; Yan et al., 2020). DL can achieve a performance level hitherto unachieved in conventional and ML algorithms. Gathering and analyzing using a long chain of time-series data enhances accuracy and increases the prediction window of FW with up-to-date DL.

In conventional agricultural research to date, the observation and selection of crops are possible only at a set time with the naked eye of breeders. Time-series data analysis from HTPP could provide valuable information. We applied up-to-date DL for semantic segmentation from HTPP data and analyzed selected pre-flowering developmental stages to forecast the growth pattern of the next growth stage in *Arabidopsis.* High-confidence F1-score (97%) was achieved using U-Net with SE-ResXt101 for semantic segmentation. This study reported that a part (17–21 DAS) of the developmental stages ($P < 0.01$) is sufficient for predicting the growth pattern of different developmental stages at 23 DAS. The result was confirmed with an independent study ($P < 0.01$). Moreover, FW prediction ($P < 0.01$) with HTPP time-series data is validated. The proposed method could be applied to forecast the growth or yield of leafy plants such as lettuce.

DATA AVAILABILITY STATEMENT

The original contributions presented in the study are included in the article/**Supplementary Material**, further inquiries can be directed to the corresponding author.

AUTHOR CONTRIBUTIONS

SC and J-BK designed the research. SC and MH performed the experiments and data analysis. SC and UL analyzed the data and wrote the manuscript. MH, YJ, and J-BK advised on the result and discussions. All the authors discussed the results and implications and commented on the manuscript.

FUNDING

This work was supported by grants from the Nuclear R&D programs of the Ministry of Science and ICT (MSIT) and the research program of KAERI, Republic of Korea.

SUPPLEMENTARY MATERIAL

The Supplementary Material for this article can be found online at: https://www.frontiersin.org/articles/10.3389/fpls.2021.721512/full#supplementary-material

REFERENCES

Al-Tamimi, N., Brien, C., Oakey, H., Berger, B., Saade, S., Ho, Y. S., et al. (2016). Salinity tolerance loci revealed in rice using high-throughput non-invasive phenotyping. *Nat. Commun.* 7:13342. doi: 10.1038/ncomms13342

Araus, J. L., and Cairns, J. E. (2014). Field high-throughput phenotyping: the new crop breeding frontier. *Trends Plant Sci.* 19, 52–61. doi: 10.1016/j.tplants.2013.09.008

Bargoti, S., and Underwood, J. P. (2017). Image segmentation for fruit detection and yield estimation in apple orchards. *J. Field Robot.* 34, 1039–1060. doi: 10.1002/rob.21699

Benke, K., and Tomkins, B. (2017). Future food-production systems: vertical farming and controlled-environment agriculture. *Sustain. Sci. Pract. Policy* 13, 13–26. doi: 10.1080/15487733.2017.1394054

Boken, V. K. (2000). Forecasting spring wheat yield using time series analysis. *Agron. J.* 92, 1047–1053. doi: 10.2134/agronj2000.9261047x

Boyes, D. C., Zayed, A. M., Ascenzi, R., McCaskill, A. J., Hoffman, N. E., Davis, K. R., et al. (2001). Growth stage–based phenotypic analysis of *arabidopsis*: a model for high throughput functional genomics in plants. *Plant Cell* 13, 1499–1510. doi: 10.1105/tpc.010011

Buslaev, A., Iglovikov, V. I., Khvedchenya, E., Parinov, A., Druzhinin, M., and Kalinin, A. A. (2020). Albumentations: fast and flexible image augmentations. *Information* 11:125.

Chai, T., and Draxler, R. R. (2014). Root mean square error (rmse) or mean absolute error (mae)?–arguments against avoiding rmse in the literature. *Geosci. Model Dev.* 7:1247. doi: 10.5194/gmd-7-1247-2014

Chang, S., Lee, U., Hong, M. J., Jo, Y. D., and Kim, J.-B. (2020). High-throughput phenotyping (htp) data reveal dosage effect at growth stages in *arabidopsis thaliana* irradiated by gamma rays. *Plants* 9:557.

Chawade, A., van Ham, J., Blomquist, H., Bagge, O., Alexandersson, E., and Ortiz, R. (2019). High-throughput field-phenotyping tools for plant breeding and precision agriculture. *Agronomy* 9:258.

Chen, D., Shi, R., Pape, J.-M., Neumann, K., Arend, D., Graner, A., et al. (2018). Predicting plant biomass accumulation from image-derived parameters. *Gigascience* 7, 1–13. doi: 10.1093/gigascience/giy001

Chen, Y., Yang, B., and Dong, J. (2006). Time-series prediction using a local linear wavelet neural network. *Neurocomputing* 69, 449–465. doi: 10.1016/j.neucom.2005.02.006

Cort, J. W., and Kenji, M. (2005). Advantages of the mean absolute error (mae) over the root mean square error (rmse) in assessing average model performance. *Clim. Res.* 30, 79–82.

Dhondt, S., Gonzalez, N., Blomme, J., De Milde, L., Van Daele, T., Van Akoleyen, D., et al. (2014). High-resolution time-resolved imaging of in vitro *arabidopsis* rosette growth. *Plant J.* 80, 172–184. doi: 10.1111/tpj.12610

Dineva, A., Kocsis, S. S., and Vajda, I. (2020). "Data-driven terminal voltage prediction of li-ion batteries under dynamic loads," in *Proceedings of the 2020 21st International Symposium on Electrical Apparatus & Technologies (SIELA)*, Bourgas, 1–5.

Fahlgren, N., Gehan, M. A., and Baxter, I. (2015). Lights, camera, action: high-throughput plant phenotyping is ready for a close-up. *Curr. Opin. Plant Biol.* 24, 93–99. doi: 10.1016/j.pbi.2015.02.006

Faragó, D., Sass, L., Valkai, I., Andrási, N., and Szabados, L. (2018). Plantsize offers an affordable, non-destructive method to measure plant size and color in vitro. *Front. Plant Sci.* 9:219. doi: 10.3389/fpls.2018.00219

Galicia, A., Talavera-Llames, R., Troncoso, A., Koprinska, I., and Martínez-Álvarez, F. (2019). Multi-step forecasting for big data time series based on ensemble learning. *Knowl. Based Syst.* 163, 830–841. doi: 10.1016/j.knosys.2018.10.009

Geng, Y., Wu, R., Wee, C. W., Xie, F., Wei, X., Chan, P. M. Y., et al. (2013). A spatio-temporal understanding of growth regulation during the salt stress response in *arabidopsis*. *Plant Cell* 25, 2132–2154. doi: 10.1105/tpc.113.112896

Godfray, H. C. J., Beddington, J. R., Crute, I. R., Haddad, L., Lawrence, D., Muir, J. F., et al. (2010). Food security: the challenge of feeding 9 billion people. *Science* 327:812. doi: 10.1126/science.1185383

Granier, C., and Vile, D. (2014). Phenotyping and beyond: modelling the relationships between traits. *Curr. Opin. Plant Biol.* 18, 96–102. doi: 10.1016/j.pbi.2014.02.009

Großkinsky, D. K., Svensgaard, J., Christensen, S., and Roitsch, T. (2015). Plant phenomics and the need for physiological phenotyping across scales to narrow the genotype-to-phenotype knowledge gap. *J. Exp. Bot.* 66, 5429–5440. doi: 10.1093/jxb/erv345

Hoeser, T., and Kuenzer, C. (2020). Object detection and image segmentation with deep learning on earth observation data: a review-part i: evolution and recent trends. *Remote Sens.* 12:1667.

Ji, C., Zou, X., Hu, Y., Liu, S., Lyu, L., and Zheng, X. (2019). Xg-sf: an xgboost classifier based on shapelet features for time series classification. *Procedia Comput. Sci.* 147, 24–28. doi: 10.1016/j.procs.2019.01.179

Jiang, Y., and Li, C. (2020). Convolutional neural networks for image-based high-throughput plant phenotyping: a review. *Plant Phenomics* 2020:4152816. doi: 10.34133/2020/4152816

Khaki, S., Wang, L., and Archontoulis, S. V. (2020). A cnn-rnn framework for crop yield prediction. *Front. Plant Sci.* 10:1750. doi: 10.3389/fpls.2019.01750

Klerkx, L., Jakku, E., and Labarthe, P. (2019). A review of social science on digital agriculture, smart farming and agriculture 4.0: new contributions and a future research agenda. *NJAS Wageningen J. Life Sci.* 90–91:100315. doi: 10.1016/j.njas.2019.100315

Laborde, D., Martin, W., Swinnen, J., and Vos, R. (2020). Covid-19 risks to global food security. *Science* 369:500. doi: 10.1126/science.abc4765

Lee, U., Chang, S., Putra, G. A., Kim, H., and Kim, D. H. (2018). An automated, high-throughput plant phenotyping system using machine learning-based plant segmentation and image analysis. *PLoS One* 13:e0196615. doi: 10.1371/journal.pone.0196615

Lin, T.-Y., Goyal, P., Girshick, R., He, K., and Dollár, P. (2017). *Focal Loss for Dense Object Detection*. Available online at: https://ui.adsabs.harvard.edu/abs/2017arXiv170802002L (accessed August 01, 2017).

Marondedze, C., Liu, X., Huang, S., Wong, C., Zhou, X., Pan, X., et al. (2018). Towards a tailored indoor horticulture: a functional genomics guided phenotypic approach. *Hort. Res.* 5:68. doi: 10.1038/s41438-018-0065-7

Milletari, F., Navab, N., and Ahmadi, S. (2016). "V-net: fully convolutional neural networks for volumetric medical image segmentation," in *Proceedings of the 2016 4th International Conference on 3D Vision (3DV)* (Stanford, CA: IEEE), 565–571.

Nagano, S., Moriyuki, S., Wakamori, K., Mineno, H., and Fukuda, H. (2019). Leaf-movement-based growth prediction model using optical flow analysis and machine learning in plant factory. *Front. Plant Sci.* 10:227. doi: 10.3389/fpls.2019.00227

Pan, J., and He, Y. (2008). "Recognition of plants by leaves digital image and neural network," in *Proceedings of the 2008 International Conference on Computer Science and Software Engineering*, Wuhan, 906–910.

R Core Team (2019). *R: A Language and Environment for Statistical Computing*. Available online at: https://www.R-project.org/ (accessed December 13, 2019).

Redell, N. (2020). *Forecastml: Time Series Forecasting With Machine Learning Methods*. Available online at: https://CRAN.R-project.org/package=forecastML (accessed May 17, 2021).

Redmond Ramin, S., Weltzien, C., Hameed, I. A., Yule, I. J., Grift, T. E., Balasundram, S. K., et al. (2018b). Research and development in agricultural robotics: a perspective of digital farming. *Int. J. Agric. Biol. Eng.* 11, 1–14. doi: 10.25165/j.ijabe.20181104.4278

Redmond Ramin, S., Fatemeh, K., Ting, K. C., Thorp, K. R., Hameed, I. A., Weltzien, C., et al. (2018a). Advances in greenhouse automation and

controlled environment agriculture: a transition to plant factories and urban agriculture. *Int. J. Agric. Biol. Eng.* 11, 1–22. doi: 10.25165/j.ijabe.20181101.3210

Ronneberger, O., Fischer, P., and Brox, T. (2015). *U-net: Convolutional Networks for Biomedical Image Segmentation*. Available online at: https://ui.adsabs.harvard.edu/abs/2015arXiv150504597R (accessed May 01, 2015).

Salas Fernandez, M. G., Bao, Y., Tang, L., and Schnable, P. S. (2017). A high-throughput, field-based phenotyping technology for tall biomass crops. *Plant Physiol.* 174:2008. doi: 10.1104/pp.17.00707

Salehi, S. S. M., Erdogmus, D., and Gholipour, A. (2017). "Tversky loss function for image segmentation using 3d fully convolutional deep networks," in *Proceedings of the International Workshop on Machine Learning in Medical Imaging* (Berlin: Springer), 379–387.

Tardieu, F., Cabrera-Bosquet, L., Pridmore, T., and Bennett, M. (2017). Plant phenomics, from sensors to knowledge. *Curr. Biol.* 27, R770–R783. doi: 10.1016/j.cub.2017.05.055

Tay, F. E. H., and Cao, L. (2001). Application of support vector machines in financial time series forecasting. *Omega* 29, 309–317. doi: 10.1016/S0305-0483(01)00026-3

van Es, S. W., van der Auweraert, E. B., Silveira, S. R., Angenent, G. C., van Dijk, A. D. J., and Immink, R. G. H. (2019). Comprehensive phenotyping reveals interactions and functions of *arabidopsis thaliana* tcp genes in yield determination. *Plant J.* 99, 316–328. doi: 10.1111/tpj.14326

Walter, A., Scharr, H., Gilmer, F., Zierer, R., Nagel, K. A., Ernst, M., et al. (2007). Dynamics of seedling growth acclimation towards altered light conditions can be quantified via growscreen: a setup and procedure designed for rapid optical phenotyping of different plant species. *New Phytol.* 174, 447–455. doi: 10.1111/j.1469-8137.2007.02002.x

Waltz, E. (2017). Digital farming attracts cash to agtech startups. *Nat. Biotechnol.* 35, 397–398. doi: 10.1038/nbt0517-397

Wang, H., Sánchez-Molina, J. A., Li, M., Berenguel, M., Yang, X. T., and Bienvenido, J. F. (2017). Leaf area index estimation for a greenhouse transpiration model using external climate conditions based on genetics algorithms, back-propagation neural networks and nonlinear autoregressive exogenous models. *Agric. Water Manage.* 183, 107–115. doi: 10.1016/j.agwat.2016.11.021

Weersink, A., Fraser, E., Pannell, D., Duncan, E., and Rotz, S. (2018). Opportunities and challenges for big data in agricultural and environmental analysis. *Annu. Rev. Resour. Economics* 10, 19–37. doi: 10.1146/annurev-resource-100516-053654

Wiese, A., Christ, M. M., Virnich, O., Schurr, U., and Walter, A. (2007). Spatio-temporal leaf growth patterns of *arabidopsis thaliana* and evidence for sugar control of the diel leaf growth cycle. *New Phytol.* 174, 752–761. doi: 10.1111/j.1469-8137.2007.02053.x

Yakubovskiy, P. (2019). *Segmentation Models*. Available online at: https://github.com/qubvel/segmentation_models (accessed February 24, 2019).

Yan, J., Mu, L., Wang, L., Ranjan, R., and Zomaya, A. Y. (2020). Temporal convolutional networks for the advance prediction of enso. *Sci. Rep.* 10:8055. doi: 10.1038/s41598-020-65070-5

Yang, W., Duan, L., Chen, G., Xiong, L., and Liu, Q. (2013). Plant phenomics and high-throughput phenotyping: accelerating rice functional genomics using multidisciplinary technologies. *Curr. Opin. Plant Biol.* 16, 180–187. doi: 10.1016/j.pbi.2013.03.005

Yu, C., Wang, J., Peng, C., Gao, C., Yu, G., and Sang, N. (2018). *Learning a Discriminative Feature Network for Semantic Segmentation*. Available online at: https://ui.adsabs.harvard.edu/abs/2018arXiv180409337Y (accessed April 01, 2018).

Zhang, R., Du, L., Xiao, Q., and Liu, J. (2020). Comparison of backbones for semantic segmentation network. *J. Phys. Conf. Ser.* 1544:012196. doi: 10.1088/1742-6596/1544/1/012196

Zhu, W., Huang, Y., Zeng, L., Chen, X., Liu, Y., Qian, Z., et al. (2019). Anatomynet: deep learning for fast and fully automated whole-volume segmentation of head and neck anatomy. *Med. Phys.* 46, 576–589. doi: 10.1002/mp.13300

Conflict of Interest: The authors declare that the research was conducted in the absence of any commercial or financial relationships that could be construed as a potential conflict of interest.

Publisher's Note: All claims expressed in this article are solely those of the authors and do not necessarily represent those of their affiliated organizations, or those of the publisher, the editors and the reviewers. Any product that may be evaluated in this article, or claim that may be made by its manufacturer, is not guaranteed or endorsed by the publisher.

frontiers in Plant Science

ORIGINAL RESEARCH
published: 23 November 2021
doi: 10.3389/fpls.2021.768717

Nutrient Dosing Framework for an Emission-Free Urban Hydroponic Production

*Tae In Ahn, Jai-Eok Park, Je Hyeong Jung, Sang Min Kim, Gyhye Yoo, Hyoung Seok Kim and Ju Young Lee**

Smart Farm Research Center, KIST Gangneung Institute of Natural Products, Gangneung, South Korea

The urban hydroponic production system is accelerating industrialization in step with the potentials for reducing environmental impact. In contrast, establishing sustainable fertilizer dosing techniques still lags behind the pace of expansion of the system. The reproducibility of root-zone nutrient dynamics in the system is poorly understood, and managing nutrients has so far primarily relied on periodic discharge or dumping of highly concentrated nutrient solutions. Here, we assayed root-zone nutrient concentration changes using three possible nutrient dosing types. Three *Brassica* species were hydroponically cultivated in a controlled environment to apply the nutrient absorption and transpiration parameters to the simulation analysis. We found that nutrient dosing based on total ion concentration could provide more reproducible root-zone nutrient dynamics. Our findings highlight the nutrient absorption parameter domain in management practice. This simplifies conventional nutrient management into an optimization problem. Collectively, our framework can be extended to fertilizer-emission-free urban hydroponic production.

Keywords: sustainability, vertical farming, fertilizer, root-zone, hydroponics, urban agriculture

OPEN ACCESS

Edited by:
Eiji Goto,
Chiba University, Japan

Reviewed by:
Roberta Bulgari,
University of Turin, Italy
Giacomo Cocetta,
University of Milan, Italy

****Correspondence:***
Ju Young Lee
jyl7318@kist.re.kr

Specialty section:
This article was submitted to Crop and Product Physiology, a section of the journal Frontiers in Plant Science

Received: *01 September 2021*
Accepted: *28 October 2021*
Published: *23 November 2021*

Citation:
Ahn TI, Park J-E, Jung JH, Kim SM, Yoo G, Kim HS and Lee JY (2021) Nutrient Dosing Framework for an Emission-Free Urban Hydroponic Production. Front. Plant Sci. 12:768717. doi: 10.3389/fpls.2021.768717

INTRODUCTION

Soil-based agriculture is facing substantial challenges such as the loss of arable land, water scarcity, nutrient leaching, and the carbon costs of transporting products. Under these circumstances, as a complementary solution, urban agriculture and vertical farming are currently being explored (Benke and Tomkins, 2017; O'Sullivan et al., 2019). The vertical farming system uses resources independently of the soil surface and expects optimal land use and environmental friendliness. In line with this, the industry is also gearing up. Recently, there has been significant investment in the urban and vertical farming industry. Traditional agribusiness, biotech, and holding companies are entering a global race for new agricultural technologies (O'Sullivan et al., 2019). Inspired by the potential of sustainability, researchers have started to explore urban vertical farming production (Seto and Ramankutty, 2016; Eshed and Lippman, 2019; Eldridge et al., 2020; Kwon et al., 2020; SharathKumar et al., 2020). However, at the same time, there are criticisms about technical pitfalls that prevent vertical farming from substantially contributing to environmental

sustainability (Russo and Cirella, 2019). In general, a vertical farming system requires a highly controlled environment in essential factors for plant growth such as light, temperature, water, and mineral nutrients (Kozai and Niu, 2016). The technological status of urban agriculture and vertical farming as a complementary approach to traditional farming is still in its infancy, and there is no solid technological framework for sustainable resource management.

A hydroponic cultivation system, a core technology of urban agriculture, also entails unsolved issues. Inevitably, in hydroponics, fertilizer and water are used intensively. For example, as standard conditions, 2–14 mM of nitrate is prepared in the smaller rooted volume (van Delden et al., 2020). However, still, periodic discharge or dumping of waste fertilizer solution is a trade-off for nutrient management. The repeated emission of concentrated nutrient solutions to the environment has long been an unsolved issue inherent to the conventional greenhouse-based hydroponic sites. Until now, most farms in the countries where there is no legal mandate do not want to take the management risk from blocking the wastewater. In South Korea, hydroponic fertilizers equivalent to nearly 7,400 kg/ha/year are consumed, and 25–30% of the supply is discharged outside the farms (Lee and Kim, 2019).

On the contrary, only about 5% of the farms use wastewater recycling systems. In Almería, Spain, one of the highest areas of greenhouse-based hydroponics, 12% in 3,000 ha of farms uses a recycling system (Massa et al., 2020). This trade-off between the nutrient solution discharge and the nutrient management is related to the concerns about unwanted deviations from standard nutrient conditions and microbial risk. In microbial risk management, a sterilizer could provide a solution (Ahn et al., 2021). On the other hand, in the root-zone, multiple essential nutrients show dynamic changes with perturbations in water absorption, one of the major driving factors of root-zone nutrient variations (Van Noordwijk, 1990; Le Bot et al., 1998). As a result, in hydroponic systems, which are most advantageous for manipulating root-zone nutrition for experiments or cropping, various root-zone nutrient fluctuations have been reported (Zekki et al., 1996; Massa et al., 2011; Signore et al., 2016; Miller et al., 2020).

Due to these seemingly complicated aspects, most hydroponic systems referenced empirical management strategies such as leaching fraction and a suitable period of reuse (Jones, 2005). In rooting medium culture, due to temporal and spatial variations in mass flow, heterogeneity of nutrient distribution remains high (De Rijck and Schrevens, 1998b; Bougoul and Boulard, 2006). Thus, this adds one more layer of complexity to the problem. Instead, in water-based hydroponic cultivation systems, the volume of water and the concentration of nutrients are the most basic and measurable physicochemical factors in root-zone management (Jones, 2005). Thus, root-zone conditioning is inevitably approached based on volume and concentration. In many studies, water level, electrical conductivity (EC, i.e., total ionic concentration), and pH have been used as standard indicators (Fanasca et al., 2006; Signore et al., 2016; Lu et al., 2017). However, it is poorly understood how the nutrient dosing methods could manage the nutrient dynamics. Previous studies have focused on on-line measurements, and several applicable technologies were provided, but it is still challenging to replace conventional nutrient management in terms of technical stability or essential ion measurements (Bratov et al., 2010; Bamsey et al., 2012). These lack of framework for understanding nutrient reproducibility according to nutrient management limits our ability to deduce resource management techniques for zero emissions.

Here we designed a hydroponic simulation model for the Michaelis–Menten equation-based simple hydroponic system with stochastic variations in transpiration rate to address this problem. Three Brassica species (curly kale, lacinato kale, and pakchoi) were hydroponically cultivated in a controlled environment to apply the nutrient absorption and transpiration parameters to the simulation model. Three commonly applicable nutrient dosing methods in the combination of volume, EC, and time were applied in the simulation study. By applying stochastic transpiration variations and the estimated parameters to the hydroponic simulation model with three nutrient dosing methods (volume-, time-, and EC + volume-based dosing), we were able to theoretically predict that the reproducible root-zone nutrient dynamics could be acquired by the EC + volume-basis nutrient dosing method. The reproducible root-zone nutrient dynamics under the stochastic transpiration variations suggest that the root-zone nutrient variations could be managed at the nutrient absorption parameter domain. Our systematic assessment shows that optimization analyses present a novel method to determine the nutrient dosing composition for standard nutrient conditions in the root-zone without periodic dumping or discharge of waste fertilizer solutions.

MATERIALS AND METHODS

Nutrient Absorption Measurement Under a Controlled Environment

Three *Brassica* plant species were used for the nutrient absorption experiment. Pakchoi (*Brassica rapa* subsp. chinensis), lacinato kale (*Brassica oleracea* L., var. acephala), and curly kale (*Brassica oleracea* L., var. sabellica) were cultivated under a controlled environment system at the Korea Institute of Science and Technology (SMART U-FARM, KIST, Gangneung, South Korea). The three *Brassica* species were simultaneously sown and grown hydroponically for 10 days. At 11 days after sowing, 84 plants of each *Brassica* species were selected and transplanted to the hydroponic growing system consisted of a single nutrient container (0.3 m^3) and cultivated for 54 days. The temperature in the growing room was controlled at 20 ± 1°C (night) and 23 ± 1°C (daytime). LED lamps (KLB-40-2C, red:blue: white = 10:3:2 ratio, KAST Engineering, South Korea) were used for daytime lighting. The LED lamps' wavelength was composed of red (660 nm), blue (440 nm), and warm white. The average photosynthetic photon flux density (PPFD) in the growing bed was 120 ± 5 μmol m^{-2} s^{-1}. Diurnal light conditions were applied (14 h daytime and 10 h dark). The average relative humidity was 73 ± 5% at night and 60 ± 4% at daytime. Carbon dioxide (CO_2) was supplied at 714 ± 40 ppm.

Macronutrient absorption was calculated by referring to Dr. Yamazaki's method (N/W) (Wada, 2019). The N/W method calculates the absorption amount based on the container's initial nutrient concentration and volume and a concentration and a volume of each nutrient at the end of the given period (**Figure 1A**). On a weekly basis, the initial macronutrients (K, Ca, Mg, NO_3, H_2PO_4, and SO_4) concentrations were analyzed, and the water volume of the nutrient solution container was measured as the initial condition of the system. For NO_3^-, $H_2PO_4^-$, and SO_4^{2-} analysis, ion chromatography was performed (730 Professional IC, Metrohm, Switzerland). K^+, Ca^{2+}, and Mg^{2+} were analyzed using an inductively coupled plasma-optical emission spectrophotometer (ICP-OES, PerkinElmer SCIEX, United States). All the analytical procedures were validated using certified internal reference materials and the average concentration values were obtained by three repeated measurements. The replenishment of the nutrient solution during the week was not performed. At the end of the week, the final macronutrient concentrations were analyzed, and the water volume of the nutrient solution container was measured as the final condition of the system. After the final value was measured, the container's nutrient solution was replaced entirely with the fresh nutrient solution. The initial nutrient condition composition of macro-elements (K, Ca, Mg, NO_3, H_2PO_4, and SO_4) was established by referring to the percentage equivalent ratios of anions and cations in Steiner's universal nutrient solution (Steiner, 1980; Jones, 2005). The total ion equivalent concentration of the initial nutrient solution was provided at 26.1 ± 3.8 meq L^{-1} (7.5 ± 1.0, 3.0 ± 1.4, 2.5 ± 1.1, 4.0 ± 0.4, 1.9 ± 0.4, and 1.4 ± 0.2 mM of NO_3^-, $H_2PO_4^-$, SO_4^{2-}, K^+, Ca^{2+}, and Mg^{2+}) and the initial nutrient conditions distributing around Steiner's standard ratio (NO_3^-: 60%, $H_2PO_4^-$: 5%, SO_4^{2-}: 35%, K^+: 35%, Ca^{2+}: 45%, Mg^{2+}: 20%) were established to estimate the average level of nutrient absorption parameters. The micronutrients in the nutrient solution were Fe, B, Mn, Cu, Zn, and Mo at 2.80, 0.32, 0.77, 0.04, 0.02, and 0.02 ppm, respectively.

Hydroponic System Model

In the present study, a simple hydroponic system model was designed. The simulation scale of nutrients and water in the model was taken equal to the experiment's hydroponic system specification. In the model, we considered nutrient dosing methods, nutrient absorption kinetics, the transpiration rate,

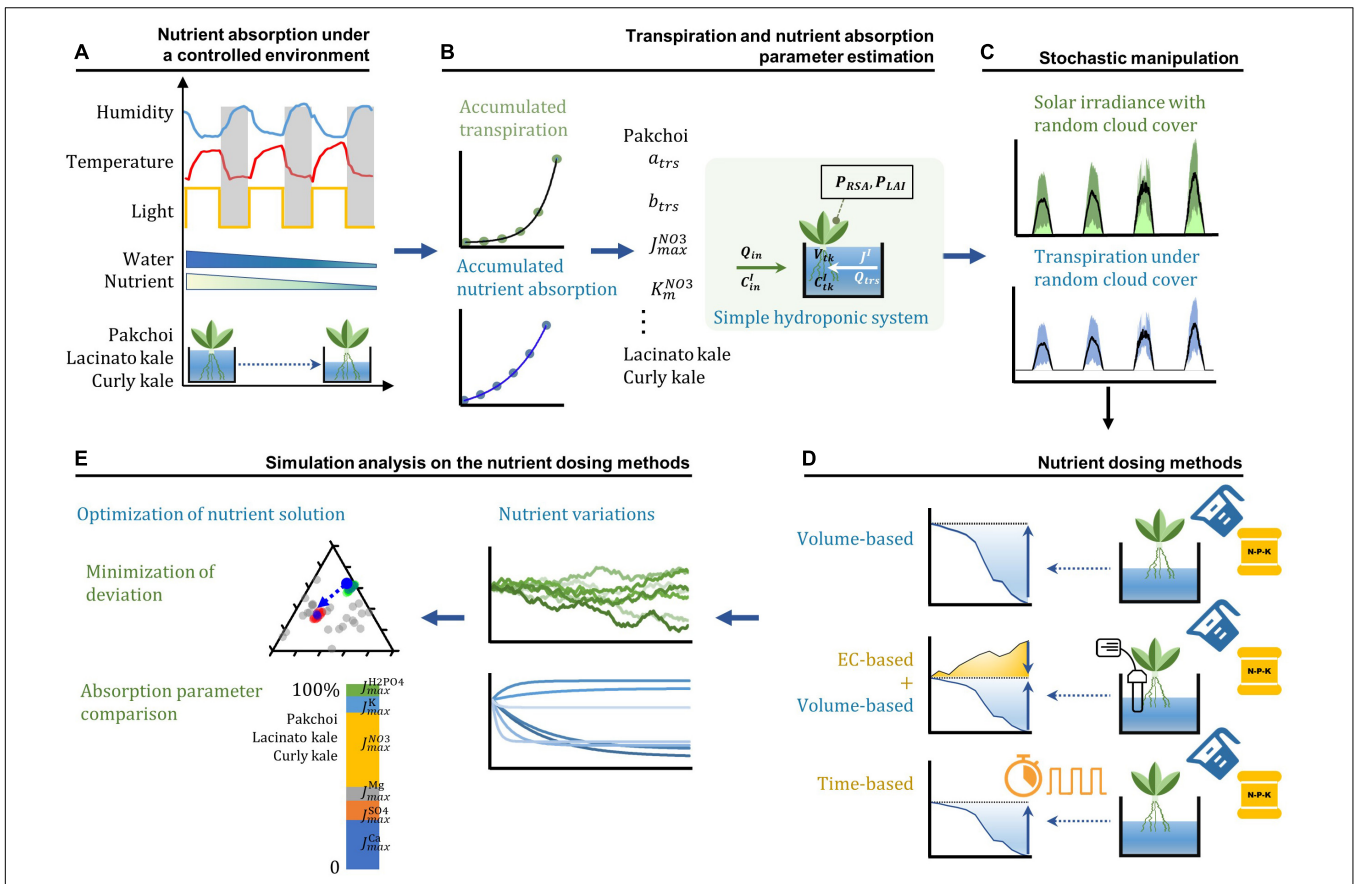

FIGURE 1 | The workflow of the theoretical and experimental analysis setup. **(A)** Nutrient absorption measurement of three *Brassica* species under a controlled environment. **(B)** Parameter estimation process under the simple hydroponic system model by using the progress curve analysis. **(C)** Stochastic manipulation of solar irradiance with a random walk generated cloud cover and subsequent transpiration rate variations in the simple hydroponic system model. **(D)** Three nutrient dosing processes in the simulation analysis. **(E)** Simulation analysis of the nutrient dosing effects on the nutrient variations and nutrient solution optimization.

and nutrient and water absorption capacity variations due to plant growth.

The nutrient dynamics in the hydroponic system can be expressed as follows:

$$V_{tk}\frac{dC^I_{tk}}{dt} = Q_{in}C^I_{in} - J^I \quad (1)$$

where V_{tk} is the water volume (m^3) in the nutrient solution tank of the hydroponic system, C is the nutrient concentration (mol m^{-3}), superscript I is the type of nutrients (K, Ca, Mg, NO_3, H_2PO_4, and SO_4), and Q is the flow rate (m^3 h^{-1}) of water to the nutrient solution tank. Subscript *tk* and *in* represent nutrient solution tank and dosing, respectively, and indicate the variables' location.

Water volume in the nutrient solution tank of the hydroponic system can be expressed as follows:

$$\frac{dV_{tk}}{dt} = Q_{in} - Q_{trs} \quad (2)$$

where Q_{trs} is the transpiration rate per plant (m^3 h^{-1} $plant^{-1}$).

The Michaelis-Menten equation has been used widely in representing the plant's nutrient absorption behavior (Le Bot et al., 1998). The following equation can express nutrient absorption variation along with plant growth:

$$J^I = P_{RSA}\frac{J^I_{max}C^I}{K^I_m + C^I} \quad (3)$$

where P_{RSA} is root surface area (m^2), J^I is the nutrient absorption rate (mol m^{-2} h^{-1}), J^I_{max} (mol m^{-2} h^{-1}) is the maximum absorption rate of nutrient I, and K^I_m (mol) is the Michaelis-Menten parameter. In this model, the nutrient absorption dynamics are described by the function of nutrient concentrations and root growth (Silberbush et al., 2005).

The root surface area P_{RSA} was assumed to smooth cylinders and calculated with root length and constant mean radius, and the root length variation is modeled using a logistic function of time (Barber, 1995):

$$P_{RL} = \frac{R_{max}}{1 + K_1 e^{-k_1 t}} \quad (4)$$

$$P_{RSA} = 2\pi r_0 P_{RL} \quad (5)$$

where P_{RL} is the root length (m), R_{max} is the maximal root length (m), K_1 and k_1 are coefficients, r_0 is the mean root radius (m), and t is the elapsed time (h).

For the transpiration model, the Penman–Monteith equation can be used to predict transpiration by crops.

We used the empirical version of the Penmen–Monteith equation (Bailey et al., 1993; Choi and Shin, 2020). In this model, the transpiration rate is mainly determined by the solar irradiance, the vapor pressure deficit (VPD), and plant growth by the following equation:

$$Q_{trs} = a_{trs}\left(1 - e^{-k_{ext}P_{LAI}P_{VPD}}\right)K^+ + b_{trs}P_{LAI}P_{VPD} \quad (6)$$

$$P_{LAI} = \frac{a_{LAI}}{\left[1 + e^{\frac{x_0 - t}{b_{LAI}}}\right]} \quad (7)$$

where a_{trs} and b_{trs} are empirical coefficients, k_{ext} is the extinction coefficient in the plant canopy, K^+ is the solar irradiance (W m^{-2}), P_{LAI} is the leaf area index (LAI), and P_{VPD} is VPD (kPa). The Boltzmann sigmoid equation was used to express LAI variations. a_{LAI}, b_{LAI}, and x_0 are the empirical coefficient.

The parameters used in this model were estimated by a progress curve analysis that estimates the value that minimized the root mean square error (RMSE) between the measured and simulated values. In the parameter estimation process, PPFD and relative humidity variations during the day/night cycle were converted to a radiometric unit (W m^{-2}) and VPD (kPa). W m^{-2} was obtained by dividing PPFD by the conversion constant of warm-white fluorescent (Thimijan and Heins, 1983). VPD was calculated by the vapor pressure equation (Choi and Shin, 2020). Transpiration and nutrient absorption data measured in the controlled environment condition were applied for the estimation of the parameters (**Figure 1B**).

Stochastic Manipulation of Transpiration Rate

Under the hydroponic system model's verified condition, the stochastic changes in the transpiration rate were applied (**Figure 1C**). The transpiration model used in this study could be mainly driven by solar irradiance and VPD. Thus, the stochastic seasonal variations in solar radiation and VPD could generate dynamic changes in the transpiration, nutrient concentration, and water content in the hydroponic system. The dynamic changes in incoming solar radiation could be modeled by the total cloud cover model based on solar elevation (Holtslag and Van Ulden, 1983). The framework for stochastic changes in the incoming solar radiation model and VPD was referred to water dynamics model of an automated soilless irrigation system (Ahn et al., 2021). In this model, solar irradiance is the incoming solar radiation at ground level under the total cloud cover, and the dynamic weather changes were simulated by moving the cloud cover in a random walk process. In the case of stochastic changes in VPD, the model simulates a random walk process between 0.5 and 2.0 kPa. However, in this study, the model parameter estimation was conducted under controlled environmental conditions, and the solar irradiance level could largely deviate from the experimental condition. Thus, the solar irradiance was reduced to distribute the simulated transpiration around the measured transpiration rate.

Simulation Analysis

We examined the reproducibility of the root-zone nutrient dynamics according to the nutrient dosing methods with these models. Three conventional nutrient dosing methods were considered in this analysis: (1) volume-based, (2) time-based, and (3) EC + volume-based (**Figure 1D**). The volume-based dosing method routinely supplies the standard nutrient solution based on the nutrient solution's initial volume. The consumed water and nutrients are compensated at the dosing time by supplying

the standard nutrient solution to the container's initial nutrient solution volume. The time-based dosing method supplies a fixed amount of nutrients at a fixed rate. EC + volume-based dosing method estimates total ionic concentration and compensates consumed total mineral nutrients to the initial value, and supplies water to the container's initial nutrient solution volume.

Under the reproducible nutrient dynamics condition in this simulation analysis, the optimization analysis was conducted to seek the standard nutrient solution for the least deviating from the initial root-zone nutrient condition (**Figure 1E**). The optimization analysis was carried out in the same way as the parameter estimation by the progress curve analysis in this study. During the process, the molar nutrient concentrations were converted to the percentage molar ratios between the nutrients. Therefore, in this way, it was made to be approached by the scaling relationship of a plant stoichiometric perspective. The mean values of estimated nutrient absorption parameters from three *Brassica* species were converted to the percentage molar ratios and compared in this perspective.

RESULTS

The overall increase in weekly transpiration and nutrient absorption rate was observed in the three *Brassica* species as the cultivation proceeded (**Figure 2**). Differences among the three *Brassica* species' transpiration and nutrient absorption rates were observed to be in the order of pakchoi > lacinato kale > curly kale. NO_3 was the most absorbed nutrient in all plants. The difference in absorption rate among individual nutrients was similar in all plant species, except SO_4. SO_4 absorption amounts were distinctively higher in lacinato and curly kale than in pakchoi.

Using the measured data in **Figure 2A**, the transpiration parameters were estimated. The estimated transpiration parameters for pakchoi, lacinato kale, and curly kale simulated the amount of accumulated transpiration at the RMSE 1.35×10^{-5}, 1.62×10^{-5}, and 2.09×10^{-5} m^3 $plant^{-1}$, respectively (**Figure 3A**). The amount of accumulated transpiration was in the order, pakchoi > lacinato kale > curly kale, similar to the measurements. The calibrated transpiration model provided a good description of the water volume behavior in the nutrient container of pakchoi, curly kale, and lacinato kale at an RMSE of 1.43×10^{-2}, 8.78×10^{-3}, 1.35×10^{-2} m^3 (**Figure 3B**). As explained in the "Materials and Methods" section, the water stored in the nutrient container was replaced weekly, and the simulation model showed the periodical replacement of reservoir water and subsequent water consumption by transpiration until the next water replacement.

The estimated Michaelis-Menten parameters for nutrient absorption simulated the accumulated nutrient absorption with good agreement with the measured data (**Figure 4A**). RMSEs for the three species ranged from 4.60×10^{-5} to 8.09×10^{-5} mol $plant^{-1}$ in K, 3.06×10^{-5} to 4.14×10^{-5} mol $plant^{-1}$ in Ca, 1.73×10^{-5} to 5.38×10^{-5} mol $plant^{-1}$ in Mg, 4.62×10^{-4} to 5.09×10^{-4} mol $plant^{-1}$ in NO_3, 2.70×10^{-5} to 8.42×10^{-5} mol $plant^{-1}$ in H_2PO_4, and 2.56×10^{-5} to 9.31×10^{-5} mol $plant^{-1}$ in SO_4. With these nutrient absorption model calibrations, the simulated nutrient concentrations showed a good description of the measured nutrient concentration behavior in the water reservoir (**Figure 4B**). The percentage molar ratio of the initial nutrient conditions after the weekly used nutrient solution was distributed around Steiner's standard percentage molar ratios (**Figure 4C**).

The effect of the three nutrient dosing methods (volume-, time-, and EC + volume-based) under stochastic transpiration variations is shown in **Figures 5A–C**. Here, the pakchoi model parameters, which have the highest absorption capacities for nutrients and transpiration, were used as a representative for analyzing the nutrient dosing effect. The root-zone response to volume-based dosing was not monotonic (**Figure 5A**). As the simulation proceeded, various routes of root-zone nutrient changes were simulated in volume-based dosing conditions. The EC + volume- and time-based methods showed reproducible and deterministic changes in the root-zone nutrients (**Figures 5B,C**). However, while time-based dosing showed similar variations to EC + volume-based dosing, overall decreasing tendencies in nutrient concentration were observed (**Figure 5B**). The percent coefficient of variation (% CV) summarizes the variation attributes of each dosing method (**Figure 5D**). The EC + volume- and time-based methods showed the lowest % CV. **Figures 5A–C** also illustrates the nutrient dosing rates. Volume-based dosing showed an irregular dosing rate, time-base dosing showed a constant dosing rate, and EC + volume-based dosing rate gradually increased as the simulation proceeded. During the simulation analysis, most of the stochastic transpiration rates generated by the random-walk cloud cover distributed within a similar range of the measured transpiration rate (**Figure 5E**).

Figure 6 illustrates EC + volume-based dosing to control the root-zone nutrients according to the standard nutrient composition input. When the nutrient dosing composition was the same as the standard nutrient composition, the three *Brassica* species' root-zone nutrient variations were reproducible and deterministic (**Figure 6A**), as shown in **Figure 5C**. However, they inevitably deviated from the initial nutrient composition (i.e., standard nutrient composition) (**Figure 5C**). On the other hand, the nutrient dosing composition acquired by optimization analysis to achieve minimal deviation of the root-zone nutrients from the standard composition provided approximately constant root-zone nutrients close to the initial nutrient conditions (i.e., standard nutrient composition) (**Figures 6B,D**). The conversion of the root-zone nutrient variations, optimized nutrient dosing composition, and the standard nutrient composition into mutual nutrient ratios displayed a plant stoichiometric scaling relationship among the nutrients (**Figures 6E,F**). The ternary graph of the percentage molar ratio of nutrients distinctively visualized effects of input nutrient ratio on the output nutrient ratio. **Figure 6** also summarizes the relationship between the dosing nutrient composition and the standard nutrient composition. This result shows that a dosing nutrient composition identical to the standard nutrient composition does not result in standard nutrient conditions in the root-zone. The dosing nutrient compositions determined by the optimization analysis were nutrient solutions that least deviated from the

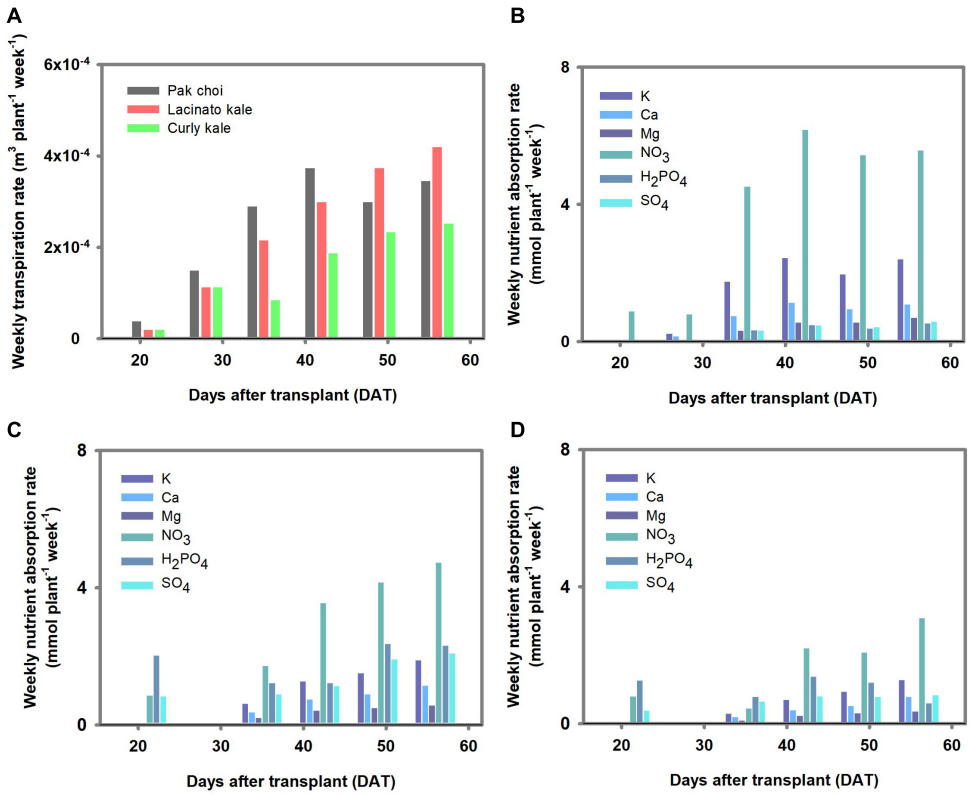

FIGURE 2 | Transpiration and nutrient absorption rate estimated in the controlled environment experiment. **(A)** Weekly transpiration rate of three *Brassica* species. The weekly nutrient absorption rate of pakchoi **(B)**, lacinato kale **(C)**, and curly kale **(D)**.

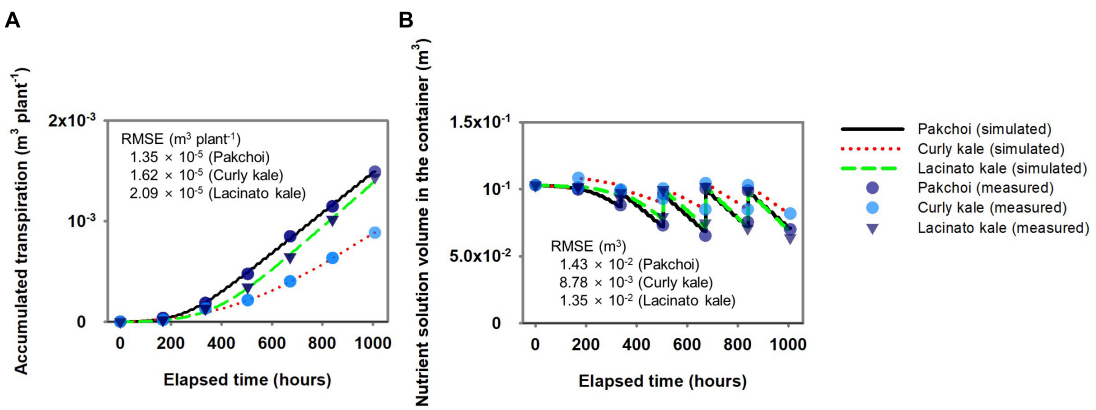

FIGURE 3 | Comparison between simulated and measured accumulated transpiration **(A)** and subsequent changes of nutrient solution volume changes in the nutrient solution container **(B)** for verifying the simple hydroponic system model.

standard nutrient conditions. The hydroponic systems in which the three *Brassica* species were cropped were simulated using the estimated nutrient uptake parameters.

Figures 7A,C illustrates the means, standard deviations, and % CV of the three *Brassica* species' J_{max} parameters. **Figures 7B,D** shows the conversion of the J_{max} parameters to percentage molar ratio and summarizes the means, standard deviations, and % CV of the three *Brassica* species' J_{max} ratios. The J_{max} for NO_3 was the highest of three *Brassica*'s means, and the mean J_{max} for K, SO_4, Ca, Mg, and H_2PO_4 followed in that order. However, relatively high % CVs were observed for K, Ca, Mg, NO_3, and H_2PO_4 which differ the % CVs of percentage molar ratio of J_{max} between nutrients. The J_{max} conversion to percantage molar ratio reduced the % CV for K, Ca, Mg, NO_3, and H_2PO_4, and increased that of SO_4. Overall, the mean % CV for V_{max} was reduced from 61 to 41% when J_{max} was converted to percentage molar ratio.

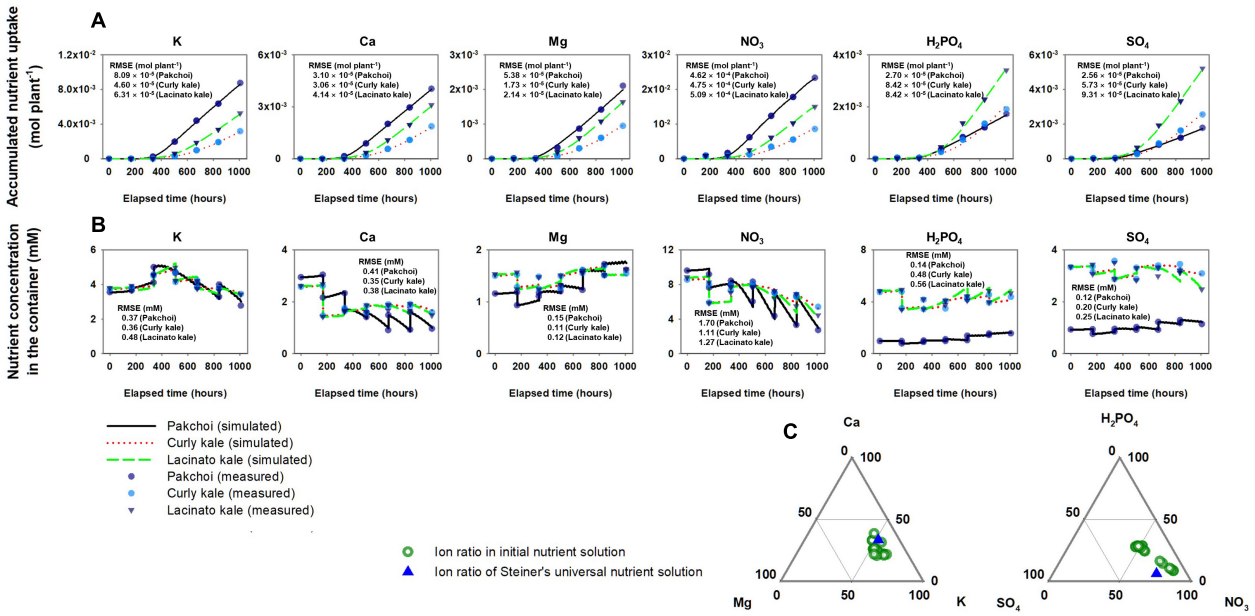

FIGURE 4 | Comparison between simulated and measured accumulated nutrient absorption of three *Brassica* species **(A)** and subsequent nutrients molar concentrations in the hydroponic system's nutrient solution container **(B)**. **(C)** Distribution of percentage molar ratio of cations and anions in the nutrient solution container's initial nutrient solution after replacing the weekly used nutrient solution around the Steiner's standard percentage molar ratios.

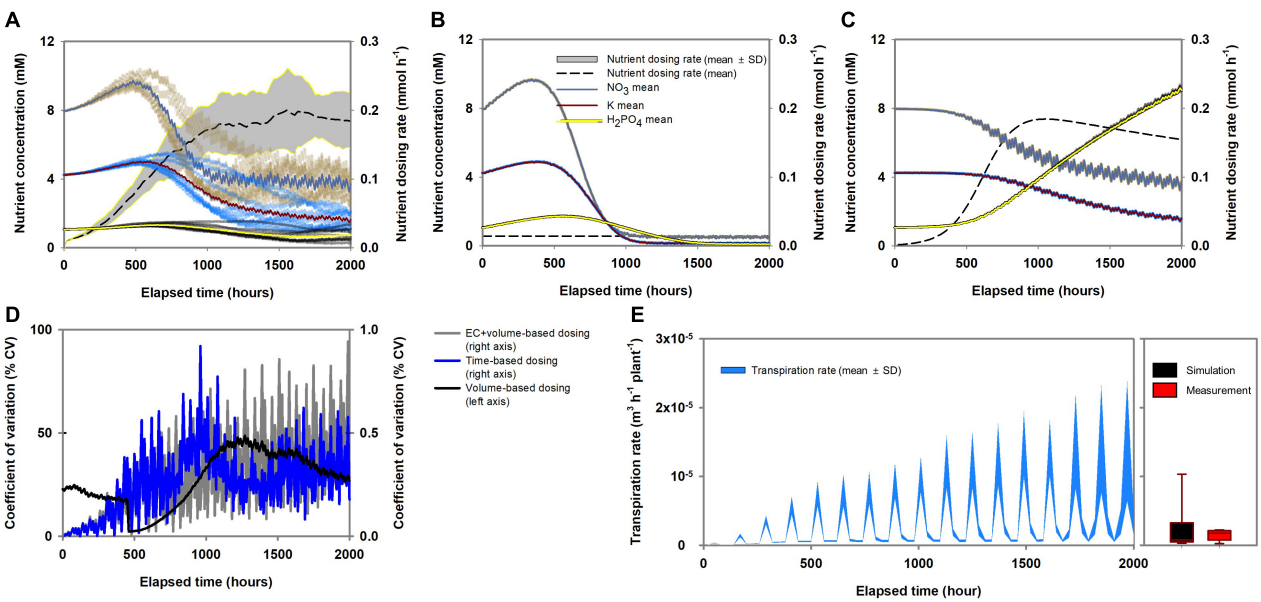

FIGURE 5 | Characteristics of variations in root-zone nutrient concentration according to the nutrient dosing methods (pakchoi parameter applied simulation): **(A)** volume-based, **(B)** time-based, and **(C)** EC + volume-based methods. **(D)** The percent coefficient of variation of root-zone nutrient concentration according to the nutrient dosing methods. **(E)** Level of stochastic changes in the transpiration rate during the simulation analysis and box-plot comparing the distribution of the simulated transpiration rate (pakchoi parameter applied simulation) and the measured transpiration rate of pakchoi.

DISCUSSION

Our theoretical analyses on nutrient dosing and root-zone nutrients provide insight into root-zone nutrient dynamics. Currently, nutrient dosing and time-dependent root-zone nutrient dynamics are considered as steady-state. However, by systematically varying the transpiration rate in the Michaelis-Menten nutrient absorption-based hydroponic system model, we could theoretically predict the appropriate nutrient dosing method for acquiring reproducible root-zone nutrient dynamics.

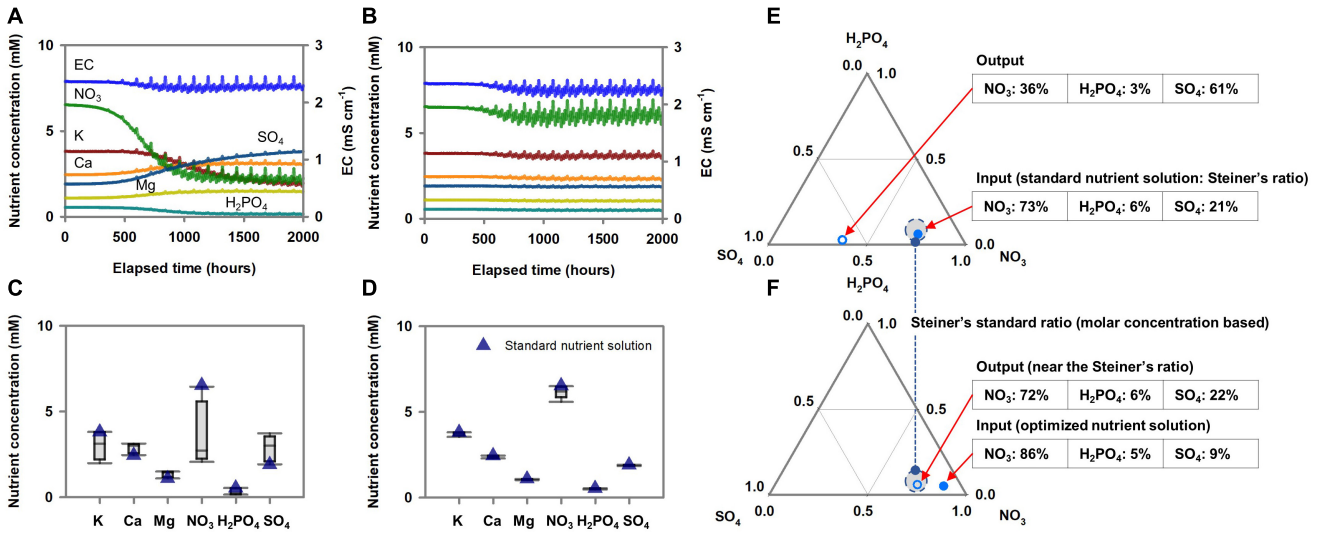

FIGURE 6 | Optimization results of a standard nutrient solution for acquiring the reproducible and least deviating root-zone nutrient dynamics from the initial nutrient condition under the EC+volume-based nutrient dosing method. **(A)** Changes in root-zone nutrients concentration when the nutrient dosing was performed as a nutrient solution with a conventional standard nutrient solution. **(B)** Changes in root-zone nutrients concentration when the nutrient dosing was performed as an optimized nutrient solution. **(C)** Box-plot of the nutrient distribution during the nutrient dosing simulation with a nutrient solution with a conventional standard nutrient concentration. **(D)** Box-plot of the nutrient distribution during the nutrient dosing simulation with an optimized nutrient solution. **(E)** The percentage molar ratio's final simulation output under the nutrient dosing condition of a conventional standard nutrient ratio input (Steiner's ratio). **(F)** The percentage molar ratio's final simulation output under the nutrient dosing condition of an optimized nutrient ratio input.

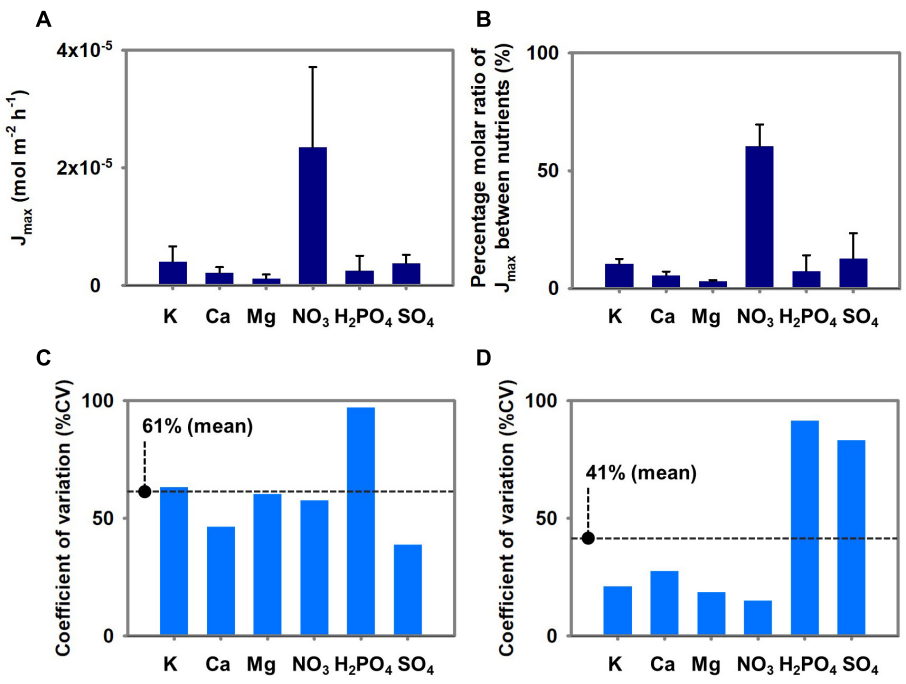

FIGURE 7 | (A) Mean ± SD of J_{max} of three *Brassica* species (pakchoi, lacinato kale, and curly kale). **(B)** Percentage molar ratio between J_{max} of the nutrients. **(C)** The percent coefficient of variation among the J_{max} of three *Brassica* species. **(D)** The percent coefficient of variation among the percentage molar ratio between J_{max} of the nutrients.

To our knowledge, only a few studies have theoretically analyzed root-zone nutrient dynamics in the hydroponic system. Heinen (1997) constructed a hydroponic simulation model and analyzed the system's solute flux and distribution characteristics. Silberbush and Ben-Asher (2001) and Silberbush et al. (2005) developed a simplified hydroponic system model and analyzed nutrient concentration changes and ballast ion accumulation (Na and Cl). Hydroponic systems are essential for plant science and agricultural technologies because of their advantages in manipulating root-zone nutrients. However, root-zone nutrients are sensitive to perturbations. By elucidating plant stoichiometry and nutrient dynamics, root-zone nutrient dynamics offer new avenues for research and exploitation of dynamics in agricultural systems. However, little is known on the reproducibility of root-zone nutrient variations, which is essential for harnessing plant nutritional dynamics.

Our hydroponic system model with stochastic transpiration variation will enable us to examine the consequences of nutrient dosing in the root-zone. In addition to water absorption by plants, the root-zone nutrients could be affected at the microscopic scale. In the solute pathway from the external solution into root cells, ion diffusivity (Leitner et al., 2010), metabolic activity (Swift et al., 2020), and ion interaction (Munns and Tester, 2008) can affect nutrient influx, subsequently changing nutrient conditions in the root zone. However, in our study, we focused on the root-zone nutrient perturbation caused by transpiration since water absorption is a significant source of root-zone nutrients (Van Noordwijk, 1990; Le Bot et al., 1998). Macroscopic-scale nutrient variations caused by transpiration are frequently reported in in-field cultivation experiments (Shin and Son, 2016).

The reproducibility of nutrient dynamics determined by volume-, time-, and EC + volume-based dosing methods under stochastic transpiration variations revealed clearly distinct trends (**Figures 5A–C**). The reproducibility observed in the EC + volume- and time-based dosing methods suggests that the root-zone inconsistencies caused by the transpiration variations could be eliminated through periodic compensation of total nutrient absorption or a constant nutrient influx at the hydroponic system boundary. However, while the time-based periodical dosing showed reproducibility in terms of root-zone nutrients, the overall nutrients showed decreasing tendencies (**Figure 5B**). Notably, with time-based dosing, most nutrients displayed a steady-state. However, depending on the dosing interval or amount, the level of steady-state nutrients could be generally lower or higher than the initial root-zone nutrients. This observation is consistent with the findings of an agricultural experiment involving constant and periodical Mn and Zn dosing (Tzerakis et al., 2012). In the aforementioned study, Mn and Zn showed a gradual increase in the root-zone solution, leveling off after a certain period. In discrete time, a steady-state indicates that influx and efflux are equal in a system. A system that follows a Michaelis-Menten-based mechanism could have a steady-state solution (Golicnik, 2011). Thus, it could be concluded that the time-based nutrient dosing provided constant and periodical influx to the system, and the efflux, i.e., the nutrient absorption rate, approached the constant and periodical influx. However, in this case, the constant nutrient dosing could not follow the increasing nutrient absorption capacity of the plant. Therefore, fluctuations in the root-zone nutrients from their initial condition were observed.

As reported in previous studies, transpiration could destabilize the ratio between nutrient and water absorption; hence, root-zone nutrients significantly fluctuate along with water absorption variations (Van Noordwijk, 1990; Le Bot et al., 1998). The transpiration phenomenon is indicative of plant characteristics such as leaf area and stomatal conductivity; however, under normal growth conditions, transpiration is primarily driven by atmospheric environmental conditions (Pieruschka et al., 2010). Therefore, although we conducted experiment under controlled environmental conditions, the stochastic aspects between atmospheric dynamics and transpiration need to be considered in the simulation analysis. The root-zone nutrient variations observed under volume-based dosing conditions suggest the method is unsuitable for providing reproducible root-zone nutrient conditions. In the present study, we created stochastic transpiration variation by random-walk cloud cover in a periodic solar radiation model, revealing that although transpiration is a periodic phenomenon, root-zone nutrients will diverge even under stochastic fluctuations within the transpiration cycle. The volume-based dosing rate is determined by the water volume removed from the root-zone (Signore et al., 2016) while the standard nutrient composition is transported by the water flux to the system. Consequently, nutrient influx varies with transpiration variation and an irregular nutrient influx applied at the system boundary of the root-zone. Such root-zone nutrient behaviors has been reported in a study involving volume-based nutrient dosing (Signore et al., 2016). The root-zone nutrients displayed a wide range of variation when the nutrient dosing treatments were performed based on the water volume, indicating that root-zone nutrients can follow different time-series changes depending on the transpiration variations.

Similar to time-based dosing, EC + volume-based nutrient dosing generated reproducible time-series changes in the root-zone nutrients (**Figure 5C**). The dosing rate gradually increased as the simulation proceeded, indicating that the EC + volume-based nutrient dosing compensated for the increasing capacity for total nutrient absorption by plants. In contrast to the time-based nutrient dosing, nutrient dosing rates varied with plant growth; the total nutrients in the root-zone removed by the plant were periodically compensated by dosing. The kinetics of nutrient transport in plant roots are mostly determined by nutrient transporters (Swift et al., 2020). Therefore, total nutrient absorption approximately follows the influx kinetics of the total nutrients into the root cells. On the kinetics of nutrient transport in plant roots, nutrient selectivity could be conceptualized as the individual nutrient influx as regulated by the proportion of each nutrient's transporter on the root surface and transporter affinity (Menge et al., 2011). Therefore, periodical compensation of total nutrient absorption by EC + volume-based dosing could reveal the proportion of nutrient absorption transporters.

Consequently, both constant periodical time-based and EC + volume-based dosing minimize the perturbation caused by

transpiration variations and reveal the kinetics aspect of nutrient absorption. However, time-based dosing does not account for the plant's increasing nutrient absorption capacity in dosing equations. As a result, reproducibility but with overall decreases or increases from the initial root-zone variation is observed depending on the dosing interval or amount (**Figure 5B**). In contrast, EC + volume-based dosing periodically matched the total nutrient influx to the root cell. From a theoretical perspective, these results suggest that this dosing practice can eliminate the two unknown variables effects (transpiration and total nutrient absorption variations) from the root-zone system boundary. Therefore, this indicates that the uncertainty in the root-zone nutrient dynamics could be filtered down to the level of the relative variations between the proportions of Michaelis-Menten parameters. Accordingly, the dosing nutrient composition for minimal deviation of root zone nutrients from the standard nutrient composition could be acquired by an optimization analysis (**Figures 6B,D,F**). Specifically, investigating optimal nutrient proportions in the dosing nutrient solution, which result in root-zone nutrients deviating the least from the standard nutrient composition, corresponds to a process for matching dosing nutrient proportions to the Michaelis-Menten parameter proportions.

This new perspective suggests that an optimization analysis can be used as a novel method to determine the nutrient dosing composition for generating the standard nutrient conditions in the root-zone. Conventionally in plant science, the standard nutrient solution has been routinely supplied to establish standardized root-zone nutrient conditions (De Rijck and Schrevens, 1998a). However, our simulation analysis indicates that a difference in nutrient dosing practice can lead to alterations in root-zone nutrients even when dosing with standard nutrient compositions. Furthermore, in the EC + volume-based dosing, a dosing nutrient composition identical to the standard nutrient composition does not result in standard nutrient conditions in the root-zone (**Figures 6A,C,E**). However, based on its reproducibility and proportional approach to the dosing nutrient composition and the Michaelis-Menten parameters, a dosing nutrient composition that results in minimal deviation of the root zone nutrients from the standard nutrient composition could be acquired (**Figures 6B,D,F**). Thus, in an on-site hydroponic system, a standardized and simplified nutrient management process might also be deduced from this perspective; for example, in a hydroponic system in operation, simple feedback of the nutrient proportion differences between the used solution and target composition proportion into the next dosing solution could expect the formation of stabilized root zone nutrient variability centered on the target proportion.

The variation in the Michaelis-Menten nutrient uptake parameters and how they affect the root-zone nutrients were not addressed as this was beyond the scope of the present study. However, we note the scaling relationships of nutrient and parameter proportions considered in our study. In the experiment, pakchoi, lacinato kale, and curly kale's nutrient absorption capacity varied widely among the species (**Figures 2B**, **4A**). On the contrary, significant reductions in % CVs were observed when the J_{max} of the three *Brassica* species were converted into a ratio between K, Ca, or Mg, NO_3, and H_2PO_4 's J_{max} (**Figure 7D**). On the other hand, the % CV of the J_{max} proportion increased with SO_4. These proportion variations resulted in the stoichiometric proximity of K, Ca, Mg, NO_3, and H_2PO_4, in the three *Brassica* species. We studied three *Brassica* species, and these are not meant to represent all vegetable species. However, the relative proportion of plant nutrients has been examined by plant stoichiometry, providing a scaling relationship of nutrient balances from plant nutrient variations (Parent et al., 2013). In the past, many standard nutrient solutions have been developed and widely used for plant science and agricultural cropping. These nutrient solutions have some differences in macronutrient concentrations; however, for most of them, the relative proportions of cations and anions indicate stoichiometric proximity (De Rijck and Schrevens, 1998a). Nevertheless, the mechanisms of stoichiometric homeostasis and the nutrient solutions' physiological costs remain under investigation (Rouached and Rhee, 2017). The scaling relationship observed from a stoichiometric perspective across plant systems by the proportion approaches suggests a potential for an integrated framework for plant nutrient dynamics research.

CONCLUSION

Our simulation analysis provided some clarity regarding root-zone nutrient dynamics using Michaelis-Menten parameters. Subsequently, based on the reproducibility of nutrient dosing, our simulation analysis predicted a proportion approach to the dosing nutrient composition and Michaelis-Menten parameters as a novel method of manipulating root-zone nutrient dynamics. This may turn conventional nutrient management practices into a simplified optimization problem. From the reduced complexity, we can expect to have a theoretical background to build a seamless framework for exploiting plant nutrient dynamics in the agronomic field and plant research. The framework presented here may provide a platform extended to fertilizer-emission-free agricultural production and plant stoichiometric research.

DATA AVAILABILITY STATEMENT

The raw data supporting the conclusions of this article will be made available by the authors, without undue reservation.

AUTHOR CONTRIBUTIONS

TA and JL designed the research. J-EP and GY performed the research. JJ, SK, and HK analyzed the data. TA wrote the article. All authors contributed to the article and approved the submitted version.

FUNDING

This work was supported by Korea Institute of Planning and Evaluation for Technology in Food, Agriculture and Forestry

(IPET) and Korea Smart Farm R&D Foundation (KosFarm) through Smart Farm Innovation Technology Development Program, funded by Ministry of Agriculture, Food and Rural Affairs (MAFRA) and Ministry of Science and ICT (MSIT), Rural Development Administration (RDA) (Nos. 421006-03-1-HD040-KIST and 421039-03-1-HD020-KIST).

REFERENCES

Ahn, T. I., Yang, J.-S., Park, S. H., Im, Y.-H., and Lee, J. Y. (2021). Nutrient recirculating soilless culture system as a predictable and stable way of microbial risk management. *J. Clean Prod.* 298:126747. doi: 10.1016/j.jclepro.2021.126747

Bailey, B. J., Montero, J. I., Biel, C., Wilkinson, D. J., Anton, A., and Jolliet, O. (1993). Transpiration of *Ficus benjamina*: comparison of measurements with predictions of the Penman Monteith model and a simplified version. *Agric. For. Meteorol.* 65, 229–243. doi: 10.1016/01681923(93)90006-4

Bamsey, M., Graham, T., Thompson, C., Berinstain, A., Scott, A., and Dixon, M. (2012). Ion-specific nutrient management in closed systems: the necessity for ion-selective sensors in terrestrial and space-based agriculture and water management systems. *Sensors* 12, 13349–13392. doi: 10.3390/s121013349

Barber, S. A. (1995). *Soil Nutrient Bioavailability: A Mechanistic Approach*. New York, NY: John Wiley and Sons.

Benke, K., and Tomkins, B. (2017). Future food-production systems: vertical farming and controlled-environment agriculture. *Sustain. Sci. Pract. Policy* 13, 13–26. doi: 10.1080/15487733.2017.1394054

Bougoul, S., and Boulard, T. (2006). Water dynamics in two rockwool slab growing substrates of contrasting densities. *Sci. Hortic.* 107, 399–404. doi: 10.1016/j.scienta.2005.11.007

Bratov, A., Abramova, N., and Ipatov, A. (2010). Recent trends in potentiometric sensor arrays-a review. *Anal. Chim. Acta* 678, 149–159.

Choi, Y. B., and Shin, J. H. (2020). Development of a transpiration model for precise irrigation control in tomato cultivation. *Sci. Hortic.* 267:109358. doi: 10.1016/j.scienta.2020.109358

De Rijck, G., and Schrevens, E. (1998b). Distribution of nutrients and water in rockwool slabs. *Sci. Hortic.* 72, 277–285. doi: 10.1016/s0304-4238(97)00144-1

De Rijck, G., and Schrevens, E. (1998a). Comparison of the mineral composition of twelve standard nutrient solutions. *J. Plant Nutr.* 21, 2115–2125. doi: 10.1080/01904169809365548

Eldridge, B. M., Manzoni, L. R., Graham, C. A., Rodgers, B., Farmer, J. R., and Dodd, A. N. (2020). Getting to the roots of aeroponic indoor farming. *New Phytol.* 228, 1183–1192. doi: 10.1111/nph.16780

Eshed, Y., and Lippman, Z. B. (2019). Revolutions in agriculture chart a course for targeted breeding of old and new crops. *Science* 366:eaax0025. doi: 10.1126/science.aax0025

Fanasca, S., Colla, G., Maiani, G., Venneria, E., Rouphael, Y., Azzini, E., et al. (2006). Changes in antioxidant content of tomato fruits in response to cultivar and nutrient solution composition. *J. Agric. Food Chem.* 54, 4319–4325. doi: 10.1021/jf0602572

Golicnik, M. (2011). Exact and approximate solutions for the decades-old Michaelis-Menten equation: progress-curve analysis through integrated rate equations. *Biochem. Mol. Biol. Educ.* 39, 117–125.

Heinen, M. (1997). *Dynamics of Water and Nutrients in Closed, Recirculating Cropping Systems in Glasshouse Horticulture. With Special Attention to Lettuce Grown in Irrigated Sand Beds*. Ph. D. Thesis. Wageningen: Wageningen Agricultural University.

Holtslag, A. A. M., and Van Ulden, A. P. (1983). A simple scheme for daytime estimates of the surface fluxes from routine weather data. *J. Clim. Appl. Meteorol.* 22, 517–529. doi: 10.1175/1520-04501983022<0517:ASSFDE<2.0.CO;2

Jones, J. B. (2005). *Hydroponics: A Practical Guide for the Soilless Grower*. Boca Raton, FL: CRC Press.

Kozai, T., and Niu, G. (2016). "Chapter 1 – Introduction," in *Plant Factory*, eds T. Kozai, G. Niu, and M. Takagaki (San Diego, CA: Academic Press), 3–5.

Kwon, C.-T., Heo, J., Lemmon, Z. H., Capua, Y., Hutton, S. F., Van Eck, J., et al. (2020). Rapid customization of Solanaceae fruit crops for urban agriculture. *Nat. Biotechnol.* 38, 182–188. doi: 10.1038/s41587-019-0361-2

Le Bot, J., Adamowicz, S., and Robin, P. (1998). Modelling plant nutrition of horticultural crops: a review. *Sci. Hortic.* 74, 47–82. doi: 10.1016/s0304-4238(98)00082-x

Lee, S., and Kim, Y. C. (2019). Water treatment for closed hydroponic systems. *J. Korean Soc. Environ. Eng.* 41, 501–513. doi: 10.4491/KSEE.2019.41.9.501

Leitner, D., Klepsch, S., Ptashnyk, M., Marchant, A., Kirk, G. J. D., Schnepf, A., et al. (2010). A dynamic model of nutrient uptake by root hairs. *New Phytol.* 185, 792–802. doi: 10.1111/j.1469-8137.2009.03128.x

Lu, N., Bernardo, E. L., Tippayadarapanich, C., Takagaki, M., Kagawa, N., and Yamori, W. (2017). Growth and accumulation of secondary metabolites in perilla as affected by photosynthetic photon flux density and electrical conductivity of the nutrient solution. *Front. Plant Sci.* 8:708. doi: 10.3389/fpls.2017.00708

Massa, D., Incrocci, L., Maggini, R., Bibbiani, C., Carmassi, G., Malorgio, F., et al. (2011). Simulation of crop water and mineral relations in greenhouse soilless culture. *Environ. Model. Softw.* 26, 711–722. doi: 10.1016/j.envsoft.2011.01.004

Massa, D., Magán, J. J., Montesano, F. F., and Tzortzakis, N. (2020). Minimizing water and nutrient losses from soilless cropping in southern Europe. *Agric. Water Manag.* 241:106395. doi: 10.1016/j.agwat.2020.106395

Menge, D. N. L., Ballantyne, F., and Weitz, J. S. (2011). Dynamics of nutrient uptake strategies: lessons from the tortoise and the hare. *Theor. Ecol.* 4, 163–177. doi: 10.1007/s12080-010-0110-0

Miller, A., Adhikari, R., and Nemali, K. (2020). Recycling nutrient solution can reduce growth due to nutrient deficiencies in hydroponic production. *Front. Plant Sci.* 11:607643. doi: 10.3389/fpls.2020.607643

Munns, R., and Tester, M. (2008). Mechanisms of salinity tolerance. *Annu. Rev. Plant Biol.* 59, 651–681. doi: 10.1146/annurev.arplant.59.032607.092911

O'Sullivan, C. A., Bonnett, G. D., McIntyre, C. L., Hochman, Z., and Wasson, A. P. (2019). Strategies to improve the productivity, product diversity and profitability of urban agriculture. *Agric. Syst.* 174, 133–144. doi: 10.1016/j.agsy.2019.05.007

Parent, S. -É, Parent, L. E., Egozcue, J. J., Rozane, D.-E., Hernandes, A., Lapointe, L., et al. (2013). The plant ionome revisited by the nutrient balance concept. *Front. Plant Sci.* 4:39. doi: 10.3389/fpls.2013.00039

Pieruschka, R., Huber, G., and Berry, J. A. (2010). Control of transpiration by radiation. *Proc. Natl. Acad. Sci. U.S.A.* 107:13372. doi: 10.1073/pnas.0913177107

Rouached, H., and Rhee, S. Y. (2017). System-level understanding of plant mineral nutrition in the big data era. *Curr. Opin. Syst. Biol.* 4, 71–77. doi: 10.1016/j.coisb.2017.07.008

Russo, A., and Cirella, G. T. (2019). Edible urbanism 5.0. *Palgrave Commun.* 5:163. doi: 10.1057/s41599-019-0377-8

Seto, K. C., and Ramankutty, N. (2016). Hidden linkages between urbanization and food systems. *Science* 352, 943–945. doi: 10.1126/science.aaf7439

SharathKumar, M., Heuvelink, E., and Marcelis, L. F. M. (2020). Vertical farming: moving from genetic to environmental modification. *Trends Plant. Sci.* 25, 724–727. doi: 10.1016/j.tplants.2020.05.012

Shin, J. H., and Son, J. E. (2016). Application of a modified irrigation method using compensated radiation integral, substrate moisture content, and electrical conductivity for soilless cultures of paprika. *Sci. Hortic.* 198, 170–175. doi: 10.1016/j.scienta.2015.11.015

Signore, A., Serio, F., and Santamaria, P. (2016). A targeted management of the nutrient solution in a soilless tomato crop according to plant needs. *Front. Plant Sci.* 7:391. doi: 10.3389/fpls.2016.00391

Silberbush, M., and Ben-Asher, J. (2001). Simulation study of nutrient uptake by plants from soilless cultures as affected by salinity buildup and transpiration. *Plant Soil* 233, 59–69. doi: 10.1023/A:1010382321883

Silberbush, M., Ben-Asher, J., and Ephrath, J. E. (2005). A model for nutrient and water flow and their uptake by plants grown in a soilless culture. *Plant Soil* 271, 309–319. doi: 10.1007/s11104-004-3093-z

Steiner, A. A. (1980). The selective capacity of plants for ions and its importance for the composition and treatment of the nutrient solution. *Acta Hortic.* 98, 87–97.

Swift, J., Alvarez, J. M., Araus, V., Gutiérrez, R. A., and Coruzzi, G. M. (2020). Nutrient dose-responsive transcriptome changes driven by Michaelis–Menten kinetics underlie plant growth rates. *Proc. Natl. Acad. Sci. U.S.A.* 117, 12531–12540. doi: 10.1073/pnas.1918619117

Thimijan, R., and Heins, R. (1983). Photometric, radiometric, and quantum light units of measure: a review of procedures for interconversion. *Hortscience* 18, 818–822.

Tzerakis, C., Savvas, D., and Sigrimis, N. (2012). Responses of cucumber grown in recirculating nutrient solution to gradual Mn and Zn accumulation in the root zone owing to excessive supply via the irrigation water. *J. Plant Nutr. Soil Sci.* 175, 125–134. doi: 10.1002/jpln.201100035

van Delden, S. H., Nazarideljou, M. J., and Marcelis, L. F. M. (2020). Nutrient solutions for *Arabidopsis thaliana*: a study on nutrient solution composition in hydroponics systems. *Plant Methods* 16:72. doi: 10.1186/s13007-020-00606-4

Van Noordwijk, M. (1990). "Synchronisation of supply and demand is necessary to increase efficiency of nutrient use in soilless horticulture," in *Proceedings of the Eleventh International Plant Nutrition Colloquium, 30 July–4 August 1989, Wageningen, The Netherlands: Plant Nutrition — Physiology and Applications*, ed. M. L. van Beusichem (Dordrecht: Springer), 525–531.

Wada, T. (2019). "Chapter 1.1 - Theory and technology to control the nutrient solution of hydroponics," in *Plant Factory Using Artificial Light*, eds M. Anpo, H. Fukuda, and T. Wada (Amsterdam: Elsevier), 5–14. doi: 10.1016/B978-0-12-813973-8.00001-4

Zekki, H., Gauthier, L., and Gosselin, A. (1996). Growth, productivity, and mineral composition of hydroponically cultivated greenhouse tomatoes, with or without nutrient solution recycling. *J. Am. Soc. Hortic. Sci.* 121, 1082–1088.

Conflict of Interest: The authors declare that the research was conducted in the absence of any commercial or financial relationships that could be construed as a potential conflict of interest.

Publisher's Note: All claims expressed in this article are solely those of the authors and do not necessarily represent those of their affiliated organizations, or those of the publisher, the editors and the reviewers. Any product that may be evaluated in this article, or claim that may be made by its manufacturer, is not guaranteed or endorsed by the publisher.

frontiers in Plant Science

ORIGINAL RESEARCH
published: 26 November 2021
doi: 10.3389/fpls.2021.778205

Manipulation of Intraday Durations of Blue- and Red-Light Irradiation to Improve Cos Lettuce Growth

Tomohiro Jishi[1,2], Ryo Matsuda[1] and Kazuhiro Fujiwara[1]*

[1]*Department of Biological and Environmental Engineering, Graduate School of Agricultural and Life Sciences, The University of Tokyo, Tokyo, Japan,* [2]*Grid Innovation Research Laboratory, ENIC Division, Central Research Institute of Electric Power Industry, Abiko, Japan*

The morphology of plants growing under combined blue- and red-light irradiation is affected by the presence or absence of time slots of blue- and red-light mono-irradiation. The purposes of this study were to investigate the morphology and growth of cos lettuce grown under light irradiation combining several durations of blue and red light simultaneously and independent mono-irradiations of blue and red light during the day, and to clarify the effects of the durations of blue-light mono-irradiation and blue-light irradiation. Young cos lettuce seedlings were grown under 24-h blue-light irradiation with a photosynthetic photon flux density (PPFD) of 110 μmol m^{-2} s^{-1} (B + 0R) or under 24-h blue-light irradiation with a PPFD of 100 μmol m^{-2} s^{-1} supplemented with 8 (B + 8R), 16 (B + 16R), and 24-h (B + 24R) red-light irradiation with PPFDs of 30, 15, and 10 μmol m^{-2} s^{-1}, respectively (Experiment 1). The daily light integral was 9.50 mol m^{-2} in all treatments. In Experiment 1, leaf elongation was promoted as the duration of red-light irradiation decreased and the duration of blue-light mono-irradiation increased. The maximum shoot dry weight was observed under the B + 8R treatment. Growth was likely promoted by the expansion of the light-receptive area caused by moderate leaf elongation without tilting. In Experiment 2, young cos lettuce seedlings were grown as for Experiment 1, but blue- and red-light irradiation intensities were reversed (R + 0B, R + 8B, R + 16B, and R + 24B). Leaf elongation was promoted by the absence of blue-light irradiation (R + 0B). The leaf surface was increasingly flattened, and the shoot dry weight was enhanced, as the duration of blue-light irradiation increased. Thus, cos lettuce leaf morphology may be manipulated by adjusting each duration of blue-light mono-irradiation, red-light mono-irradiation, and blue- and red-light simultaneous irradiation, which can, in turn, promote cos lettuce growth.

Keywords: artificial light, leaf elongation, leaf morphology, photomorphogenesis, light receptors

OPEN ACCESS

Edited by:
Jung Eek Son,
Seoul National University, South Korea

Reviewed by:
Dimitrios Fanourakis,
Technological Educational Institute of Crete, Greece
Luigi Gennaro Izzo,
University of Naples Federico II, Italy

****Correspondence:***
Tomohiro Jishi
jishi@criepi.denken.or.jp

Specialty section:
This article was submitted to Crop and Product Physiology, a section of the journal Frontiers in Plant Science

Received: *16 September 2021*
Accepted: *05 November 2021*
Published: *26 November 2021*

Citation:
Jishi T, Matsuda R and Fujiwara K (2021) Manipulation of Intraday Durations of Blue- and Red-Light Irradiation to Improve Cos Lettuce Growth. Front. Plant Sci. 12:778205. doi: 10.3389/fpls.2021.778205

INTRODUCTION

The effects of lighting patterns on plant growth have been studied to improve plant cultivation with artificial light. A combination of blue and red light can prevent spindly growth (Hoenecke et al., 1992; Yorio et al., 2001), epinasty (Seif et al., 2021), and achieve a high photosynthetic rate and high growth rate (Yorio et al., 1998; Hogewoning et al.,

2010) and improve disease and nutritional status assessment (Moosavi-Nezhad et al., 2021). Consequently, lighting patterns using blue and red light have been well-studied. When plants are irradiated with blue and red light simultaneously, growth rates are highest at a blue/red photosynthetic photon flux density (PPFD) ratio of 80–90/20–10 (e.g., Hernández and Kubota, 2016) at an identical total PPFD. In these studies, the spectral photon flux density distribution (SPFD) was constant during the light period. However, recently, there have been attempts to promote plant growth using lighting patterns by applying different SPFDs during different hours of the day (Jishi et al., 2016; Ohtake et al., 2018).

Jishi et al. (2021) grew cos lettuce under various blue- and red-light combinations. Lighting patterns that include 12 h of blue-light mono-irradiation (i.e., irradiation with only blue light without other colors of light) promote leaf elongation, probably owing to the phytochrome reaction. The phytochrome photostationary state (PSS) is the ratio of active phytochrome to total phytochrome; a low PSS promotes leaf and stem elongation through the shade-avoidance response (Smith and Whitelam, 1997; Kong et al., 2020). The PSS under blue-light mono-irradiation is significantly lower than that under blue- and red-light simultaneous irradiation; therefore, blue-light mono-irradiation is considered to promote leaf elongation. Jishi et al. (2021) also reported that moderate leaf elongation caused by 12 h of blue-light mono-irradiation promotes growth, probably because of the expansion of the light-receptive area and the greater amount of light received, although excessive leaf elongation causes the plants to collapse and does not promote growth.

The degree of leaf elongation may be controlled by adjusting the duration of blue-light mono-irradiation (Jishi et al., 2016). The effects of blue-light mono-irradiation on plant morphology are mediated by the phytochrome reaction, and blue-light irradiation (i.e., irradiation with blue light, with or without other colors of light irradiation) affects plant morphology through the blue-light receptors of phototropin and cryptochrome (Lin, 2002). Plant morphology may also be controlled by adjusting the blue-light irradiation duration.

In the present study, we conducted a pair of cos lettuce cultivation experiments in which blue- and red-light irradiation were combined. Experiment 1 comprised four treatments with identical durations of blue-light irradiation and different durations of blue-light mono-irradiation to investigate the effects of blue-light mono-irradiation duration and possible role of the phytochrome-mediated reaction. Experiment 2 comprised four treatments with identical durations of blue-light mono-irradiation and different durations of blue-light irradiation to investigate the effects of blue-light irradiation duration and possible role of the blue-light-receptor-mediated reaction. In addition, we discuss the blue- and red-light irradiation methods that effectively promote cos lettuce growth.

MATERIALS AND METHODS

Lighting Patterns

The PPFD values described here were measured at 2 cm above the surface of the urethane cube, in which the cos lettuce seedlings were planted, using a light quantum sensor (LI-190SA; LI-COR, Lincoln, NE, United States).

In Experiment 1, to investigate the effects of the duration of blue-light mono-irradiation, seedlings were grown under 24-h blue light with a PPFD of 110 μmol m^{-2} s^{-1} (B + 0R) or under 24-h blue-light irradiation with a PPFD of 100 μmol m^{-2} s^{-1} supplemented with 8 (B + 8R), 16 (B + 16R), or 24-h (B + 24R) red-light irradiation with PPFDs of 30, 15, and 10 μmol m^{-2} s^{-1}, respectively (**Figure 1**). The durations of blue-light mono-irradiation were 24 (B + 0R), 16 (B + 8R), 8 (B + 16R), and 0-h (B + 24R). The daily averaged PPFD was 110 μmol m^{-2} s^{-1} [daily light integral (DLI): 9.50 mol m^{-2}] for all treatments. The daily averaged PPFDs of blue and red light were 100 and 10 μmol m^{-2} s^{-1}, respectively, for B + 8R, B + 16R, and B + 24R, which included red-light irradiation.

In Experiment 2, to investigate the effects of the duration of blue-light irradiation, seedlings were grown under 24-h red-light irradiation with a PPFD of 110 μmol m^{-2} s^{-1} (R + 0B) or under 24-h red-light irradiation with a PPFD of 100 μmol m^{-2} s^{-1} supplemented with 8 (R + 8B), 16 (R + 16B), or 24-h (R + 24B) blue-light irradiation with PPFDs of 30, 15, and 10 μmol m^{-2} s^{-1}, respectively (**Figure 2**). The daily averaged PPFD was 110 μmol m^{-2} s^{-1} for all treatments. The daily averaged PPFDs of blue and red light were 10 and 100 μmol m^{-2} s^{-1}, respectively, for R + 8B, R + 16B, and R + 24B, which included blue-light irradiation.

Plant Material

Cos lettuce (*Lactuca sativa* L. "Cos lettuce"; Takii Seed Co., Ltd., Kyoto, Japan) seeds were sown on watered urethane cubes

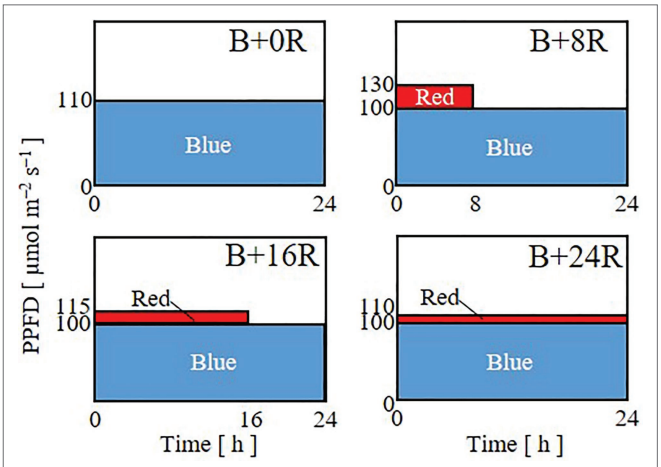

FIGURE 1 | Lighting patterns used in Experiment 1. Plants were subjected to 24-h blue-light irradiation with a PPFD of 110 μmol m^{-2} s^{-1} (B + 0R) or under 8 (B + 8R), 16 (B + 16R), or 24-h (B + 24R) red-light irradiation with PPFDs of 30, 15, and 10 μmol m^{-2} s^{-1}, respectively, supplemented with 24-h blue-light irradiation with a PPFD of 100 μmol m^{-2} s^{-1}.

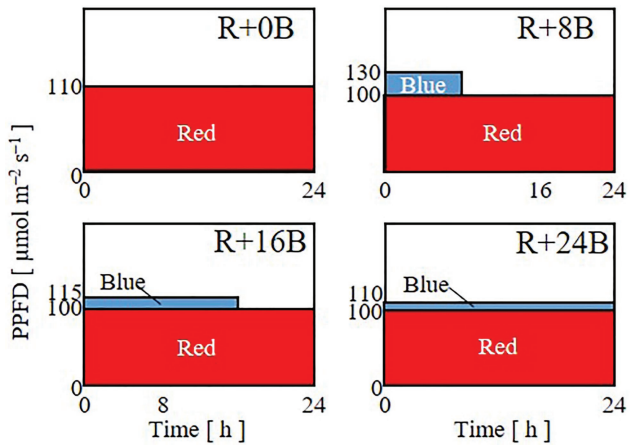

FIGURE 2 | Lighting patterns used in Experiment 2. Plants were subjected to 24-h red-light irradiation with a PPFD of 110 μmol m^{-2} s^{-1} (R + 0B) or under 8 (R + 8B), 16 (R + 16B), or 24-h (R + 24B) blue-light irradiation with PPFDs of 30, 15, and 10 μmol m^{-2} s^{-1}, respectively, supplemented with 24-h red-light irradiation with a PPFD of 100 μmol m^{-2} s^{-1}.

and germinated in a temperature-controlled chamber (MIR-553; SANYO Electric Co., Ltd., Osaka, Japan) at 25 ± 1°C under a 16-h light/8-h dark cycle. Light was provided with white LEDs at a PPFD of 100 μmol m^{-2} s^{-1}. Seven days after sowing, seedlings with approximately 1-cm-long first true leaves were selected for the cultivation experiments.

Cultivation Experiments

Sixteen cos lettuce seedlings were transplanted individually into four holes made in four plastic boards of each urethane cube. Each of the four plastic boards was placed on a 5-L plastic container filled with a continuously aerated nutrient solution (half-strength Otsuka-A nutrient solution; OAT Agrio Co., Ltd., Tokyo, Japan) with electrical conductivity of 0.13 ± 0.01 S m^{-1}. The internal spaces of two temperature-controlled chambers were partitioned into upper and lower compartments with cardboard and black paper to prevent light contamination between compartments. Four seedlings were cultivated in each of the four compartments for each treatment. The temperature was maintained at 25 ± 1°C throughout the day in all compartments. The CO_2 concentration and relative humidity were not measured or controlled but were expected to have been similar among all compartments because the external air was continuously introduced into each compartment using air pumps from the same space. At 14 days after transplanting (21 days after sowing), all seedlings were harvested and measured. The total leaf area per plant was measured using an area meter (AAM-9; Hayashi Denko Co., Ltd., Tokyo, Japan). The shoots were dried for 1 h at 100°C and then dried at 80°C for 3 days before measurement of the shoot dry weight. The length and width of the largest leaf on each seedling were measured using a ruler. The cultivation experiments were repeated twice for each of the eight treatments, and the compartments were changed for each replication.

Lighting Sources

An LED panel with indicator-type white LEDs (NSPW310DS-b2W; Nichia Corp., Tokushima, Japan) was used for seedling growth before the cultivation experiments. Panels with blue (HBL3-3S55-LE; Toricon, Shimane, Japan) and red (SRK1-3A80-LE; Toricon) LEDs were used for the cultivation experiments. The relative SPFDs of the white, blue, and red LED lights are shown in **Figure 3**. The SPFD was measured with a spectroradiometer (MS-720; EKO Instruments Co., Ltd., Tokyo, Japan). DC power supplies (PAS60-4.5 for blue LEDs, and PMC35-1 for red and white LEDs; Kikusui Electronics Corp., Yokohama, Japan) were used to supply electrical currents to the LEDs, and the PPFD values of blue and red light were adjusted through current control. Digital timers (H5CX; OMRON Corp., Kyoto, Japan) were connected to the DC power supplies and used to remotely control the durations of blue and red irradiation.

RESULTS

Experiment 1: Effects of Blue-Light Mono-Irradiation Duration

As the blue-light mono-irradiation duration increased, the leaves became more elongated (**Figure 4**). The average values of shoot fresh weight, shoot dry weight, and total leaf area were highest under B + 16R and lowest under B + 24R (**Figures 5A–C**). Leaf widths were similar among the treatments, but leaf lengths tended to increase along with blue-light mono-irradiation; thus, the leaf length/width ratio tended to be greater as the blue-light mono-irradiation duration increased (**Figures 5D–F**).

Experiment 2: Effects of Blue-Light Irradiation Duration

The leaves were elongated and twisted under R + B0 (**Figure 6**). In the blue-light irradiation treatments, the longer the blue-light irradiation, the flatter the appearance of the leaves, with no curling into bowl shapes. Shoot fresh weight, shoot dry weight, and total leaf area tended to be greater as the blue-light irradiation duration increased (**Figures 7A–C**). Leaf length was greatest under R + B0, and in the blue-light irradiation treatments; it increased along with the blue-light irradiation duration (**Figure 7D**). Leaf width tended to be greater as the blue-light irradiation duration increased (**Figure 7E**). As a result, the leaf length/width ratio was significantly greater under R + B0 and similar among the other treatments (**Figure 7F**).

DISCUSSION

Experiment 1: Effects of Blue-Light Mono-Irradiation Duration

The leaf length may be increased under the longer blue-light mono-irradiation durations because of the resulting low PSS (**Table 1**; Sager et al., 1988), as shown by the elongation of cucumber stems (Hernández and Kubota, 2016) and lettuce leaves (Jishi et al., 2021) exposed to blue-light mono-irradiation.

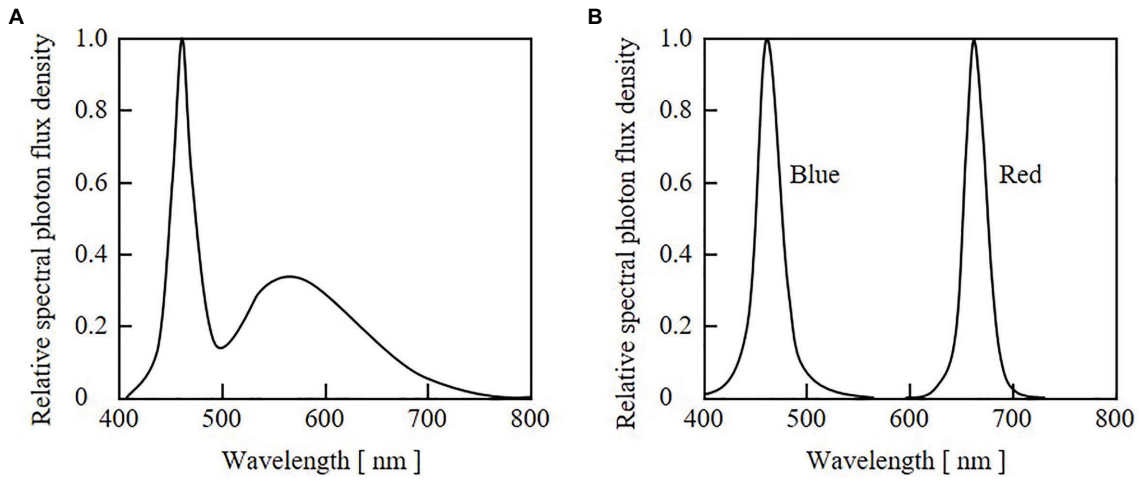

FIGURE 3 | Relative spectral photon flux density distributions of light from white LEDs used for seedling cultivation **(A)** and from blue and red LEDs used for growth experiments **(B)**.

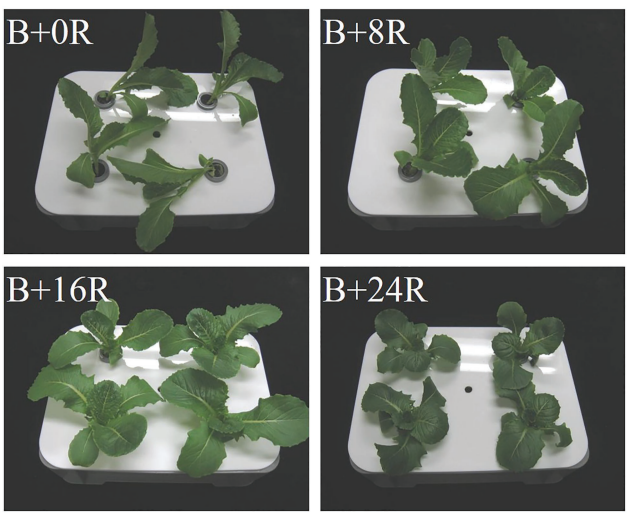

FIGURE 4 | Cos lettuce plants grown under irradiation conditions described in **Figure 1** (Experiment 1).

This result corroborates the finding by Jishi et al. (2016) that the longer the duration of both red-light mono-irradiation and blue-light mono-irradiation, the greater the promotion of cos lettuce leaf elongation. The present results clearly showed that leaf elongation was increasingly promoted by a longer duration of blue-light mono-irradiation. Thus, the degree of elongation mediated by the phytochrome reaction may be regulated by the duration of low PSS, such as blue-light mono-irradiation.

The leaf widths were similar among the treatments, suggesting that the longer blue-light mono-irradiation duration resulted in elongated leaves rather than enlarged leaves. The leaf lengths under B + 0R and B + 8R were similar, but seedlings appeared spindlier under B + 0R than under B + 8R (**Figure 4**). The seedlings grown under B + 0R collapsed owing to excessive elongation, and their dry matter production was low (**Figure 5B**) probably because of the low amount of light received. Therefore, leaf length under B + 0R may have the potential to increase as a photomorphogenic response, but the biomass may have been insufficient to allow an increase in leaf length.

The differences in shoot fresh weight, shoot dry weight, and total leaf area may result from differences in the amount of light received. Under B + 16R, the leaf surfaces facing the light source and the light-receptive area were high, whereas under B + 0R and B + 8R, the seedlings were tilted owing to excessive elongation. However, under B + 24R, the leaves did not elongate notably and the light-receptive area was small. As a result, the degree of leaf elongation was moderate under B + 16R for the purpose of promoting growth. Additionally, moderate durations of blue- and red-light irradiation vary depending on other environmental conditions. For example, the higher the DLI, the more plant elongation is suppressed (Johkan et al., 2012). If a similar experiment was conducted with a higher DLI, then elongation would be suppressed in all treatments and the leaf morphology of seedlings grown under B + 8R or B + 0R would be relatively "moderate." The degree of plant elongation may be moderated by adjusting the duration of blue-light mono-irradiation in accordance with other environmental conditions, such as DLI.

Experiment 2: Effects of Blue-Light Irradiation Duration

The significantly greater leaf length under R + B0 may result from the absence of the inhibitory effects of blue-light irradiation on elongation through the cryptochrome reaction (Ahmad et al., 1995; Zhao et al., 2007). The leaf length/width ratios, which were affected by blue-light mono-irradiation in Experiment 1, probably through the phytochrome reaction, were similar under R + 8B, R + 16B, and R + 24B in Experiment 2. This

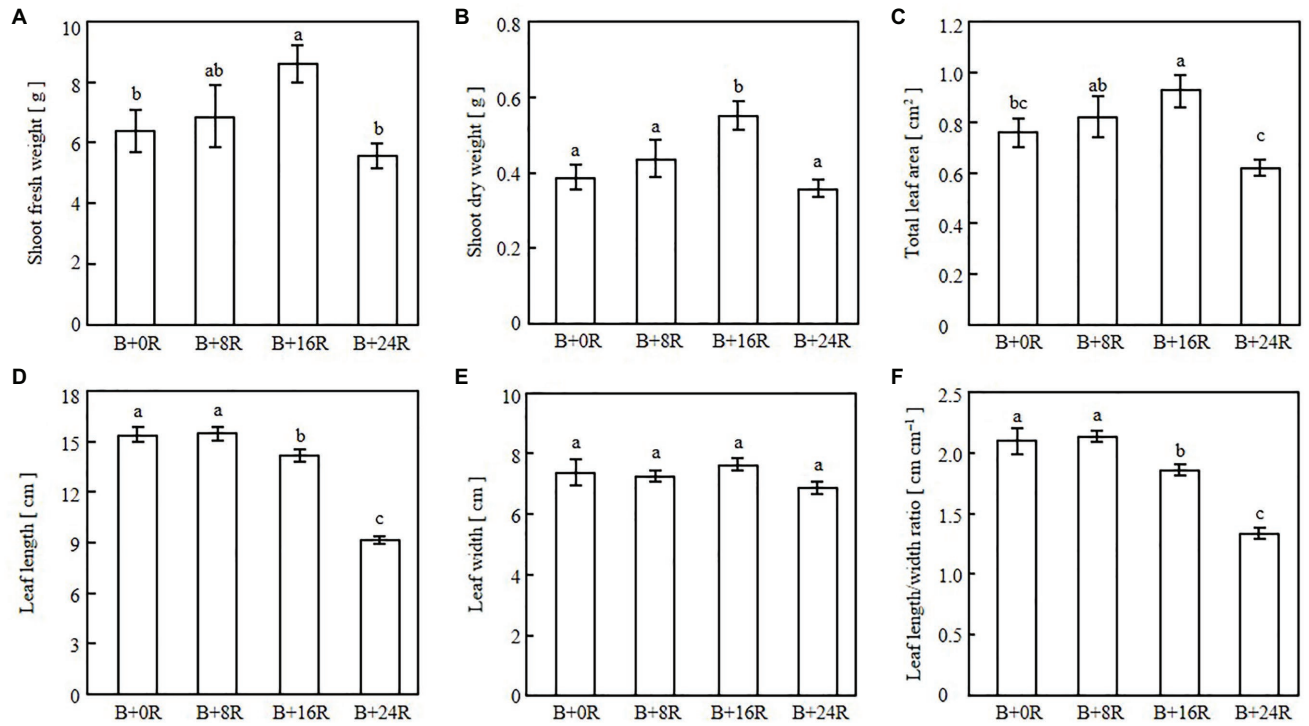

FIGURE 5 | Shoot fresh weight **(A)**, shoot dry weight **(B)**, total leaf area **(C)**, leaf length **(D)**, leaf width **(E)**, and leaf length/width ratio **(F)** of cos lettuce seedlings grown under irradiation conditions described in **Figure 1** (Experiment 1). Bars represent SEMs ($n = 8$). Different lower-case letters above bars within a panel indicate a significant difference ($p < 0.05$, Tukey–Kramer HSD test).

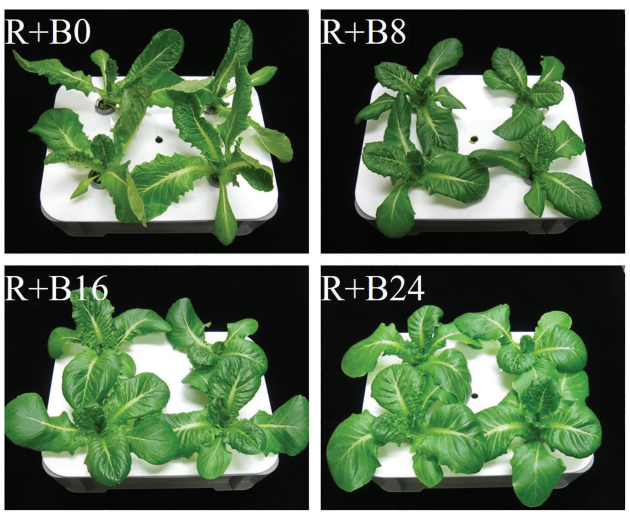

FIGURE 6 | Cos lettuce plants grown under irradiation conditions described in **Figure 2** (Experiment 2).

suggests that the elongation-suppressive effect of the cryptochrome is affected by the presence or absence of blue-light irradiation during the day, but the effects of blue-light irradiation duration are small. The effects of blue-light DLI cannot be discussed for the present experiment because the blue-light DLI was identical among treatments. The blue-light DLI in this study (0.86 mol m^{-2}) may be sufficiently high to saturate the cryptochrome reaction. Wheeler et al. (1991) investigated the effects of blue-light PPFD in irradiated light on soybean grown under a 12-h light period. These authors found that stem elongation was suppressed as the blue-light PPFD increased up to 30 µmol m^{-2} s^{-1} (1.30 mol m^{-2}), at which point the suppressive effect was saturated.

The differences in shoot fresh weight, shoot dry weight, and total leaf area resulted from differences in the amounts of light received. The treatments with a longer blue-light irradiation duration resulted in flatter leaves, which potentially have a greater light-receptive area by orienting the leaf surface toward the light source compared with that of epinastic leaves. Under R + B0, some leaves turned and did not face the light source, which likely also decreased the light-receptive area. Among the three treatments including blue-light irradiation, leaf length and width increased together with blue-light irradiation duration, whereas the leaf length/width ratio was similar. This may be because the development of flattened leaves was caused by the phototropin reaction, and the gain in biomass was caused by the increased light-receptive area of the flattened leaves.

The flattening of leaves with increase in blue-light irradiation duration may be a phototropin-mediated response (Inoue et al., 2008). Although the blue-light DLI was identical among treatments, the degree of leaf flatness was affected by the duration of

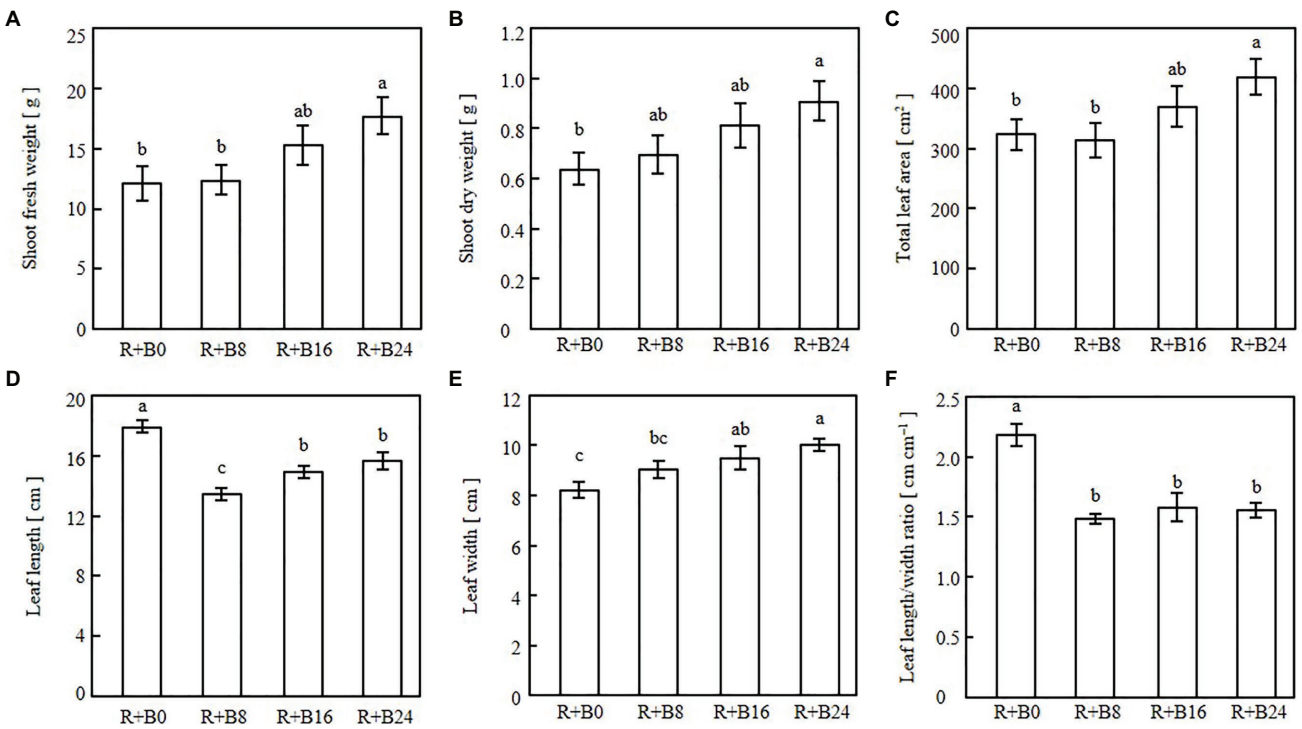

FIGURE 7 | Shoot fresh weights **(A)**, shoot dry weights **(B)**, total leaf areas **(C)**, leaf lengths **(D)**, leaf widths **(E)**, and leaf length/width ratios **(F)** of cos lettuce seedlings under irradiation conditions described in **Figure 2** (Experiment 2). Bars represent SEMs ($n = 8$). Different lower-case letters above bars within a panel indicate a significant difference ($p < 0.05$, Tukey–Kramer HSD test).

TABLE 1 | Phytochrome photostationary state (PSS) values under several photosynthetic photon flux density (PPFD) combinations of blue- and red-LED light irradiation for each time slot of treatments in the present study.

Blue-/red-light PPFD (μmol m^{-2} s^{-1})	Treatment including the time slot with blue-/red-light PPFD	PSS
110/0, 100/0	B+0R, B+8R, B+16R, and B+24R	0.55
100/30	B+8R	0.86
100/15	B+16R	0.83
100/10	B+24R	0.80
30/100	R+8B	0.90
15/100	R+16B	0.90
10/100	R+24B	0.91
0/110, 0/100	R+0B, R+8B, R+16B, and R+24B	0.91

*The PSS values were calculated from the spectral photon flux densities (**Figure 3**) and photochemical cross-section data of Sager et al. (1988).*

blue-light irradiation; therefore, the phototropin reaction may be affected by the duration of blue-light irradiation rather than by blue-light DLI. Thus, the phototropin reaction induced by blue light may not follow the reciprocity law, whereas the phytochrome reaction is induced by end-of-day far-red light irradiation (Zou et al., 2021). However, 10 μmol m^{-2} s^{-1}, the lowest blue-light PPFD applied in the present study, may have been sufficient to saturate the phototropin reaction. Thus, it is possible that the phototropin reaction follows the reciprocity law at a significantly lower blue-light DLI and PPFD than applied in the present study.

Lighting Patterns to Promote Growth

Adjusting the duration of blue-light mono-irradiation to moderately elongate leaves is one way to increase the amount of light received and promote growth. However, leaf elongation is effective in increasing light-receptive areas only when leaves do not shade each other. Normally, immediately after planting of a crop, there is ample space between seedlings; during this phase, leaf elongation effectively promotes growth until shading occurs. In comparison, under high plant densities in which shading occurs earlier than in the present study, differences in growth may not be observed as strikingly as in the present study.

Another method to regulate phytochrome-mediated elongation is far-red-light irradiation (Meng and Runkle, 2019). Far-red-light irradiation has the advantages that the PSS can be changed markedly by adjusting the far-red photon flux density and that it does not require timers to control the duration of blue- or red-light irradiation independently. When using far-red light irradiation, attention must be paid to the following: far-red light has a low photosynthetic efficiency; it is difficult to control the PSS because a small difference in the far-red PFD greatly affects the PSS; and the PSS differs between the upper and lower parts of the canopy owing to the greater penetration

of far-red light compared with red light. On the basis of this study's results, the degree of elongation is also likely to be regulated by adjusting the duration of the far-red-light irradiation during the light period. Blue-light mono-irradiation and far-red irradiation should be used separately or in combination, depending on the purpose.

Long-blue-light irradiation during the day promotes the development of flat leaves and growth. The blue-light DLI was 0.86 mol m^{-2} in the present study, and leaf flattening may be further promoted by a greater blue-light DLI. However, because the emission wavelength bands of AlGaInP-based devices, which have relatively high luminous efficiency levels, are in the red region of 640–680 nm (Jung et al., 2021) near the absorption peak of chlorophyll, it is better to increase the red-light DLI for the purpose of increasing the amount of photosynthesis per the amount of light received with equal energy consumption. The price of the light source (initial investment cost) also cannot be ignored as well as the electricity cost for lighting (running cost). Light sources with wavelengths that are in high demand for general home lighting are low-priced as a result of mass production. Even if the relative SPFD is not optimal for plant growth, the use of inexpensive light sources may maximize profits in commercial plant factories. The wavelength band of the light source should be selected with consideration of the estimated photosynthetic rate and photoreceptor reactions based on the absorption spectrum of the photoreceptors.

Photosynthesis is suppressed and growth slows if the light environment does not change during a close to 24-h cycle (Dodd et al., 2005). One reason that growth was suppressed under B + 24R during Experiment 1 may have been because it was not a 24-h cycle. However, because growth was not particularly suppressed under R + B24 during Experiment 2, the effects of the circadian rhythms should have been small. Alternatively, cyclic changes in the PSS or the presence or absence of red light may be the main circadian rhythm-related signals.

We have discussed the photoreceptor reaction as the response of plants to a light environment comprising different SPFDs in different durations. However, detailed physiological experiments, such as those using mutants, are needed to test these hypotheses. In addition, growth analysis is useful to examine the effect of the light environment on growth rate through morphology. Conducting such studies in the future, and the possible manipulation of plant responses using a time-varying lighting method, are predicted to lead to further advances in light irradiation in plant factories.

CONCLUSION

The leaf morphology and growth of cos lettuce were affected by the durations of blue- and red-light irradiation. Leaf elongation increased along with the blue-light mono-irradiation duration, and leaf flattening increased along with the blue-light irradiation duration. These morphological traits can be applied to increase the amount of light received, thereby promoting the growth of cos lettuce.

DATA AVAILABILITY STATEMENT

The raw data supporting the conclusions of this article will be made available by the authors, without undue reservation.

AUTHOR CONTRIBUTIONS

TJ conducted the experiments and wrote the manuscript. RM and KF supervised the experiments, provided editorial advice, and revised the manuscript. All authors contributed to the article and approved the submitted version.

REFERENCES

Ahmad, M., Lin, C., and Cashmore, R. A. (1995). Mutations throughout an *Arabidopsis* blue-light photoreceptor impair blue-light-responsive anthocyanin accumulation and inhibition of hypocotyl elongation. *Plant J.* 8, 653–658. doi: 10.1046/j.1365-313X.1995.08050653.x

Dodd, A. N., Salathia, N., Hall, A., Kévei, E., Tóth, R., Nagy, F., et al. (2005). Plant circadian clocks increase photosynthesis, growth, survival, and competitive advantage. *Science* 309, 630–633. doi: 10.1126/science.1115581

Hernández, R., and Kubota, C. (2016). Physiological responses of cucumber seedlings under different blue and red photon flux ratios using LEDs. *Environ. Exp. Bot.* 121, 66–74. doi: 10.1016/j.envexpbot.2015.04.001

Hoenecke, M. E., Bula, R. J., and Tibbitts, T. W. (1992). Importance of "blue" photon levels for lettuce seedlings grown under red-light-emitting diodes. *HortScience* 27, 427–430. doi: 10.21273/HORTSCI.27.5.427

Hogewoning, S. W., Trouwborst, G., Maljaars, H., Poorter, H., Van Ieperen, W., and Harbinson, J. (2010). Blue light dose–responses of leaf photosynthesis, morphology, and chemical composition of Cucumis sativus grown under different combinations of red and blue light. *J. Exp. Bot.* 61, 3107–3117. doi: 10.1093/jxb/erq132

Inoue, S., Kinoshita, T., Takemiya, A., Doi, M., and Shimazaki, K. (2008). Leaf positioning of *Arabidopsis* in response to blue light. *Mol. Plant* 1, 15–26. doi: 10.1093/mp/ssm001

Jishi, T., Kimura, K., Matsuda, R., and Fujiwara, K. (2016). Effects of temporally shifted irradiation of blue and red LED light on cos lettuce growth and morphology. *Sci. Hortic.* 198, 227–232. doi: 10.1016/j.scienta.2015.12.005

Jishi, T., Matsuda, R., and Fujiwara, K. (2021). Blue light monochromatic irradiation for 12 hours in lighting pattern with combinations of blue and red light elongates young cos lettuce leaves and promotes growth under high daily light integral. *HortScience* 56, 940–945. doi: 10.21273/HORTSCI15959-21

Johkan, M., Shoji, K., Goto, F., Hahida, S., and Yoshihara, T. (2012). Effect of green light wavelength and intensity on photomorphogenesis and photosynthesis in *Lactuca sativa*. *Environ. Exp. Bot.* 75, 128–133. doi: 10.1016/j.envexpbot.2011.08.010

Jung, B. O., Lee, W., Kim, J., Choi, M., Shin, H., Joo, M., et al. (2021). Enhancement in external quantum efficiency of AlGaInP red μ-LED using chemical solution treatment process. *Sci. Rep.* 11:4535. doi: 10.1038/s41598-021-83933-3

Kong, Y., Schiestel, K., and Zheng, Y. (2020). Maximum elongation growth promoted as a shade-avoidance response by blue light is related to deactivated phytochrome: a comparison with red light in four microgreen species. *Can. J. Plant Sci.* 100, 314–326. doi: 10.1139/cjps-2019-0082

Lin, C. (2002). Blue light receptors and signal transduction. *Plant Cell* 14, 207–225. doi: 10.1105/tpc.000646

Meng, Q., and Runkle, E. (2019). Far-red radiation interacts with relative and absolute blue and red photon flux densities to regulate growth, morphology, and pigmentation of lettuce and basil seedlings. *Sci. Hortic.* 255, 269–280. doi: 10.1016/j.scienta.2019.05.030

Moosavi-Nezhad, M., Salehi, R., Aliniaeifard, S., Tsaniklidis, G., Woltering, E. J., Fanourakis, D., et al. (2021). Blue light improves photosynthetic performance during healing and acclimatization of grafted watermelon seedlings. *Int. J. Mol. Sci.* 22:8043. doi: 10.3390/ijms22158043

Ohtake, N., Ishikura, M., Suzuki, H., Yamori, W., and Goto, E. (2018). Continuous irradiation with alternating red and blue light enhances plant growth while keeping nutritional quality in lettuce. *HortScience* 53, 1804–1809. doi: 10.21273/HORTSCI13469-18

Sager, J. C., Smith, W. O., Edwards, J. L., and Cyr, K. L. (1988). Photosynthetic efficiency and phytochrome photoequilibria determination using spectral data. *Trans. ASAE* 31, 1882–1889. doi: 10.13031/2013.30952

Seif, M., Aliniaeifard, S., Arab, M., Mehrjerdi, M. Z., Shomali, A., Fanourakis, D., et al. (2021). Monochromatic red light during plant growth decreases the size and improves the functionality of stomata in chrysanthemum. *Funct. Plant Biol.* 48, 515–528. doi: 10.1071/FP20280

Smith, H., and Whitelam, G. C. (1997). The shade avoidance syndrome: multiple responses mediated by multiple phytochromes. *Plant Cell Environ.* 20, 840–844. doi: 10.1046/j.1365-3040.1997.d01-104.x

Wheeler, R. M., Mackowiak, C. L., and Sager, J. C. (1991). Soybean stem growth under high-pressure sodium with supplemental blue lighting. *Agron. J.* 83, 903–906. doi: 10.2134/agronj1991.00021962008300050024x

Yorio, N. C., Goins, G. D., Kagie, H. R., Wheeler, R. M., and Sager, J. C. (2001). Improving spinach, radish, and lettuce growth under red light-emitting diodes (LEDs) with blue light supplementation. *HortScience* 36, 380–383. doi: 10.21273/HORTSCI.36.2.380

Yorio, N. C., Wheeler, R. M., Goins, G. D., Sanwo-lewandowski, M. M., Mackowiak, C. L., Brown, C. S., et al. (1998). Blue light requirements for crop plants used in bioregenerative life support systems. *Life Support Biosph. Sci.* 5, 119–128.

Zhao, X., Yu, X., Foo, E., Symons, G. M., Lopez, J., Bendehakkalu, K. T., et al. (2007). A study of gibberellin homeostasis and cryptochrome-mediated blue light inhibition of hypocotyl elongation. *Plant Physiol.* 145, 106–118. doi: 10.1104/pp.107.099838

Zou, J., Fanourakis, D., Tsaniklidis, G., Cheng, R., Yang, Q., and Li, T. (2021). Lettuce growth, morphology and critical leaf trait responses to far-red light during cultivation are low fluence and obey the reciprocity law. *Sci. Hortic.* 289:110455. doi: 10.1016/j.scienta.2021.110455

Conflict of Interest: The authors declare that the research was conducted in the absence of any commercial or financial relationships that could be construed as potential conflict of interest.

Publisher's Note: All claims expressed in this article are solely those of the authors and do not necessarily represent those of their affiliated organizations, or those of the publisher, the editors and the reviewers. Any product that may be evaluated in this article, or claim that may be made by its manufacturer, is not guaranteed or endorsed by the publisher.

frontiers in Plant Science

ORIGINAL RESEARCH
published: 22 December 2021
doi: 10.3389/fpls.2021.786309

Monitoring of Salinity, Temperature, and Drought Stress in Grafted Watermelon Seedlings Using Chlorophyll Fluorescence

Yu Kyeong Shin[1], Shiva Ram Bhandari[1,2] and Jun Gu Lee[1,2,3]**

[1]*Department of Horticulture, College of Agriculture & Life Sciences, Jeonbuk National University, Jeonju, South Korea,* [2]*Core Research Institute of Intelligent Robots, Jeonbuk National University, Jeonju, South Korea,* [3]*Institute of Agricultural Science & Technology, Jeonbuk National University, Jeonju, South Korea*

OPEN ACCESS

Edited by:
Jung Eek Son,
Seoul National University,
South Korea

Reviewed by:
Weverton Pereira Rodrigues,
Universidade Estadual da Região Tocantina do Maranhão (UEMASUL), Brazil
Ilektra Sperdouli,
Hellenic Agricultural Organisation (HAO), Greece
Michael Moustakas,
Aristotle University of Thessaloniki, Greece

***Correspondence:**
Jun Gu Lee
jungu@jbnu.ac.kr
Shiva Ram Bhandari
shivarbhandari@gmail.com

Specialty section:
This article was submitted to Technical Advances in Plant Science, a section of the journal Frontiers in Plant Science

Received: *30 September 2021*
Accepted: *18 November 2021*
Published: *22 December 2021*

Citation:
Shin YK, Bhandari SR and Lee JG (2021) Monitoring of Salinity, Temperature, and Drought Stress in Grafted Watermelon Seedlings Using Chlorophyll Fluorescence. Front. Plant Sci. 12:786309. doi: 10.3389/fpls.2021.786309

Chlorophyll fluorescence (*CF*) is used to measure the physiological status of plants affected by biotic and abiotic stresses. Therefore, we aimed to identify the changes in *CF* parameters in grafted watermelon seedlings exposed to salt, drought, and high and low temperatures. Grafted watermelon seedlings at the true three-leaf stage were subjected to salinity levels (0, 50, 100, 150, and 200 mM) and temperature [low (8°C), moderate (24°C), and high (40°C)] stresses for 12 days under controlled environmental conditions independently. Eight *CF* parameters were measured at 2-day intervals using the FluorCam machine quenching protocol of the FluorCam machine. The seedlings were also exposed to drought stress for 3 days independent of salinity and temperature stress; *CF* parameters were measured at 1-day intervals. In addition, growth parameters, proline, and chlorophyll content were evaluated in all three experiments. The *CF* parameters were differentially influenced depending on the type and extent of the stress conditions. The results showed a notable effect of salinity levels on *CF* parameters, predominantly in maximum quantum yield (Fv/Fm), non-photochemical quenching (NPQ), the ratio of the fluorescence decrease (Rfd), and quantum yield of non-regulated energy dissipation in PSII [Y(NO)]. High temperature had significant effects on Rfd and NPQ, whereas low temperature showed significant results in most *CF* parameters: Fv/Fm, Y(NO), NPQ, Rfd, the efficiency of excitation capture of open photosystem II (PSII) center (Fv′/Fm′), and effective quantum yield of photochemical energy conversion in PSII [Y(PSII)]. Only NPQ and Rfd were significantly influenced by severe drought stress. Approximately, all the growth parameters were significantly influenced by the stress level. Proline content increased with an increase in stress levels in all three experiments, whereas the chlorophyll (a and b) content either decreased or increased depending upon the stressor. The results provided here may be useful for understanding the effect of abiotic stresses on *CF* parameters and the selection of index *CF* parameters to detect abiotic stresses in grafted watermelon seedlings.

Keywords: proline, abiotic stress, maximum quantum yield, growth parameter, chlorophyll

INTRODUCTION

Plants experience a range of stresses during their life cycle and exhibit physiological, biochemical, and molecular responses to biotic and abiotic stresses (Fahad et al., 2017; Nadeem et al., 2018). These stressors affect the plants negatively in different ways, depending on the extent and duration of the stress (Shin et al., 2020a; Giordano et al., 2021). The ultimate effects of stressors are reduction in growth by decreasing the photosynthesis rate, changes in bioactive compounds, and overall yield (Toscano et al., 2019; Giordano et al., 2021). Among the different abiotic stresses, salt, temperature, and drought stress are some of the important abiotic stresses experienced by plants during cultivation (Kalaji et al., 2016). The effects of each abiotic stress slightly differ from each other to some extent, although their ultimate effects are the reduction in growth *via* reduced photosynthesis rate, alteration in phytochemicals, and overall yield. The effects of stressors in plants have been studied in a range of plants at different stages of their life cycle (Bhandari et al., 2018; Shin et al., 2020a,b).

Salinity stress disrupts membrane permeability and stomatal closure, and imbalances ion concentrations; this reduces the photosynthetic rate as well as the levels of photosynthetic pigments, growth, and yields by up to 20% worldwide (De Oliveira et al., 2013). Salinity stress influences the relationship between salinity level and water, stomatal closure, leaf wilting, premature aging of leaves due to salinity accumulation, and decreased growth and yield (Garg et al., 2020; Lotfi et al., 2020). Salinity stress can be due to either a short-term exposure or a long-term stress due to continuous nutrient and salinity accumulation in the rhizome, affecting growth and fruit production (Negrão et al., 2017). Plants may receive either high- or low-temperature stresses during cultivation; their effects are dependent on the plant genotypes (Korkmaz and Dufault, 2001; Hou et al., 2016; Rajametov et al., 2021). In particular, high-and low-temperature stress causes various physiological changes in plants, such as damage to the cellular structure of plants, reduction of chlorophyll levels, and deterioration of photosynthetic function (Garstka et al., 2007; Mattila et al., 2020). High temperatures severely affect the structure and functions of cell membranes, causing early bolting, dehydration of soil moisture content, and disruption of ion movement, which reduces photosynthesis and ~50% reduction in total yield in different crops (Fahad et al., 2017; Nadeem et al., 2018). Under high temperature stress, plants accumulate reactive oxygen species (ROS), such as hydrogen peroxide (Soengas et al., 2018; Hassan et al., 2020). Furthermore, the electron transport ability during photosynthesis is reduced, reducing the energy utilization capacity of photosystem II (Song et al., 2014). In contrast, excessively low temperatures are responsible for chilling injuries in plants and damage to the photosynthetic apparatus (Lee et al., 2021). Soil water content has a crucial role, and optimum water content is required for plant growth under normal conditions. A reduction in soil water content, causing drought stress in plants, disrupts the uptake of minerals and other essential nutrients (Yordanov et al., 2000). Sometimes, sudden changes in temperature levels during the life cycle of plants cause thermal shock which may induce the expression of some genes which in turn results in the increased synthesis of some proteins: heat shock proteins (Gupta et al., 2010). These proteins are responsible to bind and stabilize misfolded proteins. Such proteins are also induced by the other stress factors such as osmotic potential, salinity, drought, and high intensity irradiations (Swindell et al., 2007). Furthermore, plants also undergo various *in vitro* phenotypic and *in vivo* physiological changes both internally and externally when subjected to drought stress, and activate multiple defense mechanisms for protection and survival (Yordanov et al., 2000; Kapoor et al., 2020; Tabassum et al., 2021). In addition, drought stress is known to limit photosynthetic activity (Shafiq et al., 2021). Drought stress caused by inadequate watering induces physiological changes in plants, such as cell dehydration, osmotic pressure imbalance, and plant growth retardation (Jia et al., 2021). Depending on abiotic stressors, such as salinity, drought, high, and low temperatures, plants show various phenotypic and physiological responses *in vivo* according to various crops, genetic resources, varieties, growth stages, and stress tolerance levels (He et al., 2018). Photo-inhibition caused by environmental stress on photosystem II is closely related to the photosynthetic performance of plants (Murata et al., 2007). Therefore, studying the effects of abiotic stress in plants is an important step in the production of high-yield and nutritionally improved crops (Fahad et al., 2017; Liang et al., 2020).

Both destructive and non-destructive methods have been used to detect abiotic stress and their responses in plants (Gorbe and Calatayud, 2012; Kalaji et al., 2016; Bhandari et al., 2018; Susič et al., 2018; Shin et al., 2020b). Among them, chlorophyll fluorescence (*CF*) imaging is one of the most common non-destructive techniques that has been applied to detect abiotic stresses in a range of plants (Moustakas et al., 2021). The *CF* parameters provide information on the mechanical detail and extent of damage in plants due to stress. Protocols capable of measuring various chlorophyll fluorescence parameters include the chlorophyll fluorescence induction curve (OJIP), the Kautsky effect (chlorophyll a fluorescence induction), and quenching effects (Lichtenthaler and Babani, 2000; Zushi et al., 2012; Yao et al., 2018; Shin et al., 2020a).

Watermelon (*Citrullus lanatus*) is a high-income economic crop, with 3.08 million hectares of cultivated area and 100 million tons of worldwide production (FAO, 2019). It has been found that the overall yield and fruit quality of watermelon are severely affected by biological and environmental stressors during cultivation (Toscano et al., 2019; Giordano et al., 2021). To solve this problem, the development of particular stress-resistant cultivars has been pursued; however, it requires diverse strategies, sufficient time, and human resources (Bulgari et al., 2019). As an alternative, the use of stress-resistant stock cultivars and grafted seedlings for high quality and yield is steadily increasing (Kumar et al., 2017). As the use of grafted seedlings has increased in response to various stressors, the domestic seedling market is developing into specialized seedling production facilities with expertise in facility gardening, smart farms, and grafting machines (Kwack et al., 2021). The development of the seedling industry reflects various cultivation management

objectives, such as of soil-borne diseases in the growing environment, climate change, and increases in fruit production (Rahmatian et al., 2014; Spanò et al., 2020). Furthermore, seedling industries have been used small container (plug tray having different sizes) for the efficient production of seedlings as it occupies small space and cost effective. The various abiotic factors affecting grafted seedlings include lack of nutrients, salinity accumulation, drought, water, and high and low temperatures (Coskun et al., 2016; Nievola et al., 2017; Hussain et al., 2018). Both grafted and non-grafted seedlings have been used for watermelon cultivation; however, the use of grafted seedlings has been increasing because of their high yield (Lee et al., 2010). Several studies related to the effects of abiotic stress in watermelon have been performed (Yetişir and Uygur, 2009; Hou et al., 2016; Yanyan et al., 2018; Lu et al., 2020, 2021). However, the effects of salinity, temperature, and drought stresses independently in a single cultivar during a different treatment schedule have not been performed in detail.

Therefore, this study was performed to evaluate the effects of salt, temperature, and drought stress on *CF* parameters, photosynthetic pigments (chlorophyll a and b), stress-related compounds (proline), and growth performance in grafted watermelon seedlings during progressive exposure to the respective stressors, and to select possible index *CF* parameters for the detection of salt, temperature, and drought stress.

MATERIALS AND METHODS

Plant Material and Seedling Preparation

For the preparation of watermelon (*Citrullus lanatus*) grafted seedlings, the scion cultivar 'Seo Tae Ja' (Asia Seed Co. Ltd., Seoul, South Korea) and stock cultivar 'Seol Jung Mae Plus' (Tae Seong Seed Co. Ltd., Yeonggwang, South Korea) which was resistant to temperature stress were used. The scion seeds were sowed in 128-cell plug trays (54.4 cm × 28.2 cm × 5.4 cm); stock seeds were sowed in 40-cell plug trays (54.4 cm × 28.2 cm × 5.4 cm) filled with bed soil (Chorok-i, Nongwoobio Co. Ltd., Suwon, South Korea). Grafted seedlings were made from the scion and stock using the single cotyledon grafting method, according to Hassell et al. (2008), and were used in experiments when the true leaves of the scion reached the three-leaf stage. Watermelon-grafted seedlings were grown by a professional seedling company (Sol-Rae Seedling Farm, Iksan, South Korea) in a greenhouse with the standard protocol developed for experimental plant materials until the three true-leaf stages.

Experimental Design and Growth Conditions

The experiment was performed under three different stress conditions: salt, temperature, and drought stress independently. A detailed experimental plan is presented in **Figure 1**. For the salt and temperature stress treatments, the grafted seedlings were grown in a closed light box (120 cm × 65 cm × 45 cm; l × b × h) under a fluorescent lamp (Philips, TLD 32 W/865RS) with a photosynthetic photon flux density (PPFD) of 210 ± 10 μmol m^{-2} s^{-1}, 24/18°C (day/night) temperature, 14/10-h (day/night) photoperiod, and 60 ± 3% relative humidity for 3 days of acclimatization. In the salt stress treatment, 35 seedlings were used for each treatment. The seedlings were treated with five different NaCl concentrations (0, 50, 100, 150, and 200 mM). Three liters of the respective NaCl solution were kept in different trays before irrigation, and the seedlings were irrigated once a day for 10 min in the morning until the end of the experiment. The seedlings were grown under the same conditions for 12 days. Drought stress treatment followed the same conditions for acclimatization. For the drought stress experiment, one set of grafted seedlings was irrigated every day with the nutrient solution EC 1.5 dS^{-1} using the sub-irrigation method for 20 min as the control (well-irrigated), whereas another set of seedlings was not irrigated (non-irrigation) after the start of the experiment for 3 days and assumed to be drought stressed. The conditions of the closed light box were similar to those of the salt stress experiment. The drought stress treatment was performed only for 3 days as the seedlings under drought stress showed permanent wilting symptoms with severe leaf deformation and stunted plant growth. In the temperature stress treatment, the seedlings were grown under the same light conditions, 24/20°C (day/night) temperature, 14/10-h (day/night) photoperiod, and non-controlled relative humidity for 3 days for acclimatization of the seedlings. The seedlings were then grown under three temperature conditions: low [8/4°C (day/night)], moderate [24/20°C (day/night)], and high [40/36°C (day/night)] for 12 days at the same light conditions. Irrigation was performed daily in the morning using the sub-irrigation method. Three liters of water was kept in each tray and the plug tray was embedded for 20 min in every morning and transferred to the respective temperature controller system.

Measurement of Chlorophyll Fluorescence Parameters

An open FluorCam 800 (Photon System Instruments, Drasow, Czech Republic) was used for imaging of *CF* kinetics from the upper surface of all true leaves from the intact seedlings according to Shin et al. (2020b). Cool white 6,500 K in the LED panels (130 mm × 130 mm) was used as the light source at an angle of 45°. Seedlings were adapted in dark condition for 20 min before the measurement of *CF* parameters. The distance between the camera lens and the seedling canopy was maintained at 15–20 cm. In summary, eight *CF* parameters were assessed according to Shin et al. (2020b) using the following protocols: quenching act 2, shutter speed 20 μs, sensitivity 20%, actinic light 240 μmol m^{-2} s^{-1}, and the saturating flash light 300 μmol m^{-2} s^{-1}. Detailed information on each *CF* parameter is provided in **Table 1**. For the salinity and temperature stress treatments, seven watermelon-grafted seedlings (from 35 seedlings per treatment) were randomly selected for each time point (0, 2, 4, 6, 8, 10, and 12 days after the initiation of salinity stress) and used to measure the *CF* parameters. In contrast, the *CF* parameters were measured every day until day 3 of the drought stress initiation. Five seedlings (from 20 seedlings per treatment) were randomly selected for each

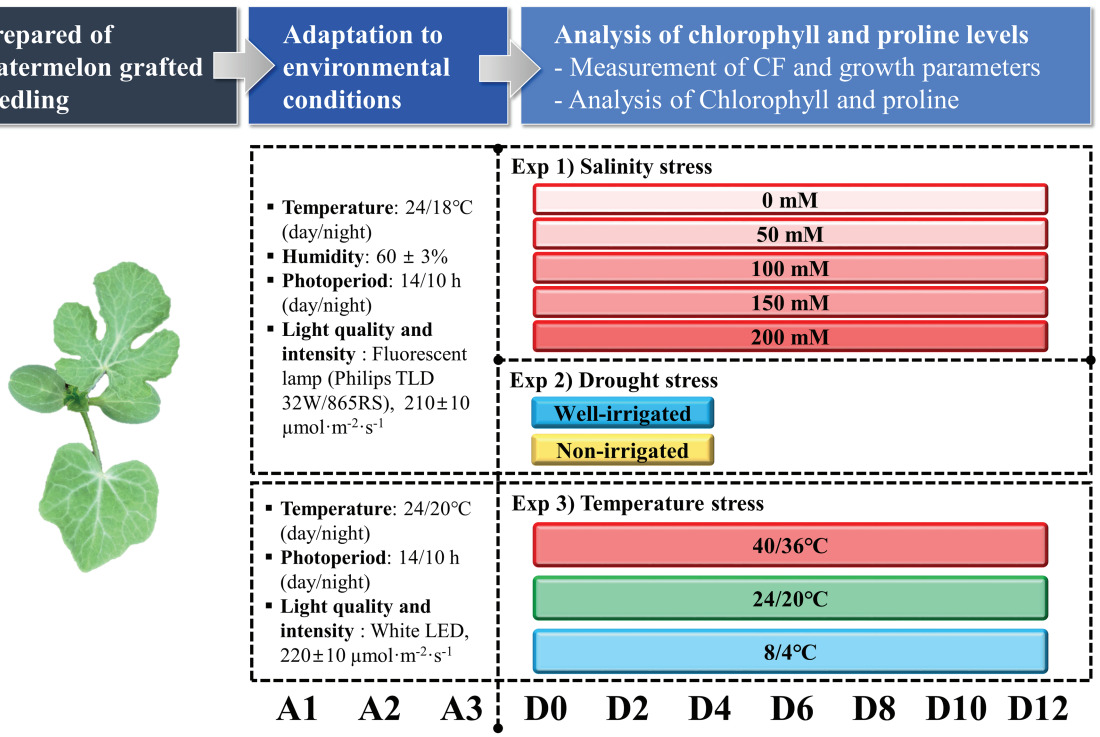

FIGURE 1 | Overview of individual experimental processes and measurement timeline. A1, A2, and A3 represent the respective acclimatization times. D0–D12 represents the days after the treatment time.

TABLE 1 | Chlorophyll fluorescence parameters used in this study.

Parameter	Formula	Description
Fv/Fm	(Fm – F0)/Fm	Maximum quantum yield of PSII photochemistry measured in the dark-adapted state
Fv′/Fm′	(Fm′ – F0')/Fm′	Exciton transfer efficiency from antenna pigments to the reaction center of photosystem II (PSII) in the light-adapted state
Y(PSII)	(Fm′ – Fs)/Fm′	Effective quantum yield of photochemical energy conversion in PSII
NPQ	(Fm – Fm′)/Fm′	Non-photochemical quenching of maximum fluorescence
qP	(Fm′ – Fs)/(Fm′ – F′0)	Photochemical quenching of PSII
qN	(Fm – F′m)/(Fm – F′0)	Coefficient of non-photochemical quenching of variable fluorescence
Y(NO)	1/[NPQ + 1 + qL(Fm/F0–1)]	Quantum yield of non-regulated energy dissipation in PSII
Rfd	(Fm – Fs)/Fs	Ratio of fluorescence decline

measurement time (0, 1, 2, and 3 days) and used for the analysis of *CF* parameters.

Measurement of Growth Parameters and Soil Moisture Content

Growth parameters included the number of leaves, shoot fresh and dry weights of the scion, plant height of scion and stock, and root fresh weight. Plant height was measured using a set of digital calipers (CD-20APX; Mitutoyo Co., Kanagawa, Japan) to evaluate the growth performance of the grafted seedlings. Fresh shoot and root weights were measured using a digital weighing machine (UX420H; Shimadzu Corp., Kyoto, Japan). The relative water content of the soil in a single plug tray was measured by drying the soil samples at 105°C for 72 h according to Shin et al. (2021a). The seedlings from 0, 6, and 12 of treatment time after measuring *CF* and growth parameters were collected separately, freeze-dried and used for chlorophyll and proline analysis in salinity and temperature stress treatments, whereas the samples from all the treatment times (0, 1, 2, and 3 days after the initiation of treatment) were used in the drought stress experiment. Seven seedlings from each treatment and time were mixed independently, freeze-dried, ground into a fine powder, and stored at −20°C for the analysis of chlorophyll and proline content.

Analysis of Chlorophyll and Proline Content

Chlorophyll a and b were measured according to Shin et al. (2020b) using a microplate reader (Multiskan Go; Thermo Scientific Inc.). Twenty milligrams of freeze-dried and finely

powdered samples were mixed with 10 ml MeOH (Avantor Performance Materials Co., Center Valley, PA, United States) for 2 h at room temperature (~25°C), and the aliquot was centrifuged at 2,400 × *g* for 10 min. The supernatant was filtered using a 0.45 μm syringe filter, and the absorbance was measured at 652 and 665 nm using a microplate reader.

The method for analysis of proline content was adopted from Shin et al. (2020b). A total of 50 mg of freeze-dried and powdered samples was mixed in 5 ml of 3% aqueous sulfosalicyclic acid dehydrate (Sigma-Aldrich, St. Louis, MO, United States), extracted for 1 h by shaking at 200 rpm, centrifuged (2,400 × *g* for 10 min), and filtered. The supernatant of the sample (500 μl), acetic acid from Sigma-Aldrich (500 μl), and acid ninhydrin from Sigma-Aldrich (500 μl) were mixed simultaneously in a 15-ml tube, kept in a water bath (at 95°C) for 1 h, and cooled rapidly on ice for 10 min. After adding 1 ml of toluene (Sigma-Aldrich) to the supernatant, the mixture was vortexed and centrifuged at 2,400 × *g* for 10 min. Thereafter, the toluene phase (200 μl) was added in a 96-well plate, and the absorbance was measured using a microplate reader at 520 nm. Proline content was quantified using a commercial L-proline (Sigma-Aldrich) standard with a linear range of 0–100 μg ml^{-1}.

Statistical Analyses

The results of growth parameters and *CF* parameters in salinity and temperature stress treatments are reported as the mean of seven biological replications, whereas the results were reported as the mean of five biological replications in drought stress treatment. The chlorophyll and proline contents were reported as the mean of three replicates in all the three experiments. Statistical analyses were performed using RStudio ver. 4.0.2 (R Studio Desktop, Boston, MA, United States). Statistical analysis followed by Duncan's multiple range test was used to analyze the statistical differences among the mean values at $p < 0.05$. The interactive effect of respective treatments and treatment time were analyzed using a mixed model of one-way analysis of variance.

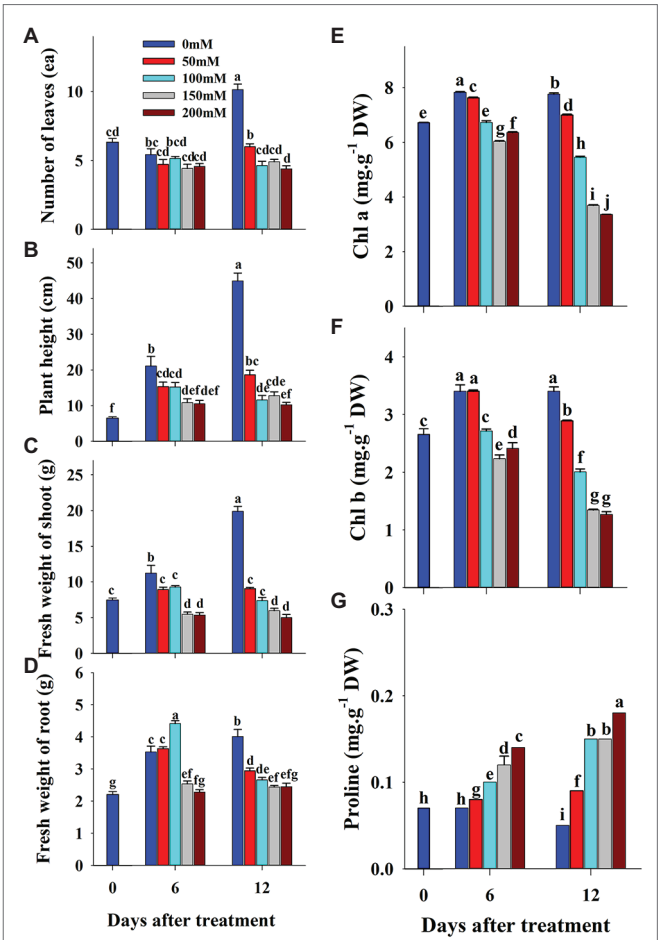

FIGURE 2 | Changes in growth parameters **(A–D)**, chlorophyll **(E,F)** and proline **(G)** content of grafted watermelon seedlings grown under salinity stress during the progressive treatment time. Each bar represents the mean ± SD of seven biological replicates in growth parameters, and three replicates in chlorophyll and proline content. Different letters within a figure indicate a significant difference at $p < 0.05$ by Duncan's multiple range test.

RESULTS

Effect of Salinity Level on Growth and *CF* Parameters

The effect of salinity level on growth parameters (number of leaves, plant height, shoot fresh weight, and root fresh weight) is presented in **Figures 2A–D**. The growth parameters were measured at 0, 6, and 12 days of the experiment. The visual appearance was poor at salinity levels of 150 and 200 mM (**Figure 3**). Growth parameters gradually decreased with increasing salinity levels during the progressive treatment. The effect of salinity level was highest at 12 days after treatment initiation. The number of leaves significantly decreased at all salinity levels compared to the control at day 12 of treatment. Plant height, shoot fresh weight, and root fresh weight were also significantly lower in the seedlings grown under salinity stress than in the control. The effect of salinity level on plant height was relatively higher than on other growth parameters.

The photochemical and non-photochemical quenching *CF* parameters measured at 2-day intervals were affected by salinity levels during the progressive treatment time (**Figure 4**). Except for Y(NO), all the other *CF* parameters decreased at higher salinity levels during the progressive treatment time. Fv/Fm, maximum quantum yield of PSII, showed non-significant changes until the end of the experiment (12 days of treatment time) at 0-, 50-, and 100-mM salinity levels. However, it decreased significantly at 150- and 200-mM salinity level from 8 day of treatment. Fv′/Fm′ also decreased at higher salinity levels in the later stage of treatment time; however, the magnitude of the decrease was lower than that of Fv/Fm. NPQ, an important non-photochemical quenching parameter, was not affected at the 50-mM salinity level throughout the experiment. It showed a gradual decrease from 6, 8, and 10 days after treatment at salinity levels of 200, 150, and 100 mM, respectively. Y(NO), a component that indicates the effectiveness of the photo-protection mechanism, started to increase from 8 days after treatment

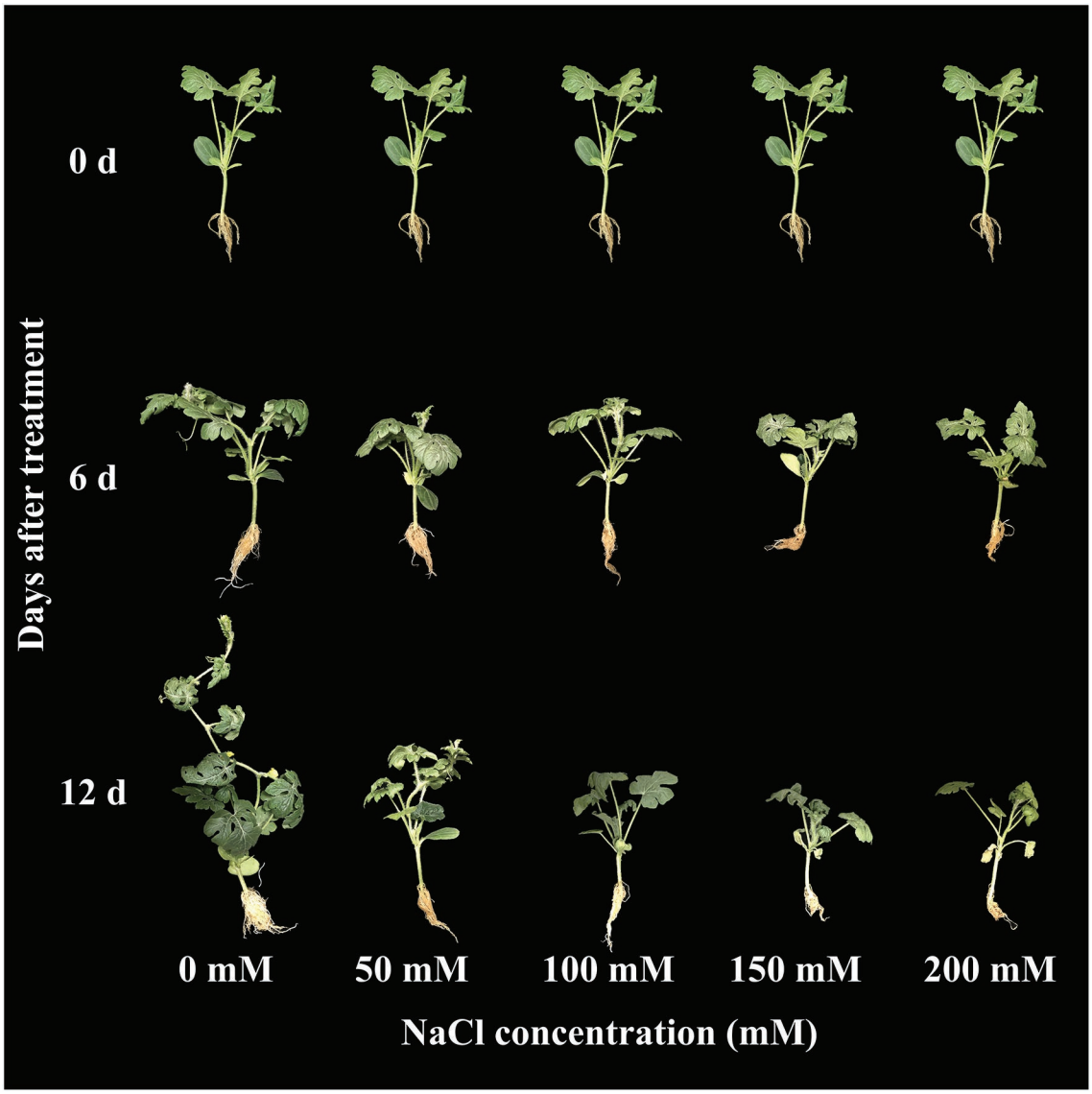

FIGURE 3 | Changes in visual appearance of grafted watermelon seedlings grown under different salinity levels during the progressive treatment time.

only at higher salinity levels (150 and 200 mM). Rfd also showed a similar changing pattern as in the NPQ at the respective salinity levels. qP, qN, and Y(PSII) also decreased with an increase in salinity level (>50 mM) from the 4 day of treatment. In summary, the results showed significant differences in all *CF* parameters according to salinity level, treatment duration, and their interactive effects (**Table 2**).

Effect of Temperature Stress on Growth and Chlorophyll Fluorescence Parameters

The effects of low, moderate, and high temperature on growth parameters at 0, 6, and 12 days of treatment are presented in **Figure 5**. All the growth parameters were lower in both the high and low temperature conditions compared to the control in respective treatment times. The total number of leaves and root fresh weight were statistically higher at the end of the experiment than in the beginning in both moderate and high temperature conditions; however, it remained constant throughout the experimental time at low temperature. Plant height and shoot fresh weight increased under moderate and high temperature conditions, whereas they increased at 6 days of treatment time and decreased with further treatment time at low temperature. Among the three treatment conditions, low temperatures showed significantly lower values of growth parameters at the end of the experiment. Although the growth parameters were highly reduced in the low-temperature treatment, the visual appearance of seedlings was as good as that in seedlings at moderate temperature (**Figure 6**). The leaves of seedlings grown under higher temperatures showed yellow burning leaves.

The *CF* parameters were differentially affected by the temperature conditions. Among the three temperature conditions, low temperature showed the highest effect on all *CF* parameters (**Figure 7**). Fv/Fm values continuously decreased from 0.81 at 0 day to 0.45 at the end of the experiment under low temperature treatment; they remained steady throughout the treatment time in high- and moderate-temperature conditions. A similar decreasing pattern was also observed in Fv′/Fm′ and Y(PSII) values in the seedlings at low temperatures. Rfd and NPQ were significantly affected by both high and low temperatures, showing a gradual decrease during progressive treatment time. In contrast, qP and qN showed non-significant changes under all temperature conditions. Only low temperature had a significant effect on Y(NO) levels, which increased gradually from the beginning and were highest at the end of the experiment. Overall, the effect of temperature stress, treatment time, and their interaction showed significant results for nearly all the *CF* parameters except for qP (**Table 3**).

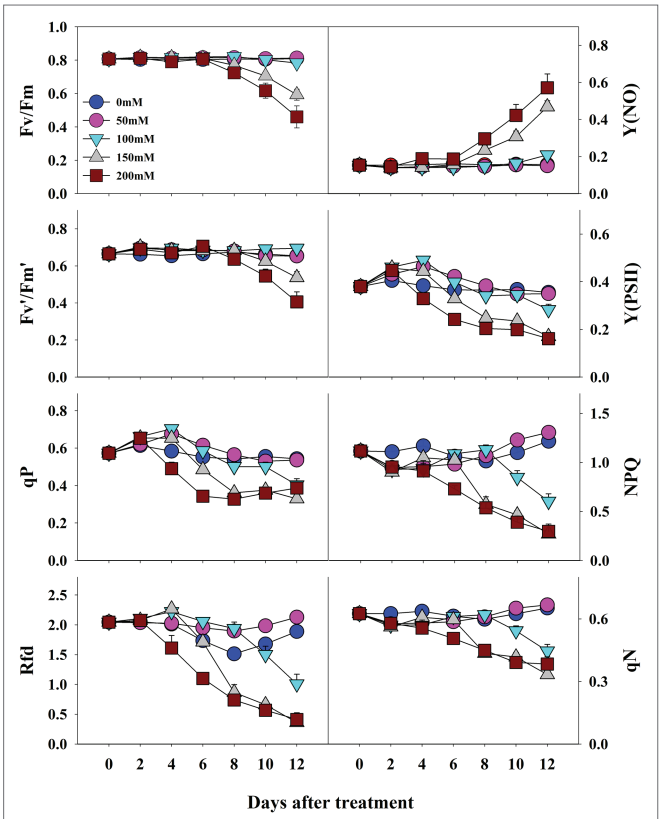

FIGURE 4 | Changes in *CF* parameters in grafted watermelon seedlings grown under different salt concentration levels during the progressive treatment time. Each plot point represents the mean ± SD of seven biological replicates. Refer **Table 1** for the description of each parameter.

Effect of Drought Stress on Growth and Chlorophyll Fluorescence Parameters

The changes in soil water content and growth parameters of watermelon seedlings during the progressive treatment time (0–3 days after treatment) under control (well-irrigation) and drought-stress (no-irrigation) treatments are presented in **Figure 8**. The water content in the soil gradually decreased from 77% (1st day of treatment) to 37% (3rd day of treatment time) under drought stress. The shoot fresh weight and number of leaves were statistically lower in drought-stressed seedlings than in control seedlings on the 3rd day of the experiment. In contrast, plant height showed statistically similar values between control and drought stress groups at the respective treatment times, although the value was lower in drought-stressed seedlings than in the control at the end of the experiment. The shoot of the scion began to wither continuously after the initiation of drought stress, and the stock began to wilt on the 2nd day (**Figure 9**). On the 3rd day of drought stress, the seedlings had permanent wilting symptoms showing cotyledons and curling of first three true leaves downward and upward, respectively; therefore, further treatment was not performed.

Most of the *CF* parameters did not differ significantly between control and drought-stressed seedlings during the respective treatment times (**Figure 10**). Fv/Fm remained unchanged throughout the experiment between control and drought stress treatment, while Fv′/Fm′, Y(NO), qN, and NPQ showed significant changes only at the end of the experiment (3rd day of treatment time). In contrast, Y(PSII), qP, and Rfd in drought stressed seedlings showed some decrement when compared to

TABLE 2 | Summary of analysis of *CF* parameters of watermelon grafted seedlings at five salinity levels (0, 50, 100, 150, and 200 mM) and seven treatment times (0, 2, 4, 6, 8, 10, and 12 days).

Parameters	Salinity level (S)		Treatment time (T)		S × T	
	F-Value	Significance	F-Value	Significance	F-Value	Significance
Fv/Fm	33.83	***	23.45	***	9.04	***
Fv′/Fm′	16.107	***	19.26	***	6.84	***
Y(PSII)	63.04	***	68.74	***	7.37	***
NPQ	80.57	***	15.70	***	15.62	***
qN	62.88	***	15.09	***	12.10	***
qP	41.987	***	46.18	***	6.05	***
Rfd	73.12	***	56.85	***	12.99	***
Y(NO)	46.05	***	30.95	***	10.03	***

*** *indicate significance at $p < 0.001$. Detailed information on each CF parameter is provided in* ***Table 1****.*

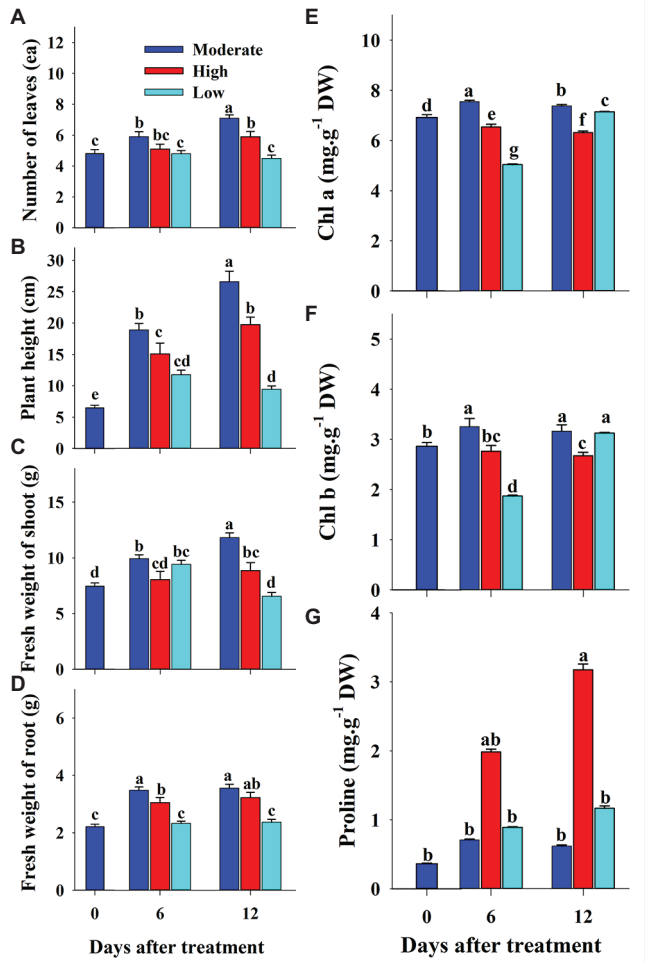

FIGURE 5 | Changes in growth parameters **(A–D)**, chlorophyll **(E,F)** and proline **(G)** content of grafted watermelon seedlings grown under moderate, high, and low temperatures during the progressive treatment time. Each bar represents the mean ± SD of seven biological replicates in growth parameters, and three replicates in chlorophyll and proline content. Different letters within a figure indicate a significant difference at $p < 0.05$ by Duncan's multiple range test.

control seedlings at respective treatment time showing the statistically lower value at the end of the treatment time. At overall, except for Fv/Fm, all *CF* parameters were significantly affected by drought stress, treatment time, and their interaction (**Table 4**).

Effect of Salinity, Temperature, and Drought Stress on Chlorophyll and Proline Content

Chlorophyll and proline content were differentially affected by salinity, drought, and temperature stress. Content levels of both chlorophyll a and b decreased with increasing salinity levels and treatment time (**Figures 2E,F**). Chlorophyll a was decreased significantly with the increase of salinity level until 150 mM, and increased at 200 mM salinity level at 6 days of treatment time, while it continuously decreased with the increase of salinity level at 12 days of treatment time. Chlorophyll b followed somewhat similar pattern as shown in chlorophyll content at 6 days of treatment time while it was statistically similar in higher concentration (150 and 200 mM) at 12 days of treatment time. Chlorophyll b was more sensitive to salinity levels than chlorophyll a. It showed 29 and 63% of decrement in 6 and 12 days of treatment time, respectively in 200 mM salinity level compared to the control. Temperature stress also had a significant effect on both chlorophyll a and b content. Seedlings exposed to both high and low temperature conditions had statistically lower chlorophyll content levels at both 6 and 12 days of treatment compared to the control (**Figures 5E,F**). However, they were differentially affected by high and low temperatures. High temperature showed a continuous decrease in levels of both chlorophylls as the treatment time progressed, whereas both chlorophylls content decreased at day 6 and was restored at day 12 of low temperature stress. The effect of high temperature stress on the chlorophyll content was lower than that of the salinity stress treatment showing only 13 and 14% of decrement in 6 and 12 days of treatment time, respectively. Levels of both chlorophyll a and b increased at day 12 of treatment at low temperatures when compared with those at high temperatures. Seedlings under drought stress showed significantly higher chlorophyll a content levels than the control at the 1st day and decreased from the 2nd day on, whereas chlorophyll b levels were lower in drought-stressed seedlings than in the control from the 1st day of treatment to the end of the experiment (**Figures 8E,F**).

The level of proline, an important stress indicator, increased with increases in salinity level at both 6 and 12 days of treatment time (**Figure 2G**), and the highest proline levels were found in the 200 mM-salinity level-treatment seedlings. Similarly, temperature stress also caused a significant change in proline content (**Figure 5G**). Plants subjected to both the high and low temperature treatment had higher proline content compared to the control at both the 6 and 12 day of treatment time (**Figure 8G**). High temperature stress showed the highest proline accumulation in both the 6 and 12 day of treatment time. Drought stress also resulted in higher proline content in stressed seedlings than in the control at different treatment times. Overall, the effect of each stressor, treatment time, and their interaction had significant effects on both chlorophyll and proline content (**Table 5**). Temperature stress showed the most significant changes (*F*-value: 5387; $p > 0.001$) in proline content within the stress levels of respective experiments, while both the chlorophyll a and b were highly affected by salinity stress than by the water and temperature stress.

DISCUSSION

Effect of Salt, Temperature, and Drought Stress on Growth Parameters

Plants experience many biotic and abiotic stresses during their life cycle. Salt, temperature, and drought stress are important abiotic stresses that have adverse effects on plant growth and productivity. This study summarizes the effects of salt, temperature, and drought stress on growth and *CF* parameters

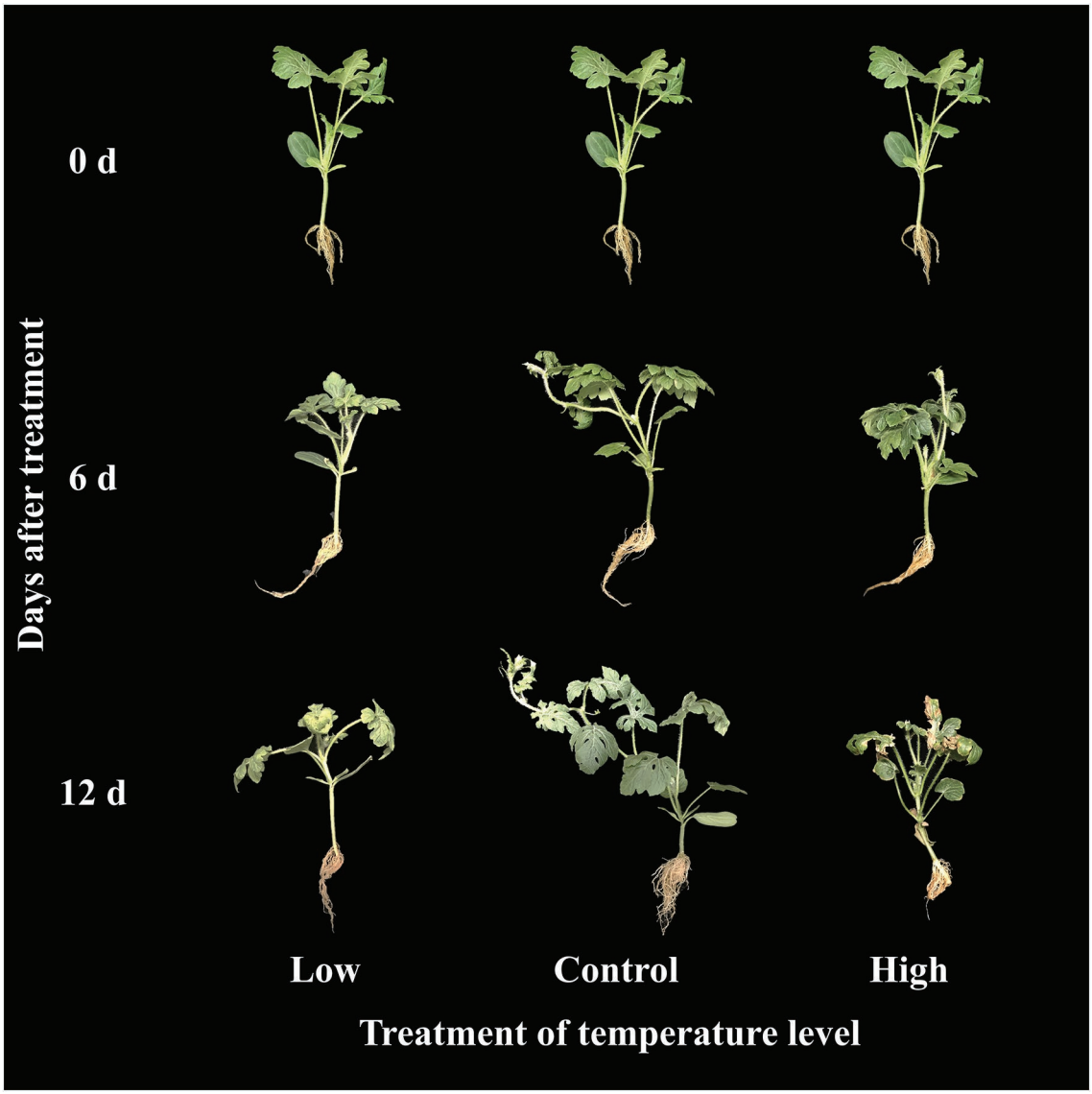

FIGURE 6 | Changes in visual appearance of grafted watermelon seedlings grown under different temperature conditions during the progressive treatment time.

along with chlorophyll and proline content in grafted watermelon seedlings at three true-leaf stages. The results showed the differential effects of each stress on growth performance and the photosynthetic apparatus. The magnitude of the effect was dependent on the type of stress and the duration of seedling exposure to stress. We found a significant decrease in growth parameter values under all stress conditions, which was consistent with previous reports in a range of plants, including watermelon (Hou et al., 2016; Bhandari et al., 2018; Yanyan et al., 2018; Lee et al., 2021; Shin et al., 2021a).

Similar to several previous studies in various plants (Bhandari et al., 2018; Shin et al., 2020a, 2021b), growth parameter values were significantly reduced in all three experiments. However, the magnitude of the variation was dependent on the stressor. There were clear differences between the control and salinity-stressed seedlings. Changes in leaf phenotype and roots of plants subjected to salinity stress and a decrease in fresh shoot weight of scions were previously observed in watermelon, *Arabidopsis*, lettuce, and tomato (Kamanga et al., 2020; Rolly et al., 2020; Shin et al., 2020a; Song et al., 2020). In addition, the poor growth status showing leaf deformation and stunted seedling growth under drought stress conditions was similar to the previous report by Zhang et al. (2011) that might be due to physiological changes in the leaves, nodes, and stems, including decreased chlorophyll content and inhibition of photosynthesis due to lack of water (Zhang et al., 2019). Similar results have been reported for tomato, watermelon, and other plants (Omprakash et al., 2017; Moles et al., 2018; Li et al., 2019). These results were similar to those of previous studies, which found that the chlorophyll content of plants affected by drought stress was reduced in watermelon, tomato, lettuce, and *Arabidopsis* affected by drought stress (Banks et al., 2018;

Yao et al., 2018; Malambane et al., 2021; Shin et al., 2021a). Our results also showed a decrease in growth parameters under high and low temperature conditions, which is in accordance with Hou et al. (2016). In addition, high-temperature and low-temperature stress causes damage to the cellular structure of plants, reduction of chlorophyll, and deterioration of photosynthetic function (Garstka et al., 2007; Mattila et al., 2020). The result showed more prominent effect of low temperature compared to the high temperature stress this was because the stock cultivar used in this study was resistant to the high temperature. Phenotypic changes in the leaves and roots of plants subjected to low-temperature stress and a decrease in fresh shoot weight of scions were also observed in *Arabidopsis* and watermelon seedlings (Mattila et al., 2020; Lu et al., 2021).

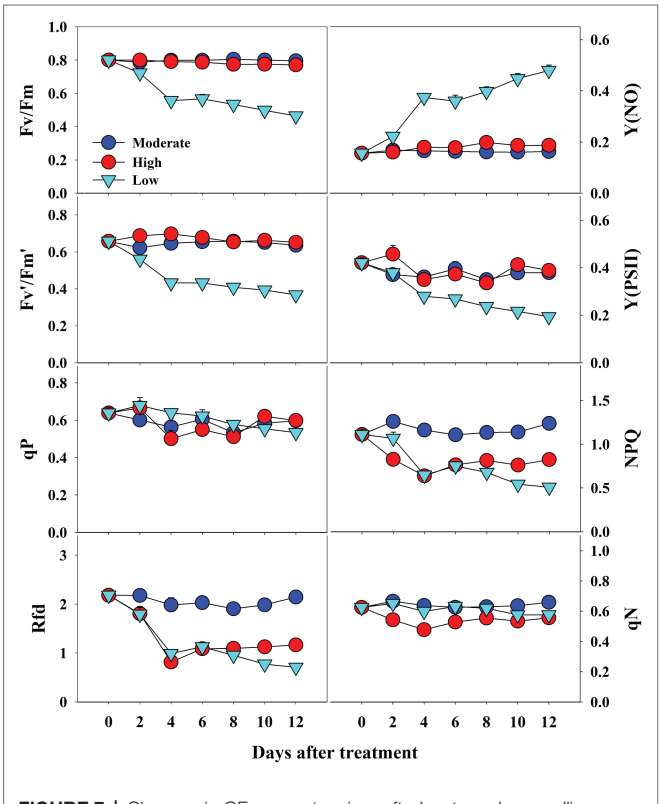

FIGURE 7 | Changes in *CF* parameters in grafted watermelon seedlings grown under moderate, high and low temperature during progressive treatment time. Each plot point represents the mean ± SD of seven biological replicates. Refer **Table 1** for the description of each parameter.

Effect of Salt, Temperature, and Drought Stress on *CF* Parameters

CF analysis can sensitively detect changes in photosynthetic activities in plants and has been used to study the response of plants to biotic and abiotic stresses (Gorbe and Calatayud, 2012; Shin et al., 2020a,b, 2021a). *CF* has been widely used as a non-destructive evaluation technique to evaluate the photosynthetic level of plants under salinity stress (Morant-Manceau et al., 2004; Bhandari et al., 2018; Shin et al., 2020b). However, the response to different stresses is highly dependent on the magnitude, type, and duration of stress undergone by the plants, and on plant genotypes. In this study, *CF* parameters responded differentially depending on the type of stress, although the general trends of some parameters were similar. Plants exposed to stressful conditions exhibited a decreasing trend in photochemical quenching and an increase in non-photochemical quenching parameters, although non-photochemical quenching parameters also decrease at severe stressful conditions (Murchie and Lawson, 2013).

Fv/Fm, an important photochemical quenching parameter that determines the maximum quantum efficiency under dark conditions, showed a similar value (~0.80) throughout the experimental period under control conditions in all three experiments. These results are consistent with a large number of other studies on unstressed plants (He et al., 2009; Bhandari et al., 2018; Shin et al., 2020b, 2021a). Salt stress induced a decrease in Fv/Fm values, but the decrease was significant only at higher salinity levels after 8 days of treatment. Similar results were also previously found in a range of plants, including watermelon (Hou et al., 2016; Shin et al., 2020b). In accordance with Bhandari et al. (2018), we found a significant decrease in Fv/Fm values in seedlings grown under low temperature, whereas high temperature did not affect Fv/Fm until the end of the experiment, indicating that higher temperatures did not damage the primary photochemical reaction sites; stroma of chloroplasts and thylakoid lamellae which are the primary sites

TABLE 3 | Summary of analysis of *CF* parameter of watermelon grafted seedlings at three temperature levels (8/4°C, 24/20°C, and 40/36°C day/night temperature) and seven treatment times (0, 2, 4, 6, 8, 10, and 12 days).

Parameters	Temperature level (T)		Treatment time (T)		T × T	
	F-Value	Significance	F-Value	Significance	F-Value	Significance
Fv/Fm	310.56	***	13.81	***	11.71	***
Fv'/Fm'	393.25	***	12.27	***	9.39	***
Y(PSII)	28.54	***	5.57	***	2.47	*
NPQ	83.63	***	7.37	***	5.98	***
qN	66.59	***	5.08	***	4.56	***
qP	2.41	NS	2.72	*	1.46	NS
Rfd	77.74	***	11.73	***	3.94	***
Y(NO)	253.10	***	14.75	***	11.84	***

*, and *** indicate significance at $p < 0.05$, and $p < 0.001$, respectively. NS: non-significant. Detailed information on each CF parameter is provided in ***Table 1***.

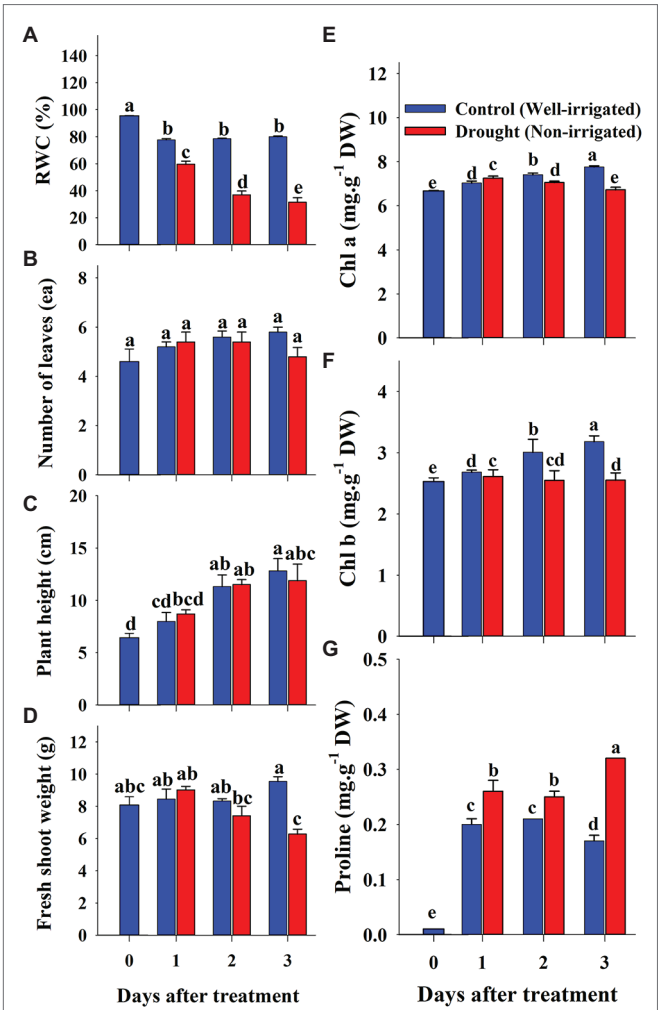

FIGURE 8 | Changes in growth parameters **(A–D)**, chlorophyll **(E,F)** and proline **(G)** content of grafted watermelon seedlings grown under drought stress during the progressive treatment time. Each bar represents the mean ± SD of five biological replicates in growth parameters, and three replicates in chlorophyll and proline content. Different letters within a figure indicate a significant difference at $p < 0.05$ by Duncan's multiple range test. RWC: relative water content.

of heat injury (Wise et al., 2004). In the drought stress treatment, we found non-significant changes in Fv/Fm throughout the treatment period. Such differential effects on Fv/Fm by abiotic stresses have also been observed in a range of plants (Fahad et al., 2017; Giordano et al., 2021), however, this is the first report that provides information on Fv/Fm values under three stress factors at the same time.

The other photochemical quenching parameters [Fv′/Fm′, Y(PSII), and qP] were also affected when exposed to stress conditions. All of them exhibited similar trends as in the case of Fv/Fm, although the magnitude was different, showing lower values when exposed to higher salt stress (>50 mM). In the case of temperature stress treatment, we found significantly lower values of Fv′/Fm′ and Y(PSII) from days 2 and 4 of treatment onward, respectively. In contrast, qP showed non-significant changes. Furthermore, only Y(PSII) values exhibited significant differences between control and drought-stressed seedlings, and even in that case, the difference was statistically significant at the end of the experiment. The decrease in the Fv′/Fm′ values in the seedlings grown under lower temperatures might be due to chilling injury caused by cold stress under the given conditions (Hou et al., 2016). All the photo chemical quenching parameters were affected by temperature stress suggesting the disturbed homeostasis *via* the modification in carbon metabolism enzymes, starch accumulation, and sucrose synthesis, by down regulating the genes in carbohydrate metabolism (Ruan et al., 2010).

Values of the non-photochemical quenching parameters NPQ and qN decreased with increasing salinity level and treatment time. In this case, we also found a significant effect at higher salinity levels (>50 mM). The adverse effect was observed at 150- and 200-mM salinity levels. In the second experiment with temperature stress conditions, both the high and low temperatures had non-significant effects on qN when compared to the control at the respective treatment time. In contrast, both high and low temperatures exhibited significant differences in NPQ values at the respective treatment times. NPQ levels generally increase under stressful conditions and decrease under severe stressful conditions (Murchie and Lawson, 2013), and the magnitude of changes depends on the plant species and the level of stress (Yao et al., 2018; Shin et al., 2020a). Seedlings grown under high salinity level and low and high temperatures showed a significant decrease in NPQ levels when compared to control seedlings during the respective treatment time, indicating a reduction in the heat dissipation capacity, limitations of CO_2 assimilation, and imbalance of photochemical activity in photosystem II (Huang et al., 2019). In addition, our results also indicated the incapacity of the protection mechanism due to senescence for the downregulation during those periods (Ors et al., 2021). Furthermore, non-significant changes in NPQ levels until the end of the experiment under drought conditions indicated that the photochemical activity in the photosystem was not severely influenced until that period.

Y(NO) is an important *CF* parameter that indicates the effectives of the photo-protective mechanisms (NPQ) in plants. The increase in Y(NO) levels at a higher salinity levels and at lower temperature conditions implied that the seedlings received extreme stress during the experiment, and the NPQ was decreased under extreme stress conditions (Murchie and Lawson, 2013; Huang et al., 2019). These results are consistent with previous reports on watermelon and tomato seedlings (Hou et al., 2016; Shin et al., 2020a). Similar to the effects on NPQ, Y(NO) levels also exhibited non-significant changes until the 2nd day of treatment time in drought stress treatment, implying that the photosynthetic activity was normal until that period. Rfd, an indicator of plant vitality under stressful conditions (Murchie and Lawson, 2013), showed a significant decrease in high salinity levels from day 4 of the experiment on salinity stress experiment. Our results were consistent with those of Shin et al. (2020b), who also found a significant decrease in Rfd levels in tomato seedlings exposed to extreme salinity stress. Both the high-and low-temperature stress also showed a significant decrease in Rfd levels from the beginning

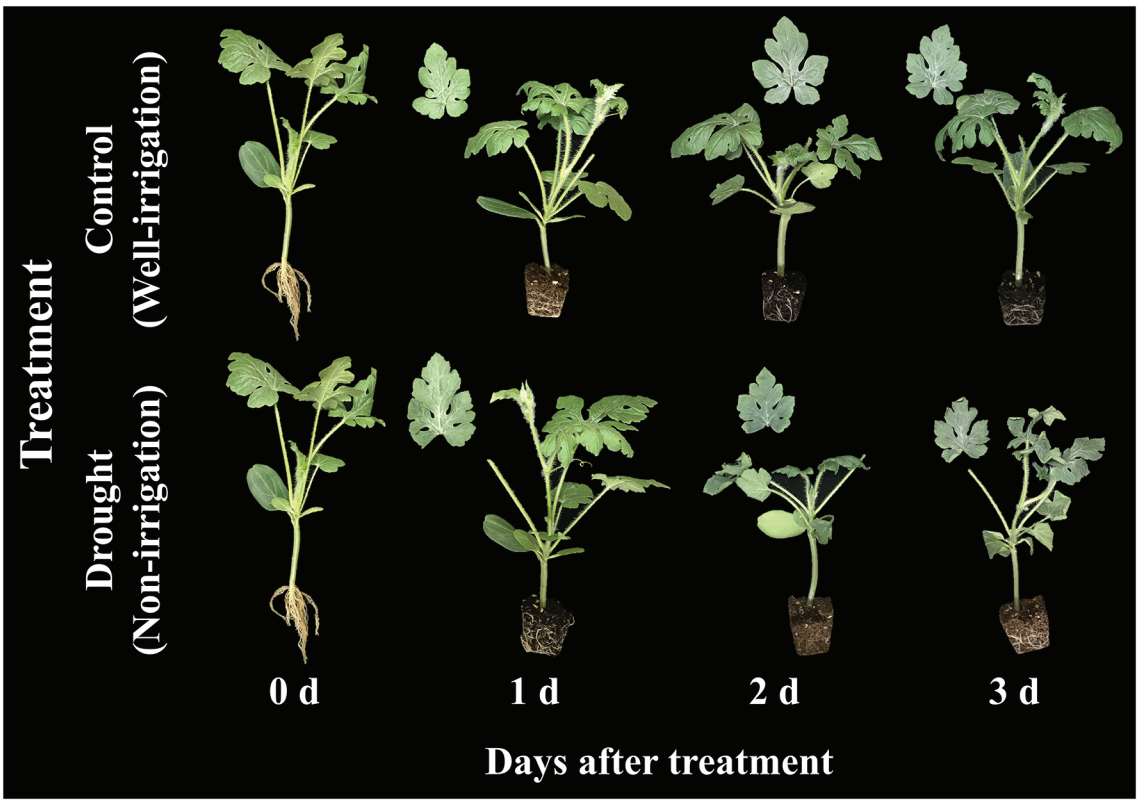

FIGURE 9 | Changes in visual appearance of grafted watermelon seedlings grown under control and drought stress conditions during the progressive treatment time.

of the experiment; however, low temperature had a more prominent effect on Rfd levels, in accordance with Hou et al. (2016). Drought stress had minimal effect only at the end of the experiment, suggesting that the photosynthetic protective mechanism of watermelon seedlings is affected only under extreme drought conditions (soil water level < 40%). NPQ, which was the common parameter significantly affected by each of the stressor, is presented as a representative chlorophyll fluorescence images to understand the spatial heterogeneity (**Figure 11**). The results showed the obvious spatial variation in *CF* images but differently depending upon the stressor.

The response of *CF* parameters to salt, temperature, and drought stress conditions were different from each other. Fv/Fm, NPQ, Rfd, and Y(NO) showed significant changes during the progressive treatment time at higher salinity levels, suggesting the possible use of these parameters to detect salinity stress. Only two *CF* parameters; Rfd and NPQ were significantly affected under high temperature conditions even the cultivar was high-temperature resistant, while six parameters [Fv/Fm, Fv′/Fm′, Rfd, Y(NO), Y(PSII), and NPQ] were affected significantly under low temperature conditions. So, two parameters (Rfd and NPQ) can be used to detect low-and high-temperature stress, as these parameters decreased significantly from the beginning of the experiment under both temperature conditions. Furthermore, Rfd and NPQ levels decreased significantly at the end of the experiment in the drought stress treatment and could be considered for detecting drought stress. Further studies on seedlings of many watermelon genotypes exposed to long-term stress and higher light conditions might be required to detect the effect of genotype, and the impact of initial severe stress as genotype is also a key factor for the tolerance of stress conditions.

Effect of Salt, Temperature, and Drought Stress on Chlorophyll and Proline Content

Proline, one of the osmoprotectants (glycine, proline, betaine, and soluble sugars) is an important compatible solute found in plants (Farooq et al., 2008). It is generally elevated in large amounts in plants under stressful conditions. It is found in plants in small quantities even under non-stressed conditions (Trovato et al., 2008; Gupta et al., 2014). It helps to maintain membrane integrity by maintaining turgor pressure to sustain the growth of the plant (Gupta et al., 2014). The level of proline content is highly dependent on plant genotypes and stressors (Nikolaeva et al., 2010). Proline increased with the increase in stress level in all three experiments compared to the respective control seedlings, and the magnitude of increment was dependent on the stressor. We found a significant increase in proline content with increasing salinity and progressive treatment time. The highest proline levels were found in the seedlings treated with the highest salinity level, similar to previous reports on lettuce, tomato, and citrus (Shin et al., 2020a,b; Martínez-Cuenca et al., 2021). The elevation of proline levels at

different salinity levels indicated that seedlings grown at the salinity level experienced high stress levels. Our results showed that the seedlings grown under both high and low temperatures had statistically higher proline content than the control at both 6 and 12 days of treatment. However, the highest proline content was observed at high temperatures, which is consistent with previous results in paprika seedlings (Bhandari et al., 2018). The over accumulation of proline under high temperature stress was responsible to regulate the osmotic activities and protect cellular structure by maintain the membrane stability and by buffering the cellular redox potential (Farooq et al., 2008). So the status of the plants was maintained with normal photosynthesis showing non-significant changes in Fv/Fm. Similarly, seedlings experiencing drought stress also showed statistically higher proline content; however, the magnitude of increase was lower than that in previous reports (Li et al., 2019; Shin et al., 2021a), which might be due to the difference in genotypes and less treatment time. These results suggest that a responsive mechanism exists due to salt, temperature, and drought stress in grafted watermelon seedlings, which along with other compounds also helps to generate an efficient antioxidant system to cope with ROS species, increase the protein stability, and stabilize the structure of the membrane bilayer (Mirzaei et al., 2012). Comparative analysis showed that the highest proline accumulation and its fluctuation occurred under temperature stress, followed by salinity stress and drought stress.

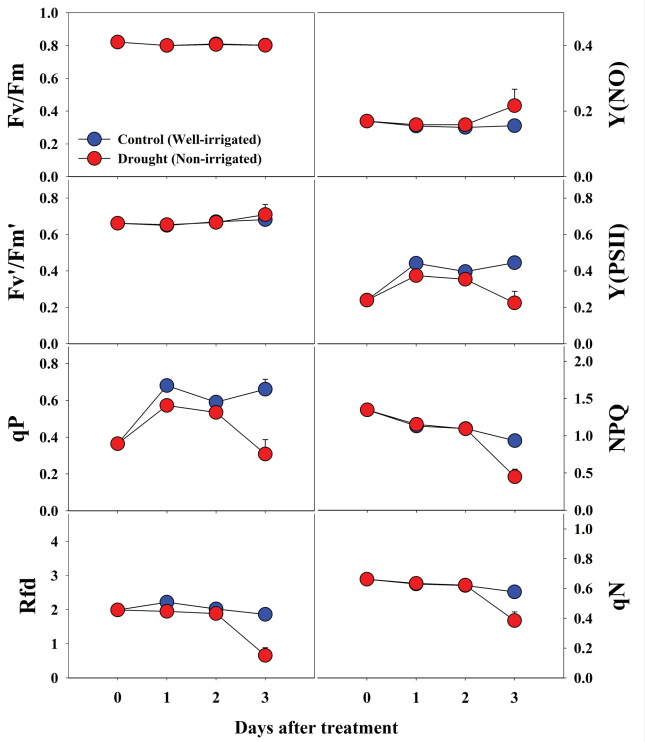

FIGURE 10 | Changes in *CF* parameters in grafted watermelon seedlings grown under control and drought stress conditions during the progressive treatment time. Each plot point represents the mean ± SD of seven biological replicates. Refer to **Table 1** for the description of each parameter.

Chlorophylls are photosynthetic pigments that are responsible for the photosynthetic efficiency of plants and are ultimately responsible for primary production (Gitelson et al., 2003). Chlorophyll a and b levels were measured in all three experiments, and we found significant changes in the levels of both chlorophylls with increasing stress levels. The levels of both chlorophyll a and b decreased with increasing salinity levels during the progressive treatment time, consistent with previous reports in different vegetables, including watermelon (Taïbi et al., 2016; Yanyan et al., 2018; Shin et al., 2020a, 2021a). The lower content levels of the chlorophylls at higher salinity levels was probably due to damage to the chloroplast membrane and structure, increased activity of chlorophyllase, and photo-oxidation of chlorophyll due to the excessive accumulation of salt in the soil (Taffouo et al., 2010; Silveira and Carvalho, 2016). Temperature stress treatment showed a somewhat different accumulation pattern of chlorophylls, and the effect was lower than that of salinity stress. As watermelon is a thermophilic crop, it is less affected at high temperatures than at low temperatures, and seedlings grown at low temperatures exhibited relatively higher chlorophyll content than those grown at high temperatures. Our results were consistent with previous reports by Hou et al. (2016), who also found lower chlorophyll content in watermelon seedlings grown at cold temperatures. This is because plants exposed to low temperatures experience chilling

TABLE 4 | Summary of analysis of *CF* parameters of watermelon grafted seedlings at two water levels (well-irrigated and non-irrigated) and four treatment times (0, 1, 2, and 3 days).

Parameters	Water level (W)		Treatment time (T)		W × T	
	F-Value	Significance	F-Value	Significance	F-Value	Significance
Fv/Fm	2.93	NS	1.11	NS	0.82	NS
Fv′/Fm′	8.25	**	17.58	***	6.51	**
Y(PSII)	89.41	***	3.82	*	21.22	***
NPQ	15.16	***	32.80	***	17.95	***
qN	39.51	***	57.78	***	41.52	***
qP	86.86	***	6.30	**	22.35	***
Rfd	68.04	***	26.91	***	23.86	***
Y(NO)	39.22	***	15.50	***	22.35	***

*, **, and *** *indicate significance at* $p<0.05$, $p<0.01$, *and* $p<0.001$, *respectively. NS: non-significant. Detailed information on each CF parameter is provided in* ***Table 1***.

TABLE 5 | Summary of analysis of chlorophyll and proline of watermelon grafted seedlings at various salinity, drought, and temperature levels, and multiple treatment times.

Treatment	Parameter	Stress level (S)		Measurement treatment time (T)		S × T	
		F-Value	Significance	F-Value	Significance	F-Value	Significance
Salt	Chl a	9,147	***	7,891	***	1875	***
	Chl b	697.41	***	492.61	***	64.66	***
	Proline	963.06	***	62.02	***	11.93	***
Drought	Chl a	36.09	***	68.58	***	98.83	***
	Chl b	12.13	**	45.45	***	37.76	***
	Proline	889.36	***	285.41	***	61.56	***
Temperature	Chl a	572	***	203.4	***	532	***
	Chl b	73.41	***	44.46	***	97.33	***
	Proline	5387.5	***	399.7	***	469.2	***

** and *** indicate significance at $p < 0.01$ and $p < 0.001$, respectively. Chl: chlorophyll.

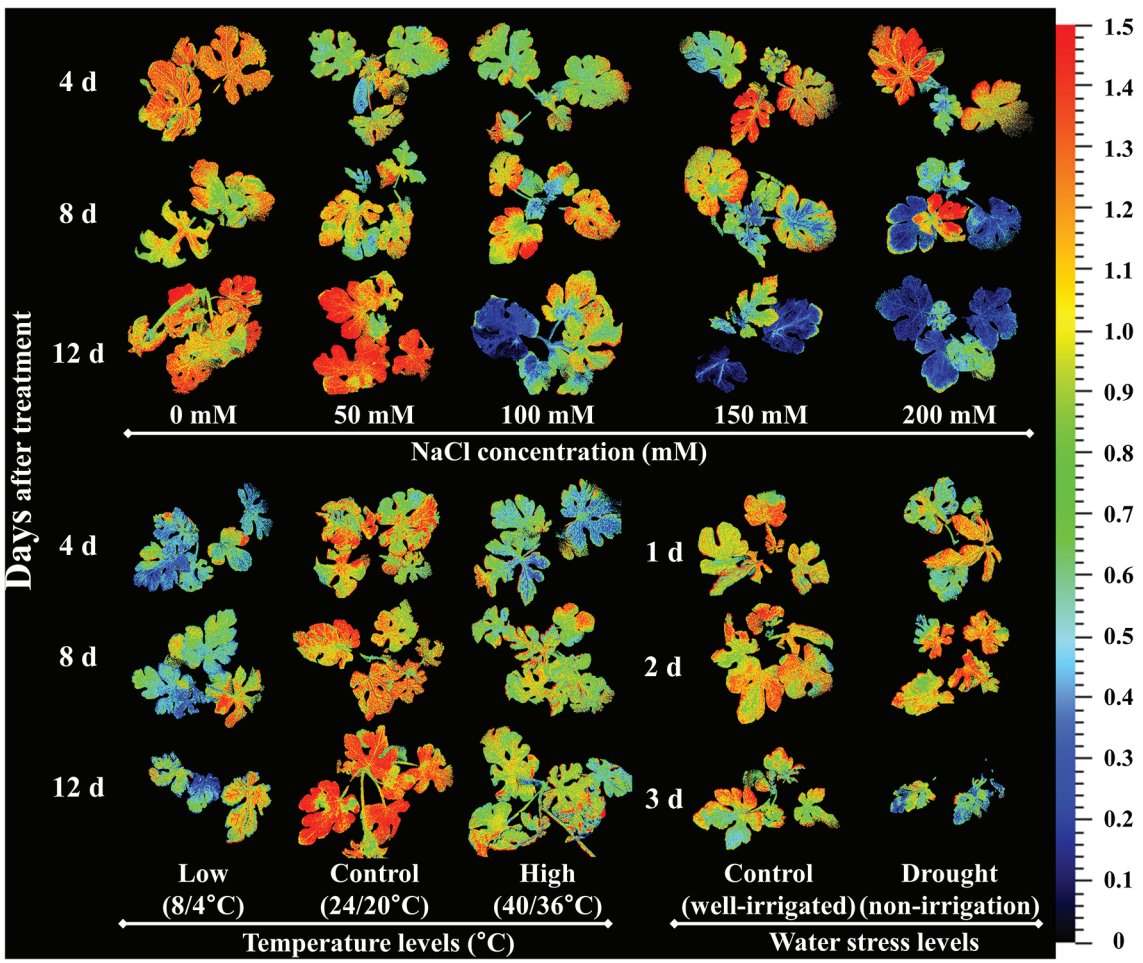

FIGURE 11 | Representative chlorophyll fluorescence images of non-photochemical quenching (NPQ) under the salinity, drought, and temperature stress treatment in different time after each stress initiation in watermelon seedlings.

injury, which enhances ion imbalance, reduction in antioxidant activity, and low chlorophyll content (Lu et al., 2020; Mlinarić et al., 2021). Chlorophyll content in drought-stressed seedlings was least affected among the three treatment types, although significant changes were observed between control and drought-stressed seedlings during the respective treatment schedule. In the drought stress experiment, the treatment was conducted for only 3 days as the status of the seedling was poor after that period. Previous reports also showed that chlorophyll levels in plants decrease after severe stress; however,

some authors have reported an increase in chlorophyll content for some time and decrement after exposure to severe stress conditions (Partelli et al., 2009; Bhandari et al., 2018; Shin et al., 2020b, 2021a).

CONCLUSION

This study showed the potential of using *CF* imaging to detect abiotic stressors (salinity, high and low temperature, and drought) in grafted watermelon seedlings (**Figure 11**). The response of the seedlings to various abiotic stresses was observed through changes in *CF* and growth parameters, chlorophyll, and proline content. The changes were dependent on the type of stressor and duration. Most *CF* parameters were affected only at the higher salinity stress (>50 mM), with the most influential parameters being Fv/Fm, NPQ, Rfd, and Y(NO) increased during the progressive treatment time. Low temperature had a prominent effect on nearly all the *CF* parameters compared to the high temperature stress, suggesting that the low temperature caused more severe photo-inhibition of photosynthesis than high temperature. Drought stress had a similar effect on *CF* parameters as in the high-temperature stress, showing significant changes only in the Rfd and NPQ. Altogether, NPQ and Rfd could be used as index parameters for the detection of three abiotic stresses. In general, values of all the growth parameters reduced, chlorophyll content levels were decreased or increased depending upon the stressor, and proline content was increased in the seedlings exposed to each stressor. These results imply that photosynthetic activity, growth performance, and chlorophyll and proline content are differentially affected by each stressor and their magnitude, which might be useful for the effective detection of each stress during the production process of watermelon-grafted seedlings. Furthermore, research on open environmental conditions having high light condition and combined application of stressors are required for understanding the comparative and synergetic effects of these stressors, respectively in photosynthetic and growth parameters in watermelon seedlings.

DATA AVAILABILITY STATEMENT

The original contributions presented in the study are included in the article/supplementary material, further inquiries can be directed to the corresponding authors.

AUTHOR CONTRIBUTIONS

YKS designed and performed the experiments, statistically analyzed and interpreted the data, and wrote the manuscript. SRB designed the experiment, analyzed and interpreted the data, and wrote the manuscript. JGL conceived the project, designed the experiment, and wrote the manuscript. All authors contributed to the article and approved the submitted version.

FUNDING

This research was funded by the Basic Science Research Program through the National Research Foundation of Korea (NRF) by the Ministry of Education (no. 2019R1A6A1A09031717).

REFERENCES

Banks, J. M. (2018). Chlorophyll fluorescence as a tool to identify drought stress in acer genotypes. *Environ. Exp. Bot.* 155, 118–127. doi: 10.1016/j.envexpbot.2018.06.022

Bhandari, S. R., Kim, Y. H., and Lee, J. G. (2018). Detection of temperature stress using chlorophyll fluorescence parameters and stress-related chlorophyll and proline content in paprika (*Capsicum annuum* L.) seedlings. *Hortic. Sci. Technol.* 36, 619–629. doi: 10.12972/kjhst.20180062

Bulgari, R., Franzoni, G., and Ferrante, A. (2019). Biostimulants application in horticultural crops under abiotic stress conditions. *Agronomy* 9:306. doi: 10.3390/agronomy9060306

Coskun, D., Britto, D. T., Huynh, W. Q., and Kronzucker, H. J. (2016). The role of silicon in higher plants under salinity and drought stress. *Front. Plant Sci.* 7:1072. doi: 10.3389/fpls.2016.01072

De Oliveira, A. B., Alencar, N. L. M., and Gomes-Filho, E. (2013). "Comparison between the water and salt stress effects on plant growth and development," in *Responses of Organisms to Water Stress*. ed. S. Akinci (London, UK: IntechOpen), 67–94.

Fahad, S., Bajwa, A. A., Nazir, U., Anjum, S. A., Farooq, A., Zohaib, A., et al. (2017). Crop production under drought and heat stress: plant responses and management options. *Front. Plant Sci.* 8:1147. doi: 10.3389/fpls.2017.01147

Food and Agriculture Organization of the United Nations (FAO) (2009). Agricultural Statistical Database for 2019. Available: http://www.fao.org/faostat/en/#data/QCL (Accessed September 15, 2021).

Farooq, M., Basra, S., Wahid, A., Cheema, Z., Cheema, M., and Khaliq, A. (2008). Physiological role of exogenously applied glycinebetaine to improve drought tolerance in fine grain aromatic rice (*Oryza sativa* L.). *J. Agron. Crop Sci.* 194, 325–333. doi: 10.1111/j.1439-037X.2008. 00323.x

Garg, A., Bordoloi, S., Ganesan, S. P., Sekharan, S., and Sahoo, L. (2020). A relook into plant wilting: observational evidence based on unsaturated soil–plant-photosynthesis interaction. *Sci. Rep.* 10, 1–15. doi: 10.1038/s41598-020-78893-z

Garstka, M., Venema, J. H., Rumak, I., Gieczewska, K., Rosiak, M., Koziol-Lipinska, J., et al. (2007). Contrasting effect of dark-chilling on chloroplast structure and arrangement of chlorophyll–protein complexes in pea and tomato: plants with a different susceptibility to non-freezing temperature. *Planta* 226, 1165–1181. doi: 10.1007/s00425-007-0562-7

Giordano, M., Petropoulos, S. A., and Rouphael, Y. (2021). Response and defence mechanisms of vegetable crops against drought, heat and salinity stress. *Agriculture* 11:463. doi: 10.3390/agriculture11050463

Gitelson, A. A., Gritz, Y., and Merzlyak, M. N. (2003). Relationships between leaf chlorophyll content and spectral reflectance and algorithms for non-destructive chlorophyll assessment in higher plant leaves. *J. Plant Physiol.* 160, 271–282. doi: 10.1078/0176-1617-00887

Gorbe, E., and Calatayud, A. (2012). Applications of chlorophyll fluorescence imaging technique in horticultural research: a review. *Sci. Hortic.* 138, 24–35. doi: 10.1016/j.scienta.2012.02.002

Gupta, S. C., Sharma, A., Mishra, M., Mishra, R. K., and Chowdhuri, D. K. (2010). Heat shock proteins in toxicology: how close and how far? *Life Sci.* 86, 377–384. doi: 10.1016/j.lfs.2009.12.015

Gupta, N., Thind, S. K., and Bains, N. S. (2014). Glycine betaine application modifies biochemical attributes of osmotic adjustment in drought stressed wheat. *Plant Growth Regul.* 72, 221–228. doi: 10.1007/s10725-013-9853-0

Hassan, A. H., Hozzein, W. N., Mousa, A. S., Rabie, W., Alkhalifah, D. H. M., Selim, S., et al. (2020). Heat stress as an innovative approach to enhance the antioxidant production in pseudooceanicola and bacillus isolates. *Sci. Rep.* 10, 1–13. doi: 10.1038/s41598-020-72054-y

Hassell, R. L., Memmott, F., and Liere, D. G. (2008). Grafting methods for watermelon production. *HortScience* 43, 1677–1679. doi: 10.21273/HORTSCI.43.6.1677

He, M., He, C.-Q., and Ding, N.-Z. (2018). Abiotic stresses: general defenses of land plants and chances for engineering multistress tolerance. *Front. Plant Sci.* 9:1771. doi: 10.3389/fpls.2018.01771

He, Y., Zhu, Z., Yang, J., Ni, X., and Zhu, B. (2009). Grafting increases the salt tolerance of tomato by improvement of photosynthesis and enhancement of antioxidant enzymes activity. *Environ. Exp. Bot.* 66, 270–278. doi: 10.1016/j.envexpbot.2009.02.007

Hou, W., Sun, A., Chen, H., Yang, F., Pan, J., and Guan, M. (2016). Effects of chilling and high temperatures on photosynthesis and chlorophyll fluorescence in leaves of watermelon seedlings. *Biol. Plant.* 60, 148–154. doi: 10.1007/s10535-015-0575-1

Huang, B., Chen, Y.-E., Zhao, Y.-Q., Ding, C.-B., Liao, J.-Q., Hu, C., et al. (2019). Exogenous melatonin alleviates oxidative damages and protects photosystem ii in maize seedlings under drought stress. *Front. Plant Sci.* 10:677. doi: 10.3389/fpls.2019.00677

Hussain, H. A., Hussain, S., Khaliq, A., Ashraf, U., Anjum, S. A., Men, S., et al. (2018). Chilling and drought stresses in crop plants: implications, cross talk, and potential management opportunities. *Front. Plant Sci.* 9:393. doi: 10.3389/fpls.2018.00393

Jia, X., Mao, K., Wang, P., Wang, Y., Jia, X., Huo, L., et al. (2021). Overexpression of mdatg8i improves water use efficiency in transgenic apple by modulating photosynthesis, osmotic balance, and autophagic activity under moderate water deficit. *Hortic. Res.* 8:81. doi: 10.1038/s41438-021-00521-2

Kalaji, H. M., Jajoo, A., Oukarroum, A., Brestic, M., Zivcak, M., Samborska, I. A., et al. (2016). Chlorophyll a fluorescence as a tool to monitor physiological status of plants under abiotic stress conditions. *Acta Physiol. Plant.* 38:102. doi: 10.1007/s11738-016-2113-y

Kamanga, R. M., Echigo, K., Yodoya, K., Mekawy, A. M. M., and Ueda, A. (2020). Salinity acclimation ameliorates salt stress in tomato (*Solanum lycopersicum* L.) seedlings by triggering a cascade of physiological processes in the leaves. *Sci. Hortic.* 270:109434. doi: 10.1016/j.scienta.2020.109434

Kapoor, D., Bhardwaj, S., Landi, M., Sharma, A., Ramakrishnan, M., and Sharma, A. (2020). The impact of drought in plant metabolism: how to exploit tolerance mechanisms to increase crop production. *Appl. Sci.* 10:5692. doi: 10.3390/app10165692

Korkmaz, A., and Dufault, R. J. (2001). Developmental consequences of cold temperature stress at transplanting on seedling and field growth and yield. I. Watermelon. *J. Am. Soc. Hortic. Sci.* 126, 404–409. doi: 10.21273/JASHS.126.4.404

Kumar, P., Rouphael, Y., Cardarelli, M., and Colla, G. (2017). Vegetable grafting as a tool to improve drought resistance and water use efficiency. *Front. Plant Sci.* 8:1130. doi: 10.3389/fpls.2017.01130

Kwack, Y., An, S., and Kim, S. K. (2021). Development of growth model for grafted hot pepper seedlings as affected by air temperature and light intensity. *Sustainability* 13:5895. doi: 10.3390/su13115895

Lee, J.-M., Kubota, C., Tsao, S., Bie, Z., Echevarria, P. H., Morra, L., et al. (2010). Current status of vegetable grafting: diffusion, grafting techniques, automation. *Sci. Hortic.* 127, 93–105. doi: 10.1016/j.scienta.2010.08.003

Lee, H. J., Lee, J. H., Wi, S., Jang, Y., An, S., Choi, C. K., et al. (2021). Exogenously applied glutamic acid confers improved yield through increased photosynthesis efficiency and antioxidant defense system under chilling stress condition in *Solanum lycopersicum* L. Cv. Dotaerang dia. *Sci. Hortic.* 277:109817. doi: 10.1016/j.scienta.2020.109817

Li, H., Mo, Y., Cui, Q., Yang, X., Guo, Y., Wei, C., et al. (2019). Transcriptomic and physiological analyses reveal drought adaptation strategies in drought-tolerant and-susceptible watermelon genotypes. *Plant Sci.* 278, 32–43. doi: 10.1016/j.plantsci.2018.10.016

Liang, G., Liu, J., Zhang, J., and Guo, J. (2020). Effects of drought stress on photosynthetic and physiological parameters of tomato. *J. Am. Soc. Hortic. Sci.* 145, 12–17. doi: 10.21273/JASHS04725-19

Lichtenthaler, H. K., and Babani, F. (2000). Detection of photosynthetic activity and water stressby imaging the red chlorophyll fluorescence. *Plant Physiol. Biochem.* 38, 889–895. doi: 10.1016/S0981-9428(00)01199-2

Lotfi, R., Ghassemi-Golezani, K., and Pessarakli, M. (2020). Salicylic acid regulates photosynthetic electron transfer and stomatal conductance of mung bean (*Vigna radiata* L.) under salinity stress. *Biocatal. Agric. Biotechnol.* 26:101635. doi: 10.1016/j.bcab.2020.101635

Lu, J., Nawaz, M. A., Wei, N., Cheng, F., and Bie, Z. (2020). Suboptimal temperature acclimation enhances chilling tolerance by improving photosynthetic adaptability and osmoregulation ability in watermelon. *Hortic. Plant J.* 6, 49–60. doi: 10.1016/j.hpj.2020.01.001

Lu, J., Shireen, F., Cheng, F., and Bie, Z. (2021). High relative humidity improve chilling tolerance by maintaining leaf water potential in watermelon seedlings. *Plant Physiol. Biochem.* 166, 818–826. doi: 10.1016/j.plaphy.2021.06.037

Malambane, G., Batlang, U., Ramolekwa, K., Tsujimoto, H., and Akashi, K. (2021). Growth chamber and field evaluation of physiological factors of two watermelon genotypes. *Plant Stress* 2:100017. doi: 10.1016/j.stress.2021.100017

Martínez-Cuenca, M.-R., Primo-Capella, A., and Forner-Giner, M. A. (2021). Screening of 'king'mandarin (*Citrus nobilis* Lour)× *Poncirus trifoliata* ((L.) raf.) hybrids as salt stress-tolerant citrus rootstocks. *Hortic. Environ. Biotechnol.* 62, 337–351. doi: 10.1007/s13580-020-00291-1

Mattila, H., Mishra, K. B., Kuusisto, I., Mishra, A., Novotná, K., Šebela, D., et al. (2020). Effects of low temperature on photoinhibition and singlet oxygen production in four natural accessions of arabidopsis. *Planta* 252:19. doi: 10.1007/s00425-020-03423-0

Mirzaei, M., Pascovici, D., Atwell, B. J., and Haynes, P. A. (2012). Differential regulation of aquaporins, small GTPases and V-ATPases proteins in rice leaves subjected to drought stress and recovery. *Proteomics* 12, 864–877. doi: 10.1002/pmic.201100389

Mlinarić, S., Cesar, V., and Lepeduš, H. (2021). Antioxidative response and photosynthetic regulatory mechanisms in common fig leaves after short-term chilling stress. *Ann. Appl. Biol.* 178, 315–327. doi: 10.1111/aab.12671

Moles, T. M., Mariotti, L., De Pedro, L. F., Guglielminetti, L., Picciarelli, P., and Scartazza, A. (2018). Drought induced changes of leaf-to-root relationships in two tomato genotypes. *Plant Physiol. Biochem.* 128, 24–31. doi: 10.1016/j.plaphy.2018.05.008

Morant-Manceau, A., Pradier, E., and Tremblin, G. (2004). Osmotic adjustment, gas exchanges and chlorophyll fluorescence of a hexaploid triticale and its parental species under salt stress. *J. Plant Physiol.* 161, 25–33. doi: 10.1078/0176-1617-00963

Moustakas, M., Calatayud, A., and Guidi, L. (2021). Editorial: Chlorophyll fluorescence imaging analysis in biotic and abiotic stress. *Front. Plant Sci.* 12:658500. doi: 10.3389/fpls.2021.658500

Murata, N., Takahashi, S., Nishiyama, Y., and Allakhverdiev, S. I. (2007). Photoinhibition of photosystem II under environmental stress. *Biochim. Biophys. Acta Bioenerg.* 1767, 414–421. doi: 10.1016/j.bbabio.2006.11.019

Murchie, E. H., and Lawson, T. (2013). Chlorophyll fluorescence analysis: A guide to good practice and understanding some new applications. *J. Exp. Bot.* 64, 3983–3998. doi: 10.1093/jxb/ert208

Nadeem, M., Li, J., Wang, M., Shah, L., Lu, S., Wang, X., et al. (2018). Unraveling field crops sensitivity to heat stress:mechanisms, approaches, and future prospects. *Agronomy* 8:128. doi: 10.3390/agronomy8070128

Negrão, S., Schmöckel, S., and Tester, M. (2017). Evaluating physiological responses of plants to salinity stress. *Ann. Bot.* 119, 1–11. doi: 10.1093/aob/mcw191

Nievola, C. C., Carvalho, C. P., Carvalho, V., and Rodrigues, E. (2017). Rapid responses of plants to temperature changes. *Temperature* 4, 371–405. doi: 10.1080/23328940.2017.1377812

Nikolaeva, M., Maevskaya, S., Shugaev, A., and Bukhov, N. (2010). Effect of drought on chlorophyll content and antioxidant enzyme activities in leaves of three wheat cultivars varying in productivity. *Russ. J. Plant Physiol.* 57, 87–95. doi: 10.1134/S1021443710010127

Omprakash, Gobu, R., Bisen, P., Baghel, M., and Chourasia, K. N. (2017). Resistance/tolerance mechanism under water deficit (drought) condition in plants. *Int. J. Curr. Microbiol. App. Sci.* 6, 66–78. doi: 10.20546/ijcmas.2017.604.009

Ors, S., Ekinci, M., Yildirim, E., Sahin, U., Turan, M., and Dursun, A. (2021). Interactive effects of salinity and drought stress on photosynthetic characteristics

and physiology of tomato (*Lycopersicon esculentum* L.) seedlings. *S. Afr. J. Bot.* 137, 335–339. doi: 10.1016/j.sajb.2020.10.031

Partelli, F. L., Vieira, H. D., Viana, A. P., Batista-Santos, P., Rodrigues, A. P., Leitão, A. E., et al. (2009). Low temperature impact on photosynthetic parameters of coffee genotypes. *Pesqui. Agropecu. Bras.* 44, 1404–1415. doi: 10.1590/S0100-204X2009001100006

Rahmatian, A., Delshad, M., and Salehi, R. (2014). Effect of grafting on growth, yield and fruit quality of single and double stemmed tomato plants grown hydroponically. *Hortic. Environ. Biotechnol.* 55, 115–119. doi: 10.1007/s13580-014-0167-6

Rajametov, S. N., Yang, E. Y., Jeong, H. B., Cho, M. C., Chae, S. Y., and Paudel, N. (2021). Heat treatment in two tomato cultivars: A study of the effect on physiological and growth recovery. *Horticulturae* 7:119. doi: 10.3390/horticulturae7050119

Rolly, N. K., Imran, Q. M., Lee, I.-J., and Yun, B.-W. (2020). Salinity stress-mediated suppression of expression of salt overly sensitive signaling pathway genes suggests negative regulation by atbzip62 transcription factor in *Arabidopsis thaliana*. *Int. J. Mol. Sci.* 21:1726. doi: 10.3390/ijms21051726

Ruan, Y.-L., Jin, Y., Yang, Y.-J., Li, G.-J., and Boyer, J. S. (2010). Sugar input, metabolism, and signaling mediated by invertase: roles in development, yield potential, and response to drought and heat. *Mol. Plant* 3, 942–955. doi: 10.1093/mp/ssq044

Shafiq, B. A., Nawaz, F., Majeed, S., Aurangzaib, M., Al Mamun, A., Ahsan, M., et al. (2021). Sulfate-based fertilizers regulate nutrient uptake, photosynthetic gas exchange, and enzymatic antioxidants to increase sunflower growth and yield under drought stress. *J. Soil Sci. Plant Nutr.* 21, 2229–2241. doi: 10.1007/s42729-021-00516-x

Shin, Y. K., Bhandari, S. R., Cho, M. C., and Lee, J. G. (2020a). Evaluation of chlorophyll fluorescence parameters and proline content in tomato seedlings grown under different salt stress conditions. *Hortic. Environ. Biotechnol.* 61, 433–443. doi: 10.1007/s13580-020-00231-z

Shin, Y. K., Bhandari, S. R., Jo, J. S., Song, J. W., Cho, M. C., Yang, E. Y., et al. (2020b). Response to salt stress in lettuce: changes in chlorophyll fluorescence parameters, phytochemical contents, and antioxidant activities. *Agronomy* 10:1627. doi: 10.3390/agronomy10111627

Shin, Y. K., Bhandari, S. R., Jo, J. S., Song, J. W., and Lee, J. G. (2021a). Effect of drought stress on chlorophyll fluorescence parameters, phytochemical contents, and antioxidant activities in lettuce seedlings. *Horticulturae* 7:238. doi: 10.3390/horticulturae7080238

Shin, Y. K., Jo, J. S., Cho, M.-C., Yang, E.-Y., Ahn, Y. K., and Lee, J. G. (2021b). Application of chlorophyll fluorescence parameters to diagnose salinity tolerance in the seedling of tomato genetic resources. *J. Bio-Env. Con.* 30, 165–173. doi: 10.12791/KSBEC.2021.30.2.165

Silveira, J. A., and Carvalho, F. E. (2016). Proteomics, photosynthesis and salt resistance in crops: An integrative view. *J. Proteome* 143, 24–35. doi: 10.1016/j.jprot.2016.03.013

Soengas, P., Rodríguez, V. M., Velasco, P., and Cartea, M. E. (2018). Effect of temperature stress on antioxidant defenses in *Brassica oleracea*. *ACS Omega.* 3, 5237–5243. doi: 10.1021/acsomega.8b00242

Song, Y., Chen, Q., Ci, D., Shao, X., and Zhang, D. (2014). Effects of high temperature on photosynthesis and related gene expression in poplar. *BMC Plant Biol.* 14:111. doi: 10.1186/1471-2229-14-111

Song, Q., Joshi, M., and Joshi, V. (2020). Transcriptomic analysis of short-term salt stress response in watermelon seedlings. *Int. J. Mol. Sci.* 21:6036. doi: 10.3390/ijms21176036

Spanò, R., Ferrara, M., Gallitelli, D., and Mascia, T. (2020). The role of grafting in the resistance of tomato to viruses. *Plan. Theory* 9:1042. doi: 10.3390/plants9081042

Susič, N., Žibrat, U., Širca, S., Strajnar, P., Razinger, J., Knapič, M., et al. (2018). Discrimination between abiotic and biotic drought stress in tomatoes using hyperspectral imaging. *Sens. Actuators B: Chem.* 273, 842–852. doi: 10.1016/j.snb.2018.06.121

Swindell, W. R., Huebner, M., and Weber, A. P. (2007). Transcriptonal profiling of Arabidopsis heat shock proteins and transcription factors reveals extensive overlap between heat and non-heat stress response pathways. *BMC Genomics* 8:125. doi: 10.1186/1471-2164-8-125

Tabassum, S., Ossola, A., Marchin, R., Ellsworth, D. S., and Leishman, M. (2021). Assessing the relationship between trait-based and horticultural classifications of plant responses to drought. *Urban For. Urban Green.* 61:127109. doi: 10.1016/j.ufug.2021.127109

Taffouo, V. D., Nouck, A. H., Dibong, S. D., and Amougou, A. (2010). Effects of salinity stress on seedlings growth, mineral nutrients and total chlorophyll of some tomato (*Lycopersicum esculentum* L.) cultivars. *Afr. J. Biotechnol.* 9. 5366–5372. doi: 10.5897/AJB10.798

Taïbi, K., Taïbi, F., Abderrahim, L. A., Ennajah, A., Belkhodja, M., and Mulet, J. M. (2016). Effect of salt stress on growth, chlorophyll content, lipid peroxidation and antioxidant defence systems in *Phaseolus vulgaris* L. *S. Afr. J. Bot.* 105, 306–312. doi: 10.1016/j.sajb.2016.03.011

Toscano, S., Trivellini, A., Cocetta, G., Bulgari, R., Francini, A., Romano, D., et al. (2019). Effect of preharvest abiotic stresses on the accumulation of bioactive compounds in horticultural produce. *Front. Plant Sci.* 10:1212. doi: 10.3389/fpls.2019.01212

Trovato, M., Mattioli, R., and Costantino, P. (2008). Multiple roles of proline in plant stress tolerance and development. *Rend. Lincei* 19, 325–346. doi: 10.1007/s12210-008-0022-8

Wise, R., Olson, A., Schrader, S., and Sharkey, T. (2004). Electron transport is the functional limitation of photosynthesis in field-grown pima cotton plants at high temperature. *Plant Cell Environ.* 27, 717–724. doi: 10.1111/j.1365-3040.2004.01171.x

Yanyan, Y., Shuoshuo, W., Min, W., Biao, G., and Qinghua, S. (2018). Effect of different rootstocks on the salt stress tolerance in watermelon seedlings. *Hortic. Plant J.* 4, 239–249. doi: 10.1016/j.hpj.2018.08.003

Yao, J., Sun, D., Cen, H., Xu, H., Weng, H., Yuan, F., et al. (2018). Phenotyping of *Arabidopsis* drought stress response using kinetic chlorophyll fluorescence and multicolor fluorescence imaging. *Front. Plant Sci.* 9:603. doi: 10.3389/fpls.2018.00603

Yetişir, H., and Uygur, V. (2009). Plant growth and mineral element content of different gourd species and watermelon under salinity stress. *Turk. J. Agric. For.* 33, 65–77. doi: 10.3906/tar-0805-23

Yordanov, I., Velikova, V., and Tsonev, T. (2000). Plant responses to drought, acclimation, and stress tolerance. *Photosynthetica* 38, 171–186. doi: 10.1023/A:1007201411474

Zhang, H., Gong, G., Guo, S., Ren, Y., Xu, Y., and Ling, K. S. (2011). Screening the USDA watermelon germplasm collection for drought tolerance at the seedling stage. *Amer. Soc. Hortic. Sci.* 46, 1245–1248. doi: 10.21273/HORTSCI.46.9.1245

Zhang, F., Zhu, K., Wang, Y., Zhang, Z., Lu, F., Yu, H., et al. (2019). Changes in photosynthetic and chlorophyll fluorescence characteristics of sorghum under drought and waterlogging stress. *Photosynthetica* 57, 1156–1164. doi: 10.32615/ps.2019.136

Zushi, K., Kajiwara, S., and Matsuzoe, N. (2012). Chlorophyll a fluorescence ojip transient as a tool to characterize and evaluate response to heat and chilling stress in tomato leaf and fruit. *Sci. Hortic.* 148, 39–46. doi: 10.1016/j.scienta.2012.09.022

Conflict of Interest: The authors declare that the research was conducted in the absence of any commercial or financial relationships that could be construed as a potential conflict of interest.

Publisher's Note: All claims expressed in this article are solely those of the authors and do not necessarily represent those of their affiliated organizations, or those of the publisher, the editors and the reviewers. Any product that may be evaluated in this article, or claim that may be made by its manufacturer, is not guaranteed or endorsed by the publisher.

frontiers in Plant Science

ORIGINAL RESEARCH
published: 22 December 2021
doi: 10.3389/fpls.2021.786555

Time-Course of Changes in Photosynthesis and Secondary Metabolites in Canola (*Brassica napus*) Under Different UV-B Irradiation Levels in a Plant Factory With Artificial Light

Jin-Hui Lee[1], *Seina Shibata*[1] *and Eiji Goto*[1,2]*

[1] Graduate School of Horticulture, Chiba University, Matsudo, Japan, [2] Plant Molecular Research Center, Chiba University, Chiba, Japan

OPEN ACCESS

Edited by:
Carl-Otto Ottosen,
Aarhus University, Denmark

Reviewed by:
Rodrigo Loyola,
Instituto de Investigaciones Agropecuarias (INIA), Chile
Oksana Sytar,
Taras Shevchenko National University of Kyiv, Ukraine

***Correspondence:**
Eiji Goto
goto@faculty.chiba-u.jp

Specialty section:
This article was submitted to Crop and Product Physiology, a section of the journal Frontiers in Plant Science

Received: 30 September 2021
Accepted: 08 November 2021
Published: 22 December 2021

Citation:
Lee J-H, Shibata S and Goto E (2021) Time-Course of Changes in Photosynthesis and Secondary Metabolites in Canola (Brassica napus) Under Different UV-B Irradiation Levels in a Plant Factory With Artificial Light. Front. Plant Sci. 12:786555. doi: 10.3389/fpls.2021.786555

This study aimed to evaluate short-duration (24 h) UV-B irradiation as a preharvest abiotic stressor in canola plants. Moreover, we quantified the expression levels of genes related to bioactive compounds synthesis in response to UV-B radiation. Canola seedlings were cultivated in a plant factory under artificial light (200 μmol m^{-2} s^{-1} photosynthetic photon flux density; white LED lamps; 16 h on/8 h off), 25°C/20°C daytime/nighttime air temperature, and 70% relative humidity. Eighteen days after sowing, the seedlings were subjected to supplemental UV-B treatment. The control plants received no UV-B irradiation. The plants were exposed to 3, 5, or 7 W m^{-2} UV-B irradiation. There were no significant differences in shoot fresh weight between the UV-B-irradiated and control plants. With increasing UV-B irradiation intensity and exposure time, the H_2O_2 content gradually increased, the expression levels of genes related to photosynthesis downregulated, and phenylpropanoid and flavonoid production, and also total phenolic, flavonoid, antioxidant, and anthocyanin concentrations were significantly enhanced. The genes related to secondary metabolite biosynthesis were immediately upregulated after UV-B irradiation. The relative gene expression patterns identified using qRT-PCR corroborated the variations in gene expression that were revealed using microarray analysis. The time point at which the genes were induced varied with the gene location along the biosynthetic pathway. To the best of our knowledge, this is the first study to demonstrate a temporal difference between the accumulation of antioxidants and the induction of genes related to the synthesis of this compound in UV-B-treated canola plants. Our results demonstrated that short-term UV-B irradiation could augment antioxidant biosynthesis in canola without sacrificing crop yield or quality.

Keywords: antioxidant capacity, bioactive compounds, environmental stress, phytochemical, microarray

INTRODUCTION

Phytochemicals are naturally occurring, bioactive, and non-nutrient compounds in plants (Visioli et al., 2011). They include polyphenols, terpenoids, alkaloids, carotenoids, aromatic glucosinolates, among others. Some of these promote human health, as they are anti-inflammatory, anticancer, antioxidant, and so on (Reddy et al., 2003; Scalbert et al., 2011). Research interest in foods containing functional antioxidant phytochemicals has recently grown. The quantity and quality of phytochemicals may be improved through various environmental controls. Plant factories and vertical farms can precisely regulate the ambient environment and are suitable as production systems for crops rich in phytochemicals (Goto, 2011).

Plants control a wide range of physiological processes and use UV radiation as an environmental signal. The three types of UV radiation are UV-C (100–280 nm), UV-B (280–315 nm), and UV-A (315–400 nm) (Madronich et al., 1998). However, only UV-A and UV-B radiations reach the surface of the Earth, as UV-C is absorbed mainly by the tropospheric ozone layer. As UV-B irradiation range is highly energetic and has a short wavelength, it can generate excessive reactive oxygen species (ROS) in plants exposed to high levels of it. Excessive ROS can damage DNA, proteins, membranes, and the photosynthetic apparatus. Hence, they can adversely affect plant growth and development (Tevini et al., 1981; Flint and Caldwell, 1984; Tevini and Steinmüller, 1987; Jenkins, 2009). In contrast, low-level UV-B irradiation promotes morphological responses in plants, such as leaf growth, stomatal differentiation, and the inhibition of hypocotyl elongation. Therefore, the morphophysiological responses of plants to UV irradiation vary with intensity and exposure duration. However, even at the same UV irradiation intensity and exposure time plant responses vary with species, genotype, resistance, sensitivity, leaf thickness, and other factors (Rozema et al., 1997; Kataria et al., 2014; Lee and Oh, 2015). According to a previous report (Sytar et al., 2018), the sensitivity of lettuce to UV was different depending on the species, and the content of secondary metabolites (total phenol, flavonoid, anthocyanin, and phenolic acids) also varied when different lettuce species were exposed to the same UV conditions.

Plants may adapt to augmented UV-B irradiation by increasing secondary metabolite production. UV-B-responsive genes are induced *via* UV resistance locus 8 (UVR8)-dependent UV-B signaling pathway, and promote the accumulation of phenolic compounds, such as hydroxycinnamic, ferulic, caffeic, and sinapic acids and flavonoid compounds, such as luteolin, kaempferol, and quercetin (Jenkins, 2009; Wargent et al., 2009; Neugart et al., 2014; Escobar et al., 2017). The overall responses of plants to UV-B irradiation are governed by acclimatization mechanisms, such as the accumulation of compounds that absorb UV-B radiation, and they protect the photosynthetic apparatus from injury (Allen et al., 1998; Chang et al., 2009). The long-term effects of UV-B irradiation on plants have been extensively investigated, and the findings of these studies helped predict the consequences of increasing UV exposure. Nevertheless, few studies have focused on the impact of short-term UV-B exposure on plants. As the photosynthesis process is sensitive to UV-B irradiation, most plant species are affected by it and their growth may be impaired in response to prolonged UV exposure. Therefore, research is being conducted on increasing the phytochemical content of plants without inhibiting their growth. It was recently discovered that short-term (several days) UV-B irradiation might serve as a preharvest treatment to obtain plant products rich in antioxidants (Pandey and Pandey-Rai, 2014; Inostroza-Blancheteau et al., 2016). Studies on the effects of short-term UV-B irradiation may help elucidate UV-induced signaling pathways and trends in genes and/or parameters that immediately respond to UV irradiation.

Previous research showed that upregulation of the expression of genes related to bioactive secondary metabolites synthesis triggered by UV-B exposure may vary with duration. Inostroza-Blancheteau et al. (2016) found that *PAL*, *CHS*, and *F3'H* expression levels were upregulated within 6 h of UV-B exposure. Elevated total phenolic content was observed in highbush blueberry leaves (*Vaccinium corymbosum* L. cv. Bluegold) exposed to UV-B for 24 h. In addition, Neugart and Bumke-Vogt (2021) investigated the effects on major genes expression of the phenylpropanoid pathway, contents of the flavonoid groups, and hydroxycinnamic acid derivatives after short-term UV-B irradiation and before the harvest of various *Brassica* species (*B. rapa, B. nigra, B. oleracea, B. juncea, B. napus*, and *B. carinata*). The response during the acclimation period after the UV-B irradiation (2 and 24 h) was investigated, but the response immediately after the UV-B irradiation was not confirmed. If we conduct a study to check the changes in gene expression and the content of bioactive compounds immediately after UV exposure, it is expected that the temporal differences between gene expression and the synthesis of bioactive compounds in response to UV irradiation are elucidated.

Hence, this study aimed to identify UV-B treatment conditions conducive to the accumulation of bioactive compounds without inhibiting plant growth. Furthermore, this study was performed to confirm the expression patterns of photosynthesis and secondary metabolites biosynthesis related genes and the increasing patterns of bioactive compounds according to UV-B exposure time in canola plants.

MATERIALS AND METHODS

Plant Materials and Cultivation Conditions

The experiments were conducted at Chiba University, Japan, in a closed plant production system with multilayer cultivation shelves. Canola (*Brassica napus* L. cv. Kizakino-natane) was the plant material. It was used as a model for research on the growth, gene expression, and accumulation of bioactive compounds in a *Brassica* leaf vegetable cultivated under various environmental conditions (Goto et al., 2020; Son et al., 2020). The seeds were germinated on Kimtowels (NIPPONPAPER CRECIA Co. Ltd., Tokyo, Japan). One day after sowing (DAS), the germinated seeds were transplanted to M-size polyurethane sponges (M Hydroponics Laboratory Co. Inc., Aichi, Japan). The seedlings

were then transplanted to 18.6-L hydroponic containers (San Box No. 26B; SANKO Co. Ltd., Tokyo, Japan) under white LED lamps (LDL40S-N/19/21; Panasonic Corp., Osaka, Japan) and cultivated until 18 DAS. A quarter-strength Otsuka A formulation (OAT house A treatment; OAT Agrio Co. Ltd., Tokyo, Japan) was the nutrient solution used in all the experiments. The pH and electrical conductivity of the nutrient solution were ∼6.4-6.5 and ∼1.0-1.1 dS m^{-1}, respectively. The environmental conditions were 200 μmol m^{-2} s^{-1} photosynthetic photon flux density, 16-h light/8-h dark, 25°C/20°C daytime/nighttime air temperature, 70% RH, and 1,000 μmol mol^{-1} CO_2.

UV-B Treatment

The 18-DAS seedlings were subjected to UV-B irradiation at three intensities, including relatively low (intensity 3 W m^{-2}; daily dose 259.2 kJ m^{-2}), medium (intensity 5 W m^{-2}; daily dose 432 kJ m^{-2}), and high (intensity 7 W m^{-2}; daily dose 604.8 kJ m^{-2}) (**Figure 1A**). The UV-B energy levels used in this study were determined through preliminary experiments. When UV-B levels of 3, 5, and 7 W m^{-2} were applied to 18-DAS canola plants for 3 days, changes in gene expression of *PAL*, *CHS*, *rbcL*, and *rbcS*, and morphological changes such as a decrease in leaf area and increase in specific leaf weight (leaf thickness) were observed in leaves in response to UV-B levels (data not shown). Therefore, the three levels of UV-B used in our study were thought to be effective treatments for inducing both gene expression and bioactive compounds synthesis in canola plants for only 1 day. This study was conducted to confirm the initial response by short-term UV-B irradiation for 1 day. Each UV-B irradiation intensity was regulated by covering the UV-B lamp with Al foil. UV-B irradiation was applied to the canola plants for 24 h. The UV-B irradiation source was a UV-B lamp (TL20W/01 RS; Philips, Hamburg, Germany). **Figure 1A** shows the spectral radiant flux of the UV-B lamp. The UV-B lamp spectrum was measured with a spectroradiometer (USR-45D; Ushio Inc., Tokyo, Japan). Ten samples were performed during 24 h. The duration of the UV-B treatments and the sampling intervals are shown in **Figure 1B**. Shoot fresh weights were determined immediately before and after 24 h UV-B treatment.

Total Phenolic Concentration and Antioxidant Capacity Determination

Canola leaf samples were dried under vacuum in a freezer (FDU-1110; Tokyo Rikakikai Co. Ltd., Tokyo, Japan) at −45°C for 24 h and pulverized in an MM400 ball mill (Retsch GmbH, Haan, Germany) at 20 Hz for 2 min. Dried powder (0.01 g) was extracted with 1 mL of 80% (v/v) acetone. The third leaves of each canola plant that were subjected to different UV-B irradiation intensities were used in the analysis. The UV-B irradiation times were 0, 0.25, 0.5, 1, 2, 5, 8, 12, 16, and 24 h. Total phenolics and antioxidants were extracted from ∼200 mg fresh leaf sample with 80% (v/v) acetone according to the methods of Miller and Rice-Evans (1996) and Ainsworth and Gillespie (2007), respectively. The total phenolic concentration and the antioxidant capacity were determined with a spectrophotometer (V-750; JASCO Corp., Tokyo, Japan) at 765 nm and 730 nm, respectively. Results were expressed as milligrams gallic acid equivalents (GAE) per gram of fresh weight for the total phenolic concentration (GAE mg g^{-1} FW). To determine the antioxidant capacity, acetone extracts were diluted 10-fold, and the results were expressed as millimoles trolox-equivalents per gram fresh weight (TEAC mM g^{-1} FW).

Flavonoid Concentration Determination

The third leaves of each canola plant were exposed to UV-B irradiation for 0, 0.25, 0.5, 1, 2, 5, 8, 12, 16, or 24 h and were used for this analysis. Approximately, 200 mg of leaf tissue was dried under vacuum in a freezer (FDU-1110; Tokyo Rikakikai Co. Ltd.) at −45°C for 24 h and pulverized in an MM400 ball mill (Retsch GmbH) at 20 Hz for 2 min. About 7 mg dried powder was extracted with 1 ml of 70% (v/v) ethanol and the extracts were sonicated at 30 Hz for 6 min, incubated in the dark at 4°C overnight, and centrifuged at 13,000 × *g* for 2 min at room temperature (20–25°C). The extract (150 μl) was then added to a mixture of 750 μl distilled water plus 45 μl of 5% (w/v) $NaNO_2$. The solution was then vortexed and maintained in the dark at room temperature (20–25°C) for 6 min. Then, 90 μl of 10% (w/v) $AlCl_3$ was added to the solution, and the mixture was incubated for 5 min. Then, 300 μl of 1 M NaOH and 165 μl of distilled water were added to the solution. The optical density of the reaction mixture was measured in a spectrophotometer (V-750; JASCO Corp.) at 510 nm. The flavonoid concentration was expressed as milligrams catechin equivalents per gram dry weight (mg catechin/g DW).

Anthocyanin Concentration Determination

Approximately, 400-500 mg fresh second leaf tissue was collected from plants subjected to UV-B irradiation for 0.25, 0.5, 1, 2, 5, 8, 12, 16, or 24 h. The leaf tissue was stored at −80°C until the analysis. The anthocyanins were analyzed according to the method of Mancinelli and Schwartz (1984) with certain modifications. The plant tissues were extracted overnight at 4°C in 400 μl of 1% (v/v) HCl in methanol. Two hundred microliters of distilled water plus 500 μl chloroform were added to the extracts and the mixtures were centrifuged at 13,000 × *g* for 2 min at room temperature (20–25°C). The chloroform layer was separated, 400 μl of the top layer was transferred to a fresh microtube, and 600 μl of 1% (v/v) HCl in methanol was added to it. The anthocyanin concentrations were calculated using the following formula:

$$A530 - 0.25 \times A657 \quad (1)$$

where, the factor 0.25 compensates for the contribution of the chlorophylls to A530. Cyanidin-3-glucoside was a reference standard.

Hydrogen Peroxide Content Determination

The hydrogen peroxide content of the canola plants was determined according to the method of Velikova et al. (2000). Fresh leaf tissue (0.2 g) was ground twice in the MM400 ball mill

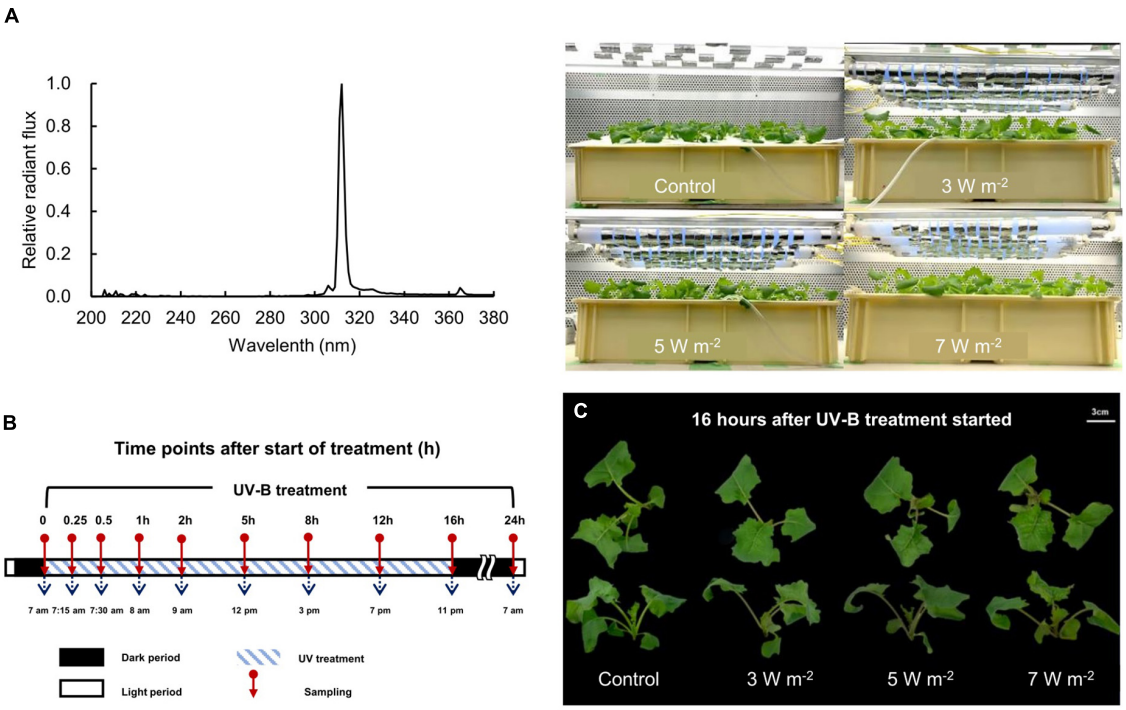

FIGURE 1 | A spectral radiant flux of UV-B lamp (TL20W/01 RS; Philips, Hamburg, Germany) measured with a spectroradiometer (USR-45D; Ushio Inc., Tokyo, Japan) and photographs of canola plants under UV-B lamps **(A)**, UV-B sampling and exposure times **(B)**, and canola plants after 16 h UV-B treatment **(C)**. UV-B irradiation intensity was set to 3, 5, and 7 W m^{-2} by overlapping Al foil on the lamp tube. Sampling was conducted at 0, 0.25, 0.5, 1, 2, 5, 8, 12, 16, and 24 h to investigate time-dependent responses to UV-B irradiation. UV-B irradiation intensities at top of the cultivation panel were set to 3, 5, and 7 W m^{-2}. White bar = 3 cm.

(Retsch GmbH) at 30 Hz for 1 min each time. Then 2 mL of 0.1% (w/v) trichloroacetic acid (TCA) was added to the microtube containing the leaf sample. The extract was centrifuged at 12,000 × *g* for 15 min at room temperature (20–25°C). The supernatant (0.5 mL) was added to 0.5 mL of 10 mM potassium phosphate buffer (pH 7.0) plus 1 ml of 1 M KI. The absorbance was measured in a spectrophotometer (V-750; JASCO Corp.) at 390 nm. H_2O_2 in the leaf extracts was estimated *via* an equation used to determine standard H_2O_2 concentrations. The H_2O_2 was expressed as micromoles H_2O_2 equivalents per gram fresh weight (μmol H_2O_2/g FW).

Gene Expression Quantification

The third leaves were sampled at 0, 0.25, 0.5, 1, 2, 5, 8, 12, 16, and 24 h UV-B irradiation to investigate time-dependent changes in gene expression. Approximately, 100-150 mg fresh leaf sample was collected and stored at −80°C until the analysis. The RNeasy Plant Mini Kit (Qiagen N.V., Venlo, Netherlands) was used to extract total RNA. The oligonucleotide primers used in the experiments were constructed according to information obtained from the GenBank database (**Supplementary Table 1**). Complementary DNA (cDNA) was synthesized with a PrimeScript RT Reagent Kit (Perfect Real Time; Takara Bio Inc., Kusatsu, Shiga, Japan) in a GeneAmp PCR System 9700 (Thermo Fisher Scientific, Waltham, MA, United States). The PCR was performed in a Thermal Cycler Dice Real Time System (TP970; Takara Bio Inc.) set to 37°C for 15 min followed by incubation at 85°C for 5 s, termination of the reaction, and cooling at 4°C. TB Green Premix ex Taq (Tli RNaseH Plus; Takara Bio Inc.) was used for the PCR. The PCR conditions for the amplification were 95°C for 5 s (hold), 40 cycles of 95°C for 5 s→60°C for 30 s (two-step PCR), one cycle of 95°C for 15 s→60°C for 30 s→95°C for 15 s (dissociation). The following mRNAs were amplified: phenylalanine ammonia-lyase (*PAL*), cinnamic acid 4-hydroxylase (*C4H*), 4-coumaroyl-CoA ligase (*4CL*), ferulate 5-hydroxylase (*F5H*), chalcone synthase (*CHS*), chalcone isomerase (*CHI*), flavanone 3-hydroxylase (*F3H*), flavonoid 3′-hydroxylase (*F3′H*), flavonol synthase (*FLS*), dihydroflavonol 4-reductase (*DFR*), anthocyanidin synthase (*ANS*), constitutively photomorphogenic (*COP1*), elongated hypocotyl 5 (*HY5*), light-harvesting complex II chlorophyll a/b-binding protein gene (*Lhcb*), ribulose-1,5-bisphosphate carboxylase/oxygenase large subunit (*rbcL*), and ribulose-1,5-bisphosphate carboxylase/oxygenase small subunit (*rbcS*). The mRNA expression levels were normalized against that of the actin (*ACT*) reference gene. Relative gene expression was calculated using the $\log_2$ treatment:control ratio.

Microarray Analysis

To explore genome-wide expression changes, samples were selected from plants exposed to 5 W m^{-2} UV-B irradiation

for 0.5, 2, 8, 16, and 24 h. Total RNA (1–5 μg) was isolated from each sample with an Agilent Quick Amp Labeling Kit (Agilent Technologies, Palo Alto, CA, United States) and used in the microarray analysis. After fragmentation, the cDNA (1.65 μg) was hybridized using Agilent microarray protocols. The hybridized probes were scanned with an Agilent G4900DA SG12494263. The ratios of normalized fluorescence values were obtained by calculating the $\log_2$ treatment:control expression ratios.

The differentially expressed genes (DEGs) were used to evaluate differential gene expression of 5 W m^{-2} UV-B irradiation. To analyze reliable data, the noise was excluded (signal evaluation). Flag values of microarray analyzed with Agilent software are as follows: [0] signal was not detected, [1] signal detected but difficult to evaluate, and [2] signal detected. Results of variations in gene expression only involved data with flag values [2]. After data signal evaluation, gene ontology (GO) terms were retrieved and data with confirmed GO function were used for DEGs analysis. Gene differences between those values were calculated based on the Log2 ratio. The result was shown as the number of upregulated (Log2 fold change ≥ 1) and downregulated genes (Log2 fold change ≤ -1).

Statistical Analysis

The means were subjected to one-way ANOVA in SPSS v. 24 (IBM Corp., Armonk, NY, United States). There were four biological replicates and one plant per replicate. The displayed data are the means and ±SE per treatment. The means were compared using the Tukey–Kramer test. Treatment means were considered significantly different at $p < 0.05$.

RESULTS

Growth Characteristics After UV-B Exposure

After 16 h UV-B irradiation exposure, the stems of the canola plants turned red. Stem redness intensified with UV-B irradiation intensity (**Figure 1C**). At higher UV-B irradiation intensity levels, the fresh weight of the canola plant decreased after 24 h. However, none of the UV-B treatments (3, 5, or 7 W m^{-2}) notably affected canola growth relative to the control after 24 h (**Supplementary Figure 1**).

Total Phenolic, Flavonoid, and Anthocyanin Concentrations, and Antioxidant Capacity in Response to UV-B

The total phenolic concentration and antioxidant capacity of the canola leaves varied with UV-B exposure time and irradiation level (**Figure 2**). The total phenolic concentration increased 2 h after the onset of UV-B irradiation and continuously increased over time (**Figure 2A**). The plants subjected to 3, 5, and 7 W m^{-2} UV-B irradiation for 16 h showed a 1.43-, 1.53-, and 1.66-fold increase, respectively, in total phenolic concentrations compared with the control plants. The total phenolic concentration increased with UV-B irradiation intensity, showing a 1.82-fold increase in the plants subjected to 7 W m^{-2} UV-B irradiation for 24 h compared with the control. After 24 h, the plants exposed to 7 W m^{-2} UV-B irradiation presented a 1.75-fold increase in antioxidant capacity compared with the control plants (**Figure 2B**).

The total flavonoid concentration in the canola leaves varied with UV-B irradiation intensity and exposure time (**Figure 2C**). The total flavonoid concentration increased 8 h after the onset of UV-B irradiation and continuously increased. They reached their maxima after 24 h UV-B irradiation but did not significantly differ among UV-B irradiation intensity levels.

The plants subjected to 3, 5, and 7 W m^{-2} UV-B irradiation showed 2.59-, 2.63-, and 5.15-fold increase, respectively, in anthocyanin concentrations after 16 h of the treatment compared with the control plants (**Figure 2D**). The plants exposed to 7 W m^{-2} UV-B irradiation for 24 h showed an 11.21-fold increase in anthocyanin concentrations compared with the control plants. The stems and leaves of the canola plants turned red after 16 h UV-B exposure.

Hydrogen Peroxide Production in Response to UV-B

In this work, the association between H_2O_2 content and plant UV-B exposure was like that for anthocyanin (**Figure 3**). The H_2O_2 content significantly increased 8 h after the onset of UV-B irradiation and continuously increased. The plants subjected to 7 W m^{-2} UV-B irradiation for 24 h showed maximum H_2O_2 content, representing a 4.97-fold increase compared with the control plants.

Expression of Genes Related to UVR8-Dependent UV-B Signaling Pathway

The expression levels of *COP1* and *HY5* were significantly induced by UV-B irradiation (**Figure 4**). The levels of *COP1* and *HY5* were upregulated after the onset of UV-B irradiation and reached maxima at 2 h; thereafter, *COP1* and *HY5* levels were substantially downregulated.

Expression of UV-B-Responsive Genes Related to Phenylpropanoid and Flavonoid Biosynthesis

To identify DEGs from microarray data, genes were determined to be differentially expressed in the UV-B samples compared with the control samples (**Supplementary Figure 2**). GO annotation was used to functionally analyze the canola plant. Approximately, 2,500 gene transcripts were assessed after the signal evaluation was applied during 24 h of UV-B exposure (**Supplementary Figure 2**). Differential gene expression analysis showed a total of 291, 398, 197, 192, and 305 at 0.5, 2, 8, 16, and 24 h of UV-B exposure, respectively. Among them, 188 and 181 upregulated genes showed significantly highest fold changes at 0.5 and 2 h of UV irradiation. The number of downregulated genes was 217, showing the highest fold change at 2 h of UV irradiation.

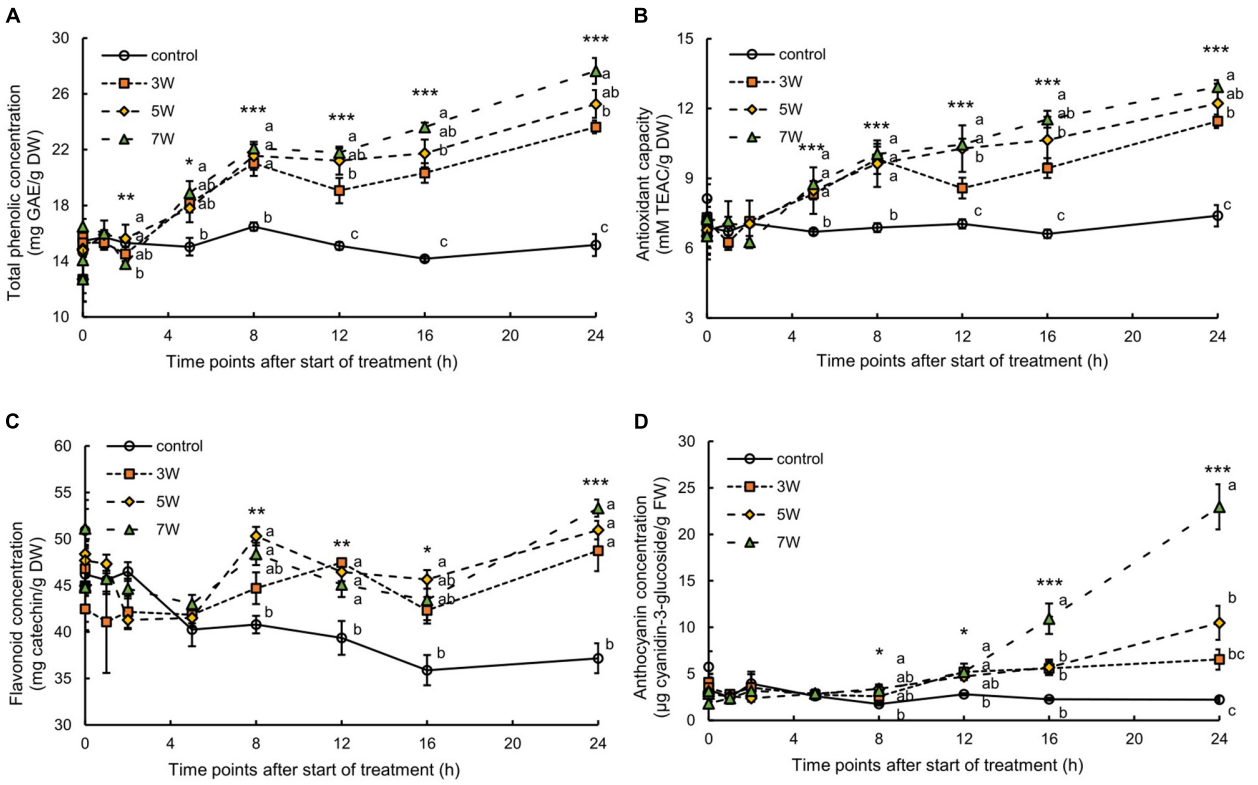

FIGURE 2 | Time courses of total phenolic concentration **(A)**, antioxidant capacity **(B)**, flavonoid concentration **(C)**, and anthocyanin concentration **(D)** in canola subjected to 3, 5, and 7 W m^{-2} UV-B irradiation intensity. Third (total phenolic and antioxidant capacity and flavonoid) and second (anthocyanin) leaves from the bottom of each canola plant were subjected to various UV-B irradiation intensities. Vertical bars indicate SE ($n = 4$). Different letters (a, b, and c) indicate a significant difference using Tukey–Kramer test (*$p < 0.05$, **$p < 0.01$, and ***$p < 0.001$, respectively).

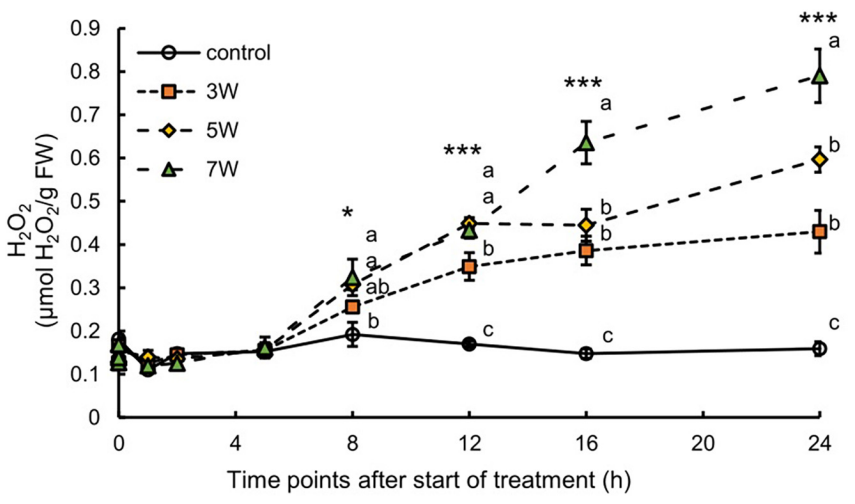

FIGURE 3 | Time courses of H_2O_2 content in canola subjected to 3, 5, and 7 W m^{-2} UV-B irradiation intensity. Second leaves from the bottom of each canola plant were subjected to various UV-B irradiation intensities. Vertical bars indicate SE ($n = 4$). Different letters (a, b, and c) indicate a significant difference using Tukey–Kramer test (*$p < 0.05$, **$p < 0.01$, and ***$p < 0.001$, respectively).

Table 1 shows the results of the microarray analyses of the variations in the expression levels of the genes related to phenylpropanoid and flavonoid biosynthesis, respectively. The relative gene expression patterns identified using RT-PCR corroborated the variations in gene expression revealed by microarray analysis. *PAL* was continuously expressed between

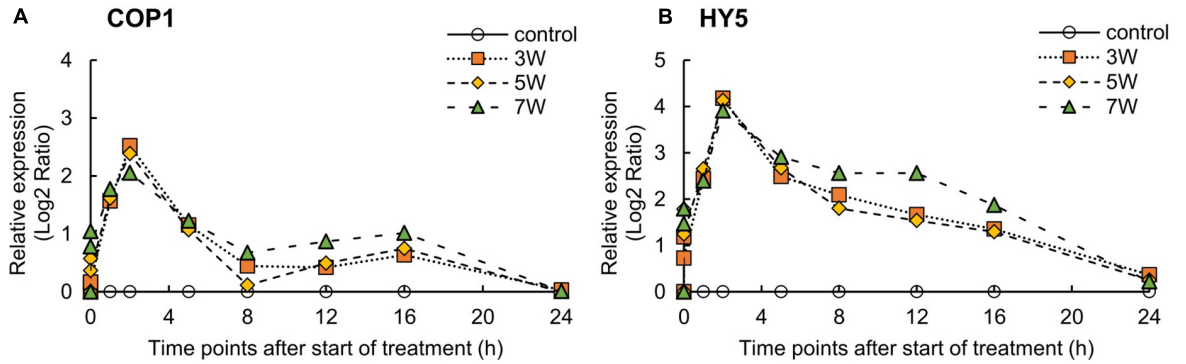

FIGURE 4 | Time courses of *COP1* **(A)** and *HY5* **(B)** mRNA expression in canola plants. Vertical bars indicate SE (n = 4). Third leaves from the bottom of each canola plant were subjected to various UV-B irradiation intensities. UV-B irradiation intensities at the top of the cultivation panel were set to 3, 5, and 7 W m^{-2}. Line graphs indicate log_2 fold changes (treatment:control) in gene expression levels.

2 h and 16 h UV-B irradiation. The expression levels of *C3′H* and *CCoAOMT* were significantly upregulated after 2 h UV-B exposure. *F5H* expression was upregulated after 8 h UV-B treatment. The downstream *SGT* expression was upregulated throughout the UV-B irradiation period. The expression levels of all flavonoid genes, except *FLS* and *ANS,* continuously varied between 2 and 16 h of UV-B treatment (**Table 1**).

The expression levels of the genes encoding secondary metabolites and the shikimate pathway were analyzed (**Supplementary Figure 3**). Relative gene expression varied with UV-B irradiation intensity and exposure time. The *PAL* and *C4H* expression levels reached maxima after 2 h UV-B treatment (**Figure 5**). *PAL* and *C4H* encode the first and second key enzymes in the phenylpropanoid pathway. In the plants subjected to 7 W m^{-2} UV-B irradiation, *PAL* and *C4H* expression levels were downregulated at a slower rate than in the plants subjected to the other UV-B irradiation intensity levels. The trend in *4CL* expression in response to UV-B irradiation resembled those for *PAL*, *C4H,* and *F5H* expression, which peaked after 5 h UV-B treatment and increased once again after 16 h UV-B exposure. The plants exposed to 7 W m^{-2} UV-B irradiation maintained high *F5H* expression levels between 5 and 12 h UV-B exposure. *CHS* expression reached maxima at 5 h (3 W m^{-2}) and 8 h (5 and 7 W m^{-2}) UV-B treatment and decreased thereafter. *CHI* expression reached a peak after 2 h at all the UV-B irradiation intensity levels and decreased thereafter. *F3H* expression reached a peak at 5 h after UV-B treatment and decreased thereafter. *F3'H* expression reached a maximum after 5 h UV-B irradiation and remained at high levels between 5 and 12 h UV-B treatment. *FLS* expression reached peaks at 2 h (5 and 7 W m^{-2}) and 5 h (3 W m^{-2}) UV-B exposure and decreased thereafter. *DFR* expression reached a maximum at 5 h UV-B exposure and decreased to a minimum after 16 h. In the plants subjected to 5 and 7 W m^{-2} UV-B irradiation, *DFR* expression reached maxima after 5 h UV-B treatment and decreased thereafter. *ANS* expression showed a trend similar to that of *DFR* only until 5 h UV-B treatment. At all UV-B irradiation intensities, *ANS* expression was dramatically downregulated after 8 h and was upregulated thereafter.

Expression of Genes Related to Photosynthesis in Response to UV-B Radiation

Figure 6 shows the log_2 ratios of the expression levels of the photosynthesis-related genes, namely *Lhcb1*, *rbcL*, and *rbcS,* within 24 h of UV-B irradiation. Relative *Lhcb1* expression was reduced under all UV-B treatments. However, the timing of the decrease in *Lhcb1* expression varied with UV-B irradiation intensity. Nevertheless, all UV-B irradiation intensities lowered gene photosynthesis-related gene expression after 8 h UV-B treatment. Then, *Lhcb1* expression was upregulated after 16 h UV-B exposure.

The *rbcL* expression levels varied with UV-B irradiation intensity. For 3 and 7 W m^{-2} UV-B irradiation treatments, *rbcL* expression was rapidly upregulated after 2 h, downregulated after 8 h, and showed expression levels similar to those of the control thereafter.

The *rbcS* expression levels also varied with UV-B irradiation intensity. For 3 and 7 W m^{-2} treatments, *rbcS* expression was rapidly upregulated after 4 h and downregulated after 8 h. Under the 5 W m^{-2} UV-B treatment, however, *rbcS* expression was immediately upregulated at 8 h and downregulated thereafter. Nevertheless, the variations in the expression levels did not significantly differ among photosynthesis-related genes (data not shown).

DISCUSSION

Effect of UV-B Irradiation on Growth

The growth of the canola plants was not significantly affected by short-term (24 h) UV-B treatment (**Supplementary Figure 1**). Ravindran et al. (2010) reported that UV-B exposure for 2 days (20 W m^{-2}, 2 h per day; daily dose 144 kJ m^{-2}) did not affect the growth parameters (shoot length, fresh weight, dry weight, or leaf area) of *Indigofera tinctoria,* whereas 4-day UV-B irradiation reduced growth. When tobacco was subjected to various UV-B irradiation doses (0, 37, 740, 1,480, and 2,960 J m^{-2}) for

TABLE 1 | Gene expression variation related to phenylpropanoid and flavonoid biosynthesis in canola subjected to UV-B irradiation.

Genename [EC No.]	Description	Time points after start of treatment (h)				
		0.5	2	8	16	24
PAL [EC:4.3.1.24]	Phenylalanine ammonia-lyase	0.41	3.01	2.92	1.94	0.30
C4H [EC:1.14.1491]	Cinnamate 4-hydroxylase isoform	0.42	3.90	2.39	2.50	0.89
4CL [EC:6.2.1.12]	4-Coumarate-CoA ligase	0.08	0.48	0.11	−0.01	−0.84
C3'H [EC:1.14.14.96]	*p*-Coumaroyl ester 3′-hydroxylase	−0.08	2.29	0.93	−0.25	0.02
CCoAOMT [EC:2.1.1.104]	Caffeoyl-Coenzyme A 3-O-Methyltransferase	−0.27	2.72	0.27	0.08	−0.04
CCR [EC:1.2.1.44]	Cinnamoyl-CoA reductase	−0.73	0.10	0.47	1.02	−0.89
F5H [EC:1.14.-.-]	Ferulate 5-hydroxylase	−0.64	0.93	1.69	2.68	0.39
POX [EC:1.11.1.7]	Peroxidase	0.22	−0.49	−0.69	−0.45	−0.61
SGT [EC:2.4.1.120]	Sinapate glucosyltransferase	0.15	3.36	4.86	3.48	1.61
SCT [EC:3.4.16– 2.3.1.91]	1-O-sinapoylglucose:choline sinapoyltransferase	−0.11	−0.12	−0.13	−0.01	−0.40
CHS [EC:2.3.1.74]	Chalcone synthase	−0.02	2.73	5.76	3.49	2.91
CHI [EC:5.5.1.6]	Chalcone isomerase	0.13	3.44	5.54	3.01	2.60
F3H [EC:1.14.11.9]	Flavanone 3-hydroxylase	0.14	1.77	2.74	2.93	1.16
F3'H [EC:1.14.13.21]	Flavonoid 3′-hydroxylase	0.92	5.99	8.67	9.43	9.46
FLS [EC:1.14.11.23 1.14.20.6]	Flavonol synthase	−0.32	−0.33	−0.06	0.75	−1.67
DFR [EC:1.1.1.219 1.1.1.234]	Dihydroflavonol 4-reductase	−0.49	0.51	2.51	3.28	4.26
ANS [EC:1.14.11.19 1.14.20.4]	Anthocyanidin synthase	0.27	−0.17	−0.29	0.09	0.13

Values indicate log_2 ratios (n = 1) obtained by calculating treatment:control gene expression ratios. UV-B irradiation intensity at the top of the cultivation panel was set to 5 W m^{-2}.

Positive values that increased by ≥ 1.0 are in pink. To analyze reliable data, the noise was excluded (signal evaluation). Flag values of microarray analyzed with Agilent software are as follows: [0] signal not detected, [1] signal detected difficult to evaluate, and [2] signal detected. Results of variations in gene expression only involved data with flag values [2].

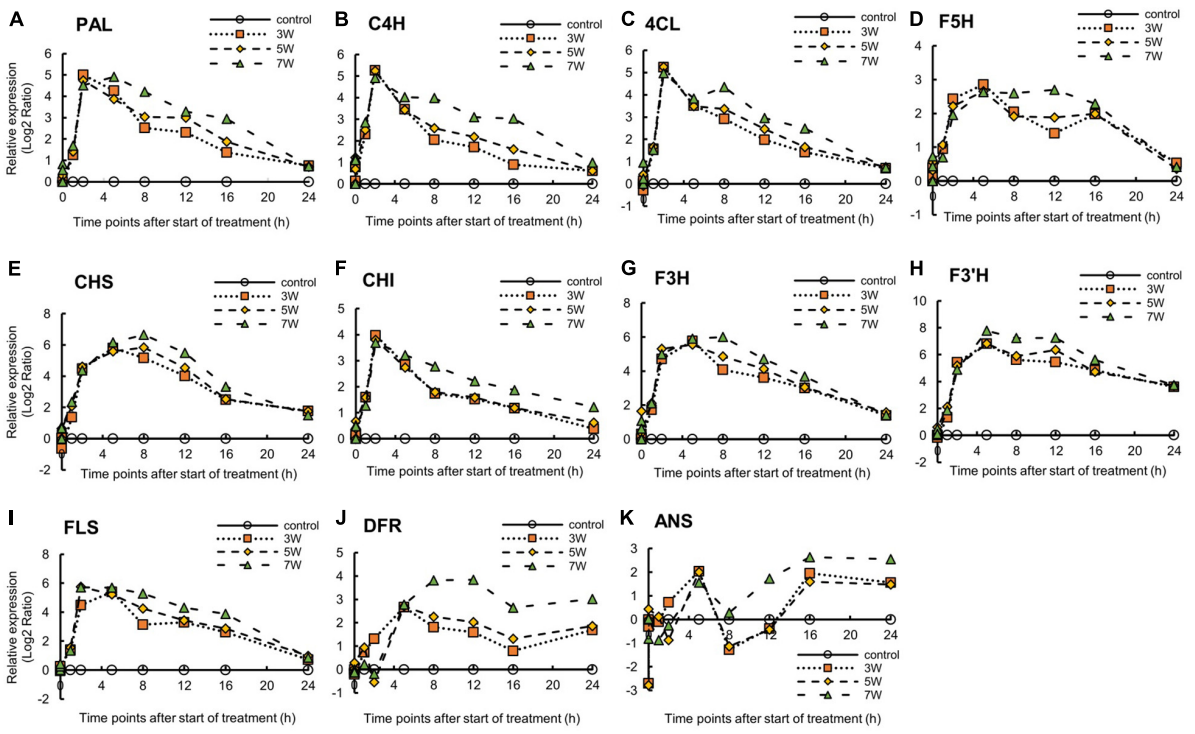

FIGURE 5 | Time courses of *PAL* **(A)**, *C4H* **(B)**, *4CL* **(C)**, *F5H* **(D)**, *CHS* **(E)**, *CHI* **(F)**, *F3H* **(G)**, *F3'H* **(H)**, *FLS* **(I)**, *DFR* **(J)**, and *ANS* **(K)** mRNA expression in canola (*n* = 4). Third leaves from the bottom of each canola plant were subjected to various UV-B irradiation intensities. UV-B irradiation intensities at top of the cultivation panel were set to 3, 5, and 7 W m^{-2}. Line graphs indicate log_2 fold changes (treatment:control) in gene expression levels.

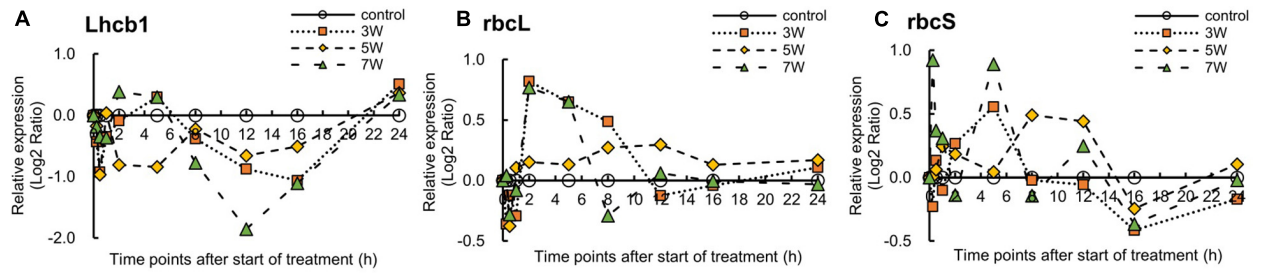

FIGURE 6 | Time courses of **(A)** *Lhcb1*, **(B)** *rbcL*, and **(C)** *rbcS* mRNA expression in canola (n = 4). Third leaves from the bottom of each canola plant were subjected to various UV-B irradiation intensities. UV-B irradiation intensities at top of the cultivation panel were set to 3, 5, and 7 W m^{-2}. Line graphs indicate log_2 fold changes (treatment:control) in gene expression levels.

4 days, cell proliferation significantly declined. Cell death was also significantly induced after 4 days of UV-B irradiation at all intensities (Takahashi et al., 2015). These results indicate that exposure to 3, 5, and 7 W m^{-2} UV-B irradiation for 24 h did not adversely affect canola plant growth. These treatments were not intense enough to cause permanent oxidative damage to the plants. However, long-term UV-B treatment may adversely affect plant growth, and the responses to it may vary with plant species, developmental stage, and leaf thickness (Piluzza and Bullitta, 2011; Wang et al., 2018).

Effects of UV-B Irradiation on Bioactive Compounds and Hydrogen Peroxide

High-intensity UV light can damage DNA, proteins, and the photosynthetic apparatus, including the chloroplasts. These injuries can adversely affect plant growth and development (Diffey, 1991). However, low-intensity UV irradiation may induce various protective mechanisms in plants, including the accumulation of low-molecular-weight compounds, such as antioxidants that suppress oxidative damage and maintain redox homeostasis (Bharti and Khurana, 1997). UV-B irradiation can induce the biosynthesis of phenylpropanoids and flavonoids that absorb UV (Jenkins, 2009; Robson et al., 2015). In the leaf epidermis, phenolics reduce oxidative damage and protect the photosynthetic apparatus by inhibiting the penetration of UV-B irradiation into the inner photosynthetic layers (Agati and Tattini, 2010).

Here, short-term UV-B irradiation at 3, 5, and 7 W m^{-2} activated secondary metabolite biosynthesis pathways and promoted antioxidant accumulation in canola plants (**Figures 2**, **3**). The concentrations of secondary metabolites, such as total phenolics, antioxidants, total flavonoids, anthocyanins, and H_2O_2, significantly increased in response to all UV-B exposure levels (**Figures 2**, **3**). These results suggested that the stems and leaves of canola plants turned red because the concentration of anthocyanins was significantly increased by UV-B irradiation; thus, anthocyanin expression may be associated with higher UV-B irradiation levels (**Figure 2D**). Furthermore, the results of total phenolic and antioxidant capacity showed almost similar trends, which agreed with results of previous studies that showed a positive linear relation between total phenolic content and antioxidant capacity (ABTS and DPPH) (Javanmardi et al., 2003; Pennycooke et al., 2005; Piluzza and Bullitta, 2011).

Based on the homeostasis between ROS and antioxidants, ROS is continuously generated in different cellular compartments as by-products of various metabolic pathways, such as plant respiration and photosynthesis, even under normal conditions (Berni et al., 2019). A constant adjustment of ROS concentration is achieved by non-enzymatic secondary metabolites such as CAT, APX, GPX, and GR; therefore, plants have a normal metabolism (Kapoor et al., 2015). However, when plants were subjected to a stressful environment (biotic and abiotic), an imbalance between ROS and antioxidants occurs, resulting in a rapid increase in ROS concentration and inducing irreversible oxidative processes such as cell death by "oxidative burst" (Sharma et al., 2012). However, the appropriate concentration of ROS acts as a signaling molecule participating in important developmental and physiological processes and responds to highly generated ROS by generating secondary metabolites such as polyphenol, terpene, and vitamins (Sharma et al., 2012; Xia et al., 2015). In particular, H_2O_2 plays a central role in signaling pathways because of its relatively long lifetime and can freely diffuse across membranes through aquaporins (Bienert et al., 2007; Møller et al., 2007). Moreover, at the appropriate levels, ROS may act as signaling molecules in various intracellular processes and induce antioxidant biosynthesis.

In this study, the concentration of H_2O_2 showed a tendency to increase as energy increased, but all UV treatments did not significantly affect plant growth and morphological changes. Therefore, the amount of ROS generated was not high enough to inhibit canola growth and was within the appropriate range. The observed increases in the bioactive compound content at 3, 5, and 7 W m^{-2} UV-B irradiation indicated that these radiation levels were within a suitable range to stimulate antioxidant biosynthesis in canola. Previous studies reported that the UV levels they used increased the bioactive compound content in plants (Lois, 1994). *Arabidopsis* plants were exposed to various levels of UV-B irradiation intensity (0.10, 0.15, 0.24, 0.37, and 0.8 W m^{-2}) for 30 h and flavonoid accumulation was the highest at 0.15 W m^{-2} UV-B irradiation (Lois, 1994). However, exposure to high UV levels may actually decrease the bioactive compound content by impairing cellular function. Similar results were obtained for

sweet basil leaves exposed to various levels of UV-B irradiation intensity (0, 2.3, 3.6, and 4.8 W m^{-2}) (Ghasemzadeh et al., 2016). The concentrations of total phenolics, total flavonoids, and individual flavonoids, and phenolic acids were the highest at 3.6 W m^{-2} UV-B irradiation but significantly declined at 4.8 W m^{-2} UV-B irradiation. In *Medicago sativa,* antioxidant and flavonoid compounds significantly increased in response to lower UV-B irradiation levels (17.35 μW cm^{-2} d^{-1}), whereas higher UV-B irradiation levels caused severe damage and adversely affected growth and development (Gao et al., 2019). The foregoing results suggest that, below certain UV exposure thresholds, the content of bioactive compounds, such as flavonoids, may be proportional to the UV dose. In this study, there is a possibility that 7 W m^{-2} UV-B irradiation was the optimal UV-B exposure level, whereas 10 W m^{-2} reduced the bioactive compound content in canola.

Effects of UV-B Irradiation on Expression of the Secondary Metabolites Biosynthesis-Related Genes

The expression of the genes encoding antistress and antioxidant compounds is regulated by the UVR8 pathway (Hideg et al., 2013). The cytoplasmic UVR8 photoreceptor is an active dimer and it becomes a monomer during UV-B absorption. UV-B-induced UVR8 photoreceptor monomers directly reacted with E3 ubiquitin ligase "constitutively photomorphogenic 1" (COP1) and promoted "elongated hypocotyl 5" (HY5) transcription in *Arabidopsis* nuclei (Brown et al., 2005; Favory et al., 2009; Wu et al., 2012). In *Arabidopsis*, the accumulation of HY5 transcripts promoted flavonoid biosynthesis by activating chalcone synthase (CHS) and prevented UV-B absorption by epidermal tissue (Bharti and Khurana, 1997; Kliebenstein et al., 2002; Brown and Jenkins, 2008). Photomorphogenic responses, such as an increase in leaf thickness, axillary branching, and the induction of UV-absorbing compounds, are mediated by the activation of UV-B photoreceptor UV "resistance locus 8" (UVR8) in response to low-to-moderate UV-B irradiation levels (0.1-21 μmol m^{-2} s^{-1} and 1.77-1.07 W m^{-2}) (Hectors et al., 2007; Brown and Jenkins, 2008; Rizzini et al., 2011). *COP1* and *HY5* transcription were induced in *Arabidopsis* by low UV-B flux rates (0.1 μmol m^{-2} s^{-1}) (Brown and Jenkins, 2008). In this study, the expression levels of *COP1* and *HY5* were upregulated immediately after UV-B exposure and attained the highest expression levels after 2 h. UV-B-absorbing compounds were also affected by UVR8 pathway activation and accumulated in the canola plants (**Figure 2**). However, high UV-B irradiation levels may induce ROS biosynthesis, which damages DNA, proteins, membranes, and so on, and impedes plant growth and development (Brown and Jenkins, 2008; Hideg et al., 2013). Here, the UV-exposed plants were not harmed, and their bioactive compound content had significantly increased. These results suggest that the canola plants were subjected to only low-to-moderate levels of UV-B irradiation.

The genes *PAL, C4H, 4CL, F5H, CHS, CHI, F3H, F3'H, FLS, DFR,* and *ANS* are key genes in the phenylpropanoid and flavonoid biosynthesis pathways. *PAL* leads to the main bifurcation in phenylpropanoid metabolism and is an upstream gene. *F3'H, DFR*, and *ANS* are downstream genes in flavonoid biosynthesis. The times to peak expression differed among genes; genes with downregulated expression required a long time to reach maximum expression (**Figure 5**); however, with variable gene expression (**Table 1**), the trends in upregulation were like those encoding phenylpropanoids (*PAL*, *C4H,* and *F5H*) and flavonoids (*CHS*, *CHI*, *F3H*, *F3'H,* and *DFR*) according to qRT-PCR (**Figure 5**). When *Chrysanthemum morifolium* was exposed to UV-B irradiation for different durations, *HY5* expression was rapidly upregulated after 1 h, whereas the expression levels of *CHS, CHI, F3H,* and *FLS* increased after 6 h (Yang et al., 2018). Similar trends were reported in a previous study analyzing *CHS, CHI, F3H, DFR,* and *ANS* expression in radish sprouts (Su et al., 2016). *CHS, CHI,* and *F3H* are located upstream in the flavonoid biosynthesis pathway, and their expression levels were upregulated after 12 h UV-B exposure. However, the expression levels of downstream *DFR* and *ANS* were upregulated after 24 h UV-B irradiation. Moreover, the expression levels of phenylpropanoid and flavonoid-related genes were consistently upregulated at 7 W m^{-2} UV-B irradiation. At 7 W m^{-2} UV-B irradiation, gene expression levels decreased at a slower rate than at 3 and 5 W m^{-2} UV-B irradiation. Therefore, 7 W m^{-2} UV-B irradiation stimulated gene expression more effectively than 3 or 5 W m^{-2}, regardless of the duration of UV-B exposure.

Microarray analysis was used for the whole-genome exploration of gene expression profiles in canola plants. Quantitative RT-PCR results supported the microarray data. In the microarray analysis, many DEGs, down- or upregulated, were observed during 24 h of UV-B irradiation (**Supplementary Figure 2**). These genes identified in this study have been implicated in secondary metabolite syntheses (**Table 1**). The DEGs were significantly upregulated at the 0.5 and 2 h of UV-B exposure relative to the other time point. The significantly upregulated DEGs with unknown genes were from the 0.5 and 2 h of UV-B irradiation. These results suggested that DEGs were involved in the complex molecular mechanisms necessary for resistance to UV irradiation in canola plants. In addition, even in the quantitative RT-PCR results (**Figures 4**, **5**), genes of the UVR8 pathway and the upper group of the secondary metabolite rapidly increased after 2 h of UV exposure. The DEGs results indicated that numerous genes in UV-B treated plants have undergone molecular biological changes on 0.5 and 2 h of UV-B irradiation. Even at 0.5 h, the number of upregulated genes was large. It is possible that unanalyzed (or unconfirmed) genes were expressed and ultimately led to upregulation.

The time points at which the expression levels of genes were upregulated varied with plant species. UV-B irradiation induced genes related to phenylpropanoid and flavonoid biosynthesis, which increased polyphenol antioxidant content. The results of the gene expression analyses were consistent with those for the characteristics of the bioactive compounds (**Figure 2**). The observed increases in the bioactive compound content in plants subjected to 3, 5, and 7 W m^{-2} UV-B irradiation indicated that all UV-B exposure levels were within a range suitable to stimulate antioxidant phenolic compound biosynthesis in canola. All UV-B treatments increased the production of these

bioactive compounds by upregulating the expression levels of several key genes in the biosynthetic pathways for these compounds. However, there were significant time lags between the observed increases in the levels of these compounds and upregulation of the expression levels of genes encoding them. The expression levels of *PAL, C4H*, and *4CL* were dramatically increased after 2 h UV-B irradiation. The relative expression of *F5H* reached a peak after 5 h UV-B irradiation (**Figure 5**). The total phenolic concentration coincided with the peaks in *F5H* expression and significantly increased, starting at 5 h UV-B irradiation (**Figure 2A**). The flavonoid biosynthesis genes (*CHS, F3H, F3'H*, and *FLS*) were induced in response to HY5 transcript accumulation following UV-B irradiation, and their peak expression levels occurred after 5-8 h UV-B irradiation. The expression levels of *ANS* and *DFR* reached their maxima at 12-16 h UV-B treatment. According to a previous report, some genes involved in the biosynthesis of the phenylpropanoid pathway are not expressed continuously when exposed to UV-B irradiation, but genes are expressed rapidly for a short period and then return to the basal level (Höll et al., 2019; Meyer et al., 2021). Our results also showed a tendency to decrease to the basal level after each gene expression peaked.

Total flavonoid concentration and relative anthocyanin content increased at 5-8 h and 12-16 h UV-B irradiation, respectively (**Figure 2**). Regardless of the time points at which the expression levels of the gene reached their maxima, the bioactive compound content continued to rise. These reactions may have been defense responses in anticipation of future exposure to the same abiotic stress. If UV irradiation is interrupted, the plant may use its "memory capacity" to continue increasing the bioactive compound content (Bruce et al., 2007). Time differences between gene expression and bioactive compound biosynthesis were reported for wheat leaves under drought stress (Ma et al., 2014). Their *CHS, CHI, F3H, FLS, DFR,* and *ANS* expression levels reached their maxima at 12-16 h after UV. Timely application of short-term, moderate-intensity UV-B irradiation to leafy vegetables 1-2 days preharvest might enhance antioxidant phytochemical production without yield or quality loss in horticultural crops raised in plant factories and vertical farms under artificial light. Thus, bioactive compound biosynthesis might have continued to increase in canola even after the 24-h UV-B treatment.

Effects of UV-B Irradiation on Expression of the Photosynthetic Metabolites Biosynthesis-Related Genes

The photosynthesis-related genes *Lhcb1, rbcL*, and *rbcS* were differentially expressed throughout the entire UV-B irradiation period (**Figure 6**). The *Lhcb1, rbcL*, and *rbcS* expression levels in pea plants were reduced by UV-B treatment (Strid et al., 1994). *Lhcb1* encodes the chlorophyll a/b-binding protein of the photosystem (PS) - light-harvesting antenna complex and maintains the photosynthetic apparatus (Andersson et al., 2003). *Lhcb1* also modulates stomatal movement and promotes plant stress tolerance (Xu et al., 2012). In this study, *Lhcb1* expression was rapidly downregulated under all UV-B treatments after 8 h and upregulated after 24 h UV-B treatment (**Figure 6A**). These results suggest that short-term UV-B exposure had a negative effect on the photosynthetic machinery. Kalbina and Strid (2006) reported that *Lhcb1* mRNA expression was reduced in *Arabidopsis* by short-term UV-B irradiation. $O_2^{\cdot -}$ and H_2O_2 are secondary messengers involved in the downregulation of the expression of photosynthetic genes, such as *Lhcb* (Kalbina and Strid, 2006). Hence, the generated ROS might have downregulated *Lhcb1* expression in this study.

The CO_2 fixation is achieved through photosynthesis, and the enzyme Rubisco is involved in this complex process. It was reported that this highly sensitive mechanism may be inhibited by UV-B irradiation (Fedina et al., 2010). The rbcS (Rubisco small subunit) and rbcL (Rubisco large subunit) proteins are susceptible to degradation. However, the expression levels of *rbcS* and *rbcL* are upregulated to compensate for the damage caused to their protein products by oxidative stress (Xiong et al., 2010). Here, *rbcS* expression was upregulated after 2 h and downregulated after 8 h UV-B treatment (**Figure 6C**); however, *rbcL* expression was upregulated after 4 h and downregulated after 16 h UV-B treatment. The times of peak expression differed slightly between *rbcS* and *rbcL*. Nevertheless, the rbcS and rbcL protein levels were drastically downregulated by UV-B treatment. It is therefore possible that rbcS and rbcL mRNA levels were rapidly upregulated to regenerate the lost photosynthetic proteins (Xiong et al., 2010). Enhanced gene transcription might compensate for ROS-mediated protein damage/loss and help maintain the photosynthetic machinery subjected to UV-B irradiation. Increased *rbcS* and *rbcL* transcription have also been reported to cause drought and salinity stress, which promote oxidative stress (Lilley et al., 1996; Fu et al., 2007). Thus, *rbcS* and *rbcL* expression levels were rapidly upregulated to compensate for the decreases in photosynthetic protein content caused by UV-B exposure. Nevertheless, prolonged UV-B exposure might delay or even suppress upregulation of *rbcS* and *rbcL* expression.

In canola, short-term UV-B irradiation downregulated the expression of genes implicated in photosynthesis but did not adversely affect plant growth (**Supplementary Figure 1**). However, if UV-B irradiation continues for $>$ 2 days, plant growth would significantly decrease.

CONCLUSION

This study demonstrated that the genes regulating secondary metabolite biosynthesis in canola were affected by UV-B irradiation intensity and duration. UV-B irradiation for $\leq$ 24 h was merely a mild stressor for canola and did not damage its photosynthetic machinery or hinder its growth. To minimize UV-B-induced damage, phenylpropanoid and flavonoid biosynthesis were rapidly activated, and antioxidant phytochemicals accumulated. The expression levels of the genes governing targeted secondary metabolic pathways significantly differed with UV-B exposure duration. There were also temporal differences between gene expression and bioactive compound accumulation. The concentrations of all antioxidants increased in response to the peak expression levels of the genes regulating the

phenylpropanoid and flavonoid pathways. The plants subjected to 7 W m^{-2} UV-B irradiation showed 1. 82-, 1. 75-, and 11.21-fold increase in total phenolic, flavonoid, and anthocyanin concentrations, respectively, compared with the unexposed controls because of the inherent "memory mechanism" of the plant. To the best of our knowledge, this work is the first to demonstrate a temporal difference between the accumulation of antioxidants and the induction of the genes encoding them in UV-B-treated canola plants. Based on the discoveries in this work, timely application of short-term, moderate-intensity UV-B irradiation to canola and other leafy vegetables at 1-2 days preharvest might enhance the biosynthesis of health-promoting antioxidants without compromising crop yield or quality.

As biosynthesis and accumulation of bioactive compounds are regulated by complex temporal and spatial patterns, more in-depth studies are needed on temporal differences between gene expression and target bioactive compounds' accumulation. Short-term UV irradiation could be a widely used technique for controlling the activation timing of target compounds in plant factories and vertical farms.

DATA AVAILABILITY STATEMENT

The datasets presented in this study can be found in online repositories. The names of the repository/repositories and accession number(s) can be found at: https://www.ebi.ac.uk/arrayexpress/E-MTAB-11034.

AUTHOR CONTRIBUTIONS

J-HL and SS: performance of experiments, sample collection, and analyses of chemical data. J-HL: writing – original draft preparation. EG: writing – review and editing, conceptualization, experimental design, supervision, and funding acquisition. All authors read and agreed to the final version of the manuscript.

FUNDING

This work was supported by the Ministry of Economy, Trade, and Industry of Japan in the form of a grant-in-aid from the project "Development of Fundamental Technologies for the Production of High-Value Materials Using Transgenic Plants."

SUPPLEMENTARY MATERIAL

The Supplementary Material for this article can be found online at: https://www.frontiersin.org/articles/10.3389/fpls.2021.786555/full#supplementary-material

REFERENCES

Agati, G., and Tattini, M. (2010). Multiple functional roles of flavonoids in photoprotection. *New Phytol.* 186, 786–793. doi: 10.1111/j.1469-8137.2010.03269.x

Ainsworth, E. A., and Gillespie, K. M. (2007). Estimation of total phenolic content and other oxidation substrates in plant tissues using folin–ciocalteu reagent. *Nat. Protoc.* 2, 875–877. doi: 10.1038/nprot.2007.102

Allen, D. J., Nogués, S., and Baker, N. R. (1998). Ozone depletion and increased UV-B radiation: is there a real threat to photosynthesis? *J. Exp. Bot.* 49, 1775–1788. doi: 10.1093/jxb/49.328.1775

Andersson, J., Wentworth, M., Walters, R. G., Howard, C. A., Ruban, A. V., Horton, P., et al. (2003). Absence of the Lhcb1 and Lhcb2 proteins of the light-harvesting complex of the photosystem II—effects on photosynthesis, grana stacking and fitness. *Plant J.* 35, 350–361. doi: 10.1046/j.1365-313X.2003.01811.x

Berni, R., Luyckx, M., Xu, X., Legay, S., Sergeant, K., Hausman, J. F., et al. (2019). Reactive oxygen species and heavy metal stress in plants: impact on the cell wall and secondary metabolism. *Environ. Exp. Bot.* 161, 98–106. doi: 10.1016/j.envexpbot.2018.10.017

Bharti, A. K., and Khurana, J. P. (1997). Mutants of Arabidopsis as tools to understand the regulation of phenylpropanoid pathway and UVB protection mechanisms. *Photochem. Photobiol.* 65, 765–776. doi: 10.1111/j.1751-1097.1997.tb01923.x

Bienert, G. P., Møller, A. L., Kristiansen, K. A., Schulz, A., Møller, I. M., Schjoerring, J. K., et al. (2007). Specific aquaporins facilitate the diffusion of hydrogen peroxide across membranes. *J. Biol. Chem.* 282, 1183–1192. doi: 10.1074/jbc.M603761200

Brown, B. A., and Jenkins, G. I. (2008). UV-B signaling pathways with different fluence-rate response profiles are distinguished in mature Arabidopsis leaf tissue by requirement for UVR8, HY5, and HYH. *Plant Physiol.* 146, 576–588. doi: 10.1104/pp.107.108456

Brown, B. A., Cloix, C., Jiang, G. H., Kaiserli, E., Herzyk, P., Kliebenstein, D. J., et al. (2005). A UV-B-specific signaling component orchestrates plant UV protection. *Proc. Natl Acad. Sci. U.S.A.* 102, 18225–18230. doi: 10.1073/pnas.0507187102

Bruce, J. A. T., Matthes, C. M., Napier, A. J., and Pickett, A. J. (2007). Stressful 'memories' of plants: evidence and possible mechanisms. *Plant Sci.* 173, 603–608. doi: 10.1016/j.plantsci.2007.09.002

Chang, X., Alderson, P. G., and Wright, C. J. (2009). Enhanced UV-B radiation alters basil (*Ocimum basilicum* L.) growth and stimulates the synthesis of volatile oils. *J. Hortic. For.* 1, 27–031.

Diffey, B. L. (1991). Solar ultraviolet radiation effects on biological systems. *Phys. Med. Biol.* 36, 299–328. doi: 10.1088/0031-9155/36/3/001

Escobar, A. L., Alberdi, M., Acevedo, P., Machado, M., Nunes-Nesi, A., Inostroza-Blancheteau, C., et al. (2017). Distinct physiological and metabolic reprogramming by highbush blueberry (*Vaccinium corymbosum*) cultivars revealed during long-term UV-B radiation. *Physiol. Plant.* 160, 46–64. doi: 10.1111/ppl.12536

Favory, J. J., Stec, A., Gruber, H., Rizzini, L., Oravecz, A., Funk, M., et al. (2009). Interaction of COP1 and UVR8 regulates UV-B-induced photomorphogenesis and stress acclimation in Arabidopsis. *EMBO J.* 28, 591–601. doi: 10.1038/emboj.2009.4

Fedina, I., Hidema, J., Velitchkova, M., Georgieva, K., and Nedeva, D. (2010). UV-B induced stress responses in three rice cultivars. *Biol. Plant.* 54, 571–574. doi: 10.1007/s10535-010-0102-3

Flint, S. D., and Caldwell, M. M. (1984). Partial inhibition of in vitro pollen germination by simulated solar ultraviolet-B radiation. *Ecology* 65, 792–795. doi: 10.2307/1938051

Fu, B. Y., Xiong, J. H., Zhu, L. H., Zhao, X. Q., Xu, H. X., Gao, Y. M., et al. (2007). Identification of functional candidate genes for drought tolerance in rice. *Mol. Genet. Genomics* 278, 599–609. doi: 10.1007/s00438-007-0276-3

Gao, L., Liu, Y., Wang, X., Li, Y., and Han, R. (2019). Lower levels of UV-B light trigger the adaptive responses by inducing plant antioxidant metabolism and flavonoid biosynthesis in *Medicago sativa* seedlings. *Funct. Plant Biol.* 46, 896–906. doi: 10.1071/FP19007

Ghasemzadeh, A., Ashkani, S., Baghdadi, A., Pazoki, A., Jaafar, H. Z., and Rahmat, A. (2016). Improvement in flavonoids and phenolic acids production and pharmaceutical quality of sweet basil (*Ocimum basilicum* L.) by ultraviolet-B irradiation. *Molecules* 21:1203. doi: 10.3390/molecules21091203

Goto, E. (2011). Production of pharmaceutical materials using genetically modified plants grown under artificial lighting. *Acta Hortic.* 907, 45–52. doi: 10.17660/ActaHortic.2011.907.3

Goto, E., Ide, M., Saito, Y., and Hikosaka, S. (2020). Enhancement of gene expression related to phytochemical accumulation in plant leaves via exposure to environmental stresses in a plant factory. *Acta Hortic.* 1296, 265–272. doi: 10.17660/ActaHortic.2020.1296.34

Hectors, K., Prinsen, E., De Coen, W., Jansen, M. A. K., and Guisez, Y. (2007). Arabidopsis thaliana plants acclimated to low dose rates of ultraviolet B radiation show specific changes in morphology and gene expression in the absence of stress symptoms. *New Phytol.* 175, 255–270. doi: 10.1111/j.1469-8137.2007.02092.x

Hideg, E., Jansen, M. A., and Strid, A. (2013). UV-B exposure, ROS, and stress: inseparable companions or loosely linked associates? *Trends Plant Sci.* 18, 107–115. doi: 10.1016/j.tplants.2012.09.003

Höll, J., Lindner, S., Walter, H., Joshi, D., Poschet, G., Pfleger, S., et al. (2019). Impact of pulsed UV-B stress exposure on plant performance: how recovery periods stimulate secondary metabolism while reducing adaptive growth attenuation. *Plant Cell Environ.* 42, 801–814. doi: 10.1111/pce.13409

Inostroza-Blancheteau, C., Acevedo, P., Loyola, R., Arce-Johnson, P., Alberdi, M., and Reyes-Díaz, M. (2016). Short-term UV-B radiation affects photosynthetic performance and antioxidant gene expression in highbush blueberry leaves. *Plant Physiol. Biochem.* 107, 301–309. doi: 10.1016/j.plaphy.2016.06.019

Javanmardi, J., Stushnoff, C., Locke, E., and Vivanco, J. M. (2003). Antioxidant activity and total phenolic content of Iranian Ocimum accessions. *Food Chem.* 83, 547–550. doi: 10.1016/S0308-8146(03)00151-1

Jenkins, G. I. (2009). Signal transduction in responses to UV-B radiation. *Annu. Rev. Plant Biol.* 60, 407–431. doi: 10.1146/annurev.arplant.59.032607.092953

Kalbina, I., and Strid, A. (2006). The role of NADPH oxidase and MAP kinase phosphatase in UV-B-dependent gene expression in Arabidopsis. *Plant Cell Environ.* 29, 1783–1793. doi: 10.1111/j.1365-3040.2006.01555.x

Kapoor, D., Sharma, R., Handa, N., Kaur, H., Rattan, A., Yadav, P., et al. (2015). Redox homeostasis in plants under abiotic stress: role of electron carriers, energy metabolism mediators and proteinaceous thiols. *Front. Environ. Sci.* 3:13. doi: 10.3389/fenvs.2015.00013

Kataria, S., Jajoo, A., and Guruprasad, K. N. (2014). Impact of increasing ultraviolet-B (UV-B) radiation on photosynthetic processes. *J. Photochem. Photobiol. B* 137, 55–66. doi: 10.1016/j.jphotobiol.2014.02.004

Kliebenstein, D. J., Lim, J. E., Landry, L. G., and Last, R. L. (2002). Arabidopsis *UVR8* regulates ultraviolet-B signal transduction and tolerance and contains sequence similarity to human *Regulator of Chromatin Condensation 1*. *Plant Physiol.* 130, 234–243. doi: 10.1104/pp.005041

Lee, J.-H., and Oh, M.-M. (2015). Short-term low temperature increases phenolic antioxidant levels in kale. *Hortic. Environ. Biotechnol.* 56, 588–596. doi: 10.1007/s13580-015-0056-7

Lilley, J. M., Ludlow, M. M., McCouch, S. R., and O'Toole, J. C. (1996). Locating QTL for osmotic adjustment and dehydration tolerance in rice. *J. Exp. Bot.* 47, 1427–1436. doi: 10.1093/jxb/47.9.1427

Lois, R. (1994). Accumulation of UV-absorbing flavonoids induced by UV-B radiation in *Arabidopsis thaliana* L. *Planta* 194, 498–503. doi: 10.1007/BF00714462

Ma, D., Sun, D., Wang, C., Li, Y., and Guo, T. (2014). Expression of flavonoid biosynthesis genes and accumulation of flavonoid in wheat leaves in response to drought stress. *Plant Physiol. Biochem.* 80, 60–66. doi: 10.1016/j.plaphy.2014.03.024

Madronich, S., McKenzie, R. L., Björn, L. O., and Caldwell, M. M. (1998). Changes in biologically active ultraviolet radiation reaching the Earth's surface. *J. Photochem. Photobiol. B* 46, 5–19. doi: 10.1016/S1011-1344(98)00182-1

Mancinelli, A. L., and Schwartz, O. M. (1984). The photoregulation of anthocyanin synthesis IX. The photosensitivity of the response in dark and light-grown tomato seedlings. *Plant Cell Physiol.* 25, 93–105.

Meyer, P., Van de Poel, B., and De Coninck, B. (2021). UV-B light and its application potential to reduce disease and pest incidence in crops. *Hortic. Res.* 8, 1–20. doi: 10.1038/s41438-021-00629-5

Miller, N. J., and Rice-Evans, C. A. (1996). Spectrophotometric determination of antioxidant activity. *Redox Rep.* 2, 161–171. doi: 10.1080/13510002.1996.11747044

Møller, I. M., Jensen, P. E., and Hansson, A. (2007). Oxidative modifications to cellular components in plants. *Annu. Rev. Plant. Biol.* 58, 459–481. doi: 10.1146/annurev.arplant.58.032806.103946

Neugart, S., and Bumke-Vogt, C. (2021). Flavonoid glycosides in Brassica species respond to UV-B depending on exposure time and adaptation time. *Molecules* 26:494. doi: 10.3390/molecules26020494

Neugart, S., Fiol, M., Schreiner, M., Rohn, S., Zrenner, R., Kroh, L. W., et al. (2014). Interaction of moderate UV-B exposure and temperature on the formation of structurally different flavonol glycosides and hydroxycinnamic acid derivatives in kale (*Brassica oleracea* var sabellica). *J. Agric. Food Chem.* 62, 4054–4062. doi: 10.1021/jf4054066

Pandey, N., and Pandey-Rai, S. (2014). Short term UV-B radiation-mediated transcriptional responses and altered secondary metabolism of in vitro propagated plantlets of *Artemisia annua* L. *Plant Cell Tissue Organ Cult.* 116, 371–385. doi: 10.1007/s11240-013-0413-0

Pennycooke, J. C., Cox, S., and Stushnoff, C. (2005). Relationship of cold acclimation, total phenolic content and antioxidant capacity with chilling tolerance in petunia (Petunia× hybrida). *Environ. Exp. Bot.* 53, 225–232. doi: 10.1016/j.envexpbot.2004.04.002

Piluzza, G., and Bullitta, S. (2011). Correlations between phenolic content and antioxidant properties in twenty-four plant species of traditional ethnoveterinary use in the Mediterranean area. *Pharm. Biol.* 49, 240–247. doi: 10.3109/13880209.2010.501083

Ravindran, K. C., Indrajith, A., Pratheesh, P. V., Sanjiviraja, K., and Balakrishnan, V. (2010). Effect of ultraviolet-B radiation on biochemical and antioxidant defence system in *Indigofera tinctoria* L. seedlings. *Int. J. Eng. Sci. Technol.* 2, 226–232. doi: 10.4314/ijest.v2i5.60154

Reddy, L., Odhav, B., and Bhoola, K. D. (2003). Natural products for cancer prevention: a global perspective. *Pharmacol. Ther.* 99, 1–13. doi: 10.1016/S0163-7258(03)00042-1

Rizzini, L., Favory, J. J., Cloix, C., Faggionato, D., O'Hara, A., Kaiserli, E., et al. (2011). Perception of UV-B by the Arabidopsis UVR8 protein. *Science* 332, 103–106. doi: 10.1126/science.1200660

Robson, T. M., Klem, K., Urban, O., and Jansen, M. A. (2015). Re-interpreting plant morphological responses to UV-B radiation. *Plant Cell Environ.* 38, 856–866. doi: 10.1111/pce.12374

Rozema, J., Chardonnens, A., Tosserams, M., Hafkenscheid, R., and Bruijnzeel, S. (1997). Leaf thickness and UV-B absorbing pigments of plants in relation to an elevational gradient along the Blue Mountains. Jamaica. *Plant Ecol.* 128, 151–159. doi: 10.1023/A:1009719109153

Scalbert, A., Andres-Lacueva, C., Arita, M., Kroon, P., Manach, C., Urpi-Sarda, M., et al. (2011). Databases on food phytochemicals and their health-promoting effects. *J. Agric. Food Chem.* 59, 4331–4348. doi: 10.1021/jf200591d

Sharma, P., Jha, A. B., Dubey, R. S., and Pessarakli, M. (2012). Reactive oxygen species, oxidative damage, and antioxidative defense mechanism in plants under stressful conditions. *J. Bot.* 26. doi: 10.1155/2012/217037

Son, K.-H., Ide, M., and Goto, E. (2020). Growth characteristics and phytochemicals of canola (*Brassica napus*) grown under UV radiation and low root zone temperature in a controlled environment. *Hortic. Environ. Biotechnol.* 61, 267–277. doi: 10.1007/s13580-019-00219-4

Strid, A., Chow, W. S., and Anderson, J. M. (1994). UV-B damage and protection at the molecular level in plants. *Photosynth. Res.* 39, 475–489. doi: 10.1007/BF00014600

Su, N., Lu, Y., Wu, Q., Liu, Y., Xia, Y., Xia, K., et al. (2016). UV-B-induced anthocyanin accumulation in hypocotyls of radish sprouts continues in the dark after irradiation. *J. Sci. Food Agric.* 96, 886–892. doi: 10.1002/jsfa.7161

Sytar, O., Zivcak, M., Bruckova, K., Brestic, M., Hemmerich, I., Rauh, C., et al. (2018). Shift in accumulation of flavonoids and phenolic acids in lettuce attributable to changes in ultraviolet radiation and temperature. *Sci. Hortic.* 239, 193–204. doi: 10.1016/j.scienta.2018.05.020

Takahashi, S., Kojo, K. H., Kutsuna, N., Endo, M., Toki, S., Isoda, H., et al. (2015). Differential responses to high- and low-dose ultraviolet-B stress in tobacco Bright Yellow-2 cells. *Front. Plant Sci.* 6:254. doi: 10.3389/fpls.2015.00254

Tevini, M., and Steinmüller, D. (1987). Influence of light, UV-B radiation, and herbicides on wax biosynthesis of cucumber seedling. *J. Plant Physiol.* 131, 111–121. doi: 10.1016/S0176-1617(87)80272-9

Tevini, M., Iwanzik, W., and Thoma, U. (1981). Some effects of enhanced UV-B irradiation on the growth and composition of plants. *Planta* 153, 388–394. doi: 10.1007/BF00384258

Velikova, V., Yordanov, I., and Edreva, A. (2000). Oxidative stress and some antioxidant systems in acid rain-treated bean plants: protective role of exogenous polyamines. *Plant Sci.* 151, 59–66. doi: 10.1016/S0168-9452(99)00197-1

Visioli, F., De La Lastra, C. A., Andres-Lacueva, C., Aviram, M., Calhau, C., Cassano, A., et al. (2011). Polyphenols and human health: a prospectus. *Crit. Rev. Food Sci. Nutr.* 51, 524–546. doi: 10.1080/10408391003698677

Wang, Y., Meng, G., Chen, S., Chen, Y., Jiang, J., and Wang, Y. P. (2018). Correlation analysis of phenolic contents and antioxidation in yellow-and black-seeded *Brassica napus*. *Molecules* 23:1815. doi: 10.3390/molecules23071815

Wargent, J. J., Moore, J. P., Roland-Ennos, A., and Paul, N. D. (2009). Ultraviolet radiation as a limiting factor in leaf expansion and development. *Photochem. Photobiol.* 85, 279–286. doi: 10.1111/j.1751-1097.2008.00433.x

Wu, D., Hu, Q., Yan, Z., Chen, W., Yan, C. Y., Huang, X., et al. (2012). Structural basis of ultraviolet-B perception by UVR8. *Nature* 484, 214–219. doi: 10.1038/nature10931

Xia, X. J., Zhou, Y. H., Shi, K., Zhou, J., Foyer, C. H., and Yu, J. Q. (2015). Interplay between reactive oxygen species and hormones in the control of plant development and stress tolerance. *J. Exp. Bot.* 66, 2839–2856. doi: 10.1093/jxb/erv089

Xiong, J. H., Fu, B. Y., Xu, H. X., and Li, Y. S. (2010). Proteomic analysis of PEG-simulated drought stress responsive proteins of rice leaves using a pyramiding rice line at the seedling stage. *Bot. Stud.* 51, 137–145.

Xu, Y. H., Liu, R., Yan, L., Liu, Z. Q., Jiang, S. C., Shen, Y. Y., et al. (2012). Light-harvesting chlorophyll a/b-binding proteins are required for stomatal response to abscisic acid in Arabidopsis. *J. Exp. Bot.* 63, 1095–1106. doi: 10.1093/jxb/err315

Yang, Y., Yang, X., Jang, Z., Chen, Z., Ruo, X., Jin, W., et al. (2018). UV RESISTANCE LOCUS 8 from Chrysanthemum morifolium Ramat (CmUVR8) plays important roles in UV-B signal transduction and UV-B-induced accumulation of flavonoids. *Front. Plant Sci.* 9:955. doi: 10.3389/fpls.2018.00955

Conflict of Interest: The authors declare that the research was conducted in the absence of any commercial or financial relationships that could be construed as a potential conflict of interest.

Publisher's Note: All claims expressed in this article are solely those of the authors and do not necessarily represent those of their affiliated organizations, or those of the publisher, the editors and the reviewers. Any product that may be evaluated in this article, or claim that may be made by its manufacturer, is not guaranteed or endorsed by the publisher.

frontiers in Plant Science

ORIGINAL RESEARCH
published: 03 March 2022
doi: 10.3389/fpls.2022.706042

Using Machine Learning Models to Predict Hydroponically Grown Lettuce Yield

Ali Mokhtar[1,2,3], Wessam El-Ssawy[1,4], Hongming He[2,3], Nadhir Al-Anasari[5]*, Saad Sh. Sammen[6], Yeboah Gyasi-Agyei[7] and Mohamed Abuarab[1]*

[1] Department of Agricultural Engineering, Faculty of Agriculture, Cairo University, Giza, Egypt, [2] State Key Laboratory of Soil Erosion and Dry Land Farming on Loess Plateau, Institute of Soil and Water Conservation, Chinese Academy of Sciences and Ministry of Water Resources at Northwest University of Agriculture and Forestry, Xianyang, China, [3] School of Geographic Sciences, East China Normal University, Shanghai, China, [4] Irrigation and Drainage Department, Agricultural Engineering Research Institute, Agricultural Research Center, Giza, Egypt, [5] Department of Civil Engineering, Environmental and Natural Resources Engineering, Lulea University of Technology, Lulea, Sweden, [6] Department of Civil Engineering, College of Engineering, University of Diyala, Baquba, Iraq, [7] School of Engineering and Built Environment, Griffith University, Nathan, QLD, Australia

Prediction of crop yield is an essential task for maximizing the global food supply, particularly in developing countries. This study investigated lettuce yield (fresh weight) prediction using four machine learning (ML) models, namely, support vector regressor (SVR), extreme gradient boosting (XGB), random forest (RF), and deep neural network (DNN). It was cultivated in three hydroponics systems (i.e., suspended nutrient film technique system, pyramidal aeroponic system, and tower aeroponic system), which interacted with three different magnetic unit strengths under a controlled greenhouse environment during the growing season in 2018 and 2019. Three scenarios consisting of the combinations of input variables (i.e., leaf number, water consumption, dry weight, stem length, and stem diameter) were assessed. The XGB model with scenario 3 (all input variables) yielded the lowest root mean square error (RMSE) of 8.88 g followed by SVR with the same scenario that achieved 9.55 g, and the highest result was by RF with scenario 1 (i.e., leaf number and water consumption) that achieved 12.89 g. All model scenarios having Scatter Index (SI) (i.e., RMSE divided by the average values of the observed yield) values less than 0.1 were classified as excellent in predicting fresh lettuce yield. Based on all of the performance statistics, the two best models were SVR with scenario 3 and DNN with scenario 2 (i.e., leaf number, water consumption, and dry weight). However, DNN with scenario 2 requiring less input variables is preferred. The potential of the DNN model to predict fresh lettuce yield is promising, and it can be applied on a large scale as a rapid tool for decision-makers to manage crop yield.

Keywords: machine learning, deep learning, DNN, yield prediction, food safety 2

OPEN ACCESS

Edited by:
Francesco Orsini, University of Bologna, Italy

Reviewed by:
Ana María Mendez-Espinoza, Instituto de Investigaciones Agropecuarias, Chile
Laura Carotti, University of Bologna, Italy
Toyoki Kozai, Japan Plant Factory Association, Japan

***Correspondence:**
Wessam El-Ssawy
eng_wess50@yahoo.com
Nadhir Al-Anasari
nadhir.alansari@ltu.se

Specialty section:
This article was submitted to Technical Advances in Plant Science, a section of the journal Frontiers in Plant Science

Received: *06 May 2021*
Accepted: *18 January 2022*
Published: *03 March 2022*

Citation:
Mokhtar A, El-Ssawy W, He H, Al-Anasari N, Sammen SS, Gyasi-Agyei Y and Abuarab M (2022) Using Machine Learning Models to Predict Hydroponically Grown Lettuce Yield. Front. Plant Sci. 13:706042. doi: 10.3389/fpls.2022.706042

INTRODUCTION

The changing conditions of climate and weather patterns during the past years have fueled the current problems of land and water scarcity and continue to cause harm in the agricultural sector (Majid et al., 2021). Globally, the agricultural sector is the largest consumer of water comprising about 70% of the total demand, but 70% of this is returned as wastewater through the different processes (Kloas et al., 2015; Murad et al., 2017). While *per capita* drinking water is about 2–5 L/day, it requires about 5,000 L of water to produce daily dietary needs per person (Manju et al., 2017). The

development of sustainable plans has become a global focus, and a circular economy is the order of the day (Wei et al., 2019).

Without a doubt, the use of modern technologies has increased ability of mankind to meet the latest challenges of limited resources. Hydroponic systems are considered as an alternative to traditional agricultural systems (Majid et al., 2021). Safety, sustainability, and policy issues associated with water and agriculture are fundamental to Egyptian interests. Irrigated agriculture is the main user of water resources in most parts of the world. Stress on water availability and associated impacts among competing user groups in the region are increasing due to population growth, development, environmental, and wildlife concerns (Abd-Rbo et al., 2015). Therefore, the application of modern agricultural techniques of hydroponic and aeroponics without the need for soil is on the increase (Mehra et al., 2018). Hydroponic systems can increase water productivity and maintain the quality of production. Therefore, they should be implemented on any scale to support the environment and agriculture (El-Ssawy et al., 2020). Artificial intelligence (AI), such as neural networks, has been applied in hydrology to deal with complex phenomena (Elbeltagi et al., 2020; Abdel-Fattah and Abdo, 2020; Mokhtar et al., 2021) and is also used to control the growth of hydroponic plants (Mehra et al., 2018). For some systems, such as the nutrient film technique (NFT), a fresh solution of nutrients is continuously supplied to the crops to compensate for the uptake of nutrients and water by the plants. In some systems, the input of nutrients is based on the nutrient/water uptake ratio concept, i.e., nutrient weight per unit volume of water absorbed (Sonneveld and Voogt, 2001; Neocleous and Savvas, 2019).

Lettuce grows much faster in aeroponics compared to a floating system, probably due to the higher dissolved oxygen level in the nutrient solution (Puccinelli et al., 2021). Hydroponic systems can be automated using Internet of Things technology, and machine learning (ML), a subset of AI, is very beneficial in this regard. However, the use of ML in hydroponic/aeroponic systems to automate plant growth has received less research (Araújo et al., 2019). Recently, there have been many approaches to estimate crop yield based on conventional methods, including models of process-oriented crop simulation and statistical-based models analyzing crop production and explanatory variables (Johnson, 2014; Cai et al., 2019). Conventional statistical-based methods or specific response functions linking yield and independent variables provide an alternative to forecast yield due to their simpler computation and higher interpretation power (Qader et al., 2018). However, there are some problems with conventional empirical prediction models because they tend to be applicable to local conditions and the generalization for other areas is limited (Qader et al., 2018; Folberth et al., 2019). ML is a "black-box" with complicated functions but has the capability for dealing with complex relationships between the independent and the dependent variables (Kamir et al., 2020; Cao et al., 2021). In recent years, ML techniques have been used in agricultural research fields, such as classification of crop and monitoring of growth and prediction of yield in some countries (Sadeghipour et al., 2013; Shah et al., 2019; Wolanin et al., 2019). The ground is now set for future sustainable agriculture that is data-driven to feed AI and robots (Saiz-Rubio and Rovira-Más, 2020).

The ML is improving the ability of computers to perform actions on their own after they have been trained for a specific task. For machines to think like humans, they should first learn like human beings. The mind of a human being makes decisions based on past experiences, i.e., the data of the past that one has been exposed to. ML algorithms have different uses in hydroponics, such as to control plant growth, electrical conductivity (EC) values, and the constituents of the nutrient solution (Mehra et al., 2018). It instructs computers to perform complicated tasks through regression, diagnosis, planning, and recognition by learning from historical data. Thus, data and algorithms are considered fundamental to performance of ML models. Higher quality data and larger data sizes are instrumental for the accuracy of ML models. It is also necessary to apply suitable algorithms to achieve solutions to different problems containing different types of datasets (Kang et al., 2020). For example, Johnson (2014) applied a regression tree (RT) for predicting yields of soybean and maize at the county-level in the United States. In Australia, Cai et al. (2019) compared the three improved ML models [i.e., support vector machine (SVM), random forest (RF), and neural network (NN)] and the method of traditional regression [i.e., Least Absolute Shrinkage and Selection Operator (LASSO)] for the prediction of wheat yield. Their results showed that ML methods were better than the traditional regression method.

Jeong et al. (2016) predicted the yield of wheat, maize, and potato by applying RF and multiple linear regression (MLR). They concluded that RF was better than MLR in predicting crop yields. Fukuda et al. (2013) also applied RF to predict yields of mango fruit with a successful outcome. Deep learning (DL), a subset of NN, has multiple layers and progressively extracts higher-level features from the raw input data (Lecun et al., 2015; Khaki and Wang, 2019). You et al. (2017) used convolutional neural networks (CNNs) and recurrent neural networks (RNNs) to predict soybean yield based on a sequence of remotely sensed images. Furthermore, a deep neural network (DNN) was applied to predict maize yield during 2008–2016, and the results showed that DNN was clearly better than LASSO, shallow neural network (SNN), and RT (Khaki and Wang, 2019). Kim et al. (2019) applied a DNN model to predict corn and soybean yield during 2006–2015. In Argentina, Khaki and Wang (2019) developed a DNN for predicting soybean yields.

The initial cost for establishing a hydroponic system is very high, making it imperative to predict crop yield before establishment using models, such as ML. Therefore, the objectives of this study were to (1) apply four ML models to predict fresh head weight (yield) of lettuce under controlled greenhouse conditions subject to three input scenarios consisting of the combinations of input variables and (2) identify the best model scenarios.

MATERIALS AND METHODS

Experimental Treatments

The experiment was conducted in a controlled greenhouse (2.0 m wide, 3.5 m long, and 2.5 m height) environment

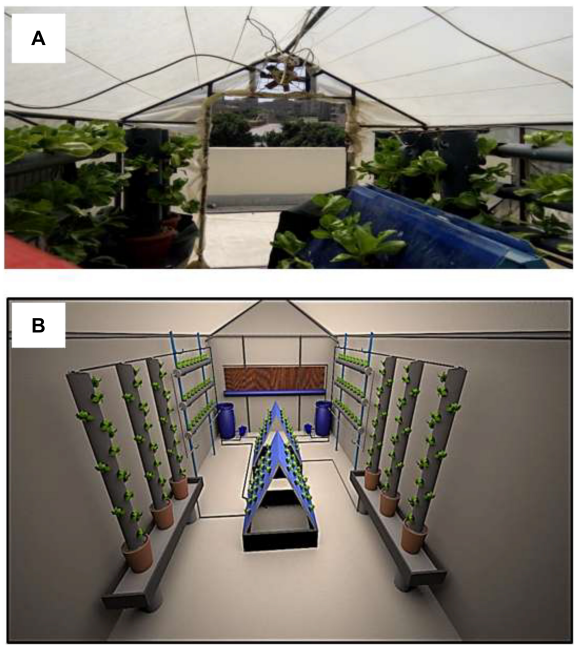

FIGURE 1 | Components of the experimental setup. **(A)** Photograph. **(B)** Computer graphics.

made with an iron frame covered with a polyethylene sheet at the Agricultural Engineering Research Institute, Agricultural Research Center, Giza, Egypt, during the growing season in 2018 and 2019. It contained three hydroponics systems (i.e., suspended NFT system, pyramidal aeroponic system, and tower aeroponic system) as shown in **Figure 1**, subjected to three different magnetic levels (MWL1 = 3,800 gauss, MWL2 = 5,250 gauss, and MWL3 = 6,300 gauss) (**Figure 2**). The nutrient solution was pumped from an irrigation storage tank through 16-mm polyethylene pipes connected to each system by a 1-hp pump, and the irrigation rate was 10 L/day for 6 h.

The suspended NFT system consisted of 150-cm-high vertical iron stands that support three horizontal pipes each of 250 cm length and 10.16 cm diameter. Each pipe had holes with 5 cm diameter at 20-cm intervals containing the hydroponic cups that housed the plants. The pyramidal aeroponic system consisted of 1 m^2 iron frames, two put together to make a V-shaped structure and placed on an iron tank (1 m wide, 1 m long, and 0.5 cm deep). The iron frames were covered with high-density plastic sheets on both sides forming a triangular pyramid, the plants being housed in the plastic sheet. A gutter at the bottom of the pyramid collected the nutrient solution which was then redirected to the irrigation storage tank. Four foggers of 0.5 m diameter, discharging at 6 L/h under 2 bar pressure, were installed inside the system. The tower aeroponic system was made of pipes of 15.24 cm diameter and 1.5 m height. Also with this system, the plants were placed at 20 cm intervals in hydroponic cups within holes of 5 cm diameter. The nutrient solution was pumped from a tank to the foggers installed above the system through a polyethylene pipe of 16 mm diameter. The same type of foggers was used for both the pyramidal and the tower aeroponic systems.

The lettuce (cv. *LimorHyb*.) plants were obtained from the Institute of Horticulture Research, Giza, Egypt. In the hydroponic systems, the plants were grown in high-density sponges of 3 cm thick. They were cultivated for 3 weeks in 5 cm deep cups filled with nutrient solution to generate complete rooting. The plants were placed in different hydroponics systems after rooting on April 01, 2018, and March 01, 2019. Irrigation water was sourced from two tanks filled with a nutrient solution in the environmentally controlled greenhouse. The EC of the nutrient solution was approximately 1.5 dS/m which also had the following chemical properties: N = 51, P = 219.29, K = 358.3, Ca = 135, Mg = 45, Fe = 2.7, Mn = 0.75, Cu = 0.375, Zn = 0.113, B = 0.188, and Mo = 0.009 (Jackson and McGonigle, 2005).

Climate Conditions

The range of temperature during the two seasons was 23–25 and 20–22°C, and the relative humidity was 60–65%. These weather conditions were controlled and monitored by the greenhouse tools (i.e., cooling pad, suction van, and monitoring sensor) and were checked by a Hygrometer Thermo-Anemometer Model 407412 (accuracy ±0.8°C and ±3%) and monitoring sensor CSP60BA252M with a nominal resistance of 2,500 ohms. Light intensity was 1981:1992 in the lux unit, and it was measured by light meter Model YK-10LX (accuracy ±5% and 4 days).

Plant Variables and Scenarios

The systems were designed to contain 64 plants per square meter in each system. The harvest occurred after 50 days from planting in the systems at the same time. For each harvest, three plants were taken from each system. Then, the explanatory features, or variables used interchangeably, of leaf number, stem length, stem diameter, and dry weight, as well as the water consumption, and the dependent feature of fresh head weight (yield) were recorded. Descriptive statistical analysis of the collected data during the growing season of 2 years is shown in **Table 1** for the three complete datasets. The explanatory features were divided into three scenarios: scenario 1 (leaf number and water consumption), scenario 2 (leaf number, water consumption, and dry weight), and scenario 3 (leaf number, water consumption, dry weight, stem length, and stem diameter, i.e., all input variables) (**Table 2**).

Machine Learning Models

Support Vector Machine

The SVM is a supervised learning algorithm that can also be used as a regression model. The main objective is to minimize the errors and individualize the hyperplane that increases the tolerance limit. The approximated function in the algorithm of SVM is given as follows:

$$f(x) = \omega\varphi(x) + b \quad (1)$$

where φ (x) is a feature space of higher dimension converted from the input vector x, ω represents the weights vector, and b are thresholds that are estimated by minimizing the following

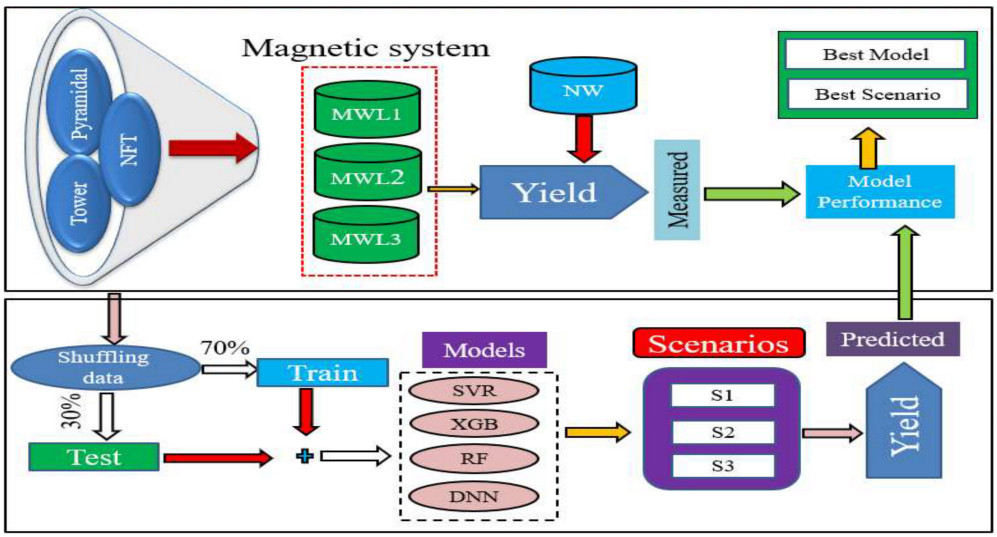

FIGURE 2 | Flowchart of the treatments implemented and models applied.

regularized risk function:

$$R(C) = C\frac{1}{n}\sum_{i=1}^{n} L(d_i, y_i) + \frac{1}{2} \parallel \omega \parallel^2 \quad (2)$$

where C is the penalty parameter of the error, d_i is the desired value, n is the number of observations, and $C\frac{1}{n}\sum_{i=1}^{n} L(d_i, y_i)$ is the empirical error in which the function L_ε is determined as follows:

$$L_\varepsilon(d, y) = |d - y| - \varepsilon \; |d - y| \geq \varepsilon \;\; or \;\; 0 \;\; otherwise \quad (3)$$

where $\frac{1}{2} \parallel \omega \parallel^2$ is the so-called regularization term and ε is the tube size. The approximated function of Equation (1) is expressed in an explicit form by introducing Lagrange multipliers and exploiting the optimality constraints as follows:

$$f(x, \alpha_i, \alpha_i^*) = \sum_{i=1}^{n} (\alpha_i - \alpha_i^*) k(x, x_i) + b \quad (4)$$

where $k(x, x_i)$ is the kernel function. Vapnik (2016) and Fan et al. (2018) have provided detailed information and the computational procedures of the SVM algorithm.

TABLE 1 | Descriptive statistical analysis of the collected data.

	Mean	Max	Min	SD	Q1	Q3
Stem diameter	22.05	28.20	17.00	2.84	19.98	23.98
Leaf number	26.88	37.00	21.00	3.51	24.00	29.00
Stem length	41.15	52.00	32.00	4.28	38.00	43.00
Dry weight	18.20	27.90	13.10	3.17	16.25	19.05
water/area	0.32	0.42	0.25	0.05	0.26	0.34
Fresh head weight	329.81	416.20	275.20	36.48	301.73	346.10

Extreme Gradient Boosting

The extreme gradient boosting (XGB) algorithm proposed by Chen and Guestrin (2016) is a novel implementation method for Gradient Boosting Machine which is based on RTs. The algorithm depends on the "boosting" idea which combines all the predictions of a set of "weak" learners to develop a "strong" learner during strategies of additive training. The general function for the prediction at step t is given as follows:

$$fi^{(t)} = \sum_{k=1}^{t} f_k(x_i) = f_i^{(t-1)} + f_t(x_i) \quad (5)$$

where $ft\ (x_i)$ is the learner at step t, $f_i\ (t)$ and $f_i\ (t\text{-}1)$ are the predictions at steps t and $t\text{-}1$, and x_i is the input variable.

To avoid the overfitting problem without any influence on the model computational speed, the XGB applies the analytic expression given below to evaluate the "goodness" of the model

TABLE 2 | Summary of the combination of the input variables for the applied models.

Scenario	Model				Input variables combination
1	SVR1	XGB1	RF1	DNN1	Leaf number, water consumption
2	SVR2	XGB2	RF2	DNN2	Leaf number, water consumption, dry weight
3	SVR3	XGB3	RF3	DNN3	Leaf number, water consumption, dry weight, stem length, stem diameter

SVR1, XGB1, RF1, and DNN1 for the first scenario, 2 is the second scenario, and 3 is the third scenario.

from the original function:

$$Obj^{(t)} = \sum_{k=1}^{n} l\left(\bar{y_i}, y_i\right) + \sum_{k=1}^{t} \Omega\left(f_i\right) \quad (6)$$

where l is the loss function, n is the number of observations, and Ω is the regularization term which is defined as follows:

$$\Omega\left(f\right) = \gamma T + \frac{1}{2}\lambda||\omega||^2 \quad (7)$$

where ω is the vector of scores in the leaves, λ is the regularization parameter, and γ is the minimum loss needed to further partition the leaf node. More information and procedures of the computation of the XGB algorithm can be found in the study by Chen and Guestrin (1994).

Random Forest

The RF model was developed by Breiman (2001) and uses the "bagging" idea to ensemble a collection of decision trees with controlled variance. The RF model is commonly used for regression and prediction problems. An RF regression is a specific type of bootstrap ensembles. It deals with random binary trees that use a subset of the observations *via* bootstrapping, where a random subset of the training dataset is sampled from the raw dataset and utilized to evolve the model. The detailed computational procedure of the RF model can be found in the studies by Breiman (2001) and Ferreira and da Cunha (2020). To get the best score, an RF was trained using 200 trees, 5 max depth, and the default values of the other hyperparameters. During the tuning phase, the following sets of hyperparameters and their respective values were used: n estimators (number of trees) (100, 200, 300, and 500) and max depth (1, 2, 5, and 10).

Deep Neural Network

The DNN is a powerful DL model (Montes-Atenas et al., 2016; Achieng, 2019). It is an artificial neural network (ANN) with multiple layers between the input layers, hidden layers, and output layers to learn more complex non-linear relationships between input and output. In this study, the rectified linear unit (ReLU) was applied as an activation function which is commonly employed to establish input-output relationships and defined as follows (Xu et al., 2015; Ghimire et al., 2019):

$$ReLu(s) = \left\{ \begin{array}{l} x(x > 0 \\ 0(x \leq 0 \end{array} \right\} \quad (8)$$

The loss function in the DNN model is expressed as follows:

$$loss = \frac{1}{2n}\sum_{i=1}^{n}\left(T_i - T_i^{'}\right)^2 \quad (9)$$

where n is the number of observation data T, and $T'$is the estimated value by the DNN model which can be defined for a three-hidden-layer DNN model with the ReLU activation function as follows:

$$T' = ReLu\varpi_4(\varpi_3(ReLu(\varpi_2(ReLu)(\varpi_1 + b_1)) + b_3)) + b_4 \quad (10)$$

where ω_1, ω_2, ω_3, and ω_4 are the weights in the network and b_1, b_2, b_3, and b_4 are the bias terms.

Performance Evaluation of the Models

In this study, the mean absolute error (MAE), the root mean square error (RMSE), and the mean bias error (MBE) were used to evaluate the applied models. In addition, uncertainty with a 95% confidence level (U95) was estimated (Gueymard, 2014; Behar et al., 2015). The model deviations and the T-statistic test (Tstat) were used to evaluate the significant differences between the predicted and the observed yield (Stone, 1994; Gueymard, 2014). The performance statistics are defined as follows:

$$MAE = \frac{1}{n}\sum_{i=1}^{n}|O_i - P_i| \quad (11)$$

$$RMSE = \sqrt{\frac{1}{n}\sum\left(P_i - O_i\right)^2} \quad (12)$$

$$MBE = \frac{1}{n}\sum_{i=1}^{n}(O_i - P_i) \quad (13)$$

$$SI = \frac{RMSE}{O^{-}} \quad (14)$$

$$T_{stat} = \sqrt{\frac{(1-n)\,MBE^2}{RMSE^2 - MBE^2}} \quad (15)$$

$$U_{95} = 1.96\sqrt{\left(SD^2 + RMSE^2\right)} \quad (16)$$

where $\bar{O}$ represents the average values of the observed yield, O_i and P_i are the observed and predicted yield, respectively, and i is the number of observations. SD is the standard deviation of the difference between the observed and estimated values. The range of the Scatter Index (SI) for the classification of the models is "excellent" if SI $<$ 0.1, "good" if 0.1 $<$ SI $<$ 0.2, "fair" if 0.2 $<$ SI $<$ 0.3, and "poor" if SI $>$ 0.3. Notably, the MBE and T-statistics take both negative and positive values.

In this study, the datasets were divided into 70% for training and 30% for testing. The ML models were implemented using the Python programming language library Scikit-learn 0.22.1. A virtual machine was established on Google Cloud Platform which was used for the computations. The hyperparameter tuning was performed using a grid search method for each model to get the best score as well as the best parameter sets that gave the lowest prediction errors in the testing stages (Al-Fugara et al., 2020; Fan et al., 2021). For support vector regressor (SVR), two different kernels (i.e., radial basis function and linear) were applied, as well as regularization parameter C from the set (1, 2, 3, 4, and 5), and maintained the default values of the remaining hyperparameters. To get the best score, an XGB was applied by using 400 trees, 10 max depths, a learning rate of 0.1, and the other hyperparameters that are the default values. The following sets of hyperparameters were applied: n estimators (number of trees) (100, 200, 300, 400, and 500);

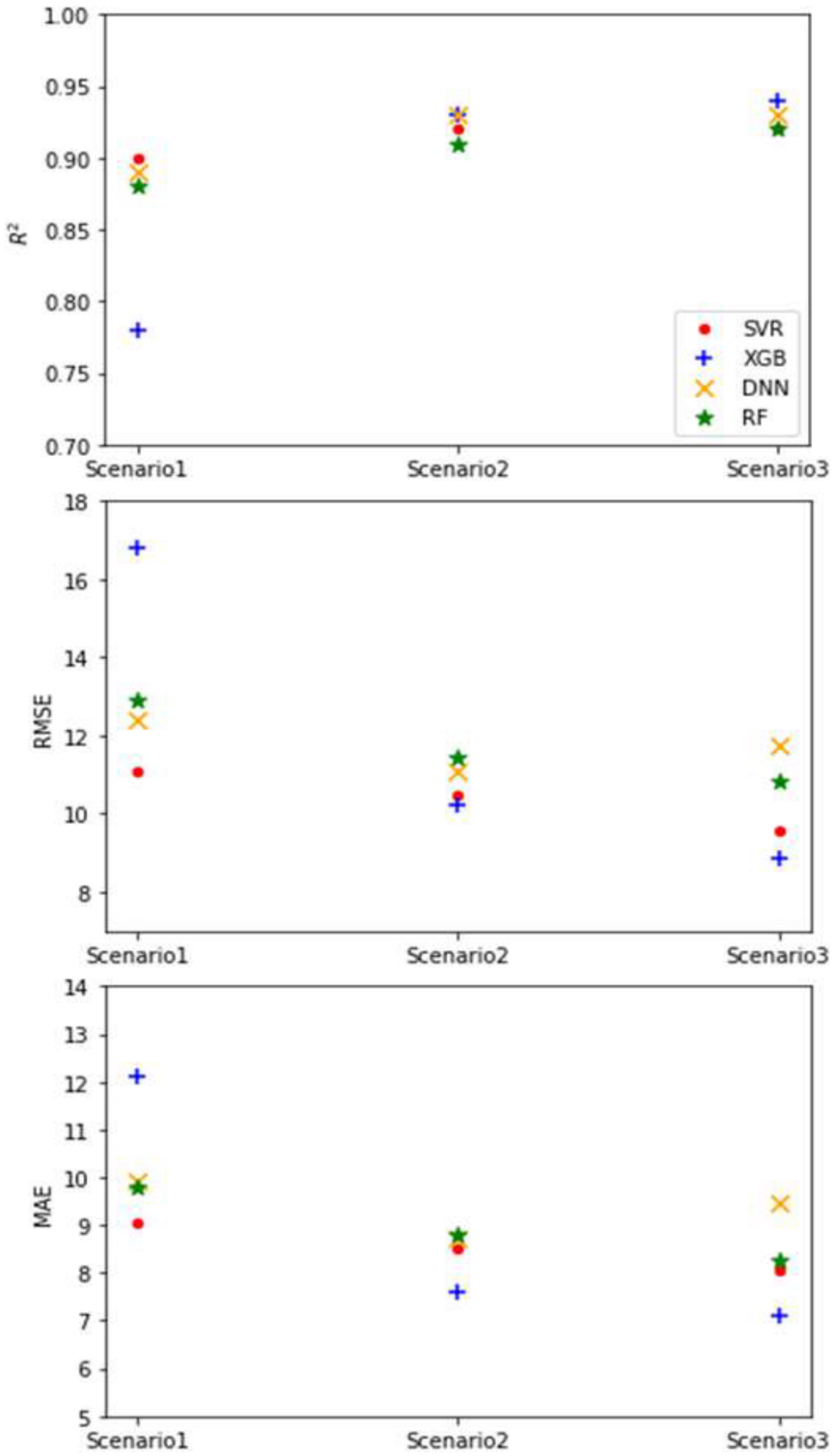

FIGURE 3 | The performance statistics values for different model scenarios.

max depth (1, 2, 5, 10, and 12); and learning rate (0.05, 0.1, and 0.5). RF was trained using 400 trees, where 10 max depth and the default values of the other hyperparameters were used. During the hyperparameter tuning stage, the following sets of hyperparameters were assessed: number of trees (100, 200, 300, 400, and 500) and max depth (1, 2, 5, 10, and 12). For the DNN

model, the neuron numbers in the four hidden layers were 256, 128, 128, and 64 neurons, respectively, and the iterations (epochs) were optimized as 500 epochs.

RESULTS AND DISCUSSION

Evaluation of the Machine Learning Models

The results of the application of the ML models are shown in **Figure 3**. The XGB model with scenario 3 yielded the lowest RMSE value of 8.88 g followed by SVR with scenario 3 at 9.55 g, and the highest value was in XGB with scenario 1. With regard to MAE, XGB reported the lowest value with scenario 3 as 7.1 g, and the same model yielded the highest value with scenario 1 as 12.1 g. In terms of the coefficient of determination (R^2), all model scenarios registered more than 0.88 except for XGB with scenario 1 which recorded a modest value of 0.78 (**Figure 3**).

The lowest T-statistic was recorded by SVR with scenario 2, and the highest was recorded by DNN with scenario 2. For the uncertainty, XGB with scenario 3 recorded the lowest value as 24.8, and the highest value of 46.8 was recorded by the same model but with scenario 1, following the same trend as RMSE and MAE. In terms of the MBE, the highest value was reported by the DNN model with scenario 3 as 3.95 g followed by DNN with scenario 2 as 3.8 g. All model scenarios produced SI values of <0.1, which is an indication of excellent performance by all models. This may be related to the strong correlation between the input and output variables. However, the selection of input variables is one of the most important aspects for ML models to achieve better results.

The ML models performed well at the controlled environment level. Our methodology is scalable, simple, and inexpensive for estimating lettuce fresh weight. It is observed that the prediction accuracy of the models varied and also depended on the scenario input variables. Prediction of crop yield is extremely challenging due to its dependency on multiple factors, such as crop genotype, environmental factors, management practice, and their interactions (Khaki et al., 2020). There are many studies discussing crop genotype and environmental factors, but our study is focused on the effect of plant components and water consumption on yield (fresh head weight). The DL subset of ML can be further improved by combining with crop models, adding detailed farming management data, and higher spatiotemporal input variables (Cao et al., 2021).

We predicted lettuce crop yield depending on the input variable scenarios. Scenario 1 consisted of leaf number and water consumption, scenario 2 combined leaf number, dry weight, and water consumption, and scenario 3 included all features (i.e., stem diameter, leaf number, stem length, dry weight, and water consumption). Our results are in agreement with previous studies that showed that the RF model can accurately estimate crop yields (Fukuda et al., 2013; Everingham et al., 2016). There was no overfitting during the training stage for the RF model yet it had the lowest R^2 for scenarios 2 and 3 and the second lowest value after XGB for scenario 1. In contrast, the results of Jeong et al. (2016) reported

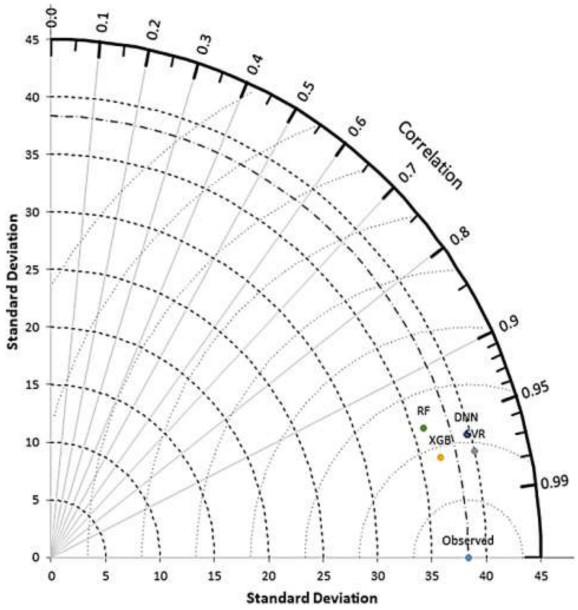

FIGURE 4 | Taylor diagram displaying a statistical comparison of the applied models used for predicting fresh head weight (yield).

that the algorithm of RF may suffer overfit to data because its algorithm consists of an ensemble of a large number of decision trees that may not be fully described mechanistically. Also, RF may cause a loss of accuracy when extreme ends are expected or responses are outside the limits of the training data (Jeong et al., 2016).

Model Comparison

As shown in **Figure 3**, the XGB model reported the lowest RMSE and MAE values of 2.69 and 2.2%, respectively, and also the highest R^2 value (0.94) for scenario 3. According to the SI statistics, the SVR model with scenario 3 had excellent performance (Li et al., 2013). The second model was XGB as judged by the RMSE (2.89%) and MAE (2.4%) performance statistics. **Figure 4** presents a Taylor diagram that shows how much the observations are matched by the predictions and the degree of compliance by the model (Taylor, 2001; Maroufpoor et al., 2019). It is clear that the best models were SVR with scenario 3 and DNN with scenario 2. However, SVR with scenario 3 (i.e., leaf number, water consumption, dry weight, stem length, and stem diameter) is superior, and DNN with scenario 2 (i.e., leaf number, water consumption, and dry weight) is equally good. It needs to be mentioned that DNN with scenario 2 has less input features than SVR with scenario 3, making DNN with scenario 2 the preferred model. Nevertheless, all four models that were applied have a high correlation coefficient in excess of 0.95, and the SD was close to the observed values.

A boxplot to compare the models based on the residuals (estimation error) is shown in **Figure 5**. Positive and negative estimation errors show under- and overestimations, respectively.

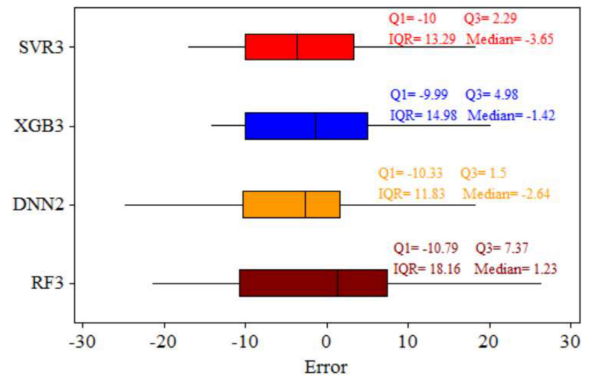

FIGURE 5 | Boxplots showing the distribution of the estimation errors in the test stage for support vector regressor (SVR), extreme gradient boosting (XGB), deep neural network (DNN), and random forest (RF) models. Q25, lower quartile of errors; Q75, upper quartile of errors; IQR, interquartile range for each model.

TABLE 3 | The performance statistics of support vector regressor (SVR), extreme gradient boosting (XGB), deep neural network (DNN), and random forest (RF) models for lettuce.

Model	Scenario	SI	T	U95	MBE
SVR	1	0.035	0.647	31.90	1.59
	2	0.032	0.015	29.35	0.034
	3	0.029	1.600	26.10	3.10
XGB	1	0.051	0.780	46.80	2.84
	2	0.031	0.110	28.70	–0.25
	3	0.027	0.540	24.80	1.04
DNN	1	0.037	0.630	34.50	1.70
	2	0.033	1.650	30.30	3.80
	3	0.035	1.630	31.90	3.95
RF	1	0.039	0.160	36.2	–0.45
	2	0.035	0.135	32.1	–0.34
	3	0.033	0.087	30.3	–0.21

SI, Scatter Index; Tstat, T-statistic test; U95, Uncertainty with a 95% confidence level; MBE, mean bias error.

The DNN with scenario 2 model appears to be the best model having the lowest error in comparison with the others. It has a lower quartile (Q1) value of –10.33, while XGB has a value of –9.99, and SVR, a value of –10. Third quartile (Q3) error analysis is better than Q1 because it contains 75% of the error. It is reported that the DNN with scenario 2 model has a difference of $\Delta Q3 = 3.48$ compared with XGB with scenario 3 which has $\Delta Q3 = 0.79$ compared with SVR3. Moreover, the smaller interquartile range (IQR = Q3–Q1) by DNNs compared with the other three models clearly show that its distribution of error is much better than the others (**Figure 5**), and it is therefore preferred.

As mentioned earlier, the highest R^2 and the lowest RMSE were recorded by XGB (0.94 and 8.88, respectively) with scenario 3, followed by DNN with scenario 2 (0.93 and 11.11, respectively). Also, XGB with scenario 3 had the lowest MAE followed by XGB with scenario 2. These results do not agree with Fan et al. (2021) who reported that the best model results were given by DNN models (R^2 = 0.816–0.954), slightly outperforming SVR models (R^2 = 0.731–0.948) during the testing stage, followed by XGB models (R^2 = 0.739–0.929) under the four-input combination, but their research was about summer maize in Northwest China. The DNN model had a high prediction performance of yield which is similar to those reported by Khaki and Wang (2019), where RMSE for the validation dataset was around 11% of their respective values. The accuracy for the prediction of the crop yield was slightly higher than that reported by Khaki and Wang (2019) because they used average yield. In **Table 3**, the SI values are lower than 0.1 for all model scenarios, meaning the accuracy of the models can be characterized as "excellent" (Li et al., 2013; Maroufpoor et al., 2019).

CONCLUSION

This study presented ML approaches for the prediction of lettuce crop yield cultivated in three different hydroponic systems which interacted with three different kinds of magnetic water. Three samples were collected from each system 50 days after transplanting, at the same time, for all systems for 2 years. The datasets were divided into 70% for the training of the four ML models (i.e., RF, XGB, SVR, and DNNs) used to predict lettuce crop yield based on the three scenarios of input plant and water features, and 30% of the remaining data were used for testing the models.

The lowest RMSE was recorded in XGB with scenario 3 followed by SVR with scenario 3, and the highest, by RF with scenario 1. The R^2 was more than 0.77 for all applied model scenarios. Based on the SI, all models performed excellently, especially XGB with scenario 3 and SVR with scenario 3. Based on all performance statistics, the two best models were SVR with scenario 3 and DNN with scenario 2. However, the latter model scenario is preferred because it requires fewer input variables.

The methods developed in this study can be further improved by combining the input variables with climate variables, farming management data, and higher resolution spatiotemporal input variables for the successful prediction of crop yield on a large scale. The ML models could be a rapid tool for predicting crop yield and disaster evaluation over a large area.

CODE AVAILABILITY

Codes and datasets generated and/or analyzed during this study are available from the corresponding author on reasonable request.

DATA AVAILABILITY STATEMENT

The original contributions presented in the study are included in the article/supplementary material, further inquiries can be directed to the corresponding authors.

ETHICS STATEMENT

This study was approved by the Agricultural Engineering Research Institute, Agricultural Research Center, and the authors certify that this study was performed in accordance with the ethical standards as laid down in the 1964 Declaration of Helsinki and its later amendments or comparable ethical standards. The participants provided their written informed consent to participate in this study.

AUTHOR CONTRIBUTIONS

WE-S collected and analyzed the research data. AM designed and applied the ML models of the research. WE-S, AM, and MA wrote the original manuscript and provided suggestions on data analysis. NA-A, SS, and YG-A edited and provided suggestions to improve the content and structure of the manuscript. All authors read and edited the final manuscript before submission.

REFERENCES

Abdel-Fattah, M. K., and Abdo, A. A. I. M. (2020). Application of neural network and time series modeling to study the suitability of drain water quality for irrigation: A case study from Egypt. *Environ. Sci. Pollut. Res.* 28, 1–17. doi: 10.1007/s11356-020-10543-3

Abd-Rbo, G., Hegab, K., El-Behairy, U. A., and El-sawy, W. (2015). Effect Micro Irrigation Systems, Irrigation Period and Seed Thickness on Barley Sprout Production. *Int. J. Sci. Res. Agricult. Sci.* 2, 086–096.

Achieng, K. O. (2019). Modelling of soil moisture retention curve using machine learning techniques: Artificial and deep neural networks vs support vector regression models. *Comp. Geosci.* 133:104320. doi: 10.1016/j.cageo.2019.104320

Al-Fugara, A., Ahmadlou, M., Al-Shabeeb, A. R., AlAyyash, S., Al-Amoush, H., and Al-Adamat, R. (2020). Spatial mapping of groundwater springs potentiality using grid search-based and genetic algorithm-based support vector regression. *Geocarto Int.* 0, 1–20. doi: 10.1080/10106049.2020.1716396

Araújo, E. M., de Lima, M. D., Barbosa, R., and Alleoni, L. R. F. (2019). Using Machine Learning and Multi-Element Analysis to Evaluate the Authenticity of Organic and Conventional Vegetables. *Food Anal. Methods* 12, 2542–2554. doi: 10.1007/s12161-019-01597-2

Behar, O., Khellaf, A., and Mohammedi, K. (2015). Comparison of solar radiation models and their validation under Algerian climate - The case of direct irradiance. *Energy Convers. Manage.* 98, 236–251. doi: 10.1016/j.enconman.2015.03.067

Breiman, L. (2001). Random forests. *Random For.* 45, 1–122. doi: 10.1201/9780429469275-8

Cai, Y., Guan, K., Lobell, D., Potgieter, A. B., Wang, S., Peng, J., et al. (2019). Integrating satellite and climate data to predict wheat yield in Australia using machine learning approaches. *Agricult. For. Meteorol.* 274, 144–159. doi: 10.1016/j.agrformet.2019.03.010

Cao, J., Zhang, Z., Tao, F., Zhang, L., Luo, Y., Zhang, J., et al. (2021). Integrating Multi-Source Data for Rice Yield Prediction across China using Machine Learning and Deep Learning Approaches. *Agricult. For. Meteorol.* 297:108275. doi: 10.1016/j.agrformet.2020.108275

Chen, T., and Guestrin, C. (2016). XGBoost: A scalable tree boosting system. *Proc. ACM SIGKDD Int. Confer. Knowledge Discov. Data Mining* 2016, 785–794. doi: 10.1145/2939672.2939785

Chen, T., and Guestrin, C. (1994). Diagnosis of tuberculosis–newer tests. *J. Assoc. Physic. India* 42:665.

Elbeltagi, A., Aslam, M. R., Malik, A., Mehdinejadiani, B., Srivastava, A., Bhatia, A. S., et al. (2020). The impact of climate changes on the water footprint of wheat and maize production in the Nile Delta, Egypt. *Sci. Total Environ.* 743:140770. doi: 10.1016/j.scitotenv.2020.140770

El-Ssawy, W., Abuarab, M., El-Mogy, M., Mohamed, K., Wasef, E., Sultan, W., et al. (2020). The Impact of Advanced Static Magnetic Units on Water Properties and the Performance of Aeroponic and NFT Systems for Lettuce. *Pol. J. Environ. Stud.* 29, 1–12.

Everingham, Y., Sexton, J., Skocaj, D., and Inman-Bamber, G. (2016). Accurate prediction of sugarcane yield using a random forest algorithm. *Agronomy Sustainable Dev.* 36:364–z. doi: 10.1007/s13593-016-0364-z

Fan, J., Wang, X., Wu, L., Zhou, H., Zhang, F., Yu, X., et al. (2018). Comparison of Support Vector Machine and Extreme Gradient Boosting for predicting daily global solar radiation using temperature and precipitation in humid subtropical climates: A case study in China. *Energy Convers. Manage.* 164, 102–111. doi: 10.1016/j.enconman.2018.02.087

Fan, J., Zheng, J., Wu, L., and Zhang, F. (2021). Estimation of daily maize transpiration using support vector machines, extreme gradient boosting, artificial and deep neural networks models. *Agricult. Water Manage.* 245:106547. doi: 10.1016/j.agwat.2020.106547

Ferreira, L. B., and da Cunha, F. F. (2020). Multi-step ahead forecasting of daily reference evapotranspiration using deep learning. *Comp. Electron. Agricult.* 178:105728. doi: 10.1016/j.compag.2020.105728

Folberth, C., Baklanov, A., Balkoviè, J., Skalskı, R., Khabarov, N., and Obersteiner, M. (2019). Spatio-temporal downscaling of gridded crop model yield estimates based on machine learning. *Agricult. For. Meteorol.* 264, 1–15. doi: 10.1016/j.agrformet.2018.09.021

Fukuda, S., Spreer, W., Yasunaga, E., Yuge, K., Sardsud, V., and Müller, J. (2013). Random Forests modelling for the estimation of mango (Mangifera indica L. cv. Chok Anan) fruit yields under different irrigation regimes. *Agricult. Water Manage.* 116, 142–150. doi: 10.1016/j.agwat.2012.07.003

Ghimire, S., Deo, R. C., Raj, N., and Mi, J. (2019). Deep learning neural networks trained with MODIS satellite-derived predictors for long-term global solar radiation prediction. *Energies* 12:en12122407. doi: 10.3390/en12122407

Gueymard, C. A. (2014). A review of validation methodologies and statistical performance indicators for modeled solar radiation data: Towards a better bankability of solar projects. *Renewable Sustain. Energy Rev.* 39, 1024–1034. doi: 10.1016/j.rser.2014.07.117

Jackson, C., and McGonigle, D. (2005). Direct monitoring of the electrostatic charge of house-flies (Musca domestica L.) as they walk on a dielectric surface. *J. Electrostat.* 2005:75. doi: 10.1016/j.elstat.2005.03.075

Jeong, J. H., Resop, J. P., Mueller, N. D., Fleisher, D. H., Yun, K., Butler, E. E., et al. (2016). Random forests for global and regional crop yield predictions. *PLoS One* 11:1–15. doi: 10.1371/journal.pone.0156571

Johnson, D. M. (2014). An assessment of pre- and within-season remotely sensed variables for forecasting corn and soybean yields in the United States. *Rem. Sens. Environ.* 141, 116–128. doi: 10.1016/j.rse.2013.10.027

Kamir, E., Waldner, F., and Hochman, Z. (2020). Estimating wheat yields in Australia using climate records, satellite image time series and machine learning methods. *ISPRS J. Photogramm. Rem. Sens.* 160, 124–135. doi: 10.1016/j.isprsjprs.2019.11.008

Kang, Z., Catal, C., and Tekinerdogan, B. (2020). Machine learning applications in production lines: A systematic literature review. *Comp. Industr. Engine.* 149:106773. doi: 10.1016/j.cie.2020.106773

Khaki, S., and Wang, L. (2019). Crop yield prediction using deep neural networks. *Front. Plant Sci.* 10:1–10. doi: 10.3389/fpls.2019.00621

Khaki, S., Wang, L., and Archontoulis, S. V. (2020). A CNN-RNN Framework for Crop Yield Prediction. *Front. Plant Sci.* 10:1–14. doi: 10.3389/fpls.2019.01750

Kim, N., Ha, K. J., Park, N. W., Cho, J., Hong, S., and Lee, Y. W. (2019). A comparison between major artificial intelligence models for crop yield prediction: Case study of the midwestern United States, 2006–2015. *ISPRS Int. J. Geo Informat.* 8, 2006–2015. doi: 10.3390/ijgi8050240

Kloas, W., Groß, R., Baganz, D., Graupner, J., Monsees, H., Schmidt, U., et al. (2015). A new concept for aquaponic systems to improve sustainability, increase productivity, and reduce environmental impacts. *Aquacult. Environ. Interact.* 7, 179–192. doi: 10.3354/aei00146

Lecun, Y., Bengio, Y., and Hinton, G. (2015). Deep learning. *Nature* 521, 436–444. doi: 10.1038/nature14539

Li, M. F., Tang, X. P., Wu, W., Liu, H., and Bin. (2013). General models for estimating daily global solar radiation for different solar radiation zones

in mainland China. *Energy Convers. Manage.* 70, 139–148. doi: 10.1016/j.enconman.2013.03.004

Majid, M., Khan, J. N., Ahmad Shah, Q. M., Masoodi, K. Z., Afroza, B., and Parvaze, S. (2021). Evaluation of hydroponic systems for the cultivation of Lettuce (Lactuca sativa L., var. Longifolia) and comparison with protected soil-based cultivation. *Agricult. Water Manage.* 245:106572. doi: 10.1016/j.agwat.2020.106572

Manju, M., Karthik, V., Hariharan, S., and Sreekar, B. (2017). Real time monitoring of the environmental parameters of an aquaponic system based on internet of things. *ICONSTEM* 2017, 943–948. doi: 10.1109/ICONSTEM.2017.8261342

Maroufpoor, S., Maroufpoor, E., Bozorg-Haddad, O., Shiri, J., and Mundher Yaseen, Z. (2019). Soil moisture simulation using hybrid artificial intelligent model: Hybridization of adaptive neuro fuzzy inference system with grey wolf optimizer algorithm. *J. Hydrol.* 575, 544–556. doi: 10.1016/j.jhydrol.2019.05.045

Mehra, M., Saxena, S., Sankaranarayanan, S., Tom, R. J., and Veeramanikandan, M. (2018). IoT based hydroponics system using Deep Neural Networks. *Comp. Electron. Agricult.* 155, 473–486. doi: 10.1016/j.compag.2018.10.015

Mokhtar, A., Jalali, M., He, H., Al-Ansari, N., Elbeltagi, A., Alsafadi, K., et al. (2021). Estimation of SPEI Meteorological Drought Using Machine Learning Algorithms. *IEEE Access* 9, 65503–65523.

Montes-Atenas, G., Seguel, F., Valencia, A., Bhatti, S. M., Khan, M. S., Soto, I., et al. (2016). Predicting bubble size and bubble rate data in water and in froth flotation-like slurry from computational fluid dynamics (CFD) by applying deep neural networks (DNN). *Int. Commun. Heat Mass Transfer* 76, 197–201. doi: 10.1016/j.icheatmasstransfer.2016.05.031

Murad, S. A. Z., Harun, A., Mohyar, S. N., Sapawi, R., and Ten, S. Y. (2017). Design of aquaponics water monitoring system using Arduino microcontroller. *AIP Confer. Proc.* 1885:5002442. doi: 10.1063/1.5002442

Neocleous, D., and Savvas, D. (2019). The effects of phosphorus supply limitation on photosynthesis, biomass production, nutritional quality, and mineral nutrition in lettuce grown in a recirculating nutrient solution. *Sci. Horticult.* 252, 379–387. doi: 10.1016/j.scienta.2019.04.007

Puccinelli, M., Landi, M., Maggini, R., Pardossi, A., and Incrocci, L. (2021). Iodine biofortification of sweet basil and lettuce grown in two hydroponic systems. *Sci. Horticult.* 276:109783. doi: 10.1016/j.scienta.2020.109783

Qader, S. H., Dash, J., and Atkinson, P. M. (2018). Forecasting wheat and barley crop production in arid and semi-arid regions using remotely sensed primary productivity and crop phenology: A case study in Iraq. *Sci. Total Environ.* 613–614, 250–262. doi: 10.1016/j.scitotenv.2017.09.057

Sadeghipour, O., Aghaei, P., and Sadeghipour, O. (2013). Improving the growth of cowpea (Vigna unguiculata L. Walp.). *Magnetized Water* 3, 37–43.

Saiz-Rubio, V., and Rovira-Más, F. (2020). From smart farming towards agriculture 5.0: A review on crop data management. *Agronomy* 10:10020207. doi: 10.3390/agronomy10020207

Shah, S. H., Angel, Y., Houborg, R., Ali, S., and McCabe, F. (2019). Spectral-spatial attention networks for hyperspectral image classification. *Rem. Sens.* 11:rs11080920. doi: 10.3390/rs11080920

Sonneveld, C., and Voogt, W. (2001). Velocity Analysis and Statics Corrections. *Seismic Data Anal.* 2001:ch3. doi: 10.1190/1.9781560801580.ch3

Stone, R. J. (1994). A nonparametric statistical procedure for ranking the overall performance of solar radiation models at multiple locations. *Energy* 19, 765–769. doi: 10.1016/0360-5442(94)90014-0

Taylor, K. E. (2001). Summarizing multiple aspects of model performance in a single diagram. *J. Geophys. Res.* 106, 7183–7192. doi: 10.1029/2000jd900719

Vapnik, V. N. (2016). Reviewed Work: A Step-by-Step Approach to Using the SAS®System for Factor Analysis and Structural Equation Modeling by Larry Hatcher. *Am. Soc. Qual. Am. Statist. Assoc.* 38, 296–297. doi: 10.2307/1270628

Wei, Y., Li, W., An, D., Li, D., Jiao, Y., and Wei, Q. (2019). Equipment and Intelligent Control System in Aquaponics: A Review. *IEEE Access* 7, 169306–169326. doi: 10.1109/ACCESS.2019.2953491

Wolanin, A., Camps-Valls, G., Gómez-Chova, L., Mateo-García, G., van der Tol, C., Zhang, Y., et al. (2019). Estimating crop primary productivity with Sentinel-2 and Landsat 8 using machine learning methods trained with radiative transfer simulations. *Rem. Sens. Environ.* 225, 441–457. doi: 10.1016/j.rse.2019.03.002

Xu, B., Wang, N., Chen, T., and Li, M. (2015). Empirical Evaluation of Rectified Activations in Convolutional Network. [Preprint].

You, J., Li, X., Low, M., Lobell, D., and Ermon, S. (2017). Deep Gaussian Process for Crop Yield Prediction Based on Remote Sensing Data Jiaxuan. *Proc. Thirty First AAAI Confer. Artific. Intellig.* 2, 569–573. doi: 10.1109/MWSCAS.2006.381794

Conflict of Interest: The authors declare that the research was conducted in the absence of any commercial or financial relationships that could be construed as a potential conflict of interest.

Publisher's Note: All claims expressed in this article are solely those of the authors and do not necessarily represent those of their affiliated organizations, or those of the publisher, the editors and the reviewers. Any product that may be evaluated in this article, or claim that may be made by its manufacturer, is not guaranteed or endorsed by the publisher.

Advantages of publishing in Frontiers

OPEN ACCESS
Articles are free to read for greatest visibility and readership

FAST PUBLICATION
Around 90 days from submission to decision

HIGH QUALITY PEER-REVIEW
Rigorous, collaborative, and constructive peer-review

TRANSPARENT PEER-REVIEW
Editors and reviewers acknowledged by name on published articles

Frontiers
Avenue du Tribunal-Fédéral 34
1005 Lausanne | Switzerland

Visit us: www.frontiersin.org
Contact us: frontiersin.org/about/contact

REPRODUCIBILITY OF RESEARCH
Support open data and methods to enhance research reproducibility

DIGITAL PUBLISHING
Articles designed for optimal readership across devices

FOLLOW US
@frontiersin

IMPACT METRICS
Advanced article metrics track visibility across digital media

EXTENSIVE PROMOTION
Marketing and promotion of impactful research

LOOP RESEARCH NETWORK
Our network increases your article's readership